



205(2), 2026



COMBUSTION ENGINES

EMITUJE TYLKO WODĘ. OCZYSZCZA POWIETRZE



REWOLUCJA



Toyota Mirai to technologia jutra dostępna już dziś.

To pierwszy samochód elektryczny na wodór o nadwoziu typu sedan.



MIRAI

Zużycie paliwa w Toyocie Mirai FCEV i emisja CO₂: metoda badawcza WLTP 182 KM e-CVT średnio [kg H₂/100 km] 0,84, emisja CO₂ średnio [g/km] 0. Zużycie paliwa i emisja spalin CO₂ w konkretnym pojeździe w warunkach drogowych może różnić się od podanych wyników pomiarów. Na zużycie paliwa i emisję CO₂ wpływa sposób prowadzenia pojazdu oraz inne czynniki (takie jak warunki drogowe, natężenie ruchu, stan pojazdu, ciśnienie w oponach, załadowanie wyposażeniem, obciążenie, liczba pasażerów itp.). Informacje o działaniach dotyczących odzysku i recyklingu samochodów wycofanych z eksploatacji: www.toyota.pl

Due to the dynamic development of machine and vehicle powertrains, the "**Combustion Engines**" scientific journal, while retaining its historical title, currently publishes works related not only to internal combustion engines, but also other powertrains, including hybrid drives, electric drives and fuel cells.

PTNSS Supporting Members Członkowie wspierający PTNSS

BOSMAL Automotive Research and Development Institute Ltd

Instytut Badań i Rozwoju
Motoryzacji BOSMAL Sp. z o.o

Motor Transport Institute

Instytut Transportu Samochodowego

Institute of Aviation

Sieć Badawcza Łukasiewicz
– Instytut Lotnictwa

Automotive Industry Institute

Sieć Badawcza Łukasiewicz
– Przemysłowy Instytut Motoryzacji

Sieć Badawcza Łukasiewicz

– Poznański Instytut Technologiczny

AVL List GmbH

Air Force Institute of Technology

Instytut Techniczny Wojsk Lotniczych

Military Institute of Armoured & Automotive Technology

Wojskowy Instytut Techniki Pancernej
i Samochodowej

Toyota Motor Poland Ltd. Sp. z o.o.

RADWAG Balances and Scales

RADWAG Wagi Elektroniczne

FOGO Sp. z o.o.

Horus Energia Sp. z o.o.

John Deere Polska Sp. z o.o.



COMBUSTION ENGINES

A Scientific Magazine

2026, 205(2)

Year LXV

PL ISSN 2300-9896

PL eISSN 2658-1442

Publisher:

Polish Scientific Society of Combustion Engines

61-131 Poznan, ul. J. Rychniewskiego 1, Poland

tel.: +48 61 6475959

E-mail: sekretariat@ptnss.pl

WebSite: <http://www.ptnss.pl>

Papers available on-line: <http://combustion-engines.eu>

Scientific Board:

- Krzysztof Wisłocki – chairman, Poland (*Poznan University of Technology*)
- Yuzo Aoyagi – Japan (*Okayama University*)
- Ewa Bardasz – USA (*National Academy of Engineering*)
- Piotr Bielaczyc – Poland (*BOSMAL Automotive Research and Development Institute Ltd.*)
- Zdzisław Chłopek – Poland (*Warsaw University of Technology*)
- Tadeu Cordeiro de Melo – Brazil (*Petrobras*)
- Jan Czerwinski – Switzerland (*CJ Consulting*)
- Radostin Dimitrov – Bulgaria (*University of Varna*)
- Friedrich Dinkelacker – Germany (*Leibniz Universität Hannover*)
- Hubert Friedl – Austria (*AVL*)
- Barouch Giechaskiel – Italy (*European Commission, JRC Italy*)
- Leslie Hill – UK (*Horiba*)
- Timothy Johnson – USA (*Corning Inc.*)
- Kazimierz Lejda – Poland (*Rzeszow University of Technology*)
- Helmut List – Austria (*AVL*)
- Toni Kinnunen – Finland (*Proventia*)
- David Kittelson – USA (*University of Minnesota*)
- Christopher Kolodziej – USA (*Delphi Automotive Systems*)
- Hu Li – UK (*University of Leeds*)
- Vaselin Mihaylov – Bulgaria (*University of Varna*)
- Federico Millo – Italy (*Politecnico Torino*)
- Jeffrey D. Naber – USA (*Michigan Technological University*)
- Andrzej Niewczas – Poland (*Motor Transport Institute*)
- Marek Orkisz – Poland (*Rzeszow University of Technology*)
- Dieter Peitsch – Germany (*TU Berlin*)
- Stefan Pischinger – Germany (*FEV Germany*)
- Andrzej Sobiesiak – Canada (*University of Windsor*)
- Stanisław Szwejca – Poland (*Częstochowa University of Technology*)
- Piotr Szymański – Netherlands (*European Commission, JRC*)
- Leonid Tartakovsky – Israel (*Technion – Israel Institute of Technology*)
- Andrzej Teodorczyk – Poland (*Warsaw University of Technology*)
- Xin Wang – China (*Beijing Institute of Technology*)
- Thomas Wallner – USA (*Argonne National Laboratory*)
- Michael P. Walsh – USA (*International Council on Clean Transportation*)
- Mirosław Wendeker – Poland (*Lublin University of Technology*)

Contents

Zimakowska-Laskowska M, Bogdanowicz A, Kniaziewicz T. Assessment of exhaust gas concentration uniformity in a marine engine duct based on dual-point sampling and CFD modelling..... 3

Sroka Z. Geopolitical factors influencing the rightsizing of combustion engines 17

Przytula I, Burchart D. Greenhouse gas assessment of urban buses based on environmental product declarations – a review 32

Longwic R, Kuzsneruk M, Klepka M. Comparative analysis of exhaust emissions from a compression-ignition engine fueled with mixtures of rapeseed oil with n-hexane and diesel fuel during selected phases of the WLTP test..... 39

Tomaniak E, Koszałka G, Marinho Maria T, Christinelli W, Hunicz J, Rodrigues dos Santos Crepaldi E. Use of digital twin to analyse the effect of graphene as a lubricant additive for diesel engines 46

Sander P, Longwic R, Tarkowski S. Analysis of the influence of the n-hexane content in the mixture with rapeseed oil on the auto-ignition delay angle of the fuel 56

Matla J, Kaźmierczak A, Grzebyk M, Hardy T. The study of hydrogen consumption in 12-meter fuel cell electric urban buses 64

Zadrag R, Socik P, Zacharewicz M, Bogdanowicz A, Sigieli N. Analysis of biodegradable additives in marine fuels and their effect on toxic exhaust emissions..... 71

Kamiński A. A mathematical study of the narrowband lambda sensor characteristics for lean and rich operation 82

Włóka A, Włostowski R, Leśny K, Kaźmierczak A. Preliminary research on the co-combustion process of ammonia in a compression-ignition engine 88

Lagowski P, Kurczyński D, Wcisło G. Assessment of the oxidative stability of biofuels for compression ignition engines..... 96

Nadaleti W, Przybyła G, Szczygiel I. Six-stroke spark-ignition engine fuelled with high-hydrogen-content fuel: a theoretical thermodynamic analysis..... 103

Stepanenko D. Study on effects of LPG addition and EGR application on the combustion and emission characteristics in a dual-fuel diesel engine 109

Lukášik P, Kadlub V. Chemical decarbonisation of diesel engine and its impact on engine oil degradation 121

Jakubowski R, Szumski M. Application of ChatGPT in the generation of a numerical performance model of a turbofan engine 130

Mateo NE, Calderon A, Agrupis S, Acidera KC, Manzano LF. Performance of a nipa-based fuel blend on a multi-blend capable engine test motorcycle towards renewable biofuel solutions 139

Nieścioruk MJ, Boroiu AA, Ozuna G, Ávila AB, Kubiak P, Wozniak M, Siczek K. The use of hydrogen to supply combustion engines – part 1 148

Gross X, Tomasz J, Skowron M, Kurc B, Rudnicka E, Szymlet N, Rymaniak Ł. The electrochemical route to sustainable transport..... 164

Porras Perucho HA, Moreira CMV, Boruc Ł, Grochowalska J, Kapusta ŁJ. Spray structures formed by a multi-nozzle injector during the injection of a multi-component surrogate synthetic fuel under flash-boiling conditions 170

Leśny K, Włostowski R, Włóka A, Kaźmierczak A. Analysis of the possibilities of using alternative fuel mixtures as a substitute for conventional fuels 177

Grochowalska J, Kapusta ŁJ. A model of a fuel spray parameter in a marine diesel engine..... 184

Szwajca F, Wislocki K. Impact of spark plug type on the cycle-to-cycle variability in an internal combustion gas engine..... 191

Laskowski P, Wojs M. Application of 3D-printed metal pistons in internal combustion engines: advantages and challenges..... 198

Skrętowicz M. Analysis of the quality of vehicle fleet data as input for modeling emissions and dispersion of pollutants emitted by combustion engine vehicles 206

Declaration of the original version
The original version of the Combustion Engines journal is the electronic version.

Cover

I – Cummins B6.7 Octane: new gasoline engine for medium-duty (northamerica.daimlertruck.com);
 background (Debdutta Dhara, Tractor Driving on Dusty Rural Pathway – pexels.com)
 IV – Mercedes-AMG Twin-Turbo 4.0-Liter V-8 (www.motorauthority.com)

Publisher:

Polish Scientific Society of Combustion Engines
 61-131 Poznan, ul. J. Rychlewskiego 1, Poland
 tel.: +48 61 6475959
 E-mail: sekretariat@ptnss.pl
 WebSite: <http://www.ptnss.pl>

The Publisher of this magazine does not endorse the products or services advertised herein. The published materials do not necessarily reflect the views and opinions of the Publisher.

© Copyright by
Polish Scientific Society of Combustion Engines
 All rights reserved.

No part of this publication may be reproduced, stored in a retrieval system or transmitted, photocopied or otherwise without prior consent of the copyright holder.

The journal is under the patronage of the Transport Committee and the Machine Building Committee of the Polish Academy of Sciences



The journal is registered and listed in the Polish and international database



Papers published in the
Combustion Engines

quarterly receive 70 points as stated by the Notification of the Minister of Science dated 5 January 2024.

Editorial:

Institute of Powertrains and Aviation
 Poznan University of Technology
 61-138 Poznan, Piotrowo 3 Street
 tel.: +48 61 2244505, +48 61 2244502
 E-mail: papers@ptnss.pl

Prof. Jerzy Merkisz, DSc., DEng. (Editor-in-chief)
 Prof. Miłostaw Kozak, DSc., DEng.
 Prof. Jacek Pielecha, DSc., DEng. (Editorial Secretary for Science)
 Prof. Ireneusz Pielecha, DSc., DEng.
 Prof. Jacek Hunicz, DSc., DEng.
 Prof. Liping Yang, DSc., DEng.
 Prof. Pravesh Chandra Shukla, DSc., DEng.
 Di Zhu, DEng.
 Wojciech Cieślak, DSc., DEng.
 Filip Szwajca, DEng. (Technical Editors)
 Joseph Woodburn, DEng. (Proofreading Editor)
 Wojciech Serdecki, DSc., DEng. (Statistical Editor)

Assessment of exhaust gas concentration uniformity in a marine engine duct based on dual-point sampling and CFD modelling

ARTICLE INFO

The paper presents an analysis of the flow of pollutants in the exhaust pipe of a marine diesel engine, based on measurements taken at two measurement points 2.5 meters apart. The concentrations of the basic exhaust components – CO, NO_x, HC, and O₂ – were recorded during engine operation at different load levels, ranging from 30 to 686 kW. The aim of the analysis was to determine whether significant changes in the chemical composition of the exhaust gases occur in the section of the exhaust pipe between the two points. The results showed that the differences in the recorded concentrations were negligible, which confirms the homogeneity of the gas composition in the tested section and allows treating this section of the pipe as a conduit with established flow properties. Based on the measurements, a CFD model of exhaust flow was developed, representing the distribution of velocity and pressure in the exhaust pipe of a marine combustion engine. This model will be used to analyze mixing processes, possible local accumulation, and the effect of the geometry and operating conditions of the engine on the distribution of pollutants in the exhaust system.

Received: 10 June 2025

Revised: 2 August 2025

Accepted: 2 August 2025

Available online: 16 September 2025

Key words: *marine diesel engine, exhaust gas composition, CFD modeling, pollutant dispersion, multi-point measurement*

This is an open access article under the CC BY license (<http://creativecommons.org/licenses/by/4.0/>)

1. Introduction

Marine engines, especially fossil fuel-powered piston combustion engines, are among the main sources of air pollution emissions in port areas and coastal zones. In actual operation conditions, vessels emit significant amounts of nitrogen oxides (NO_x), sulphur oxides (SO_x), particulate matter (PM), volatile organic compounds (VOCs), and carbon dioxide (CO₂), which have a significant impact on air quality, human health, and the heat balance of the atmosphere [1, 14, 25]. Due to the high concentration of emission sources in ports and limited atmospheric exchange under typical local weather conditions, modelling the spread of pollutants from marine vessels is an important tool to support environmental and design decisions. However, the effectiveness of emission dispersion models depends largely on the quality of input data, particularly the chemical composition and spatial distribution of exhaust gases leaving the exhaust system. In emission modelling for numerical simulations (e.g. CFD or GIS-CFD), one of the most commonly adopted simplifications is the assumption of uniform exhaust gas composition across the pipe cross-section. This simplification is commonly used in conditions of limited access to measurement data, but its validity is not always verified experimentally. As indicated by Deng et al. [5], local differences in concentrations resulting from turbulent flow, non-mixing, or secondary transformations can lead to errors in estimating the spread of pollutants in the environment. The aim of this work is to empirically assess the spatial homogeneity of the chemical composition of exhaust gases in a straight section of the exhaust pipe of a ship engine. As part of the research, the concentrations of selected exhaust gas components (NO_x, CO, HC, O₂) were measured at two measuring points located along the axis of the pipe, at a distance of 2.5 m. The recording was made in operating conditions for different engine load levels. The recorded data were subjected to statistical and time analy-

sis, and their interpretation was supported their interpretation was supported by CFD simulation representing flow conditions. The obtained results allow us to assess the validity of simplifying the emission distribution to a one-dimensional profile and indicate whether data from a single point can be considered representative for modeling pollutant dispersion.

2. Literature studies

Pollutant emissions from vessels are a significant source of environmental burden, especially in port areas and areas with high shipping traffic. The most important emission components are nitrogen oxides (NO_x), sulphur oxides (SO_x), particulate matter (PM), volatile organic compounds (VOCs), and CO₂ [1, 14, 25, 27]. Such emissions stem directly from combustion processes in ship engine chambers [5, 8]. In response to increasing environmental requirements, both regulatory restrictions (e.g. MARPOL Annex VI standards) and emission reduction technologies are being introduced. The most commonly used of these are selective catalytic reduction (SCR), exhaust gas recirculation (EGR) systems, particulate matter traps (DPF), fuel type changes (e.g. LNG, MGO), and – increasingly – hybrid systems and alternative power sources, especially in short-sea shipping [2, 9, 13, 17]. However, the efficiency of these technologies depends not only on the parameters of the propulsion system itself, but also on the operating conditions, load level, and exhaust system design [13, 22]. The literature also emphasizes the importance of degradation of operating materials, such as oils or fuels, which, through the presence of particulate matter and oxidation products, can affect the combustion process and exhaust gas composition. Gil et al. [6] showed that contamination in gear oils significantly changes their lubricating properties, which in the long term may affect the performance characteristics of the propulsion system and pollutant emissions. Phenomena accompanying the flow of exhaust gases in the exhaust

pipe, such as turbulent mixing, pressure changes, losses at the joints, or the presence of local turbulences, may affect the actual effectiveness of the cleaning systems and the distribution of concentrations at the outlet of the system. Soulhac et al. [21, 22] draw attention to the need to take into account spatial inhomogeneity in emission models, especially when trying to assess the local impact of the unit on air quality. At the same time, many simplified emission models used in environmental assessments of vessels assume a homogeneous distribution of the exhaust gas composition in the outlet cross-section. In the conditions of actual operation of marine engines, this assumption is not always confirmed by experimental data [5].

For this reason, the need to verify the spatial distribution of the exhaust gas composition within the exhaust system itself is increasingly being postulated to correctly assess the boundary conditions for further modelling of the spread of pollutants.

In the case of RCCI engines fuelled with a mixture of diesel and NG, the use of an appropriate split injection strategy allows for a significant reduction in the emission of incomplete combustion products and improvement of thermal efficiency, while at the same time influencing the complexity of the emission profile [26]. This approach is used, among others, in the works of Basiri et al. [2], Lin et al. [12], and Johansson et al. [10], who use both measurement data and CFD simulations to reproduce realistic emission conditions from vessels.

Precise knowledge of the emission source characteristics, including the spatial distribution of exhaust gas composition, is therefore essential not only for the selection of emission reduction technologies, but also for the correct modelling of their spread in the environment. Similar conclusions were presented in [29], showing that the accuracy of air quality forecasts in port areas depends mainly on the level of detail and the method of obtaining emission data. Effective assessment of the impact of emissions from maritime transport on the environment requires the use of appropriate pollutant dispersion models. In recent decades, a number of computational tools have been developed to simulate the spread of gaseous and particulate pollutants in variable meteorological and geographical conditions. These models take into account, among others, wind speed and direction, turbulence, temperature, terrain, and the height of emissions above ground level [18, 21, 22]. The most used tools include AERMOD, CALPUFF, and SIRANE. AERMOD is based on a modified Gaussian model that takes into account meteorological factors and is characterized by high sensitivity to the quality of input data, such as terrain roughness or the height of the emission source [18]. The SIRANE model was developed for the urban environment and better reflects the conditions in densely built-up areas [21, 22]. The accuracy of the results obtained from dispersion models depends to a large extent on the quality of emission data. As indicated by Rezaali et al. [18], errors in the parameterization of the emission source can lead to deviations of $\pm 60\%$ in the predicted pollutant concentrations. For this reason, data assimilation techniques and model tuning based on field measurement results are increasingly used [22, 23]. In the case of emissions from

vessels, additional challenges include the variability of engine operating conditions, changes in the location of the emission source, and the dynamic geometry of the environment. The models must take into account the ship's trajectory and the interactions of the exhaust jet with local atmospheric and hydrological conditions [11, 19]. The characteristics of the initial exhaust dispersion are also crucial, depending on the exhaust pipe geometry, the muffler layout, and the gas temperature and velocity. Although CFD modelling can accurately represent these phenomena, in practice, many dispersion models are still based on generalized emission source parameters that require empirical verification. Advanced multi-zone combustion models are now an important tool supporting CFD emission simulations of complex propulsion systems such as LTC, HCCI, or RCCI [24]. Their integration with simulation tools enables more accurate source analysis of emissions under transient and low-temperature conditions.

As shown by the studies of Basiri et al. [2] and Deng et al. [5], the inhomogeneity of the exhaust gas composition in the first meters from the outlet can significantly affect the accuracy of environmental forecasts. Therefore, the importance of multi-point measurements in the immediate vicinity of the emission source is growing. Such measurements enable precise representation of the actual concentration distribution and calibration of input data for dispersion models. Only in this way is it possible to reliably predict the spread of pollutants in port and coastal areas and develop effective air quality management strategies. However, reliable representation of emission conditions in numerical models requires not only multi-point data, but also detailed consideration of design factors such as the geometry of the exhaust pipe and the shape of the outlet jet. The literature emphasizes that these elements – often marginalized in simplified models – have a significant impact on the initial concentration distribution and trajectory of the pollutant plume [5, 28]. The geometry of the exhaust system has a significant impact on the distribution of exhaust components and on the accuracy of emission measurements, which directly translates into the reliability of pollutant dispersion models. Although many emission models assume a homogeneous exhaust gas composition at the outlet, experimental studies have shown that flow conditions often contradict this. Bends, narrowing, changes in cross-section, and can induce turbulence, phase separation, and localized concentration gradients [2, 5, 15]. As a result, the shape of the emission plume – its width, direction, and mixing speed – depends not only on the engine operating conditions, but also on the design of the final section of the exhaust pipe [12]. These problems are particularly important when using CFD models, in which the assumed boundary conditions – velocity profile, temperature, composition, and spatial distribution of exhaust gases – determine the final result of the simulation [10, 16, 20, 23]. Unfortunately, many studies are based on single measurements, averaged in time and space, which can lead to errors of 20–50% in local receptors, especially in systems with complex geometry or dynamic load changes [7, 18].

For this reason, multi-point measurements, both axial and radial, are becoming increasingly important, enabling

accurate representation of the concentration distribution in the cross-section and along the duct [5]. This approach not only increases the reliability of emission data but also enables the calibration of numerical models and better representation of flow phenomena, such as recirculation or stream separation. This is of key importance, especially in validation studies and in the design of emission reduction systems. In parallel, increasing attention is being paid to the analysis of uncertainty and sensitivity of CFD models. Errors in input data – e.g., regarding mass flow or NO_x concentration – can lead to large discrepancies between simulation results and reality [18]. These analyses allow us to indicate which parameters have the greatest impact on the result and which should be controlled with greater precision. Techniques such as data assimilation, i.e., tuning the model based on actual measurements, are becoming an increasingly popular tool for reducing uncertainty [10]. Validation of models based on empirical data is an essential step in the emission modelling process. Field and laboratory studies provide key information on the actual behaviour of the exhaust stream, which can differ substantially from results based on simplified assumptions. Without such data, even the most advanced CFD models remain a tool with limited predictive value, especially in variable and difficult to generalize conditions – as is the case with ship systems [2, 5]. Considering the presented results of literature studies, the key factor influencing the accuracy of exhaust emission modelling turns out to be the spatial distribution of the exhaust gas composition within the exhaust tract. Reliable representation of emission conditions requires both considering the geometry of the exhaust system and the use of empirical data from multi-point measurements. Of particular importance are data enabling the assessment of the homogeneity of the exhaust gas composition and flow parameters, which can be used to define boundary conditions in CFD models. In response to these needs, this paper proposes an approach based on direct comparison of measurement data from two points along the exhaust pipe axis. The combination of statistical and time analyses and numerical flow simulation enabled a comprehensive assessment of the spatial variability of the exhaust gas composition. The obtained results constitute the basis for verifying the assumptions on the homogeneity of emissions and assessing the possibility of using simplified emission models in further analyses of pollutant spread.

Despite the increasing number of dispersion modelling studies in maritime transport, there is still a lack of empirical data verifying the spatial uniformity of pollutant concentrations within the exhaust systems of marine engines. This research addresses that gap by providing a detailed analysis of concentration profiles based on dual-point measurements and CFD simulations. The scientific objective is to evaluate whether the chemical composition of exhaust gases can be considered spatially homogeneous along a straight pipe section, which is crucial for setting accurate boundary conditions in emission modelling. The main contribution of this study lies in combining empirical measurements, statistical testing, and CFD modelling to validate simplified emission profile assumptions, thereby

improving the reliability of environmental impact assessments based on marine engine emissions.

3. Materials and methods

3.1. Test stand and general measurement setup

The section presents a detailed description of the test object, the configuration of the measuring station, and the conditions in which the pollutant emission data were recorded. The layout of the measuring points, the parameters of the exhaust gas analyser, and the power ranges corresponding to the analysed engine load states are described. The methods used in the analysis of empirical data are also included, with particular emphasis on descriptive statistics, significance tests, and principal component analysis. The supplement is a description of the assumptions adopted for numerical modelling (CFD), which is a tool for verifying the homogeneity of the flow and distribution of exhaust gas components in the exhaust pipe.

The tests were carried out on a marine engine type SULZER 6AL20/24, fuelled with F-75 diesel oil. It is a six-cylinder, four-stroke engine with direct fuel injection, turbocharging, and charge air cooling. The engine was fuelled with F-75 marine diesel oil and operated with a turbocharged air supply system with charge air cooling. No exhaust aftertreatment system (such as SCR or DPF) was used, as the test object was a conventional marine engine operating in a laboratory setting without emission control technologies.

The main technical data of the engine are presented in Table 1.

Table 1. Technical data laboratory stand SULZER 6AL20/24 engine [3]

Parameter	Value
Number of cylinders	6
Nominal power	420 kW (at 750 rpm rotational speed)
Nominal speed	750 rpm
Idle speed	350 rpm
Cylinder diameter	200 mm
Piston stroke	240 mm
Compression ratio	12.7
Maximum combustion pressure	10.5–11.0 MPa
Fuel injection pressure	24.5 MPa
Specific consumption	212 g/kWh

The engine was operated with a Froude water brake, which allowed for the reproduction of dynamic manoeuvring conditions typical of port navigation and short-distance voyages. Measurements were taken in real operating conditions, with variable load and variable crankshaft speed.

3.2. Measurement system and sampling layout

A portable TESTO 350 analyser was used to record the chemical composition of exhaust gases, enabling simultaneous measurement of CO, NO, NO₂, O₂, SO₂, and CO₂ concentrations. The measurement range and accuracy of the device are presented in Table 2.

Measurements were taken at two points along the exhaust pipe axis, spaced 2.5 meters apart (Fig. 1). This enabled analysis of spatial emission inhomogeneity and assessment of the accuracy of the assumptions of homogeneous emission profiles in the CFD models.

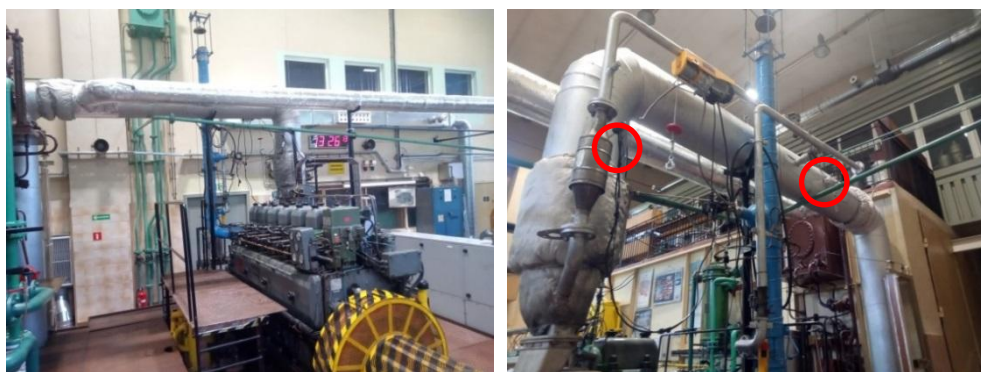


Fig. 1. Laboratory stand SULCER 6AL20/24 engine and exhaust installation

Table 2. Analyser TESTO 350 parameters [4]

Parameter	Measuring range	Tolerance
Exhaust temperature	-40 to 1000°C	±5 K
O ₂	0–25%	According to MARPOL VI
CO	0–3000 ppm	±10 ppm
NO/NO ₂	0–3000/0–500 ppm	±5 ppm/±1 ppm
SO ₂	0–3000 ppm	±5 ppm
CO ₂ (IR)	0–40%	±0.5% obj.
Absolute pressure	600–1150 hPa	±5–10 hPa

The measurements were performed using a single TESTO 350 portable analyser. The device was alternately connected to two sampling points along the exhaust pipe, with measurements taken separately under stabilised engine operating conditions. The analyser did not include a hydrocarbon (HC) measurement module; therefore, HC concentrations were not recorded in this study.

3.3. Load conditions during measurements

The measurement was performed in four load conditions, corresponding to instantaneous powers of approximately 430 kW, 494 kW, 558 kW, and 622 kW. For each load level, concentration parameters were recorded in stabilised engine operating conditions. The obtained data were characterized by low instantaneous variability, which allowed their use to assess the uniformity of the distribution of exhaust components and to analyse their variability between measurement points. The power ranges were selected to reflect typical operating conditions of the vessel – from port manoeuvres at low load to full power in cruise conditions. Such selection allows for an assessment of whether emission modelling can be based on average values for individual operating modes. Measurements were taken at two points along the exhaust pipe axis, spaced 2.5 meters apart (Fig. 1). This enabled analysis of spatial emission inhomogeneity and assessment of the accuracy of the assumptions of homogeneous emission profiles in the CFD models. The selected load points were unrelated to legislative or certification test cycles. However, they were chosen to reflect typical real-world engine operating conditions encountered during port manoeuvres and cruising. The goal was to ensure representativeness of the measurements rather than compliance with any specific regulatory protocol.

3.4. Data analysis and CFD modelling tools

Statistical analysis of the measurement data was performed in the Python environment (version 3.10), using the

pandas, seaborn, scikit-learn, and SciPy libraries. It included the calculation of descriptive statistics, coefficients of variation (CV), principal component analysis (PCA), and tests of significance of differences (ANOVA, Student's t-test, Mann–Whitney U). The analysis included data from one measurement set, recording emission parameters at two points in the exhaust pipe. This set was selected as representative due to typical engine operating conditions and characteristic load range. All sets contained a comparable number of observations, and preliminary analysis showed similar distributions and relationships, which justifies limiting the full analysis to one case without losing the generality of the conclusions. CFD simulation was performed in the OpenFOAM numerical software environment, representing the exhaust gas flow in the analysed section of the exhaust pipe. A steady-state flow model was applied using RANS (Reynolds-Averaged Navier–Stokes) turbulence modelling. Boundary conditions were assumed as constant: the volume flow and gas composition were defined at the inlet, and atmospheric pressure at the outlet. The model geometry corresponded to the actual measurement system, and the mesh was refined in the near-wall zones to improve the accuracy of flow conditions representation. It should be noted that the CFD model used in this study did not account for the pulsating nature of exhaust flow resulting from the cyclic operation of individual engine cylinders. Instead, a steady-state approximation was adopted, based on averaged flow parameters under stabilised load conditions. This simplification is consistent with the RANS modelling approach and was deemed acceptable to assess overall flow homogeneity and composition stability within a straight section of the exhaust duct.

4. Results

4.1. Statistical comparative analysis of emissions

This section presents the results of the analysis of the exhaust gas composition recorded at two measurement points located along the exhaust pipe of a marine engine. The analysis includes both a comparison of descriptive statistics and an assessment of the variability and interdependence of the concentrations of individual exhaust gas components. Additionally, statistical tests were performed to identify significant differences between the points, as well as an analysis of the time course and numerical simulation of the flow within the CFD model. The entire analysis aimed to determine whether the exhaust gas's chemical

Table 3. Descriptive statistics of exhaust gas components (O₂, CO, NO, NO₂, H₂, NO_x) at measurement points 1 and 2, including mean values, median, minimum, maximum, standard deviation, IQR and coefficient of variation (CV)

Compound	Mean	Median	Min	Max	Std	IQR	CV [%]
Point 1							
O ₂	10.997	11.0	10.98	11.02	0.012	0.015	0.11
CO	304.323	304.0	302.0	310.0	2.212	1.0	0.73
NO	1928.581	1927.0	1925.0	1935.0	3.462	5.5	0.18
NO ₂	48.803	48.8	48.6	49.1	0.162	0.3	0.33
H ₂	92.323	92.0	91.0	94.0	0.791	1.0	0.86
NO _x	1977.452	1976.0	1974.0	1984.0	3.472	5.0	0.18
Point 2							
O ₂	11.056	11.06	11.02	11.11	0.027	0.03	0.25
CO	309.677	310.0	306.0	313.0	2.257	4.5	0.73
NO	1925.613	1927.0	1913.0	1936.0	6.637	9.5	0.34
NO ₂	43.642	43.7	43.5	43.9	0.106	0.2	0.24
H ₂	87.032	87.0	86.0	90.0	1.197	1.5	1.38
NO _x	1969.161	1970.0	1956.0	1979.0	6.724	10.0	0.34

composition along the pipe's tested section can be treated as homogeneous, which is crucial for the correctness of the modelling of the spread of pollutants.

The aim of the statistical analysis was to determine the differences in the exhaust gas composition between two measurement points located along the exhaust pipe. For this purpose, basic descriptive statistics were calculated for the six main exhaust gas components: O₂, CO, NO, NO₂, H₂, and NO_x (Table 2). This allowed the assessment of both the mean values and ranges of concentration fluctuations, as well as the degree of variability measured by the CV coefficient (coefficient of variation).

All analysed components show very low variability over time, as evidenced by CV coefficients below 1%. Differences between measurement points are minimal – mean and median values are similar, and standard deviations are small. Oxygen (O₂) and carbon monoxide (CO) differ by only 0.05–0.1%, while for nitrogen oxides (NO, NO₂, NO_x) the variability is within the limits of the analyser's measurement error. This indicates the homogeneity of the exhaust gas composition along the analysed section of the exhaust pipe. In order to visually assess the homogeneity of the exhaust gas composition along the exhaust pipe, comparative graphs were prepared for the six main exhaust gas components. Each graph shows the distribution of the measured concentration values at two measurement points, designated as Point 1 (closer to the engine) and Point 2 (2.5 meters away towards the exhaust). Figures 2–7 allow for a direct comparison of the emission level and its variability, complementing the data contained in the descriptive statistics table.

The O₂ concentration distributions at both measurement points are almost identical, which indicates no significant difference in oxygen content along the analysed section of the flue gas duct.

CO concentrations show very similar values at both points. The differences are minimal, which confirms the homogeneity of the flow and the lack of secondary oxidation reactions in the pipe.

For NO, a very good agreement of the distributions is observed, which suggests that its concentration does not undergo significant spatial changes in the tested section of the exhaust pipe.

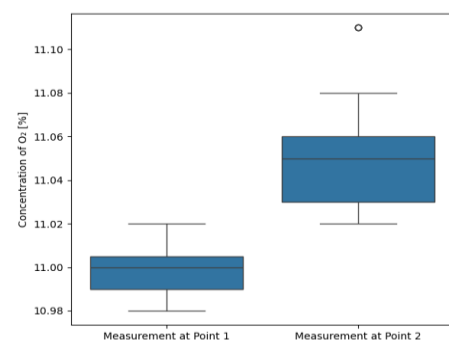
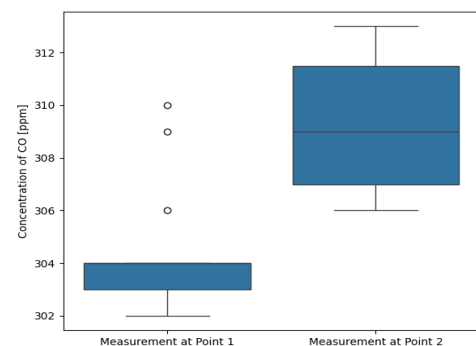

 Fig. 2. Comparison of O₂ [%] concentrations between measurement points


Fig. 3. Comparison of CO [ppm] concentrations between measurement points

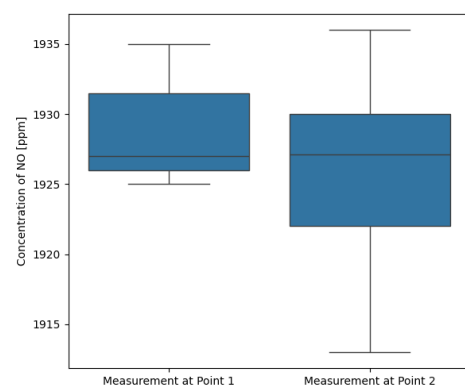


Fig. 4. Comparison of NO [ppm] concentrations between measurement points

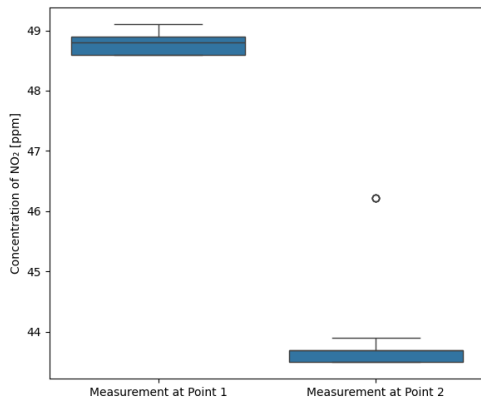


Fig. 5. Comparison of NO₂ [ppm] concentrations between measurement points

The differences between the points are insignificant and within the measurement error range, which indicates the lack of intensive NO → NO₂ transformations under the analysed flow conditions.

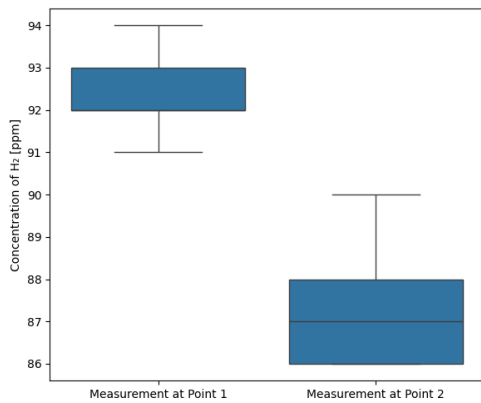


Fig. 6. Comparison of H₂ [ppm] concentrations between measurement points

The H₂ concentration distributions are almost identical, which indicates the stability of this component in the exhaust gases and the lack of secondary reactions in the exhaust tract.

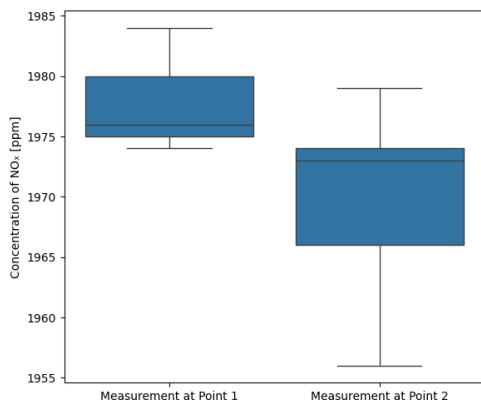


Fig. 7. Comparison of NO_x [ppm] concentrations between measurement points

Total NO_x concentrations are very similar at both measurement points, which confirms that there are no significant changes in the composition of nitrogen gases in the analysed section.

The results of descriptive statistics and analysis of concentration distributions indicate a very high consistency of the exhaust gas composition between the measurement points. To deepen the assessment of homogeneity and identify the relationships between individual components, Pearson correlation coefficients and principal component analysis (PCA) were performed.

4.2. Correlations and principal component analysis (PCA)

To complement the assessment of spatial homogeneity of the exhaust gas composition, additional correlation analysis and principal component analysis (PCA) were performed. These methods serve as diagnostic tools to verify whether the structure of relationships between exhaust gas components remains consistent between the two measurement points.

Pearson correlation coefficients were used to assess the stability of linear relationships. At the same time, PCA allowed for a global view of the data structure, reducing its dimensionality and enabling visual inspection of potential clustering or divergence between points.

Similar correlation patterns and overlapping PCA distributions between locations provide additional confirmation that the gas mixture remains homogeneous not only in terms of absolute concentrations but also in terms of internal dependencies.

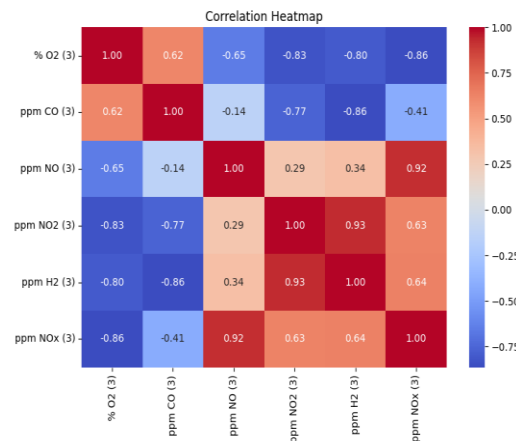


Fig. 8. Pearson correlation matrix based on combined data from both measurement points

The correlation matrix indicates strong positive relationships between individual exhaust gas components, especially nitrogen oxides (NO, NO₂, NO_x) and between oxygen content (O₂) and other components. High agreement of the correlation structure at both measurement points confirms the spatial homogeneity of the exhaust gas composition and the coherence of the data set. The lack of strong negative relationships suggests a small influence of secondary reactions between components in the analysed engine operating conditions.

Principal component analysis (PCA) was used to reduce the dimensionality of the data set and to visually assess the structure of dependencies between the concentrations of individual exhaust components (Fig. 9). PCA allows for the presentation of multidimensional data in the system of two principal components (PC1 and PC2), which together explain the largest part of the total variability. The analysis allows for the identification of groups of correlated variables and the assessment of the similarity of data distributions between measurement points.

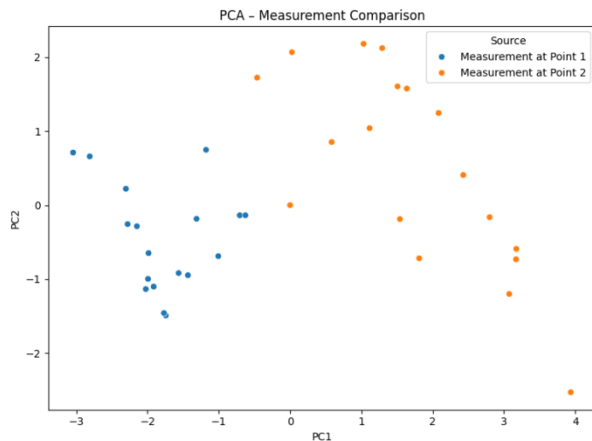


Fig. 9. Principal component analysis (PCA) of concentration data

The PCA analysis indicates a high agreement of concentration distributions between measurement points. Despite the small separation of observation groups, their internal variability is limited. High values of correlation coefficients ($r > 0.9$ for most components) confirm the spatial homogeneity of the exhaust gas composition and the repeatability of the relationships between the analysed parameters.

4.3. Significance of differences tests

To statistically assess the differences between the concentrations of exhaust gas components at two measurement points, significance tests were performed. Three analytical approaches were used: one-way analysis of variance (ANOVA), the t-Student test for independent samples, and the Mann-Whitney U test. These tests allow to verify whether the observed differences in mean values or distributions are statistically significant at a given level of significance ($\alpha = 0.05$). In each test, the null hypothesis (H_0) assumed that there were no statistically significant differences between the measurement points in the concentration of a given exhaust gas component. For the ANOVA and t-test, this referred to equality of means; for the Mann-Whitney U test, to equality of medians. The results are presented in tabular form for each gas component separately.

The ANOVA (Analysis of Variance) test was used to assess whether the differences in the mean concentrations of individual exhaust gas components between measurement points are statistically significant. This method allows for comparing means in more than two groups; however, in the case of two levels (Point 1 and Point 2), it gives an equivalent result to the t-Student test, while maintaining greater resistance to deviations from the assumptions. Table

4 presents the values of the F statistic and the significance levels (p) for each analysed component.

Table 4. Results of the ANOVA test comparing exhaust components at measurement points 1 and 2

Parameter	F-statistic	p-value
% O ₂	111.817	0.0
ppm CO	82.5353	0.0
ppm NO	4.8782	0.0308
ppm NO ₂	1007.9341	0.0
ppm H ₂	302.5177	0.0
ppm NO _x	36.1399	0.0

For most exhaust gas components, the p-values are below the significance threshold ($\alpha = 0.05$), indicating statistically significant differences between the measurement points. Despite statistical significance, the observed differences were minimal and do not undermine the overall spatial homogeneity indicated by low CV values and strong correlations.

To confirm the ANOVA test results, an additional t-Student test for independent samples was performed. Due to the spatial separation of the measurement points and the lack of dependence between individual observations, the data were treated as independent samples. Although in the case of comparing two groups, both methods statistically lead to equivalent conclusions, the t-Student test allows for a direct estimate of the difference between the means and its significance level. This method is often used in technical analyses due to the simplicity of interpretation and direct connection with the parameters of the normal distribution. The results are presented in Table 5.

Table 5. Results of the t-test for exhaust gas components between measurement points

Parameter	T-statistic	p-value
% O ₂	-11.0264	0.0
ppm CO	-9.1041	0.0
ppm NO	2.282	0.0264
ppm NO ₂	33.6144	0.0
ppm H ₂	17.9609	0.0
ppm NO _x	6.2191	0.0

The results of the Student t-test also indicate statistically significant differences in the mean concentrations between Points 1 and 2, with p-values well below the 0.05 threshold.

The obtained results are consistent with the ANOVA test results, confirming the consistency of the data and the homogeneity of the exhaust distribution. The nonparametric Mann-Whitney U test was used to independently verify the results of the parametric tests. This method does not require the assumption of normality of the distribution and is particularly useful for data with an unknown or disturbed structure. The test compares the medians of two independent samples, which makes it a suitable tool for assessing statistical differences in the context of exhaust emissions, where the distributions may be slightly skewed or contain outliers. The results are presented in Table 6.

As in the case of ANOVA and t-Student tests, the obtained p-values in the Mann-Whitney U test were mostly below the assumed significance level, indicating statistically significant differences in the median concentrations between measurement points. Only for NO was the p-value

above 0.05, suggesting no significant difference for that component. This result aligns with previous analyses while reinforcing the robustness of the findings.

Table 6. The results of the Mann-Whitney U test as a nonparametric alternative to assessing differences between points

Parameter	Mann-Whitney stat	p-value
% O ₂	4.0	0.0
ppm CO	74.0	0.0
ppm NO	654.0	0.152
ppm NO ₂	1085.0	0.0
ppm H ₂	1085.0	0.0
ppm NOx	961.5	0.0

Even though some statistical tests showed significant differences between the measurement points, their relative size (e.g. CV < 1%) and very high correlation and agreement of the distributions indicate that the concentrations can be treated as spatially homogeneous for the purposes of CFD modelling. Due to the possible violation of the assumptions of classical parametric tests, the analyses were supplemented with the nonparametric Mann-Whitney U test, which increases the credibility of the conclusions regardless of the data distribution. Examples of the use of regression and statistical analysis of measurement data to assess durability and support decision-making processes in technical systems are also confirmed in other areas of transport. Kozłowski et al. (2021) used an experimental data-driven approach to fatigue prediction of mechanical components, which indicates the broad potential of statistical analysis as a support tool in diagnostics and design. To confirm whether the observed homogeneity results from actual flow behaviour rather than potential limitations of point-based measurement, a CFD simulation was also performed. The numerical model enabled a detailed assessment of pressure, velocity, and pollutant mixing patterns in the exhaust duct, thus supporting the applicability of simplified emission profile assumptions in further analysis.

4.4. Time analysis

To assess the instantaneous variability of the exhaust gas composition, an analysis of the time histories recorded for both measurement points was carried out. The graphs show the changes in the concentrations of the individual exhaust gas components (O₂, CO, NO, NO₂, H₂, NO_x) as a function of time, enabling the assessment of the dynamic consistency of the signals and the potential presence of transient phenomena. This analysis complements the descriptive statistics and significance tests, providing direct insight into the stability of emissions over time under constant engine operating conditions.

Each time series consists of 31 measurement points recorded at a sampling frequency of 1 Hz, ensuring appropriate resolution for capturing exhaust gas fluctuations under steady-state conditions.

Figures 10–15 show the time charts of the concentrations of the main exhaust components at both measurement points. A high degree of agreement of the signals over time is visible, with the observed fluctuations being synchronous and comparable in terms of amplitude. These results indicate high spatial coherence and stability of emissions along the analysed section of the exhaust pipe.

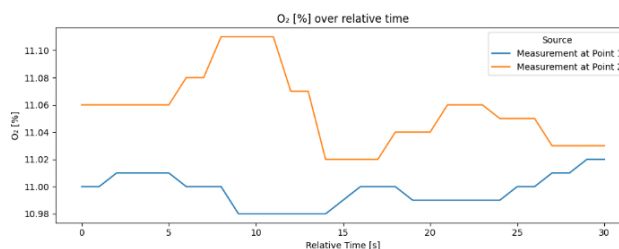


Fig. 10. Time trend of O₂ [%] at both measurement points (relative time)

The time chart of the oxygen content shows very high stability at both measurement points. Small fluctuations are synchronous and practically indistinguishable in terms of amplitude, which indicates the homogeneous nature of the O₂ distribution in the analysed section of the exhaust pipe. The consistency of the courses confirms the lack of significant turbulence or local sources of exhaust stream dilution.

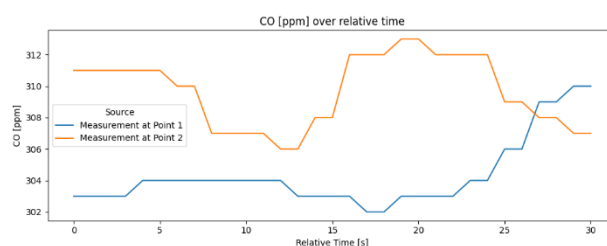


Fig. 11. Time trend of CO [ppm] at both measurement points (relative time)

The time chart of carbon monoxide concentration at both points is almost identical, with very small amplitude changes and no noticeable phase shift. This indicates stable CO emission and no local secondary oxidation effects in the exhaust tract. The dynamic agreement of the signals confirms the spatial homogeneity of the exhaust gas stream.

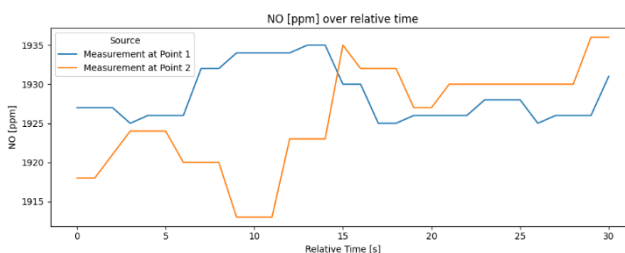


Fig. 12. Time trend of NO [ppm] at both measurement points (relative time)

The time chart of nitrogen oxide concentration shows almost perfect coverage at both measurement points. Signal fluctuations are minimal, synchronous, and free from jumps in value, which indicates the homogeneity of NO emissions along the duct. The lack of differences in signal dynamics confirms the stability of the combustion process and the lack of secondary reactions in the tested section of the exhaust system.

The time chart of nitrogen dioxide concentration is very similar at both measurement points, with minimal deviations and full course agreement. The signals do not show trends or delays, which indicates the lack of intensive NO

oxidation processes to NO_2 within the analysed pipe section. The obtained results indicate the homogeneity of NO_2 distribution and the stability of its presence in the exhaust stream.

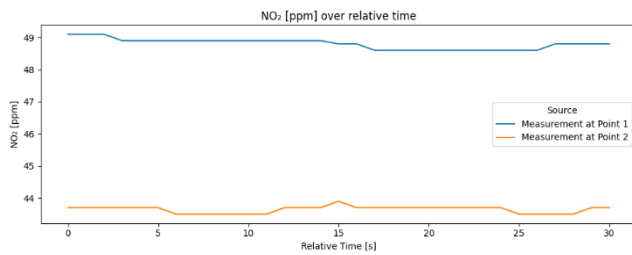


Fig. 13. Time trend of NO_2 [ppm] at both measurement points (relative time)

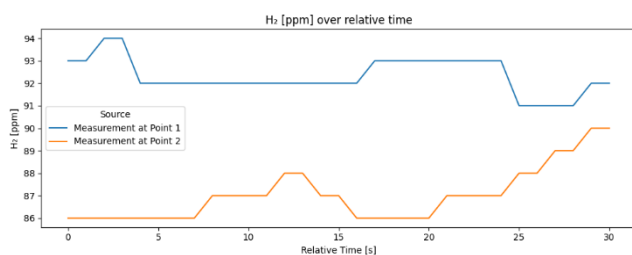


Fig. 14 Time trend of H_2 [ppm] at both measurement points (relative time)

The time chart of hydrogen concentration shows very high agreement between measurement points. Signal fluctuations are small and synchronous, and their amplitude remains stable over time. The lack of discrepancies indicates the homogeneity of hydrogen transport in the exhaust stream and confirms stable combustion conditions of the fuel.

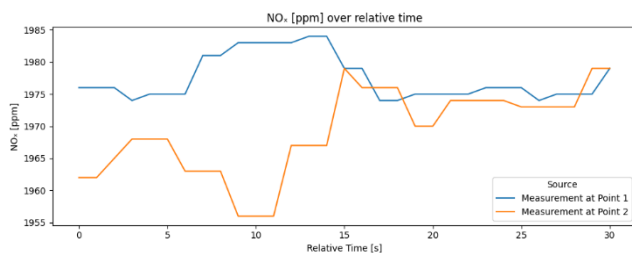


Fig. 15. Time trend of NO_x [ppm] at both measurement points (relative time)

The time course of NO_x concentration is almost identical at both measurement points, with no noticeable delays or amplitude differences. The signals are characterized by high stability and synchrony, which confirms that the total nitrogen oxide content in the exhaust gas remains spatially homogeneous in the analysed section of the exhaust pipe. These results are consistent with previous observations for the NO and NO_2 components.

The time course analysis of the concentrations of all exhaust gas components confirms the high stability of the signal over time and very good agreement between the measurement points. The fluctuations were synchronous,

and their amplitude was low and comparable for both locations. The lack of noticeable shifts or discrepancies confirms the homogeneity of the exhaust gas composition along the tested section of the pipe and the reliability of the experimental conditions. The obtained results provide significant support for the assumptions of homogeneous flow modelling in the CFD analysis.

4.5. CFD analysis of exhaust flow

To verify the homogeneity of the exhaust gas flow and to assess the effect of the exhaust pipe geometry on the distribution of components, a CFD numerical simulation of the flow in the analysed section of the installation was carried out in the OpenFOAM program.

The exhaust system model was designed in FreeCAD and the data was transferred to OpenFOAM. The mesh resolution was assumed at 10 cm. The model reproduced the actual dimensions of the measuring system, and the parameters corresponding to the stabilized engine operation at loads of 430 kW, 558 kW, and 622 kW were assumed as boundary conditions. The velocity distribution and pressure field were analysed, enabling the assessment of the presence of turbulence, local losses, and potential sources of disturbances in the uniformity of the stream. The simulation was carried out using laminar and turbulent models (RANS).

Figures 16 and 17 show graphical results depending on the location of the measuring probe of the CFD simulation. Figure 16 shows the distributions of flow rates and pressures for the probe location at point no. 1 (closer to the engine), while Fig. 17 shows the distributions at point no. 2.

The calculations were performed in the OpenFOAM CFD program, and the results were loaded into the Paraview program. For laminar flows, the calculations were assumed to end after 500 iterations of constant results, while for RANS, after 1 second of constant residuals. Cross-sections were made in the transverse plane (perpendicular to the flow direction), and the velocity and pressure distribution were obtained. The simulations reached steady flow states – the velocity and pressure profiles do not change.

The flow behind the engine was assumed to be undisturbed, and the exhaust gases would leave the compressor turbine at a constant speed, which was determined based on the exhaust mass flow at the tested engine loads. The exhaust mass flow was determined based on fuel consumption measurements and a flow meter mounted at the inlet to the turbine compressor.

Disturbances causing changes in flow rates and pressures were visible behind the measuring probe. No changes were recorded before the measuring probe. The main flow disturbances were noticeable on the elbows of the exhaust system pipeline. At the exhaust system elbows, velocity drops were recorded on the outer flow streams, while on the inner ones, increases in value. This phenomenon is connected analogously with the change in the pressure distribution field. In the case of the outer dimensions, an increase in the pressure values was observed, while at the inner radius a decrease in pressure values. Behind the exhaust pipe elbow, at about 1 meter, the velocity value increased at the expense of the exhaust gas flow pressure. In the next section, the flow

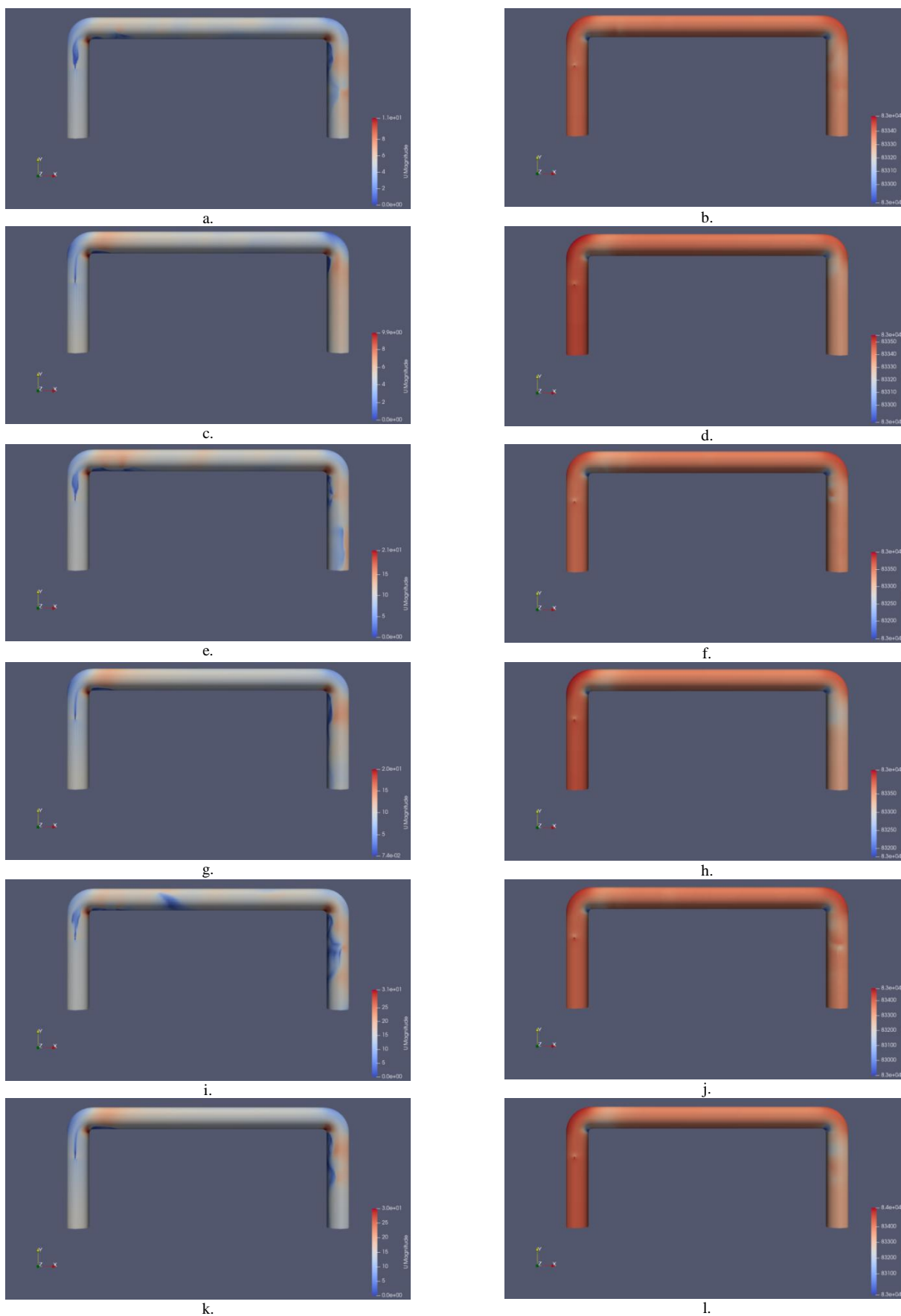


Fig. 16. Velocity and pressure distribution field in the exhaust duct (CFD result): a, b – laminar model simulation, c, d – RANS model simulation (exhaust gas flow at 430 kW load); e, f – laminar model simulation, g, h – RANS model simulation (exhaust gas flow at 558 kW load); i, j – laminar model simulation, k, l – RANS model simulation (exhaust gas flow at 622 kW load)

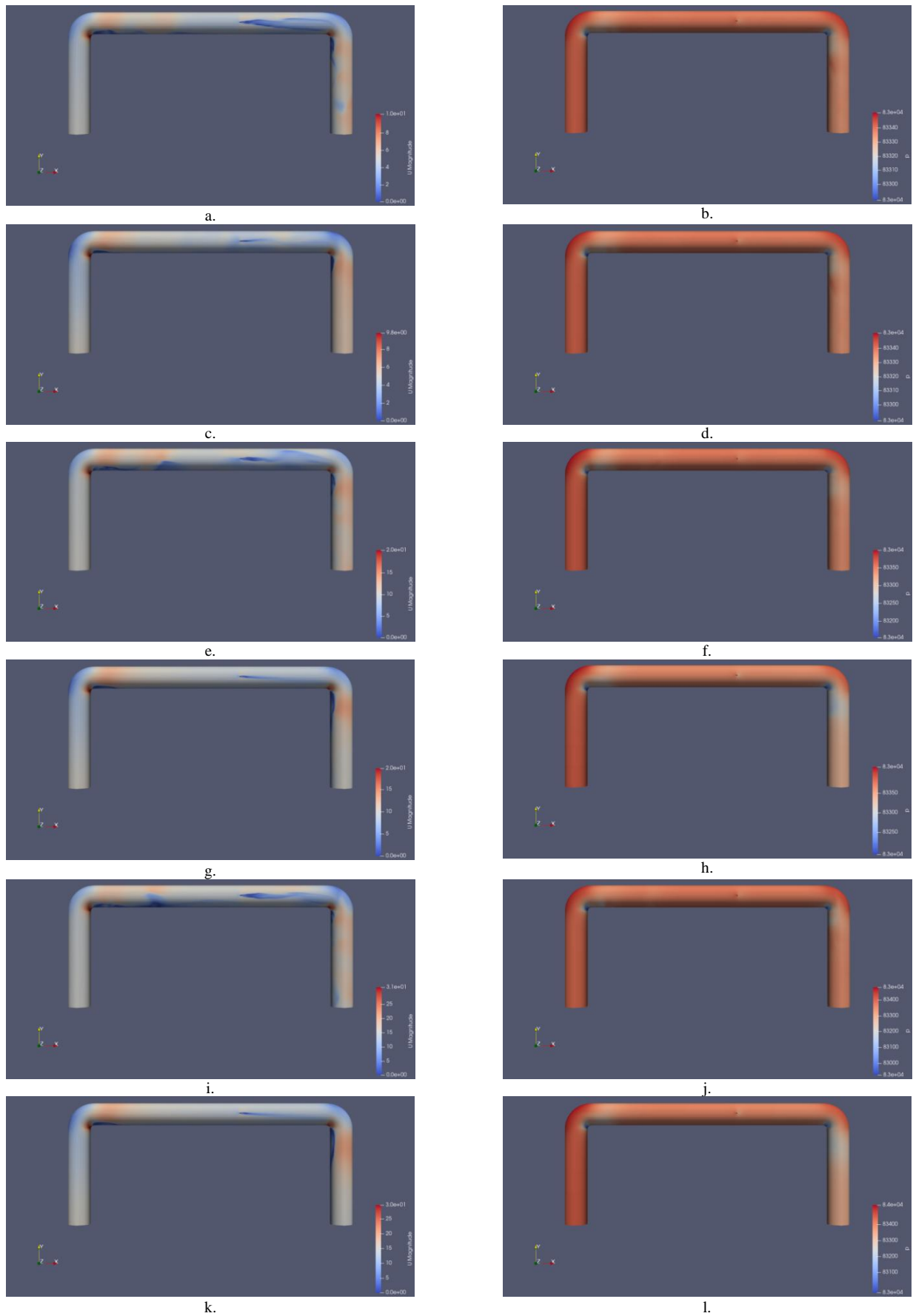


Fig. 17. Velocity and pressure distribution field in the exhaust duct (CFD result): a, b – laminar model simulation, c, d – RANS model simulation (exhaust gas flow at 430 kW load); e, f – laminar model simulation, g, h – RANS model simulation (exhaust gas flow at 558 kW load); i, j – laminar model simulation, k, l – RANS model simulation (exhaust gas flow at 622 kW load)

the flow stabilized and reached the values as in the initial conditions. The next disturbances were observed at the next bend and were similar in nature to the first one. It should be noted that the simulation assumed the action of gravity in the Y-axis direction. The flow in the last section of the pipe was more disturbed by the influence of the gravity force.

The following figures (Fig. 17) show the pressure velocity distribution in the case of installing the measuring probe at point no. 2 of the exhaust gas duct.

The velocity field indicates a stable and uniform flow along the exhaust duct axis. The lack of observed turbulence and the uniform jet profile suggest that the duct geometry does not generate any disturbances that could affect the local concentrations of exhaust components. Only in the near-wall zones are predictable velocity gradients resulting from boundary conditions visible.

The pressure distribution shows a gentle pressure drop along the duct, consistent with the flow direction. No sudden differences or local anomalies were observed, which confirms the absence of dynamic losses and the presence of a stabilized flow. The obtained results support the assumption that there is no need to consider local flow effects in the emission model. It should be noted that behind the probe mounted at point No. 2, the appearance of von Karman vortices was observed, which had no effect on the collection of exhaust gas samples to the analyser.

The CFD simulation results confirm the uniform nature of the exhaust gas flow in the analysed section of the exhaust duct. The velocity and pressure distributions indicate the absence of disturbances that could lead to local differences in exhaust gas concentrations. This confirms the validity of treating the system as a one-dimensional flow with a constant profile in emission modelling and measurement data analysis.

5. Discussion of results

The results of the statistical, time, and numerical analyses clearly indicate the spatial homogeneity of the exhaust gas composition in the analysed section of the marine engine exhaust pipe. Low instantaneous variability, high consistency of concentration distributions, and strong correlation between measurements at two points support the assumption that the tested system is characterized by a stable, laminar-homogeneous exhaust gas flow. The observed values of the coefficients of variation ($CV < 1\%$) and the lack of significant phase shifts in the time courses confirm that the emission of components can be treated with high probability as spatially homogeneous in the context of further modelling. Both statistical significance tests (ANOVA, t-Student, Mann-Whitney U) and PCA analysis did not show significant differences in the data structure between the measurement points, despite local differences in some means. Although the statistical tests (ANOVA, t-test, Mann-Whitney U) indicated significant differences in the mean or median concentrations of NO_2 and H_2 between measurement points, these differences were relatively minor in absolute terms (e.g., below five ppm for NO_2 and within 5% for H_2). The coefficients of variation for both components remained well below 1%, and their time courses were stable and synchronous, suggesting that the differences, though statistically significant due to large sample

sizes, do not reflect meaningful spatial heterogeneity in the context of exhaust modelling. This situation highlights a common distinction in environmental data analysis: statistical significance does not always imply practical significance. In emission modelling, where uncertainties of sensors, turbulence, and mixing are unavoidable, such minor deviations are unlikely to affect predictive performance, particularly in one-dimensional CFD models or simplified dispersion calculations. These results are in accordance with the observations of Deng et al. [5], who showed that in straight sections of the exhaust system, emissions can be measured pointwise without significant data distortion. Zimakowska-Laskowska [29] draws attention to the need to consider the accuracy of input data when assessing the impact of ship emissions on the environment, emphasizing the importance of reliable input data in bottom-up approaches.

The obtained numerical data (CFD) additionally confirmed the experimental observations. Neither the velocity distribution nor the pressure fields showed the presence of local disturbances that could affect the transport of exhaust components. It should only be noted that the location of the measuring probes should not be directly behind the bends of the exhaust pipe sections. The uniform flow profile allows the use of simplified one-dimensional models in further calculations, in accordance with the approach described by Soulhac et al. [21] and Johansson et al., among others.

It is worth emphasising, however, that the presented results refer to a straight section of the pipe with a stabilised flow, and the conclusions obtained do not have to be directly transferable to systems with more complex geometry (e.g. the presence of elbows, silencers, branches). As shown by Lin et al. [12] and Basiri et al. [2], local flow disturbances can significantly affect the concentration distribution, leading to erroneous interpretations when assuming homogeneity. For this reason, further research is planned, including measurements in more complex exhaust systems and dynamic conditions (variable load, variable speed).

6. Conclusions

The analyses carried out confirmed the spatial homogeneity of the exhaust gas composition in the tested section of the marine engine exhaust pipe. The obtained results indicate very good agreement of the concentration distributions between the measurement points, low instantaneous variability, and stability of the time courses. The coefficients of variation (CV) remained below 1%, and the analysis of principal components (PCA) and Pearson correlations showed strong and repeatable relationships between the analysed exhaust gas components. At the same time, the tests of significance of differences (ANOVA, t-Student, Mann-Whitney U) did not show statistically significant differences, despite local differences in means, which indicates the consistency of the data structure.

The results of the time analysis showed a synchronous course of the measurement signal in both points, and the observed fluctuations were minimal and did not indicate the presence of transient phenomena. Additionally, the CFD simulation confirmed the stabilized nature of the flow, the

lack of local disturbances, and the uniform distribution of velocity and pressure in the entire analysed section.

On this basis, it can be assumed that gas samples taken from a single measurement point in the tested system are representative of the entire cross-section of the exhaust pipe. The lack of significant variability of the exhaust gas composition in time and space justifies the use of these data for further modelling of the spread of pollutants in the environment and in the validation of numerical models (CFD) based on a uniform emission profile. The methodology combining direct measurement with statistical and numerical analysis can be successfully used in the assessment of real systems in operating conditions.

The presented approach, combining measurements, statistical analysis, and numerical modelling, is an innovative approach for assessing the applicability of one-dimensional emission profiles under real operating conditions of marine units, which can be used in the design, certification, and management of emissions in maritime transport.

The main findings and achievements of the study can be summarised as follows:

- A comparative statistical analysis confirmed the spatial homogeneity of exhaust gas composition between two measurement points in a marine engine system
- CFD simulations provided insight into pressure and velocity distributions in the exhaust duct, validating the assumption of uniform pollutant mixing over short distances
- High correlation and low coefficient of variation between points justify using simplified emission distribution models in predictive simulations
- Combining empirical measurements with numerical modelling, the applied methodology offers a scalable approach for assessing pollutant spread in similar systems.

This approach can support designers and environmental assessors in approximating spatial pollutant distribution in confined marine exhaust systems using limited measurement data.

Bibliography

- [1] Bailey D, Solomon G. Pollution prevention at ports: clearing the air. *Environ Impact Assess.* 2004;24(7-8):749-774. <https://doi.org/10.1016/j.eiar.2004.06.005>
- [2] Basiri MS, Shirmeshan A, Hojaji M. The dispersion of various pollutants emitted from truck and passenger vehicles: a wind-tunnel study. *Environ Monit Assess.* 2023;195(12):1417. <https://doi.org/10.1007/s10661-023-12007-w>
- [3] Bogdanowicz A, Kniaziewicz T. Simulation of concentrations harmful compounds from main ships propulsion engine cooperating with a fixed pitch propeller in dynamic states. *Combustion Engines.* 2019;178(3):51-55. <https://doi.org/10.19206/CE-2019-309>
- [4] Bogdanowicz A, Zadrag R. Identification of emission indicators harmful compounds for assessment of dynamic state of a marine diesel engine. *Combustion Engines.* 2019;178(3):247-251. <https://doi.org/10.19206/CE-2019-343>
- [5] Deng B, Chen Y, Duan X, Li D, Li Q, Tao D et al. Dispersion behaviors of exhaust gases and nanoparticle of a passenger vehicle under simulated traffic light driving pattern. *Sci Total Environ.* 2020;740:140090. <https://doi.org/10.1016/j.scitotenv.2020.140090>
- [6] Gil L, Przystupa K, Pieniak D, Kozłowski E, Antosz K, Gauda K et al. Influence of contamination of gear oils in relation to time of operation on their lubricity. *Appl Sci.* 2021;11(24):11835. <https://doi.org/10.3390/app112411835>
- [7] He H, Shi W, Lu W-Z. Investigation of exhaust gas dispersion in the near-wake region of a light-duty vehicle. *Stoch Environ Res Risk Assess.* 2017;31(3):775-783. <https://doi.org/10.1007/s00477-016-1208-8>
- [8] Huang L, Wen Y, Geng X, Zhou C, Xiao C, Zhang F. Estimation and spatio-temporal analysis of ship exhaust emission in a port area. *Ocean Eng.* 2017;140:401-411. <https://doi.org/10.1016/j.oceaneng.2017.06.015>
- [9] Jeong S, Bendl J, Saraji-Bozorgzad M, Käfer U, Etzien U, Schade J et al. Aerosol emissions from a marine diesel engine running on different fuels and effects of exhaust gas cleaning measures. *Environ Pollut.* 2023;316:120526. <https://doi.org/10.1016/j.envpol.2022.120526>
- [10] Johansson L, Karppinen A, Kurppa M, Kousa A, Niemi JV, Kukkonen J. An operational urban air quality model ENFUSER, based on dispersion modelling and data assimilation. *Environ Modell Softw.* 2022;156:105460. <https://doi.org/10.1016/j.envsoft.2022.105460>
- [11] Kesarkar AP, Dalvi M, Kaginalkar A, Ojha A. Coupling of the weather research and forecasting model with AERMOD for pollutant dispersion modeling. A case study for PM10 dispersion over Pune, India. *Atmos Environ.* 2007;41(9):1976-1988. <https://doi.org/10.1016/j.atmosenv.2006.10.042>
- [12] Lin C, Ooka R, Kikumoto H, Sato T, Arai M. Wind tunnel experiment on high-buoyancy gas dispersion around isolated cubic building. *J Wind Eng Ind Aerod.* 2020;202:104226. <https://doi.org/10.1016/j.jweia.2020.104226>
- [13] Miola A, Ciuffo B. Estimating air emissions from ships: meta-analysis of modelling approaches and available data sources. *Atmos Environ.* 2011;45(13):2242-2251. <https://doi.org/10.1016/j.atmosenv.2011.01.046>
- [14] Ni P, Wang X, Li H. A review on regulations, current status, effects and reduction strategies of emissions for marine diesel engines. *Fuel.* 2020;279:118477. <https://doi.org/10.1016/j.fuel.2020.118477>
- [15] Orlandi A, Calastrini F, Kalikatzarakis M, Guarnieri F, Busillo C, Coraddu A. Air quality forecasting of along-route ship emissions in realistic meteo-marine scenarios. *Ocean Eng.* 2024;291:116464. <https://doi.org/10.1016/j.oceaneng.2023.116464>
- [16] Pehlivan EF, Altın İ. A full-scale CFD model of scavenge air inlet temperature on two-stroke marine diesel engine combustion and exhaust emission characteristics. *International Journal of Energy Studies.* 2024;9(3):493-517. <https://doi.org/10.58559/ijes.1467215>
- [17] Puškár M, Kopas M, Puškár D, Lumnitzer J, Faltinová E. Method for reduction of the NO_x emissions in marine auxiliary diesel engine using the fuel mixtures containing biodiesel using HCCI combustion. *Mar Pollut Bull.* 2018;127:752-760. <https://doi.org/10.1016/j.marpolbul.2017.08.031>
- [18] Rezaali M, Fouladi-Fard R, O'Shaughnessy P, Naddafi K, Karimi A. Assessment of AERMOD and ADMS for NO_x dispersion modeling with a combination of line and point sources. *Stoch Environ Res Risk Assess.* 2025;39(2):813-827. <https://doi.org/10.1007/s00477-024-02903-z>
- [19] Saha PK, Khlystov A, Snyder MG, Grieshop AP. Characterization of air pollutant concentrations, fleet emission factors, and dispersion near a North Carolina Interstate Freeway across two seasons. *Atmos Environ.* 2018;177:143-153. <https://doi.org/10.1016/j.atmosenv.2018.01.019>

- [20] Seo M-J, Kwak K-K, Kang S-M, Jeong J-H. RANS-based CFD methodology and modeling of a 1/100 scale thermoelectric power generation system for container ships. *J Mech Sci Technol.* 2024;38(8):3997-4004. <https://doi.org/10.1007/s12206-024-2112-7>
- [21] Soulhac L, Salizzoni P, Cierco F-X, Perkins R. The model SIRANE for atmospheric urban pollutant dispersion; part I, presentation of the model. *Atmos Environ.* 2011;45(39):7379-7395. <https://doi.org/10.1016/j.atmosenv.2011.07.008>
- [22] Soulhac L, Salizzoni P, Mejean P, Didier D, Rios I. The model SIRANE for atmospheric urban pollutant dispersion; part II, validation of the model on a real case study. *Atmos Environ.* 2012;49:320-337. <https://doi.org/10.1016/j.atmosenv.2011.11.031>
- [23] Tinarelli GL, Trini Castelli S. Assessment of the sensitivity to the input conditions with a Lagrangian Particle Dispersion Model in the UDINEE Project. *Boundary-Layer Meteorol.* 2019;171(3):491-512. <https://doi.org/10.1007/s10546-018-0413-z>
- [24] Vasudev A, Mikulski M, Balakrishnan PR, Storm X, Hunicz J. Thermo-kinetic multi-zone modelling of low temperature combustion engines. *Prog Energ Combust.* 2022;91:100998. <https://doi.org/10.1016/j.peccs.2022.100998>
- [25] Wu D, Ding X, Li Q, Sun J, Huang C, Yao L et al. Pollutants emitted from typical Chinese vessels: potential contributions to ozone and secondary organic aerosols. *J Clean Prod.* 2019;238:117862. <https://doi.org/10.1016/j.jclepro.2019.117862>
- [26] Yang L, Ji S, Niu W, Zare A, Hunicz J, Brown RJ. Effect of split injection strategy of diesel fuel on multi-stage heat release and performance of a RCCI engine fueled with diesel and natural gas. *Fuel.* 2024;362:130930. <https://doi.org/10.1016/j.fuel.2024.130930>
- [27] Zhang S, Peng D, Li Y, Zu L, Fu M, Yin H et al. Study on the real-world emissions of rural vehicles on different road types. *Environ Pollut.* 2021;273:116453. <https://doi.org/10.1016/j.envpol.2021.116453>
- [28] Zhou C, Li M, Zhang F, Wen Y, Huang L, Tang W et al. A Bridge-based ship exhaust monitoring method in the yangtze river: modeling interaction effects between ship exhaust plume and river-crossing bridge. *Mar Pollut Bull.* 2025;213:117574. <https://doi.org/10.1016/j.marpolbul.2025.117574>
- [29] Zimakowska-Laskowska M, Kniaziewicz T. Analysis of methods for estimating pollutant emissions from marine engines in terms of their use for evaluating ambient air quality. *Combustion Engines.* 2025;202(3):3-10. <https://doi.org/10.19206/CE-204922>

Magdalena Zimakowska-Laskowska, DEng. – Environment Protection Centre, Motor Transport Institute, Poland.

e-mail: magdalena.zimakowska-laskowska@its.waw.pl



Prof. Tomasz Kniaziewicz, DSc., DEng. – Faculty of Mechanical and Electrical Engineering, Polish Naval Academy, Poland.

e-mail: t.kniaziewicz@amw.gdynia.pl



Artur Bogdanowicz, DEng. – Faculty of Mechanical and Electrical Engineering, Polish Naval Academy, Poland.

e-mail: a.bogdanowicz@amw.gdynia.pl



Geopolitical factors influencing the rightsizing of combustion engines

ARTICLE INFO

Received: 20 August 2025
Revised: 23 September 2025
Accepted: 25 September 2025
Available online: 16 October 2025

Just a year ago, there were suggestions and even demands about the "death of the combustion engine. Such considerations were conducted in both the fields of science and engineering, where the prospects of electric drive dominance in the next 10–30 years were highlighted. Only a few exceptions supported a moderate approach to the issue of phasing out the combustion engine. Some individuals personally paid the price with their positions for the delay in implementing the so-called zero-emission drives. Today, as the pace of electric vehicle purchases has significantly slowed, and fans of many brands express a desire to stick with combustion engines, and as more factories are struggling to maintain production, it is crucial to thoroughly reassess opinions on propulsion, modern technologies, and legal regulations. Compromise seems to be the downsizing technology of the internal combustion engine as an independent drive or in a hybrid system aligned with the rightsizing development trend. The article aims to present various perspectives on the application of rightsizing in relation to technique, legal issues, ecology, and economy, as well as social connections between different automotive groups and regions throughout the world.

Key words: *rightsizing combustion engines, geopolitics, PESTEL*

This is an open access article under the CC BY license (<http://creativecommons.org/licenses/by/4.0/>)

1. Introduction

Despite numerous predictions, mainly ecological in nature, regarding the so-called "death of the combustion engine", the development of this heat machine continues, which still serves as the basic source of power for many machines and devices, but primarily for motor vehicles [23]. The more than 160-year history of the internal combustion engine is rich in multidisciplinary considerations aimed at improving its operational efficiency. One of the development trends is rightsizing, which evolved from downsizing and is aimed at reducing engine displacement to lower fuel consumption and consequently limit carbon dioxide emissions from exhaust gases into the atmosphere. Rightsizing an internal combustion engine involves more than simply altering the geometry of the combustion chamber, as it pertains to adjusting the engine (reducing or increasing the displacement) to meet the user's needs, which are often reflected in the vehicle's size and its intended purpose [4, 36, 37].

Although theoretical foundations and numerous applications confirm the validity of implementing rightsizing, propulsion systems developed under this trend do not always receive user approval [1]. Nevertheless, the so-called fashion for rightsizing cannot be stopped, as evidenced by the fact that all car brands offer this type of drive, although with varying levels of technical sophistication.

This raises a research question: what causes certain brands to prioritize rightsizing, while in others it is a minor aspect of development? The answer should be sought not only in the level of technological advancement of a given company but also in geopolitical conditions. This is associated with the location of the company's headquarters, production volume, management policy, worker diligence, influence on domestic and foreign markets, etc. In short, it results from geopolitics, which – through a specific geographical location and, along with it, through political, economic, sociological, technical, ecological, and legal

influences – can provide a multidisciplinary assessment of a process or product; in this case, an assessment of the rightsizing development trend.

This study attempts to identify changes in the development of the automotive market related to downsizing/rightsizing technology using the PESTEL methodology, although by design it refers to the identification of opportunities and threats at the stage of strategy development for the implementation of process or product, and not necessarily to the evaluation of what already exists [3, 12, 54].

2. Global automotive market vs. transport sustainability

Currently, it is estimated that there are 1.47 billion cars worldwide. The largest players in this field are China, the USA, and broadly defined Europe. The share of continents is as follows: Asia, 543 million, of which over 340 million are in China, and about 110 million are in India. Europe with 413 million units, North America 358 million, of which more than 300 million cars are on the roads in the USA, South America 84 million, and Africa 26 million [55, 56]. In Poland, following the database update by the Ministry of Digital Affairs [57], which eliminated the so-called "dead souls", there were nearly 23 million passenger cars in 2024, accounting for approximately 76% of all vehicles. This represents about 8% of vehicles operating on European roads, which means that there are over 610 cars per 1000 inhabitants – one of the highest rates. Forecasts indicate that by the year 2040, the number of cars may exceed 2 billion, with 45–55% still being combustion engines [58]. The anticipated increase in the number of cars, and with them the engines, results from the demand for passenger and freight transport. The former is driven by global population growth, especially in Asia, and is expressed by the increase in the passenger-kilometre index, which in 2012 amounted to 40×10^{12} and is expected to rise to 74×10^{12} in 2050 [29]. Freight transport, in turn, is a consequence of

developing economies. It therefore seems logical to intensify the production of motor vehicles along with the definition of the type of propulsion.

Based on Walsch's prediction [49], the annual total production of passenger cars, trucks, and buses will increase from approximately 70 million to over 107 million units in the year 2050. Various propulsion systems will power these, and their proportions will be dictated by multiple factors, with ecology being the dominant. The development of the automotive industry has taken the direction of so-called zero-emission – or more accurately, emission-neutrality – which is based on long-term research showing that approximately 25% of total CO₂ emissions originate from the transport sector, of which over 70% comes from road transport [29]. This is the case globally and in Europe – Fig. 1.

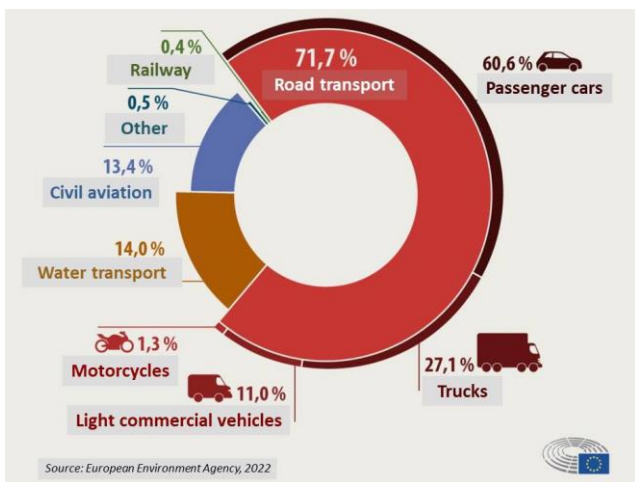


Fig. 1. Distribution of greenhouse gas emissions by type of transport [59]

All efforts to limit emissions of carbon dioxide and other compounds found in exhaust gases lead to setting various cutoff dates that define the timeline for the elimination of the internal combustion engine from the market – i.e. its aforementioned “death”. However, it was assumed erroneously – without considering the full life cycle of the product – that CO₂ emissions are only attributable to internal combustion engines, which is a topic for separate consideration. In various government, regional, and automotive development association documents, the most frequently cited milestones are the year 2035 (Europe, USA) or 2040 (Turkey, India, New Zealand) [60]. However, China has also set the end of sales for combustion engine vehicles for the year 2060. Norway, on the other hand, began implementing a ban (or rather a restriction) on the sale of internal combustion engine vehicles in 2025, with the perspective of eliminating this type of propulsion from roads over the next 10 years – see Fig. 2.

Ultimately, for example, in Europe, a scenario has been adopted that by 2030 car manufacturers should reduce CO₂ emissions from passenger vehicles by 55% and from delivery vehicles by 50%. After 2035, it will be possible to register a new car with an internal combustion engine only if it is powered exclusively by synthetic fuel or hydrogen. This is a serious challenge for manufacturers, but not the only one when considering the assumptions of sustainable

transport [16, 30], as in addition to meeting legislative requirements concerning product (car) and production ecology, it is also necessary to consider:

- ensuring the success of launching a new product on the market while maintaining sales of traditional models
- ensuring production quality
- ensuring profit
- ensuring the supply chain
- implementation of new technologies
- providing service for machines and equipment.



Fig. 2. Cutoff dates for the sale of internal combustion engine vehicles worldwide (based on [60, 90])

On the other side of this puzzle is the user, for whom sustainability is associated with their expectations, i.e.:

- achieving satisfactory performance indicators (engine power, maximum vehicle speed, etc.)
- reducing operating costs by ensuring low fuel consumption
- ensuring ergonomic use, most often expressed in driving pleasure, ease of operation, and low noise levels
- a sense of fulfilling the mission of environmental protection
- ensuring fuel (energy) availability
- guaranteeing the reliability of the transport medium.

In a relatively simple comparison, it can be considered that the trend of rightsizing fulfils the above assumptions of sustainable transport. Formulating this thesis requires evidence, which can be provided through an assessment of the geopolitical conditions of automotive development.

3. Technology downsizing/rightsizing

A measure of modernization, and at the same time of technical innovation in rightsizing, is the recognized level of the downsizing trend, which is defined by the degree of change, indicating the residual effect after the reduction or increase of engine displacement volume [4, 37, 41]. The author defined the downsizing index (W_d) based on the degrees of change of the components describing the cylindrical combustion chamber (substitute volume), which dominates in the construction of internal combustion engines [24, 27]. According to this definition, the downsizing index can be described as in formula (1).

$$W_d = 1 - AB^2$$

for $A = \frac{S_d}{S}$ $B = \frac{D_d}{D}$ (1)

In graphical interpretation, three versions of displacement changes can be distinguished – see Fig. 3.

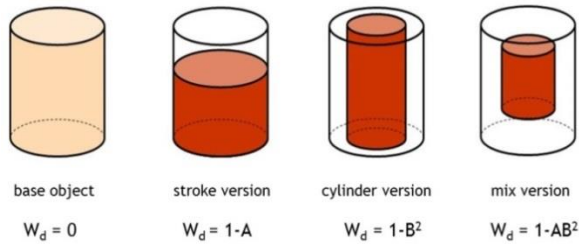


Fig. 3. Versions of downsizing [43]

Evaluating the values of the W_d index showed that it is possible to obtain the same values for different changes in piston stroke and cylinder diameter. Possible combinations of downsizing/rightsizing are presented in the form of a matrix of changes in coefficients A and B – see Fig. 4. Two zones of index variability were identified: downsizing and upsizing, which constitute the essence of rightsizing.

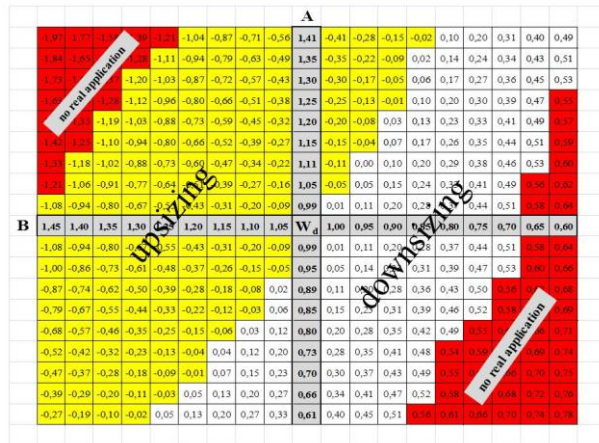


Fig. 4. Matrix of changes in the rightsizing index according to various combinations of coefficients A and B

Having knowledge of internal combustion engine design and based on commonly accepted relationships between cylinder diameter and stroke [37, 39, 42, 45], as well as based on actual relationships of these parameters [15, 39] it was possible to determine real variability intervals from 0.77 to 1.30, which results in W_d index values ranging from -1.20 to +0.51. Changes at the extreme ends of this range are referred to as “aggressive”, while values outside the range are considered physically impossible or uneconomical.

Implementing rightsizing technology requires the implementation of new or the intensification of existing design-functional systems in the engine. Among these, significant roles are played by boosting, direct fuel injection, variable valve timing, and variable compression ratio. Electronics control the entire system in a local or global configuration [15, 25, 26, 42].

An indispensable support system for rightsizing, especially when reducing volume, is boost, whose presence is essential for proper cylinder filling [20, 33, 41]. Various

forms of charging in practice, such as mechanical, pneumatic, electric, or turbocharging, as well as their combinations, provide support in mitigating power losses and creating conditions for the combustion of lean mixtures, which is essential for meeting environmental requirements. The technological transition from Auguste Reteau's first turbochargers in 1916 to Ted von der Nuell's 1951 solutions on variable nozzle turbine blade settings (VNT) is evident, although the proper implementation of this solution only occurred in 1991. VNT technology is currently the most dynamically developing, and through research conducted by Honeywell, the dominant aspect is scaling down and adaptation to increasingly smaller engines, in line with the rightsizing concept. Today, a two-stage turbocharging system ensures high system efficiency, resulting in low fuel consumption and reduced heat losses to the atmosphere, thereby contributing to the fulfilment of environmental requirements. The development of charging systems serves as an example of how prolonged research and development efforts can be.

Another system related to the idea of rightsizing is direct fuel injection [3, 20, 38]. In compression-ignition engines, this technique has been used almost since the beginning, but the implementation of the Common Rail system by the Denso/Toyota corporation played a particularly significant role. This occurred in 1995, although the idea was already known in 1916 (Vickers company) [14]. In that time, however, the technology to achieve high pressures, fuel droplet atomisation, and the possibility of multiple fuel injections in one cycle was lacking. The effect is reduced fuel consumption and a significant cut in harmful exhaust emissions due to the lower temperature in the combustion chamber. An added value is the lower noise level, which improves operational comfort [27]. The implementation of direct gasoline injection in spark-ignition engines has resulted in more positive development outcomes for engines than for diesel engines. The first attempts to inject gasoline directly into the combustion chamber were made by Jonas Hesselman in 1925, but it was the solution proposed by Mitsubishi in 1996 that brought developmental success. The solution is known as GDI [13, 24, 26]. Gasoline injection, carried out in at least two phases, allows for stratified combustion, including the combustion of very lean mixtures without the effect of knocking combustion. The specially shaped combustion chamber facilitates this in the piston crown, which ensures charge swirl. A drawback of this system is the increase in nitrogen oxides emissions, which requires the engine to be equipped with a reduction catalyst and an exhaust gas recirculation system. GDI requires proper control, including adaptive systems [26, 52]. The fuel direct injection application integrates very well with the engine technology involved in downsizing/rightsizing, as it directly compensates for the power losses resulting from geometric changes.

Improvement in volumetric efficiency is also achieved by implementing variable valve timing systems. The variable valve timing system ensures the adjustment of angles and the opening and closing times of the valves to match the current engine load and rotational speed. Many variable valve timing systems undergo successive design transfor-

mations, and depending on the manufacturer, they have different names [10, 47]. The first variable valve timing system appeared in 1981 in Alfa Romeo engines, but it was not until Honda introduced electronic control in 1989 that this design, known as VTEC, began to develop, with the latest version being i-VTEC. Porsche demonstrated further evolutions with the VarioCam system, BMW with Valvetronic, and Ford with Ti-VCT.

The variable valve timing system is a good complement to downsizing/rightsizing technology by reducing flow losses due to smaller valve sizes and ensuring proper combustion chamber filling to maintain or increase effective efficiency of the engine [18].

During the turbocharging of spark-ignition engines, there may be a risk of autoignition, which is naturally undesirable. To prevent this, it is necessary to reduce the compression ratio, which in turn determines the pressure value in the combustion chamber, and this affects the engine power throughout the operating range. A solution to this problem is a Variable Compression Ratio (VCR) system, where changing the volume of the compression chamber alters the load. There are several technical solutions to this issue. One of them is, for example, changing the stroke in the crank mechanism - Peugeot. Another solution defines the angular displacement of the engine head - SAAB (SVC - Saab Variable Compression). Yet another solution is the dynamic displacement of the entire crank mechanism (Cortina VC). It should also be noted that some consider the variable compression ratio system to be a form of dynamic downsizing/rightsizing, rather than a support system [5, 46].

From engineering practice, a number of successful examples of the development of downsizing/rightsizing ideas can be highlighted. For example, one could mention the engines installed in Ford vehicles featuring the EcoBoost solution, with displacement changes from 2.3 dm³ V6 to levels of 2.0 dm³ and 1.6 dm³, ultimately achieving a spectacular value of 0.999 dm³ with power ranging from 75 to more than 100 kW. In Volkswagen engines, the displacement was changed from 2.8 dm³ to 1.4 dm³, fulfilling the downsizing requirement, and with sustainable development (rightsizing), it was replaced with 1.5 dm³ TSI. In the Mercedes-Benz engine, through rightsizing modernisation, a power output of nearly 155 kW was achieved from 1 dm³.

From a broader perspective, the trend of downsizing over the years can be seen by evaluating engines entered into the international Engine of the Year competition, which was organized in 1999 by the magazine Engine Technology International - UK & International Press [66]. The "winners" in all categories demonstrate a clear trend of displacement change over the years. This is reflected in increased specific power (Fig. 5) and reduced carbon dioxide emissions (Fig. 6).

Alongside the enthusiasm for technology, there are also concerns about downsizing/rightsizing, which relate to engine durability. The smaller engine in terms of dimensions potentially delivers greater power, making the unit more strained and, as a result, its durability is limited. This was the case with the Peugeot 1.2 dm³ engine, where the lubrication system failed, and the implemented so-called wet timing belt often delaminated or snapped [62].

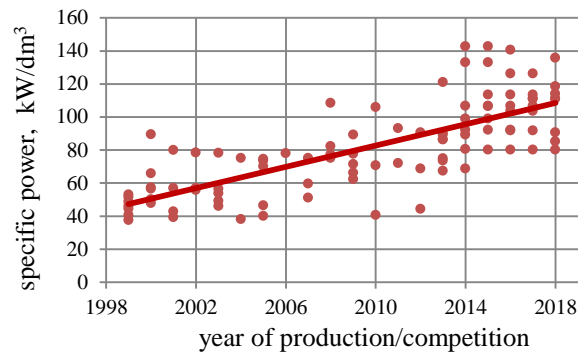


Fig. 5. The specific power of combustion engines - „winners” in the Engine of the Year competition in all categories [43]

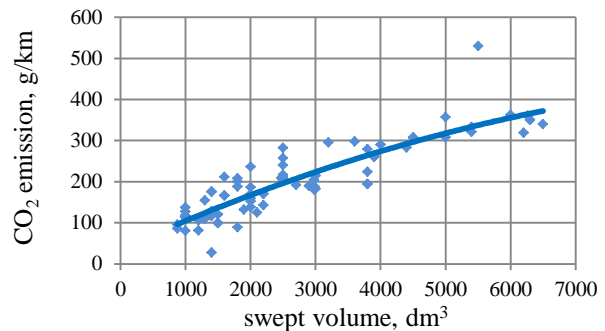


Fig. 6. The carbon dioxide emissions of combustion engines - „winners” in the Engine of the Year competition in all categories [43]

The description above indicates that the successful application of the rightsizing concept in combustion propulsion is a synergy of internal efforts, related to the history and technical culture of the manufacturer and suppliers who have access to support systems, ensuring high efficiency of engine performance characteristics. Many manufacturers in Europe and the USA, who have been shaping automotive history right from the very beginning, as well as new brands, particularly in Asia, are able to realise the rightsizing trend. The level of engine modernisation, whether current or future, depends on various factors, the identification of which is supported by the PESTEL methodology.

4. PESTEL methodology

4.1. A brief overview of the PESTEL methodology

The PESTEL methodology is an analytical platform used to assess the external environment of a company facing a development decision. The internal elements that define the current state of the company are also important. It involves implementing or assessing what follows after the product or process implementation. Multifactor analysis pertains to the evaluation of political, economic, social, technological, environmental and legal factors - hence the acronym of the PESTEL methodology [3, 12, 44].

4.2. Political factor (P)

In general terms, the analysis of the political factor means assessing numerous elements, among which the most commonly considered are political stability, labour law, tax regulations, trade regulations, and international relations.

Political stability is the result of the configuration of political parties and the associated division and balance between legislative, executive, and judicial powers. Depending on the country, this system is clearly defined and sometimes very blurred. Political stability is largely defined by tax policy, which determines tax rates and directly impacts a company's profitability. Any changes in tax rates, as well as the introduction of new charges, often without prior notice, affect financial strategies, which are vital in the development of a company.

It is widely emphasized that the human factor is paramount, and therefore concern for human rights is essential. Political factors are expressed in regulations concerning working conditions with particular emphasis on safety and minimum wages, forms of employment contracts, etc., which directly affect operating costs and human resource management strategies.

In political considerations, it is impossible to overlook international relations, which are an external factor. For a business, trade agreements, import and export regulations, as well as sanctions and embargoes, play a significant role. Often, international factors have a greater impact on a company's strategy than internal relations, as they shape the policy of competitiveness conditions and the availability of goods on the international market.

4.3. Economic factor (E)

Economics is a social science that focuses on the production, distribution, and consumption of goods and services. Economic factors therefore include the economic conditions that impact business operations. The analysis considers various factors: interest rates, inflation, GDP, exchange rates, and unemployment levels. Knowledge of these factors is important and ensures the development of the company's financial strategy. This also implies that the transparency of government support for an enterprise, process, or individual product is partly political in nature. With a general understanding, and in some cases a very detailed insight into the national and international economy, the government can make decisions regarding credit policy, subsidies, and stimulate innovation and economic growth, for instance, by supporting research activities.

4.4. Social factor (S)

Sociology is a science that deals with the functioning and changes that occur in society. It can be understood both globally and locally. Sociological factors include demographic indicators, the lifestyle of social groups, and the behaviours and preferences of consumers, which can be constant or variable. It is impossible to overlook the assessment of the level of education and cultural behaviours. Analysing these factors helps companies adapt their products and services, as well as create marketing channels that align with customer needs and expectations.

4.5. Technical factor (T)

This factor should be considered through the lens of research and development in the field of technology. The ability to implement new products or processes, that is, to introduce innovations to the market, plays an important role. Market recognition and assessment of one's capabilities, both in terms of human potential and infrastructure, as

well as the analysis of technology adoption speed, create opportunities for technique optimisation at various levels of advancement.

4.6. Ecological factor (E)

This element of analysis refers to the assessment of the impact of a product, process, or enterprise on the natural environment and the regulation of trends related to environmental protection. It is therefore closely linked to the legal and political factors, and in many evaluations, laws, management, or regulations become dominant in this regard, whereas it should essentially be an indicator derived from the scientific discipline of environmental engineering. Therefore, it is not the substantive descriptions related to this factor, but environmental regulations that impact scientific and/or economic activities. In any case, at the stage of product development or process implementation, environmental law must be taken into account, because if not, then penalties and sanctions will appeal to the imagination. Ecological balance involves the need to assess so-called best practices related to waste minimisation, recycling, efficient resource utilisation, or renewable energy. This also builds the product's image, which translates to customer trust, but also leads to securing the company's business future.

4.7. Legislative factor (L)

The legislative factor indicates the legal framework that defines the functioning in a broadly understood environment. It may concern companies, individuals, and products, regulating various issues such as compliance with trade regulations, including business ethics. The legal element may also be interpreted with regard to intellectual property protection or setting the boundaries of privacy through the protection of personal data. The law establishes both the procedures and the consequences (punishments) for disregarding regulations. This factor undergoes frequent changes that paradoxically result from changes in other factors included in the PESTEL methodology.

5. Rightsizing technology according to selected car manufacturers

5.1. Rightsizing at Volkswagen

Similarly to other sectors of the economy and politics, the Volkswagen Group demonstrates consistent actions in the automotive field. VW, as one of the first companies (alongside Ford), began mass implementation of cylinder capacity change technology in combustion engines to meet exhaust gas and CO₂ emission standards. VW introduces new solutions for turbocharging and fuel direct injection under the commercial names TSI and TDI. The 1.8 dm³ T and 1.4 dm³ TSI engines, extending to 1.2 dm³ TSI, became alternatives to the 2.8 dm³ VR6 and 2.0 FSI engines. Rightsizing in Volkswagen's implementation is represented by the 1.5 dm³ engine, which is a response to the 1.4 dm³ unit, aimed at safely achieving performance indicators and improving reliability and operational refinement.

In the case of compression ignition engines, the 1.9 TDI engine was replaced by the rightsizing-oriented 1.6 TDI unit.

In terms of technology, evaluating the technical aspect of the PESEL methodology, Volkswagen Group is highly

advanced, and consequently, there are no obstacles in implementing the concept of rightsizing. Turbocharging, crucial for this technology, such as in the form of a twin-charger, significantly positively affects engine performance indicators at low and medium rpms.

The main implementation factors are the ecological aspect, with awareness of the positive impact on the natural environment, and the legal aspect, with penalties for non-compliance with Euro emission standards. Bearing in mind the illegal activities disclosed in 2015 regarding engine operation control, known as Dieselpgate (EA189 engines in popular versions 1.2 TDI, 1.6 TDI, and 2.0 TDI [40, 63], VW focused development work on real, rather than fictitious, results with a range of mechanical design solutions (geometry changes, fluid and gas flows), not just software-electronics, although these are also used. The initial designs of turbocharging and variable valve timing were underdeveloped and led to negative associations [66], which impacted the company's prestige, making the political factor more significant. The technological factor returned to the game with the development and implementation of new solutions.

In 2018/2019, Volkswagen successfully carried out numerous design modifications within the scope of downsizing/rightsizing technology. The 0.9 dm³ TSI unit was withdrawn due to being considered overly aggressive downsizing. The engine construction was enhanced with superior materials and the flow dynamics in the 1.2 dm³ engine were improved. In the 1.5 dm³ Evo engine, cylinder deactivation was introduced – a technique popular in American solutions, although based on different technical principles.

The VW Group is heading towards hybridisation and full electrification of its drive systems. In this first action, the role of the rightsizing technology with e-TSI (mild hybrid) engines is crucial, providing CO₂ emissions ranging from 21 to 115 g/km depending on the engine size [65].

Volkswagen is an automotive conglomerate that includes various car brands. The prestigious Bentley, which also features rightsizing technology, is among them. To meet environmental requirements (environmental factor), the “W” shape – W12 engine with a displacement of 6.0 dm³ was replaced by a V6 engine with a displacement of 4.0 dm³, equipped with twin-charger technology, which – along with other solutions, reduces CO₂ emissions from 300 to below 250 g/km. The unit is more than 100 kg lighter, which translates to lower fuel consumption. For affluent users of this brand (a sociological factor), the vehicle must have an eco-friendly unit. Additionally, driving comfort has been improved by improving the dynamics, which is a result of a more favourable external characteristic in areas of low engine speeds. The implementation of downsizing/rightsizing techniques has improved the company's prestige after Dieselpgate, reflecting on the political assessment at both a local and international level.

The Volkswagen Group manufactures and exports units, including those with downsizing/rightsizing technology, to almost every country in the world, which makes geopolitics extremely significant in the group's development strategy, as sometimes different plans need to be considered, for

example, between Europe and countries in Africa or South America.

In summary, it is important to note that Volkswagen is adopting downsizing/rightsizing technology mainly because of political reasons – the aspiration to become a world leader with a significant impact on international markets. Then, due to the ecological factor – pro-environmental awareness and the resulting need for climate protection and the economic factor, combined with the sociological factor – smaller engines mean lower operational costs, as well as production costs, with a very well-functioning technological factor due to years of experience and continuous investments in the R&D sector.

5.2. Rightsizing at Ford

One could argue that the idea of downsizing/rightsizing started at Ford with the introduction of environmentally friendly initiatives under the collective name EcoBoost. The cascade of displacement changes is indeed spectacular, starting from the 5.4 dm³ V8 engine through various forms, down to the 0.999 dm³ engine. EcoBoost is a collection of innovative technical solutions that include not only a change in displacement, but also fuel direct injection, turbocharging, and variable valve timing. In some units, such as 1.5 dm³, with a 3-cylinder construction, cylinder deactivation has also been implemented. The use of lightweight aluminium alloys was a significant factor, undeniably improving both the thermal efficiency and the mass balance. The set of solutions that have been implemented allows for operation with lean mixtures, lowering fuel consumption, and thus reducing CO₂ emissions. In the PESTEL analysis, the technological factor for Ford appears evident due to the company's tradition and continuous investment in R&D. However, the most crucial criterion for implementing rightsizing technology is ecology and the legal factor, with potential penalties for exceeding emission standards. In the American environment, and not only there, the social factor gains importance, where operating costs, as well as insuring vehicles with lower engine displacements, play a significant role [6, 11]. For the numerous Ford factories scattered around the world, maintaining jobs and combating unemployment is also significant. Therefore, the sociological factor, along with the implementation of new technical solutions, becomes crucial. Ford is a leading global player in the automotive sector, and with the implementation of downsizing/rightsizing, the company's prestige has been maintained or even enhanced. Awards, such as multiple victories in the Engine of the Year competition [66], serve as proof of this.

Since 2021, Ford's vehicle propulsion development strategy has been moving towards hybridisation using units with altered displacement volumes. An example might be the F150 Powerboost Hybrid with a 3.5-litre twin-turbo engine and cylinder deactivation compared to the earlier V8 5.0 dm³ (Coyote – which already used cylinder deactivation) and the later 3.7 dm³ V6 engine.

To conclude, it is worth mentioning that the technical factor with EcoBoost technology has positioned the Ford brand in the group of the most aggressive downsizing in the A, B, and C automotive segments. This leadership is also

the result of political influences that elevate the company's prestige and sustain international markets.

5.3. Rightsizing at Toyota

Toyota, in its core strategy, successfully creates vehicles with drives in the mass segment. A glance at the sales statistics reveals that three models from this brand are among the top 10 best-selling cars globally, securing the 2nd, 3rd, and 8th positions [59]. The same applies to the Polish market [68].

Downsizing/rightsizing at Toyota occurred with consideration for the political factor, stemming from a unique position in the fleet market with low operating costs, as well as the technological factor due to a high level of reliability. By introducing 1.2 dm³ turbo engines to replace the 2.0 D-4D, as well as 1.0 dm³ VVT-i and 1.5 hybrid instead of 1.3 dm³, the CO₂ emission level was effectively reduced to just 75 g/km. The technique of variable valve timing, encapsulated in the acronym VVT-i, has gained significant importance, ensuring an improvement in the filling coefficient [45].

An interesting technological solution is the TNGA system with the Miller/Atkinson cycle in 1.8 and 2.0 dm³ Hybrid units. Higher thermodynamic efficiency was achieved with energy recovery and improved engine operating flexibility. This ensures more favourable ecological and economic indicators, which positively influence customer perception, positioning the sociological factor well in the implementation of rightsizing technology. Another example of downsizing is the 1.0 dm³ engine, where the added value in the technological factor turned out to be the reduced weight, which translates to lower operating costs, and this is reflected in the social factor through user satisfaction.

Another example of Toyota's operations using downsizing/rightsizing technology is the niche model 0.6 dm³, produced in collaboration with Daihatsu. These engines are used in the segment of so-called kei cars, which meet local regulations concerning engine displacement and vehicle dimensions. Smaller Toyota engines also respond to legal regulations and environmental conditions in the European and American markets.

In summary, when implementing downsizing/rightsizing technology by Toyota, it is important to highlight the significance of the following factors: political (the company's prestige in global markets, especially in the mass sector, and the purchasing support of the Japanese government for domestically produced cars), sociological (popularity among Japanese people), economic (low operating costs), ecological (conscious environmental responsibility with low CO₂ emissions), and technological (a range of innovative technical solutions quickly implemented to maintain the company's prestige and significant investments in the R&D sector – recently in alternative fuels involving ammonia and hydrogen within the Japan Petroleum and Carbon Neutral Fuels Energy Centre) [69].

5.4. Rightsizing at Mercedes-Benz

Mercedes-Benz, as a group (Mercedes, AMG, EQ and Maybach) with a recognised high standing in terms of reliability, quality, and luxury, approached the issue of downsizing/rightsizing primarily by considering two PESTEL

factors: political and sociological. These actions have been supported by others and classified under legal and environmental factors. In this way, one can distinguish, for example, the development work on the modernisation of the V6 2.5 dm³ unit and the creation of the downsized R4 2.0 dm³ engine, powering, among others, the popular Mercedes E model. Another example of downsizing is the V8 engine with a displacement of 4.7 dm³, with a biturbo charging technique, which was replaced by the R6 3.0 dm³ unit with twin-scroll turbocharging, supporting a mild hybrid system to achieve the full effect of rightsizing.

Implementing modern turbocharging systems has become a marketing hallmark of downsizing technology as executed by Mercedes-Benz, which, together with improving the direct injection system, has reduced CO₂ emissions from 300 to 180 g/km or less [70].

In geopolitical considerations regarding the determinants of rightsizing in Mercedes-Benz vehicle drives, the local market with the so-called flagship user plays an important role. Mercedes-Benz customers often have their own cost policy known as TCO, where rightsizing is the answer to low operating and service costs, as well as emission costs of CO₂, in the overall context of a given institution. Mercedes-Benz follows such corporate strategies, but places greater emphasis on analysing the development of regional markets, particularly the Asian and American ones, where the so-called drive modularity plays a significant role. The economic aspect is crucial in China, as it is linked to high consumer expenses due to elevated tariffs and CO₂ emission taxes. Therefore, Mercedes-Benz launched the downsized 1.5 dm³ engine equipped with ISG technology. On the other hand, the USA is prestigious for Mercedes-Benz. To a large extent, this market must be considered from the social factor perspective, arising from the habitual preference for so-called large capacities in big cars, which is in opposition to the ecological and legal factor, related to penalties for non-compliance with CO₂ emission standards. After all, it was in the USA, specifically in California, that numerous efforts to protect our climate began, alongside today's standards and various forecasts developed by CARB as well as CAFE which define fuel consumption and indirectly indicate CO₂ emissions. Environmental standards in the USA serve as guidelines for the developmental work of Mercedes-Benz. Some Americans accepted the mentioned switch from a V8 engine to an R4, but Mercedes-Benz went further and developed EQ Boost hybrid units, observing the work of competitors such as Ford and Toyota and sales results in the USA [71].

The transition (although not completely) from the almost flagship V6 and V8 units to inline engines, reinforced by a range of technical systems to maintain performance levels, has also been expressed in the prestigious S-class models, where the environmental awareness of users is significantly higher than the others. This therefore has a sociological dimension in the PESTEL framework.

In summary, following a broad assessment of the political factor regarding the continued prevalence of internal combustion propulsion as a still significant source of vehicle drive, Mercedes-Benz in 2024 altered its seemingly rigid "electric first" declaration in favour of developing

hybrid designs incorporating internal combustion engines within the rightsizing concept [72].

6. Geopolitical conditions of rightsizing in selected regions of the world

6.1. Rightsizing in Europe

The implementation of the downsizing/rightsizing concept in Europe is primarily associated with the Volkswagen Group (chapter 4.1), whose power units are found in vehicle brands forming the group such as VW, Audi, Skoda or Seat. Dominant factors are ecology and law. The same applies to other companies: Peugeot, Citroen, Opel, and Fiat, which formed the Stellantis group, possessing their own technologies and having a significant place in the history of automotive development. The Stellantis group also includes American companies: Chrysler, Dodge, Jeep, which strongly contribute to the development strategy with a social factor. The development package includes modifications such as 1.6 or 1.8 dm³ units to 1.2 or 1.0 dm³ units in Opel or Peugeot models. The effect is a reduction in CO₂ emissions from 160 to approximately 120 g/km.

Rapid implementation of certain technical solutions, along with downsizing such as the wet timing belt and insufficient lubricant flow, caused the 1.2 dm³ Pure Tech engine to earn a very poor reputation due to numerous damages and failures. The prestige of the Peugeot company has been severely damaged. Hence, the significant effort and creation of the 1.2 PureTech GEN3 model in a hybrid solution, thereby enhancing the technical factor. Additionally, to improve the company's image, the sociological factor was altered by extending the warranty period from 6 to 10 years.

In turn, Renault has focused its attention on underdeveloped countries located in Africa, Asia or South America, where it is possible to "bypass" restrictive legal regulations and maintain existing product technology, thus surviving in the market, which proved to be effective during the COVID-19 coronavirus pandemic. In this way, the high labour costs (an economic and sociological factor) have also been transferred from Europe to Turkey and Morocco. This move aligns with the framework of so-called "bad bank structures," which are used to survive difficult times and avoid the risk of company collapse [73]. The second development path for the Renault company, including downsizing/rightsizing products, is a venture carried out jointly with the Chinese company Geely as Geely Horse Powertrain Ltd [75]. Among the products, there are ultra-low emission CO₂ engines as standalone power units: 1.0 dm³ TCe and 1.2 dm³ TCe as well as used in hybrid systems: 1.2 E-Tech full hybrid. They are sold, among others, to Africa and Asia – India [74]. The Stellantis group adopts a similar practice [76]. This indicates that when evaluating downsizing/rightsizing technology from both an economic and partly political standpoint, the entire approach can only be seen as temporary rather than permanent. The sociological factor, in turn, has a positive dimension through the reduction of unemployment and the creation of new jobs – although only a few of these concern Europe, such as Spain and Romania.

Europe, having faced several fuel crises, clearly emphasises the economic factor in numerous development strategies, taking fuel prices into account. Investments in research on alternative fuels for combustion engines, such as historically LPG or CNG, but also currently ammonia and hydrogen, play a crucial role, as these, combined with downsizing techniques, contribute to meeting European emission standards. An example might be the Fiat 0.9 dm³ TwinAir (Multi-AIR) CNG engine, which has been awarded multiple times in the Engine of the Year competition [68]. The presented unit is a twin-cylinder with a JTS injection system, dual spark plug, and an innovative timing system ensuring combustion of mixtures close to stoichiometric. In practical engineering terms, this leads to about 10% decrease in fuel usage. Such aggressive downsizing requires strong support from other systems, like the SCR system for nitrogen oxides reduction and the GPF – particulate filter. This all results in increased operating costs, which affects user enthusiasm and is reflected in sociological factors.

In summary, it can be noted that in Europe, the main factors determining the implementation of downsizing/rightsizing technologies are environmental, legal, and economic regulations. The economic factor has a clear dimension in tax and insurance reliefs, which additionally introduces a sociological factor into effect – the client's choice.

6.2. Rightsizing in the USA

The automotive industry in the USA, with giants such as GMC, Ford, Chevrolet, and Cadillac, plays a crucial role in implementing numerous technological innovations. History places American automotive companies at the top podium in terms of technology. Hence, the technical factor did not raise any doubts during the implementation of downsizing/rightsizing technologies, especially considering that cylinder deactivation – classified as downsizing technology – was first introduced in the Cadillac V8 as early as the 1980s [77]. Ecology is the main driving force behind the implementation of the rightsizing concept. The government agency EPA, as well as the Californian state environmental body CARB, and CAFE regulations have a significant potential to influence environmental awareness and shape the foundations of automotive development. American standards (Californian) are considered the strictest in the world – Table 1.

Table 1. Sample exhaust gas emission standards in different regions around the world

Region	Current standard	Sample emission values, g/km			CO ₂ emissions	Test
		CO	NO _x	PM		
USA	Tier 3	0.62	0.018	0.0019	82.5 – activities CAFE from 2026	FTP-75 and US06
Europe	Euro 6(d)	1.00	0.060	0.0050	93.5 for the fleet	RDE
Asia – China	China VI B	1.00	0.035	0.0045	93.6	RDE

The ecological factor in the USA is clearly intertwined with the sociological factor, expressed by the growing

awareness of car users towards climate protection. The full support of the state for maintaining the prestige of American companies, including automotive ones, is not without significance, as evidenced by the significant dedicated resources and subsequent federal takeover of GM and the creation of GMC. For Americans, the economy is also of significant importance and it may even parallel ecology in the development of the automotive industry, as customers demand low-cost operation of their vehicles. Although inexpensive operation primarily means cheap fuel, design solutions that ensure lower fuel consumption are also taken into account. Fuel for combustion engines comes from various sources, which the USA strongly seeks, sometimes involving itself in armed conflicts over oil and gas deposits. Energy security of a country and region is an important development factor, represented by both political and sociological dimensions [32].

In summary, the USA acts as a distinctive catalyst for innovation in the field of downsizing/rightsizing technology, demonstrated by the increase in the market share of engines with a capacity below 3.0 dm^3 from around 30% in 2000 to approximately 59% in 2020 [19]. Nevertheless, in the context of strong lobbying for electromobility, the idea of rightsizing combustion engines is seen as a transitional phase.

6.3. Rightsizing in Asia-China

For 20 years, the automotive market in China has been one of the most rapidly developing markets in the world. The most important factor in development is the broadly understood "policy" that defines the local market, Asian markets, and influences the strategic decisions of other producers on a global scale. China strongly influences legal and economic regulations, as well as consumer preferences, reinforcing the position of the sociological factor. For Chinese, the overall national strategy "Made in China: New Energy Vehicles" is important [31, 78]. Actions for environmental protection are included in the country's development strategy and in individual sectors. However, they are selective and do not consider the entire product life cycle. Hence, for example, the fight against low emissions from transportation means while simultaneously having high emissions at the stage of automotive component production [7, 8]. China, with government support, has ensured technological development by providing education at various levels, establishing an international grant system, and building dedicated research and development centres. This brings tangible results, as well as downsizing/rightsizing technology. Implementing the idea of rightsizing involves discussions on the country's prestige and technological dominance in the world, as well as fiscal policy. It should be emphasized that in China, the market for manufacturers of cars with internal combustion engines is made up of well-known global brands such as Toyota, Mercedes-Benz Group, BMW and VW [79].

Chinese manufacturers such as BYD, Geely, and Great Wall focus primarily on an electric strategy for vehicles [76]. Similarly, it is the case with corporations like BAIC Motor or SAIC, although they are supported by global companies – Mercedes-Benz in the former case, and VW and GM in the latter. The implementation of downsiz-

ing/rightsizing technology in China is influenced by financial and sociological factors due to taxes (such as the Consumption Tax as well as Vehicle and Vessel Tax Law), which are heavily dependent on engine displacement. In the range from 1% for units below 1.0 dm^3 to 40% – above 3.0 dm^3 [12, 31, 48]. Naturally, these two extreme scenarios are not compatible with each other regarding performance indices and technically cannot be aligned, yet the tax system significantly impacts customer choices, shaping production policy as a result. The current exhaust emission standard in China, China VI B (Table 1) practically eliminated large displacement internal combustion engines in favour of smaller turbocharged units, supported by after-treatment systems such as SCR. The Chinese customer expects a prestigious car today with low operating costs – hence various responses from the external market such as the Mercedes E (1.5 dm^3 R4 Turbo – EQ Boost). In the popular car segment, Toyota (1.5 dm^3 R3 Hybrid) or VW (1.4 dm^3 TSI).

It is worth noting the production of combustion engines beyond the automotive sphere, i.e., for power generators. This is an important production sector due to the highly diverse energy infrastructure in China and the need for power in areas lacking transmission lines or due to power instability [80]. The engines are intended for stationary devices, and in this case, no one has attempted to implement the downsizing/rightsizing concept, unlike mobile units, which are designed not only with environmental protection in mind, but also with weight reduction in mind. In this case, technical and sociological factors play an important role.

In fulfilling the "Made in China" strategy, the Chinese aim to also dominate the shipbuilding industry, accounting for 50% of the global order book [81]. In this context, the technology of downsizing/rightsizing internal combustion engines, which remain a primary source of propulsion, gains significant importance. There are three reasons. The first, mentioned above, is political in nature, stemming from Chinese pride and the nation's prestige. The second is an ecological factor due to the movement of ships across different zones, where international IMO standards apply, especially concerning NO_x emissions and the sulphur content in fuel [82]. There are also local standards like DECA, concerning the emissions of harmful substances, sulphur content in fuel, and noise levels in ports, along the coast, and rivers, where combustion engines are also used. Environmental factors have led to the implementation of downsizing technology, primarily in hybrid systems and additionally using LNG or ammonia as secondary or primary fuel. This is the case in companies such as CSSC Guangzhou Marine Diesel Engine Co., Ltd. or the R&D CSSC Power Research Institute, although many do not consider it 'classic' downsizing, but rather actions aimed at environmental protection in models with smaller engine displacement. Research and domestic production have led China to take steps towards independence from major players in the field of marine propulsion technology like MAN or Wärtsilä, thereby making the political factor the third reason for the changes being made. Currently, there is full cooperation between the Chinese industry and foreign companies, such

as the MAN-B&W 11G95ME-C engine, which was replaced with the 8G90ME-C10.5 model with a reduced number of cylinders and, although with limited power, completely sufficient to drive container ships – a classic example of rightsizing.

China produces many engines for external markets, specifically for countries with a similar economic structure, where the economic factor plays a significant role, focusing on operating costs, service, and low taxes, as well as small insurance premiums, much like other Asian and African countries.

In China, there is another important area that concerns vehicles and their propulsion systems – the issue of military solutions. It is classified as a political factor. In the military, emissions and fuel consumption standards do not apply, so ecological and economic factors are irrelevant. However, the equipment must be reliable and easy to service. Downsizing/rightsizing technology does not favour such criteria, but if one considers the drive mass and the widespread (not only in China) miniaturisation of military vehicle platforms to reduce the target area for enemy missiles, downsizing should be considered. Thus, the miniaturisation and reliability demonstrated by the creation of twin systems with hybrid configurations are an intriguing solution, such as the Mengshi EREV (Range Extender), where a 1.5 dm³ turbo engine is used as a generator to charge the main electric drive motors, or the ISDe 200-41 Cummins 6.7 dm³ engines, which replaced the L-series units with a volume of 8.9 dm³, but through turbocharging (HPCR system) along with electronic control, comparable performance indicators were achieved.

In summary, the deployment of downsizing/rightsizing technology in China ensures:

- industrial sovereignty, expressed as a political factor
- impact on global markets – political factor
- reduction of harmful substance emissions – factors: technical, ecological, and legal
- reduction of fuel consumption – factors: economic and sociological
- social prestige – a sociological factor.

6.4. Rightsizing in Asia–India

India is a country classified as part of the developing nations, with the largest population and the highest birth rate. This means that the transportation needs for people and goods in India are increasing exponentially from 4.25×10^{12} in 2005 to nearly 25×10^{12} in 2025, and if the current pace is maintained, the passenger-kilometre (PKM) ratio could reach an astronomical value of 588×10^{12} [83].

All PESTEL factors in the automotive sector, and downsizing in particular, gained significant importance after 2000, when the first emission standards known as BS-I (Bharat Stage) based on European standards were introduced – hence the economic factor [84]. In the history of these actions taken by the government of India, the omission of the BS-V standard and the introduction of BS-VI – the equivalent of the Euro 6 standard, but not only in large cities, rather across the entire country (political and sociological factor) was spectacular. The current standard requires the use of higher quality fuels (lower sulphur content of 10 ppm instead of 50 ppm) and advanced exhaust purifi-

cation systems – an ecological factor. The ecological factor is not widely recognised and is considered a necessary evil, particularly in the context of the use of older vehicles, which stems from the poverty of the population. The government announced a programme to revitalise transportation resources, thus introducing a strong political and legislative factor. The concept of rightsizing fits well into this scenario, especially because the dominant modes of transport in India are two- and three-wheeled vehicles, which require small power units. Engines with a capacity of 0.8 to 1.2 cubic decimetres are very popular and should be improved by adding support systems to reduce fuel consumption and emissions. An example might be the Maruti Suzuki 1.2 dm³ engine modified with turbocharging, fuel direct injection, and reduced displacement to 0.998 dm³, known as Boosterjet [85].

A similar action was taken by the local car manufacturer Tata by changing the 1.5 dm³ engine to a 1.2 dm³ GDI or a 1.2 dm³ powered by natural gas CNG. Ever stricter emission standards are eliminating compression ignition engines and replacing them with petrol engines featuring new modification packages, including downsizing. The ecological factor combined with the sociological one can be observed in the attitude of the new generation of Indians, who are better educated than their parents, taking into account pro-environmental actions, which is expressed both in government initiatives and in the lives of ordinary citizens. Another factor influencing the implementation of downsizing/rightsizing technology is taxation – a smaller engine displacement means a lower tax. Therefore, the sociological and economic factors are taken into account. In summary, India is tracking innovative solutions in foreign markets, striving to achieve a higher level of technological independence similar to that of China. The downsizing/rightsizing of the combustion engine primarily stems from economic factors combined with social and ecological reception, in conjunction with government policy on lower taxes.

6.5. Rightsizing in South America

In terms of the implementation of automotive and new technology, South America is mainly based on four factors: political, economic, sociological, and technical. Emission standards for exhaust gases are less stringent than in Europe and the USA and apply to a wide range of engines primarily powered by ethanol. The use of this biofuel was not and is not driven by environmental concerns, but rather by economic reasons and regional policy, from which arose the desire to develop agricultural regions and reduce unemployment [86]. Unfortunately, on this path, there was a loss leading to environmental degradation due to monoculture cultivation, primarily of sugarcane and corn used as a base for alcohol production. In addition, Brazil, for example, applies the highest amount of agricultural chemicals globally, improving crop yields but adversely affecting groundwater, rivers, and air quality. In such conditions, the sociological factor expressed through the work for farmers is positive, but the overall balance is diminished due to poorer financial results, i.e., the economic factor which takes into account the reduction in soil quality, leading to lower yields. Nevertheless, South America is focusing on biofuels, seeing it as an eco-friendly initiative [86].

In South America, there are no legal penalties for non-compliance with emission standards, or at least no one enforces them, which means there are no incentives to implement new technologies such as rightsizing. What is important, however, is the low costs of purchasing, operating, and servicing vehicles. In South America, small units prevail, which is why it serves as a good research ground for companies like VW and Stellantis.

Additionally, by placing factories on this continent, unemployment is reduced and such actions are supported by the governments of individual countries offering various tax reliefs to manufacturers. Therefore, an essential factor in endorsing the concept of downsizing/rightsizing is political and social influence. An example is the Rota 2030 programme in Brazil [87]. Fiats equipped with 1.0 dm³ FireFly engines (either turbocharged or mHEV in a hybrid setup), VW 1.0 dm³ TSI with BlueMotion technology, or Chevrolet 1.0 dm³ 16V M-TEC II, are driven on South American roads.

In summary, South America is receptive to adopting downsizing/rightsizing technology, but it carries this out with the participation of international firms, heavily influenced by economic and political factors.

6.6. Rightsizing in Africa

Having a general understanding of the political, economic, and social structures, as well as the climate in Africa, it is clear that the continent views automotive issues quite differently compared to Europe or the USA, and even more so when it comes to implementing new technologies. However, when considering the development of the automotive industry, it should be viewed through the lens of economics, with high car costs and low fuel prices, as well as through the sociological factor (unemployment, low levels of education) [88].

Automotive giants dominate Africa, and they set the tone for all changes. Africa itself is not interested in implementing eco-friendly technologies, given the general economic difficulties. Small vehicles dominate the roads in Africa, not necessarily because of downsizing, but due to the economic situation. The most popular brands with small engines in the range of 1.3 to 1.5 dm³ belong to companies such as Toyota, VW, Nissan or Renault [89]. Only in slightly more developed countries such as South Africa, Egypt, or Morocco, social factors related to the awareness of unemployment and policies determining the location of factories and services are beginning to play a role in the choice of vehicle types. In addition, there is some pressure (not much, but still) from tourists who, when arriving in Africa, are environmentally conscious and would like to travel in vehicles that meet emission standards. This is a factor at the boundary of sociology and ecology. The lack of definitive research on the automotive industry in Africa means that analysts rely solely on estimated data, indicating that more than 60% of cars and their engines in Africa are old machines and are used until they reach technical failure, with little or no service support [2]. This creates a major challenge in terms of modernising these units (retrofit) with the implementation of downsizing/rightsizing technology. This must be a systemic action that takes into account a whole range of other activities, such as the development of educa-

tion to improve the overall technical culture. This strategy has potential given the global preference for electromobility, due to the severely limited availability of electricity, even when using solar sources in Africa.

In summary, the development of the automotive industry in Africa should be viewed through the lens of the growth of foreign companies. Small power units that serve as the driving force for numerous cars are the result of economic measures and have nothing to do with the development of downsizing/rightsizing technology, which contrary to appearances, is very demanding.

7. Conclusions

The entire world is declaratively moving towards climate neutrality, which in the case of transportation means stricter emission standards for harmful substances and carbon dioxide, as well as setting deadlines for the sale of new combustion engine vehicles. In this area of activity, there is a collision between the challenges faced by manufacturers and the expectations of vehicle users, referred to as sustainable transport, all within a specific geo-environment.

Although electromobility is named the future of automotive innovation, its role in climate protection is questionable when considering the full lifecycle of products and processes. This ensures that the world will continue to recognise combustion engines as an important source of vehicle propulsion, which in turn means maintaining the continuity of work on improving the design and technology of this heat machine. One of the development trends that should be considered is engine downsizing, which was introduced into engineering practice more than 15 years ago. Today, it operates in the form of rightsizing and, depending on geopolitical conditions, may occur independently or in conjunction with hybrid systems.

This study evaluates the current status and development potential of downsizing/rightsizing combustion engines, viewed through the PESTEL methodological framework, with examples from selected manufacturers across different global regions.

The analysis of individual factors and their elements among the automotive manufacturers evaluated above showed that downsizing/rightsizing is considered by all, namely VW, Ford, Toyota, and Mercedes-Benz, but to varying degrees. For every company, prestige is important: a political factor. Each of these companies wants or needs to include all technological trends in their offerings, and therefore downsizing/rightsizing, which leads to improved drive efficiency. It is important to maintain a strong position in both the local market and international relations and potentially shape this market.

The political factor is consistent with the economic and social, where people with their purchasing preferences predominate, influencing consumption. The contribution of these factors varies between individual companies. VW, Ford, and Toyota are heavily reliant on the economical vehicle operation formula provided by downsizing/rightsizing, making the development of this technology more significant than for Mercedes-Benz. The evaluation of a vehicle user's education with a certain level of technical culture and thus the awareness of what downsizing/rightsizing technology involves (a technical factor) is im-

portant for VW and Ford customers, but is less significant or not at all important for Toyota and Mercedes-Benz customers.

Evaluating the technical factor and the ecological awareness of manufacturers, each of the analysed companies has a high level of development and invests in the R&D sector, which is most evident during successive automotive trade fairs, where solutions related to combustion engines are presented, and rightsizing is included in each of these solutions.

All evaluated manufacturers consider the legislative factor, and VW pays the most attention to it, especially after the Dieseltgate scandal, which instilled a particular respect for legal frameworks and the penalties associated with them. Each of these companies protects its intellectual property, which is expressed, for instance, through marketing names such as VW – TSI or TFSI, Ford – EcoBoost, with information on engine displacement. Mercedes-Benz incorporates downsizing in the EQ Boost hybrid unit, while Toyota does not use a trade name, considering downsizing/rightsizing as part of the overall development strategy for combustion engines.

The analysis of geopolitical conditions for downsizing/rightsizing technology in different regions of the world highlights the importance of political stability and tax regulations, as well as the significance of international relations for the development of this trend in Europe, the USA and China.

The political factor of the government practically does not influence the development of downsizing/rightsizing technology in South America and Africa, where car manufacturers already present in the market play a leading role in this respect. In India, international relations are important because this market is one of the fastest growing in the automotive sector, but is highly dependent on user prefer-

ences, where purchase and running costs play a significant role.

The social factor, considering demographics, education, and lifestyle, is very strong in Africa compared to other PESTEL factors, where, for example, awareness of climate protection, legal frameworks, or intellectual property protection related to new technologies are not considered at all or only to a minimal extent.

A significant factor for Africa, as well as South America and parts of Asia, is the combined political and social element related to unemployment. Relocating factories to these regions not only provides social support but also offers the opportunity for the gradual implementation of new technologies due to customer preferences for low-cost operation, which downsizing/rightsizing ensures. However, these must be driven by a lower level of technological advancement, particularly in relation to variable valve timing systems or complex turbocharging systems, which is due to the low level of service or the lack of infrastructure in this area. However, this is a significant area for development, especially in the context of modernising old units that are being imported in large quantities from Europe and the USA.

This analysis does not claim to be the definitive interpretation of the material; on the contrary, it is expected to spark a wide-ranging discussion, and the Author himself promises a more in-depth evaluation.

Acknowledgements

This project was supported by the Wrocław University of Science and Technology – GEO-3EM research centre – Energy-Ecology-Education, Marshal's office project number RPDS.01.01.00-02-0001/16). We also thank to Autocomp Management Ltd. – Research and Development Centre – Producer of simulators on the military and civilian market from Poland.

Nomenclature

A, B	change coefficients in downsizing	PESTEL	methodology due to Political, Economic, Social, Technological, Environmental and Legal factors
CAFE	Corporate Average Fuel Economy,	PKM	passenger-kilometre
CARB	California Air Resources Board	PureTech	Stellantis's (formerly Peugeot and Citroen) brand name for gasoline engines
CNG	compressed natural gas	R&D	research and development
C-TEC	engine code	S	piston stroke – initial state
D	cylinder diameter – initial stat	S _d	piston stroke in an engine after downsizing
D _d	the cylinder diameter in an engine after downsizing	SCR	selective catalytic reduction
DECA	China Domestic Emission Control Area	SVC	Saab Variable Compression
EcoBoost	Ford's brand name for gasoline engines	TCO	total cost of ownership
EPA	Environmental Protection Agency	TDI	turbocharged direct injection
FSI	fuel stratified injection	Ti-VCT	twin independent variable camshaft timing
GDI	gasoline direct injection	TNGA	Toyota New Global Architecture
GDP	gross domestic product	TSI	turbocharged stratified injection
HPCR	high-pressure common rail	VCR	variable compression ratio
IMO	International Maritime Organization	VNT	variable nozzle turbine
ISG	integrated starter generator	VTEC	variable valve timing and lift electronic control
i-VTEC	intelligent system VTEC operating proactively	VVT-i	variable valve timing with intelligence
LPG	liquefied petroleum gas	W _d	downsizing index

Bibliography

- [1] Aaron C. The real impact of engine downsizing: benefits and drawbacks explained. <https://autopartswd.com/engine-downsizing-impact/> (accessed on July 28, 2025).
- [2] Baskin A, de Jong R, Dumitrescu E, Akumu J, Stannah VR, Mwangi A et al. A global overview of used light duty vehicles report: flow, scale and regulation, united nations environment programme, Dec 28; 2020. <https://www.unep.org/resources/report/global-trade-used-vehicles-report> (accessed on July 28, 2025).
- [3] Belsare HV. PESTLE analysis. *Int J Adv Res.* 2025;13(2): 608-612. <https://doi.org/10.21474/IJAR01/20411>
- [4] Brzeżański M, Śliwiński K, Downsizing – a new direction of automobile engine development. *Combustion Engines* 2004;119(2):3-11. <https://doi.org/10.19206/CE-117413>
- [5] Cassiani M, Bittencourt ML, Galli LA, Villalva SG. Variable compression ratio engines. *SAE Technical Papers.* 2009-36-0245. 2009. <https://doi.org/10.4271/2009-36-0245>
- [6] California Code of Regulations Title 10 – Investment Chapter 5 – Insurance Commissioner Subchapter 4.7 – Private Passenger Automobile Rating Factors, Article 3 – Rating Factors Section 2632.5 – Rating Factors.
- [7] Chen Y, Lawell CYCL, Wang Y. The Chinese automobile industry and government policy. *Res Transportation Econ.* 2021;84(28):100849. <https://doi.org/10.1016/j.retrec.2020>
- [8] Chen Y, Dai X, Fu P, Luo G, Shi P. A review of China's automotive industry policy: recent developments and future trends. *J Traffic Transp Eng.* 2024;11(5):867-895. <https://doi.org/10.1016/j.jtte.2024.09.001>
- [9] Dahodwala M, Joshi S, Krishnamoorthy H, Koehler EW, Franke M. Evaluation of system configurations for downsizing a heavy-duty diesel engine for non-road applications. *SAE Int J Engines.* 2016;9(4): 2272-2285. <https://doi.org/10.4271/2016-01-8058>
- [10] Danciu BA, Giannakopoulos GK, Bode M, Frouzakis CHE. Direct numerical simulation of hydrogen combustion in a real-size IC engine. *Cornell Univeristy, Arxiv Physics, Fluid Dynamics.* 2025. <https://doi.org/10.48550/arXiv.2502.16318>
- [11] Directive 2009/103/EC of the European Parliament and of the Council of 16 September 2009 relating to insurance against civil liability in respect of the use of motor vehicles, and the enforcement of the obligation to insure against such liability. <https://eur-lex.europa.eu/eli/dir/2009/103/oj/eng>
- [12] Dziemianowicz W, Szmigiel-Rawska K, Nowicka P, Dąbrowska A. Planowanie strategiczne. MRR. Warszawa 2012.
- [13] Falfari S, Bianchi GM, Cazzoli G. Thermal efficiency enhancement for future rightsized boosted GDI engines – effectiveness of the operation point strategies depending on the engine type. *SAE Technical Papers.* 2021-24-0009. 2021. <https://doi.org/10.4271/2021-24-0009>
- [14] Fisher CH. Carburation, spark-ignition engines fuel injection systems. Vol III, Chapman&Hall, London 1966.
- [15] Fraser N, Bassett M. Extreme engine downsizing with a single turbocharger – 100 kW/l and 30 bar BMEP. *Seminar Proceedings IMechE.* London, February 2011;3145.
- [16] Fraser ADJ. How low can we go? Challenges and opportunities of engine downsizing to reduce CO₂ emissions, *Seminar Proceedings IMechE,* Londyn 2011;3145.
- [17] Friedl H, Kapus P. Trends in gasoline engines technology. *Combustion Engines.* 2005;121(2):3-19. <https://doi.org/10.19206/CE-117402>
- [18] Galloni E, Fontana G, Palmaccio R. Effects of exhaust gas recycle in a downsized gasoline engine. *Appl Energy.* 2013; 105:99-107. <https://doi.org/10.1016/j.apenergy.2012.12.046>
- [19] Glickman B. After years of going big, American car buyers are downsizing. *The Wall Street Journal.* Dec. 23, 2024.
- [20] Gupta A, Saul J, Abdel-Gayed RG. Downsizing of a naturally aspirated engine to turbocharged gasoline direct injection variable valve timing engine. *Int J Eng Appl Sci.* 2013;4(6): 1-10.
- [21] Huang Y, Surawski NC, Zhuang Y, Zhou JL, Hong G. Dual injection: an effective and efficient technology to use renewable fuels in spark ignition engines. *Renewable and Sustainable Energy Rev.* 2021;143:110921. <https://doi.org/10.1016/j.rser.2021.110921>
- [22] Interim regulations of the people's Republic of China on consumption tax. https://www.gov.cn/zhengce/2008-12/19/content_2843852.htm (accessed on July 28, 2025).
- [23] Kalghatgi G. Is it the end of combustion and engine combustion research? Should it be? *Transp Eng.* 2022;10: 100142. <https://doi.org/10.1016/j.treng.2022.100142>
- [24] Kasedorf J. Układy wtryskowe i katalizatory. WKiŁ, Warszawa 1998.
- [25] Kemper H, Baumgarten H, Hebermann K, Yapici KI, Pischinger S. On the road towards consequent downsizing. *MTZ Worldwide.* 2003;54(5):16-18. <https://doi.org/10.1007/BF03227583>
- [26] Kneba Z, Makowski S. Zasilania i sterowanie silników, WKiŁ. Warszawa 2004.
- [27] Lejda K. Injection systems of high-speed diesel engines and development trends. *Combustion Engines.* 2005;123(4):19-30. <https://doi.org/10.19206/CE-117366>
- [28] Lejda K, Woś P. Fuel injection in automotive engineering – simulation of combustion process in direct injection diesel engine based on fuel injection characteristics. *InTech.* 2012. <https://www.intechopen.com/books/2157>
- [29] Lenz HP. The future of the combustion engines from the sight of the 28th International Vienna Motor Symposium. *Combustion Engines.* 2007;129(2):21-32. <https://doi.org/10.19206/CE-117327>
- [30] Lenz HP. 30 International Vienna Motor Symposium May 2009 – Report on the occasion of the International Congress PTNSS on Combustion Engines in Opole. *Combustion Engines.* 2009;137(2):150-154. <https://doi.org/10.19206/CE-117185>
- [31] Lu C. Analysis of China's new energy vehicle industry. *Proceedings of the 2022 7th International Conference on Financial Innovation and Economic Development.* 2022; 648:1249-1256. <https://doi.org/10.2991/aebmr.k.220307.207>
- [32] Makos J. The impact of Trump's tariffs: PESTLE breakdown. <https://pestleanalysis.com/trump-tariffs/> (accessed on Apr 04, 2025).
- [33] Mazanec JM, Vang NS, Kokjohn SL. Enabling off-highway diesel engine downsizing and performance improvement using electrically assisted turbocharging. *Int J Engine Res.* 2023;24(9):4104-4126. <https://doi.org/10.1177/14680874231181002>
- [34] Mitianiec W, Bac G. Camless hydraulic valve timing system in combustion engines. *Combustion Engines.* 2011;146(3): 28-37. <https://doi.org/10.19206/CE-117089>
- [35] Namar MM, Jahanian O, Shafaghat R, Nikzadfar K. Engine downsizing; global approach to reduce emissions. A worldwide review. *HighTech and Innovation Journal.* 2021;2(4): 384-399. <https://doi.org/10.28991/HIJ-2021-02-04-010>

- [36] Patil C, Varade S, Wadkar S. A review of engine downsizing and its effects. *Int J of Curr Eng Technol.* 2017;7(7): 319-324. <http://inpressco.com/category/ijcet>
- [37] Pielecha I, Cieślík W, Borowski P, Czajka J, Bueschke W. Reduction of the number of cylinders in internal combustion engines – contemporary trends in downsizing. *Combustion Engines.* 2014;159(4):12-25. <https://doi.org/10.19206/CE-116926>
- [38] Perceau M, Guibert P, Guilain S, Segretain F, Redlinger T. Why can Miller cycle improve the overall efficiency of gasoline engines? THIESEL – Conference on Thermo- and Fluid Dynamic Processes in Direct Injection Engines. 2020.
- [39] Pischinger S, Verbrennungskraftmaschinen I, RWTH Aachen, Aachen 2011.
- [40] Reynders D. Member of the EC – Letter from Commissioner Reynders to Volkswagen on compensation, Ares(2020) s4604327, Brussels September 17, 2020.
- [41] Rinaldini CA, Breda S, Fontanesi S, Savioli T. Two-stage turbocharging for the downsizing of SI V-engines. *Energy Procedia.* 2015;81:715-722. <https://doi.org/10.1016/j.egypro.2015.12.077>
- [42] Sroka ZJ, Dworaczyński MK, Assessment of thermodynamic cycle of internal combustion engine in terms of rightsizing. *Combustion Engines.* 2019;178(3):182-186. <https://doi.org/10.19206/CE-2019-331>
- [43] Sroka ZJ. Work cycle of internal combustion engine due to rightsizing, internal combustion engine technology and application of biodiesel fuel. *IntechOpen.* 2021. <https://doi.org/10.5772/intechopen.97144>
- [44] Stabryła A. Zarządzanie strategiczne w teorii i praktyce firmy (in Polish). PWN. Warszawa–Kraków 2000.
- [45] Szalek A, Pielecha I. The influence of engine downsizing in hybrid powertrains on the energy flow indicators under actual traffic conditions. *Energies.* 2021;14:2872. <https://doi.org/10.3390/en14102872>
- [46] Szwaja S, Szymkowiak M. The Szymkowiak’s over-expanded cycle in the rocker engine with the variable compression ratio – kinematics, *Combustion Engines.* 2022; 189(2):68-72. <https://doi.org/10.19206/CE-143157>
- [47] Vlaswinkel M, Antunes D, Willems F. Automated and risk-aware engine control calibration using constrained Bayesian optimization. Cornell Univeristy, Arxiv Physics, Electrical Engineering and Systems Science, Systems and Control. 2025. <https://doi.org/10.48550/arXiv.2503.20493>
- [48] Vehicle and vessel tax law. http://www.mof.gov.cn/zhengwuxinxi/caizhengxinwen/201901/t20190102_3112026.htm (accessed on Apr 04, 2025).
- [49] Walsch MP. Global trends in motor vehicle pollution control: a 2011 update; part 3. *Combustion Engines.* 2011; 167(4):98-103. <https://doi.org/10.19206/CE-117083>
- [50] Weissbäck M, Howlett M, Ausserhofer N, Krapf S. The efficiency engine – cost-effective alternative to downsizing. *Combustion Engines.* 2012;149(2):3-9. <https://doi.org/10.19206/CE-117034>
- [51] Wendeker M. Sterowanie napełnianiem w silniku samochodowym (in Polish). Lubelskie Towarzystwo Naukowe. Lubin 1999.
- [52] Wendeker M. Adaptacyjne sterowanie wtryskiem benzyny w silniku (in Polish). PWN. Warszawa 2000.
- [53] Wisłocki K, Pielecha I, Czajka J, Maslennikov D. The qualitative spray analysis of liquid fuel in high-pressure piezoelectric injection system, *Combustion Engines.* 2010;143(4): 31-44. <https://doi.org/10.19206/CE-117129>
- [54] <https://1stplace.pl/blog/pestel-identyfikacja-szans-i-zagrozen-rynkowych-wsparcie-w-tworzeniu-strategii/> (accessed on July 31, 2025).
- [55] <https://www.thedrive.com/guides-and-gear/how-many-cars-are-there-in-the-world> (accessed on July 31, 2025).
- [56] <https://www.chinskiraport.pl/blog/samochody-elektryczne-w-chinach/> (accessed on June 16, 2025).
- [57] <https://www.bankier.pl/moto/wiadomosc/Ile-mamy-samochodow-w-Polsce-Ubylo-niemal-5-mln-martwych-dusz-8767485.html> (accessed on July 23, 2025).
- [58] <https://www.iea.org/reports/global-ev-outlook-2025/trends-in-electric-car-markets> (accessed on July 23, 2025).
- [59] <https://www.europarl.europa.eu/topics/pl/article/20190313/STO31218/emisje-co2-z-samochodow-fakty-i-liczby-infografiki> (accessed on July 17, 2025).
- [60] <https://magazynauto.pl/wiadomosci/silnik-spalinowy-jeszcze-pozyje-analiza,aid,2761> (accessed on July 17, 2025).
- [61] <https://autoblog.spidersweb.pl/2025-norwegia-sprzedaz-samochodow-spalinowych> (accessed on July 17, 2025).
- [62] <https://www.auto-swiat.pl/wiadomosci/aktualnosci/kolejny-zwrot-akcji-w-sprawie-najbardziej-awaryjnego-silnika-ostatnich-lat-12/r22jmvq> (accessed on Sep 6, 2025).
- [63] <https://www.justice.gov/archives/opa/pr/volkswagen-spend-147-billion-settle-allegations-cheating-emissions-tests-and-deceiving> (accessed on June 28, 2025).
- [64] <https://forum.vwgolf.pl/viewtopic.php?t=616545> (accessed on Apr 16, 2025).
- [65] <https://autogaleria.pl/volkswagen-golf-1-5-etsi-mild-hybrid-dsg-test-opinia> (accessed on Oct 20, 2020).
- [66] <https://www.ukimediaevents.com/engineoftheyear/> (accessed on Aug 19, 2019).
- [67] <https://www.visualcapitalist.com/ranked-the-worlds-best-selling-cars-from-2024/> (accessed on Mar 06, 2025).
- [68] <https://moto.infor.pl/wiadomosci/rynek/7013274,te-samochody-polacy-kupuja-najczesciej-w-2025-r-auta-nowe-i-uzywane-do-3-lat.html> (accessed on July 18, 2025).
- [69] <https://www.pecj.or.jp/en/> (accessed on Aug 01, 2025).
- [70] <https://www.fleetnews.co.uk/cars/Car-CO2-and-fuel-economy-mpg-figures?manufacturer=mercedes-benz> (accessed on Aug 01, 2025).
- [71] <https://www.newsauto.pl/mercedes-technologia-eq-boost-cala-rodzina-elektryczna/> (accessed on June 07, 2025).
- [72] <https://motopass.pl/inne/mercedes-ola-kallenius-samochody-elektryczne-zmiana-decyzji/> (accessed on June 15, 2025).
- [73] <https://www.investopedia.com/terms/badbank.asp> (accessed on Oct 31, 2020).
- [74] <https://www.horse.cars/newsroom/renault-group-and-geely-announce-the-creation-of-leading-powertrain-technology-company-horse-powertrain-limited/> (accessed on May 31, 2024).
- [75] https://francuskie.pl/geely-i-renault-wprowadzaja-na-rynek-nowego-suv-a-to-historyczny-moment-dla-grupy-renault/#google_vignette (accessed on Apr 10, 2025).
- [76] https://francuskie.pl/stellantis-i-renault-inwestuja-w-maroku-tu-powstaja-dacia-sandero-i-citroen-ami/#google_vignette (accessed on Nov 11, 2024).
- [77] <https://www.cadillacforums.com/threads/1981-v8-6-4-project.622298/> (accessed on Dec 1, 2024).
- [78] <https://automobility.io/2025/03/state-of-chinas-auto-market-march-2025/> (accessed on Mar 18, 2025).
- [79] <https://global.chinadaily.com.cn/a/202305/09/WS6459eb45a310b6054fad1ee0.html> (accessed on May 09, 2025).
- [80] <https://fullbax.pl/import-agregatow-pradotworczych-z-chino-czym-warto-wiedziec/> (accessed on Dec 22, 2022)..
- [81] <https://www.construction-physics.com/p/how-china-became-the-worlds-biggest> (accessed on July 18, 2025).
- [82] <https://www.imo.org/en/mediacentre/pressbriefings/pages/imo-approves-netzero-regulations.aspx> (accessed on Apr 11, 2025).

- [83] <https://ourworldindata.org/grapher/annual-reported-passenger-kilometers?country=~IND> (accessed on Aug 01, 2025).
- [84] <https://www.spinny.com/blog/bharat-stage-emission-norms-bs-i-bs-ii-bs-iii-bs-iv-bs-vi-explained/> (accessed on Jul 18, 2025).
- [85] <https://www.suzuki.be/nl/blog/suzuki-boosterjet-en-dualjet-wat-het-en-wat-zijn-de-voordelen> (accessed on Jul 21, 2025).
- [86] <https://pl.renovablesverdes.com/Brazylia-i-Europa- nap%C4%99dzaj%C4%85-transformacj%C4%99-w- kierunku-biopaliw%3A-strategie--post%C4%99p-i-wyzwania/> (accessed on Jun 27, 2025).
- [87] <https://www.trade.gov.pl/wiedza/brazylia-bariery-wejscia/> (accessed on Oct 26, 2023).
- [88] <https://tradingeconomics.com/country-list/unemployment-rate?continent=africa> (accessed on Aug 01, 2025).
- [89] <https://www.diversityspares.com/best-engines-for-africa/> (accessed on Nov 19, 2025).
- [90] <https://pl.freepik.com/darmowe-zdjecie-wektory/mapa-%C5%9Bwiata-druku> (accessed on Sep 23, 2025).

Prof. Zbigniew J. Sroka, DSc., DEng. – Faculty of Mechanical Engineering, Wrocław University of Science and Technology, Poland.
e-mail: zbigniew.sroka@pwr.edu.pl



Greenhouse gas assessment of urban buses based on environmental product declarations – a review

ARTICLE INFO

Received: 14 June 2025
Revised: 30 September 2025
Accepted: 6 October 2025
Available online: 31 October 2025

The paper presents a review study about comparative life cycle assessment (LCA) of selected 12-meter urban buses powered by hybrid, battery-electric, and hydrogen fuel cell systems. The review is based on Environmental Product Declarations (EPDs) and follows ISO 14040/44 standards, using a cradle-to-grave approach and a functional unit of 1 passenger-kilometer. Environmental impacts are assessed across raw material extraction, production, operation, maintenance, and end-of-life stages. Results of the review show that the operation phase has the highest share of total greenhouse gas emissions, particularly when fossil-based energy is used. For electric and hydrogen buses, upstream processes also contribute significantly due to material and component complexity. The findings highlight the role of energy mix and vehicle structure in determining the total impact, stressing the importance of full life cycle assessment in evaluating sustainable transport solutions. EPD can be the first step for developing a Digital Product Passport (DPP) for the buses.

Key words: *life cycle assessment, public transport, environmental product declaration, alternative fuels*

This is an open access article under the CC BY license (<http://creativecommons.org/licenses/by/4.0/>)

1. Introduction

In recent years, environmental considerations have gained increasing importance in the public transport sector, particularly in bus transport. Faced with growing pressure to reduce greenhouse gas emissions and improve energy efficiency, local authorities and transport operators are seeking low-emission and zero-emission solutions. This shift is particularly relevant in light of the fact that road transport causes about 25% of EU greenhouse gas emissions, the second-largest source after energy. [14]. In response, a key direction in the decarbonization of urban mobility is the implementation of alternative fuels such as electricity, hydrogen, biofuels, and synthetic fuels, whose environmental impacts can vary significantly depending on the technology used and the energy source.

To reliably assess the environmental performance of buses used in public transport, it is essential to apply the Life Cycle Assessment (LCA) methodology, which enables a comprehensive evaluation of environmental impacts across all stages of a vehicle's life. This approach covers the production phase – including the extraction and processing of construction materials – as well as the operational phase, maintenance activities, and the final dismantling and disposal of the vehicle at the end of its service life. Considering all phases gives a clearer view of a transport solution's environmental burden.

LCA makes it possible to assess not only emissions generated during daily operation but also hidden environmental burdens such as natural resource consumption, emissions from component manufacturing, and the impact of maintenance processes. In the case of buses powered by alternative fuels, this method allows for the consideration of specific drivetrain technologies, energy storage systems, and technical maintenance requirements, which can significantly influence the overall environmental profile. As a result, it becomes feasible to identify the life cycle stages that contribute most significantly to the total environmental

impact and to develop strategies for effectively reducing the overall environmental footprint of bus fleets, including through material selection, energy efficiency improvements, or the implementation of circular economy principles.

The LCA method currently represents the most comprehensive tool for environmental analysis, enabling the assessment of not only greenhouse gas emissions but also a wide range of other impact categories such as resource depletion, acidification, eutrophication, and toxicity [15, 16]. Despite its complexity, the method identifies key life cycle stages and guides stakeholders in reducing impacts.

Recent years have seen a growing number of LCA studies on diesel, hybrid, battery-electric (BEB) and fuel cell buses (FCEB). These analyses confirm that the environmental performance of public transport technologies depends mainly on the electricity mix, hydrogen production pathways, vehicle lifetime, and battery size. For example, studies on Polish and Spanish bus fleets show that while BEBs significantly reduce GHG emissions, their benefits strongly depend on energy intensity per kilometer and power sector decarbonization [9, 22]. Hybrid buses can provide meaningful interim GHG reductions (~40% lower life-cycle CO₂) with negligible cost increases [9]. At the same time, research from Bangkok demonstrates that BEB and CNG buses reduce human health and ecosystem damage by up to 55% and also incur lower life-cycle costs [8]. In turn, hydrogen-based LCA studies stress that only “green” hydrogen enables substantial GHG reductions (> 70%). In contrast, conventional hydrogen offers limited advantages [11]. Comparative modelling further indicates that both BEB and FCEB can deliver significant climate benefits if powered by low-carbon energy [13].

In this context, the importance of Environmental Product Declarations (EPD) becomes evident. They support the ESG agenda by ensuring: Environmental transparency of carbon and resource indicators; Social benefits through

reduced air pollution; and Governance compliance with EU taxonomy and sustainable procurement. Embedding LCA insights into ESG frameworks allows municipalities and operators to demonstrate that bus technology choices contribute not only to decarbonization but also to broader sustainability governance in public transport.

The objective of this review study is to evaluate and compare the environmental performance of 12-meter urban buses powered by hybrid, battery-electric, and hydrogen fuel cell systems, using the Life Cycle Assessment (LCA) methodology applied in verified Environmental Product Declarations (EPDs). By adopting a boundary system and a functional unit, the analysis aims to identify the key life cycle stages contributing to total environmental impacts, with particular focus on greenhouse gas emissions, as well as to highlight the role of energy mix, vehicle design, and material composition in shaping overall results. The study also seeks to demonstrate the usefulness of EPD-based LCA as a transparent and standardized tool for supporting climate policy objectives, guiding sustainable fleet planning, and serving as a basis for future Digital Product Passports (DPPs) in the bus sector.

2. The role and relevance of environmental declarations in public transport

Type III Environmental Product Declarations (EPDs) are a key instrument for assessing the environmental performance of public transport vehicles [14]. They deliver standardized, independently verified data from Life Cycle Assessment (LCA) in line with ISO 14040/44, enabling fair comparison across technologies. The main recipients are policymakers, transport operators, manufacturers, and procurement authorities, who use EPDs to integrate environmental criteria into fleet planning, procurement, and climate strategies. Covering all stages of the life cycle – from raw material extraction to production, use, and end-of-life treatment, EPDs provide a transparent basis for sustainable decision-making. In practice, they support evidence-based policy, guide investments in low-emission fleets, and strengthen market competitiveness through verified environmental performance. They are also increasingly applied in public tenders, benchmarking of vehicle technologies, monitoring compliance with environmental standards, and as a foundation for future Digital Product Passports (DPPs). Furthermore, EPD-based assessments contribute to research and innovation by identifying environmental hotspots, thereby supporting the development of more resource-efficient and circular design solutions.

Environmental Product Declarations are voluntary manufacturer documents that require third-party verification to comply with ISO 14025 [14]. Thanks to their standardized format and credibility, they are widely applied in B2B contexts to assess the environmental impact of components and raw materials in final products. In the public transport sector – particularly in bus transportation – Environmental Product Declarations (EPDs) are still relatively uncommon. To date, only a limited number of vehicle manufacturers have chosen to develop such declarations as evidence of the reduced environmental impact of their products throughout the entire life cycle. Limited uptake results from the voluntary nature of EPDs and the effort needed for full LCA with

third-party review. Nevertheless, the growing emphasis on sustainability, coupled with increasing regulatory and public pressure for transparency in environmental performance, may encourage broader adoption of EPDs in the near future.

For public buses, an EPD includes an LCA covering all life cycle stages. As illustrated in Figure 1, the assessment begins with the extraction and transportation of raw materials, followed by the manufacturing of components and vehicle assembly. The completed vehicle is then delivered to the customer during the transportation stage, which, while less impactful, is included for completeness. The operation and maintenance stage typically represents the largest share of total emissions, particularly in conventionally fuelled buses, accounting for fuel or energy consumption and servicing over the vehicle's lifetime. Finally, the disposal stage covers end-of-life processes such as dismantling, material recycling, and waste treatment.

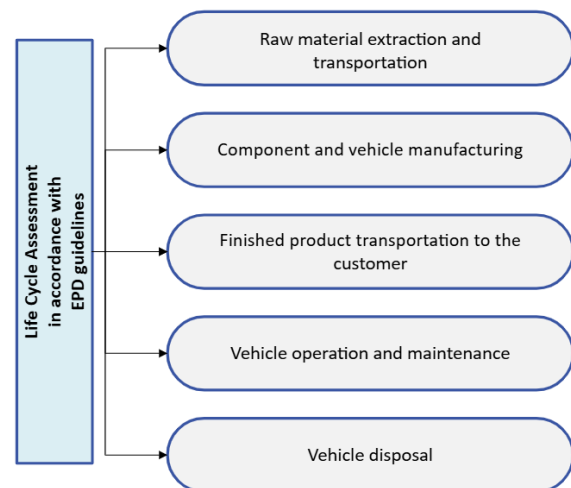


Fig. 1. Stages included in the LCA of transport vehicles in accordance with EPD guidelines



Fig. 2. Selected public transport vehicles for which EPDs have been developed

Based on data provided by the global environmental declaration program, Fig. 2 illustrates examples of Type III EPDs developed for public road transport vehicles [5]. All

listed models are 12-meter city buses designed for urban operation. The group includes vehicles equipped with a range of low-emission technologies: hybrid systems (Mercedes-Benz Citaro Hybrid, Solaris Urbino 12 Hybrid, MAN Lion's City EfficientHybrid), battery-electric drivetrains (Volvo 7900 Electric, Ebusco 3.0), as well as hydrogen fuel cell propulsion (H2.City Gold).

The development EPDs is carried out in accordance with the guidelines defined in the Product Category Rules (PCR), which provide a standardized framework for conducting LCA and presenting the resulting environmental data for a specific group of products. PCR documents ensure consistency, comparability, and transparency across EPDs by specifying in detail the methodological approach, system boundaries, data quality requirements, and reporting formats appropriate for the given product category [12].

In the case of public transport vehicles – such as single-decker and double-decker buses, as well as articulated and standard models that fall under vehicle categories M1, M2, and M3 – the applicable PCRs are developed with reference to specific regulatory foundations. In particular, they are aligned with the provisions of Regulation (EU) 2018/858 of the European Parliament and of the Council. This regulation establishes uniform technical and administrative requirements for the approval and market access of motor vehicles designed for the transport of passengers and their luggage, thereby forming the legal and technical basis for defining the life cycle boundaries, product reference flows, and functional characteristics relevant to the assessment [7]. As a result, the environmental performance evaluation of such vehicles within EPDs is not only harmonized with EU regulatory frameworks but also tailored to the operational context and functional roles of vehicles in public transport systems.

Figure 3 presents the scope of LCA-based environmental assessments for public transport vehicles. The PCR documents define, among other things, system boundaries and required impact categories, enabling comparability of declarations across different manufacturers and technologies.

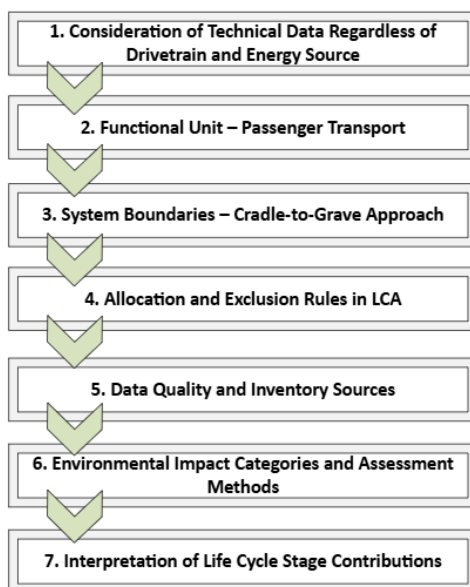


Fig. 3. PCR content for the environmental assessment of the life cycle of public transport

The process begins with the integration of full technical data regardless of the drivetrain type or energy source. This allows for the consistent assessment of all vehicle technologies – whether diesel, hybrid, electric, gas-powered, or hydrogen fuel cell – based on standardized parameters such as vehicle mass, dimensions, engine power, and passenger capacity.

The environmental performance is evaluated per a defined functional unit, typically one passenger-kilometer (1 pkm), which ensures comparability between different transport modes and operational profiles. The system boundaries are based on the cradle-to-grave model and are divided into three main life cycle phases:

- a) Upstream: extraction and processing of raw materials, manufacturing of components and subsystems, and logistics associated with the delivery of materials to the production site
- b) Core: vehicle production and final assembly within the manufacturer's facilities, including the integration of powertrain, bodywork, and systems. This stage also includes the transport of the finished product to the customer
- c) Downstream: operational use of the vehicle, covering fuel or energy consumption, maintenance and repair processes, and end-of-life scenarios such as dismantling, material recovery, recycling, and waste disposal.

Each EPD must follow clear allocation and exclusion rules as set by the applicable Product Category Rules (PCR), ensuring that only relevant environmental impacts are considered and minor contributions (typically < 1%) can be justifiably excluded. The quality and reliability of data sources are critical, with a preference for empirical data from the manufacturer or reputable life cycle inventory (LCI) databases such as Ecoinvent or GaBi.

The assessment includes multiple impact categories – such as greenhouse gas emissions (GHG), acidification potential (AP), eutrophication potential (EP), abiotic depletion potential (ADP), photochemical ozone creation potential (POCP), and water scarcity potential (WSP) – in accordance with standardized impact assessment methods. Finally, interpretation of the results should identify the relative contribution of each life cycle phase, enabling stakeholders to pinpoint environmental hotspots and implement targeted strategies for reducing the overall footprint of public transport systems.

3. Life cycle-based environmental assessment of 12-meter urban buses using EPD declarations

This chapter presents a comparison of six selected models of 12-meter urban buses, based on data obtained from their respective Environmental Product Declarations (EPDs). The analysis deliberately relies on EPDs, as they are prepared according to ISO 14025 and EN 15804 standards and provide third-party verified life-cycle data. The purpose of this approach is not to establish a new methodological framework, but to demonstrate how standardized and transparent information can be used to compare environmental performance across bus technologies. This perspective highlights the practical value of EPDs in supporting sustainable public procurement and ESG reporting, while ensuring data consistency and credibility. It should be

noted that currently, only selected manufacturers choose to develop and publish EPDs for their vehicles, despite the fact that such documents offer one of the most transparent and reliable sources of environmental information. For example, in the case of hydrogen-powered buses based on fuel cells, only one EPD was available, which limits the possibility of fully evaluating this technology. The highest number of declarations was found for battery-electric and hybrid vehicles, reflecting growing interest in these technologies in the context of sustainable public transport and the need to meet climate policy targets. A detailed comparison of the selected vehicles, including passenger capacity, lifetime mileage, material composition, and recycling indicators, is provided in Table 1.

All analyzed declarations are based on a full life cycle approach (cradle-to-grave), covering raw material extraction, component and vehicle manufacturing, distribution, use, maintenance, and end-of-life treatment.

Data were extracted directly from the interpretation sections of the declarations, compiled into comparative tables, and examined to identify both the total carbon footprint and the relative contribution of individual life cycle stages. Differences in methodological assumptions between EPDs (e.g., databases, electricity mixes, system boundaries) were documented and discussed as part of the interpretation. To ensure comparability across different propulsion technologies, only verified EPDs developed in line with ISO 14040/44 and ISO 14025 standards were included. These documents were selected as the primary data source because they provide standardized, independently verified LCA results prepared by manufacturers and reviewed by third parties.

Most vehicles have a reference life of 800,000 km, as set by Directive 2009/33/EC [6]. This value is considered representative for the typical operation of a city bus over 10–12 years. Deviations from this standard, such as in the case of the MAN Lion's City 12 C EfficientHybrid

(1 300 000 km) or the Mercedes-Benz Citaro Hybrid (600,000 km), reflect manufacturer-specific assumptions based on durability expectations and intended operational conditions.

Passenger capacities range from 88 to 110 persons, with the highest values recorded for battery-electric vehicles – likely due to the use of lighter structural materials. A higher number of passengers contributes to a lower environmental impact per pkm, which is a notable advantage in terms of life cycle performance.

An analysis of material composition reveals clear differences between technologies. Hybrid vehicles are characterized by the highest share of metals – up to 74% of total mass – which supports high material recoverability. In contrast, zero-emission vehicles (BEVs and FCEVs) contain a significantly higher proportion of complex components, particularly electrical systems, batteries, and electronic equipment. In the case of the Ebusco 3.0, these components account for up to 30% of the vehicle's total mass. While beneficial from an operational perspective (no tail-pipe emissions), this profile presents challenges at the end-of-life stage, particularly in relation to battery and composite material recycling.

The highest recyclability rates were recorded for hybrid buses: MAN – 96.4%, Solaris – 95.9%, Mercedes – 94.0%, which corresponds to their relatively simple and predictable material structures. Electric buses achieved slightly lower values: Volvo – 90.0%, Ebusco – 84.5%, mainly due to the use of composite and chemically complex battery materials. The hydrogen bus (H2.City Gold) scored 89.2%. However, full evaluation is hindered by the lack of data on overall recoverability, likely due to the absence of standardized end-of-life procedures for hydrogen storage tanks and fuel cell systems. The overall recoverability rate (including both material and energy recovery) reached the highest levels in hybrid buses – up to 99.0% – indicating strong potential for circular material flows. The lowest recovery rate was obser-

Table 1. Overview of selected 12-meter urban bus models based on Environmental Product Declarations (EPDs), including technical parameters and material recovery indicators

N°	Brand of bus	Propulsion type	Functional unit	System boundary	Passenger capacity	Travelled distance	Material composition	Recyclability rate	Recoverability rate
1	Mercedes-Benz Citaro Hybrid [3]	HEV	1 pkm	Cradle-to-Grave	101	600 000 km	72.9% metals; 9.3% polymers; 4.8% glass; 13% others	94.0%	99.0%
2	Solaris Urbino 12 hybrid [21]	HEV			102	800 000 km	66.0% metals; 12.0% electric and electronic equipment; 9.0% polymers; 13.0% others	95.9%	96.1%
3	MAN Lion's City 12 C EfficientHybrid [17]	HEV			97	1 300 000 km	74.1% metals; 10.7% polymers; 19.6% glass; 13.7% others	96.4%	98.2%
4	H2.City Gold [2]	FCEV			91	800 000 km	55.7% metals; 19.6% electric and electronic equipment; 11.0% polymers; 13.7% others	89.2%	–
5	Ebusco 3.0 [4]	BEV			110	800 000 km	46.0% metals; 30.0% battery and electric; 10.0% polymers; 14.0% others	84.5%	89.5%
6	Volvo 7900 Electric [23]	BEV			88	800 000 km	76.9% metals; 8.9% polymers; 4.8% glass; 9.4% others	90.0%	98.0%

Table 2. Total greenhouse gas emissions (GHG) and dominant life cycle phase contributions for six 12-meter urban buses according to EPD data

Nº	Type of bus	Total GHG emission [kg CO ₂ eq.]	Analysis Results	GHG emission Determinants
1	Mercedes-Benz Citaro Hybrid [3]	0.0111	The operation phase dominates GHG emissions with 91.0%, indicating that fuel combustion during use is the primary contributor. Raw material supply contributes 6.9%, with notable influence on abiotic depletion of metals (88.3%) and water deprivation (39.1%). Maintenance has a minor GHG impact (1.4%) but contributes significantly to water deprivation (38.0%).	Operation 91.0%; Raw material acquisition 6.9%
2	Solaris Urbino 12 hybrid [21]	0.011	The highest environmental impact occurs during bus operation – responsible for 89.5% of greenhouse gas emissions, 53.2% of photochemical smog, 61.8% of water pollution (eutrophication), and nearly 90.0% of fossil fuel use. In contrast, raw material extraction and manufacturing have the greatest share in mineral depletion (91.1%) and water use (74.2%). Transport and end-of-life phases have minimal impact – below 1%.	Operation 89.5%; Raw material acquisition 5.9%
3	MAN Lion's City 12 C EfficientHybrid [17]	0.0138	Reducing lifetime mileage from 1.3 million to 800,000 km lowers total GHG emissions per vehicle by 36.9% (from 1736 to 1092 kg CO ₂ -eq). However, emissions per passenger-km increase slightly (from 13.77 to 14.07 g CO ₂ -eq/pkm). The use phase still dominates with 94% of total impact in the 800,000 km case.	Operation approx. 90.0%
4	H2.City Gold [2]	0.0116	Total GHG emissions per passenger-km are 0.0116 kg CO ₂ -eq. The downstream phase dominates (82.17%), with operation alone responsible for 78.3%. Upstream contributes 16.7%, core processes 1.1%, maintenance 3.2%, and end-of-life 0.7%.	Operation 78.3%; Raw material acquisition 16.7%
5	Ebusco 3.0 [4]	0.00454	Total life cycle emissions: 399.916 kg CO ₂ -eq. Use phase dominates across all impact categories (e.g. 68.0% GHG emissions, 62.0% smog, 66.0% fossil resource use). Raw material extraction is the main contributor to water deprivation (30.0%) and mineral depletion (83.0%). Downstream processes account for 74.0% of total emissions.	Operation 68.0%; Raw material acquisition 23.0%
6	Volvo 7900 Electric [23]	0.00853	Most of the fossil climate impact comes from the operation phase due to electricity use (EU residual mix). Changing the grid mix greatly affects results: switching to Swedish grid lowers impact by ~69%, while hard coal mix nearly doubles emissions. Upstream also contributes, but less than operation.	Operation approx. 80%

ved for the Ebusco 3.0 (89.5%), which confirms the challenges related to the recovery of next-generation vehicle designs. These differences are particularly relevant in assessing compliance with circular economy principles – the higher the recovery rate, the lower the final environmental burden associated with vehicle disposal

These data were extracted directly from the interpretation sections of each Environmental Product Declaration (EPD) and provide deeper insight into the distribution of greenhouse gas (GHG) emissions across the value chain. Each analysis was conducted using the regional electricity mix applicable in Europe (typically the European residual mix), as defined in the respective EPDs, which ensures consistency in the assessment of the operation phase impact. Nevertheless, the study is subject to several methodological limitations. Since the data originate from EPDs prepared by different manufacturers, variations in databases, calculation tools, and methodological assumptions are inevitable. In particular, detailed information on energy use in battery production outside the EU is missing, as is data on non-CO₂ emissions, both of which may influence the overall environmental profile of vehicles. Furthermore, system boundaries are defined differently across individual declarations, limiting the comparability of results. The findings should therefore be considered approximate and interpreted with these constraints in mind.

Among the analysed models, Ebusco 3.0 shows the lowest total GHG emission at 0.00454 kg CO₂-eq/pkm, followed by Volvo 7900 Electric (0.00853 kg CO₂-eq/pkm) and Mercedes-Benz Citaro Hybrid (0.0111 kg CO₂-eq/pkm). The highest GHG emission is observed for the MAN

Lion's City 12 C EfficientHybrid, with 0.0138 kg CO₂-eq/pkm, primarily due to the originally declared high lifetime mileage of 1.3 million km being adjusted to the standard 800,000 km used for comparability across models. This adjustment leads to a relatively higher impact per kilometer travelled.

In all cases, the operation phase is identified as the dominant contributor to total GHG emission, ranging from approximately 68% (Ebusco 3.0) to over 91% (Citaro Hybrid and MAN Lion's City). This phase includes the energy consumed during regular vehicle use and is highly dependent on the type and carbon intensity of the energy carrier used. In battery buses, the grid mix is key – for Volvo 7900 Electric, high emissions result from a fossil-heavy EU residual mix. Similarly, the Solaris Urbino 12 Hybrid and H2.City Gold confirms the dominant role of the operation phase, responsible for approximately 89.5% and 82.2%, respectively, of total GHG emissions per pkm.

The upstream phase, covering raw material acquisition, component production, and supply chain emissions, shows varying degrees of importance depending on drivetrain technology and material composition. In Ebusco 3.0, for instance, upstream emissions account for over 23% of the GHG emission, reflecting the embedded carbon intensity of advanced materials such as composite structures and high-capacity lithium-ion batteries, for the hydrogen-powered H2.City Gold, upstream contributions reach 16.7%, largely due to the production of fuel cell components and associated electronic systems. In contrast, hybrid vehicles generally show lower upstream shares (typically below 7%), which can be attributed to their more conventional material structure.

The core phase (vehicle assembly) and downstream processes (maintenance and end-of-life treatment) typically contribute the least to overall GHG emission. These stages generally account for less than 5% of total emissions, although in some electric bus models, battery replacements and associated maintenance activities may slightly increase the downstream share.

These findings reinforce the critical role of the use phase in determining the overall climate impact of public buses and underline the importance of energy source selection and grid decarbonization in reducing operational emissions. Electrified buses demonstrate considerable potential for GHG emission reduction. However, this potential can only be fully realized when combined with low-carbon electricity sources. Furthermore, the upstream burden of alternative drivetrains must be carefully considered, especially in battery-electric and fuel cell-electric vehicles, where material intensity, component complexity, and supply chain impacts contribute significantly to life cycle emissions.

4. Summary

This study presents a comprehensive review and environmental assessment of six models of urban buses equipped with alternative propulsion systems, based on data disclosed in verified Type III Environmental Product Declarations (EPDs) and interpreted in accordance with the Life Cycle Assessment (LCA) methodology. The analysis focuses on the comparative evaluation of manufacturer-declared environmental data, allowing for the identification of trends and dependencies relevant to the sustainable development of public transport systems. Such an approach enables an objective and standardized comparison of environmental performance across technologies, which is essential for informed policy-making and strategic fleet planning in the transition to low-carbon urban mobility.

It should be emphasized that the results presented in this study are based on secondary data reported in Environmental Product Declarations (EPDs) prepared by different manufacturers and analysts. As a consequence, they may vary in terms of methodological assumptions, databases applied, and calculation tools used, which inevitably affects the comparability of results. This is particularly evident in the case of electricity mixes. According to the Product Category Rules (PCR), the use of the European residual mix is recommended; however, individual EPDs adopt different approaches – for example, plant-specific data for Mercedes, Solaris, and MAN buses, the Portuguese mix applied to the production of H2.City Gold, or the Spanish mix considered for the air-conditioning operation of the same model. Such discrepancies may significantly influence the final results, especially with regard to greenhouse gas (GHG) emissions. Therefore, the outcomes should be interpreted with these limitations in mind and treated as an approximation of the actual.

Additionally, the review results should be interpreted with caution, as they rely on secondary data from EPDs prepared by different manufacturers and analysts. Variations in methodological assumptions, databases, and electricity mixes introduce uncertainties that may influence the final outcomes, meaning the findings represent indicative rather than strictly comparable values of the environmental impacts of the analyzed technologies.

The analysis revealed significant variations in environmental performance between the different drivetrain technologies. Battery-electric buses, despite higher environmental burdens during the production phase—mainly due to the use of lithium-ion batteries and advanced electronic systems – achieved the lowest GHG emission values across the entire life cycle. These results confirm the advantages of zero-emission vehicles in long-term environmental terms, especially when operational emissions are considered. Hybrid vehicles, which exhibited relatively higher emissions during the use phase due to partial reliance on combustion engines, demonstrated the highest potential for material recovery and recyclability, reaching up to 99%. This highlights their relative strength from a circular economy perspective, particularly in the context of end-of-life strategies. The hydrogen-powered bus occupied an intermediate position in terms of both life cycle emissions and end-of-life recovery potential, combining selected benefits of both technological approaches. Importantly, for all analyzed cases, the operational phase was identified as the dominant contributor to total GHG emission – accounting for 68–91% – which underscores the critical environmental significance of the use stage and the necessity of improving energy efficiency and reducing indirect emissions.

For zero-emission buses, the electricity mix is the decisive factor. The carbon intensity of electricity used to charge batteries or produce hydrogen (e.g., via electrolysis) directly affects environmental efficiency during the operational phase. It may significantly alter the comparative advantage of each technology depending on regional grid characteristics. In the EPDs reviewed in this study, an average European electricity mix was assumed, providing a representative and harmonized basis for comparison. Nevertheless, to fully realize the decarbonization potential of these technologies, transport fleets must be powered by electricity from low-emission sources – particularly renewables and nuclear energy. In this regard, the broader transformation of the energy system constitutes an essential element of any effective strategy aimed at reducing the environmental impact of modern public transport technologies. Without a parallel transition in energy generation, even the most advanced vehicle technologies cannot achieve their intended climate benefits.

The conclusions of this review are consistent with previous research. Nordelöf et al. (2019) compared the life cycle environmental performance of city buses powered by electricity, hydrogenated vegetable oil (HVO), and diesel, confirming the overall superiority of electric drivetrains in terms of total GHG emissions and underlining the pivotal role of the energy mix in shaping environmental outcomes [18]. These observations are further complemented by Regulski [19], who demonstrated that the optimal operational lifetime of city buses is typically in the range of 10–14 years, largely influenced by material durability and economic performance, which provides an important context for interpreting environmental outcomes. Similarly, recent life cycle analyses of alternative fuel buses [20] emphasize that material composition and energy pathways critically determine both environmental and economic efficiency. Taken together, these converging insights reinforce the

validity of current EPD-based declarations and highlight their usefulness as a transparent tool for supporting sustainability-oriented decisions in urban transport planning.

In summary, the effective decarbonization of urban public transport requires a systemic, multidimensional approach that goes beyond the mere substitution of propulsion technologies. Parallel efforts must address energy supply decar-

bonization, ecodesign principles with end-of-life considerations, optimization of vehicle lifetime performance, and the implementation of transparent, standardized environmental reporting tools such as EPDs. Reducing urban transport's carbon footprint depends on a comprehensive strategy combining vehicles, energy systems, and operations.

Bibliography

- [1] Burchart-Korol D, Jursova S, Folega P, Korol J, Pustejovska P, Blaut A. Environmental life cycle assessment of electric vehicles in Poland and the Czech Republic. *J Clean Prod.* 2018;202:476-487. <https://doi.org/10.1016/j.jclepro.2018.08.145>
- [2] CaetanoBus. Environmental Product Declaration: Bus H2.City Gold. Stockholm: EPD International AB; 2024 Jun 27. Report No.: EPD-IES-0015193. <https://www.environdec.com/>
- [3] Daimler Buses GmbH. Environmental Product Declaration: Mercedes-Benz Citaro hybrid bus. Stockholm: EPD International AB; 2025 May 20. Report No.: EPD-IES-0022581. <https://www.environdec.com/>
- [4] Ebusco BV. Environmental Product Declaration: Ebusco 3.0 12-meter. Stockholm: EPD International AB; 2024 Jul 8. Report No.: EPD-IES-0012607. <https://www.environdec.com/>
- [5] EPD International. <https://www.environdec.com> (accessed on 2025 May 12).
- [6] European Parliament, Council of the European Union. Directive 2009/33/EC of the European Parliament and of the Council of 23 April 2009 on the promotion of clean and energy-efficient road transport vehicles. *Off J Eur Union.* 2009. <https://eur-lex.europa.eu/legal-content/EN/TXT/?uri=CELEX:32009L0033>
- [7] European Parliament, Council of the European Union. Regulation (EU) 2018/858 of 30 May 2018 on the approval and market surveillance of motor vehicles and their trailers, and of systems, components and separate technical units intended for such vehicles, amending Regulations (EC) No 715/2007 and (EC) No 595/2009 and repealing Directive 2007/46/EC. *Off J Eur Union.* 2018.
- [8] Gabriel NR, Martin KK, Haslam SJ, Faile JC, Kamens RM, Gheewala SH. A comparative life cycle assessment of electric, compressed natural gas, and diesel buses in Thailand. *J Clean Prod.* 2021;315:128013. <https://doi.org/10.1016/j.jclepro.2021.128013>
- [9] García A, Monsalve-Serrano J, Sari SL, Tripathi A. Life cycle CO₂ footprint reduction comparison of hybrid and electric buses for bus transit networks. *Appl Energy.* 2022;308:118354. <https://doi.org/10.1016/j.apenergy.2021.118354>
- [10] Gradin KT. Simplified life cycle assessment approaches and potential impact shifts. 2020. <http://hig.diva-portal.org/smash/record.jsf?pid=diva2:1506681> (accessed on 2025 May 12).
- [11] Iannuzzi L, Hilbert JA, Silva Lora EE. Life Cycle Assessment (LCA) for use on renewable sourced hydrogen fuel cell buses vs diesel engines buses in the city of Rosario, Argentina. *Int J Hydrogen Energy.* 2021;46(28):29694-29705. <https://doi.org/10.1016/j.ijhydene.2021.01.065>
- [12] IK Ingenieria, Irizar Group, BYD Company Limited, Volvo Bussar AB, Daimler Buses GmbH, Ebusco BV, CaetanoBus, MAN Truck & Bus SE, TEMSA, Yutong Bus Co Ltd, Solaris Bus & Coach. PCR 2016:04 – Public and private passenger buses and coaches. Version 2.0.3. Stockholm. The International EPD® System.
- [13] Lubecki A, Szczurowski J, Zarębska K. A comparative environmental Life Cycle Assessment study of hydrogen fuel, electricity and diesel fuel for public buses. *Appl Energy.* 2023;350:121766. <https://doi.org/10.1016/j.apenergy.2023.121766>
- [14] International Organization for Standardization. ISO 14025:2006 – Environmental labels and declarations – Type III environmental declarations – Principles and procedures. Geneva: ISO; 2006.
- [15] International Organization for Standardization. ISO 14040:2006 – Environmental management – Life cycle assessment – Principles and framework. Geneva: ISO; 2006.
- [16] International Organization for Standardization. ISO 14044:2006 – Environmental management – Life cycle assessment – Requirements and guidelines. Geneva: ISO; 2006
- [17] MAN Truck & Bus SE. Environmental Product Declaration: Lion's City 12 EfficientHybrid. Stockholm: EPD International AB; 2022 Dec 15. Report No.: S-P-07585. <https://www.environdec.com/>
- [18] Nordelöf A, Romare M, Tivander J. Life cycle assessment of city buses powered by electricity, hydrogenated vegetable oil or diesel. *Transp Res Part D Transp Environ.* 2019;75:211-222. <https://doi.org/10.1016/j.trd.2019.08.019>
- [19] Regulski P. Assessment of the life cycle of city buses with diesel and electric drive in the operation phase. *Combustion Engines.* 2023;193(2):117-1212. <https://doi.org/10.19206/CE-162108>
- [20] Regulski P. The material and economic assessment of the life cycle of city buses in the operational phase. *Combustion Engines.* 2023;192(1):50-54. <https://doi.org/10.19206/CE-151942>
- [21] Solaris Bus & Coach sp. z o.o. Environmental Product Declaration: Solaris Urbino 12 hybrid bus. Stockholm: EPD International AB; 2022 Mar 31. Report No.: S-P-05600. <https://www.environdec.com/>
- [22] Szczurowski J, Lubecki A, Bałys M, Brodawka E, Zarębska K. Life cycle assessment study on the public transport bus fleet electrification in the context of sustainable urban development strategy. *Sci Total Environ.* 2022;824:153872. <https://doi.org/10.1016/j.scitotenv.2022.153872>
- [23] Volvo Bussar AB. Environmental Product Declaration: Volvo 7900 Electric. Stockholm: EPD International AB; 2023 Nov 2. Report No.: S-P-11237. <https://www.environdec.com/>

Iga Przytuła, MEng. – Faculty of Transport and Aviation Engineering, Silesian University of Technology, Poland.

e-mail: iga.przytula@polsl.pl



Prof. Dorota Burchart, DSc., DEng. – Faculty of Transport and Aviation Engineering, Silesian University of Technology, Poland.

e-mail: dorota.burchat@polsl.pl



Comparative analysis of exhaust emissions from a compression-ignition engine fueled with mixtures of rapeseed oil with n-hexane and diesel fuel during selected phases of the WLTP test

ARTICLE INFO

Received: 20 June 2025

Revised: 6 October 2025

Accepted: 6 October 2025

Available online: 13 November 2025

The article presents the differences in emissions of a passenger car with a compression-ignition engine fueled by vegetable fuel – rapeseed oil with n-hexane and diesel fuel. Emission tests were carried out on a chassis dynamometer in selected phases of the World Harmonized Light Vehicle Test Procedure. Carbon monoxide, carbon dioxide, nitrogen oxides, total hydrocarbons and non-methane hydrocarbons were measured based on the WLTC Class 3b driving cycle. The effect of engine operating conditions on exhaust emissions when fueled with the fuels studied was described. A regression model was developed to estimate the level of pollutants in the exhaust gas.

Key words: *exhaust emission, WLTP, compression-ignition engine, vegetable fuel, regression model*

This is an open access article under the CC BY license (<http://creativecommons.org/licenses/by/4.0/>)

1. Introduction

In order to protect life and health, reducing the harmful effects of internal combustion engines on the environment is a priority. Reducing emissions can therefore be considered a fundamental in the context of internal combustion engine development. By developing new vehicles, internal combustion engine manufacturers must meet constantly tightening emission standards. For many years, legislative procedures have been based on the use of driving cycles. This tests both speed changes and a wide range of loads under varying operating conditions. Currently, the World-wide Harmonized Test Procedure for Light Vehicles is used, which was developed based on actual driving data to simulate the most common daily driving conditions [3, 13].

The real operating conditions of internal combustion engines are largely undefined. The essence of emission measurements, in addition to replicating real conditions, is therefore to ensure their high accuracy and repeatability. In order to eliminate factors that affect the discrepancies in the values of the results, the tests should be performed under repeatable conditions, which include the same test environment, the use of the same test method, the use of the same test equipment and instruments, and, in the case of mapping, the test cycle should also be performed by the same operator. The repeatability of the measurement results is also due to the repeatability of the operating states of the internal combustion engine. The operating states of the engine that characterize emissions are determined by the engine speed, engine load or its thermal state, and in the case where the test engine is installed in a vehicle, by the vehicle speed and motion resistance. Measurements under laboratory conditions carried out on a chassis dynamometer, ensuring the repeatability of the motion resistance, make vehicle speed the main variable determining engine operating states [1, 6, 7, 12, 13].

However, so many factors affecting the level of pollutant emissions call into question their repeatability. The cost of conducting tests is often higher than the cost of the measuring equipment and the electricity used during the tests, or the working gases used. This affects the number of measurements performed. Issues of repeatability of emission tests are described in works [2, 6, 11, 13].

In the face of costly scientific research, it is reasonable to use learning algorithms that allow the construction of predictive models that, based on available empirical data, can predict the results of future experiments with high probability. As a result, it becomes possible to reduce the number of actual studies to the most promising ones. It allows the identification of hidden relationships in complex data sets that could go unnoticed using traditional methods of analysis [5].

Research on exhaust emissions is also an extremely important aspect of the energy transition. A growing number of studies have focused on comparing emissions from alternative energy sources versus traditional internal combustion engines. This is related to the positive impact of using bio-fuels on the environment. The use of replacement fuels that do not require structural or regulatory changes to the engine requires the development of a fuel with physical properties similar to those of conventional fuel. Solutions based on esterification processes or additives to vegetable oils are well known. The use of plant-based fuels significantly reduces carbon dioxide emissions, also taking into account their absorption during the growth phase of raw materials. In compression ignition engines, a decrease in particulate matter emissions is observed. However, the use of substitute fuels can also lead to increased nitrogen oxide emissions, especially during periods of high load. It is therefore important to test fuels under real driving conditions, based on current test procedures [4, 8–10, 14–16].

This paper combines the above challenges, focusing on the evaluation of emission relationships when running on mixtures of rapeseed oil with n-hexane based on selected WLTP test phases and the development of a regression model.

2. Materials and methods

The test vehicle was a Fiat Qubo passenger car with a 1.3 Multijet four-cylinder diesel engine. The engine complied with the Euro 5 standard. Basic information about the test object is shown in Table 1.

Table 1. Parameters and technical data of the Fiat Qubo passenger car with a 1.3 Multijet engine

Parameter	Value
Engine displacement	1248 cm ³
Fuel type	Diesel
Compression ratio	16.8:1
Emission standard	Euro 5
Power	55 kW
Max. power rpm	4000 rpm
Max torque	190 Nm
Max. torque rpm	1750 rpm
Number of gears	5
1 st gear ratio	3.64:1
2 nd gear ratio	1.95:1
3 rd gear ratio	1.28:1
4 th gear ratio	0.98:1
5 th gear ratio	0.77:1
Final drive ratio	3.56:1
Tire size	185/65 R15

In the study, a mixture of rapeseed oil with a 20% addition of n-hexane (RONhex) was used. The added compound is a hydrocarbon produced during the distillation of crude oil. It is a component of the light gasoline fraction. Due to its physicochemical properties, it is used as a solvent in the chemical industry. Its addition affects the parameters of rapeseed oil, including surface tension, density, or viscosity, thus bringing its properties closer to those of conventional fuels. Its addition allows rapeseed oil to be used at ambient temperatures of sub-zero. The addition of n-hexane improves the atomization properties of the fuel in the combustion chamber, which promotes the combustion process and leads to higher engine efficiency. It also reduces the risk of damage to the injection system and other fuel system components, allowing rapeseed oil to be used without the need for engine modifications [4, 8–10]. Diesel fuel (DF) was used as the reference fuel. An auxiliary fuel tank was located in the vehicle, which allowed for a quick change of fuel mixtures and did not affect the amount of fuel in the main tank. The basic physicochemical properties of the fuels tested are presented in Table 2.

Table 2. Basic physicochemical properties of the tested fuels [9]

	Diesel Fuel	RONhex
Density at 20°C [kg/m ³]	840	879
Surface tension at 20°C [mN/m]	29.15	27.70
Kinematic viscosity index at 40°C [mm ² /s]	2.7	11.70
Flash point [°C]	72	< 40
LC cetane number [-]	51.2	75.6
Calorific value [MJ/kg]	43	9.4

The tests were conducted based on selected phases of the WLTP test. The condition of the vehicle and its preparation corresponded to the procedure recommendations. The tests were conducted on an unhomologized test stand, a diagram of which is shown in Fig. 1, which consisted of a Dynorace DF4FS-HLS two-axle chassis load dynamometer. To reproduce the driving cycle, a computer with implemented software was used, using the OBDII system to communicate with the vehicle's ECU. Using the system, the following were recorded:

- vehicle speed
- engine speed
- torque.

The test stand also included an AVL SESAM i60 FT measurement system, which recorded exhaust gas concentrations. The system's measuring probe was placed in front of the catalytic converter. During the tests, the concentration of the following substances was tested:

- concentration of carbon monoxide (CO) and carbon dioxide (CO₂)
- concentration of nitrogen oxides (NO_x divided into NO and NO₂)
- concentration of hydrocarbons (THC) and non-methane hydrocarbons (NMHC).

The stand was not built in a climate chamber, which made it impossible to control environmental conditions. Measurements were made under the following laboratory conditions:

- temperature (23.6–24.8°C)
- humidity (45–57.8%)
- atmospheric pressure (984.8–990.4 hPa).

Measurements were made based on the WLTC Class 3b driving cycle. Three runs were made for each of the fuels tested.

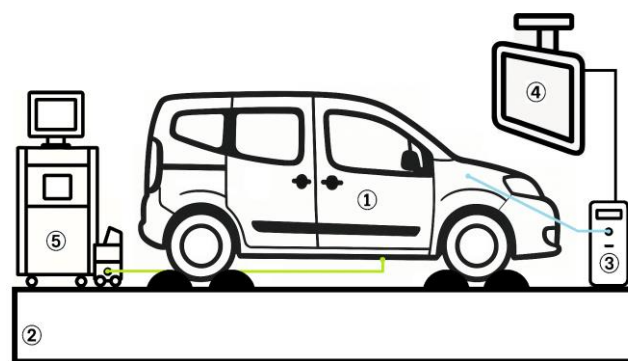


Fig. 1. Test stand (1 – Fiat Qubo passenger car, 2 – Dynorace DF4FS-HLS chassis dynamometer, 3 – PC with implemented WLTC test cycle, 4 – additional screen, 5 – AVL SEASAM i60 FT)

3. Results

The test travel speed results were linearly interpolated, and then a Savitzky-Golay filter was applied. The average travel speed (AV), standard deviation (SD) and coefficient of variation (CV) were calculated for each fuel. The results are shown in Table 3.

Table 3. Parameters of the driving cycles

Parameter	DF	RONhex
AV [km/h]	46.35	46.21
SD [km/h]	1.49	1.43
CV [%]	7.8	7.6

The results obtained (7.8% variability for DF and 7.6% variability for RONhex) indicate high repeatability of measurements. The average values of speed and torque for each fuel are shown in Fig. 2 and Fig. 3.

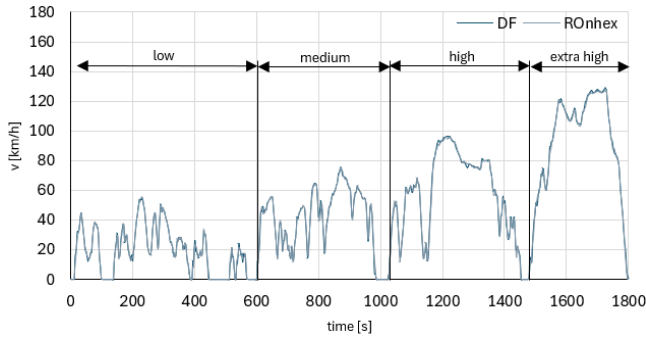


Fig. 2. Average speed during the WLTC driving cycle

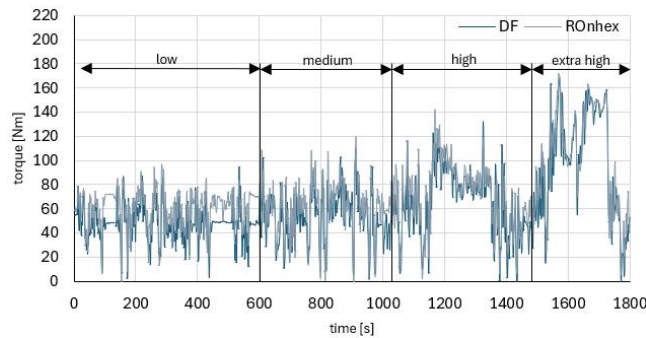


Fig. 3. Average torque during the WLTC driving cycle

In the analysis of the exhaust gas concentration results, a median filter was used to reduce impulse noise and a Savitzky-Golay filter to smooth the data. The results of the filtered and averaged measurements for each fuel type are shown in Fig. 4–17.

The highest CO concentrations were recorded for RONhex in the low phase (the average concentration reached 932.26 ppm and was 68.83% higher relative to DF in this phase) and for DF in the extra high phase (715.21 ppm and was 207.14% higher relative to RONhex). The high CO concentration in the early phases of the cycle for rapeseed oil with n-hexane addition is due to the lower temperature and incomplete combustion process, which, combined with the lower volatility of rapeseed oil, results in poorer fuel evaporation. On the other hand, the higher viscosity relative to diesel fuel negatively affects the fuel atomization process. This results in a less efficient combustion process. As the load and combustion temperature increase, this effect is offset, thanks in part to the oxygen content of the RONhex mixture, resulting in lower CO concentrations. In the case of DF, at higher loads, the fuel mixture becomes richer, and the lower oxygen content results in a higher CO concentration. The course of CO concentra-

tion over the WLTC cycle is shown in Fig. 4, while the average values over each cycle are shown in Fig. 5.

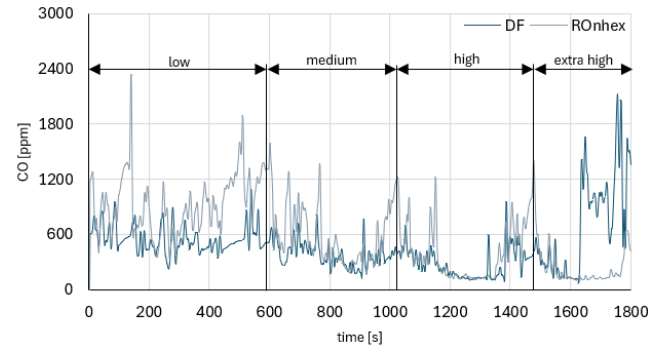


Fig. 4. CO concentration during the WLTC driving cycle

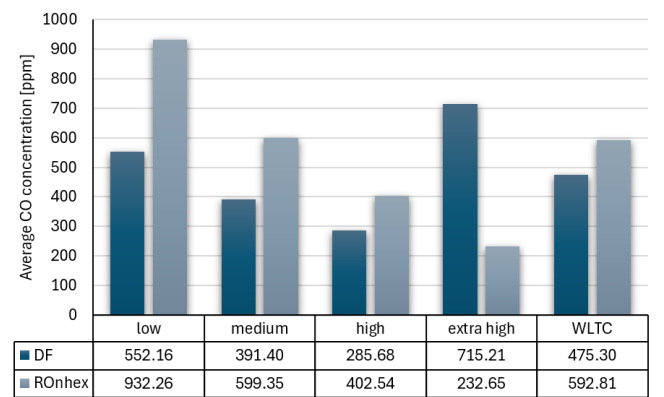


Fig. 5. Average CO concentration during each cycle

For both fuels tested, the highest CO₂ and NO_x concentrations were recorded in the phases characterized by the highest loads. The average CO₂ concentration in each phase was lower for RONhex (by 9.65% relative to DF throughout the cycle). The lower CO₂ concentration is mainly due to the difference in the chemical composition of the fuels tested. Diesel fuel contains more carbon per unit weight, which is associated with a higher heating value, as well as higher CO₂ emissions. In contrast, the increase in concentration with load is mainly due to the increased dose of fuel delivered. Figure 6 shows the course of CO₂ concentration over the WLTC cycle, and the average values for each cycle are shown in Fig. 7.

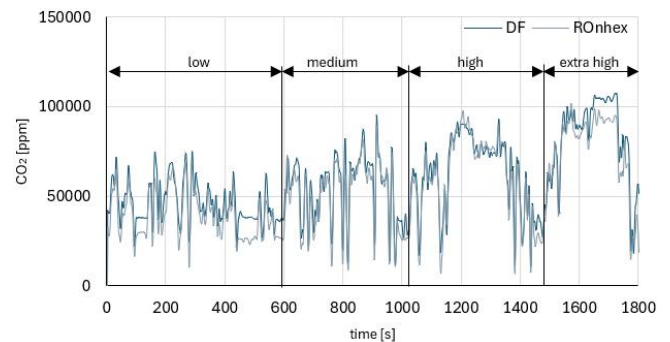


Fig. 6. CO₂ concentration during the WLTC driving cycle

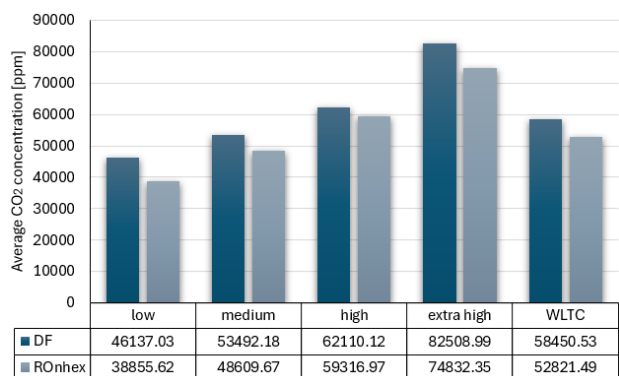


Fig. 7. Average CO₂ concentration during each cycle

The difference in average NO_x concentration throughout the cycle did not exceed 0.05%. At the same time, it was noted that in the low, medium and high phases it was lower for RONhex (by 15.9%, 8.13%, 0.77%, respectively) and in the extra high phase for DF (by 12.91%). This phenomenon is due to the difference in the chemical composition of the fuels - the presence of oxygen in rapeseed oil, and therefore the higher concentration of oxygen in the combustion process and the higher flame temperature. On the other hand, the increase in concentrations in subsequent phases is related to the increase in combustion temperature. Figures 8 and 9 show the course and average values of NO_x concentrations in each cycle.

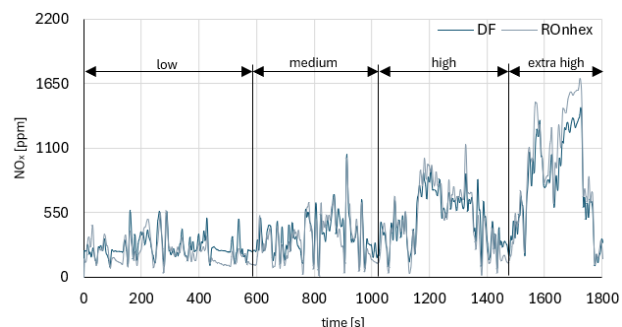


Fig. 8. NO_x concentration during the WLTC driving cycle

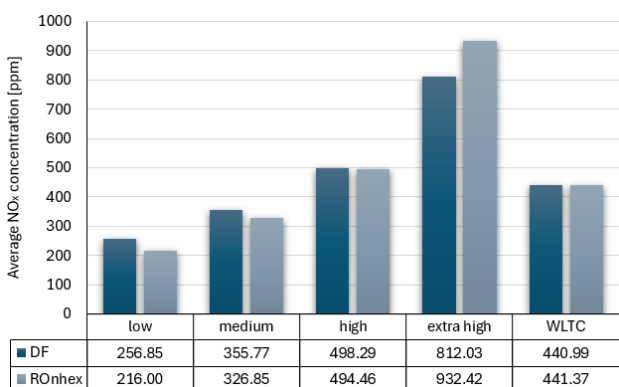


Fig. 9. Average NO_x concentration during each cycle

In the case of NO, the concentration throughout the cycle was 2.05% higher for DF than for RONhex. When considering the case of NO₂ concentration, the difference due to the presence of oxygen in the rapeseed oil, which pro-

motes the oxidation of NO to NO₂, again becomes apparent. Throughout the cycle, the NO₂ concentration was 16.26% higher for RONhex relative to DF. Figures 10 and 12 show the waveforms of NO and NO₂ concentrations during the WLTC cycle. The average values of NO and NO₂ concentrations in each cycle are shown in Fig. 11 and Fig. 13.

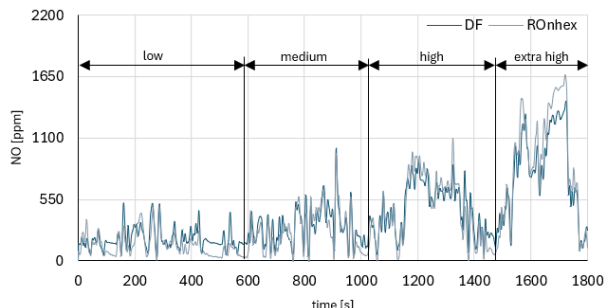


Fig. 10. NO concentration during the WLTC driving cycle

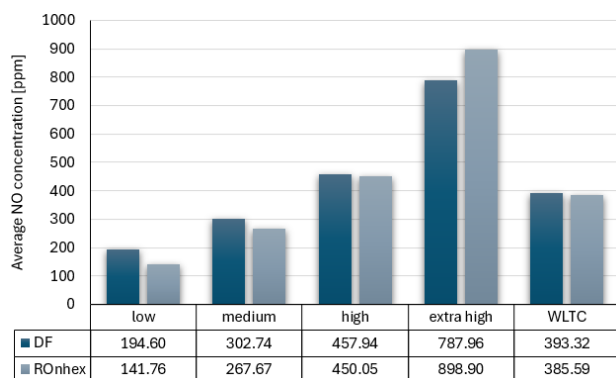


Fig. 11. Average NO concentration during each cycle

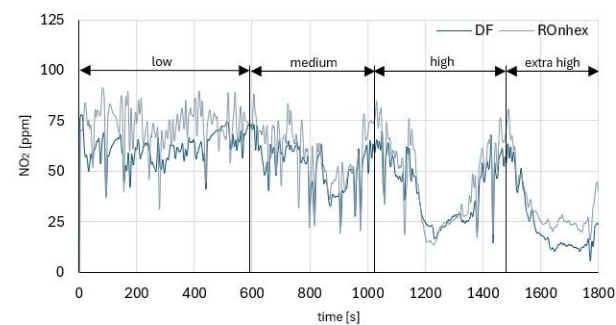


Fig. 12. NO₂ concentration during the WLTC driving cycle

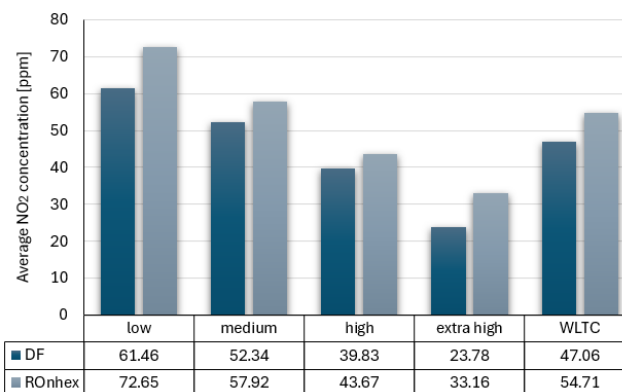


Fig. 13. Average NO₂ concentration during each cycle

For hydrocarbon exhaust concentrations, the highest concentrations were observed for RONhex in the low phase (the average concentration reached 109.76 ppm for THC and 242.77 ppm for NMHC), while for DF in the extra high phase (359.91 ppm for THC and 736.53 ppm for NMHC). For the tested concentrations in the extra high phase, a large deviation from the mean was observed in the case of DF (the extreme value of the upper distribution was 17 times higher than the average value in the case of THC, 16 times in the case of NMHC). This relationship was not observed for RONhex. The concentrations of THC and NMHC in the WLTC cycle are shown in Fig. 14 and 16, respectively. In contrast, the values of the average concentration are shown in Fig. 15 and Fig. 17.

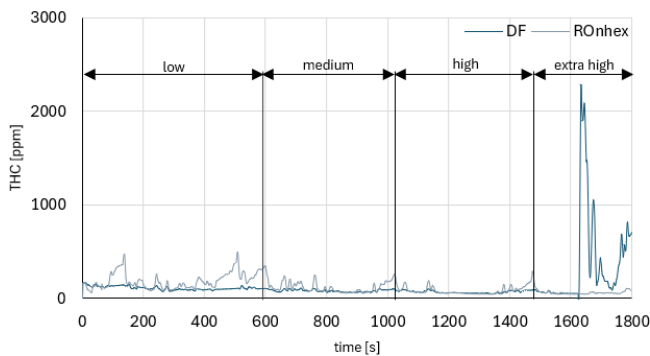


Fig. 14. THC concentration during the WLTC driving cycle

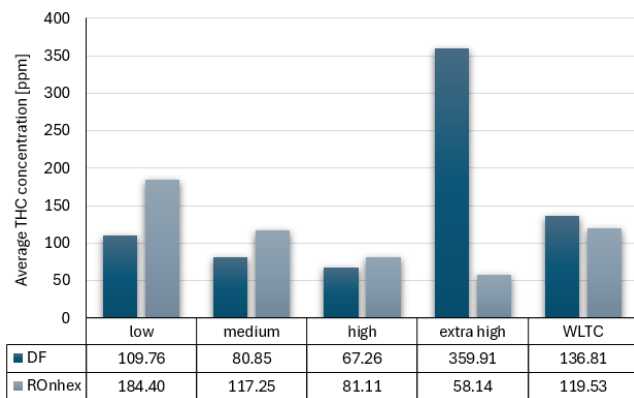


Fig. 15. Average THC concentration during each cycle

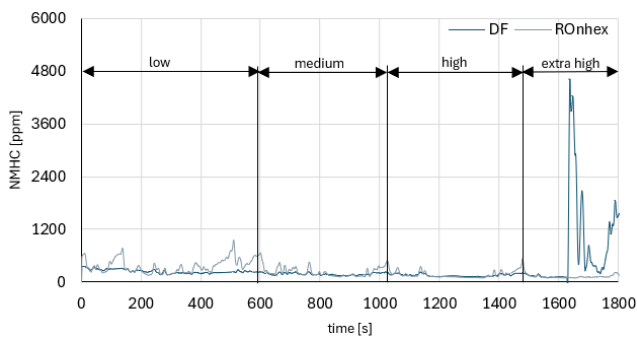


Fig. 16. NMHC concentration during the WLTC driving cycle

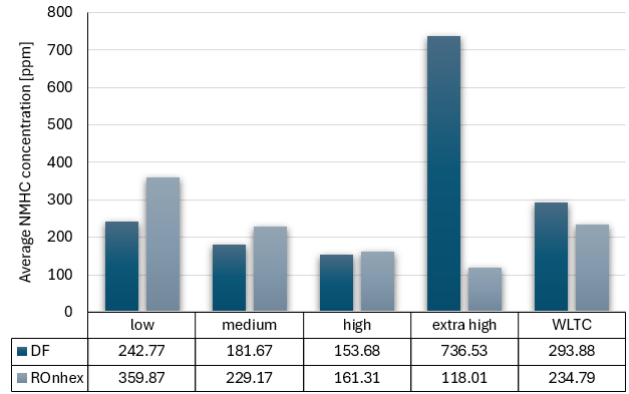


Fig. 17. Average NMHC concentration during each cycle

In further analysis, a predictive model was developed to forecast NO_x concentrations. Its purpose was to estimate the level of pollutants based on input (independent) variables - vehicle speed, engine speed and engine load. The highest R^2 coefficient of determination was obtained for both fuels tested, using the Random Forrest model. This is a versatile algorithm, used in datasets, for classification and regression purposes, due to its ability to model complex, non-linear relationships between variables. Table 3 shows the results of fitting the obtained predictive models using metrics for assessing the quality of regression models - mean absolute error (MAE), root mean squared error (RMSE). Figure 18 shows the actual and predicted values plot for both cases considered. Meanwhile, Fig. 19 and Fig. 20 correlate the above results with vehicle speed for DF and ORhex, respectively.

Table 3. Metrics for evaluating the quality of regression models

Parameter	DF	RONhex
R^2	0.9537	0.9466
MAE (ppm)	56.16	57.38
RMSE (ppm)	78.91	80.52

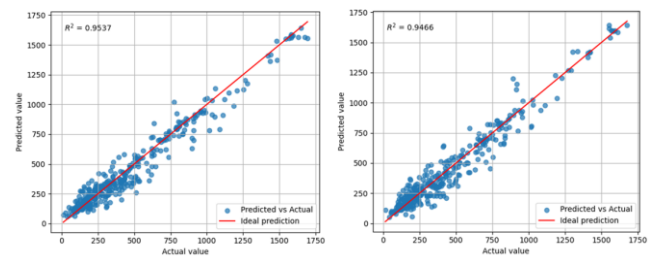


Fig. 18. Actual and predicted values plot (DF – left, RONhex – right)

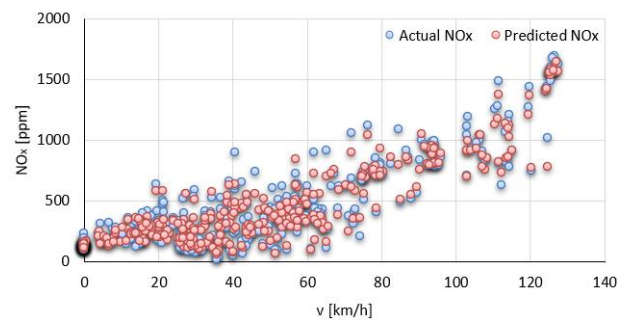


Fig. 19. Comparison of predicted values and actual NO_x concentrations for DF

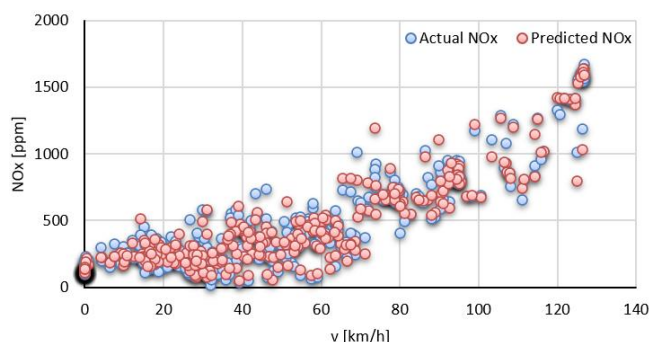


Fig. 20. Comparison of predicted and actual values of NO_x concentration for RONhex

A comparison of the model used for both fuels showed a lower coefficient of determination R^2 , and higher prediction errors for RONhex. This indicates that the model generates more stable predictions with smaller deviations from actual values for DF.

4. Conclusions

The study was able to measure the concentrations of exhaust emissions for diesel fuel and a mixture of rapeseed oil with 20% n-hexane additive, based on the WLTC driving cycle.

When measuring CO and NO_2 , the concentration of these components is higher for RONhex. Lower loads result in lower temperatures and incomplete combustion, which, combined with the lower volatility of rapeseed oil, results

in poorer fuel evaporation, and the higher viscosity compared to diesel fuel has a negative effect on the atomization process. This results in a less efficient combustion process and higher CO concentrations. As the load and combustion temperature increase, this effect is compensated by the oxygen content in RONhex, unlike DF, where at higher loads the fuel mixture becomes richer. The lower oxygen content causes an increase in CO concentration. In the case of NO_2 concentration, the oxygen content in rapeseed oil promotes the oxidation of NO to NO_2 , resulting in a higher concentration than in DF.

Similarly, in the case of hydrocarbon exhaust concentrations, RONhex had the highest concentrations in phase I of the cycle, in contrast to DF, whose maximum concentration in the last phase of the cycle was significantly higher than the average value (almost 17 times for THC and 16 for NMHC) and the values obtained for RONhex. CO_2 and NO concentrations increased with vehicle load and were higher for DF.

The study developed a predictive model to predict NO_x concentration values based on vehicle speed, engine speed and engine load. The model used had a high predictive capability.

A further stage of research envisages the analysis of individual cycle phases, especially in the context of studying the stability of the combustion process in phases characterized by low loads for RONhex. The research is also planned to continue by applying more complex predictive models.

Nomenclature

AV	average	OBDII	on-board diagnostic II
CI	compression ignition	RMSE	root mean squared error
CO	carbon oxides	RONhex	rapeseed oil with 20% n-hexane
CO_2	carbon dioxides	SD	standard deviation
CV	coefficient of variation	THC	total hydrocarbons
DF	diesel fuel	v	vehicle speed
ECU	engine control unit	WLTC	Worldwide Harmonized Light Vehicles Test Cycle
MAE	mean absolute error	WLTP	Worldwide Harmonized Light Vehicles Test Procedure
NMHC	non-methane hydrocarbons		
NO_x	nitrogen oxides		

Bibliography

- [1] Adamiak B, Andrych-Zalewska M, Merksiz J, Chłopek Z. The uniqueness of pollutant emission and fuel consumption test results for road vehicles tested on a chassis dynamometer. *Ekspluat Niezawodn.* 2025;27(1). <http://doi.org/10.17531/ein/195747>
- [2] Chłopek Z, Rostkowski J. Non-repeatability of exhaust emission test results. *Combustion Engines.* 2015;163(4):92-100.
- [3] Giakoumis E, Zachiotis A. Investigation of a diesel-engined vehicle's performance and emissions during the WLTC driving cycle – comparison with the NEDC. *Energies.* 2017; 10(2):240. <https://doi.org/10.3390/en10020240>
- [4] Górski K, Sander P, Longwic R. The assessment of ecological parameters of diesel engine supplied with mixtures of canola oil with n-hexane. *IOP Conf Ser: Mater Sci Eng.* 2018;421:042025. <https://doi.org/10.1088/1757-899X/421/4/042025>
- [5] Hassan MA, Salem H, Bailek N, Kisi O. Random forest ensemble-based predictions of on-road vehicular emissions and fuel consumption in developing urban areas. *Sustainability.* 2023;15(2):1503. <https://doi.org/10.3390/su15021503>
- [6] Jaworski A, Kuszewski H, Ustrzycki A, Balawender K, Lejda K, Woś P. Analysis of the repeatability of the exhaust pollutants emission research results for cold and hot starts under controlled driving cycle conditions. *Environ Sci Pollut Res.* 2018;25(18):17862-17877. <https://doi.org/10.1007/s11356-018-1983-5>
- [7] Koszałka G, Szczotka A, Suchecki A. Comparison of fuel consumption and exhaust emissions in WLTP and NEDC procedures. *Combustion Engines.* 2019;179(4):186-191. <http://doi.org/10.19206/CE-2019-431>
- [8] Longwic R. Diesel engine operations with alternative fuels. Taylor & Francis Group. 2024. <https://doi.org/10.1201/9781003466291>

- [9] Longwic R, Sander P. The course of combustion process under real conditions of work of a traction diesel engine supplied by mixtures of canola oil containing n-hexane. IOP Conf Ser: Mater Sci Eng. 2018;421:042050. <https://doi.org/10.1088/1757-899X/421/4/042050>
- [10] Longwic R, Sander P, Jańczuk B, Zdziennicka A, Szymczyk K. Modification of canola oil physicochemical properties by hexane and ethanol with regards of its application in diesel engine. Energies. 2021;14(15). <https://doi.org/10.3390/en14154469>
- [11] Merkisz J, Sordyl A, Chłopek Z. Non-repeatability of the WLTP vehicle test results. Archives of Transport. 2024; 71(3):25-49. <https://doi.org/10.61089/aot2024.fjw8a575>
- [12] Sordyl A, Chłopek Z, Merkisz J. Correlation relationships of processes in the combustion engine in the RDE test. Combustion Engines. 2024;199(4):112-125. <https://doi.org/10.19206/CE-192877>
- [13] Sordyl A, Chłopek Z, Merkisz J. Correlation studies of processes: vehicle velocity, pollutant emissions, and vehicle fuel consumption in the worldwide light-duty test cycle. Transport Problems. 2024;19(2):229-41. <http://doi.org/10.20858/tp.2023.19.2.18>
- [14] Struś M, Poprawski W. Efficiency of the diesel engine fuelled with the advanced biofuel Biodiesel. Combustion Engines. 2021;186(3):89-95. <https://doi.org/10.19206/CE-140972>
- [15] Wasilewski J, Krzaczek P, Szyszlak-Bargłowicz J, Zając G et al. Evaluation of nitrogen oxide (NO) and particulate matter (PM) emissions from waste biodiesel combustion. Energies. 2024;17(2):328. <https://doi.org/10.3390/en17020328>
- [16] Zakrzewska D, Chłopek Z, Szczepański K. The criteria for qualifying fuels as a replacement fuels for internal combustion engines. Combustion Engines. 2024;199(4):60-66. <https://doi.org/10.19206/CE-186848>

Prof. Rafał Longwic, DSc., DEng. – Department of Automotive Vehicles, Lublin University of Technology, Poland.
e-mail: r.longwic@pollub.pl



Michał Kuszneruk, MEng. – Department of Automotive Vehicles, Lublin University of Technology, Poland.
e-mail: m.kuszneruk@pollub.pl



Mateusz Klepka, MEng. – Department of Automotive Vehicles, Lublin University of Technology, Poland.
e-mail: mateusz.klepka@pollub.edu.pl



Use of a digital twin to analyze the effect of graphene as a lubricant additive for diesel engines

ARTICLE INFO

Received: 11 June 2025
Revised: 31 August 2025
Accepted: 6 October 2025
Available online: 13 November 2025

The effect of two graphene additives to engine oil on diesel engine efficiency was studied. The first additive was a commercially available additive based on graphene oxide (GO). The additive was tested on a small automotive diesel engine. The use of the additive concentration recommended by the manufacturer at 3% in the engine oil resulted in a reduction of the specific fuel consumption from 0.2% to 0.7%, depending on the engine operating conditions. The second additive, currently under development, was based on graphene nanoplatelets (GNP). The additive was tested on a medium-sized diesel engine in a truck. The use of the equivalent GNP concentration of 0.1% resulted in a reduction of fuel consumption in the ESC test by 0.4%. Increasing the concentration of this additive to 0.2% GNP did not result in a further reduction in fuel consumption. Because the engine efficiency benefits resulting from the use of improved oils were close to the measurement uncertainties, the applicability of machine learning using engine on-board diagnostics (OBD) readings to analyze the impact of lubricant additives was investigated. The use of Random Forest, machine learning digital twins, was able to reproduce the OBD instantaneous fuel consumption with excellent accuracy. Further analysis with SHAPLEY values helped to identify the more important engine parameters that affected instantaneous fuel consumption.

Key words: *energy efficiency, engine oil, graphene oxide, graphene nanoplatelets, fuel consumption, machine learning, Shapley values (SHAP)*

This is an open access article under the CC BY license (<http://creativecommons.org/licenses/by/4.0/>)

1. Introduction

Reducing mechanical losses in internal combustion engines is crucial for enhancing efficiency and lowering emissions. Engine oil properties significantly influence these losses [7, 9, 21]. Lower-viscosity oils can decrease hydrodynamic friction, improving fuel economy. However, they may also reduce oil film thickness, potentially increasing wear under certain conditions. To mitigate this, different additives to oil are employed to form protective tribofilms, reducing boundary friction and wear. Studies have shown that combining low-viscosity base oils with effective additives like molybdenum dithiocarbamate (MoDTC) can optimize the balance between friction reduction and component protection, leading to improved engine performance and longevity. Unfortunately, MoDTC, which is a very effective friction modifier, is not used in diesel engines with the Diesel Particulate Filter (DPF) due to its harmful effect on the DPF [8, 22, 23].

Recent advances in nanotechnology have introduced novel lubricant additives, among which graphene-based materials have gained considerable attention due to their outstanding tribological and thermal properties. Graphene oxide (GO) and graphene nanoplatelets (GNP) are among the most commonly investigated forms of graphene for lubricant applications. GO, with its oxygen-containing functional groups, offers good dispersibility in polar and non-polar base oils, enabling the formation of a stable suspension and tribological film. On the other hand, GNPs – few-layer graphene structures with high surface area – demonstrate excellent mechanical strength, load-bearing capacity, and low shear characteristics, making them effective

in reducing boundary friction and wear under high-load conditions [1, 3, 12, 15, 17, 18].

Machine learning techniques have shown increased use in helping engine tests. They are able to find complex, nonlinear relationships in data that may be difficult to catch with traditional statistical methods. Machine learning can identify the importance of even those features that have a smaller impact on the output and take them into account in creating predictions [4–6, 10, 16, 19, 24]. The use of digital twins can reduce the number of costly experimental tests and help with the analysis of instantaneous variations. Engine transients, e.g. transients when the engine goes from one operation regime to another, are neglected in stationary tests but may contain relevant information on real driving conditions.

In the current work, two graphene-based lubricant additives were investigated using diesel engine dynamometer tests. Since the expected fuel savings by using improved oils are almost the same as experimental test variability, instantaneous reading of the engine On-Board Diagnostics (OBD) and random Forest machine learning digital twins were used for a more detailed analysis of the effect of the lubricant additives.

2. Tests of a commercially available graphene additive

A commercially available additive with claims of graphene was added to a SAE 5W-30 oil, fully synthetic, Low SAPS. TGA analysis suggests that the additive contains Oxide of Graphene (GO). It was not possible to determine the Graphene concentration in the additive. 3% in volume

of additive was added to the engine oil, as recommended by the supplier, for the engine tests. Due to the additive's relatively lower viscosity, oil kinetic viscosities kV40 and kV100 were reduced by about 4%. See details in [11].

An automotive 4-cylinder Diesel engine, 1.25 L, 66 kW, TCDI, Common Rail injection system, air cooling and EGR was tested on a dynamometer with controlled coolant and oil temperatures. The following OBD parameters were recorded at 5 Hz frequency: time, acceleration pedal position, engine rotational speed, total fuel injection, coolant temperature, boost pressure, fuel pressure in the rail, exhaust temperature after DPF, and DPF filling. Potentially interesting parameters, such as injection timing, were not available via OBD on this engine. The dynamometer tests were done at two accelerator pedal positions: 100% and 30%, and engine speeds: 2000 to 4000 rpm. The test sequence was: a) baseline oil, b) addition of 3% VV of the graphene-based additive, as recommended by the additive supplier. Before pouring the additive, the same oil volume was removed from the crankcase to maintain the engine oil volume constant. Maximum engine torque and power increased 0.8% and 0.4% with the oil additive, but as fuel consumption also showed a small increase with the additive, BSFC decreased on average by only 0.2% [11].

Tests for oil without an additive and with the additive were repeated at least 3 times. The repetitions were always done on different days. For simplicity, the dataset was defined as sequential time, including only the OBD acquisitions. Figure 1 shows the test sequence with the reference oil (without an additive). Figure 2 shows the map of engine rotational speed and pedal position covered during the tests.

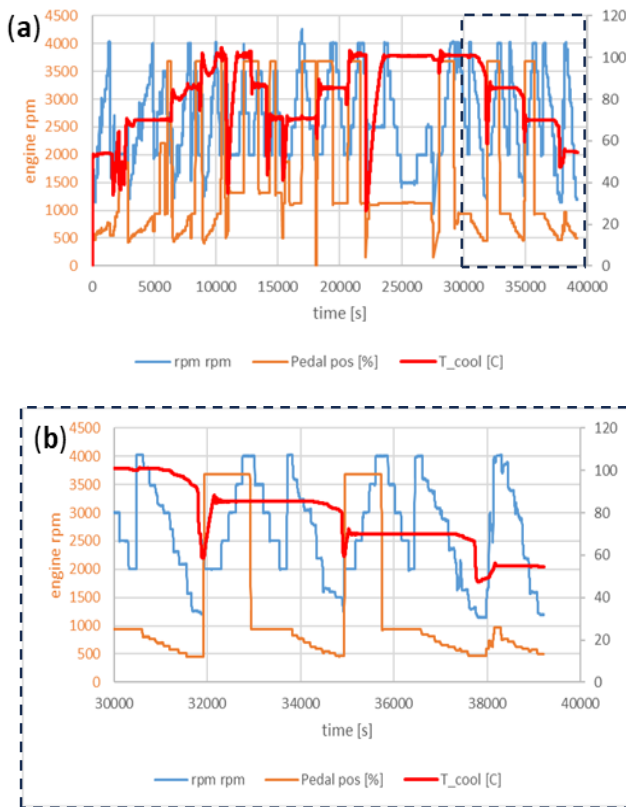


Fig. 1. Test sequence with the reference oil: (a) complete sequence, (b) zoom on the last replications

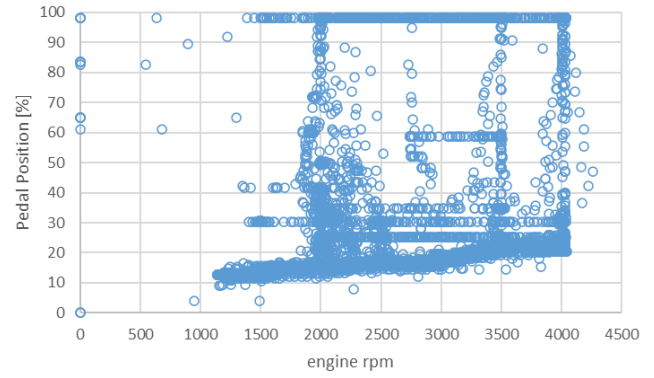


Fig. 2. Map of engine rotational speed and pedal position along the tests with the reference oil

Pearson and Spearman correlations were calculated to select the variables used as input to train the digital twin. Pearson assumes a linear numerical regression, while Spearman is more flexible and calculates the correlation based on the variable ranking. Table 1 shows the Pearson correlation between variables, and Table 2 shows the Pearson and Spearman correlation factors for the instantaneous fuel consumption. Pearson and Spearman's rankings are similar, but notice that some differences exist. See discussion of Shapley values in the MDD case ahead.

Table 1. Pearson correlation coefficients between the variables

rpm	1.00	0.25	0.13	0.41	0.64	0.19	0.11	0.25	0.52
Pedal Pos	0.25	1.00	0.08	0.97	0.83	0.99	0.43	0.26	0.92
T_cool	0.13	0.08	1.00	0.11	0.06	0.07	0.15	0.75	0.09
P_boost	0.41	0.97	0.11	1.00	0.84	0.95	0.26	0.34	0.91
P_rail	0.64	0.83	0.06	0.84	1.00	0.80	0.35	0.32	0.96
Fuel Inj	0.19	0.99	0.07	0.95	0.80	1.00	0.44	0.26	0.90
T_afterDPF	0.11	0.43	0.15	0.26	0.35	0.44	1.00	0.35	0.44
DPF_fill	0.25	0.26	0.75	0.34	0.32	0.26	0.35	1.00	0.27
Fuel Cons.	0.52	0.92	0.09	0.91	0.96	0.90	0.44	0.27	1.00

Table 2. Pearson and Spearman correlations to the instantaneous fuel consumption

	Pearson	Spearman	
rpm	0.52	0.69	1.0
Pedal Pos	0.92	0.89	0.8
T_cool	0.09	0.19	0.6
P_boost	0.91	0.92	0.5
P_rail	0.96	0.98	0.4
Fuel Injection	0.90	0.70	0.2
T_afterDPF	0.44	0.19	0.1
DPF_filling	0.27	0.37	0.0

The correlation coefficients show some obvious relations, fuel consumption is directly dependent on fuel injection, boost pressure, etc. To verify the digital twin's capacity to make predictions with as few parameters as possible, the following parameters were selected to predict the instantaneous fuel injection:

- inputs: engine rotational speed, pedal position, cooling temperature
- output, “target” in the machine learning jargon: fuel injection or fuel consumption, the latter calculated from the OBD fuel injection and engine rotational speed.

The machine learning digital twin is created (“trained” in the AI jargon), having variables for input and, in our case, one for output to be predicted (Fig. 3–5).

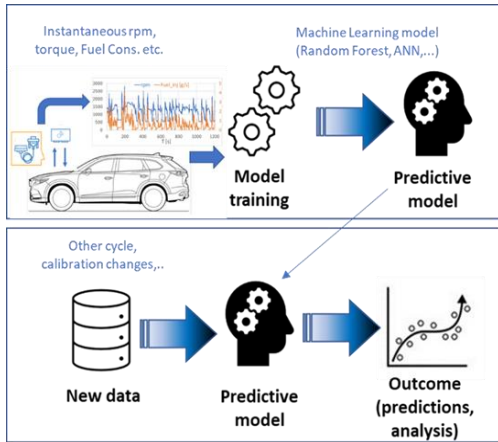


Fig. 3. Scheme of the machine learning approach used in this work (reproduced from [19])

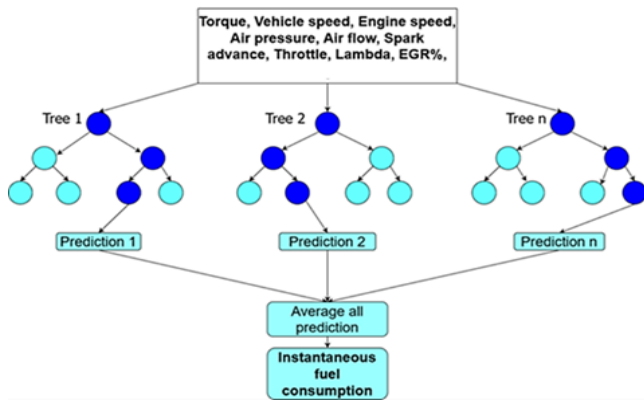


Fig. 4. Scheme of the machine learning Random Forest model (reproduced from [19])

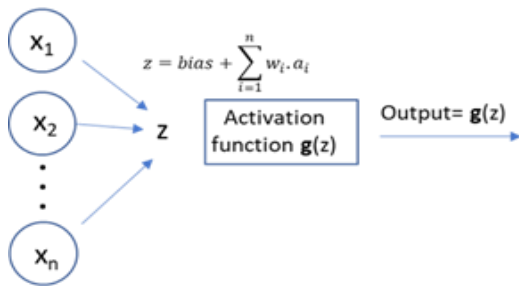


Fig. 5. Scheme of the Random Forest model (reproduced from [19])

In all replications, the model correlation between the real ECU instantaneous fuel injection and the model was very good, with a coefficient of correlation R^2 of almost 1.0 and an accumulated error smaller than 0.1%. See two examples in Fig. 6 and Fig. 7. Such good correlation was already verified in the author's previous publications, even for transient emission and RDE cycles [14]. More robust validation is whether the model trained on a given day can predict the test on another day, which was also obtained with the developed digital twin. Figure 7 shows that the model prediction for the 2024Feb06 test using the model trained with the

baseline 2023 dataset showed an almost perfect correlation, R^2 : 0.9994, and the accumulated error on accumulated fuel injected along the replication was lower than 0.1%. The time frames in Fig. 6–9 refer to the respective test replication (06_02 and 07_02). They are part of the complete test sequence shown in Fig. 1, but with time starting at the start of the respective replication.

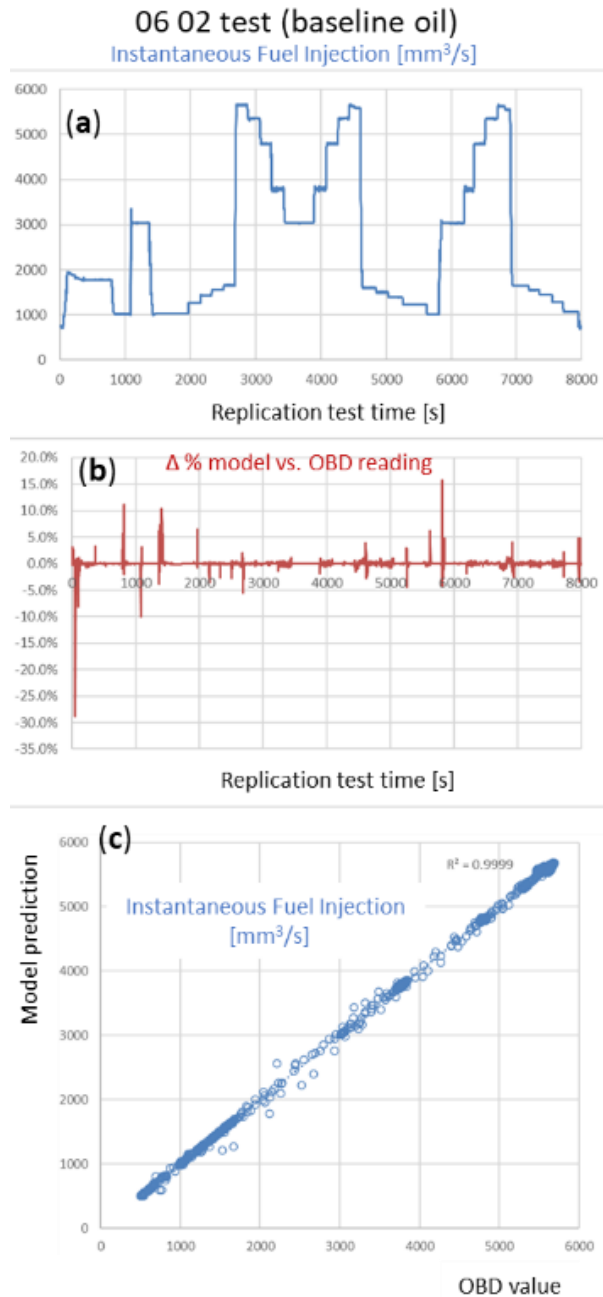


Fig. 6. Digital twin predictions for the reference test

As already mentioned, using the dynamometer stand measurements, BSFC reduction was almost within the experimental uncertainties [11]. To investigate if the use of digital twins could provide a more resolute comparison, the following method was carried out:

- instantaneous fuel consumption was calculated using the fuel injection and engine rotational speed

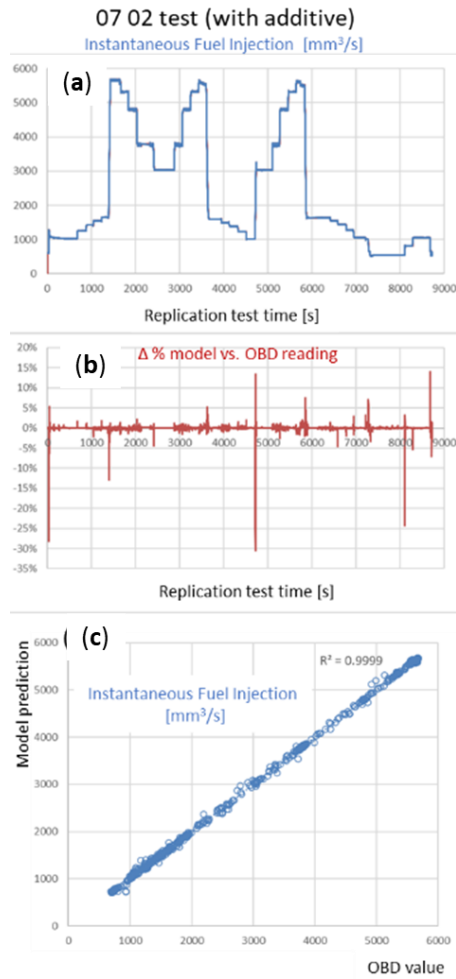


Fig. 7. Digital twin predictions for test with 3% additive

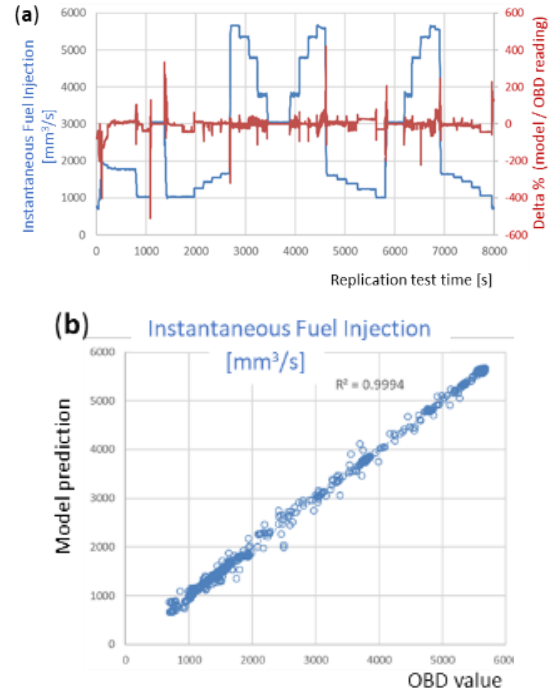


Fig. 8. Prediction for the 06Feb2024 replication with the model trained with Dec2023 replications

- 2 digital twins were trained for tests done on consecutive days, one with the baseline oil, and the other with the addition of the 3% V/V graphene additive. Both models were able to fully reproduce the respective datasets, as discussed before
- then, the model trained with the baseline oil was used to predict the test with the graphene additive and vice versa.

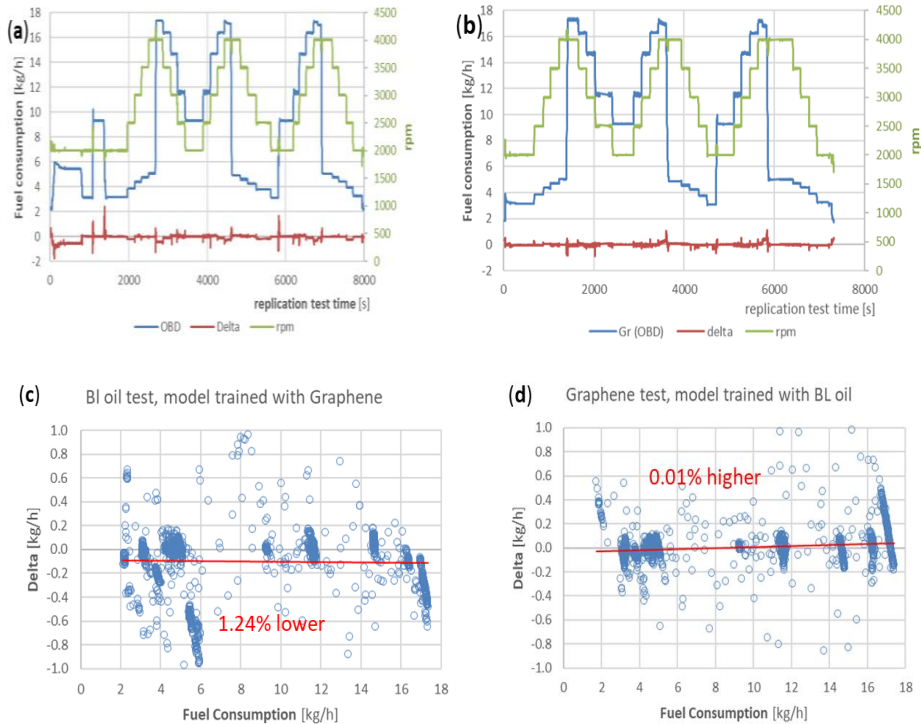


Fig. 9. Tentative to use the digital twins to predict the influence of graphene on instantaneous fuel consumption: (a) and (c) reference oil test, model trained with graphene; (b) and (d) test with graphene, model trained with the baseline oil

The expectation was that the model trained with graphene would reduce the fuel consumption when applied to the baseline oil, and the opposite when the baseline oil model was applied to the test with graphene. However, the results were inconclusive. While the model trained with graphene reduced 1.24% the fuel consumption of the baseline test, the use of the baseline oil model showed almost no change when applied to the test with graphene. See Fig. 9.

3. Tests of a GPN-based additive

After testing the GO additive on the small diesel engine, the project moved to the use of an in-house graphene-developed additive based on graphene nanoplatelets (GNP) with a higher graphene concentration. Table 3 and Fig. 10 show the GNP main characteristics. See details in [20]. The higher graphene concentration allowed a reduction in the additive volume, leading to a lower impact on the kinematic viscosity of less than 1%.

Table 3. GNP characterisation

Characteristic	Unit	Mean	Q90
Number of layers – $\langle N \rangle_{2D}$ (nm)	–	9	11
Surface density of point defects – nD	10^{10} cm^{-2}	2.8	4.3
Lateral size – L_a	nm	71.1	99.4
D to G peak intensity ratio (I_D/I_G)	–	0.28	0.44

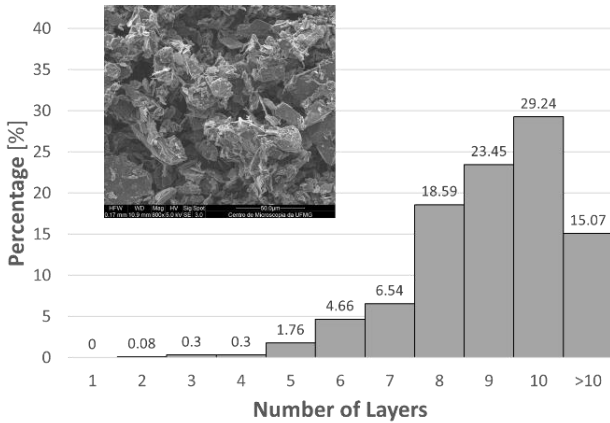


Fig. 10. GNP number of layers, adapted from [20]

A Medium-Duty Diesel (MDD) engine of 4.8 L, 4-cyl., 136 kW and 700 Nm was used in the tests. Both the DPF sensor and the coasting strategies were turned off during the tests. The dynamometer tests were carried out in the following sequence: a) baseline oil, b) addition of the equivalent of 0.1% graphene, c) another 0.1%, reaching a total of 0.2% of graphene. The test cycle followed the European Stationary Cycle (ESC) – see Fig. 11. Four other operation regimes, at engine rotational speed of maximum power and 25, 50, 75 and 100% of load were added to the test program for completeness.

On the combined ESC values, 0.4% and 0.3% fuel saving were observed with 0.1% and 0.2% graphene additives, respectively – see [11]. The possibilities of using AI in the results obtained in MDD tests were initially investigated in [14]. Digital twins were able to reproduce the OBD values accurately. In the current work, an improved digital twin and the calculation of SHAP values were used to under-

stand better the potential and limitations of using AI on fuel consumption tests.

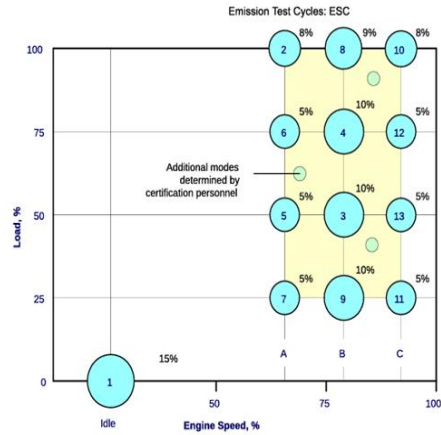


Fig. 11. ESC cycle

On the ESC cycle, the engine must be operated for 2 minutes at each regime point. At each point, the first 20 seconds are neglected to allow engine stabilization. But even after stabilization, it is not uncommon that some engine parameters present instantaneous variations. For example, Fig. 12 shows turbo pressure variations, which may affect instantaneous power, fuel consumption etc. Figure 13 shows in more detail step 11, neglecting the first 20 seconds as defined in the ESC procedure. The step average is 1791 hPa and 7.0 kg/h, respectively, for turbo pressure and fuel consumption. However, it can be noted that there is lower fuel consumption when the P_{turbo} is higher than the average and higher fuel consumption when the P_{turbo} is lower than the average. Such a correlation, although small, is not considered if only the average values are considered.

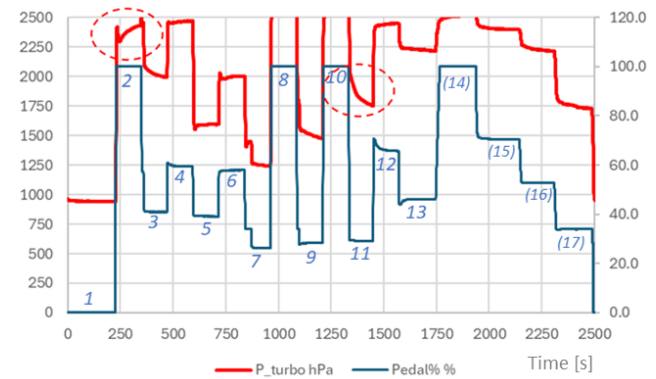


Fig. 12. OBD turbo pressure and pedal position along a tests sequence; notice some instantaneous variations even on stationary conditions

Table 4 shows the four higher Pearson correlation coefficients used as input to train the digital twin. These chosen parameters are engine speed, coolant temperature, turbo-charger pressure and calculated torque, so-called rpm, T_{cool} , P_{turbo} and $CalcTorque$, respectively. No significant difference was found in the correlation coefficients between the baseline oil and the ones with graphene additives.

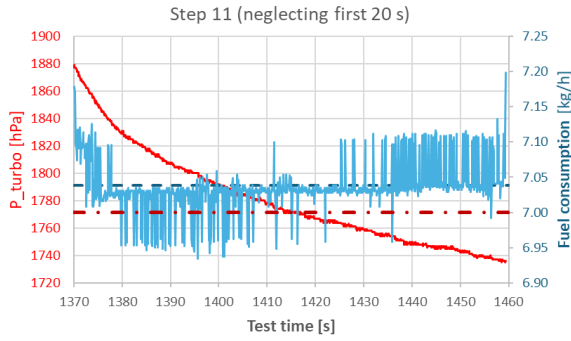


Fig. 13. Turbo pressure and fuel consumption for step 11 – see Fig. 12

Some of the parameters may indeed be an indirect consequence of fuel consumption. For the carried-out tests, with the engine already hot, the engine cooling temperature was probably affected by the torque (and not vice versa). The higher torques caused, of course, higher fuel consumption. See discussion ahead.

The developed digital twins were able not only to reproduce the test used for training accurately but also to predict the instantaneous fuel consumption of a different replication – see Fig. 14–18.

Table 4. Pearson correlation coefficients for the four parameters used to train the digital twin

	baseline oil						+ 0.1% graphene						+ 0.2% graphene							
	BL_18	BL_19	BL_20	BL_22	BL_25	BL_26	0.1_29	0.1_30	0.1_32	0.1_33	0.1_35	0.1_36	0.1_38	0.1_39	0.2_41	0.2_42	0.2_44	0.2_45	0.2_47	0.2_48
rpm	0.58	0.56	0.54	0.56	0.53	0.51	0.57	0.52	0.51	0.51	0.53	0.54	0.54	0.48	0.53	0.54	0.55	0.53	0.56	0.53
Tcool	0.67	0.64	0.63	0.61	0.60	0.59	0.62	0.59	0.58	0.58	0.57	0.58	0.61	0.59	0.57	0.59	0.60	0.60	0.61	0.56
P_turbo	0.93	0.93	0.93	0.93	0.92	0.92	0.93	0.93	0.93	0.93	0.93	0.93	0.93	0.93	0.93	0.93	0.93	0.93	0.93	0.93
CalcTorque	0.92	0.92	0.92	0.92	0.92	0.92	0.93	0.92	0.93	0.92	0.92	0.92	0.92	0.92	0.92	0.92	0.92	0.92	0.92	0.92

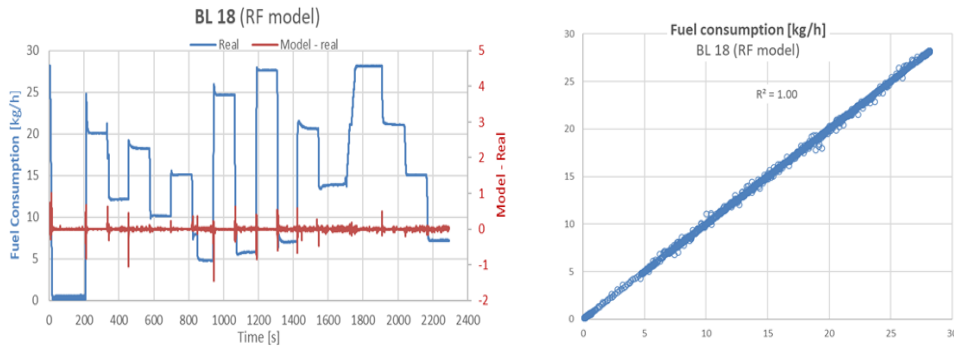


Fig. 14. RF digital twin for the baseline oil replication #18

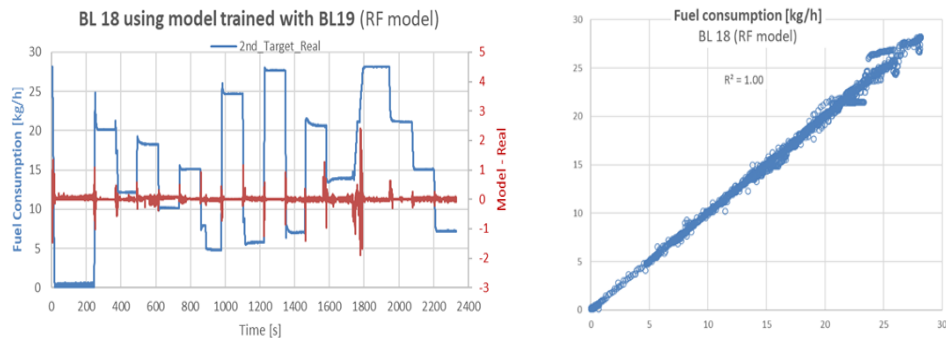


Fig. 15. RF digital twin, trained with replication BL #19, for the BL #18

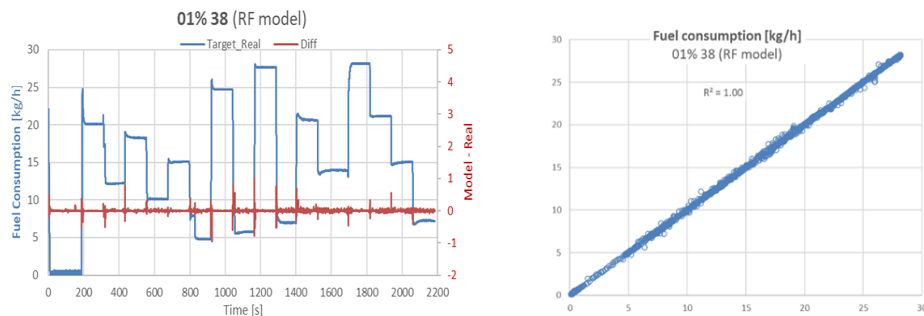


Fig. 16. RF digital twin trained with replication #38 with 0.1% GNP

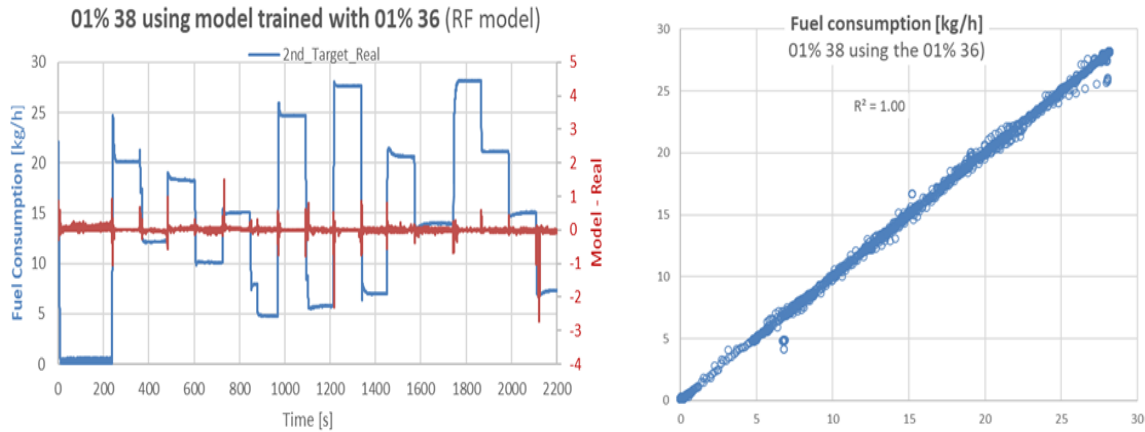


Fig. 17. RF digital twin, trained with replication 01% #36, for the 0.1% #38

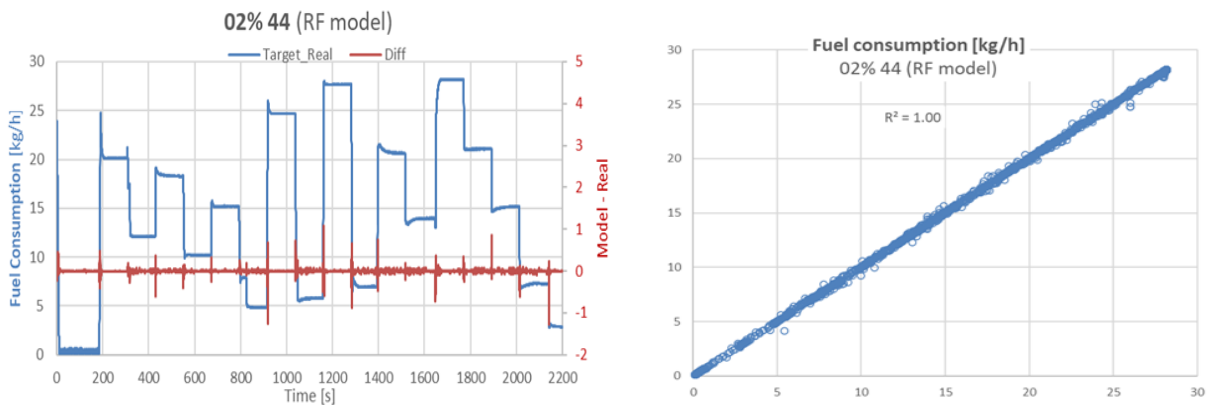


Fig. 18. RF digital twin, trained with replication 0.2% #44

4. Use of SHAP values to analyze the digital twin model

The correlation factor calculations were carried out in the datasets and do not necessarily reflect the impact on the model output. SHAP (SHapley Additive exPlanations) is a method used to explain how machine learning models make predictions. It is based on ideas from cooperative game theory, especially Shapley values, which fairly measure each player’s contribution in a group. In machine learning, SHAP looks at how important each feature (or input) is to a specific prediction. It shows how much each feature pushes the prediction higher or lower by comparing the result with and without that feature [2, 13].

SHAP helps explain both individual predictions (local explanations) and overall model behavior (global explanations). This is especially useful for complex models like neural networks or ensemble methods, where understanding how they work is often difficult. Because SHAP adds up all feature contributions to match the model’s output, it makes model decisions easier to trust and understand [2, 13].

Figure 19 presents a SHAP summary plot, which illustrates the impact of each feature on the model output across the entire dataset. Each point in the plot represents a SHAP value for an individual prediction, showing how much that feature contributed to increasing or decreasing the prediction.

The features are ranked vertically by their overall importance (mean absolute SHAP value), with the most influential features at the top. In this case, Pedal%, P_turbo, and rpm are the most impactful features in predicting the model output. The color of each point represents the original value of the feature for that observation, ranging from low (blue) to high (red). For example, for Pedal%, high feature values (in red) are generally associated with a strong positive impact on the model output, whereas lower values (in blue) tend to have a negative contribution.

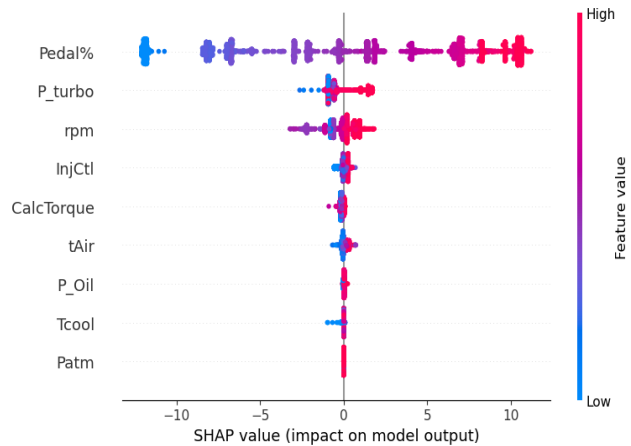


Fig. 19. SHAP Summary Plot for Feature Impact and Direction

The horizontal dispersion of points for each feature reflects the range of SHAP values and thus the variability in that feature's influence. Features like Pedal% and P_turbo show wide distributions, indicating that their impact on predictions varies significantly across the dataset. This visualization helps to understand not only which features are most important but also how their values influence the model's behavior, enabling better transparency and interpretability of the predictions.

Figure 20 shows the SHAP bar plot for the baseline test. The plot summarises the average impact of each feature on the model's predictions, measured by the mean absolute SHAP value. Pearson and Spearman correlations are also shown for comparison. The Pedal% is the most influential feature, followed by P_turbo and rpm, indicating their strong contribution to model output. Other features like InjCtl, CalcTorque, and tAir have a moderate influence, while P_Oil, Tcool, and Patm contribute minimally. This plot provides a clear overview of the importance of global features, supporting model interpretation and validation.

Notice that several parameters with high Pearson and Spearman correlation have little or no impact on the digital twin. A remarkable example is the CalcTorque with correlation factors close to 0.9, but very little effect on the model output.

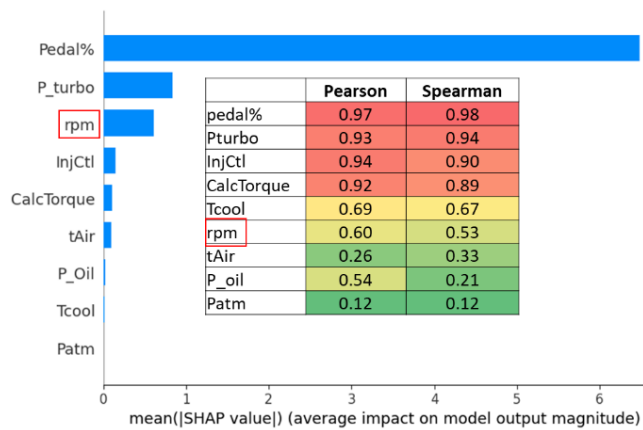


Fig. 20. Global Feature Importance Based on SHAP Values

5. Discussion and conclusions

Even under stationary conditions, normal variations in engine combustion cause instantaneous changes in engine parameters and outputs, such as power and fuel consumption. Such instantaneous variations contribute to experimental errors and may contain some relevant information that is lost when only the average values are considered. The use of instantaneous readings, either by dynamometer measurement equipment or by OBD readings, can help a more resolute analysis.

The use of machine learning models using instantaneous readings from the engine OBD showed promising results. The models are able not only to reproduce the test replication used for training but also other replications. The use of the OBD reading, digital twin and SHAP values also allowed a better assessment of the parameters impacting the engine efficiency that would be difficult to assess using conventional test methods. After the SHAP analysis men-

tioned before, a dataset combining three replications of each variant, Baseline, 0.1 and 0.2% GNP, was created by merging the individual tests. The created dataset had 208181 instantaneous OBD readings. The digital twin used as input only the Pedal%, rpm and the GNP concentration. The digital twin accuracy was excellent, $R^2 = 1.00$, Mean Squared Error, MSE, $1.6E-3$ and the accumulated fuel consumption error was lower than 0.01% (Fig. 23 and Fig. 24).

The impact of the GNP additive was very low in the carried, stationary tests. Indeed, it is known that the impact of lubricant formulation is low on diesel engines operating at higher loads. The same GNP additive, L66_2, was tested with success on SI vehicles under the FTP75 cycle [20]. Improved additives and truck transient tests are ongoing and will be covered in future publications.

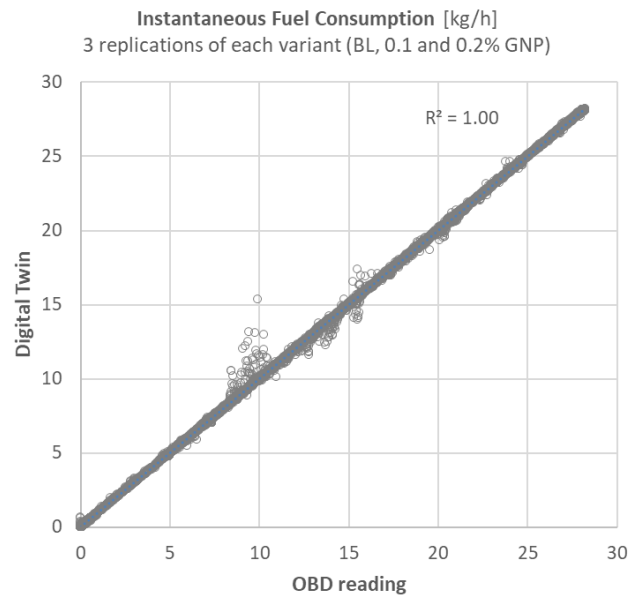


Fig. 21. Digital twin of three replications of each lubricant variant, trained only with Pedal%, rpm and GNP concentration as input

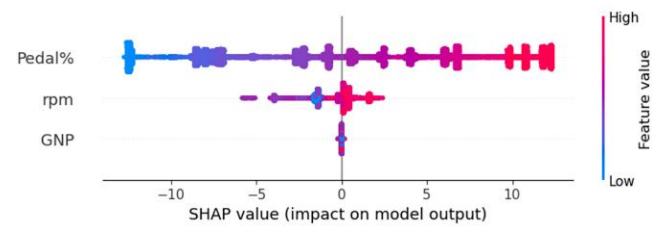


Fig. 22. SHAP summary for the digital twin with three replications of each lubricant variant

The main conclusions from the research conducted are as follows:

- the use of Random Forest, machine learning digital twins, allowed for the reproduction of the actual values of fuel consumption with very good accuracy
- use of Pearson and Spearman correlations to select the model input parameters can lead to the inclusion of unnecessary parameters, which not only increases computer resources but can also lead to erroneous analysis

– use of SHAP values can better indicate the parameters influencing the output and a better understanding of the physical system and the digital twin model, somehow

“opening” the AI black box, which will be explored in more complex and transient tests.

Nomenclature

AI artificial intelligence
BL baseline
DPF diesel particulate filter
ESC european stationary cycle
GNP graphene nanoplatelets
GO graphene oxide
MDD medium-duty diesel

MoDTC molybdenum dithiocarbamate
OBD on-board diagnostics
RDE real driving emissions
SAPS sulphated ash, phosphorous, and sulphur
SHAP Shapley additive explanations
TCDI turbo common rail direct injection
TGA thermogravimetric analysis

Bibliography

- [1] Ali M, Xianjun H, Abdelkareem M, Gulzar M, Elsheikh A. Novel approach of the graphene nanolubricant for energy saving via antifriction/wear in automobile engines. *Trib Int.* 2018;124:209-229. <https://doi.org/10.1016/j.triboint.2018.04.004>
- [2] Clement T, Kemmerzell N, Abdelaal M, Amberg M. XAIR: A systematic metareview of explainable AI (XAI) aligned to the software development process. *Mach Learn Knowl Extr.* 2023;5(1):78-108. <https://doi.org/10.3390/make5010006>
- [3] Franzosi D, de Queiroz JCF, Tomanik E, Christinelli W, Profito FJ, Souza RM. Exploring the potential of graphene nanoplatelets as a lubricant additive: topography evolution and performance under boundary lubrication conditions. *Trib Int.* 2024;192:109282. <https://doi.org/10.1016/j.triboint.2024.109282>
- [4] Gong J, Shang J, Li L, Zhang C, He J, Ma J. A comparative study on fuel consumption prediction methods of heavy-duty diesel trucks considering 21 influencing factors. *Energies.* 2021;14(23):8106. <https://doi.org/10.3390/en14238106>
- [5] He Y, Rutland C. Application of artificial neural networks in engine modelling. *Int J Engine Res.* 2005;5(4):281-296. <https://doi.org/10.1243/146808704323224204>
- [6] Hien NLH, Kor AL. Analysis and prediction model of fuel consumption and carbon dioxide emissions of light-duty vehicles. *Appl Sci.* 2022;12(2):803. <https://doi.org/10.3390/app12020803>
- [7] Idzior M. Aging of engine oils and their influence on the wear of an internal combustion engine. *Combustion Engines.* 2021;185(2):15-20. <https://doi.org/10.19206/CE-138033>
- [8] Ito A, Chubachi Y, Yamamoto T, Tanaka N, Moriizumi Y, Yari K et al. A study on effects of low viscosity engine oil and MoDTC on piston friction losses in a DI diesel engine. *SAE Technical Paper* 2015-01-2044. 2015. <https://doi.org/10.4271/2015-01-2044>
- [9] Kallas MM, Sabek MS, Saoud Y. Experimental comparison of the effect of using synthetic, semi-synthetic, and mineral engine oil on gasoline engine parts wear. *Advances in Tribology.* 2024;5997292. <https://doi.org/10.1155/2024/5997292>
- [10] Katreddi S, Thiruvengadam A. Trip based modeling of fuel consumption in modern heavy-duty vehicles using artificial intelligence. *Energies.* 2021;14(24):8592. <https://doi.org/10.3390/en14248592>
- [11] Koszalka G, Tomanik E, Maria TM, Christinelli W, Grabon W. Effect of graphene as a lubricant additive for diesel engines. *Energies.* 2025;18:257. <https://doi.org/10.3390/en18020257>
- [12] Liu Y, Ge X, Li J. Graphene lubrication. *Appl Mater Today.* 2020;20:100662. <https://doi.org/10.1016/j.apmt.2020.100662>
- [13] Lundberg SM, Lee SI. A unified approach to interpreting model predictions. In: *Advances in neural information processing systems* 30; Guyon I, Luxburg UV, Bengio S, Wallach H, Fergus R, Vishwanathan S, Garnett R (eds). Curran Associates, Inc. Red Hook, NY. 2017;4765-4774.
- [14] Maria TM, Tomanik E, Ivanytska A, Miedviedieva N. Engine emissions test analysis model based on instantaneous OBD reading and AI. In: Slavinska O, Danchuk V, Kunytska O, Hulchak O. (eds). *Intelligent Transport Systems: Ecology, Safety, Quality, Comfort ITSESQC 2024. Lecture Notes in Networks and Systems*, 1336. Springer, Cham 2025. https://doi.org/10.1007/978-3-031-87379-9_15
- [15] Nyholm N, Espallargas N. Functionalized carbon nanostructures as lubricant additives – a review. *Carbon.* 2023;201:1200-1228. <https://doi.org/10.1016/j.carbon.2022.10.035>
- [16] Perrotta F, Parry T, Neves L. Application of machine learning for fuel consumption modelling of trucks. In *Proceedings of the 2017 IEEE International Conference on Big Data*, Boston, MA, USA, 11-14 December 2017;3810-3815.
- [17] Rasheed AK. Heat transfer and tribological performance of graphene nanolubricant in ICE. *Trib Int.* 2016;103:504-515. <https://doi.org/10.1016/j.triboint.2016.08.007>
- [18] Tomanik E, Christinelli W, Souza RM, Oliveira VL, Ferreira F, Zhmud B. Review of graphene-based materials for tribological engineering applications. *Eng.* 2023;4(4):2764-2811. <https://doi.org/10.3390/eng4040157>
- [19] Tomanik E, Jimenez-Reyes AJ, Tomanik V, Tormos B. Machine-learning-based digital twins for transient vehicle cycles and their potential for predicting fuel consumption. *Vehicles.* 2023;5(2):583-604. <https://doi.org/10.3390/vehicles5020032>
- [20] Tomanik E, Christinelli W, Garcia PS, Rajala S, Crepaldi J, Franzosi D et al. Effect of graphene nanoplatelets as lubricant additive on fuel consumption during vehicle emission tests. *Eng.* 2025;6(1):18. <https://doi.org/10.3390/eng6010018>
- [21] Tormos B, Pla B, Bastidas S, Ramirez L, Pérez T. Fuel economy optimization from the interaction between engine oil and driving conditions. *Trib Int.* 2019;138:263-270. <https://doi.org/10.1016/j.triboint.2019.05.042>
- [22] Vaghar MM, Moosavian A, Ehteram MA. An experimental and theoretical investigation on the effects of piston clearance and oil viscosity on cranktrain friction. *P I Mech E-J Pro.* 2021;235(6):2230-2239. <https://doi.org/10.1177/09544089211036227>

- [23] Zhang H, Gong J, Ma Y, Sun W, Sun K, Bai S. Investigation of the influence of lubricating oil viscosity on the wear-reducing characteristics of cylinder liner surface texture. *Appl Sci.* 2024;14:10943.
<https://doi.org/10.3390/app142310943>

Dr Eduardo Tomanik – Surface Phenomena Laboratory, Polytechnic School, University of Sao Paulo, Brazil.
e-mail: eduardo.tomanik@usp.br



- [24] Ziółkowski J, Oszczypała M, Małachowski J, Szkutnik-Rogoż J. Use of artificial neural networks to predict fuel consumption on the basis of technical parameters of vehicles. *Energies.* 2021;14(9):2639.
<https://doi.org/10.3390/en14092639>

Dr Wania Christinelli – Gerdaugraphene, Brazil.
e-mail: wania.christinelli@gerdaugraphene.com



Prof. Grzegorz Koszałka, DSc., DEng. – Faculty of Mechanical Engineering, Lublin University of Technology, Poland.
e-mail: g.koszalka@pollub.pl



Prof. Jacek Hunicz, DSc., DEng. – Faculty of Mechanical Engineering, Lublin University of Technology, Poland.
e-mail: j.hunicz@pollub.pl



Thiago Marinho Maria – Kinix Consulting Ltda, Brazil.
e-mail: thi.marinho10@gmail.com



Ellen Rodrigues dos Santos Crepaldi – Independent Researcher, Brazil.
e-mail: rsantos.ellen@outlook.com



Analysis of the influence of the n-hexane content in the mixture with rapeseed oil on the auto-ignition delay angle of the fuel

ARTICLE INFO

Increasing emission-reduction requirements and EU renewable-energy targets have created a demand for biofuels that can be operated in diesel engines without modification. Current production routes – FAME and HVO – although markedly improving the physicochemical properties of rapeseed oil, are carried out in capital-intensive industrial plants and depend on continuous feedstock supply. To simplify the production chain, rapeseed oil was diluted with the inert hydrocarbon n-hexane; the resulting decrease in viscosity and flash point facilitated spray formation and ignition initiation. The effect of n-hexane content (v/v) in blends with rapeseed oil on the ignition-delay angle in a direct-injection diesel engine was analysed. Cylinder-pressure traces were used to determine the crank-angle interval between the start of injection and the start of combustion, and the results were compared with data for commercial diesel fuel and neat rapeseed oil. A progressive increase in the n-hexane fraction was found to shorten the ignition-delay angle relative to neat rapeseed oil, bringing it closer to the value observed for diesel fuel. The results confirm the suitability of the investigated blends as an alternative fuel and indicate that they can be used in currently operated diesel engines without costly modifications.

Received: 20 June 2025

Revised: 11 September 2025

Accepted: 6 October 2025

Available online: 14 November 2025

Key words: *diesel engine, rapeseed oil, combustion, auto-ignition delay, n-hexane*This is an open access article under the CC BY license (<http://creativecommons.org/licenses/by/4.0/>)

1. Introduction

For nearly a century and a half, vehicles equipped with internal combustion engines powered by liquid fuels, most commonly hydrocarbons, have been a widespread means of transportation [25, 28]. Along with the growing environmental awareness of societies and the resulting tightening of exhaust emission standards, numerous research centers have been working on improving both fuel supply systems and the design of internal combustion engines themselves. Another important direction of research aimed at meeting strict emission regulations is the enhancement of fuel properties used in combustion engines [5, 11, 23, 30]. The physicochemical properties of fuels have a direct impact on the injection and combustion processes [3, 5, 16, 17, 26, 31, 34].

Achieving proper technical parameters in the operation of a compression ignition (CI) engine – namely, low fuel consumption, reduced emissions of toxic exhaust components, and desirable torque characteristics – depends primarily on the correct course of the combustion process. Despite decades of research, combustion in CI engines remains one of the least understood processes due to the complexity and interdependence of phenomena such as fuel injection and atomization, droplet evaporation, mixing with air, pre-flame reactions, and the initiation and development of combustion itself. These difficulties are largely due to the heterogeneous nature of the fuel–air mixture, which is characteristic of compression ignition [2, 15, 18, 20, 32, 33].

One of the key parameters describing the combustion process in a CI engine is the ignition delay – the period between the start of fuel injection and the onset of combustion, which causes a rapid increase in pressure and temperature within the cylinder. The ignition delay angle, expressed in degrees of crankshaft rotation (CA), significantly influences the entire combustion process: pressure rise rate, cold start capability, operating stability, and exhaust emissions.

It can be defined as the difference between the start of injection angle (α_{pw}) and the start of combustion angle (α_{ps}) [6, 10, 13, 33].

The ignition delay consists of two parts: the physical delay (τ_f), related to the formation and evaporation of the fuel spray, and the chemical delay (τ_{ch}), associated with the chemical reactions leading to the formation of ignition kernels [4, 29, 33]:

$$\tau_s = \tau_f + \tau_{ch} \quad (1)$$

For hydrocarbon fuels, the chemical delay can be described as the sum of three phases [2, 33]:

$$\tau_{ch} = \tau_1 + \tau_2 + \tau_3 \quad (2)$$

where: τ_1 – cool flame delay, τ_2 – blue flame delay (chemiluminescence), τ_3 – hot flame delay (main combustion phase).

The length of the ignition delay is influenced by various physical and chemical parameters, including air temperature and pressure, the fuel's cetane number, piston speed, and engine design. A general mathematical expression describing this phenomenon is: [29, 33]:

$$\tau_s = A\rho^{-n}e^{E_A/RT} \quad (3)$$

where: τ_s – ignition delay period [ms], ρ – air pressure (fuel–air mixture) [bar], E_A – apparent activation energy [J/mol], R – universal gas constant [J/(mol·K)], T – air temperature (fuel–air mixture) [K], A – fuel-dependent constants, n – engine speed.

According to the formula proposed by Hardenberg and Hase, the ignition delay τ_s of a fuel in compression ignition engines can be determined using equation (4). This equation expresses the ignition delay as a function of compression temperature T , pressure p , and engine speed n [8, 9].

$$\tau_s = \frac{n}{6} \left(0.36 + 0.22 \cdot \bar{S}_p \right) \exp \left[E_A \left(\frac{1}{RT} - \frac{1}{17190} \right) + \left(\frac{21.2}{p-12.4} \right)^{0.63} \right] \quad (4)$$

where: \bar{S}_p – mean piston speed [m/s], R – gas constant, 8.3134 J/(mol·K), E_A – apparent activation energy.

$$E_A = \frac{618.840}{LC+25} \quad [\text{J/mol}] \quad (5)$$

where: LC – cetane number.

$$\tau'_{id} = \frac{\tau_{id}(\alpha^{\circ}OWK)}{0.006-n} \quad [\text{m/s}] \quad (6)$$

The values of T and p can be estimated by assuming a polytropic compression process, using the following equations:

$$T_{TC} = T_i \cdot r_c^{(m-1)} \quad (7)$$

$$p_{TC} = p_i \cdot r_c^m \quad (8)$$

where: m – polytropic compression exponent, r_c – compression ratio, subscript “i” – denotes intake air parameters [8, 9].

A higher cetane number corresponds to a lower activation energy, which translates into a shorter ignition delay. For practical purposes, equation (6) is also used to convert the delay angle into time [1, 29, 33].

In the context of alternative fuel research, a key factor is how the physicochemical properties of the fuel affect ignition delay. Rapeseed oil, which has a slightly lower cetane number than diesel fuel, exhibits a significantly longer ignition delay, as confirmed by numerous studies [14, 22, 23]. This is attributed to its higher heat of vaporization, greater viscosity, and lower chemical reactivity. In practice, this results in a longer time needed for the formation of initial ignition sites, which can hinder cold starts and negatively affect emissions of nitrogen oxides and particulate matter.

However, there are only a few studies [33] in which attempts have been made to explain the influence of chemical composition on the duration of the ignition delay period. Zablocki pointed out that the ignition delay varies depending on the properties of the fuel itself, which are determined by the chemical structure of its molecules. He identified a relationship between the ignition delay and the number of carbon atoms in the molecule for normal paraffinic, naphthenic, and olefinic hydrocarbons. The characteristics of the ignition delay process indicate that, as the number of carbon atoms in the fuel molecule increases, the ignition delay decreases. This leads to the conclusion that fuels containing large amounts of olefinic and paraffinic hydrocarbons are characterized by short ignition delay periods (τ_s), due to the ease of hydrocarbon chain decomposition at elevated temperatures.

The air temperature intake during the filling process also has a significant impact on the ignition delay time. The lower the air temperature, the longer the ignition delay. The combustion characteristics of a compression ignition engine cause the intake air temperature to be strongly correlated with the compression ratio [12, 33].

A few other factors, including the cetane number, temperature at the end of compression, intake air density, fuel injection timing, combustion chamber design, and engine speed, also influence ignition delay. These aspects make ignition delay a complex phenomenon.

The authors undertook a study aimed at modifying the physicochemical properties of rapeseed oil by adding a reactive solvent – n-hexane – in various volume proportions. The conducted analyses demonstrated that n-hexane had a positive effect on the operational properties of rapeseed oil, most notably by significantly reducing its viscosity [19, 36]. This reduction in viscosity can considerably enhance fuel atomization and evaporation in the combustion chamber, which in turn influences the ignition process and overall energy efficiency of the fuel in a diesel engine [7, 21, 23].

To mitigate this unfavorable effect, the present study introduced a 10% volume addition of n-hexane to rapeseed oil. n-Hexane, a hydrocarbon with a low boiling point, high volatility, and high reactivity, was intended to improve the ignition characteristics of the blend. Tests showed that this additive reduced the ignition delay compared to pure rapeseed oil, although the values still did not reach those typical of diesel fuel.

The experiments were conducted on a compression ignition engine using a chassis dynamometer, allowing the simulation of real-world operating conditions. Data analysis revealed that the rapeseed oil and 10% n-hexane blend exhibited a shorter ignition delay angle than pure rapeseed oil, indicating improved ignition behavior. However, the values remained higher than those for diesel fuel, confirming that while the modification had a positive impact, it did not eliminate the differences [19, 35, 36].

The aim of the study was to determine the influence of the physicochemical properties of the modified rapeseed oil on the ignition process, with particular emphasis on ignition delay as one of the main factors determining the efficiency, emissions, and reliability of a diesel engine.

2. Materials and methods

Rapeseed oil (Ro), called Kujawski (ZT "Kruszwica" S.A., Poland), n-hexane (ReagentPlus \geq 99%, Sigma-Aldrich) were used for measurements and the mixture preparation. The following fuels were studied:

- diesel oil – Df
- rapeseed oil – Ro
- mixture of rapeseed oil with 10% n-hexane – Ro-Hex10.

Diesel fuel (Df) meeting the requirements of EN590 [27] commercial rapeseed oil (Ro), non-reactive solvent n-hexane were used for testing. n-Hexane (C₆H₁₄) is an organic chemical compound from the group of alkanos. n-Hexane isomers are very little reactive and often used as solvents in organic reactions because they are highly non-polar. On the basis of rapeseed oil (Ro) mixtures with n-hexane were made in proportions of 10% (RoHex10). The main physicochemical properties of the tested fuels are presented in Table 1.

Table 1. Basic physicochemical parameters of the tested fuels [19]

Fuel type	Density 20°C [kg/m ³]	Kinematic Viscosity 20°C [mm ² /s]	Surface tension 20°C [mN/m]	Calorific value [MJ/kg]
Ro	916.00	34.89	34.15	37.10
RoHex10	895.43	19.64	30.08	30.77
Df	840.00	2.70	29.15	43.84

The engine tests were carried out on a diesel engine equipped with a common rail injection system, installed in a Fiat Qubo vehicle that met Euro 5 emission standards. The vehicle was fitted with a five-speed manual gearbox. The test vehicle was additionally equipped with an external, independent fuel tank and an auxiliary fuel pump, which allowed for quick replacement of the tested fuels. The modification of the vehicle's fuel system was concerned only with the low-pressure side (approximately 0.3 MPa). When switching to the auxiliary (low-pressure) fuel system, the main fuel supply was automatically disconnected. The high-pressure fuel system was not modified, which ensured that the fuel pressure in this part of the system remained constant for all tests. The technical specifications of the engine and a view of the test vehicle are presented in Table 2.

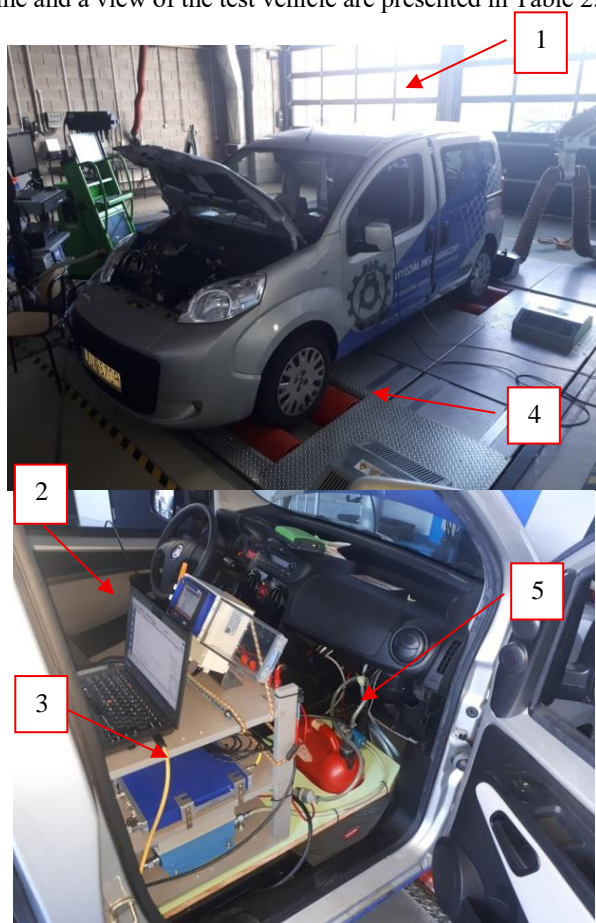


Fig. 1. Research station simulating vehicle motion under traction conditions: 1 – Fiat Qubo test car with 1.3 Multijet engine; 2 – computer with installed AVL IndiCom V2.7 software; 3 – Indimicro 602 engine indicator system; 4 – DF4FS-HLS chassis dynamometer; 5 – additional fuel system tank

An AVL pressure indication system – IndiMicro 602 – was used during the experiments, allowing for real-time

acquisition of fast-changing engine parameters. Measurements of the diesel engine's performance under conditions simulating vehicle operation in traction mode were carried out using a DF4FS-HLS chassis dynamometer. The test bench used in the study is shown in Fig. 1.

Table 2. Technical specifications of the 1.3 Multijet engine in the Fiat Qubo test vehicle

Parameter	Characteristics
Name	Fiat Qubo
Production year	2015
Engine capacity	1248 cm ³
Cylinder number and arrangement	4, in line
Cylinder diameter	69.6 mm
Piston stroke	82 mm
Compression ratio	16.8:1
Max power	55 kW CEE/75 KM CEE
Max torque	190 Nm CEE/kgm CEE
Idle speed	850 ±20 rpm
Engine speed at maximum torque	1750 rpm
Fuel injection/fuel supply system	Common Rail/diesel fuel
Exhaust after-treatment systems	EGR, DPF

The operation of an internal combustion engine in a traction vehicle occurs primarily under varying load and speed conditions, which significantly affect the combustion process. To evaluate the characteristics of this process – particularly its dynamics, efficiency, and in-cylinder pressure development – tests were conducted under conditions that reflected real-world vehicle operation. The experimental setup was described in detail in the study [18].

The WLTP (Worldwide Harmonised Light Vehicles Test Procedure) [21], a standardized driving cycle that reflects typical vehicle speed profiles, was used as the basis for the tests. The measurements were conducted on a direct-drive chassis dynamometer, where rolling resistance was simulated using the dynamometer's loading system. Based on the analysis of the WLTP cycle, two representative steady-state engine operating points were selected, corresponding to vehicle speeds of 50 km/h (approx. 1580 rpm) and 90 km/h (approx. 2860 rpm) in fourth gear (direct transmission ratio).

Dynamic conditions were reproduced by measuring the engine's maximum torque during the acceleration phase. This allowed for the analysis of key combustion parameters such as the in-cylinder pressure trace, pressure rise rate, start of injection (SOI), peak pressure location (Pmax), and the complete course of the combustion cycle, enabling the evaluation of combustion efficiency and stability under varying load conditions.

In addition to analyzing ignition delay, the start of fuel injection and the actual start of the combustion process were also evaluated. The start of injection was determined from the injector control signal, while the onset of combustion was identified primarily based on the heat release rate. The ignition initiation point was defined as the crank angle corresponding to approximately 5% of the total fuel mass burned, which represents a characteristic transition from ignition to the main combustion phase. This point coincided with the beginning of intensive heat release and a sudden increase in combustion pressure, corresponding to the actual initiation of combustion reactions of the air-fuel mixture in the cylinder combustion chamber.

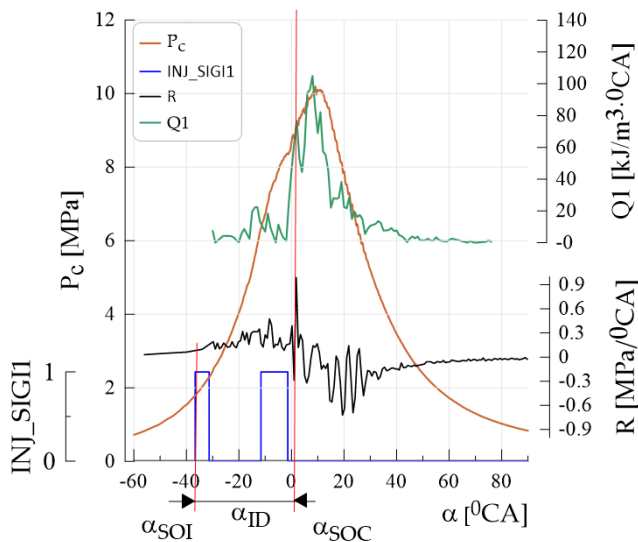


Fig. 3. Graphical interpretation of parameters necessary to calculate the self-ignition angle: α_{SOI} (Start of Injection), α_{SOC} (Start of Combustion) and α_{ID} (Ignition Delay). The course of the main injection and combustion parameters heat release rate (Q1), heat generation curves (II), combustion pressure (Pc), rate of pressure rise (R) and fuel injector control signal (INJ_SIG1) are presented

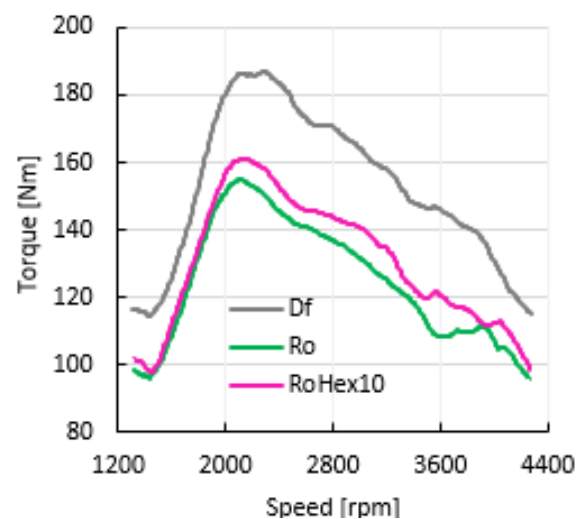
3. Results and discussion

In the experimental phase of the study, a fuel mixture Ro10hex – rapeseed oil with the addition of 10% n-hexane (fuel 3) – was used. The analysis of the physicochemical properties of this mixture showed that further increasing the share of n-hexane did not result in a significant improvement in viscosity; therefore, additional testing in this area was discontinued. The performance of the diesel engine powered by this mixture was compared with results obtained using conventional diesel fuel (Df, fuel 1) and refined rapeseed oil (Ro, fuel 2). The maximum torque and power values were determined based on engine tests (Fig. 4). For diesel fuel (Df), the torque reached 186.9 Nm at 2235 rpm, and the maximum power was 56.3 kW at 3849 rpm. For refined rapeseed oil (Ro), these values were 155.8 Nm at 2102 rpm and 45.7 kW at 3907 rpm, respectively, serving as a reference point for evaluating the performance of the alternative fuel blend. The use of the Ro10hex mixture allowed the engine to achieve a torque of 161.0 Nm at 2116 rpm and a power output of 47.7 kW at 4035 rpm, representing an increase of approximately 3.3% in torque and 4.4% in power compared to Ro. It should be noted, however, that both Ro and Ro10hex were characterized by extended ignition delay times, which is typical of biofuels with lower cetane numbers and lower reactivity. The longer ignition delay influences the timing of the combustion phase and may partly explain the lower torque and power values compared to diesel fuel.

The difference between rapeseed oil-based fuel (Ro) and the Ro10hex blend (rapeseed oil with the addition of 10% n-hexane) in terms of maximum torque and power output is relatively small. However, the course of the torque and power curves indicates that within the useful engine speed range, the difference between the Ro10hex and Ro curves becomes noticeably greater (Fig. 4). This suggests that the addition of n-hexane improves the engine's performance parameters compared to pure rapeseed oil. Such

improvement may positively affect vehicle dynamics, especially during acceleration and operation under medium load conditions. These changes may also contribute to better environmental performance of rapeseed-based fuel, as confirmed in the authors' previous studies [19]. Indicated that while the addition of n-hexane slightly increases the heating value of rapeseed oil, it significantly improves key properties such as surface tension and viscosity. These changes can have a meaningful impact on combustion quality and ignition characteristics. Both Ro and Ro10hex produced lower torque and power than diesel fuel, primarily due to their lower chemical reactivity and different combustion profiles. Nevertheless, the analysis confirmed that n-hexane enhances the performance of rapeseed oil as an alternative fuel, improving engine output and vehicle dynamics across the useful speed range.

a)



b)

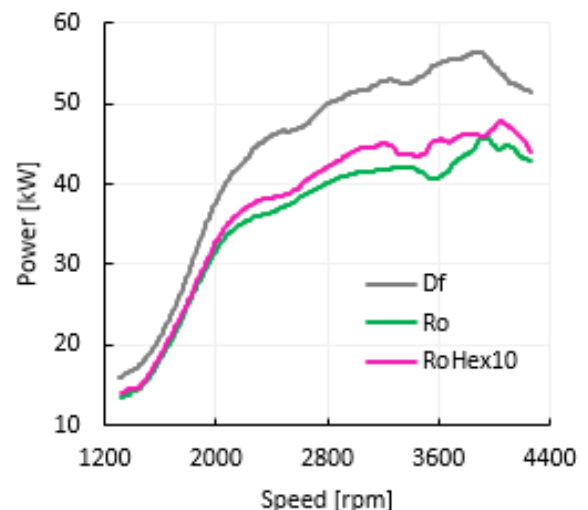


Fig. 4. The values of the Torque (a) and Power (b) values depending on the rotational speed, engine with Diesel supplied with the tested fuels, i.e. Df, Ro and Ro10hex

In the experimental studies that were conducted, clear differences were observed in ignition delay (ID) values depending on the type of fuel used. Diesel fuel (Df), due to

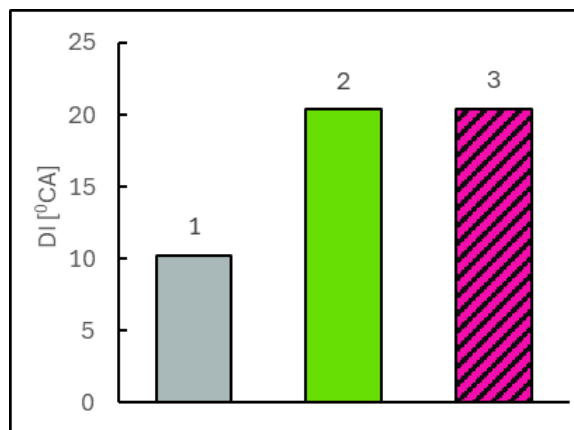
its favorable physicochemical properties (high cetane number, high reactivity), exhibited the shortest ignition delay times among all analyzed fuels – 10.25°CA at 50 km/h and 25.97°CA at 90 km/h, respectively. For refined rapeseed oil (Ro), ID values were significantly higher – 20.4°CA and 36.88°CA – confirming the lower chemical reactivity of plant-based biofuels and their slower ignition initiation. The use of the Ro10hex blend (rapeseed oil with 10% n-hexane) resulted in a noticeable, although limited, improvement in ignition properties. At 50 km/h, the ignition delay was 20.42°CA, practically unchanged from Ro. Only at 90 km/h was a reduction observed, down to 35.77°CA, which represents a decrease of approximately 3.0% compared to the base fuel (Fig. 5).

Figure 7 shows the heat release profiles as a function of crank angle for the tested fuels: diesel fuel (Df), refined rapeseed oil (Ro), and the mixture of rapeseed oil with 10% n-hexane (Ro10hex), at two vehicle speeds (50 km/h – part a, and 90 km/h – part b). In part a, corresponding to lower engine load (50 km/h), a distinct kinetic combustion phase is observed for Df, represented by a sharp peak just before top dead center (TDC). This indicates that combustion begins almost immediately after injection. In contrast, Ro and Ro10hex show almost no kinetic combustion phase – their curves rise more slowly and reach maximum values much later, confirming the predominance of diffusion combustion in these biofuels. It is also evident that the Ro10hex curve precedes the Ro curve slightly, suggesting improved fuel volatility due to the addition of n-hexane. In part b (90 km/h), similar trends are observed – the kinetic combustion phase for Df appears clearly before TDC and is the most dynamic. Both Ro and Ro10hex demonstrate delayed and more prolonged heat release, with peak values occurring after TDC. The Ro10hex curve lies between those of Df and Ro, indicating a partial improvement in combustion characteristics compared to pure rapeseed oil. At both engine loads, the addition of n-hexane leads to a slightly earlier onset and greater intensity of heat release, confirming improved ignition and combustion behavior. This has a positive impact on thermal efficiency and contributes to lower peak mechanical loads in the engine. Despite these limitations, it was found that under stationary conditions, Ro and Ro10hex released a greater total amount of heat compared to Df, and the addition of n-hexane increased both the heat released and the degree of fuel combustion. This effect partially compensated for the adverse effects of delayed ignition, resulting in improved engine performance when running on Ro10hex compared to pure rapeseed oil, as confirmed by the analysis of power and torque curves.

The experimental findings are consistent with literature data, which indicate that ignition delay is directly influenced by cetane number, ignition temperature, pressure-temperature conditions in the combustion chamber, and injection dynamics. In light of established models (e.g., Hardenberg and Hase), it is confirmed that fuels with lower chemical reactivity and weaker autoignition properties, such as vegetable-based biofuels, tend to exhibit longer ignition delays. The addition of components that improve volatility and ignition behaviour – such as n-hexane – can enhance their operating properties. However, fully match-

ing the performance of conventional diesel fuel remains a technical challenge. The results of the auto-ignition delay are shown in Fig. 5. The experimental studies revealed clear differences in the values of the maximum rate of pressure rise (R_{max}) depending on the type of fuel used. Diesel fuel (Df), due to its favorable physicochemical properties, showed the lowest R_{max} values at both tested speeds – 0.308 MPa/°CA at 50 km/h and 0.399 MPa/°CA at 90 km/h – indicating a more controlled and smoother combustion process. This was also influenced by combustion taking place mainly in the kinetic phase (Fig. 7).

a)



b)

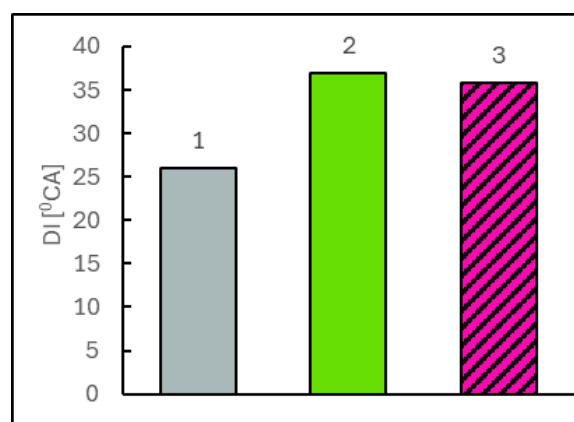


Fig. 5. The values of the ignition delay (ID) for vehicle speeds of 50 km/h (a) and 90 km/h (b) fuelled with the test fuels: Df – diesel fuel (bar 1); Ro – the rapeseed oil (bar 2), Rohex10 – the mixture of rapeseed oil with 10% n-hexane (bar 3)

The torque characteristics obtained during tests on a Dynorace chassis dynamometer (Fig. 4a) show a noticeably faster decrease in engine torque after reaching its maximum value compared to the reference characteristics provided by the manufacturer (Fiat Powertrain Technologies). According to catalogue data and engine-bench measurements (engine dynamometer), the torque of the 1.3 Multijet 55.15 kW engine is approximately 190 Nm in the range of 1500–3000 rpm, whereas in tests on a chassis dynamometer a decrease in engine torque was observed already at approximately 2000 rpm. This difference is typical and has been reported in scientific studies – it results from driveline losses occurring during chassis-dynamometer operation,

different engine-cooling conditions, and consequently a different course of the boost-control process.

For refined rapeseed oil (Ro), the rate of pressure rise was significantly higher – 0.507 MPa/°CA at 50 km/h and 0.540 MPa/°CA at 90 km/h – confirming that the combustion of plant-based biofuel is characterized by a more rapid pressure increase and, consequently, greater loading of the piston-crank system. This was due to the delayed start of combustion compared to Df, leading to the dominance of diffusion combustion. The use of the mixture of rapeseed oil with 10% n-hexane (Ro10hex) resulted in a noticeable reduction in the intensity of the pressure rise compared to pure rapeseed oil. At 50 km/h, the R_{max} value was 0.396 MPa/°CA, and at 90 km/h 0.417 MPa/°CA, representing a decrease of approximately 22% and 23%, respectively, compared to pure Ro. This result confirms the positive effect of n-hexane in improving the combustion process of the fuel blend. The ignition delay of these fuels had a decisive influence on these results, as the delay determined the accumulation of the fuel-air mixture prior to the start of combustion and, consequently, the magnitude of the pressure rise. The results of the maximum rate of pressure rise are shown in Fig. 6.

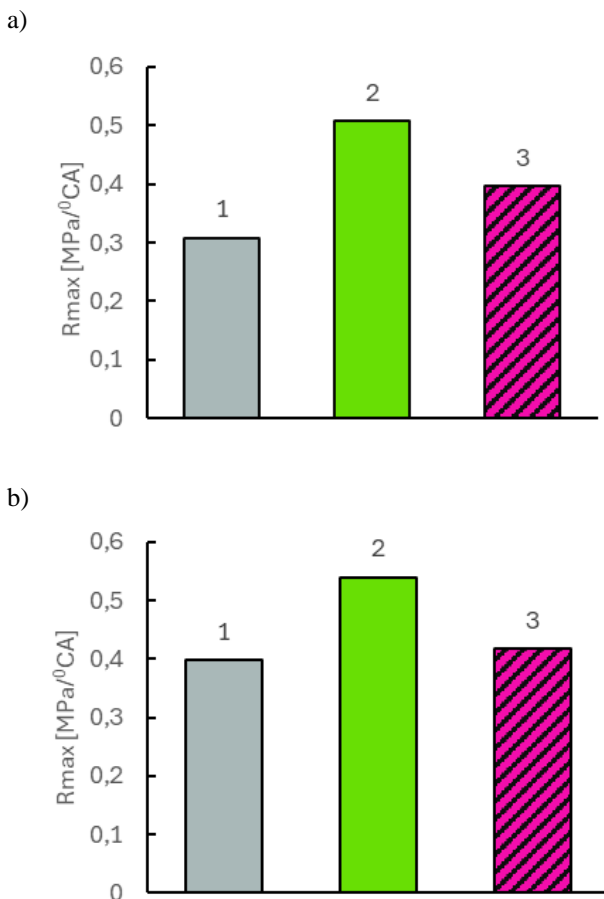


Fig. 6. The values of maximum rate of pressure rise (R_{max}) for vehicle speeds of 50 km/h (a) and 90 km/h (b) fuelled with the test fuels: Df – diesel fuel (bar 1); Ro – the rapeseed oil (bar 2), Rohex10 – the mixture of rapeseed oil with 10% n-hexane (bar 3)

The experimental studies were carried out on a diesel engine whose ECU operated on factory-calibrated control

maps designed for diesel fuel supply. The use of alternative fuels (Ro, RoHex10), characterized by lower energy content, required corrections of the control strategy by modifying injection parameters, mainly by extending the injection duration and increasing the fuel dose. This resulted in higher specific fuel consumption while maintaining comparable torque values. In this way, the ECU adapted the combustion process to the so-called “driver wish”, i.e., the driver’s demand, ensuring the required torque on the crankshaft. The physicochemical properties of rapeseed fuels (Ro, RoHex10), different from those of diesel fuel (Df), caused the observed variations in ignition delay (Fig. 5) and significantly influenced the course of the combustion process (Figs. 6 and 7). Consequently, combustion was characterized by a higher share of the diffusion phase and a less stable course compared to diesel fuel. The effect of these differences was reflected in the torque and power curves (Fig. 4). It can therefore be concluded that the EDC system played an essential compensatory role – by automatically adjusting injection parameters to the properties of alternative fuels, it enabled the maintenance of the required operating parameters of the engine despite differences in calorific value and chemical reactivity of the fuels.

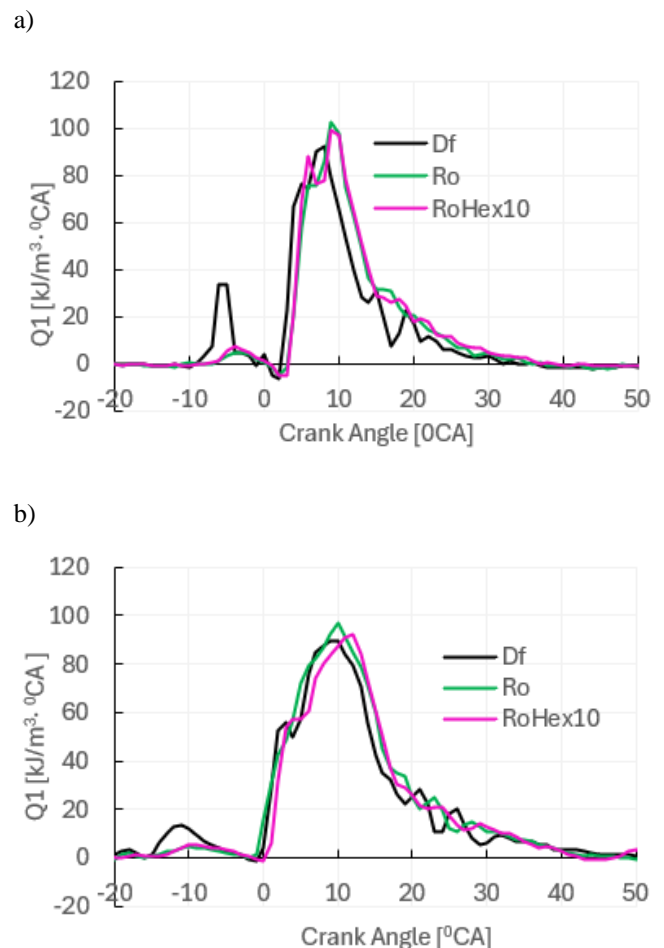


Fig. 7. The values of Heat release ($Q1$) for vehicle speeds of 50 km/h (a) and 90 km/h (b) fuelled with the test fuels: Df – diesel fuel; Ro – the rapeseed oil, Ro10hex – the mixture of rapeseed oil with 10% n-hexane

At partial loads, the ECU compensates for the fuel's lower energy content by extending the injection time and increasing the dose, which, within the limits of adaptation, allows comparable torque to be maintained. However, under maximum power demand (full utilization of the "driver wish" function), the ECU already provides the maximum injection dose specified in the control maps, taking into account boost pressure, exhaust gas temperature, and smoke limits. When using fuel with a lower calorific value, the maximum dose corresponds to a lower amount of chemical energy, which makes it impossible to reach the nominal engine power. This results in reduced maximum speed, slower acceleration, and potentially increased exhaust smoke due to less efficient combustion of the larger fuel dose. Ultimately, at partial loads, the differences are masked by ECU adaptation, while under full load, the lack of correction margin causes a drop in maximum power proportional to the energy deficit of the fuel

4. Conclusions

Based on the experimental investigations conducted, it was found that the use of the Ro10hex blend – consisting of rapeseed oil with a 10% addition of n-hexane – leads to a relative improvement in the operational parameters of a diesel engine compared to pure rapeseed oil. An increase in maximum power by approximately 4.4% and torque by 3.3% was observed, indicating the positive effect of n-hexane on the combustion process. Additionally, at higher engine speeds, a slight reduction in ignition delay (ID) was recorded, suggesting an improvement in the autoignition properties of the fuel.

However, it should be emphasized that despite these beneficial effects, both pure rapeseed oil (Ro) and its mix-

ture with n-hexane (Ro10hex) still showed significantly inferior performance parameters compared to conventional diesel fuel. This was particularly evident in the ignition delay time, which for Ro and Ro10hex was considerably longer. The analysis indicates that this is due to a different combustion mechanism: in the case of diesel fuel, combustion begins with a clearly defined kinetic phase that occurs before top dead center (TDC), whereas for Ro and Ro10hex the combustion process is predominantly diffusive and begins only after the fuel has been fully atomized and mixed with air. As a result, the peak combustion pressure occurs significantly after TDC, which negatively affects the thermodynamic efficiency of the cycle. This phenomenon was also accompanied by a more abrupt rise in combustion pressure, particularly noticeable for pure rapeseed oil, which led to increased mechanical loading of the piston-crank system.

From a physicochemical perspective, n-hexane clearly improves the practical usability of rapeseed oil as a fuel – particularly by reducing its viscosity – bringing its physical properties closer to those of diesel fuel (although not reaching its nominal values). However, the relatively high ignition temperature of rapeseed oil means that the onset of combustion for the Ro10hex mixture remains significantly delayed compared to diesel fuel. Therefore, it is justified to continue research aimed at further modifying the composition of the blend by incorporating additives that improve combustion properties, especially those that lower the ignition temperature and reduce ignition delay time, ultimately aligning the combustion characteristics more closely with those of conventional diesel fuels.

Nomenclature

CI compression ignition
DI direct injection
Hex n-heksan

ID ignition delay
Ro Rapeseed oil
TDC top dead center

Bibliography

- [1] Al-Shahrani AS. Theoretical analysis of ignition in die sel engines. *Journal of Power and Energy Engineering*. 2017; 5(6). <https://doi.org/10.4236/jpee.2017.56001>
- [2] Baczewski K, Kałdoński T. Paliwa do silników o zapłonie samoczynnym. WKŁ. Warszawa 2008.
- [3] Bayindirli C, Celik M. Investigation of combustion and emission characteristics of n-hexane and n-hexadecane additives in diesel fuel. *J Mech Sci Tech*. 2019;33:1937-1946. <https://doi.org/10.1007/s12206-019-0344-8>
- [4] Cheng C, Faurskov Cordtz R, Dyhr Pedersen T, Winther K, Langballe Førbj N, Schramm J. Investiga-tion of combustion characteristics, physical and chemical ignition delay of methanol fuel in a heavy-duty turbo-charged compression ignition engine. *Fuel*. 2023;348:128536. <https://doi.org/10.1016/j.fuel.2023.128536>.
- [5] Cisek J, Borowski A, Całkowska J, Wichary Ł. Effect of nitrON® cetane-detergent additive to B7 fuel on energy parameters and exhaust gas composition of a 6Dg locomotive with a Caterpillar C27 engine. *Combustion Engines*. 2021; 186(3):51-58. <https://doi.org/10.19206/CE-140113>
- [6] Crua C, Kennaird DA, Sazhin SS, Heikai MR, Gold MR. Diesel autoignition at elevated in-cylinder pressures. *Int J Engine Res*. 2004;5(4):365-374. <https://doi.org/10.1243/146808704323224259>
- [7] Górski K, Sander P, Longwic R. The assessment of ecological parameters of diesel engine supplied with mixtures of canola oil with n-hexane. *IOP Conf Ser Mater Sci Eng*. 2018;421(4): 042025. <https://doi.org/10.1088/1757-899X/421/4/042025>
- [8] Hardenberg HO, Hase FW. An empirical formula for computing the pressure rise delay of a fuel from its cetane number and from the relevant parameters of direct-injection diesel engines. *SAE Technical Paper*. 790493. 1979. <https://doi.org/10.4271/790493>
- [9] Hardenberg HO, Hase FW. Empirical formula for computing the pressure rise delay of a fuel from its cetane number and from the relevant parameters of direct-injection diesel engines. *SAE Preprint* 1979.
- [10] Internal combustion engine fundamentals. *Choice Reviews Online*. 1988;26. <https://doi.org/10.5860/choice.26-0943>

- [11] Jaroń A, Borucka A, Sobecki G. Assessment of the possibility of using nanomaterials as fuel additives in combustion engines. *Combustion Engines*. 2022;189. <https://doi.org/10.19206/CE-143824>
- [12] Jo S, Park S, Kim HJ, Lee JT. Combustion improvement and emission reduction through control of ethanol ratio and intake air temperature in reactivity controlled compression ignition combustion engine. *Appl Energy*. 2019;250:1418-1431. <https://doi.org/10.1016/j.apenergy.2019.05.012>
- [13] Kowalewicz A. Application of biofuels to compression ignition engines. *Mech Mech Eng*. 2005;9:69-90.
- [14] Kowalewicz A, Lotko W. Alternative fuels for automotive I.C. engines and some results of application to S.I. and C.I. engine. *Proceedings of the Third Asia-Pacific International Symposium on Combustion and Energy Utilization* n.d. 2005; 1. <https://doi.org/10.1243/095440705X6399>
- [15] Kryštofa S, Górski K, Longwic R, Smigins R, Kryštofa L. Increasing parameters of diesel engines by their transformation for methanol conversion products. *Energies*. 2021; 14(6):1710. <https://doi.org/10.3390/en14061710>
- [16] Krzemiński A, Jaworski A, Kuszewski H, Woś P. A comparative study on selected physical properties of diesel-ethanol-dodecanol blends. *Combustion Engines*. 2024;196(1):99-105. <https://doi.org/10.19206/CE-170267>
- [17] Longwic R. Diesel engine operations with alternative fuels. Boca Raton: CRC Press. 2024. <https://doi.org/10.1201/9781003466291>
- [18] Longwic R, Sander P. The characteristics of the combustion process occurring under real operating conditions of traction. *IOP Conf Ser Mater Sci Eng*. 2016;148:012071. <https://doi.org/10.1088/1757-899X/148/1/012071>
- [19] Longwic R, Sander P, Jańczuk B, Zdziennicka A, Szymczyk K. Modification of canola oil physicochemical properties by hexane and ethanol with regards of its application in diesel engine. *Energies*. 2021;14(15):4469. <https://doi.org/10.3390/en14154469>
- [20] Longwic R, Sander P, Lotko W, Gorski K, Janczuk B, Zdziennicka A et al. Self-ignition of rapeseed and n-hexane mixtures in diesel engine. *Przem Chem*. 2020;99:206-210. <https://doi.org/doi.org/10.15199/62.2020.2.3>
- [21] Longwic R, Sander P, Zdziennicka A, Szymczyk K, Jańczuk B. Combustion process of canola oil and n-hexane mixtures in dynamic diesel engine operating conditions. *Appl Sci*. 2020; 421(4):042025. <https://doi.org/10.3390/app10010080>
- [22] Lotko W. Studium zastosowań paliw alternatywnych do silników o zapłonie samoczynnym. Radom 1999.
- [23] Lotko W. Self-ignition delay and control parameters of diesel engines for different vehicle feeding systems and different fuels. *Adv Sci Technol Res J*. 2021;15(1):245-254. <https://doi.org/10.12913/22998624/132474>
- [24] Martins J, Brito FP. Alternative fuels for internal combustion engines. *Energies*. 2020;13. <https://doi.org/10.3390/en13164086>
- [25] Mohammed O, Suleiman E. The history of the internal combustion engine. *Annals of the Faculty of Engineering Hunedoara*. 2017;3.
- [26] Pirouzfard V, Zarringhalam Moghaddam A, Mirza B. Physicochemical properties and combustion performance of gas oil-fuel additives. *J Energy Resour Technol*. 2012;134(4):041101. <https://doi.org/10.1115/1.4007483>
- [27] Polska norma PN-EN 590:2013. n.d.
- [28] Rățiu S. The history of the internal combustion engine. *Annals of the Faculty of Engineering Hunedoara*. 2003;3.
- [29] Rosseel E, Sierens R. The physical and the chemical part of the ignition delay in diesel engines. *SAE Technical Paper*. 961123. 1996. <https://doi.org/10.4271/961123>
- [30] Singh AP, Mustafi NN, Sharma YC, Agarwal AK. Introduction to alternative fuels and their utilization strategies in internal combustion engines. *Energy, Environment, and Sustainability*. 2020. https://doi.org/10.1007/978-981-15-0418-1_1
- [31] Sun B, Zhao S, Zhai Y, Liu Q, Wu G, Wu H. Effect of fuel physicochemical properties on spray and particulate emissions. *ACS Omega*. 2022;7(48):44251-44265. <https://doi.org/10.1021/acsomega.2c05747>
- [32] Wajand JA, Wajand JT. *Tłokowe silniki spalinowe średnio i szybkoobrotowe*. Warszawa: WNT 2005.
- [33] Zabłocki M. *Wtrysk i spalanie w silnikach wysokoprężnych*. Wydawnictwo Komunikacji i Łączności. Warszawa 1976.
- [34] Zaharin MSM, Abdullah NR, Najafi G, Sharudin H, Yusaf T. Effects of physicochemical properties of biodiesel fuel blends with alcohol on diesel engine performance and exhaust emissions: a review. *Renew Sustain Energy Rev*. 2017;79:475-493. <https://doi.org/10.1016/j.rser.2017.05.035>
- [35] Zdziennicka A, Szymczyk K, Jańczuk B, Longwic R, Sander P. Adhesion of canola and diesel oils to some parts of diesel engine in the light of surface tension components and parameters of these substrates. *Int J Adhes Adhes*. 2015;60:23-30. <https://doi.org/10.1016/j.ijadhadh.2015.03.001>
- [36] Zdziennicka A, Szymczyk K, Jańczuk B, Longwic R, Sander P. Surface, volumetric, and wetting properties of oleic, linoleic, and linolenic acids with regards to application of canola oil in diesel engines. *Appl Sci*. 2019;9(17):3445. <https://doi.org/10.3390/app9173445>

Przemysław Sander, DEng. – Faculty of Mechanical Engineering, Lublin University of Technology, Poland.
e-mail: p.sander@pollub.pl



Sławomir Tarkowski, DEng. – Faculty of Mechanical Engineering, Lublin University of Technology, Poland.
e-mail: s.tarkowski@pollub.pl



Prof. Rafał Longwic, DSc., DEng. – Faculty of Mechanical Engineering, Lublin University of Technology, Poland.
e-mail: r.longwic@pollub.pl



The study of hydrogen consumption in 12-meter fuel cell electric urban buses

ARTICLE INFO

Received: 17 June 2025
Revised: 4 October 2025
Accepted: 6 October 2025
Available online: 14 November 2025

The fuel consumption aspect of fuel cell electric buses (FCEBs) in urban transportation is a significant research and economic issue. Following article presents the results of hydrogen consumption studies for a fleet of 12-meter FCEB under real life operating conditions in a Polish public transport company on selected routes and evaluates their operational suitability. The analysis includes factors such as the impact of weather conditions, number of stops, elevation gain, and average slope of the route. The article also discusses the challenges associated with implementing hydrogen technology in public transport and the future development prospects for this sector. The results obtained were compared with other studies in this research area.

Key words: *hydrogen consumption, hydrogen bus, FCEV, fuel cell, urban conditions*

This is an open access article under the CC BY license (<http://creativecommons.org/licenses/by/4.0/>)

1. Introduction

Key aspects regarding the vehicles used in the fleets of urban public transport companies are related to their purchase cost, quality, service costs, ergonomics, or reliability. As practice shows, a significant part of the cost of service is fuel consumption, so this is the primary factor for assessing the operational suitability of a given bus [2].

The transformation of fleets of urban public transport companies is a key challenge for both the Polish and European economies. Road transport is responsible for about 24% of total greenhouse gas emissions in the European Union [11], making it a crucial area of development. Moreover, bearing in mind the increased demand and limited supply of petroleum resources, as well as the geopolitical situation, it can be concluded that these are the factors that define strategic action for the development of low emission technologies. One of the main goals of the European Union is to popularize alternative fuels and the transportation means that use them to increase energy independence. Hydrogen, as the fuel of the future, is playing an increasingly important role in the decarbonization of public transportation. Fuel cell powered city buses offers zero emissions (except for water vapors) and significant noise reduction, which translates into environmental and health benefits especially in crowded European cities. In addition, the development of this technology could make a significant contribution to reducing fossil fuel imports in the future.

A key advantage of hydrogen buses is their larger range compared to electric buses powered solely by batteries. What is more, the tanks of FCEVs can be filled with hydrogen in just a few minutes, a time similar to refuel conventional vehicles [14].

2. Legal background

Since the research presented in this article was performed entirely in Poland, the legal aspects refers precisely to the regulations in force in this country and in the European Union. The Act on Electromobility and Alternative Fuels and the "Polish Hydrogen Strategy to 2030 (with a perspective to 2040)" are two main documents defining legislative framework in Poland that presupposes a comprehensive

development of the country hydrogen network [21, 28]. They regulate, in particular, the deployment of vehicle charging infrastructure, CNG refueling, and the possession of zero emission vehicles in the fleets of companies providing public services.

In order to implement the hydrogen economy, the Hydrogen Strategy identifies priority areas for state intervention. These include building a minimum of 32 publicly accessible refueling stations and related infrastructure, developing low carbon hydrogen production technologies (primarily through RES electrolysis), enhancing national industrial competences and expanding the use of hydrogen in industry, transportation, and energy sectors. The plan calls for the creation of a national production capacity for hydrogen powered vehicles, the deployment of hydrogen fleets in urban areas, and the promotion of pilot projects in the field of public transportation. The strategy also emphasizes the creation of at least five regional "hydrogen valleys" as integrated ecosystems linking hydrogen production, storage, distribution and utilization in order to enable the creation of a coherent hydrogen market on a national scale.

The 2020 "European Hydrogen Strategy" and the European Green Deal both state that hydrogen will be crucial in the process of reaching climate neutrality by 2050 [3, 4]. The "Fit for 55" package, which includes the RED III Directive, AFIR, ETS, and new vehicle emission standards, among other measures, establishes aggressive goals for deploying alternative fuels and boosting the contribution of RES [7, 18, 26]. In the area of the market for decarbonized gases, significant is also the proposed directive on renewable gases, including hydrogen, which will set rules for their certification and integration into the energy market. In addition to promoting investments in hydrogen technologies, the new rules are meant to guarantee that these technologies adhere to sustainable development principles. A significant factor that might accelerate the commercialization of hydrogen in the transportation industry is the establishment of consistent, transparent and uniform regulations throughout the whole European Union.

3. Fuel consumption measurement methods

For many years, the fuel consumption of buses was measured by empirical methods on the basis of refueling to full before and after completing a route and comparing this difference with the distance traveled [1]. This method, despite its simplicity, does not provide a true picture of the vehicle operation in urban conditions, where acceleration and braking cycles in combination with load variability play an important role [16]. With advances in technology and the introduction of legislative requirements, it has become necessary to implement more precise and repeatable methods of fuel consumption measurement in buses.

In the European Union, the most important legal act regulating the measurement of fuel consumption and emissions in trucks and buses is Regulation (EU) 2017/2400 [25], which makes the use of the VECTO simulation tool mandatory, which from January 1, 2019 applies, amongst others, to new models of buses for passenger transport exceeding total mass of 5 tons. VECTO is not a classic road test, but a software tool that, using actual vehicle technical data (e.g. weight, drivetrain type, rolling resistance, engine parameters), simulates fuel consumption and CO₂ emissions over standard driving cycles. For city buses, the so called "Urban Bus" cycle is typically used, which takes into account frequent stops, low speeds and varying loads characteristic of urban traffic.

The Standardized On-Road Test cycles are becoming increasingly important in the practice of evaluating fuel consumption in city and intercity buses [19]. These tests, while not part of the formal approval procedure in the European Union, are a widely accepted industry standard, used primarily to compare fuel consumption between different bus models under real world conditions. SORT is a set of three differentiated driving cycles designed to reflect typical operational profiles of buses in a variety of operating conditions, from city driving to intercity conditions. As a result, SORT test results provide more useful data for operators and decision makers who want to compare the fuel efficiency of competing bus models under similar operating conditions. The SORT tests include three driving scenarios:

SORT 1 – simulates urban driving with a very high frequency of stops and starts. Typical for densely built-up areas of central cities;

SORT 2 – corresponds to suburban conditions, with fewer stops and higher average speed;

SORT 3 – replicates intercity or expressway driving conditions, with infrequent stops and relatively high travel speeds.

Each of the SORT cycles is implemented with certain parameters: number of stops, stopping time, section length, average and maximum speeds, as well as vehicle weight (with simulated passenger load). Measurement of fuel consumption is carried out using precision measuring devices mounted on the vehicle [13]. An important element is the maintenance of consistent test conditions, which makes it possible to obtain results that are comparable regardless of location or operator.

The development of alternative propulsion systems, such as hybrid, electric and gas powered buses, has forced

change in the approach to measuring fuel consumption. In the case of hybrids, both conventional fuel consumption and electricity consumption are taken into account [17, 20]. VECTO and type approval procedures often take into account the so called fuel energy equivalent, converting fossil fuel to electric energy equivalent, which allows comparison of vehicles with different power sources. In such case energy consumption is expressed in kWh per 100 km. For conventional diesel fuel its gravimetric density is 12.2 kWh/kg while for gaseous hydrogen pressurized to 350 bar it is 33.3 kWh/kg [23].

4. Hydrogen refueling infrastructures

At the moment, there are 8 publicly accessible hydrogen refueling stations in Poland, operated by two operators: Orlen S.A. and PAK-PCE Stacje H₂ Sp. z o.o. (see Fig. 1).

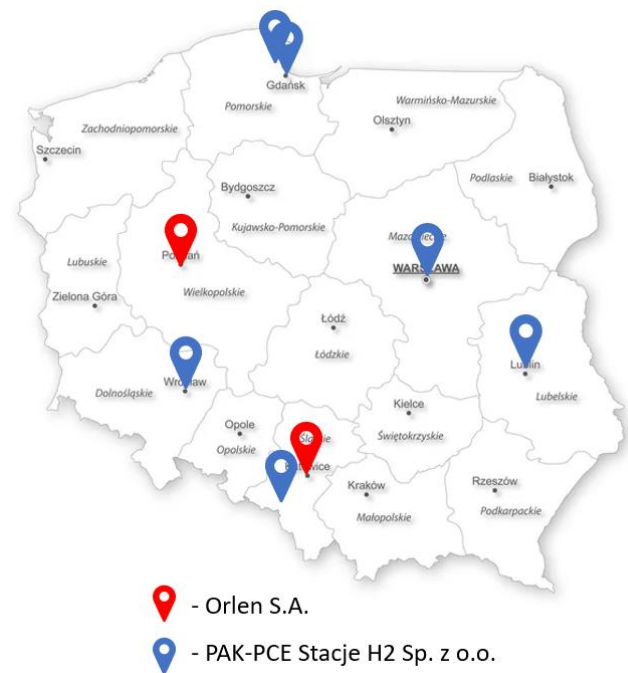


Fig. 1. Publicly accessible hydrogen refueling stations in Poland [12,22]

As a rule, the use of these stations requires appropriate precautions, but hydrogen refueling itself is quite similar to pouring CNG and does not require any additional authorizations. The process of filling a hydrogen tank usually takes from a few to several minutes. For buses, the applicable standard is the so called H35, indicating a maximum pressure of 350 bar and a maximum filling rate of 120 g/s. These values are defined by the SAE J2601 standard in force throughout the European Union [24].

In the case of the research presented in this paper, since no publicly available hydrogen refueling station was available in the region, the refueling of buses tanks was carried out using a so called mobile refueling station (see Fig. 2).

Due to its construction and the lack of a hydrogen pressurization system, the maximum refueling pressure was limited to 200 bar only, which in practice resulted in a limitation of the maximum range of the vehicles.



Fig. 2. Mobile hydrogen refueling station

5. Scope of research

5.1. Fleet

The classification of buses by size is a conventional classification that usually refers to their length [15]. According to one of the accepted classifications, the following types of buses are distinguished: MINI (up to 7.5 m), MIDI (7.5 to 10.5 m), MAXI (10.5 to 13 m) and MEGA (over 13 m). Now all FCEBs in Poland are classified as MAXI.

The research subject was the fleet of fourteen Solaris Urbino 12 Hydrogen buses (see Fig. 3) serving urban bus routes within the city public transportation company. Selected parameters of tested vehicles are presented in Table 1.

Table 1. Selected parameters of tested bus model [5]

Model	Solaris Urbino 12 Hydrogen
Length [mm]	12,000
Width [mm]	2550
Height [mm]	3000
Gross mass [kg]	19,200
Fuel cell power [kW]	70
Traction battery [kWh]	30.47
Electric motor power [kW]	2 × 125
Hydrogen tank capacity [kg]	37.5 (5 × 312 L)
Hydrogen tank max. pressure at 15°C [bar]	350
Heating system	AC with CO ₂ heat pump
Max. range [km]	350



Fig. 3. Tested bus model – Solaris Urbino 12 Hydrogen

5.2. Routes

The evaluation of hydrogen consumption under operating conditions was carried out for three bus lines on which the selected buses operated during February of 2025. The

trips were performed from Monday to Friday during day-time.

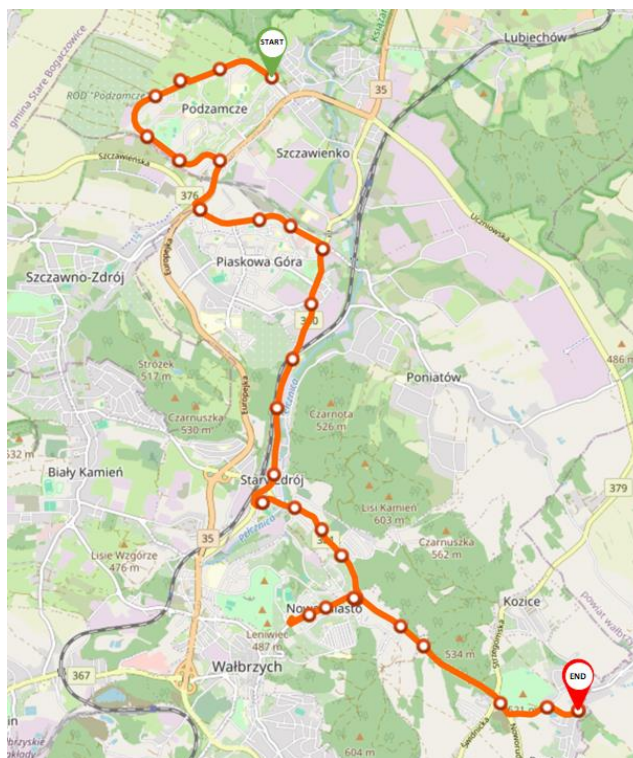


Fig. 4. Course of route 1



Fig. 5. Profile of route 1

Table 2. Route 1 parameters

Parameter	Value
Length [km]	15.6
Number of stops [-]	28
Elevation gain [m]	113
Total climb [m]	217
Total descent [m]	126
Avg. slope [%]	0.72

The first route is the longest of the routes considered, with a one way length of 15.6 kilometers. At the same time, it is the route with the smallest number of stops equal to 28. The average slope of the route is 0.72%, which ranks it in the middle of the other routes in this regard.

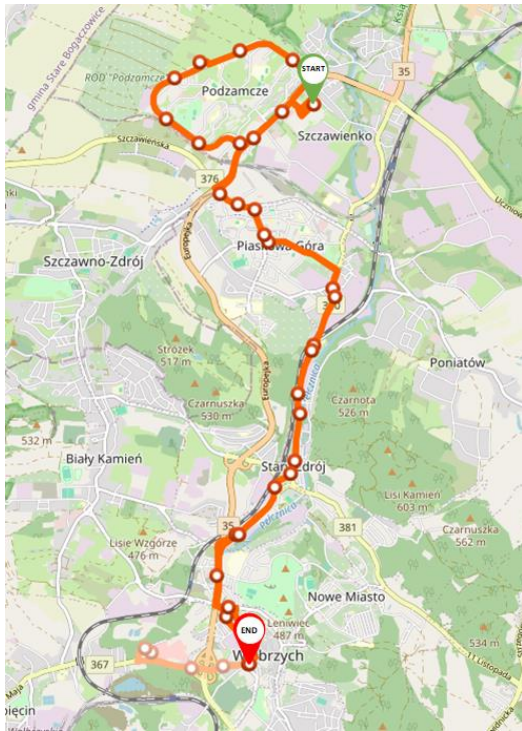


Fig. 6. Course of route 2

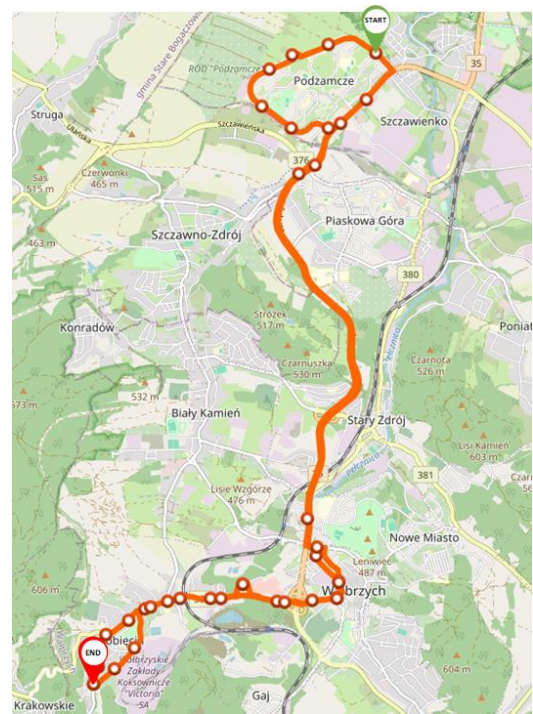


Fig. 8. Course of route 3



Fig. 7. Profile of route 2



Fig. 9. Profile of route 3

Table 3. Route 2 parameters

Parameter	Value
Length [km]	13.7
Number of stops [-]	33
Elevation gain [m]	73
Total climb [m]	128
Total descent [m]	60
Avg. slope [%]	0.53

Route number two is the shortest among all analyzed routes, with a length of 13.7 kilometers. It is also the route with the smallest average slope of 0.53% and the lowest elevation of 73 meters. Moreover, the total climb of 128 meters is significantly less from the others by means of approx. 100 m. The number of stops on the route is 33, placing it in the mid-range when compared to the other options.

Table 4. Route 3 parameters

Parameter	Value
Length [km]	14.4
Number of stops [-]	36
Elevation gain [m]	130
Total climb [m]	231
Total descent [m]	102
Avg. slope [%]	0.90

The third route under consideration is characterized by the highest number of stops of 36 and the highest elevation of 130 meters. Its distance is 14.4 kilometers, and the average gradient is 0.90%. Noteworthy, this route features the longest stretch without stops measuring approximately 5 kilometers. The profile of this route is characterized by the smoothest elevation changes along its entire course.

5.3. Weather conditions

In the operation of FCEBs ambient temperature plays an important role in both the efficiency of the fuel cell system and the energy requirements of onboard systems. It has

a particularly noticeable impact during transitional periods, when atmospheric conditions change noticeably. During the period under review (February), outdoor temperatures remained below zero typically for the winter.

The fuel cell in most FCEBs models operates optimally in the temperature range of 60–80°C. During winter months, such as February, low ambient temperature increases the time required to reach its operating value. Until internal conditions stabilize, the system operates with reduced efficiency, resulting in increased instantaneous fuel consumption. Low temperature operation can also affect the hydrogen management system, including the moisture condition of the proton membrane, whose excessive dehydration or condensation can limit the efficiency of chemical conversion [27].

For research purposes, archival data from the Institute of Meteorology and Water Management for the monitoring station located in Szczawno-Zdrój was used [6].

5. Results and discussion

Due to the number of vehicles tested amounting to 14 units, data of hydrogen consumption was collected on the basis of readings from the onboard system. Presented results refer to hydrogen consumption in February, as the month with the most relevant experimental data. The results of considerations are presented in table number 5.

Table 5. Average hydrogen consumption in February

Parameter	Route 1	Route 2	Route 3
Length [km]	15.6	13.7	14.4
Number of stops [-]	28	33	36
Elevation gain [m]	113	73	130
Total climb [m]	217	128	231
Total descent [m]	126	60	102
Avg. slope [%]	0.72	0.53	0.90
Total distance [km]	3199	4831	6037
Total H ₂ [kg]	284.63	424.13	549.75
Avg. H ₂ consumption [kg/100 km]	8.90	8.78	9.11

The green color indicates the parameters that favor the lowest fuel consumption, while the red color indicates the parameters that are least desirable in this sense. Yellow color indicates the values that are in between. The lowest average hydrogen consumption (8.78 kg/100 km) was observed for route number 2, which features the lowest elevation gain, average slope and total climb. It is also the shortest route among those considered. As the study showed, an increase in the number of stops correlates with increased fuel consumption, which suggests that this is a factor that has a direct impact on this parameter. The same applies to elevation gain and total climb, which was to be expected given the conversion of kinetic into potential energy. The highest hydrogen demand was recorded for the route 3 with the highest elevation gain, total climb and average slope. It was also the route with the most amount of stops.

Figure 10 shows the average daily fuel consumption for the three routes investigated in relation to the average daily ambient temperature.

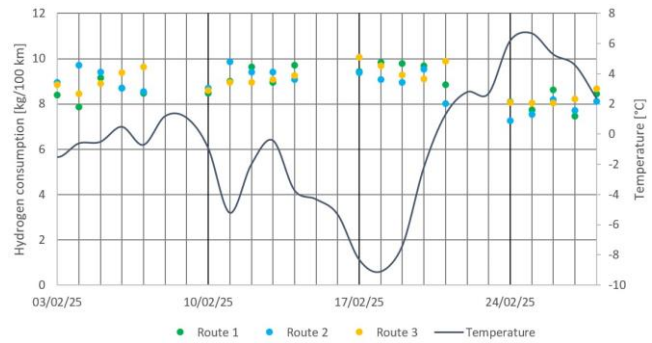


Fig. 10. Average fuel consumption in relation to temperature

The temperature remained mainly below zero for the first three weeks of research with a noticeable drop in third week, however despite the evident drop in temperature, there was no significant change in hydrogen consumption. In the final fourth week there an increase in temperature was observed, which correlated with a noticeable reduction in fuel consumption during this time. The most likely reason for this is the changing energy demand from auxiliary systems, in particular the heating and ventilation system. In February, at low temperatures, the heating of the passenger compartment is one of the main energy loads. FCEBs, unlike internal combustion vehicles, do not produce a large amount of waste heat, so all heating energy must be supplied from the battery or from auxiliary heating systems.

As spring time approaches, the demand for heating gradually decreases, which should result in a reduction in the energy load on the propulsion system. In addition, there is still no significant use of air conditioning during this period, which means that the onboard systems do not generate significant additional energy losses. With these arguments in mind, it makes sense to carry out further research in this area for the following months. In March and April, when the average outside temperatures start to rise, the cell should reach its operating temperature faster and its operation becomes more stable. Thus, the influence of weather conditions on the energy generation process should decrease. This means that less energy is used to warm up the system to a ready state, and the process of converting hydrogen into electricity itself is carried out with higher efficiency.

Finally, the results of the study were compared with those obtained by other research teams as can be seen in Table 6. The results obtained do not differ significantly from the others, which proves that the methodology used is correct and can be applied in further studies.

Table 6. Results of comparable studies [8–10]

Location	Date	Bus model	Avg. H ₂ consumption [kg/100 km]
Bolzano, Italy	2021 16 months	Mercedes Citaro O530	9.31
		Solaris Urbino 12 Hydrogen	10.07
California, USA	2013 14 months	Van Hool A300L FC	9.74
9 cities in Europe	2017 72 months	Mercedes Citaro O530	9.00

Acknowledgements

The authors would like to express their gratitude to MZUK in Walbrzych for providing the exploitation data for this publication.

Nomenclature

AC	air conditioning	FCEV	fuel cell electric vehicle
AFIR	alternative fuel infrastructure regulation	RED	renewable energy directive
CNG	compressed natural gas	RES	renewable energy sources
ETS	emissions trading system	SORT	standardized on road test
EU	European Union	VECTO	vehicle energy consumption calculation tool
FCEB	fuel cell electric bus		

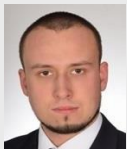
Bibliography

- [1] Chłopek Z, Gis W, Menes E. Wprowadzenie do tematyki oceny zużycia paliwa przez autobusy komunikacji miejskiej. *Transport Samochodowy* 2004.
- [2] Chłopek Z, Tułodziecki M, Sypowicz R. Badania zużycia paliwa przez autobusy komunikacji miejskiej. *Zeszyty Naukowe Instytutu Pojazdów*. 2004;4:101-108.
- [3] Communication from the Commission to the European Parliament, the Council, the European Economic and Social Committee and the Committee of the Regions: “Fit for 55”: delivering the EU’s 2030 Climate Target on the way to climate neutrality. 2021.
- [4] Communication from the Commission to the European Parliament, the Council the European Economic and Social Committee and the Committee of the Regions: A hydrogen strategy for a climate-neutral Europe. 2020.
- [5] Dane techniczne autobusu Solaris Urbino 12 Hydrogen. https://www.solarisbus.com/public/assets/Biuro_prasowe/2021_10_Transexpo_Kielce/Dane_techiczne_Urbino_12_hydrogen_Transexpo_PL.pdf (accessed on 20.08.2025).
- [6] Dane z bazy danych Systemu Hydrologii IMGW-PIB z posterunku w Szczawnie-Zdroju. <https://rafalracyznski.com.pl/imgw-archiwum/> (accessed on 21.05.2025)
- [7] Directive (EU) 2023/2413 of the European Parliament and of the Council of 18 October 2023 amending Directive (EU) 2018/2001, Regulation (EU) 2018/1999 and Directive 98/70/EC as regards the promotion of energy from renewable sources, and repealing Council.
- [8] Dolman M, Madden B. Strategies for joint procurement of fuel cell buses: a study for the fuel cells and hydrogen joint undertaking. *Fuel Cells Hydrogen Joint Undertaking* 2018.
- [9] Estrada Poggio A, Balest J, Zubaryeva A, Sparber W. Monitored data and social perceptions analysis of battery electric and hydrogen fuelled buses in urban and suburban areas. *J Energy Storage*. 2023;72:108411. <https://doi.org/10.1016/j.est.2023.108411>
- [10] Eudy L, Post M, Jeffers M. Zero emission bay area (ZEBA) fuel cell bus demonstration results: fifth report. Golden, CO 2016. <https://doi.org/10.2172/1260344>
- [11] European Commission. Climate Action Progress Report. 2023.
- [12] Ewidencja Infrastruktury Paliw Alternatywnych. Bazy ładowania i tankowania. <https://eipa.udt.gov.pl/> (accessed on 02.06.2025)
- [13] Fuć P, Rymaniak L, Ziółkowski A, Andrzejewski M, Daszkiewicz P. Pollutant emissions analysis of a hybrid drive bus in a SORT 2 test. *IOP Conf Ser Mater Sci Eng* 2018;421:042020. <https://doi.org/10.1088/1757-899X/421/4/042020>
- [14] Gis W, Menes E, Waśkiewicz J. Elektryfikacja i wodorozacja transportu samochodowego w Polsce. *Syst Logistyczne Wojsk*. 2016;44:83-94.
- [15] Gładysz A, Czech P, Łazarz B, Matyja T, Juzek M. Uwarunkowania techniczne dotyczące pojazdów wykorzystywanych w regularnym przewozie osób na przykładzie terytorialnych linii trolejbusowych (in Polish). *Autobusy Tech Eksploat Syst Transp*. 2016;17:1688-1693.
- [16] Huseyin B, Orkun O. The development and optimization of the bus driving cycle for public transportation and mobility systems. *Therm Sci*. 2025;29:641-650. <https://doi.org/10.2298/TSCI240922001B>
- [17] Kozłowski E, Zimakowska-Laskowska M, Dudziak A, Wiśniowski P, Laskowski P, Stankiewicz M et al. Analysis of instantaneous energy consumption and recuperation based on measurements from SORT runs. *Appl Sci*. 2025;15:1681. <https://doi.org/10.3390/app15041681>
- [18] Lilico A, Drury D. European Parliament: Directorate-General for Internal Policies of the Union. In *The EU Emissions Trading System: Method and Effects of Free Allowance Allocation—In-Depth Analysis* 2023.
- [19] Magryta P, Grabowski Ł, Barański G, Wendeker M. Toxic emission during road tests of urban bus. *Adv Sci Technol Res J*. 2023;17:16-26. <https://doi.org/10.12913/22998624/172413>
- [20] Milushev GS, Kirilova-Blaogoeva KS. Accredited testing of energy consumption of electrical vehicles according to e-sort protocol. 28th Int. Sci. Symp. *Metrol. Metrol. Assur*. 2018;220-225.
- [21] Ministry of Climate and Environment. Polish Hydrogen Strategy until 2030 with an outlook until 2040. Poland 2021.
- [22] ORLEN otworzył stację wodorową w Poznaniu. <https://www.orklen.pl/pl/o-firmie/media/komunikaty-prasowe/2024/Czerwiec-2024/orklen-otworzyl-stacje-wodorowa-w-poznaniu> (accessed on 23.05.2025)
- [23] Pistidda C. Solid-state hydrogen storage for a decarbonized society. *Hydrogen*. 2021;2:428-443. <https://doi.org/10.3390/hydrogen2040024>
- [24] Reddi K, Elgowainy A, Rustagi N, Gupta E. Impact of hydrogen SAE J2601 fueling methods on fueling time of light-duty fuel cell electric vehicles. *Int J Hydrogen Energy* 2017;42:16675-16685. <https://doi.org/10.1016/j.ijhydene.2017.04.233>
- [25] Regulation (EU) 2017/2400 of 12 December 2017 implementing Regulation (EC) No 595/2009 of the European Parliament and of the Council as regards the determination of the CO₂ emissions and fuel consumption of heavy-duty vehicles and amending Directive 2007/
- [26] Regulation (EU) 2023/1804 of the European Parliament and

of the Council of 13 September 2023 on the deployment of alternative fuels infrastructure, and repealing Directive 2014/94/EU.

- [27] Tawalbeh M, Alarab S, Al-Othman A, Javed RMN. The operating parameters, structural composition, and fuel sustainability aspects of PEM fuel cells: a mini review. *Fuels*. 2022;3:449-474. <https://doi.org/10.3390/fuels3030028>
- [28] The Act on Electromobility and Alternative Fuels. n.d.

Jędrzej Matla, MEng. – PhD student, Wrocław University of Science and Technology.
e-mail: jedrzej.matla@pwr.edu.pl



Prof. Andrzej R. Kaźmierczak, DSc., DEng. – Faculty of Mechanical Engineering, Wrocław University of Science and Technology
e-mail: andrzej.kazmierczak@pwr.edu.pl



Michał Grzebyk, MEng. – PhD student, Wrocław University of Science and Technology.
e-mail: michal.grzebyk@pwr.edu.pl



Tomasz Hardy, DSc., DEng. – Faculty of Mechanical and Power Engineering, Wrocław University of Science and Technology
e-mail: tomasz.hardy@pwr.edu.pl



Analysis of biodegradable additives in marine fuels and their effect on toxic exhaust emissions

ARTICLE INFO

This study investigates the influence of biodegradable additives, specifically butyl alcohol, ethyl alcohol, and demineralized water, on the emission of toxic compounds from marine diesel engines. Experiments were conducted using a Sulzer 6AL20/24 engine fueled with conventional diesel and two fuel blends containing alcohols and water. Emissions of NO_x, CO, CO₂, and O₂ were measured and analyzed via statistical modeling. Results indicate that component fuels can reduce NO_x emissions by up to 7.5%, mainly due to the cooling effect of water in the fuel mixture. However, effects on CO emissions were less consistent, varying with engine load and fuel composition. CO₂ emissions remained similar across fuels, while the presence of oxygenated compounds influenced oxygen levels. The findings support the potential of biodegradable fuel additives in reducing marine engine emissions. However, further studies are necessary to optimize combustion and meet environmental regulations.

Received: 8 July 2025

Revised: 26 September 2025

Accepted: 7 October 2025

Available online: 14 November 2025

Key words: marine diesel combustion engine, biodegradable fuels, butanol, exhaust emissions, emission modelling

This is an open access article under the CC BY license (<http://creativecommons.org/licenses/by/4.0/>)

1. Introduction

Maritime transportation is a major pillar of the global economy, accounting for about 80% of global trade by volume [26, 32]. The operation of internal combustion engines on vessels involves significant emissions of pollutants, including nitrogen oxides (NO_x), sulfur oxides (SO_x), particulate matter (PM), polycyclic aromatic hydrocarbons (PAHs) and other toxic compounds [21, 22]. These compounds have negative effects on both human health and the environment, contributing to climate change, acidification of ecosystems and degradation of air quality in coastal areas [31].

The International Maritime Organization (IMO) is introducing increasingly stringent standards for the emissions of harmful compounds from reciprocating internal combustion engines, including restrictions on NO_x (Fig. 1) and SO_x emissions (MARPOL Annex VI agreement, including Tier I, II and III standards) [16, 32, 33]. The IMO is not the only organization placing restrictions on toxic emissions. The EPA (U.S. Environmental Protection Agency) is introducing stricter standards for particulate matter (PM), nitrogen oxides and carbon dioxide (Tier IV) emissions – a 60% reduction from the previous standard [34]. The European Union is not lagging behind EPA regulations. The EU is introducing further restrictions on carbon monoxide (CO), hydrocarbons (HC), nitrogen oxides (NO_x) and particulate matter emissions – the Stage 5 document [3, 16]. The document talks about a 72% reduction in nitrogen oxides and hydrocarbon emissions compared to Stage IIIa, and a 93% reduction in PM. One should not forget the global player, the People's Republic of China. China currently has Stage 2 regulations, which are very similar to EPA Tier 3 [3].

With standards being introduced, there is growing interest in alternative fuels and additives that can reduce exhaust gas toxicity [35]. One area of intense research is biodegradable fuel additives, including fatty acid methyl esters

(FAMES), higher alcohols (e.g., butanol), ethers or biopolymers [1, 29].

Studies have shown that the use of biodegradable fuel additives can lead to reductions in emissions of particulate matter, hydrocarbons and PAHs, mainly through improved combustion and higher oxygen content in the fuel mixture [13, 15, 20]. The effect of such additives on the emission of NO_x and other toxic components of exhaust gases under the operating conditions of marine engines is still not clearly defined, especially considering the specificity of loads and the variety of engine types used in shipping [8, 29].

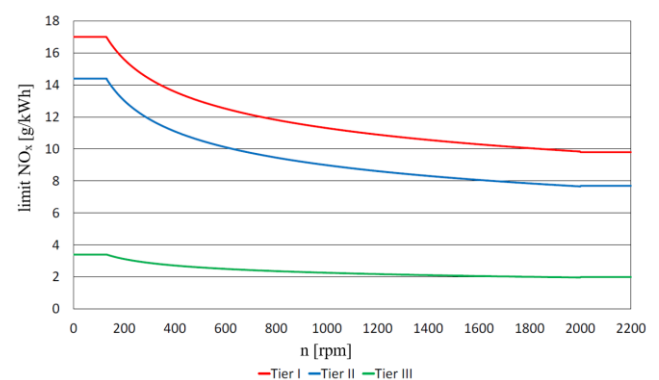


Fig. 1. Maximum allowable NO_x emissions according to MARPOL regulations with a breakdown into Tier I, II and III standards depending on nominal engine speed [32, 35]

The purpose of this study is to analyze the possibility of using biodegradable additives (butyl alcohol, methyl alcohol, demineralized water) in marine fuels and to evaluate their impact on the emission of toxic compounds in the exhaust gas of marine internal combustion engines. Particular emphasis was placed on the compounds of greatest environmental and health importance, such as NO_x and CO.

The results of the study can make an important contribution to the process of adapting shipping to increasingly stringent emission standards, and are a continuation of the authors' previous work [6, 7, 30].

2. Characteristic of harmful compounds emitted by engines

Exhaust gas is formed by the oxidation of hydrocarbons contained in the fuel with oxygen from the air. Under actual conditions, the combustion process is partial and incomplete, leading to the emission of products (Fig. 2) such as nitrogen oxides (NO_x), carbon oxides (CO_x), unburned hydrocarbons (HC), particulate matter (PM) and sulfur oxides (SO_x) [13]. The proportion of toxic components is 0.2–0.26% of the exhaust mass, with total specific emissions reaching 16–22 g/kWh [23, 25]. When operating a marine engine at a nominal power of 50,000 kW, the mass of toxic substances emitted will be 20–25 tons per day.

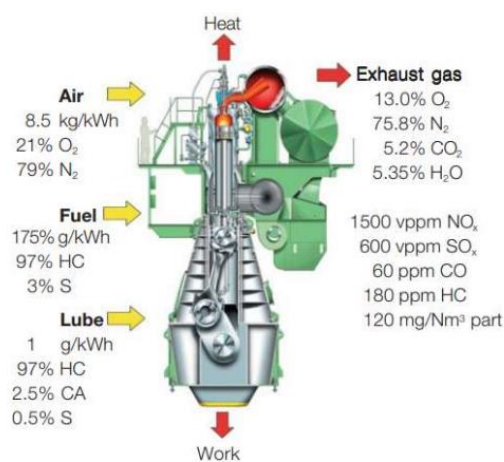


Fig. 2. Flow process and typical exhaust gas composition from marine engines [11]

Nitrogen oxides are formed by the reaction of nitrogen with oxygen at high temperatures. The concentration of nitrogen oxides increases exponentially relative to the maximum combustion temperature [23]. Mechanisms of NO_x formation include the Zeldovich model (thermal), the Fenimore mechanism (so-called fast NO) and the process of NO_x formation from nitrogen contained in the fuel [23]. NO_x emissions in medium-speed engines are about 13.8 g/kWh (59 kg/ton), and in slow-speed engines they reach 18.7 g/kWh (84 kg/ton) [16, 17, 23, 25, 27]. NO_x compounds have high toxicity – nitric oxide (NO) has an affinity for hemoglobin 1.500 times greater than oxygen, which limits the blood's ability to carry oxygen [23]. NO_2 concentrations above 0.12 mg/dm³ cause irritation of mucous membranes, and at 0.38–1.33 mg/dm³ can lead to death [19, 23].

Carbon monoxide is formed under conditions of local oxygen deficiency ($\lambda < 1$), low load and underheating of the engine, and as a result of late injection or improper fuel atomization [23]. For marine reciprocating engines, CO emissions average 1.8–2.1 g/kWh [14]. CO binds to hemoglobin about 210–300 times more strongly than oxygen, causing hypoxia [12, 14, 17, 18, 21, 23].

Unburned hydrocarbons in the flue gas are formed as a result of incomplete combustion, as well as wall and gap effects. The crevice effect is related to the extinguishing of the flame in the narrow spaces between combustion chamber components [27]. HC emissions are about 0.5–0.6 g/kWh [23, 27] and increase in proportion to lubricating oil consumption – a doubling of consumption results in a 6–18% increase in HC emissions [23]. Unburned hydrocarbons have irritant and toxic effects, leading to, among other things, damage to the bone marrow and circulatory system [12, 23].

Particulate matter (PM) consists of both soluble fractions (SOF), containing heavy aromatic and aliphatic hydrocarbons, and insoluble fractions, which are dominated by soot, sulfates and metals from fuel and wear products of engine components [13]. Soot forms under conditions of local oxygen deficiency at temperatures of 1900–2300 K, reaching a diameter of 0.1–0.5 μm as early as about 1 ms after the onset of combustion [23]. The proportion of oil-based particles in the total PM mass varies from 2% to as much as 40%, depending on the source [23, 27]. Although soot itself is not highly toxic, its porous structure makes it adsorb other toxic compounds, making it particularly dangerous to the respiratory system [19, 23].

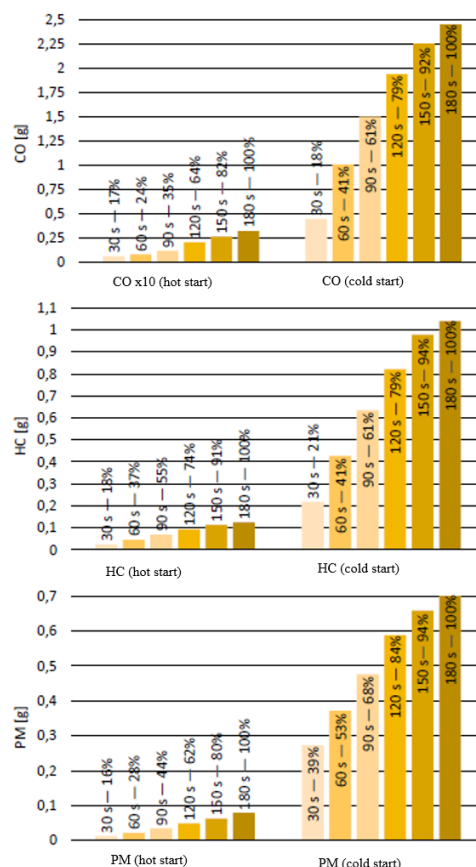


Fig. 3. Comparison of the contribution of individual operating periods to the total emissions during idle running (cold start) [4]

Sulfur oxides (SO_x) are formed by the oxidation of sulfur contained in fuel. The predominant product is SO_2 , of which 2–4% is oxidized to SO_3 , forming sulfuric acid in the

atmosphere and contributing to acid precipitation [19, 23]. SO₂ emissions are calculated according to the relationship: $eSO_2 = 20\%S$ [kg/ton of fuel] or $eSO_2 = 4.2\%S$ [g/kWh], where %S is the mass proportion of sulfur in the fuel [21, 23]. It is interesting to note that increased sulfur content in the fuel may contribute to a decrease in NO_x emissions, since sulfur takes up some of the available oxygen, reducing its contribution to the formation of nitrogen oxides [23, 30].

The thermal condition of the engine has a significant impact on emissions. During a cold start, CO, HC and PM emissions are many times higher than during a hot start. In the first 60 seconds of cold engine operation, up to 53% of the total PM emissions are produced, and about 41% of CO and HC emissions are related to the entire 180-second duty cycle. For a hot start, emissions are stable and much lower (Fig. 3) [2, 23].

3. Alternative fuels used in compression-ignition piston internal combustion engines

In the context of reducing emissions of toxic exhaust components from compression-ignition reciprocating internal combustion engines, alternative fuels, including alcohols as biofuels, are becoming increasingly important. The use of these fuels is driven by the need to meet increasingly stringent emission standards [18, 23].

Alcohol fuels, such as ethanol and butanol, are being researched because of their aerobic properties, which promote improved combustion, reducing hydrocarbon (HC) and carbon monoxide (CO) emissions. Ethanol has a high cetane number and a good ability to mix with diesel fuel. However, its use leads to a lower heating value of the fuel mixture. It requires appropriate modifications in the design of the engine injection system [23, 30]. Butanol, thanks to its higher calorific value and lower hygroscopicity compared to ethanol, is a more favorable component for creating fuel mixtures. In contrast, its share in the mixture can significantly affect the stability of engine operation and combustion parameters [10, 23, 30]. The use of alcohols also requires consideration of their effect on the physicochemical properties of the fuel, such as viscosity, density and flash point, which directly affects the performance of the fuel system and the dynamics of the combustion process [10, 23].

In parallel, work is being carried out on the use of biofuels, particularly higher fatty acid methyl esters (FAME), which are mainly made from vegetable oils such as rapeseed oil. Biofuels of this type have a high oxygen content, which is conducive to reducing CO and HC emissions, as well as lowering exhaust smoke emissions. Nevertheless, an increase in nitrogen oxide (NO_x) emissions is observed under certain engine operating conditions, due to the higher combustion temperature of the fuel-air mixture and the presence of oxygen in the structure of the fuel molecules [11, 17, 23, 28]. Methyl esters exhibit a lower heating value compared to diesel fuel, as well as higher viscosity and density, which affect the characteristics of the fuel injection process and its atomization in the combustion chamber [9, 23]. Also important are the performance characteristics of biofuels, such as susceptibility to oxidation, hygroscopicity and corrosive properties, which may limit their long-term

use without requiring changes in the design of fuel supply systems [10, 23].

The results of the study indicate that the use of rapeseed oil methyl esters (REE) and ethyl alcohol (EtOh) in the developed BIOXDIESEL fuel (variants M1 to M4 – shown in Table 1) by Struś [28] leads to a slight reduction in the indexed power and torque of CI engines, which is a consequence of the lower calorific value of these fuels compared to conventional diesel fuel. At the same time, a favorable effect of biofuels on the reduction of exhaust smoke emissions, stability of engine operation and reduction of emissions of particulate matter, carbon monoxide and unburned hydrocarbons is observed, confirming their potential in reducing toxic emissions [5, 11, 18, 28]. However, in the case of biodegradable fuels, it is necessary to take into account the increase in NO_x emissions, which poses a significant challenge in terms of meeting current emission standards [5, 16, 28].

Table 1. Comparison of physicochemical properties of varieties of Biodiesel fuel and diesel oil, where M1 70% DF + 30% REE, M2 70% DF + 4% EtOh + 26% REE, M3 70% DF + 6% EtOh + 24% REE, M4 70% DF + 10% EtOh + 20% REE [8]

Property	DF	M1	M2	M3	M4
Density T ₀ = 15 °C [kg/dm ³]	0.835	0.848	0.845	0.844	0.840
Kinematic viscosity T ₀ = 40 °C [mm ² /s]	2.66	3.52	2.40	2.40	2.33
Cetane index	52.5	51	50.5	50	49
Flash point [°C]	65	58	32	26	22
Cloud point [°C]	-16	-15	-19	-23	-22
Cold filter plugging point (CFPP) [°C]	-31	-29	-33	-34	-37
Pour point [°C]	-40	-35	-37	-38	-41
Water content in fuel [mg/kg]	44.4	66	92.4	97.1	103

To summarize, the use of alternative fuels, both alcohol and biofuels, is an important research direction for reducing emissions of harmful compounds from marine reciprocating internal combustion engines. Despite some operational and technological limitations, these fuels allow significant reductions in emissions of selected toxic components of exhaust gases, which can be of significant importance in the context of the implementation of environmentally friendly strategies in marine transportation [5, 23, 28].

4. Research plan and research object

4.1. Research plan

The research was carried out according to a simplified experiment plan. The simplified experiment plan contains 9 combinations resulting from 3 input quantities, where each quantity (speed – n, torque – M, fuel mixture – PAL) can take integer values in the range $\langle -1, 1 \rangle$. Based on previously conducted studies [6, 7, 30], the values of the parameters constituting a simplified experimental plan were determined. The assumed values of the input parameters are shown in Table 2, where the name of the fuel that was fed to the engine during the test is denoted by PAL. Three types of fuel were supplied to the engine: diesel fuel and two mixtures containing diesel fuel (DF), butyl alcohol (BOh), ethyl alcohol (EtOh), and water (W). The fuels used in the

test contained the following volume percentages of the individual components:

- DF 100% DF
- M1 60% DF, 35% BOh, 3% EtOh, 2% W
- M2 60% DF, 35% BOh, 1% EtOh, 4% W.

Table 2. The experimental plan

Test	A	B	C	n [rpm]	M [kNm]	PAL
1	0	1	-1	700	4.62	DF
2	1	1	1	750	4.62	M2
3	0	0	0	700	2.96	M1
4	1	0	-1	750	2.96	DF
5	0	-1	1	700	0.98	M2
6	-1	0	1	650	2.96	M2
7	1	-1	0	750	0.98	M1
8	-1	1	0	650	4.62	M1
9	-1	-1	-1	650	0.98	DF

The experimental plan was chosen due to its high cost-effectiveness. It is particularly advantageous when measurements are expensive and must be limited to only those strictly necessary. Using this plan, the researcher was able to conduct as few as nine tests, which nevertheless allowed for a satisfactory analysis of the obtained results. In this plan [7, 30]:

- A represents the crankshaft rotational speed
- B represents the torque
- C represents the fuel mixture.

The coded levels -1, 0, and +1 indicate the lowest, intermediate, and highest values of parameters A, B, and C, respectively [7, 30].

The output values are all recorded for engine and exhaust parameters. For the study, the following output parameters were determined:

- exhaust gas temperature t_{exh} [°C]
- nitrogen oxides concentration in the exhaust gas NO_x [ppm]
- nitrogen oxide concentration in the exhaust gas NO [ppm]
- nitrogen dioxide concentration in the exhaust gas NO_2 [ppm]
- carbon monoxide concentration in the exhaust gas CO [ppm]
- carbon dioxide concentration in the exhaust gas CO_2 [%].

4.2. Research object and measurement equipment

The tests were conducted on a Sulzer 6AL20/24 compression-ignition engine (Fig. 4), which features an in-line cylinder arrangement and a four-stroke cycle. The engine has four valves per cylinder, direct fuel injection and is turbocharged. The basic specifications of the engine are shown in Table 3. The engine is coupled to a Froudea-type DPY6D hydraulic brake.

The composition of the exhaust gas was recorded using a Testo 350 electrochemical analyzer. The concentration

values of a given substance in the exhaust gas were monitored and recorded using the software supplied with the analyzer. The Testo 350 analyzer can measure the following compounds: O_2 , CO_2 , CO, NO, NO_2 , SO_2 .

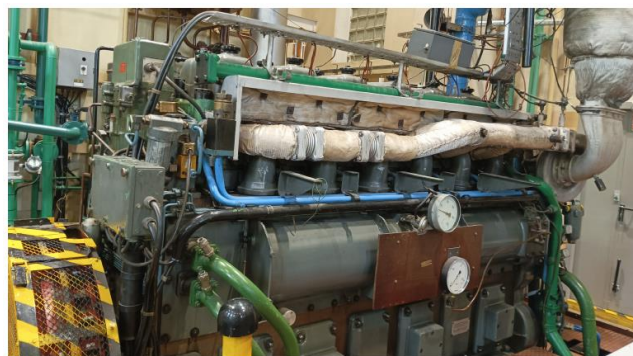


Fig. 4. Laboratory engine stand

The engine's operating parameters were recorded by a set of measuring instruments installed in the intake, exhaust, oil and cooling systems.

Table 3. Technical data of the engine used in the tests

Configuration	6L, 4-S
Rated power	420 kW
Rated speed	750 rpm
Compression ratio	12.7
Mean effective pressure	1.47 MPa
Mean piston speed	6 m/s
Piston stroke	240 mm
Cylinder bore	200 mm
Specific fuel consumption	212 g/kWh

5. Results

5.1. Test results

During the tests conducted, the differences of ambient temperature and pressure values for all measurement points did not exceed 5%. Thus, further calculations were referred to averaged values, i.e. an ambient temperature of 20°C and an ambient pressure of 1013 hPa. The emission values of O_2 , CO_2 , CO and NO_x compounds were calculated as the arithmetic average of the recorded values at the time of measurement, with the average NO_x being the sum of the average NO and NO_2 . The concentration of SO_2 in the flue gas was not determined due to the negligibly small proportion of sulfur in the fuel.

The mass emission of a given substance in the exhaust was calculated using the following formula:

$$E_x = u_x \cdot c_x \cdot \dot{m}_{\text{spal}} \quad (1)$$

where: E_x – mass emission rate of substance [$\frac{\text{kg}}{\text{s}}$], u_x – conversion factor for substance x [23], c_x – concentration of substance x in the exhaust gases, expressed in [%] for O_2 and CO_2 , and in [ppm] for CO and NO_x , \dot{m}_{spal} – exhaust gas mass flow rate [$\frac{\text{kg}}{\text{s}}$].

The specific emission of the given substance was calculated according to the following formula:

$$e_x = 3.6 \cdot 10^9 \cdot \frac{E_x}{P_e} \quad (2)$$

where: e_x – specific emission of substance x [$\frac{g}{kWh}$], P_e – useful power output [W].

The averaged emission values of oxygen, carbon dioxide, carbon monoxide, and nitrogen oxides are presented in Tables 4 and 5.

Table 4. Average emission values at measurement points

Measurement point (n/M/PAL)	C_{NO_x} [ppm]	C_{CO} [ppm]	C_{O_2} [%]	C_{CO_2} [%]
650/2.96/M2	1471	190	11.07	6.94
750/4.62/M2	1409	158	11.30	7.21
700/2.96/M1	1528	137	11.82	6.83
650/4.62/M1	1355	459	10.30	7.65
750/2.96/DF	1448	143	12.02	6.71
750/0.98/M1	1049	175	12.98	5.67
650/4.62/DF	1492	344	10.73	7.67
700/0.98/M2	1110	209	13.08	5.63
650/0.98/DF	1188	241	13.00	6.02

5.2. Emissions model

Based on the collected measurement data, a statistical analysis was performed using the Statistica 8.0 software. The program was supplied with measurement results of harmful exhaust gas emissions, including concentrations of NO_x , CO, O_2 , and CO_2 , as well as engine operating parameters such as rotational speed, torque, and the type of fuel used. Statistica enabled the development of extrapolation models describing the emission values of the analyzed substances as a function of the input variables.

A linear-quadratic model was applied in the analysis. Compared to other models, the selected model was characterized by high coefficients of determination (R^2) and low mean square errors (MS). The final model equations took the form of a polynomial consisting of seven monomials with the greatest impact on the output value.

The variables included in the models comprised both linear terms (n, M, PAL) and quadratic terms (n^2 , M^2 , PAL^2), as well as linear-linear interactions ($n \cdot M$, $n \cdot PAL$, $M \cdot PAL$), linear-quadratic interactions (e.g. $n^2 \cdot M$, $M^2 \cdot PAL$), and quadratic-quadratic interactions (e.g. $n^2 \cdot M^2$).

The accuracy of the models was evaluated based on plots comparing the approximated values with the actual measured values; the closer the points were located to the

regression line, the better the model fit was considered to be. For a more comprehensive analysis, three-dimensional plots were generated to illustrate the relationship between the emissions of individual compounds and the engine's rotational speed, torque, and the specific fuel type (PAL). Pareto charts were prepared to assess the influence of individual monomials on the emission values.

Rotational speed values were adopted in the range of 650–750 rpm. At the same time, the water content in the fuel was selected from the set {0%, 2%, 4%}, with constant torque values of {0.98, 2.96, 4.62}.

5.3. Analysis of nitrogen oxide concentrations

The conducted analysis of the influence of engine rotational speed, torque, and the type of fuel combusted on nitrogen oxides (NO_x) emissions demonstrated that the torque generated by the engine has the greatest impact on NO_x emissions (Fig. 5). Higher torque leads to an increase in the mean effective pressure and a larger fuel dose, which raises the combustion temperature and promotes higher NO_x emissions. The notation (Fig. 5) "L" indicates that the coefficient value is assigned to the linear term of the polynomial, "Q" – to the quadratic term, and "by" – in relation to a reference value.

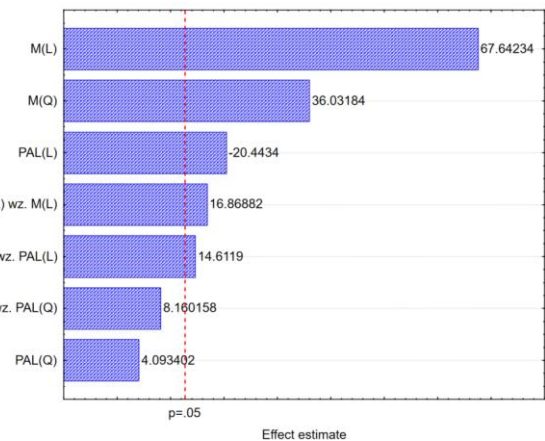


Fig. 5. Pareto charts of effect for NO_x

The type of fuel also has a significant impact on nitrogen oxides (NO_x) emissions, both as an independent variable and through interactions with engine torque. It was shown that a higher water content in the fuel mixture ($M2$ – 4% water) at lower engine loads ($M < 3$ kNm) results in a reduction of NO_x emissions by approximately 100 ppm compared to conventional diesel fuel. However, at higher

Table 5. Average values of mass emission intensity and unit emission of compounds: at measurement points

Measurement point (n/M/PAL)	E_{NO_x} [kg/h]	E_{CO} [kg/h]	E_{O_2} [kg/h]	E_{CO_2} [kg/h]	e_{NO_x} [g/kWh]	e_{CO} [g/kWh]	e_{O_2} [g/kWh]	e_{NO_x} [g/kWh]
650/2.96/M2	3.206	0.252	168.0	144.8	16.138	1.269	845.6	728.8
750/4.62/M2	4.981	0.340	278.1	243.9	13.903	0.949	776.3	680.9
700/2.96/M1	3.669	0.200	197.6	157.0	16.722	0.913	900.7	715.4
650/4.62/M1	3.866	0.797	204.6	208.9	12.526	2.583	663.0	676.9
750/2.96/DF	3.346	0.201	193.4	148.4	15.258	0.917	881.9	676.8
750/0.98/M1	1.679	0.171	144.7	86.9	20.953	2.128	1805.2	1084.0
650/4.62/DF	4.231	0.594	211.8	208.2	13.456	1.888	673.8	662.1
700/0.98/M2	1.644	0.188	134.9	79.8	20.803	2.384	1706.9	1009.9
650/0.98/DF	1.578	0.195	120.2	76.5	22.820	2.818	1738.7	1106.8

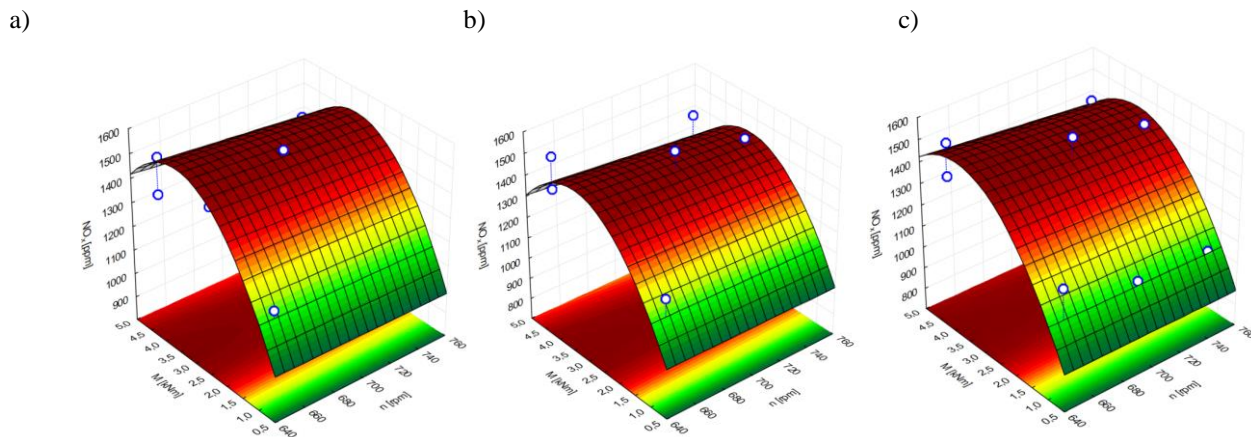


Fig. 6. Dependence of NO_x emission values depending on n and M for a) DF, b) M1, c) M2

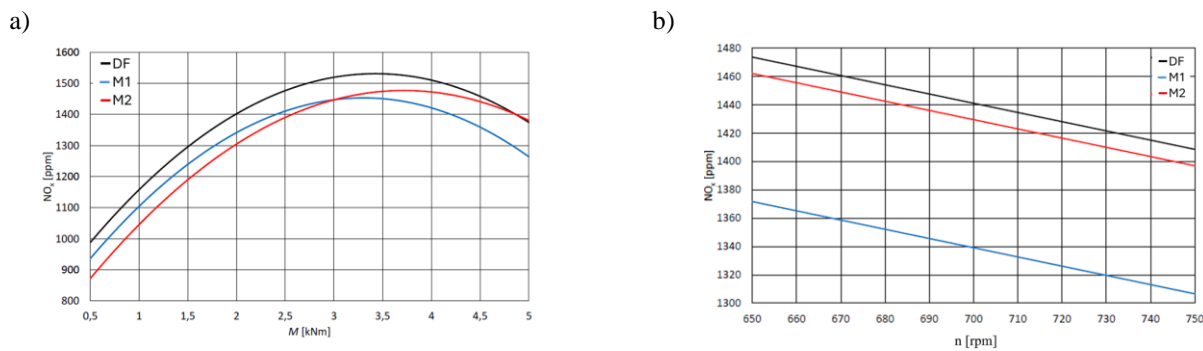


Fig. 7. Dependence of NO_x emission values at a) constant speed $n = 700$ rpm, b) constant torque $M = 4.62$ kNm depending on the fuel DF, M1, M2

loads ($M > 3$ kNm), fueling with mixture M1 (containing 2% water by volume) is more advantageous, also leading to a reduction in NO_x emissions of about 100 ppm (Fig. 6 a–c, Fig. 7 a–b).

It was observed that at a constant torque, NO_x emissions decrease with increasing engine speed, which a linear relationship can approximate. In higher torque ranges, the reduction in NO_x emissions results from the fact that the air excess ratio is lower, which limits the amount of oxygen available to react with nitrogen, despite higher combustion temperatures (Fig. 7 a–b).

The model fit was evaluated based on the coefficient of determination ($R^2 = 0.94208$) and the mean square error ($MS = 15807.11$), indicating a high agreement between the model and the measured data (Fig. 8).

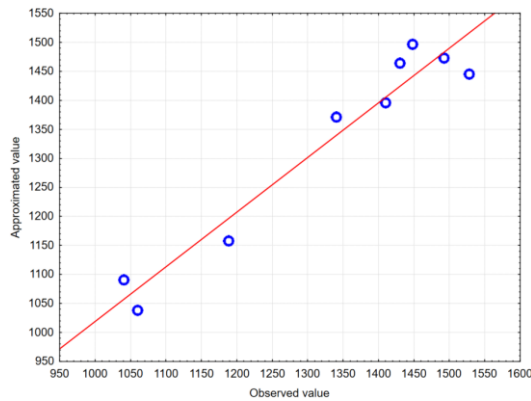


Fig. 8. Plot of observed versus approximated values for NO_x

5.4. Analysis of carbon monoxide concentrations

The analysis of carbon monoxide emission variations was carried out based on a polynomial model (Fig. 9) with a high fit to the experimental data ($R^2 = 0.98454$, $MS = 1422.536$).

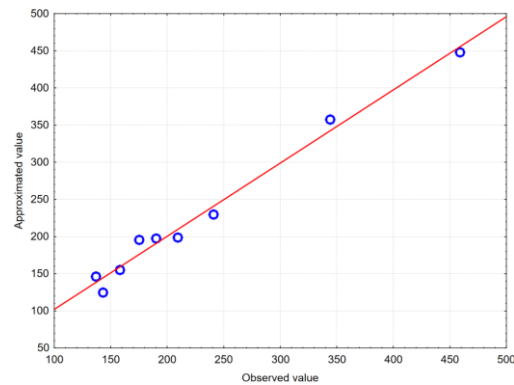


Fig. 9. Plot of observed versus approximated values for CO

The Pareto chart indicates that the quadratic relationship with torque has the greatest impact on CO emissions. Significant effects are also observed for interactions between torque and the water content in the fuel, both in linear and quadratic terms, as well as for the quadratic influence of engine speed (Fig. 10).

The research results indicate that CO emissions when fueling with diesel fuel (ON) are lower than when using the M1 blend. In the case of fuel M2, the emission pattern of

CO differs from that of ON and M1 – at low engine loads, emissions are significantly higher. In contrast, at higher loads, the CO emission level decreases.

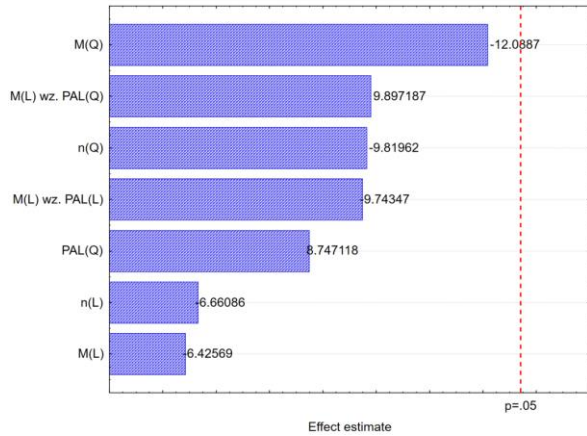


Fig. 10. Pareto charts of effect for CO

The increased CO emissions observed with M1 are attributed to a reduction in combustion temperature caused by the presence of water in the fuel. However, the mechanism behind the localized decrease in CO concentration observed at medium engine operating conditions when using the M2 blend remains unexplained (Fig. 11–12). This phenomenon may result from the catalytic effect of water, which accelerates hydrocarbon oxidation reactions.

On average, CO emissions during operation with the M1 blend are higher than the values recorded for diesel fuel (ON) by approximately 50 ppm at low loads, increasing to about 100 ppm at higher loads. In contrast, the use of fuel M2 enables a reduction in CO emissions by an average of approximately 210 ppm compared to ON, particularly at a constant engine load of 4.62 kNm (Fig. 12).

5.5. Analysis of carbon dioxide concentrations

The developed model describing the concentration of carbon dioxide (CO₂) in the exhaust gases accounts for the dependence of this compound’s emissions on engine operating parameters such as rotational speed, torque, as well as on the composition of the fuel used, including the water content.

Carbon dioxide is a product of the complete and total combustion of the carbon contained in the fuel; therefore, its emissions are directly correlated with the amount of fuel burned. For this reason, the linear torque variable exerts the greatest influence on the CO₂ emission level, which was clearly confirmed by the Pareto chart analysis (Fig. 13).

This chart also indicates a significant, though less dominant, influence of higher-order interactions between engine operating parameters and the composition of the fuel mixture.

The model achieved an excellent fit to the experimental data, as confirmed by statistical indicators: a coefficient of determination R² of 0.99993 and a low mean square error (MS) value of 0.0003594. The high degree of fit demonstrates the model’s strong predictive accuracy in the field of CO₂ emissions (Fig. 14).

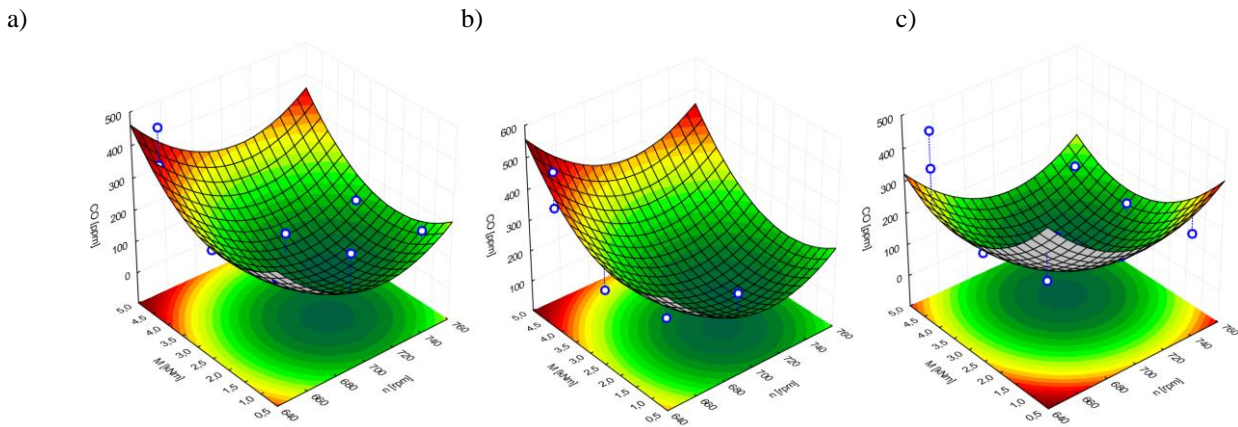


Fig. 11. Dependence of CO emission values depending on n and M for a) DF, b) M1, c) M2

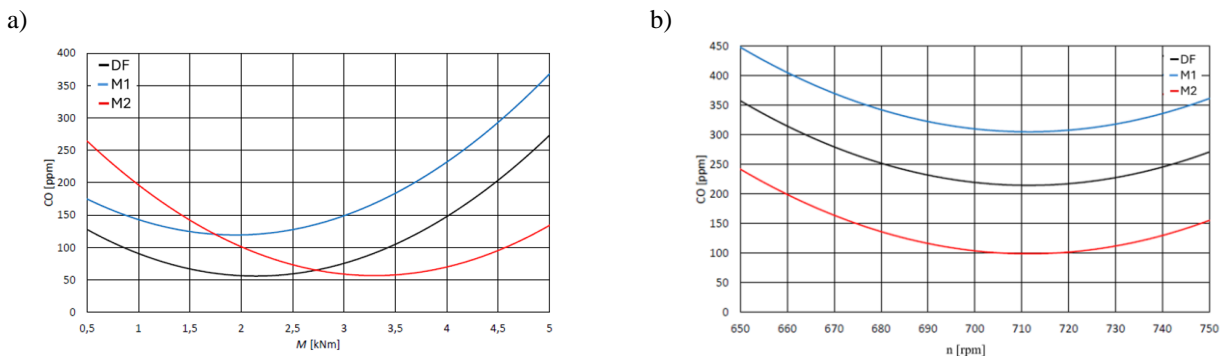


Fig. 12. Dependence of CO emission values at a) constant speed n = 700 rpm, b) constant torque M = 4.62 kNm depending on the fuel DF, M1, M2

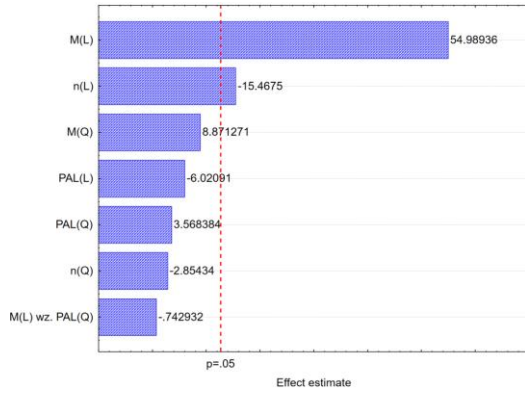


Fig. 13. Pareto charts of effect for CO₂

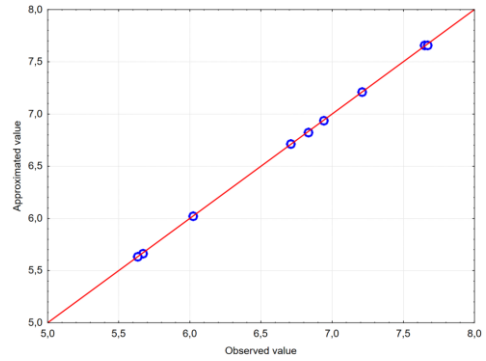


Fig. 14. Plot of observed versus approximated values for CO₂

A comparative analysis of CO₂ emissions for different fuels revealed that the concentration levels of this compound remain similar regardless of the type of fuel used (Fig. 15–16). The lowest emissions were recorded when the engine was fueled with conventional diesel fuel (DF). In contrast, the highest emissions were observed during operation with the M2 blend. However, these differences are relatively minor, suggesting that the influence of fuel composition on CO₂ emissions is limited, especially when compared to the significant variations observed in the emissions of other compounds such as NO_x or CO.

5.6. Analysis of oxide concentrations

The model describing the concentration of oxygen (O₂) in the engine exhaust gases exhibits a very high degree of agreement with the experimental results (Fig. 17), with a coefficient of determination R² = 0.99891 and a mean square error (MS) of 0.0094743.

The polynomial equation accounts for the influence of crankshaft rotational speed, torque, and the composition of the fuel mixture. The linear dependence on torque exerts the strongest effect on the O₂ level in the exhaust gases (Fig. 18). An increase in torque leads to a reduction in the air excess ratio (λ), resulting in greater utilization of oxygen during combustion and a decrease in its concentration in the exhaust gases.

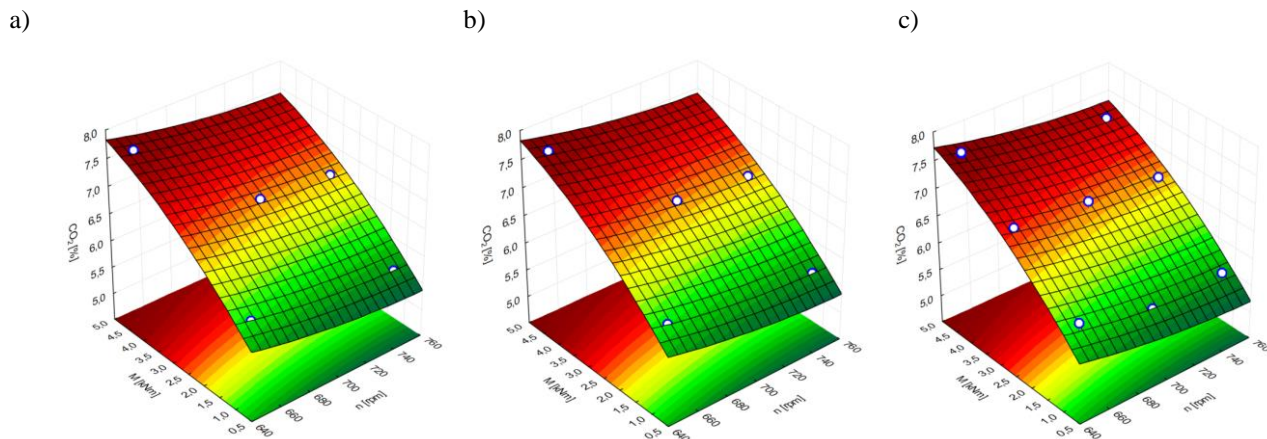


Fig. 15. Dependence of CO₂ emission values depending on n and M for a) DF, b) M1, c) M2

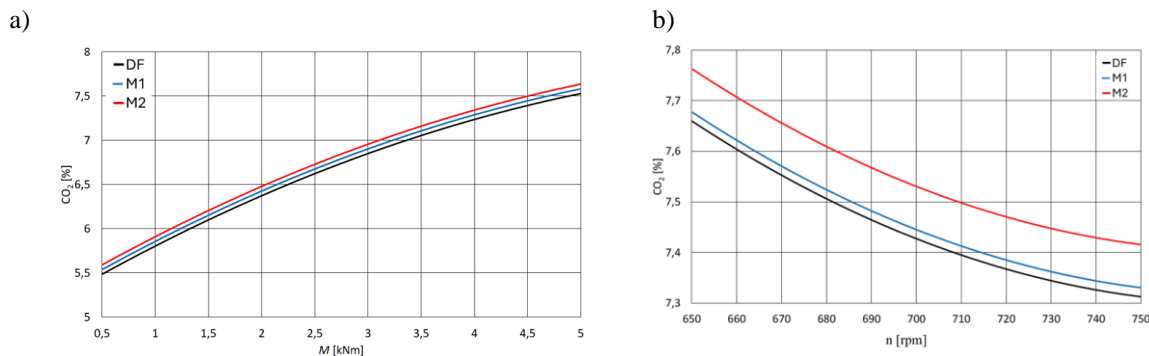


Fig. 16. Dependence of CO₂ emission values at a) constant speed n = 700 rpm, b) constant torque M = 4.62 kNm depending on the fuel DF, M1, M2

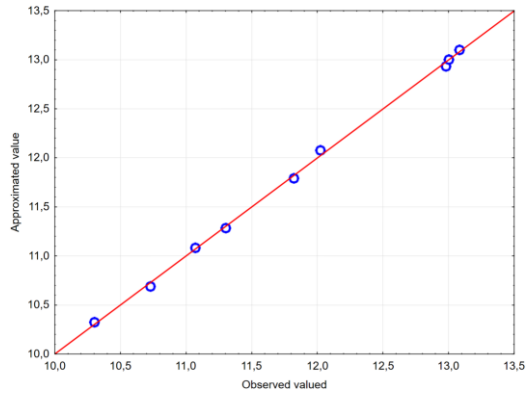


Fig. 17. Plot of observed versus approximated values for O₂

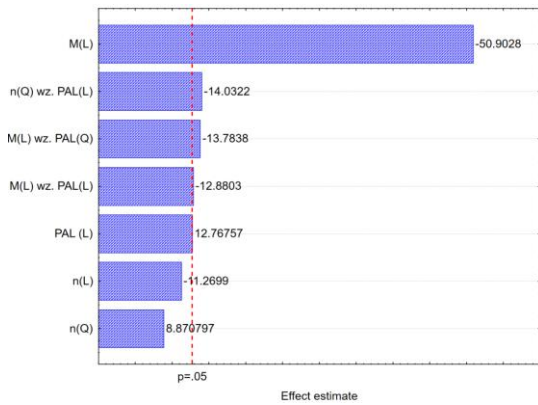


Fig. 18. Pareto charts of effect for O₂

Analyses (Fig. 19 and Fig. 20) showed that when operating on diesel fuel, the oxygen concentration decreases with increasing engine load, and this effect is more pronounced for the M1 and M2 blends. This results from the lower calorific value of butanol, which necessitates an increased fuel injection quantity into the cylinder to maintain the desired power output. The maximum O₂ concentration is observed in the range of 690–720 rpm, corresponding to the highest value of the air excess ratio.

6. Conclusion

The conducted analysis demonstrated that the use of component fuels containing butyl alcohol and water contributes to a reduction in the emissions of toxic exhaust gas constituents in marine engines. However, the nature of these changes is complex and depends on engine operating conditions.

Nitrogen oxides (NO_x) emissions were generally lower when using component fuels compared to conventional diesel fuel. The greatest reduction in NO_x emissions, reaching up to 7.5%, was achieved when operating on the M2 blend under lower torque conditions. However, at higher engine loads, the use of the M1 blend proved more advantageous. A key factor in reducing NO_x emissions is the introduction of water into the fuel blend, which lowers the maximum combustion temperature, thereby limiting the formation of NO_x, as its emission increases exponentially with rising temperatures in the combustion chamber.

In the case of carbon monoxide (CO) emissions, the results were less unequivocal. When the engine was fueled with M1, an increase in CO emissions was observed compared to operation on diesel fuel. For low engine loads, using the M2 blend resulted in higher CO emissions than with diesel; however, at higher torque values, emissions decreased and were lower than during operation on diesel. This may be related to the reduction in combustion temperature caused by the presence of water in the blend or to a potential catalytic effect of water, accelerating hydrocarbon oxidation reactions.

The concentration of oxygen (O₂) in the exhaust gases decreased with increasing engine torque, which is associated with a reduction in the air excess ratio due to the need for higher fuel injection quantities. However, for the M1 and M2 blends, the oxygen content in the exhaust gases at higher loads was higher than that observed when operating on diesel fuel. This is most likely related to the presence of oxygen in the butanol molecule, which participates in the combustion process, partially substituting for oxygen from the intake air.

Carbon dioxide (CO₂) emissions were similar across all tested fuels, which results from the fact that CO₂ is the final product of complete carbon combustion. The differences in

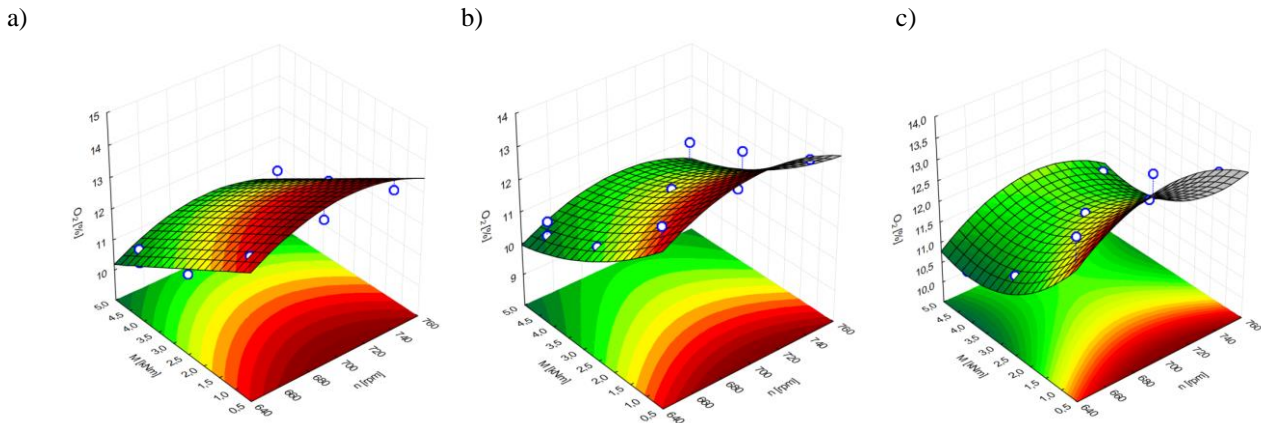


Fig. 19. Dependence of O₂ emission values depending on n and M for a) DF, b) M1, c) M2

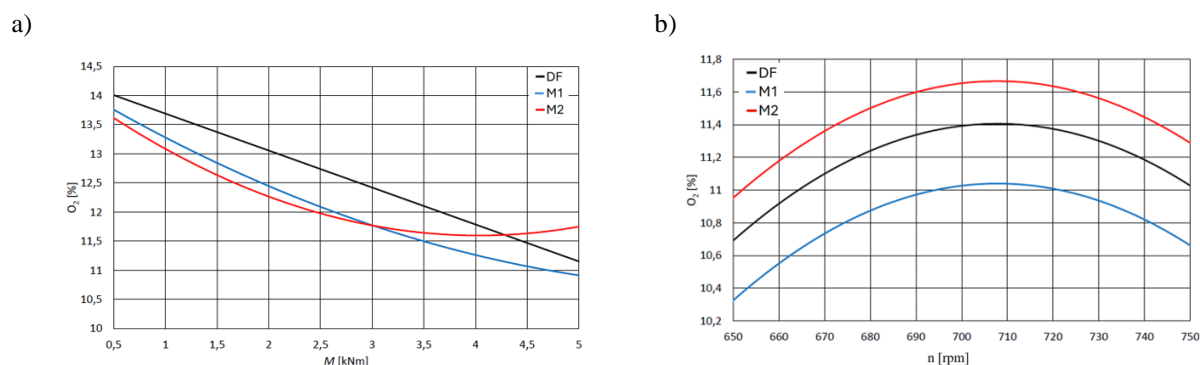


Fig. 20. Dependence of O₂ emission values at a) constant speed $n = 700$ rpm, b) constant torque $M = 4.62$ kNm depending on the fuel DF, M1, M2

emissions between fuels were minor, confirming that to obtain a given amount of energy, a comparable amount of carbon must be burned, regardless of the type of fuel used.

In conclusion, the research results suggest that the use of component fuels, particularly those containing water and butyl alcohol, may contribute to reducing emissions of harmful exhaust compounds while maintaining comparable

engine operating parameters. However, due to the complexity of combustion processes and the influence of numerous operational variables, further experiments are necessary to elucidate the mechanisms underlying these phenomena fully and to ensure optimal operating conditions for marine engines while meeting environmental protection requirements.

Nomenclature

EPA	U.S. Environmental Protection Agency	MS	mean square error
EtOH	ethyl alcohol	PAHs	polycyclic aromatic hydrocarbons
FAMES	fatty acid methyl esters	PM	particulate matter
HC	hydrocarbons	R ²	coefficient of determination
IMO	International Maritime Organization	REE	rapeseed oil methyl esters
MARPOL	International Convention for the Prevention of Pollution from Ships		

Bibliography

- [1] Alhawtali S, El-Harbawi M, Al-Awadi AS, El Blidi L, Alrashed MM, Yin CY. Enhanced adsorption of methylene blue using phosphoric acid-activated hydrothermal carbon microspheres synthesized from a variety of palm-based bio-wastes. *Coatings*. 2023;13(7):1287. <https://doi.org/10.3390/coatings13071287>
- [2] Andrych-Zalewska M, Chłopek Z, Lasocki J, Merksiz J, Pielecha J. A stochastic approach to the analysis of pollutant emissions and fuel consumption of motor vehicles driven in real traffic. *Appl Sci*. 2024;14(23):11346. <https://doi.org/10.3390/app142311346>
- [3] Aytak Y. Exhaust emission regulations for marine applications. 2021. <https://www.cummins.com/pl/news/2021/06/28/engine-emission-regulations-marine-applications>
- [4] Bielaczyc P, Merksiz J, Pielecha J. Stan cieplny silnika spalinowego a emisja związków szkodliwych (in Polish). Wydaw. Politechniki Poznańskiej. Poznań 2001.
- [5] Bocheński CI. Biodiesel: paliwo rolnicze (in Polish). Wydaw. SGGW. Warszawa 2003.
- [6] Bogdanowicz A, Kniżewicz T, Zadrąg R. The emission of harmful compounds from the marine diesel engine fueled by a blend of n-butanol and marine fuel. *Combustion Engines*. 2021;187(4):90-95. <https://doi.org/10.19206/CE-142031>
- [7] Bogdanowicz A, Socik P, Zadrąg R, Zacharewicz M, Wirkowski P. Multi-criteria analysis of the emission of harmful compounds from a marine diesel engine fueled with a mixture of marine fuel and n-butanol. *Combustion Engines*. 2025;203(4):9-15. <https://doi.org/10.19206/CE-207151>
- [8] Cesilla De Souza L, Eugênio Abel Seabra J. Technical-economic and environmental assessment of marine biofuels produced in Brazil. *Clean Environ Syst*. 2024;13:100195. <https://doi.org/10.1016/j.cesys.2024.100195>
- [9] Choi I, Lee C. Numerical study on nitrogen oxide and black carbon reduction of marine diesel engines using emulsified marine diesel oil. *Sustainability*. 2019;11(22):6347. <https://doi.org/10.3390/su11226347>
- [10] Damian CS, Devarajan Y, Jayabal R, Raja T. Enhancing marine diesel engine compatibility with sustainable fuels: key factors and adjustments. *Mar Pollut Bull*. 2025;215:117836. <https://doi.org/10.1016/j.marpolbul.2025.117836>
- [11] Doppalapudi AT, Azad AK, Nabi MN, Rasul MG, Khan MMK. Pragmatic investigation of the effect of ether additives on biodiesel combustion to reduce NO_x and other harmful emissions. *Fuel*. 2025;382:133712. <https://doi.org/10.1016/j.fuel.2024.133712>
- [12] Griesemer SD, Baldassarri B, Zhu R, Shen J, Pal K, Park CW et al. Wide-ranging predictions of new stable compounds powered by recommendation engines. *Sci Adv*. 2025;11(1):eadq1431. <https://doi.org/10.1126/sciadv.adq1431>
- [13] Huang J, Duan X. A comprehensive review of emission reduction technologies for marine transportation. *J Renew Sustain Energy*. 2023;15(3):032702. <https://doi.org/10.1063/5.0150010>
- [14] Kowalewicz A. Podstawy procesów spalania (in Polish). Wydawnictwa Naukowo-Techniczne. Warsaw 2000.

- [15] Kozak M. A comparison of thermogravimetric characteristics of fresh and used engine oils. *Combustion Engines*. 2019;178(3):289-292. <https://doi.org/10.19206/CE-2019-350>
- [16] Kozak M, Merkisz J. Oxygenated diesel fuels and their effect on PM emissions. *Appl Sci*. 2022;12:7709. <https://doi.org/10.3390/app12157709>
- [17] Kozak M, Lijewski P, Waligórski M. Exhaust emissions from a hybrid city bus fuelled by conventional and oxygenated fuel. *Energies*. 2022;15:1123. <https://doi.org/10.3390/en15031123>
- [18] Kozak M. Exhaust emissions from a diesel passenger car fuelled with a diesel fuel-butanol blend. *SAE Technical Paper 2011-28-0017*. 2011. <https://doi.org/10.4271/2011-28-0017>
- [19] Kozina A, Radica G, Nižetić S. Analysis of methods towards reduction of harmful pollutants from diesel engines. *J Clean Prod*. 2020;262:121105. <https://doi.org/10.1016/j.jclepro.2020.121105>
- [20] Lapuerta M, Armas O, Rodriguezfernandez J. Effect of biodiesel fuels on diesel engine emissions. *Prog Energy Combust Sci*. 2008;34(2):198-223. <https://doi.org/10.1016/j.pecs.2007.07.001>
- [21] Laskowski P, Zimakowska-Laskowska M. Simulation study of the effect of ethanol content in fuel on petrol engine performance and exhaust emissions. *Combustion Engines*. 2025;201(2):129-135. <https://doi.org/10.19206/CE-204049>
- [22] Liu A, Dua R, Hu W Min, Lin Ku A. Choosing to diet: the impact and cost-effectiveness of China's vehicle ownership restrictions. *Transp Res Part Transp Environ*. 2022;111:103456. <https://doi.org/10.1016/j.trd.2022.103456>
- [23] Merkisz J, Piaseczny L, Kniaziewicz T. *Zagadnienia emisji spalin silników okrętowych* (in Polish). Wydawnictwo Politechniki Poznańskiej. Poznan 2016.
- [24] Moshiul AM, Mohad Zaki NI, Abu Husain MK. Review of sulphur emission from international shipping-effects and regulatory global abatement steps. *Int J Mech Eng Technol*. 2019;10(2):924-933. <http://iaeme.com/Home/issue/IJMET?Volume=10&Issue=2>
- [25] Piotrowski I, Witkowski K. *Okrętowe silniki spalinowe* (in Polish). Ed. 3b. Trademar. Gdynia 2013.
- [26] Ramacher MOP, Tang L, Moldanová J, Matthias V, Karl M, Fridell E et al. The impact of ship emissions on air quality and human health in the Gothenburg area – part II: scenarios for 2040. *Atmospheric Chem Phys*. 2020;20(17):10667-10686. <https://doi.org/10.5194/acp-20-10667-2020>
- [27] Rychter T, Teodorczyk A. *Teoria silników tłokowych* (in Polish). Wydawnictwa Komunikacji i Łączności. Warszawa 2006.
- [28] Struś MS. *Ocena wpływu biopaliw na wybrane właściwości eksploatacyjne silników o zapłonie samoczynnym* (in Polish). Oficyna Wydawnicza Politechniki Wrocławskiej. Wrocław 2012.
- [29] Tan ECD, Hawkins TR, Lee U, Tao L, Meyer PA, Wang M et al. Biofuel options for marine applications: techno-economic and life-cycle analyses. *Environ Sci Technol*. 2021;55(11):7561-7570. <https://doi.org/10.1021/acs.est.0c06141>
- [30] Zacharewicz M, Socik P, Wirkowski P, Zadrag R, Bogdanowicz A. Evaluation of the impact of supplying a marine diesel engine with a mixture of diesel oil and n-butanol on its efficiency and emission of toxic compounds. *Combustion Engines*. 2023;195(4):40-47. <https://doi.org/10.19206/CE-169484>
- [31] Zhang Z, Lv J, Li W, Long J, Wang S, Tan D et al. Performance and emission evaluation of a marine diesel engine fueled with natural gas ignited by biodiesel-diesel blended fuel. *Energy*. 2022;256:124662. <https://doi.org/10.1016/j.energy.2022.124662>
- [32] IMO. Nitrogen Oxides (NOx) – Regulation 13. IMO. <https://www.imo.org>
- [33] Dz.U. 2016 poz. 761, Zmiany do Protokołu I oraz do załączników do Międzynarodowej konwencji o zapobieganiu zanieczyszczeniu morza przez statki (in Polish). ISAP. <https://isap.sejm.gov.pl/isap.nsf/DocDetails.xsp?id=WDU20160000761>
- [34] Regulations for Emissions from Heavy Equipment with Compression-Ignition (Diesel) Engines. <https://www.epa.gov/regulations-emissions-vehicles-and-engines/regulations-emissions-heavy-equipment-compression>
- [35] 2023 IMO Strategy on Reduction of GHG Emissions from Ships. IMO. <https://www.imo.org/en/OurWork/Environment/Pages/2023-IMO-Strategy-on-Reduction-of-GHG-Emissions-from-Ships.aspx>

Prof. Ryszard Zadrag, DSc., DEng. – Faculty of Mechanical and Electrical Engineering, Polish Naval Academy, Poland.
e-mail: r.zadrag@amw.gdynia.pl



Prof. Marcin Zacharewicz, DSc., DEng. – Faculty of Mechanical and Electrical Engineering, Polish Naval Academy, Poland.
e-mail: m.zacharewicz@amw.gdynia.pl



Paweł Socik, MEng. – Faculty of Mechanical and Electrical Engineering, Polish Naval Academy, Poland.
e-mail: p.socik@amw.gdynia.pl



Artur Bogdanowicz, DEng. – Faculty of Mechanical and Electrical Engineering, Polish Naval Academy, Poland.
e-mail: a.bogdanowicz@amw.gdynia.pl



Norbert Sigiel, DEng. – Faculty of Navigation and Naval Weapons, Polish Naval Academy, Poland.
e-mail: n.sigiel@amw.gdynia.pl



A mathematical study of the narrowband lambda sensor characteristics for lean and rich operation

ARTICLE INFO

Air-fuel ratio measurement is essential for efficient combustion and emission control in internal combustion engines. This study presents a mathematical model for the voltage response of narrowband zirconia lambda sensors, commonly used in older vehicles. These sensors, while cost-effective, are limited by their narrow operating range and strong temperature sensitivity – especially under rich mixture conditions. Using the Nernst equation, the study models the sensor voltage as a function of oxygen partial pressure. The sensor's heating element was experimentally characterized, and its resistance-temperature relationship was accurately described using a Rational5 function. A modified form of the Nernst equation enabled voltage-to-AFR conversion across a wide mixture spectrum. Data analysis confirmed that in lean conditions, the voltage response is nearly linear and largely unaffected by temperature, enabling accurate closed-loop control. In contrast, rich mixtures produced highly non-linear and temperature-dependent behavior, making interpretation more complex. To address this, an Arrhenius-based model was successfully applied to the rich-side response, significantly improving accuracy after temperature compensation. The model was implemented and tested on a Ford EEC V ECU with a Ford 302 GT40P engine running on LPG. Modifications to the controller allowed stable closed-loop operation up to $\lambda = 1.35$ using only a narrowband sensor. These results show that with proper modeling and calibration, narrowband lambda sensors can effectively monitor lean mixtures and offer limited utility in rich conditions. This opens new possibilities for retrofitting legacy engine systems without expensive hardware upgrades. Further research is needed to enhance rich-side precision and dynamic temperature correction.

Received: 17 June 2025

Revised: 7 July 2025

Accepted: 22 July 2025

Available online: 16 November 2025

Key words: *lambda, sensor, lean, burning, engine*This is an open access article under the CC BY license (<http://creativecommons.org/licenses/by/4.0/>)

1. Introduction

The measurement of the air-fuel ratio (AFR) is crucial for the proper operation of an internal combustion engine and the minimization of pollutant emissions. Both wide-band and narrowband lambda sensors play a key role in this process. The most commonly used solution in older vehicles is the zirconia narrowband sensor, which, despite its limited measurement range and slower response time, provides sufficient accuracy under typical operating conditions [14]. The operating principle of the lambda sensor is based on the electrochemical potential difference resulting from the unequal oxygen concentration on both sides of the oxide membrane. The mathematical description of this phenomenon follows directly from the Nernst equation [13], and its precise application in interpreting the lambda sensor voltage requires consideration of factors such as temperature, partial pressure, and the resistance characteristics of the heater [4, 2].

Technical and patent literature highlights significant challenges in interpreting the sensor signal in the range of extremely lean and rich mixtures, where the variability of oxygen partial pressure can span several orders of magnitude [1, 12]. For rich mixtures, the sensor signal is highly unstable and strongly dependent on temperature [8, 13], which limits its practical use in precise control systems. In parallel, alternative technologies such as titanium sensors or semiconductor cells with much higher thermal resistance and a broader measurement range are being developed [4, 8]; however, their application remains costly. Attempts to extend the durability and effectiveness of conventional

zirconia sensors have included the use of CFD simulations [2] and modifications to engine controller algorithms [14].

Modern approaches employ mathematical and numerical methods to model the real-time response behavior of the lambda sensor [13, 7], and also seek to establish relationships describing its characteristics as a function of partial pressure and temperature. At the same time, advanced ignition systems, such as microwave multipoint systems, are being developed, enabling operation with extremely lean mixtures – up to $\lambda = 2$ [9].

Current research places significant emphasis on maintaining an optimal air-fuel mixture over the widest possible range of engine loads and rotational speeds. This is especially important due to the strong correlation between AFR and mixture homogeneity in relation to the level of harmful emissions produced by the internal combustion engine. Additionally, alternatives such as gasoline blends with other hydrocarbons are being explored to reduce emissions [6, 15].

The aim of this article is to develop a consistent mathematical model describing the voltage characteristics of a narrowband lambda sensor across the full AFR range, with a division into operating conditions for lean and rich mixtures, while accounting for the influence of temperature and the heater resistance relationship. The conclusions drawn from the conducted research may contribute to more effective use of classic sensors in modern fuel mixture control systems and the retrofitting of older systems. Additionally, the ability to extend the operating range of a narrowband lambda sensor beyond the stoichiometric point ($\lambda = 1$) would enable improved calibration and adaptation of

engines with lambda-based control systems to operate on alternative fuels such as LPG, LNG, or ethanol – without the need for system reconstruction or the installation of additional devices. This could lead to increased efficiency and power output of vehicles running on alternative fuels, without sacrificing fuel economy. Such a solution would be feasible if the engine’s Powertrain Control Module (PCM) could be configured with different PI controller parameters for the lambda sensor response, tailored to various engine operating points – such as load, rotational speed, temperature, and others. This would allow lean mixture operation under high-load conditions, and fuel mixture leaning during low-load operation or in moments when high torque is not required. With the expansion of the control algorithm, more precise and broader emission control would become achievable. At present, in systems based on narrowband sensors, the engine controller only switches between predefined values for rich and lean conditions. Accurate signal interpretation would allow for control similar to that of wideband sensors. The relationship between emission levels and lambda values is presented in Fig. 1.

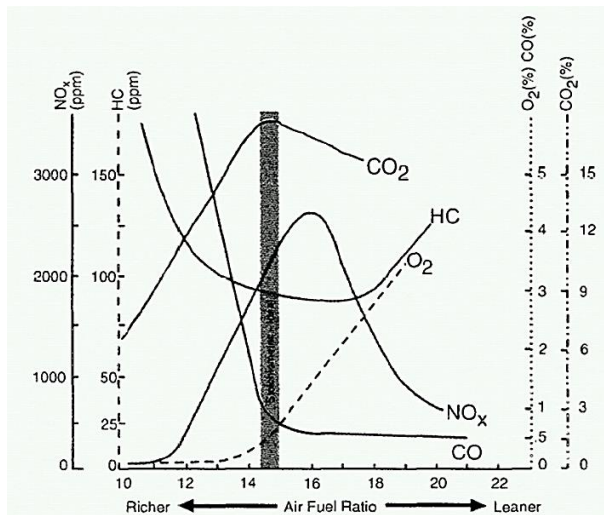


Fig. 1. AFR vs emissions [10]

2. Materials and methods

The experiment measuring the resistance of the heater in the sensor depending on its temperature was carried out on a classic zirconia lambda sensor. A planar sensor was not selected due to the fact that, in older vehicles, and for economic reasons, narrowband zirconia lambda sensors were more commonly used. Although they respond more slowly than titanium sensors, they are fully sufficient for less demanding applications, such as in everyday-use vehicles. A type K thermocouple was used to measure the temperature of the sensor. A temperature of up to 1000 °C was achieved by supplying the lambda sensor with up to 30 V from a laboratory power supply. The data analysis and calculations were carried out using OriginLab and Excel software. Likewise, all mathematical functions were determined using OriginLab. Initial formula transformations, including the Nernst equation, were performed in an OldSchool manner on paper. The identification of function formulas describing the experimental curves was done using fitting functions in OriginLab. Initial fitting parameters were se-

lected randomly, and then, using an algorithm with a fitting condition, values of the function variables were found that ensured the best fit to the plotted data. The choice of the initial fitting functions was based on the experimenter’s experience. Subsequent functions were verified in alphabetical order.

3. Basic calculations and description

The most important equation describing the operation of a lambda sensor is the Nernst equation. This equation defines the equilibrium potential of an electrode. In relation to the lambda sensor, the Nernst equation defines the voltage across the sensor’s electrodes depending on the difference in partial pressure between the exhaust system and the surrounding environment. More precisely, it is the partial pressure of oxygen that is crucial, as the sensor measures the difference in oxygen partial pressure. Air, serving as a reference value, is supplied to the lambda sensor through the signal wire. A vacuum of up to 1 bar can occur in this wire. For this reason, it is prohibited to solder the lambda sensor’s signal wires leading to its connector. Similarly, the use of products such as WD-40 or Contact Cleaner to clean the connectors of lambda sensors is also forbidden. Doing so may clog the capillaries in the signal wire, which can lead to the reversal of the voltage generated by the lambda sensor. As a result, a lean mixture may produce readings close to 1 V, while a rich mixture may cause the sensor to generate a voltage close to 0 V. A cross-section of the lambda sensor is shown in Fig. 2.

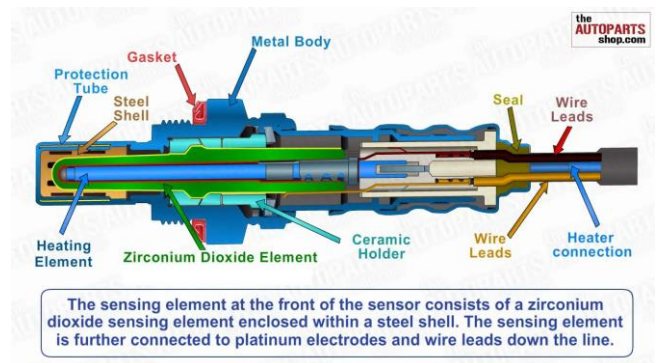


Fig. 2. Lambda sensor construction [5]

On the left side, the external shield is visible, designed to protect the cell from mechanical damage and from direct exposure to unburned fuel components. This is particularly important because large amounts of unburned fuel can cause the lambda sensor to indicate a falsely lean mixture. Just behind the protective element is the main electrode, which houses a heating element inside. Depending on the sensor model and its installation location, heaters with power ratings ranging from 3 to 24 W are used. The lowest-power heaters are typically found in planar sensors installed directly in the exhaust manifold. The purpose of the heater is to bring the sensor up to its operating temperature around 500°C as quickly as possible. Rapid heating allows the control system to switch to closed-loop mode, enabling fuel injection to be regulated based on feedback from the lambda sensor. This significantly reduces the emission of harmful substances. The zirconia electrode is mounted in a ce-

ramic holder, which is housed inside a metal tube. A real image of the sensor, both external and in cross-section, is shown in Fig. 3.



Fig. 3. Lambda sensor [11]

The Nernst equation for the lambda sensor takes the following form:

$$U = \frac{RT}{nF} \cdot \ln\left[\frac{P_a}{P_e}\right] \quad (1)$$

where: U – Lambda sensor output voltage, R – gas constant, T – temperature of the sensor/exhaust gases, n – electrons involved in the reaction = 4, F – Faraday constant, Pa – partial pressure of O₂ in the atmosphere, Pe – partial pressure of O₂ in the exhaust system.

The first issue encountered when attempting to identify the relationship with respect to lambda is the extremely different partial pressure values between the rich and lean sides of the lambda sensor's operation. In the case of the rich side, values can reach as low as 10 to the power of minus 23, whereas on the lean side, they can reach values up to the power of 3. Lambda 1 was adopted as the reference point. Another problem arises regarding the resistance of the sensor's heater. The equation clearly shows the influence of temperature on the voltage readings. Unfortunately, the full linearity of the resistance-to-temperature relationship is a fiction. To make matters worse, the equation does not define a relationship with lambda. For this reason, in order to use the equation in a control system, it becomes necessary to derive a formula describing the same voltage-generation relationship for lambda in terms of the difference in partial pressure.

To achieve this, a basic transformation of the equation was undertaken. An additional variable, k, was introduced to represent the term RT/nF. After transformations, the equation took the following form.

$$e^{(-U/k+\ln(P_a))} = P_e \quad (2)$$

$$e^{\ln(P_e)} = P_e \quad (3)$$

Having the equation transformed in this way and using tables that define the relationship between lambda and partial pressure, it became possible to attempt to identify consistent mathematical relationships and to verify whether the derived relationships are applicable.

4. Results

The first test of the correctness of the calculations was to verify whether the graph plotted using the derived equation is a logarithmic function. A test temperature of 750

degrees Celsius was assumed. Due to the very large difference in the ranges of partial pressures, correction coefficients for the lean side, rich side, and stoichiometry were applied to properly plot the curve. These coefficients indicate to the algorithm whether the system is operating on the lean or rich side. This makes it possible to filter out noise in the value ranges close to lambda 1, where the lambda sensor graph becomes almost a vertical line. The plot test confirmed that the function is indeed logarithmic. The shape of the curve is shown in Fig. 4. A total of 42 points were used to generate the graph.

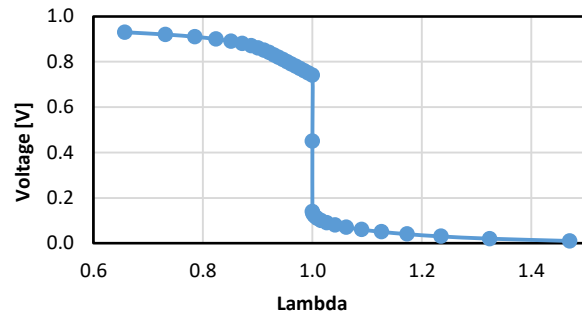


Fig. 4. Lambda vs voltage

The graph is identical to those found in textbooks. Across a very wide voltage range, the indicated air-fuel mixture remains at lambda = 1. Only at the extreme ends of the voltage scale does the lambda sensor indicate values deviating from the stoichiometric point. For rich mixtures, the voltage range is approximately 0.7 V to 0.95 V. On the lean side, the values range from around 0.15 V down to nearly 0 V. Another limitation is the 8-bit analog-to-digital converter, which is typically used in systems equipped with a narrowband lambda sensor.

The correct shape of the graph allows for further data processing. The next step was to plot and attempt to identify a function describing the relationship between the heater resistance and temperature, in order to enable compensation of the lambda sensor readings on both the lean and rich sides for a given, momentary operating temperature. The recorded measurements are presented in Fig. 5.

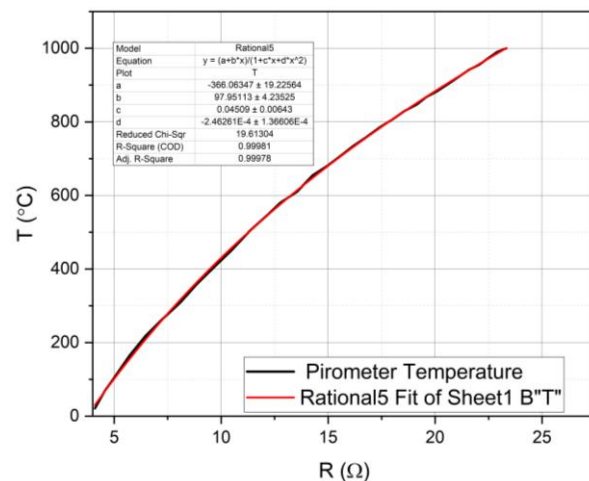


Fig. 5. Temperature vs resistance of lambda sensor heater

It was observed that the highest degree of fit is provided by the Rational5 function with appropriately selected coefficients, as shown in the graph.

The fitting function is plotted with a red line; subsequently, the relationship between lambda and the partial pressure difference was verified across the full spectrum from a lean mixture to a rich mixture. The results are presented in Fig. 6.

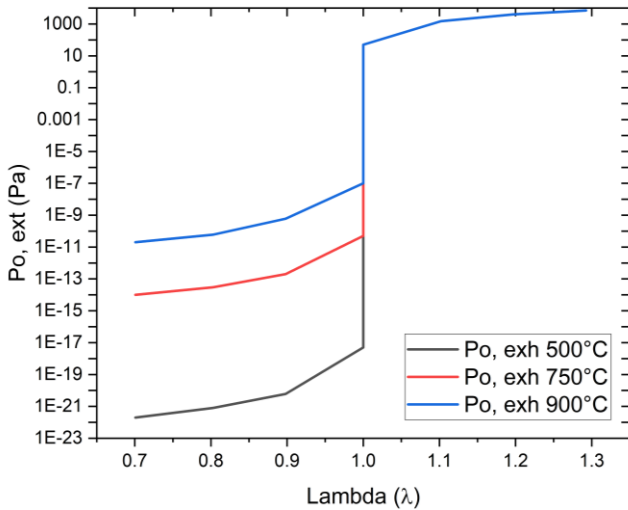


Fig. 6. Lambda vs partial pressure

The relationships were verified for the three temperatures indicated in the graph. A significant influence of temperature on the lambda sensor readings was detected on the rich side. This influence is so substantial that it greatly hinders the precise reading of rich mixtures using a narrowband sensor. For this reason, the first, more detailed calculations were carried out on the lean side. Initial results indicated a low influence of temperature on lean-side readings. More precise calculations were then performed, revealing an almost negligible impact of temperature on the sensor's readings on the lean side. This is illustrated in Fig. 7.

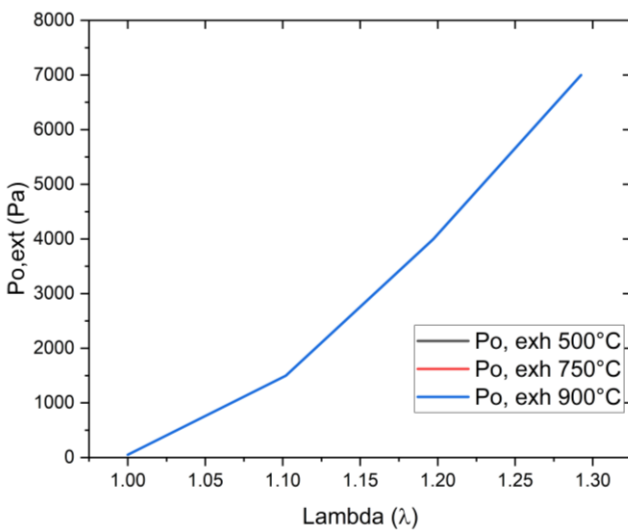


Fig. 7. Lean side of lambda sensor temperature dependence

The graphs for each temperature overlap. To better illustrate the full scope of the issue regarding the reading of lean and rich mixtures using a narrowband sensor, a graph was plotted where the y-axis represents lambda, and the x-axis indicates the difference in partial pressure as measured by the lambda sensor. The result is presented in Fig. 8.

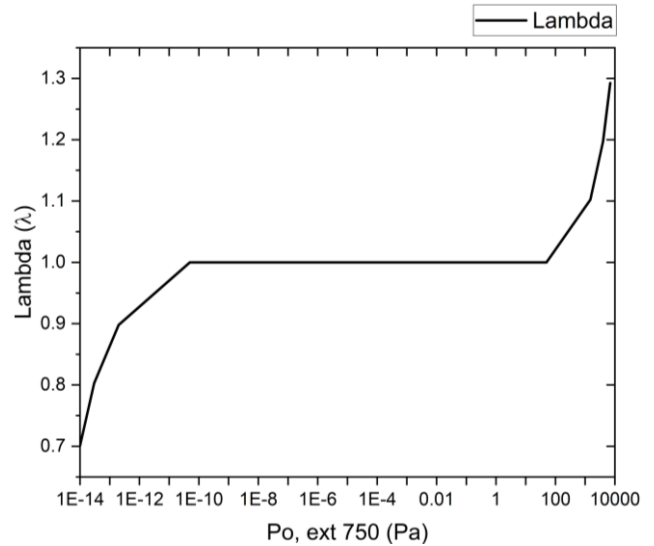


Fig. 8. Lambda vs partial pressure at 750 deg C

An important aspect is to pay close attention to the scale of the x-axis.

A closer look at the lean side of the lambda sensor readings revealed a nearly linear characteristic. For this reason, an attempt was made to determine the coefficients for the basic Rational5 function. The attempt was successful. The result is presented in Fig. 9.

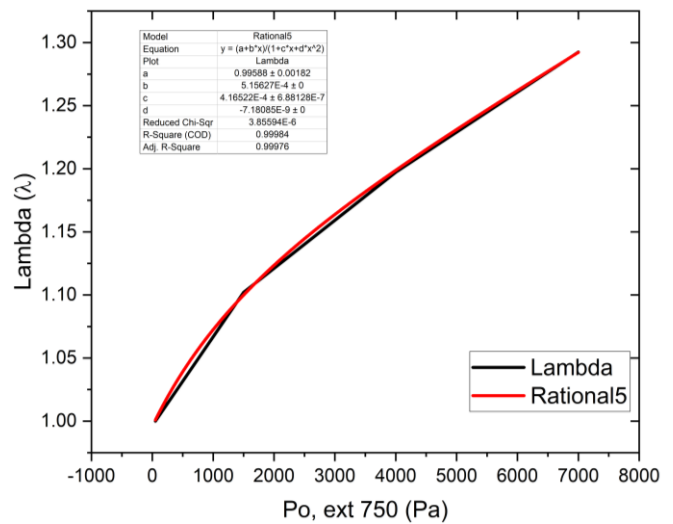


Fig. 9. Lean side of lambda sensor

This means that precise reading and control of the unit in closed-loop mode for lean mixtures is possible using a narrowband lambda sensor. The identified relationship was provisionally implemented for controlling the Ford EEC V system and a 1998 Ford 302 engine. Stable operation of the closed-loop correction system was achieved up

to the limits of stable engine operation on LPG fuel. For idle conditions, a lambda value of approximately 1.35 was reached. The controller's bias algorithm was modified to enforce only minimal voltage changes on the sensor, thereby eliminating large mixture swings. Due to the preliminary nature of this implementation, further in-depth research is required in this area, which is beyond the scope of this article. Subsequently, an attempt was made to find a function describing the lambda sensor readings on the rich side. Unfortunately, standard functions did not yield satisfactory results. However, a similarity was observed between the operating principle of the Nernst equation and the voltage generation mechanism in the lambda sensor cell, which is related to activation energy. The Arrhenius model, commonly used in semiconductor technology, turned out to be highly relevant. The similarity was not coincidental; the model very accurately describes the behavior of the sensor cell for rich mixtures. This is presented in Fig. 10.

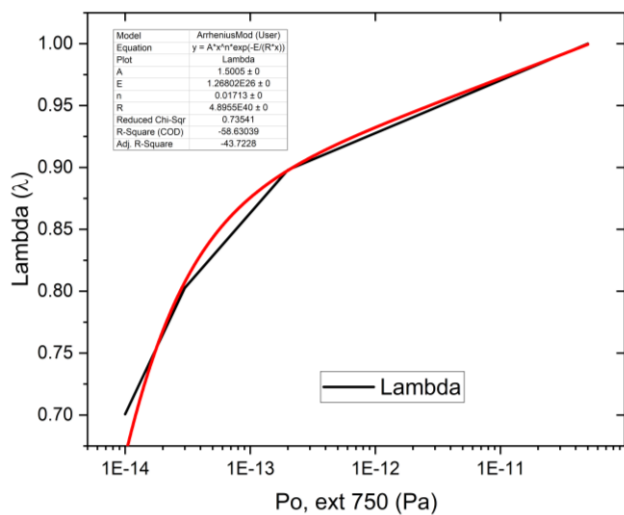


Fig. 10. Rich side of the lambda sensor

It can be observed that despite the large variation in partial pressures, it was possible to plot a curve based on the Arrhenius model. The greatest inaccuracy in the fit is seen

at a lambda value of 0.85. Above lambda 0.88, the fit is virtually perfect. The quality of the fit indicates the potential for practical application in a vehicle. After determining the coefficient values for the Arrhenius model and performing the temperature correction procedure, a complete relationship was developed, suitable for implementation in an engine control unit.

4. Summary and conclusion

The calculations, transformations, and tests performed using the narrowband sensor indicated the possibility of extending its application to include measurements in both lean and rich mixture ranges. However, measurements in the rich mixture range are associated with greater error and require more precise readings or a control system capable of maintaining a constant temperature in the lambda sensor. The downside of a system that maintains constant temperature is its inability to sustain that temperature under very high engine loads, which are typically the conditions where mixture enrichment occurs. The strong temperature dependency and very small partial pressure delta values on the rich side, combined with production variations among lambda sensors, raise doubts about achieving a reading accuracy for rich mixtures better than 10%. The situation is different on the lean side. Both the calculations and preliminary on-engine tests with the Ford 302 GT40P engine indicate proper sensor operation and the ability to accurately read lean mixture values. After algorithm adjustments, the Ford EEC V control system was able to operate correctly in closed-loop mode up to a lambda value of 1.35. The main modification to the control algorithm that was necessary for proper operation on the lean side was the adjustment of the bias and delay time. The control system is based on a PI (Proportional-Integral) controller. The bias and delay parameters are, in effect, indirect representations of the PI controller's parameters. Changes in their values affect overshoot, the functioning of the OBD II diagnostic system, and the rate of signal rise within the controller.

Further research is required to fully validate the algorithm's reliability. This, however, was beyond the scope of the present study.

Nomenclature

ADC	analog to digital converter	EEC	electric engine control
AFR	air to fuel ratio	LPG	liquid petroleum gas
CFD	computational fluid dynamics	PI	proportional-integral

Bibliography

- [1] Aravind S, Ragupathi P, Kumar DS, Vignesh G. A numerical investigation of automotive lambda sensor to improve the life span of the sensor using CFD. IOP Conf Ser Mater Sci Eng. 2020;923(1). <https://doi.org/10.1088/1757-899X/923/1/012003>
- [2] Bosch Engineering GmbH, Lambda Sensor LSU 4.9 data-sheet. 51865867 en, 1, 26. Aug. 2025
- [3] Collings N, Harris JA, Glover K. Estimating IC engine exhaust gas lambda and oxygen from the response of a universal exhaust gas oxygen sensor. Meas Sci Technol. 2013;24(9):095101. <https://doi.org/10.1088/0957-0233/24/9/095101>
- [4] Hills B. United States Patent Preparing Fire-Fighting Concentration US 4,464,267 1984;(19).
- [5] How Oxygen Sensor Works – Automotive Systems <https://youtu.be/F13aD1qJrEg?si=5diBaIOApx8ogVcH> (accessed on 10.06.2025).
- [6] Jakliński P, Czarnigowski J, Ścisłowski KJ. Study of the effect of ignition crank angle and mixture composition on the performance of a spark-ignition engine fueled with ethanol. Combustion Engines. 2024;197(2):56-63. <https://doi.org/10.19206/CE-174888>

- [7] Klett S, Piesche M, Heinzelmann S, Weyl H, Wiedenmann H, Schneider U et al. Numerical and experimental analysis of the momentum and heat transfer in exhaust gas sensors. SAE Technical Paper 2005-01-0037. 2005. <https://doi.org/10.4271/2005-01-0037>
- [8] Moos R, Izu N, Rettig F, Reiß S, Shin W, Matinfara I. Resistive oxygen gas sensors for harsh environments. Sensors. 2011;11(4):3439-3465. <https://doi.org/10.3390/s110403439>
- [9] Nishiyama A, Ikeda Y, Serizawa T. Lean limit expansion up to lambda 2 by multi-point microwave discharge igniter. 2018;247-260. Ignition Systems for Gasoline Engines: 4th International Conference December 6–7, 2018, Berlin. <https://doi.org/10.5445/IR/1000088587>
- [10] Run Lean Emissions Ecco modder forum thread <https://ecomodder.com/forum/showthread.php/run-lean-emissions-36327.html> (accessed on 10.06.2025)
- [11] Sensing the adequate mixture – the Bosch Lambda Sensor <https://www.bosch.com/stories/40-years-of-bosch-lambda-sensor/> (accessed on 10.06.2025).
- [12] Tang H, Prasad K, Sanjinés R, Lévy F. TiO₂ anatase thin films as gas sensors. Sensors and Actuators, B: Chemical. 1995. [https://doi.org/10.1016/0925-4005\(94\)01559-Z](https://doi.org/10.1016/0925-4005(94)01559-Z)
- [13] Toema M. Physics-based characterization of lambda sensor output to control emissions from natural gas fueled engines. An Abstract of a Disertation, Kansas State University, 2010.
- [14] Tutunea D, Dumitru I, Stănciuc-Oță OV. Overview of the use of oxygen sensors in automotive applications. IOP Conf Ser Mater Sci Eng. 2024;1303(1):012014. <https://doi.org/10.1088/1757-899X/1303/1/012014>
- [15] Urbański B, Przybyła G, Brodziński Ł, Savitskaya M. Reducing emissions of harmful substances in rally cars. Combustion Engines. 2024;197(2):132-8. <https://doi.org/10.19206/CE-181525>

Adam Kamiński, MEng. – Faculty of Mechanical Engineering, Wrocław University of Science and Technology, Poland.
e-mail: adam.kaminski@pwr.edu.pl



Preliminary research on the co-combustion process of ammonia in a compression-ignition engine

ARTICLE INFO

Received: 20 June 2025

Revised: 29 September 2025

Accepted: 29 September 2025

Available online: 22 November 2025

In the face of increasing requirements for exhaust emission reduction and the search for alternative fuels, ammonia is being considered as a potential fuel component in compression-ignition engines. The aim of this study was to conduct preliminary research on the co-combustion process of ammonia with diesel fuel and to assess its impact on exhaust emissions and engine performance characteristics. In the first stage, measurements of ammonia concentration in the exhaust gases were carried out to determine its presence in the exhaust stream. Next, optimal engine operating points were determined for various fuel ratios, enabling a comparative analysis of the combustion of pure diesel fuel and its mixtures with ammonia. In the final phase, key exhaust emission components were measured. The results indicate both potential benefits and challenges associated with using ammonia as a fuel additive in diesel engines. The conducted research provides a basis for further analysis aimed at optimizing the ammonia co-combustion process to improve efficiency and reduce its environmental impact.

Key words: ammonia combustion, combustion engines, combustion efficiency, alternative fuels, diesel engine decarbonization

This is an open access article under the CC BY license (<http://creativecommons.org/licenses/by/4.0/>)

1. Introduction

Rising environmental protection requirements, reductions in greenhouse gas emissions and the need to decouple the transport sector from fossil fuels have intensified the search for alternative energy carriers. This is particularly relevant for compression-ignition (CI) engines, which dominate in heavy transport, agriculture and distributed power generation, creating a demand for low-emission fuels that can be used with minimal modifications to existing technologies. In this context, ammonia (NH₃) is gaining attention as a potential fuel component or even as a standalone fuel [20].

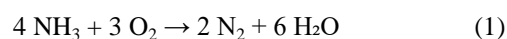
Ammonia is a chemical compound with physical and chemical properties that has been used for decades in the chemical and fertilizer industries. Its main advantages as a fuel includes: zero CO₂ emissions during combustion, the ability to store and transport it in liquid form, a well-developed distribution infrastructure and a high hydrogen content (17.6% by weight). Unlike pure hydrogen, which requires very high-pressure or low-temperature tanks, ammonia can be stored as a liquid at relatively low pressures (about 10 bar at ambient temperature), making it much more practical as an energy carrier. However, despite its advantages, using ammonia as a fuel in combustion engines involves significant limitations. Its lower heating value (18.6 MJ/kg) is more than twice as low as that of diesel fuel (about 42–45 MJ/kg), which means more mass needs to be burned to obtain the same amount of energy. Additionally, ammonia's auto-ignition temperature (~651°C) is significantly higher than that of typical CI engine fuels (about 210°C for diesel), making pure ammonia less reactive and harder to ignite under standard engine conditions [3, 11, 13, 17].

Because of these issues, co-combustion of ammonia with a conventional fuel like diesel is increasingly proposed. This hybrid approach leverages the advantages of both fuels: the high reactivity and energy density of diesel and the carbon-free combustion of ammonia. In compression

ignition (CI) engines, diesel injection can act as an ignition source for the ammonia-air mixture, promoting oxidation and improving combustion stability. By partially replacing diesel with ammonia, the overall reliance on fossil fuels can be reduced with implications for both efficiency and emissions [7, 13].

Another challenge in using ammonia effectively as an engine fuel is its low laminar flame speed, around 0.07 m/s, compared to methane or propane (0.3–0.4 m/s) and hydrogen (over 2 m/s). This low flame speed results in slower combustion of the fuel-air mixture, potentially leading to combustion irregularities, longer cycle durations and increased emissions of unburned ammonia. It is especially problematic in CI engine cyclic operation, where fast and stable combustion is essential. Therefore, research into ignition support and flame propagation acceleration strategies – such as pilot fuel injection, hydrogen blending or combustion chamber geometry modification is increasingly important [1, 19, 4, 21].

Ammonia combustion involves a complex reaction kinetics. The main combustion reaction is:



However, under practical engine conditions, with temperature gradients, uneven mixing and the presence of soot or unburned hydrocarbons – side reactions can occur, forming nitrogen oxides (NO, NO₂) and leading to unburned ammonia emissions (“NH₃ slip”). This is especially concerning due to ammonia's toxicity and pungent odor, which are noticeable even at a few ppm.

Thus, key challenges in ammonia-diesel co-combustion include selecting appropriate fuel ratios, engine operating conditions and fuel delivery techniques to optimally use the energy properties of the mixture while minimizing unwanted exhaust components. Additionally, the effects on overall efficiency – such as ignition delay, combustion duration,

peak cylinder pressure and pressure-volume curve characteristics must be considered [10, 13, 16].

An increasing number of experimental and numerical studies on ammonia combustion have been published, including fuel cells, gas burners and piston engines. These studies show that even small additions of high-reactivity fuel (e.g., diesel or hydrogen) can improve ammonia combustion and reduce unreacted molecule emissions. Still, many questions remain, especially regarding NO_x emissions under various operating conditions, flame stability and long-term engine component durability.

Ammonia (NH_3) is increasingly considered in the literature as a low-carbon energy carrier with potential use in fuel cells and combustion engines. Unlike hydrogen, ammonia is easier to store as a liquid and benefits from existing infrastructure. According to Zamfirescu and Dincer [22] producing “green ammonia” from renewable energy, can eliminate CO_2 emissions across its lifecycle.

Combustion studies highlight ammonia’s low reactivity, causing ignition issues and slow flame propagation. A laminar flame speed of ~ 0.07 m/s [6] is significantly lower than that of typical hydrocarbon fuels (0.3–0.4 m/s for methane, > 2 m/s for hydrogen), presenting a key technological challenge.

Studies have shown that even with ammonia shares of 10–30% by volume, stable engine operation is possible when diesel is used as a pilot fuel. Zhang et al. [23] reported reduced CO and HC emissions, while Reiter and Kong [14] confirmed improved ignition and combustion stability.

Lee et al. [8] pointed out a significant increase in NO_x emissions with higher ammonia content. This stems from Zeldovich reaction mechanisms and the presence of excess unburned ammonia (“ NH_3 slip”). These researchers recommend EGR systems and selective catalytic reduction (SCR) for emission control.

Ammonia combustion is governed by complex free radical kinetics involving H, OH and O radicals. Mørch et al. [12] noted that proper combustion conditions, moderate excess air and controlled peak temperatures can reduce NO_x emissions. They also highlighted that the pilot fuel injection strategy and timing significantly affect combustion efficiency. CFD models (e.g., using CHEMKIN) are increasingly applied to predict emissions for various combustion chamber setups.

Ammonia-fueled engine prototypes are being developed for road and marine transport. Toyota and Hyundai [20] are working on demonstration projects involving co-combustion of ammonia with diesel or hydrogen in commercial vehicle engines. MAN Energy Solutions is testing ammonia in medium-speed marine engines [9]. These projects focus on:

- exhaust gas recirculation (EGR) rates
- material resistance to ammonia (corrosion and degradation)
- NH_3 slip detection and mitigation.

Existing studies clearly show that pure ammonia combustion in CI engines is highly problematic. High ignition temperature, low reactivity, and slow flame speed make the use of pure ammonia technologically challenging. Co-combustion with a pilot fuel like diesel offers a promis-

ing workaround for ignition and combustion stability issues. Key factors for successful implementation include proper fuel ratio, injection timing, and combustion chamber thermal conditions. Despite growing research, experimental data on full-scale CI engines operating under realistic conditions remains limited [5, 15, 18].

The present study aims to analyze the co-combustion of ammonia with diesel in a CI engine, focusing on:

- ammonia combustion efficiency (including detection of residuals in exhaust gases)
- the impact of fuel mixture composition on key engine parameters.

Additionally, the study examines how co-combustion affects exhaust smoke, an indirect indicator of particulate matter from incomplete combustion. The experiment was conducted using an engine test bench under partial load and constant engine speed. The analysis in this preliminary study included combustion/overall efficiency derived from fuel flow, brake power and exhaust smoke. Gaseous emissions (NO_x , NH_3 , CO) and particle number (PN) were not part of the measurement scope.

2. Methodology

The tests were conducted on an engine test bench (Fig. 1) equipped with a Fiat 1.3 JTD compression-ignition engine with a nominal power output of 51 kW, a Schenck W150 eddy-current dynamometer and a data acquisition system for recording key engine operating parameters, including torque [Nm], engine speed [rpm], fuel consumption [g/h], exhaust gas temperature [$^{\circ}\text{C}$], intake air temperature, pressure and exhaust opacity (FSN). Diesel fuel consumption was measured gravimetrically using an Automex fuel balance with an accuracy of ± 0.1 g. The fuel mass flow rate was recorded in grams per hour (g/h), enabling precise calculation of specific fuel consumption and overall combustion. Ammonia was supplied to the engine in gaseous form via a custom-designed mixing system integrated into the intake manifold downstream of the charge air cooler. The ammonia source was a high-pressure cylinder (61 L) from Messer, containing Ammonia 3.8 (99.98%) and corresponding to 32 kg of gas. The operating pressure of the cylinder was 8–10 bar at room temperature (20°C), and the valve used was compliant with DIN standards for toxic gases. Ammonia was delivered in the gas phase, and its temperature was maintained within the range of 15 – 25°C to ensure repeatability of the mixing process.

The measurement of the ammonia flow rate was carried out using a rotameter EK2/NR, with simultaneous monitoring of the gas temperature. To ensure operational safety, the guidelines provided by the gas manufacturer, as well as occupational health and safety regulations related to the use of toxic substances, were strictly followed.

The load characteristics were determined at a constant engine speed of 1200 rpm and within a load range of 20 to 80 Nm. After achieving thermal stabilization of the engine at a given operating point, its performance parameters were recorded while fueled exclusively with diesel. Subsequently, ammonia was introduced into the intake system and data on the consumption of both fuels as well as exhaust smoke opacity (FSN values, converted to mg/m^3) were collected. Other gaseous pollutants (NO_x , NH_3 , CO, PN) were not

measured at this stage and will be addressed in follow-up studies.

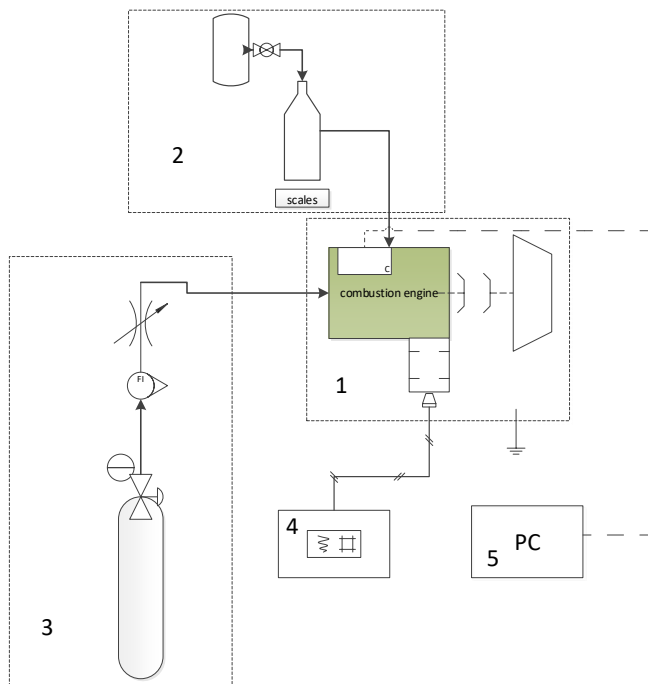


Fig. 1. Test bench schematic: 1) engine test bench, 2) fuel consumption measurement system (mass-based), 3) ammonia supply system, 4) AVL 415 smoke meter, 5) data acquisition computer

This operating point was chosen as a representative condition for low-to-medium speed operation, typical of stationary CI engines (e.g., generators, agricultural machinery). The fixed speed also ensured safe and stable conditions during preliminary trials with ammonia, enabling repeatable measurements. The selected load range corresponds to partial load operation, where efficiency and emission trade-offs are particularly relevant for practical applications.

In each case, exhaust gas opacity was measured using an AVL 415 smoke meter, which enabled the assessment of particulate matter content depending on the composition of the fuel mixture. A computer-based data acquisition system was used for data collection and recording, allowing real-time monitoring of engine performance parameters and measurement results.



Fig. 2. Test bench

The formula used to calculate the overall efficiency is as follows:

$$\eta_{\text{comb}} = \frac{P_{\text{engine}}}{\dot{m}_{\text{NH}_3} \cdot \text{LHV}_{\text{NH}_3} + \dot{m}_{\text{diesel}} \cdot \text{LHV}_{\text{diesel}}} \quad (2)$$

where: η – overall efficiency, P_{engine} – engine output power (mechanical), \dot{m}_{nh_3} , \dot{m}_{diesel} – mass flow rates of ammonia and diesel fuel [kg/s], LHV – lower heating value of the respective fuel [MJ/kg].

The conversion of Filter Smoke Number (FSN) values obtained using the AVL 415 smoke meter into units of mg/m^3 was based on an empirical relationship found in the literature:

$$\text{PM} = 1.63 \cdot e^{(1.08 \cdot \text{FSN})} \quad (3)$$

where: PM – mass concentration of particulate matter in the exhaust gas [mg/m^3], FSN – Filter Smoke Number measured directly by the smoke meter, e – base of the natural logarithm (≈ 2.718).

This formula [2] is based on standard measurement conditions for diesel engines fueled with conventional diesel. It should be noted that this conversion is approximate and does not substitute for direct gravimetric determination of particulate mass.

3. Results and experimental analysis

3.1. Influence of ammonia energy share in the fuel mixture on overall efficiency

The data were obtained based on actual efficiency measurements for individual fuel blends containing from 0 up to nearly 60% of ammonia energy share.

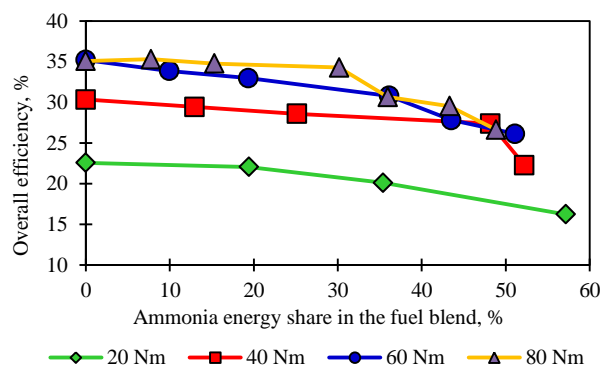


Fig. 3. Influence of the ammonia-derived energy share on overall efficiency at a constant engine speed of 1200 rpm under varying loads

For all analyzed cases, a consistent decrease in overall efficiency was observed as the percentage of ammonia energy in the fuel mixture increased. The highest efficiencies were obtained during combustion of pure diesel fuel. At the same time, the lowest were recorded for mixtures with the maximum ammonia content. Initial overall combustions (at 0% NH_3) were as follows:

1. 22.57% – 20 Nm
2. 30.33% – 40 Nm
3. 35.20% – 60 Nm
4. 35.08% – 80 Nm.

At the highest ammonia shares, the efficiencies decreased to:

1. 16.24% – 57.16% NH₃, 20 Nm
2. 22.27% – 52.21% NH₃, 40 Nm
3. 26.13% – 51.09% NH₃, 60 Nm
4. 26.64% – 48.85% NH₃, 80 Nm.

A detailed analysis of the measured parameters highlights how increasing ammonia content influences the combustion process under various load conditions. The decrease in overall efficiency with increasing ammonia energy share is clear and progresses non-linearly – most significant changes occur above ~30% NH₃. At low and medium loads (20–60 Nm), the largest absolute drops in efficiency were observed – up to 6–9 percentage points, corresponding to a relative decrease of approximately 25–30%. At the highest load (80 Nm), the efficiency drop was slightly less pronounced (from 35.08% to 26.64%) but still significant. The higher combustion chamber temperature at high load likely promotes better ammonia oxidation. The decrease in efficiency results directly from the properties of ammonia as a fuel: high ignition temperature, low lower heating value and limited reactivity under compression ignition conditions. Increasing amounts of unburned ammonia in the exhaust gases contribute to real energy losses. Despite these losses, the presence of unburned ammonia in the exhaust can be beneficial from the perspective of SCR (Selective Catalytic Reduction) systems, where ammonia acts as a reducing agent for NO_x. This opens the possibility of reducing or eliminating the need for AdBlue dosing. An integrated approach to combustion and exhaust aftertreatment may enable the implementation of ammonia-diesel co-combustion technology while maintaining acceptable efficiency and emission performance.

3.2. Influence of ammonia energy share in the fuel mixture of exhaust smoke opacity

Figure 4 presents the converted exhaust smoke opacity values expressed in mass units (mg/m³), calculated based on the FSN (Filter Smoke Number) measurement results. These values provide a more direct indication of the mass emission of particulate matter, which may be relevant from an environmental regulatory perspective. The data are detailed in Table 1.

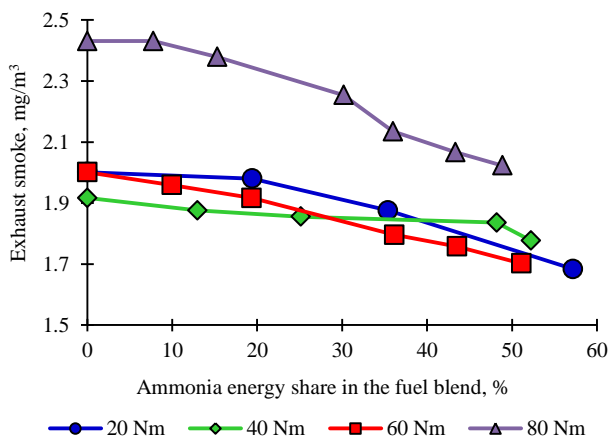


Fig. 4. Relationship between the ammonia-derived energy share (in dual-fuel operation: diesel injection + gaseous ammonia supply) and exhaust smoke opacity at 1200 rpm across different engine loads

Table 1. Effect of ammonia-derived energy share (dual-fuel mode: diesel + ammonia) on exhaust smoke (FSN and mg/m³) at different torque levels [Nm]

Nm	20						
%	0.00	19.41	35.39	57.16			
FSN	0.19	0.18	0.13	0.03			
mg/m ³	2.00	1.98	1.88	1.68			
Nm	40						
%	0.00	12.94	25.13	48.8	52.21		
FSN	0.15	0.13	0.12	0.11	0.08		
mg/m ³	1.92	1.88	1.86	1.84	1.78		
Nm	60						
%	0.00	9.93	19.34	36.12	43.53	51.09	
FSN	0.9	0.17	0.15	0.09	0.07	0.04	
mg/m ³	2.00	1.96	1.92	1.80	1.76	1.70	
Nm	80						
%	0.00	7.77	15.30	30.16	35.97	43.31	48.85
FSN	0.37	0.37	0.35	0.30	0.25	0.22	0.20
mg/m ³	2.43	2.43	2.38	2.25	2.14	2.07	2.02

The analysis below outlines the experimental findings regarding particulate emissions during ammonia-diesel co-combustion across different engine load conditions. At all load levels, a clear trend of decreasing particulate emissions (mg/m³) is observed with increasing ammonia-derived energy share in the fuel mixture. The highest absolute particulate emission values were recorded at the highest load (80 Nm), where emissions decreased from approximately 2.45 mg/m³ to 2.10 mg/m³ (a ~14% reduction). At lower loads (20–60 Nm), the relative reduction in particulate emissions was more pronounced, exceeding 15% at 20 Nm (from ~2.00 mg/m³ to ~1.65 mg/m³). Converting FSN to mg/m³ enables more accurate comparisons with emission standards. It confirms that ammonia co-combustion can positively impact the reduction of particulate mass emissions.

The following observations provide additional insight into the underlying causes and broader implications of the observed emission trends. The reduction in particulate matter with a higher ammonia energy share may be attributed to the lower carbon content in the blended fuel (hydrocarbons, ammonia), resulting in less soot formation during combustion. The presented results confirm a general trend: despite a decrease in thermal efficiency, ammonia-containing mixtures exhibit a more favorable particulate emission profile, which may be important in the context of air quality regulations and decarbonization strategies.

Reference of results to current emission standards

To enhance the practical relevance of the obtained results, the converted filter smoke number (FSN) values expressed in mass units (mg/m³) were compared with the current emission standards in force within the European Union. Although the conducted study was experimental in nature and did not follow a full homologation cycle (e.g.,

WLTP or NRTC), The measured particulate matter emissions can be approximately compared with regulatory thresholds applicable to various engine categories. Examples of particulate matter emission standards:

1. Euro 6d (for diesel passenger vehicles):
 - particulate mass: 4.5 mg/km
 - particle number: 6×10^{11} /km.
2. Stage V (for non-road mobile machinery and stationary engines):
 - for power range 19–56 kW: 15 mg/m³ (or 0.015 g/kWh)
 - for higher power ranges (e.g., 56–130 kW): limits are similar or slightly higher.

In the conducted tests, the highest measured particulate emission value (at 80 Nm torque and 0% ammonia) was approximately 2.45 mg/m³. In contrast, the lowest value for the same operating point (with 48.85% ammonia) dropped to 2.10 mg/m³. At lower loads, emissions decreased even further, reaching 1.65 mg/m³ at 20 Nm and ~57% ammonia. This indicates that all measured particulate values are significantly below the 15 mg/m³ limit defined in the Stage V standard, regardless of the ammonia energy share. Ammonia co-combustion contributes to a 10–20% reduction in particulate emissions, further distancing the results from the regulatory thresholds. Even under suboptimal conditions (highest load, low ammonia content) the powertrain remains compliant with emission standards applicable to modern non-road engines.

From an environmental regulatory perspective, the results clearly demonstrate that co-combustion of ammonia with diesel fuel can be implemented without the risk of exceeding permissible particulate matter (PM) emission limits, even at high ammonia energy shares in the fuel mixture. The measured PM emission levels remain fully compliant with Stage V standards, indicating the potential applicability of this solution in engines used in construction machinery, power generators, and off-road equipment. The reduction in PM mass emissions observed during ammonia co-combustion may be considered a significant environmental benefit of this technology, not only in terms of reducing local soot emissions but also in contributing to the mitigation of low-stack emissions and the improvement of air quality. However, it is important to note that the current data only reflect particulate emissions. The comparison to EU regulatory PM limits is illustrative. The study did not follow a certification cycle nor did it measure PN/NO_x/NH₃/CO. The lack of measurements for gaseous pollutants highlights the need for further studies before this combustion concept can be fully classified as compliant with Euro or Stage V emission regulations.

3.3. Decrease in co-combustion efficiency depending on the ammonia-derived energy share in the fuel mixture

The analysis considered the decrease in overall efficiency of a compression-ignition engine as a function of the increasing ammonia-derived energy share in the fuel mixture, across four engine load levels: 20, 40, 60 and 80 Nm (all at a constant speed of 1200 rpm). As a reference point, the efficiency values obtained with diesel-only fueling were adopted, amounting to:

- 22.57% at 1200 rpm, 20 Nm
- 30.33% at 1200 rpm, 40 Nm
- 35.20% at 1200 rpm, 60 Nm
- 35.08% at 1200 rpm, 80 Nm.

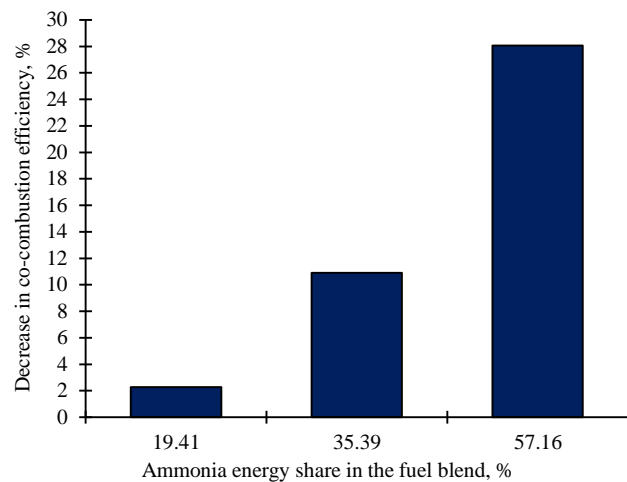


Fig. 5. Decrease in co-combustion efficiency depending on the ammonia energy share in the fuel blend at an engine speed of 1200 rpm and a load of 20 Nm

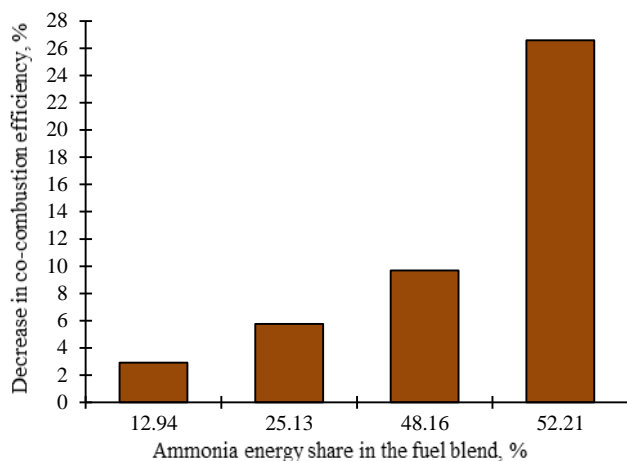


Fig. 6. Decrease in co-combustion efficiency depending on the ammonia energy share in the fuel blend at an engine speed of 1200 rpm and a load of 40 Nm

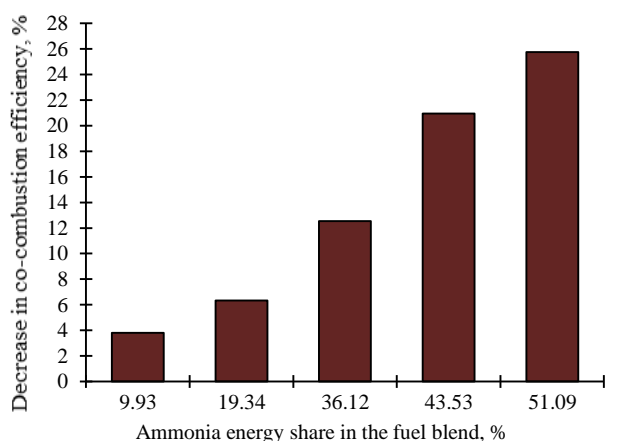


Fig. 7. Decrease in co-combustion efficiency depending on the ammonia energy share in the fuel blend at an engine speed of 1200 rpm and a load of 60 Nm

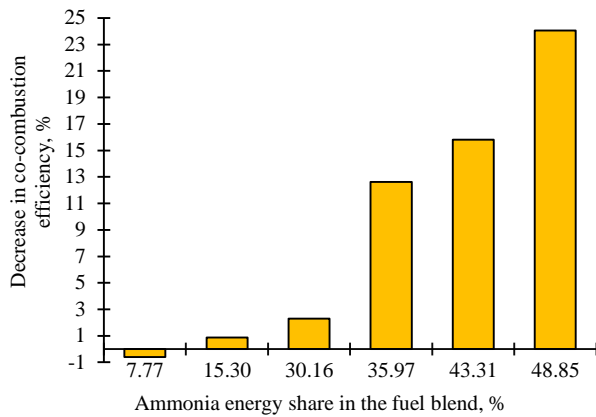


Fig. 8. Decrease in co-combustion efficiency depending on the ammonia energy share in the fuel blend at an engine speed of 1200 rpm and a load of 80 Nm

As the ammonia-derived energy share in the fuel mixture increased, a consistent decline in overall efficiency was observed. These changes are illustrated in Fig. 5–8 as a percentage drop in efficiency relative to the baseline diesel-only values.

The analysis below highlights how increasing the ammonia-derived energy share in a diesel–ammonia fuel blend affects overall efficiency under varying load conditions. It also outlines key patterns, practical implications and technical observations based on the recorded results.

A clear trend was noted across all engine operating points: increasing the ammonia energy share in the fuel blend leads to a systematic and nonlinear decline in overall efficiency, especially above 30–35% NH_3 . The largest absolute efficiency drop occurred at a load of 20 Nm, with a 28.05% decrease at 57.16% ammonia, reducing efficiency from 22.57% to 16.24%. At 40 Nm, the maximum efficiency loss was 26.57% at 52.21% NH_3 (final efficiency: 22.27%). For 60 Nm and 51.09% NH_3 , efficiency declined from 35.20% to 26.13%, a 25.77% drop. At the highest load, 80 Nm, a reduction from 35.08% to 26.64% (24.06%) was observed with 48.85% ammonia. An interesting anomaly was noted at 80 Nm with a low ammonia share (7.77%), where a slight efficiency increase of 0.6% was recorded. This effect may be attributed to favorable thermal conditions at high load enabling more complete oxidation of a small fraction of ammonia and possibly enhancing radical-driven reactions. However, given the small magnitude of this change it may also fall within the range of experimental uncertainty. Further tests are required to confirm whether this effect is systematic. At high ammonia shares, final efficiency values tend to converge across different loads, indicating that the engine operates with similar efficiency regardless of torque at elevated NH_3 levels, but with clearly higher energy losses compared to pure diesel operation. The efficiency drop is mainly attributed to incomplete ammonia combustion, resulting from its high auto-ignition temperature and lower heating value. A higher NH_3 content leads to more unburned fuel and lower usable energy output. From a practical standpoint, small to moderate ammonia admixtures (up to ~20%) may be environmentally justified, as efficiency losses remain relatively minor and are offset by the reduction in particulate emissions. Additional-

ly, the presence of unburned ammonia in the exhaust may be beneficial for selective catalytic reduction (SCR) systems. As a natural NO_x reductant, ammonia could potentially replace synthetic AdBlue, simplifying emission control systems and lowering operating costs.

4. Future research directions

4.1. Development of a method for measuring ammonia content in exhaust gases

The results of the conducted study demonstrated both the environmental potential of ammonia–diesel co-combustion (primarily in reducing particulate matter emissions) and the limitations stemming from decreased system energy efficiency. Based on these findings, several key areas have been identified for further experimental and development work.

Future research should focus on developing a dedicated analytical method – e.g., using UV-VIS spectrophotometry combined with cuvette tests. One of the main limitations of the current experiment was the inability to directly measure ammonia concentration in the exhaust due to interference with the chemical gas analyzer. The proposed approach includes:

- use of reagents that selectively react with NH_3 in the presence of NO_x and other exhaust components
- standardization of measurements using portable laboratory kits
- calibration of the method against known concentrations, with the possibility of integrating it into a sampling system directly from the exhaust line.

4.2. Optimization of diesel injection strategy

The observed efficiency drop with increasing ammonia share is largely due to inefficient combustion. Therefore, research should be conducted on modifying the diesel injection strategy, aiming to:

- adjust injection pressure and timing for both pilot and main injection events
- adapt the fuel injection control algorithm to the thermal and ignition properties of the diesel–ammonia mixture.

Such modifications could improve ignition quality and reduce the amount of unburned ammonia, thereby increasing overall efficiency.

4.3. Research on ammonia–hydrogen mixtures and use of ammonia decomposition catalysts

The use of hydrogen as a co-fuel or the application of catalysts that decompose ammonia into hydrogen and nitrogen has been proposed in the literature as a means of improving combustion stability and efficiency. Hydrogen's high reactivity can enhance ignition and flame propagation while catalytic decomposition could provide an in-cylinder source of hydrogen. Although not investigated in this study, these strategies represent complementary approaches that may support future development of ammonia-based engine technologies.

5. Conclusions

The experiments on ammonia–diesel co-combustion in a compression-ignition engine demonstrated both advantages and limitations of this approach. A clear decline in

overall efficiency was observed as the share of ammonia-derived energy increased, with the most pronounced reductions occurring above approximately 30% ammonia. These efficiency losses reached about 25–30% relative to pure diesel operation and were attributed primarily to the high ignition temperature and low reactivity of ammonia which resulted in incomplete combustion and greater energy losses. At the same time, a consistent decrease in particulate emissions was recorded with increasing ammonia content. Expressed both as FSN and in converted mass units, particulate emissions fell by more than 15% at low loads and by 10–14% at high loads which represents a significant improvement in soot-related exhaust quality. Importantly, even under the least favorable operating conditions, particu-

late matter levels remained far below the Stage V regulatory limits, suggesting that ammonia–diesel co-combustion can be applied without compromising compliance with current emission standards. The presence of unburned ammonia in the exhaust stream also indicates potential integration with selective catalytic reduction systems where ammonia could act directly as a NO_x reductant, reducing or eliminating the need for additional reagents. From a practical standpoint, moderate substitution of diesel with ammonia, up to around 20% of the energy share appears to be the most promising compromise offering notable emission benefits while limiting efficiency losses to an acceptable level.

Nomenclature

CI	compression ignition	LHV	lower heating value
EGR	exhaust gas recirculation	PM	particulate matter
FSN	filter smoke number	SCR	selective catalytic reduction

Bibliography

- Alnajideen M, Shi H, Northrop W, Emberson D, Kane S, Czyzewski P et al. Ammonia combustion and emissions in practical applications: a review. *Carbon Neutrality*. 2024; 3(1):13. <https://doi.org/10.1007/s43979-024-00088-6>
- AVL. AVL 415S Smoke meter instruction manual. Graz (Austria): AVL List GmbH; 2014.
- Giddey S, Badwal SPS, Kulkarni A. Review of electrochemical ammonia production technologies and materials. *Int J Hydrogen Energy*. 2013;38(34):14576-14594. <https://doi.org/10.1016/j.ijhydene.2013.09.054>
- Guan Y, Zhao D. Enhancing ammonia combustion with minimum hydrogen blended in presence of self excited intermittent pulsating oscillations. *Phys Fluids*. 2023;35(5): 054102. <https://doi.org/10.1063/5.0147474>
- Hari KK, Ganesan N. Experimental investigation on the impact of ammonia fuel in a low powered compression ignition engine – a study toward dual fuel engine approach. *Environ Prog Sustainable Energy*. 2025;44(3):e14580. <https://doi.org/10.1002/ep.14580>
- Hayakawa A, Goto T, Mimoto R, Arakawa Y, Kudo T, Kobayashi H. Laminar burning velocity and Markstein length of ammonia/air premixed flames at various pressures. *Fuel*. 2015;159:98-106. <https://doi.org/10.1016/j.fuel.2015.06.070>
- Jamrozik A, Tutak W, Pyrc M, Grab-Rogaliński K. Experimental study on ammonia diesel co-combustion in a dual fuel compression ignition engine. *J Energy Inst*. 2024;115: 101711. <https://doi.org/10.1016/j.joei.2024.101711>
- Lee J, Park C, Jang I, Kim M, Park G, Kim Y. Experimental research on the effect of diesel post injection conditions on the efficiency and global warming potential in a single cylinder four stroke marine engine fueled with ammonia and diesel. *Energy*. 2025;314:134244. <https://doi.org/10.1016/j.energy.2024.134244>
- MAN Energy Solutions. Ammonia as a marine fuel: perspectives for two stroke marine engines. Technical paper, MAN B&W; 2023.
- Mashruk S, Shi H, Mazzotta L, Ustun CE, Aravind B, Meloni R et al. Perspectives on NO_x emissions and impacts from ammonia combustion processes. *Energy & Fuels*. 2024;38(20):19253-19292. <https://doi.org/10.1021/acs.energyfuels.4c03381>
- Mielcarzewicz D. Technical indicators of ammonia heavy duty engines. *Rail Vehicles/Pojazdy Szynowe*. 2024;3-4:54-63. <https://doi.org/10.53502/RAIL-202183>
- Mørch CS, Bjerre A, Gøttrup MP, Sorenson SC, Schramm J. Ammonia/hydrogen mixtures in an SI engine: engine performance and analysis of a proposed fuel system. *Fuel*. 2011;90(2):854-864. <https://doi.org/10.1016/j.fuel.2010.09.042>
- Nadimi E, Przybyla G, Lewandowski MT, Adamczyk W. Effects of ammonia on combustion, emissions, and performance of the ammonia/diesel dual fuel compression ignition engine. *J Energy Inst*. 2023;107:101158. <https://doi.org/10.1016/J.JOEI.2022.101158>
- Reiter AJ, Kong SC. Combustion and emissions characteristics of compression ignition engine using dual ammonia-diesel fuel. *Fuel*. 2011;90(1):87-97. <https://doi.org/10.1016/j.fuel.2010.07.055>
- Scharl V, Sattelmayer T. Ignition and combustion characteristics of diesel piloted ammonia injections. *Fuel Communications*. 2022;11:100068. <https://doi.org/10.1016/j.jfueco.2022.100068>
- Sharma V, Panesar A, de Sercey G, Begg S. A review of ammonia combustion and emissions characteristics in spark ignition engines and future road map. *Energies*. 2025;18(1): 41. <https://doi.org/10.3390/en18010041>
- Stępień Z. Ammonia as an alternative fuel to internal combustion engines. *Combustion Engines*. 2025;200(1):117-127. <https://doi.org/10.19206/CE-200289>
- Sun J, Tang Q, Wen M, Huang L, Liu H, Yao M. Combustion characteristics and flame development of ammonia in an optical spark ignition engine. *Fuel*. 2024;375:132601. <https://doi.org/10.1016/j.fuel.2024.132601>
- Sun J, Zhao N, Zheng H. A comprehensive review of ammonia combustion: fundamental characteristics, chemical kinetics, and applications in energy systems. *Fuel*. 2025; 394:135135. <https://doi.org/10.1016/j.fuel.2025.135135>
- Tornatore C, Marchitto L, Sabia P, De Joannon M. Ammonia as green fuel in internal combustion engines: state of the art and future perspectives. *Front Mech Eng*. 2022;8:944201. <https://doi.org/10.3389/fmech.2022.944201>
- Yasiry A, Wang J, Zhang L, Dai H, Abdurraheem AAA, Shahad HAK et al. Experimental study on the effect of hy-

drogen addition on the laminar burning velocity of methane/ammonia–air flames. *Appl Sci.* 2023;13(10):5853.
<https://doi.org/10.3390/app13105853>

- [22] Zamfirescu C, Dincer I. Using ammonia as a sustainable fuel. *J Power Sources.* 2008;185(1):459-465.
<https://doi.org/10.1016/j.jpowsour.2008.02.097>

Adriana Włoka, DEng. – Faculty of Mechanical Engineering, Wrocław University of Science and Technology, Poland.
e-mail: adriana.wloka@pwr.edu.pl



- [23] Zhang X, Yalamanchi K K, Sarathy S M. Combustion chemistry of ammonia/C1 fuels: A comprehensive kinetic modeling study. *Fuel.* 2023;341:127676.
<https://doi.org/10.1016/j.fuel.2023.127676>

Kacper Leśny, DEng. – Faculty of Mechanical Engineering, Wrocław University of Science and Technology, Poland.
e-mail: kacper.lesny@pwr.edu.pl



Radosław Włostowski, DEng. – Faculty of Mechanical Engineering, Wrocław University of Science and Technology, Poland.
e-mail: radoslaw.wlostowski@pwr.edu.pl



Prof. Andrzej Kaźmierczak, DSc., DEng. – Faculty of Mechanical Engineering, Wrocław University of Science and Technology, Poland.
e-mail: andrzej.kazmierczak@pwr.edu.pl



Assessment of the oxidative stability of biofuels for compression ignition engines

ARTICLE INFO

Received: 5 August 2025
Revised: 5 October 2025
Accepted: 6 October 2025
Available online: 22 November 2025

The use of biofuels is one way of reducing the increasingly visible, harmful impact of diesel engines on the environment. At the same time, it is also a way of gradually reducing dependence on depleting oil reserves. New sources of biodiesel production are currently being sought. New types of plant-based fuels are constantly being introduced to the market. Due to their different chemical composition compared to diesel fuel, these fuels may have significantly lower oxidation resistance. Oxidation stability is one of the basic performance characteristics of fuels used in diesel engines. This article presents the results of oxidation stability tests carried out using the RapidOxy device from Anton Paar, which uses a small-scale accelerated oxidation method in accordance with PN EN 16091:2023-1. The tests were carried out on diesel fuel and biofuels of various origins. Fuels such as diesel fuel without ester additives B0, diesel fuel with 7% FAME additive designated as B7, rapeseed fatty acid methyl esters (RME) and methyl esters from animal waste (AME). The tests were carried out at various measurement temperatures ranging from 110 to 140°C.

Key words: *combustion engines, biofuels, oxidative stability*

This is an open access article under the CC BY license (<http://creativecommons.org/licenses/by/4.0/>)

1. Introduction

Internal combustion engines are currently the basis for the propulsion of various types of machines and means of transport [9, 20]. The advantages of internal combustion engines, related to their reliability, high overall efficiency, and small size depending on power, have led to their rapid development, especially in the last dozen or so years. However, combustion engines also have disadvantages which, in the current era of global pressure to protect the environment, are coming to the fore, leading to measures aimed at improving their environmental and operational parameters [14, 16]. These changes are also motivated by other, often conflicting factors, such as supporting the local economy, energy independence, and the desire to reduce emissions of particulate matter and carbon oxides into the atmosphere. Emphasis is also placed on minimizing emissions of harmful compounds into the atmosphere and improving the efficiency of the engine itself, which translates into reduced fuel consumption. These trends have a significant impact on engine design changes, but also on the types of fuels used to power engines [7, 21]. The designs of today's internal combustion engines differ significantly from their predecessors. The first self-igniting engines had low efficiency, not exceeding 30%. Today's engines, using advanced technological solutions and control systems, achieve a power output of around 60 kW from a displacement of 1 liter, and their efficiency is close to 50%. Optimizing the fuel combustion process in a compression ignition engine with multi-stage injection of hydrocarbon fuel and fuel with bio-components in a common rail system is currently the main focus of research in the field of biofuel technology and engine design, including fuel supply systems. This is due to the fact that the combustion process of the mixture in the engine's working space determines its efficiency and positive environmental impact [13, 17]. The above-mentioned factors have a significant impact on the composition and sources of fuel. Currently, there is a significant use of renewable fuels. In addition, the requirements for fuels neces-

sitate the use of new additives that significantly improve their properties. Most of the fuels currently produced and sold for compression ignition engines contain up to 7% higher fatty acid esters [6, 12]. This has necessitated the development of fuel additives designed to counteract changes in the properties of these fuels associated with changes in their composition [11, 26]. Currently, there are many engine fuel additives on the market designed to improve the performance of the final product, which can be divided into two groups. One group is used to ensure the properties necessary for the production, distribution, and storage of fuel. Fuel resistance to oxidation is particularly important in this group. The second group is designed to ensure appropriate performance properties, such as adequate lubricity, high cetane number, and combustion chamber cleanliness [4].

Currently, additive packages are used, which can be divided into two groups. The first group includes additives that improve engine performance, including those that increase the cetane number, lubricity parameters, detergent additives, and those that prevent the formation of deposits. The second group of additives improves fuel distribution and storage. These include anti-foaming, antistatic, anti-corrosion, depressants, demulsifiers, biocides and antioxidants. As mentioned earlier, one of the basic requirements for fuels in terms of storage is their resistance to oxidation, which causes fuel instability [10, 15, 25, 27].

Oxidation stability is one of the most important parameters determining the suitability of fuels for storage and warehousing. This is particularly important in view of the need to create mandatory stocks and reserve stocks of petroleum products. Long-term storage causes the product to age and thus changes its physicochemical parameters. This phenomenon contributes to the degradation and aging of motor fuels, especially diesel oils and biofuels. It affects both the operation of the engine and the durability of many of its components. Free acids formed during spontaneous oxidation have a strong corrosive effect. In addition, acidic

oxidation products can contribute to the degradation of engine components, causing increased corrosion and faster destruction of various types of seals [5]. The compounds that form during oxidation are high-molecular-weight insoluble polymers and resins that form suspensions and deposits that can cause damage and failure of the injection equipment [12, 13, 19]. They can also adversely affect the formation and combustion of the fuel mixture.

The process of diesel fuel oxidation with FAME is a complex, multi-stage chemical reaction that begins with the formation of peroxides and hydrogen peroxide. These are the primary oxidation products that subsequently participate in the formation of secondary oxidation products in the form of aldehydes, low-molecular-weight carboxylic acids, formic acid, formic acid ester, and high-molecular-weight fatty acid oligomers formed as a result of oxidative polymerization [8, 18]. The products of the secondary oxidation process cause the formation of resins, sludge and other insoluble compounds, which may, among other things, cause damage to the fuel system. The oxidative stability of fatty acid methyl esters themselves depends on the composition of the fuel and, above all, on the amount of unsaturated fatty acid esters that constitute the FAME esters. The more unsaturated bonds there are in the fatty acid chain, the lower the oxidative stability of the esters.

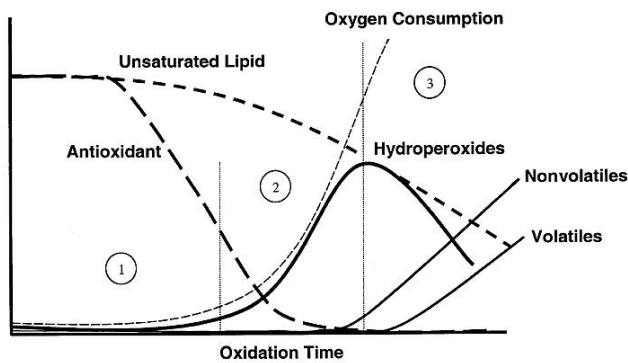


Fig. 1. Mechanism of oxidation of polyunsaturated fatty acid esters [8, 18]

The first phase is the induction period, during which oxygen consumption proceeds slowly due to the action of oxidation inhibitors. As time passes, the concentration of oxidation inhibitors decreases. The quality of fatty acid methyl esters does not undergo oxidative degradation because the free radicals that form react mainly with oxidation inhibitors. The time that fuel remains in this phase of the oxidation process depends on the reactivity of the esters and the concentration and type of oxidation inhibitors used, as well as the influence of temperature, light exposure, and oxygen availability. The second phase of the oxidation process is the phase of exponential growth of hydroperoxides and oxygen consumption, as well as a complete decrease in the concentration of oxidation inhibitors. The third phase is a rapid increase in the production of volatile acids and aldehydes, as well as the products of their secondary reactions. These form products that are precursors to the formation of deposits. In addition, the rate of decomposition of hydroperoxides in this phase is higher than the rate of their formation. The oxidative stability of fatty acid me-

thyl esters is significantly lower than that of standard or pure diesel fuel. This has a direct impact on the change in its physicochemical and tribological properties. For example, authors [18] subjected rapeseed and soybean biodiesel to oxidation in an autoclave reactor and then evaluated the functional groups, viscosity, and density of the biodiesel sample. It was found that oxidation causes the formation of two phases that tend to form a complex oil-oil emulsion. The supernatant and sediment phases were then separated and examined using Fourier transform infrared spectroscopy, which showed that polarisation influenced the separation rate. Therefore, the solid precipitate was not only induced by surface contact with the fuel but also stimulated in the liquid phase of the fatty acid methyl ester [1, 18]. Figure 2 shows the biodiesel oxidation process.

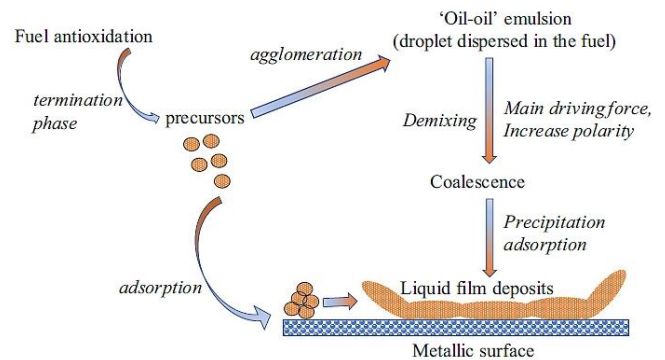


Fig. 2. Mechanism of biodiesel oxidation [1, 18]

An integrated mechanism of fatty acid methyl ester oxidation showing competing alternative reactions is shown in Fig. 3 [28, 29].

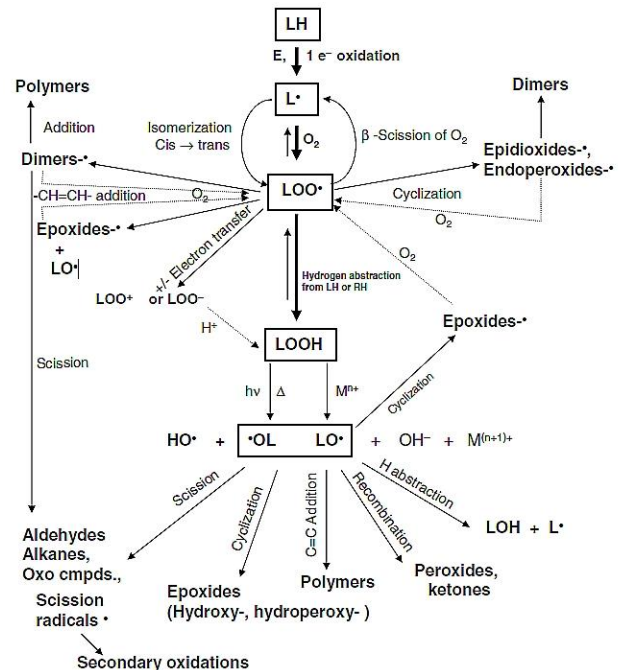


Fig. 3. Integrated scheme for the oxidation of fatty acid methyl esters [28]

Another study conducted a more comprehensive analysis of biodiesel degradation pathways using Fourier trans-

form infrared spectroscopy, nuclear magnetic resonance, and thermogravimetric analysis to monitor the biodiesel oxidation mechanism. The study showed that oxidation most often occurs as a result of reverse transesterification. In addition, impurities such as glycerol derivatives (mono-, diglycerides or glycerol) can react with methyl esters and reduce the amount of fatty acid methyl esters. The decomposition of fatty acid methyl esters can change to a perester after reaction with peroxides. Peroxides are the end products of a series of reactions occurring via a radical pathway. Oxygen radicals then react and form various carbon compounds. These include alcohols, aldehydes, ketones, or carboxylic acids. Carboxylic acid and alcohols reduce the total acidity and flash point of the fuel. All this leads to the formation of deposits that cause damage to the injection system and block fuel filters.

2. Fuels selected for testing

Fuels for supplying compression ignition engines should have good atomization, evaporation, and mixing properties with air, which affect the quality of the fuel mixture and its combustion under various load and engine speed conditions, but should also meet the requirements for oxidation resistance. Alternative fuels such as vegetable oils, vegetable oil esters, gaseous fuels, alcohols, ethers and others can also be used to power compression ignition engines. Four types of fuel were used for the tests: pure diesel fuel without ester additives (B0), B7 diesel fuel with 7% fatty acid methyl esters, rapeseed methyl esters (RME) and AME methyl esters. The results were compared to pure B0 diesel fuel. Rapeseed methyl esters (RME) in their pure form are used as fuel and as an additive to diesel fuel. On the other hand, rapeseed itself is also an edible plant, used for food production, which is why esters derived from rapeseed are classified as first-generation biofuels. AME esters were produced from animal fat waste from an animal skin processing plant. Both types of esters, RME and AME, were produced using a reactor (Fig. 4).



Fig. 4. Photo of the GW/SzW-300 reactor used for ester production (Małopolskie Center of Renewable Energy Sources „BioEnergia”, Krakow, Poland)

The reactor (can be used for the production of esters from various raw materials on a non-industrial scale and is mainly intended for individuals, farmers, transport companies, and others) can be used for the production of esters from various raw materials on a non-industrial scale and is mainly intended for individuals, farmers, transport companies, and others. The basic technical data of the GW/SzW-300 reactor are presented in Table 1 [12, 13].

Table 1. Technical data of the GW/SzW-300 reactor

Parameter	Unit	Value
Efficiency per cycle	dm ³	50
Production time per cycle	h	1.5
Supply voltage	V	230
Process temperature	°C	60/120
Rated power per cycle	kWh	5.24/5.15
Type of catalyst	–	basic/acidic
Process	–	periodic or semi-continuous
Type of process	–	single-stage or two-stage

The raw material used for the production of AME esters was waste left over from the processing of animal hides used in the footwear and clothing industries. The remaining fatty waste is difficult to use and would otherwise require disposal. The authors of the article used this waste to produce fuel that can then be used to power diesel engines [15]. Methyl alcohol and an alkaline catalyst KOH, were used, resulting in the production of methyl esters of animal origin. As part of the research, the fuels were tested in a RapidOxy apparatus at four test temperatures, i.e. 110, 120, 130, and the standard 140 °C. Photos of the tested fuels placed in measuring cylinders are presented in Fig. 5.

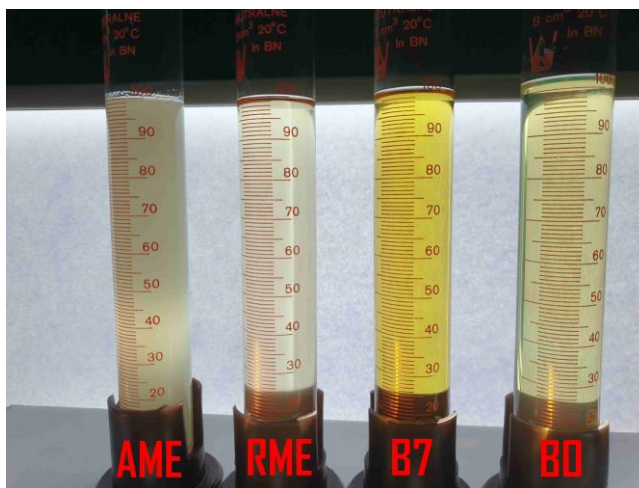


Fig. 5. Photos of the tested fuels placed in measuring cylinders are presented in Fig. 2

3. Experimental methodology

The requirement to determine the oxidative stability of fuels appeared already in the first edition of EN 590:1998 (PN EN 590:1999). EN 590 Motor vehicle fuels – Diesel fuels – Requirements and test methods is a European procedure describing physicochemical properties that all diesel fuels sold in the European Union must have for powering motor vehicles equipped with compression-ignition diesel engines.

The appearance on the market of a new type of vegetable-derived fuel, FAME, and petroleum-derived diesel with biocomponents, due to their different chemical composition, has led to difficulties in assessing their oxidative stability [23, 24]. Currently, the only universal method to assess the oxidative stability of all types of fuels in use – both oil and gasoline – is EN 16091 Liquid petroleum products – middle distillates, fatty acid methyl esters (FAME) and their blends – Determination of oxidative stability in a small-scale accelerated oxidation test, devel-

oped in April 2010. In 2023, an update to this standard was introduced. The current designation is PN EN 16091:2023-01 [22] Liquid petroleum products – Fuels and mixtures from medium petroleum distillates and fatty acid methyl esters (FAME) – Determination of oxidative stability by rapid small scale oxidation (RSSOT). This is the Polish version of the European standard EN 16091:2022. The EN 16091 method is a rapid test that allows the oxidative stability of test samples to be evaluated in a short period of time. It is intended for diesel fuels with a content of fatty acid methyl esters above 2% (V/V). Oxidative stability testing of fuels according to this standard is carried out under pressure, and the oxidation process itself is accelerated by increased test temperature and the presence of oxygen in the test chamber. The requirements of PN-EN 16091:2023-01 state that the apparatus must be equipped with [22]:

- automatic parameter control
- a fast-heating pressure vessel that reaches the test temperature in less than 300 s
- a pressure sensor capable of measuring pressure from 1 kPa to 2000 kPa with an accuracy of 1 kPa
- a temperature sensor that allows readings with an accuracy of 0.1°C
- pressure and temperature recorder in the pressure vessel, allowing recording at 1-second intervals; – Oxygen inlet and outlet valves and an automatic pressure release system at the end of the test
- a fan that cools the pressure vessel from test temperature to ambient temperature by air flow.

The instrument suitable for performing oxidative stability determinations according to this method is Anton Paar's RapidOxy apparatus, the schematic diagram of which is shown in Fig. 6, and a photo of the unit used in the study is shown in Fig. 7. The basic technical data of the apparatus is shown in Table 2.

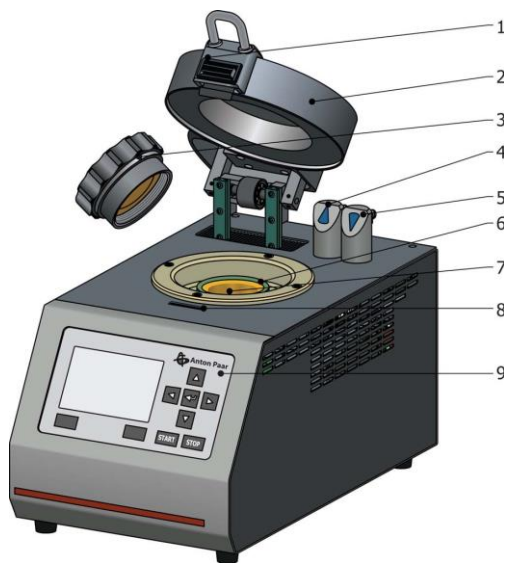


Fig. 6. Schematic of construction and photo of the RapidOxy Anton Paar device used in the study, where: 1. Unlocking mechanism for the isolation cover, 2. Protective and isolation cover, 3. Threaded cover for closing the test container 4. Oxygen outlet, 5. Oxygen inlet, 6. "O-ring" seal for the test sample chamber, 7. Test sample chamber, 8. Locking mechanism for the isolation cover, 9. Control panel with LCD display [2, 3]



Fig. 7. Photo of the RapidOxy instrument from Anton Paar used in the study

Table 2. Basic technical data of Anton Paar's RapidOxy apparatus [26]

Specification	RapidOxy Anton Paar
Standards	ASTM D7625, ASTM D7545, PN-EN 16091, IP 595
Type of samples	Liquid fuels (gasoline, diesel, bio-diesel/FAME and blends)
Operating temperature	up to 160°C or up to 200°C
Pressure range	up to 1800 kPa
Maintaining test conditions	with an accuracy of 0.5°C
Test chamber	aluminum, gold plated or stainless steel
Dimensions of the test chamber [mm].	$\varphi = 62, 53, h = 3, \Phi = 47, H = 11.4$
Sample volume	5 ml
Re-cooling	fan and active Peltier, automatically
Security	cap, protective and insulating lid, overheating cut-off
Power supply	115 V / 230 V, 50 Hz / 60 Hz, 600 W
Oxygen connection	minimum 800 kPa
Internal memory	20 test results; 16,000 pressure-temperature data sets
Interface	RS-232
Dimensions [mm].	240 × 400 × 260
Weight	11 kg
Thermal fuse	Shutting off the heater circuit; temperature threshold > 182°C (standard version); temperature threshold > 220°C (high-temperature version); maximum nominal current of 15 A at 250 V
Pressure sensor	error max. 0.6%, full scale measuring range 0–34.5 bar (500 psi); permissible operating range: 0–18 bar, error max ±3% FSS
Temperature sensor	Pt100, class 1/3 DIN B, EN 60751; measurement range 0°C to +200°C; permissible operating temperature range: room temperature –200°C; error: (class 1/3B) = $\pm(0.1 + 0.0017 \times T(^{\circ}\text{C}))$; error: 150 \pm 0.36°C; 100 \pm 0.27°C

A small sample volume of about 5 ml is required to perform the test. The course of the measurement is controlled by a microprocessor, which controls heating, cooling, flushing, and filling with oxygen before the test begins. The microprocessor measures the pressure drop. The data is stored in the device's memory, but can be transferred via an RS232 interface to a computer and displayed as a waveform of pressure and temperature as a function of time. The test itself consists of introducing 5 ml of the test sample into the test vessel. Then, after sealing it with a lid, oxygen is introduced until a pressure of 700 kPa \pm 5 kPa is reached. The control system maintains the temperature of the test cham-

ber at 25°C before starting the test. After stabilizing the pressure and temperature, the system starts the test by increasing the temperature of the chamber to 140°C. The chamber temperature should be stabilized in no more than 300 s.

Oxygen uptake by the sample during measurement is monitored by recording the pressure until a predetermined pressure drop of 10% is reached or a specified time elapses. The elapsed time until the pressure drop or the extent of the pressure drop over the specified time is directly related to the total oxygen consumption, that is, to the oxidation stability of the sample.

The standard measurement determines the induction period (IP), which is defined as the time elapsed from the start of the heating procedure of the sample vessel until the pressure drops by 10% from the maximum pressure (= zero point), measured in minutes as shown graphically in Fig. 8. The pressure in the test chamber is recorded every 1 s until the final test point is reached. The pressure drop from the maximum pressure is directly related to the oxygen uptake of the sample. According to PN EN 16091:2023-1, the minimum induction time is 60 min [2, 22].

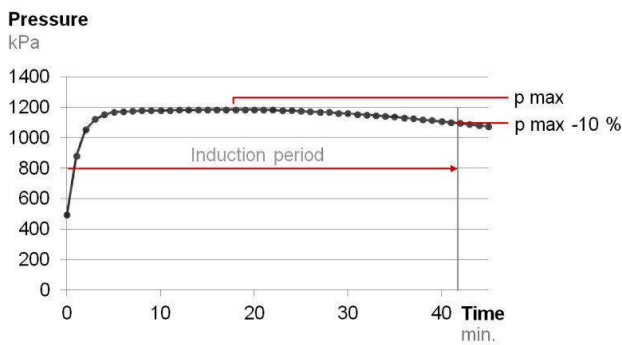


Fig. 8. Graphical representation of the determination of the induction time associated with the measurement of oxidation resistance according to PN EN 16091:2023-1 [2, 25]

3. Research results

As part of the implementation of the study, the fuels were tested in the RapidOxy apparatus at four test temperatures, i.e. 110, 120, 130 and the standard at 140°C. Table 3 shows the results.

Table 3. Numerical values of induction periods of the tested fuels determined at different temperatures

Fuel	Time in min for different temperature			
	110°C	120°C	130°C	140°C
B0	323.36	256.56	218.33	117.1
B7	326.41	225.4	192.05	96.31
RME	16.91	14.21	12.11	10.96
AME	63.15	36.83	28.18	26.65

The induction period values of the tested fuels determined at different temperatures using the Anton Paar RapidOxy tester are shown in Fig. 9.

Figures 10 to 13 show graphs of pressure over time during the test for the four fuels tested at temperatures of 110, 120, 130, and 140°C.

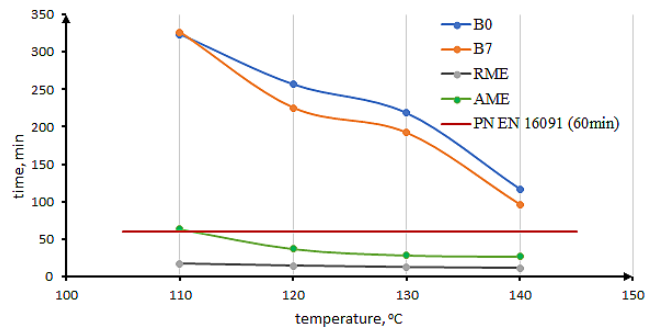


Fig. 9. Induction period values of the tested fuels determined at different temperatures using the RapidOxy tester from Anton Paar, red line – requirements of PN EN 16091:2023

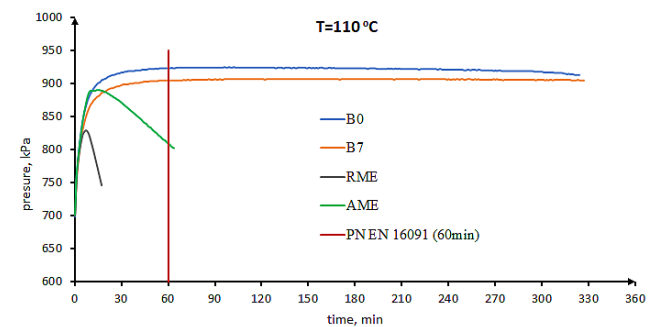


Fig. 10. Graph of pressure curves recorded during the test with the RapidOxy device at a temperature of 110°C

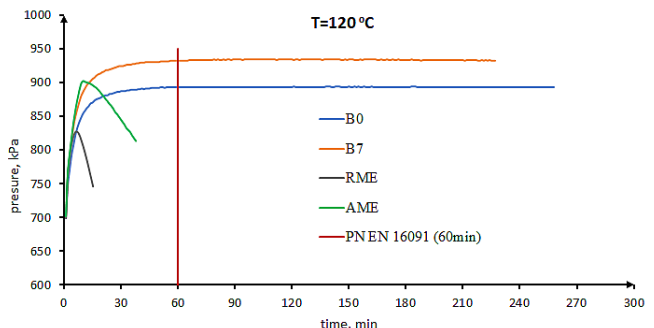


Fig. 11. Graph of pressure curves recorded during the test with the RapidOxy device at a temperature of 120°C

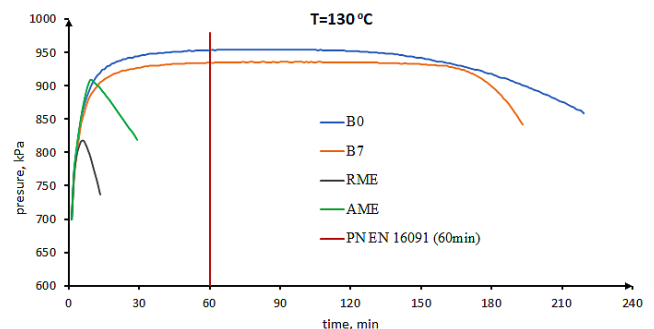


Fig. 12. Graph of pressure curves recorded during testing with the RapidOxy device at 130°C

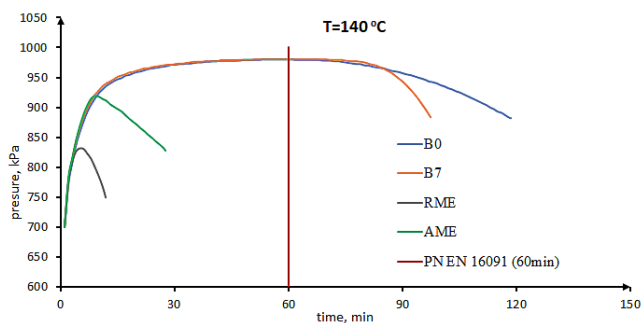


Fig. 13. Graph of pressure curves recorded during testing with the RapidOxy device at 140°C

4. Conclusions

As the test results show, pure diesel fuel without ester additives exhibited the best oxidation resistance at every test temperature. At temperatures of 110 and 120°C, it was

necessary to interrupt the test, which lasted over 5 hours. Both fuels, pure diesel fuel and oil with 7% ester content, meet the requirements of PN EN 16091:2023-1 at all tested temperatures. In the case of AME esters from animal waste, only at 110°C was the induction time within 60 minutes. With increasing temperature, a rapid decrease in this time can be observed, from 63:15 minutes to 26:65 minutes at 140°C. The lowest oxidation resistance was recorded for rapeseed oil methyl esters. At 110°C, the induction time was 16:91 min and decreased to 10:96 min at 140°C. As confirmed by the study, the oxidation resistance of diesel fuel depends on the amount of biocomponents, as well as the quality of the diesel fuel used and the antioxidant additive used. In addition, factors that can significantly accelerate oxidation processes include oxygen contained in the fuel, as well as the effects of light, temperature, and fuel storage time.

Nomenclature

AME	animal methyl esters	FAME	fatty acid methyl ester
B0	diesel fuel not containing bio-components	RME	rapeseed methyl esters
B7	diesel fuel containing 7% biodiesel	RSSOT	rapid small scale oxidation test

Bibliography

- [1] Alves-Fortunato M, Ayoub E, Bacha K, Mouret A, Dalmazzone C. Fatty acids methyl esters (FAME) autoxidation: new insights on insoluble deposit formation process in biofuels. *Fuel*. 2020;268:117074. <https://doi.org/10.1016/j.fuel.2020.117074>
- [2] Anton Paar, Brochure: ApplRaport RapidOxy.
- [3] ASTM D7525-14(2019)e1 Standard Test Method for Oxidation Stability of Spark Ignition Fuel – Rapid Small Scale Oxidation Test (RSSOT).
- [4] Baczewski K, Szczawiński P. Experimental testing of oxidation stability of diesel fuels. *Biuletyn WAT*. 2019;4. <https://doi.org/10.5604/01.3001.0013.9719>
- [5] Botella L, Bimbela F, Martín L, Arauzo J, Sánchez JL. Oxidation stability of biodiesel fuels and blends using the Rancimat and PetroOXY methods. Effect of 4-allyl-2,6-dimethoxyphenol and catechol as biodiesel additives on oxidation stability. *Front Chem*. 2014;2:43. <https://doi.org/10.3389/fchem.2014.00043>
- [6] Dhandapani S, Raja T, Murugan V, Selvaraj J, Rathinasamy V. Comprehensive review on evolution, progression, design, and exploration of electric bicycle. *The Archives of Automotive Engineering – Archiwum Motoryzacji*. 2024; 105(3):5-43. <https://doi.org/10.14669/AM/191492>
- [7] Dhande DY, Navale SJ. Experimental investigations on the performance and emissions of compression ignition engine fuelled with lower blends of neem-based biodiesel. *The Archives of Automotive Engineering – Archiwum Motoryzacji*. 2024;103(1):57-76. <https://doi.org/10.14669/AM/186109>
- [8] Eldin AK. *Lipid oxidation pathways*. AOCS Press, 2003. Illinois.
- [9] Goteti GS, Juluru PS. RCCI combustion with a partially pre-mixed concept in a diesel engine using biodiesel, di-ethyl ether, and ethanol blends. *The Archives of Automotive Engineering – Archiwum Motoryzacji*. 2025;107(1):27-48. <https://doi.org/10.14669/AM/191493>
- [10] Kamela W, Wojs MK, Orliński P. Calculation method for assessing the storage capacity of nitrogen compounds in LNT Reactors. *Energies*. 2022;15:7819. <https://doi.org/10.3390/en15207819>
- [11] Krasodomski M, Krasodomski W, Skibińska A, Żółty M. Badania porównawcze metod oznaczania stabilności termooksydacyjnej smarów plastycznych. *Przemysł Chemiczny*, 2018;9(3):370-376. <https://doi.org/10.15199/62.2018.3.6>
- [12] Kurczyński D, Łagowski P, Wcisło G. Experimental study into the effect of the second-generation BBuE biofuel use on the diesel engine parameters and exhaust composition. *Fuel*, 2021;284:118982. <https://doi.org/10.1016/j.fuel.2020.118982>
- [13] Kurczyński D, Wcisło G, Łagowski P. Experimental study of fuel consumption and exhaust gas composition of a diesel engine powered by biodiesel from waste of animal origin. *Energies*. 2021;14(12):3472. <https://doi.org/10.3390/en14123472>
- [14] Kuszewski H. Experimental investigation of the autoignition properties of ethanol–biodiesel fuel blends. *Fuel*. 2019;235:1301-1308. <https://doi.org/10.1016/j.fuel.2018.08.146>
- [15] Laskowska M, Laskowski P, Wojs, MK, Orliński P. Prediction of pollutant emissions in various cases in road transport. *Appl Sci*. 2022;12(23):11975. <https://doi.org/10.3390/app122311975>
- [16] Łagowski P, Wcisło G, Kurczyński D. Study of combustion process parameters in a diesel engine powered by biodiesel from waste of animal origin. *Energies*. 2024;17(23):5857. <https://doi.org/10.3390/en17235857>
- [17] Małek A, Karowicz R, Józwiak K. A review of technologies in the area of production, storage and use of hydrogen in the automotive industry. *The Archives of Automotive Engineering – Archiwum Motoryzacji*. 2023;102(4):41-67. <https://doi.org/10.14669/AM/177038>
- [18] Masudi A, Muraza O, Jusoh NWC, Ubaidillah U. Improvements in the stability of biodiesel fuels: recent progress and

- challenges. *Environ Sci Pollut Res.* 2023;30: 14104-14125. <https://doi.org/10.1007/s11356-022-25048-4>
- [19] Orliński P, Laskowski P, Zimakowska-Laskowska M, Mazuruk P. Assessment of the impact of the addition of bio-methanol to diesel fuel on the coking process of diesel engine injectors. *Energies.* 2022;15:688. <https://doi.org/10.3390/en15030688>
- [20] Pandian B, Harigaran A. Investigations on the performance of a single-cylinder diesel engine powered by biodiesel derived from palm oil and antioxidant additives. *The Archives of Automotive Engineering – Archiwum Motory-zacji.* 2024;106(4):18-30. <https://doi.org/10.14669/AM/193804>
- [21] Pečman J, Šarkan B, Ližbetinová L, Lupták V, Loman M, Bartuška L. Impact of acceleration style on vehicle emissions and perspectives for improvement through transportation engineering solutions. *The Archives of Automotive Engineering – Archiwum Motoryzacji.* 2024;104(2):48-62. <https://doi.org/10.14669/AM/189665>
- [22] PN-EN 16091:2023-1 Ciekłe przetwory naftowe – Paliwa i mieszaniny ze średnich destylatów naftowych i estrów metylowych kwasów tłuszczowych (FAME) – Oznaczanie stabilności oksydacyjnej metodą szybkiego utleniania w małej skali (RSSOT).
- [23] Sacha D. Evaluation of the oxidation stability of the fuel for compression ignition engines according to the proposed requirements of CEN. *Nafta-Gaz.* 2013;11.
- [24] Sacha D. Impact of antioxidant additives on the stability of fuels for diesel engines exposed to copper. *Nafta-Gaz.* 2020; 6:419-426. <https://doi.org/10.18668/NG.2020.06.07>
- [25] Sacha D. Wpływ jakości estrów metylowych kwasów tłuszczowych na niskotemperaturowe właściwości użytkowe paliw silnikowych. *Nafta-Gaz.* 2018;2:148-155. <https://doi.org/10.18668/NG.2018.02.09>
- [26] Sacha D, Skibińska A, Krasodomski W. Assessment of the possibility of using the PetroOxy instrument to determine the thermo-oxidative stability of plastic greases using the RSSOT (Rapid Small-Scale Oxidation Test) method. *Nafta-Gaz.* 2022;4:299-311. <https://doi.org/10.18668/NG.2022.04.06>
- [27] Sarin A, Arora R, Singh NP, Sharma M, Malhotra RK. Influence of metal contaminants on oxidation stability of Jatropha biodiesel. *Energy.* 2009;34(9):1271-1275. <https://doi.org/10.1016/j.energy.2009.05.018>
- [28] Schaich KM. Lipid oxidation: theoretical aspects. Shahidi F (ed.). *Bailey's industrial fat and oil products.* John Wiley, New York 2005;1:269-355. <https://doi.org/10.1002/047167849X.bio067>
- [29] Stanik W, Łaczek T. Analysis of processes occurring during the oxidation of methyl esters of higher fatty acids (FAME) and B10 diesel oil based on literature data. *Nafta-Gaz.* 2002; 10:743-749, <https://doi.org/10.18668/NG.2020.10.10>

Piotr Łagowski, DEng. – Department of Automotive Engineering and Transport, Kielce University of Technology, Poland.

e-mail: p.lagowski@tu.kielce.pl



Prof. Grzegorz Wcisło, DSc., DEng. – Department of Automotive Engineering and Transport, Kielce University of Technology, Poland.

e-mail: grzegorz.wcislo@ur.krakow.pl



Dariusz Kurczyński, DEng. – Department of Automotive Engineering and Transport, Kielce University of Technology, Poland.

e-mail: kdarek@tu.kielce.pl



Six-stroke spark-ignition engine fuelled with high-hydrogen content fuel: a theoretical thermodynamic analysis

ARTICLE INFO

This work presents a thermodynamic analysis of a six-stroke cycle implemented in Spark-Ignition (SI) engines. The cycle configuration comprises two distinct combustion phases: (1) initial combustion of a methane-hydrogen mixture under fuel-lean conditions ($\lambda > 1$), yielding exhaust gases containing residual oxygen, followed by (2) secondary hydrogen injection during the expansion phase to facilitate complete utilization of the remaining oxidizer. The investigation evaluates the system's thermodynamic performance through parametric variation of both the fuel composition (methane/hydrogen, CH_4/H_2 ratio) and the equivalence ratio during primary combustion. The results obtained indicate that the changes in the peak temperature of the second part of the cycle are small, up to 60 K relative to the mean value. The fuel mixture with $\lambda = 3.0$ showed the highest cycle efficiency at 50.73%, indicating the best performance among all cases. According to the data, better performance can be achieved by optimizing cycle parameters such as regeneration, intercooling, pressure ratios, and component efficiencies in addition to raising the maximum temperature. In conclusion, better outcomes are not always guaranteed by higher temperatures. Increasing thermal input alone is not as important as designing and optimizing cycles efficiently.

Received: 2 July 2025

Revised: 7 October 2025

Accepted: 21 October 2025

Available online: 22 November 2025

Key words: hydrogen, renewable energy, thermodynamic parameters, SI engine, 6-stroke cycle

This is an open access article under the CC BY license (<http://creativecommons.org/licenses/by/4.0/>)

1. Introduction

As the global demand for cleaner energy builds momentum, internal combustion engines (ICEs) remain a leading point of energy conversion in transportation and distributed power generation. However, their continued use falls under increasing concern due to greenhouse gas (GHG) emissions in the form of carbon dioxide (CO_2) and nitrogen oxides (NO_x), which are accountable for climate change and air pollution.

As a countermeasure, the combination of renewable energies with hydrogen-powered engines could be a promising path to a sustainable energy future, replacing the use of conventional non-renewable energy. While the combustion of hydrogen is carbon-free and increases thermal efficiency [12], it occurs at very high temperatures, which can result in high thermal NO_x formation.

However, under certain conditions, a reduction in power output can occur, and one reason for this is the need to burn hydrogen at a high excess air ratio due to the propensity of this fuel to experience excessively high cylinder pressure and knocking combustion. The higher the excess air ratio, the lower the calorific value of the fuel-air mixture feeding the combustion engine [5]. In addition, the higher combustion temperature of hydrogen can result in higher heat losses from the internal combustion engine, further reducing its efficiency, and also increasing NO_x emissions [4].

At the same time, it is worth noting that enriching natural gas or biogas with hydrogen brings tangible benefits to the performance of internal combustion engines. Previous studies have shown that hydrogen enrichment contributes to alleviating combustion instability issues in engines fuelled with gaseous blends, leading to a significant reduction in emissions [8]. Hydrogen, according to the literature, has the

ability to improve the coefficient of variation (COV) of indicated mean effective pressure (IMEP) and other properties when mixed with other fuels, such as natural gas, the latter being highly encouraged by several countries for use in internal combustion engines with a view to reducing global warming and pollutant emissions [2].

Within this framework, one alternative to sensibly improve the performance of engines burning H_2 -rich fuels or pure H_2 is to modify the thermodynamic cycle of the engine. Therefore, this paper presents a concept for implementing a six-stroke thermodynamic cycle for hydrogen combustion in an SI engine. The cycle parameters were calculated when using a hydrogen-methane mixture as fuel.

2. Properties of selected gaseous fuels

2.1. Main properties of H_2 , biomethane and biogas

Governments around the world are paying closer attention to hydrogen, methane, and biogas as cleaner fuels for internal combustion engines, particularly in the context of the movement towards sustainable energy. One notable feature of hydrogen is that it burns cleanly, releasing no CO_2 when it is used. Produced from various energy sources, it is considered a form of energy carrier. With unique properties, it is seen as promising for use in engines, such as its low density, wide flammability limits, and low minimum ignition energy. Also, certain mixtures can improve combustion stability. Special attention should be paid to its laminar burn rate, which under certain conditions can be up to six times higher than that of gasoline or methane [6, 13].

Biomethane, an upgraded form of biogas that increases its energy content, is a fuel that can be directly used in natural gas vehicles. Moreover, it can be injected into existing natural gas infrastructure and be used in transportation

in different regions [7], making it a convenient and cleaner-burning alternative to non-renewable fuels in SI engines. On the other hand, biogas is made through the anaerobic digestion of organic matter, a process that happens without oxygen. Before being used in engines, it must be upgraded to remove carbon dioxide and other impurities, the above-mentioned biomethane. It is an added benefit of being renewable, turning organic waste into a valuable source of clean energy. It stands out as a promising fuel in diesel engines, in addition to its potential for reducing emissions, although with lower performance values [1, 11].

Some of the main properties of H_2 and CH_4 include the Lower Heating Value (LHV) which range from ~ 120 MJ/kg; ~ 10.8 MJ/Nm³; ~ 50 MJ/kg; ~ 35.8 MJ/Nm³ and the density at NTP (0°C, 1 atm), equals to 0.0899 kg/m³ and 0.656 kg/m³, respectively [14]. Furthermore, another desirable property is the very fast flame propagation from H_2 , which reduces combustion duration, leading to high isochoric efficiency [10]. As for biogas, with its wide range of energy applications, trace compounds can impact its use, with special attention to concentrations of volatile organic compounds (VOCs), for example [9].

Finally, in spark ignition (SI) Engines and other types of engines, it is important, among other things, to control the rapid increase in pressure within the engine, which can lead to knock. Knock is undesirable and a major challenge in the field [13], especially with fuel blends containing H_2 .

2.2. Characteristics of the fuel-air mixture

The stoichiometric air–fuel ratio for hydrogen is 34.3 (kg/kg) compared to 14.3 for diesel and 17.2 for methane fuels. The engine's power output for a given fuel depends on the calorific value of the fuel-air mixture and the engine's thermodynamic efficiency. According to Fig. 1, the relative difference ($\Delta e_{d,v}$ in %) of the calorific value of the hydrogen-air mixture in relation to selected fuels like biogas (with 60% of CH_4 by vol.), methane, petrol and diesel oil in a range of air excess ratios. The relative difference in calorific value of the hydrogen-air mixture (e_{d,vH_2}) compared to other fuel-air mixtures ($e_{d,vf}$) is defined in Equation 1.

$$\Delta e_{d,v} = \left(1 - \frac{e_{d,vf}}{e_{d,vH_2}} \right) 100\% \quad (1)$$

where: $e_{d,vf}$, J/Nm³ – calorific value of selected fuel-air mixture, e_{d,vH_2} , J/Nm³ – calorific value of the hydrogen-air mixture.

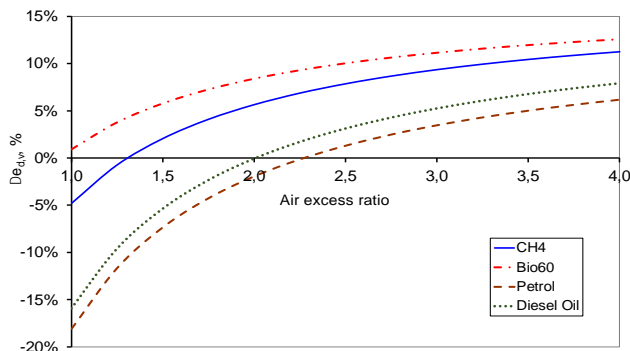


Fig. 1. Relative difference in calorific value of the fuel-air mixture of four selected fuels compared to hydrogen

The $\Delta e_{d,v}$ results are expressed in % of the calorific value of the hydrogen-air mixture under normal conditions. From the data presented in Fig. 1, it is evident that hydrogen has the same energy potential in the combustible mixture ($\Delta e_{d,v} = 0\%$) for different values of the excess air ratio. These are 1.3 for methane, 2 for diesel and 2.2 for gasoline, respectively. For a mixture of biogas and air, the calorific value is lower than that of pure hydrogen, even for a stoichiometric mixture.

3. Implementation of the six-stroke cycle in the SI engine

3.1. Introduction

The first conception of a six-stroke internal combustion engine was reported by Samuel Griffin in 1883, and many authors have since described and worked on six-stroke engines.

The basic idea from the literature is that waste heat is recovered, allowing a proportion of it to perform extra work. In a traditional six-stroke approach, the exhaust gases from the fourth stroke are not entirely exhausted into the environment (or are only partially exhausted) before compression occurs, followed by water injection to evaporate, which removes heat from the exhaust gas and the walls of the combustion chamber. Therefore, additional work is performed in the fifth stroke, and the charge is discharged to the environment in the sixth stroke [3].

3.2. Hydrogen-rich fuel utilization in a six-stroke cycle

One of the ways to sensibly improve the efficiency of engines burning H_2 -rich fuels or pure H_2 is to modify the thermodynamic cycle of the engine. The research proposed in this paper focuses on replacing the classic four-stroke cycle (4SCE) with a new six-stroke cycle (6SCE), as illustrated in Fig. 2.

The implementation of the six-stroke cycle in the SI engine is proposed as follows:

a) 1st stage of the cycle – in the first part of the cycle, the engine is fuelled with a lean air-fuel mixture. Various gaseous fuels, including those with hydrogen in their composition or pure hydrogen, are preferred. If pure hydrogen is used, a very lean mixture is required (an excess air ratio of at least three is assumed in this case). The fuel supply to the engine can be provided by a gas/air mixer or by using a gas injector in the engine intake manifold. The first part of the so-called ECO-CYCLE is realized analogously to the classic 4-stroke SI engine. After the engine is filled with a mixture of fuel and air, it is compressed and then ignited before the piston reaches top dead center (TDC). Subsequently, after the piston has passed through TDC, work is carried out in the engine cylinder, and torque is generated at the crankshaft.

b) 2nd stage of the cycle – after the work of the first part of the cycle has been carried out, the intake and exhaust valves remain closed and the exhaust gases containing oxygen are not released into the environment. At the end of the combustion process (e.g., in the expansion stage) or at the beginning of the next compression stage of the resulting exhaust gas, water injection is proposed to decrease the cylinder temperature. A partial reduction in temperature

should be achieved by injecting another dose of fuel. During this part of the cycle, direct injection of hydrogen into the engine cylinder is proposed, in such a quantity as to ensure a stoichiometric mixture with the oxygen remaining from the previous cycle in the exhaust. The resulting mixture undergoes compression, and another ignition is initiated before the piston reaches the TDC. Subsequently, another expansion occurs, and work is done in the engine cylinder, resulting in torque generation at the crankshaft.

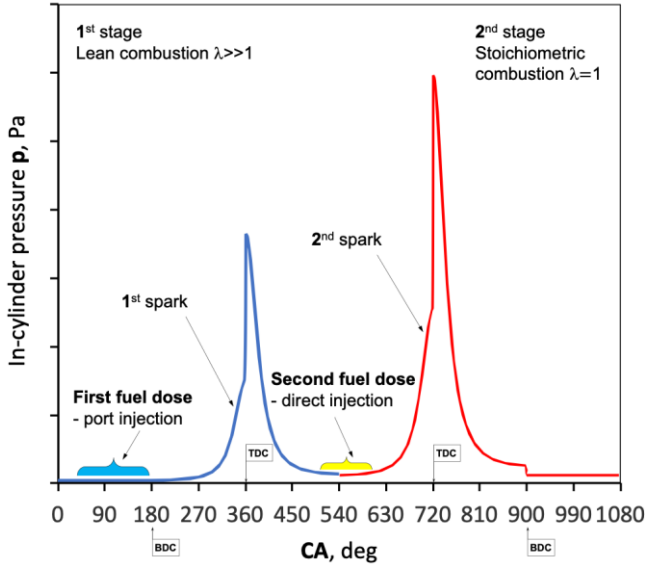


Fig. 2. The concept of six-stroke cycle implementation in a hydrogen rich fuel SI engine

To calculate the thermodynamic parameters of the 6-stroke cycle, it was necessary to determine the values of the input data. To determine the combustion stability of natural gas-hydrogen mixtures, experimental tests were carried out on a four-stroke spark-ignition engine with a compression ratio of 12.5. The content of hydrogen co-fired with methane was changed during the tests. The fuel mixture for which the engine operated stably, even with an excess air ratio above 2.5, was a mixture with 60% hydrogen by volume. For this work, simulation studies of the 6-stroke cycle were conducted for a fuel mixture of 60% H₂ and 40% CH₄. Additionally, it was assumed that the range of variation for the excess air ratio would be between 1.3 and 3.

3.3. Calculation of thermodynamic parameters of a six-stroke cycle

The following assumptions and simplifications were made to determine the thermodynamic parameters of the six-stroke cycle:

- the compression and expansion of the load (i.e. the fuel/oxidant mixture and the exhaust gas) are isentropic
- the combustion process is simulated by isochoric heat input (in the first as well as in the second stage of the cycle), without heat losses to the environment.

The shape of the 6-stroke cycle on the pV diagram, along with its characteristic points, is shown in Fig. 3.

In the first stage of the cycle the fuel is a mixture of hydrogen and methane. Considering the mole fraction of each component, they will be defined in the following equations

as H₂ and CH₄, respectively. Based on stoichiometry and considering the variable value of the excess air coefficient (λ), the actual amount of air needed to burn the fuel is presented in Equation 2:

$$n'_{a1} = \lambda \frac{(2\text{CH}_4 + \frac{1}{2}\text{H}_2)}{Z_{\text{O}_2,a}}, \frac{\text{kmol}_f}{\text{kmol}_a} \quad (2)$$

where: H₂, CH₄, – molar content of H₂ and CH₄ in the fuel, Z_{O_{2,a}}, – molar content of O₂ in the air.

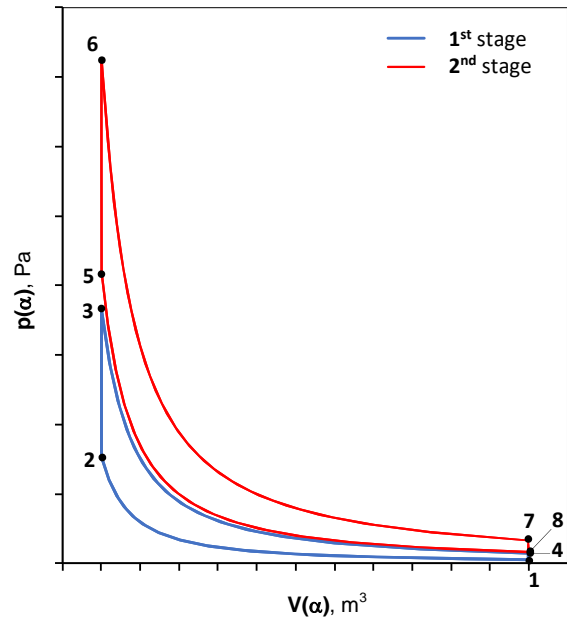


Fig. 3. The characteristic points of six-stroke cycle in p, V diagram

Using the initial cycle thermodynamic parameters, the molar quantity of working medium in the point “1” can be calculated from the Equation of state as below:

$$n_{1\text{mix}} = \frac{p_1 V_1}{(MR)T_1}, \frac{\text{kmol}_{\text{mix}}}{\text{cycle}} \quad (3)$$

where: p₁, V₁, T₁ – in cylinder parameters when the piston is in the BDC (suction stroke of 1st cycle stage).

Considering Equations (2) and (3), and the substance balance equation, the air and fuel mass for one engine cycle can be expressed by the following Equations:

$$m_{a1} = m_{f1} n'_{a1} \frac{M_a}{M_f} \left(1 + \frac{M_{\text{H}_2\text{O}}}{M_a} X_{za} \right), \frac{\text{kg}_a}{\text{cycle}} \quad (4)$$

$$m_{f1} = \frac{p_1 V_1}{\left[1 + \frac{\lambda (2\text{CH}_4 + \frac{1}{2}\text{H}_2) (1 + X_{za})}{Z_{\text{O}_2,a}} \right] (MR)T_1}, \frac{\text{kg}_f}{\text{cycle}} \quad (5)$$

where: M_a, M_f, M_{H₂O}, kg/kmol – molar weight of air, fuel and H₂O, X_{za}, kmol_{H₂O}/kmol_a – air moisture content.

The pressure during the compression and expansion stroke is calculated based on the isentropic transformation and expressed as a function of engine crank angle. These calculations finally yield the results of pressure at the 2nd and 4th points of the cycle. Cylinder volume changes for variable crankshaft angle were calculated based on the

geometry of the engine piston-crank system. In Table 1, the engine geometry adopted in the calculations is shown.

Table 1. Engine geometry

Bore, D, mm	86.0
Stroke, S, mm	69.0
Connecting rod, L, mm	117.0
Swept volume, V_s, m^3	0.000401
Number of cylinders	1.0
Compression ratio, ϵ	12.5

Once the pressure p_2 is calculated, the temperature T_2 is determined using the thermal equation of state. The energy balance is then used to calculate the temperature value T_3 using the following Equation:

$$T_3 = \frac{m_{f1} LHV_{f1}}{m_{1mix} c_v(T_{2-3})} + T_2 \quad (6)$$

where: LHV_{f1} , kJ/kg – lower heating value of the fuel, $c_v(T_{2-3})$, kJ/kgK – specific heat of the working medium during the heat supply process under constant volume, m_{1mix} , kg/cycle – mass of the working medium, the sum of fuel m_{f1} and air m_{a1} .

Then, the pressure in the circuit after the heat input is calculated by Equation 7:

$$p_3 = \frac{m_{1mix}(MR)T_3}{M_3V_2} \quad (7)$$

where: $V_2 = V_3, m^3$ – the min cycle volume (clearance volume), M_3 , kg/kmol – molar mass of the working medium for its current molar composition.

The pressure p_4 and temperature T_4 are then calculated. In the current analysis, water injection was not implemented; hence, the temperature T_4 is derived from the pressure at the end of the expansion and the amount of heat taken away by the hydrogen introduced at this point as fuel for the second part of the cycle.

The parameters for the second stage of the cycle are calculated analogously, but the oxidant is the residual oxygen from the exhaust of the first stage.

4. Results

Using the calculation methodology given in section 3, a six-stroke cycle was simulated, assuming variable combustion conditions in the first part of the cycle. The variable parameter was the excess air ratio in the 1-st cycle stage. The values were changed from 1.3 to 3 with a value step of 0.2. In Figure 4, the post-combustion temperature values are shown in the first and second stages of the 6-stroke cycle. The results are shown as a function of the excess air factor used in the first stage of the cycle. Combustion in the second cycle stage was stoichiometric. The results obtained indicate that the changes in the peak temperature of the second part of the cycle are small, up to 60 K relative to the mean value.

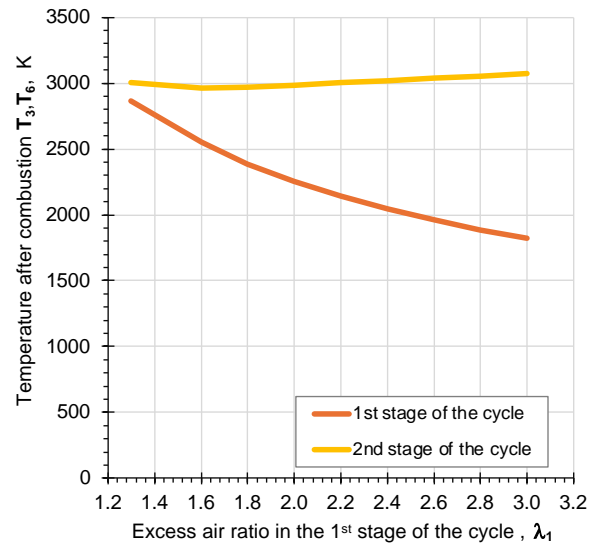


Fig. 4. Temperature after combustion of 1st and the 2nd stage the 6-stroke cycle as function of the excess air ratio in the 1st cycle stage

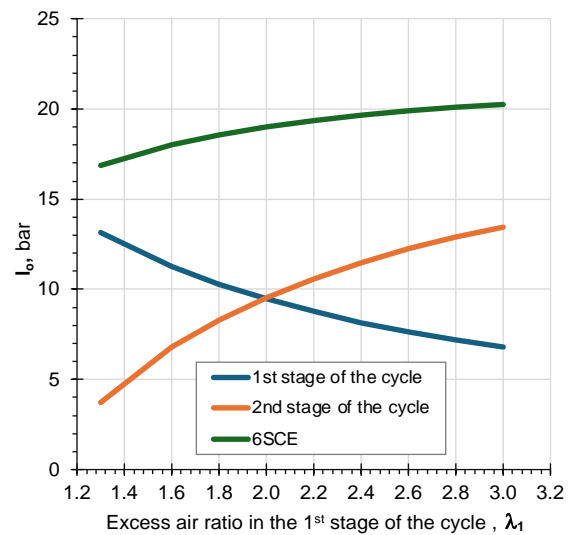


Fig. 5. Specific work of 1st, 2nd stage the 6-stroke cycle and whole cycle (6SCE) as function of the excess air ratio in the 1st cycle stage

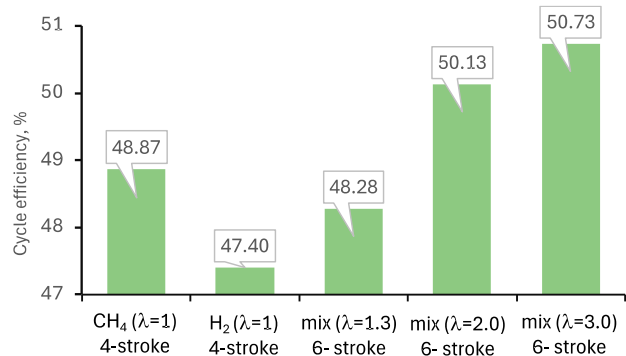


Fig. 6. Comparison between 4-stroke and 6-stroke cycle efficiency

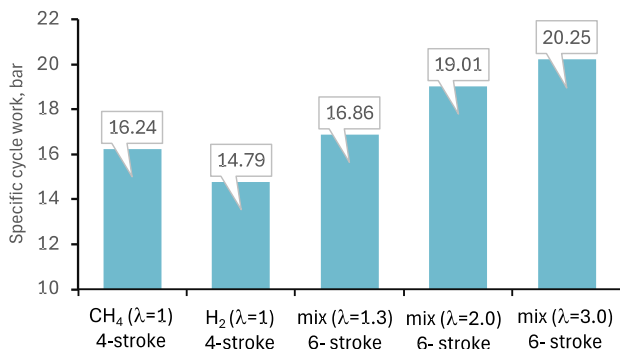


Fig. 7. Comparison between 4-stroke and 6-stroke specific cycle work

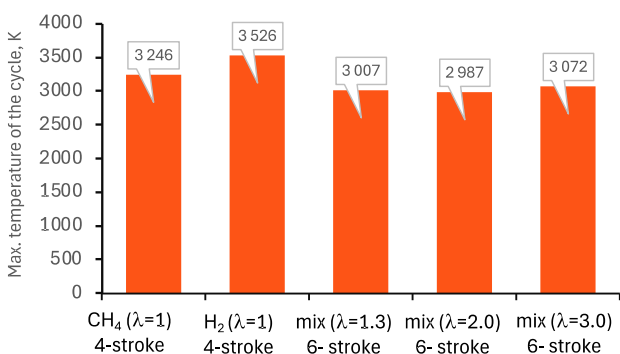


Fig. 8. Comparison between 4-stroke and 6-stroke maximum cycle temperature

In Figure 5, the specific work of the 1st, 2nd stage of the 6-stroke cycle and the whole cycle (6SCE) is shown as a function of the excess air ratio in the 1st cycle stage. The specific work was calculated as the ratio of the work performed by the working medium in the 1st and 2nd cycle stages to the engine's swept volume. As the excess air ratio increased, the specific work of the 1st stage decreased, while the specific work of the 2nd stage increased. The total specific work of the 6SCE increased slightly and then remained constant, indicating improved overall efficiency due to increased excess air.

Figures 6 to 8 express the comparison of the chosen parameters among the 4-stroke pure CH₄, 4-stroke pure H₂ combustion and the 6-stroke cycle with 60 H₂ and 40 CH₄ % by vol. in the first stage and pure H₂ stoichiometrically combusted in the second stage. From Fig. 6, the mix with $\lambda = 3.0$ showed the highest cycle efficiency at 50.73%, indicating the best performance among all cases. The pure H₂ result could be used as a baseline or a less effective configuration that might not have all the improvements. Depending on the application, the 3.33 percentage point difference in efficiency between the lowest (case H₂) and the highest (mix with $\lambda = 3.0$) can be substantial. The mix with $\lambda = 3.0$ also produced the highest specific cycle work

at 20.25 bar in Fig. 7, demonstrating the most efficient work output per cycle swept volume. The specific cycle work expresses the equivalent of the indicated mean effective pressure of a real engine. A higher value for this parameter also means a higher output power of the engine.

The combustion of the fuels analyzed in the 6-stroke cycle allows a higher power output to be achieved relative to the 4-stroke cycle without the need for supercharging or turbocharging. In addition to the previous figures on cycle efficiency and specific cycle work, Fig. 8 shows the maximum cycle temperatures for the five distinct cases (1–5). Despite having the highest temperature in the 4-stroke cycle, pure H₂ also had the lowest specific cycle work (14.79 bar) and efficiency (47.4%). On the other hand, mix with $\lambda = 3.0$ combusted in 6-stroke cycle at a moderate maximum temperature (3072 K) and had the highest efficiency (50.73%) and specific work (20.25 bar). According to the results of simulation calculations, better performance can be achieved by using a 6-stroke thermodynamic cycle. However, better outcomes are not always guaranteed by higher temperatures, due to thermodynamic and operational implications, thermal stress, etc. Increasing thermal input alone is not as important as designing and optimizing cycles efficiently.

Finally, to improve thermal efficiency in engines, in addition to the thermodynamic control and optimization of the process performed in this study, other approaches and solutions need to be developed.

Therefore, according to researchers, one such approach could be the use of multilayer coatings in the engine chamber. This technology could achieve greater thermal efficiency in internal combustion engines, and the literature points to the potential of this solution and the need for further research and analysis [15].

5. Conclusion

The mix with $\lambda = 3.0$ (in the first stage of the six-stroke cycle) exhibited the best overall performance, reaching the highest specific work (20.25 bar) and cycle efficiency (50.73%) at a moderate maximum temperature (3072 K). On the other hand, H₂ performed the worst, despite having the highest temperature (3526 K). This is less than 500,000 lower than the stoichiometric combustion of pure hydrogen in a 4-stroke cycle. As the combustion in the second part of the 6-stroke cycle is stoichiometric, the use of such a solution in an actual internal combustion engine enables the use of a three-way catalyst converter in the exhaust system. This will allow the operation of the hydrogen-burning engine with high IMEP and efficiency, as well as reduced emissions of NO_x, CO, and HC.

Acknowledgements

We would like to thank the National Council for Scientific and Technological Development – CNPq, process number 441811/2023-0, the Federal University of Pelotas and the Silesian University of Technology for the support provided to the development of this study.

Nomenclature

BDC bottom dead centre
BMEP brake mean effective pressure

CH₄ methane
COV coefficient of variation

H ₂	hydrogen	SI	spark ignition engine
IMEP	indicated mean effective pressure	T	temperature
l _o	specific cycle work	TDC	top dead center
LHV	lower heating value	V	volume
p	pressure	λ	excess air ratio

Bibliography

- [1] Ahmad A, Yadav K, Hasan S. Biogas as a sustainable and viable alternative fuel for diesel engines: a comprehensive review of production, purification, and performance evaluation. *P I Mech Eng D-J Aut.* 2024;238:325-345. <https://doi.org/10.1177/09544089241255930>
- [2] Aktaş F. Performance and emission prediction of hydrogen addition to natural gas powered engine using 0/1 dimensional thermodynamic simulation. *International Journal of Energy Studies.* 2022;7:67-81.
- [3] Conklin C, Szybist P. A highly efficient six-stroke internal combustion engine cycle with water injection for in-cylinder exhaust heat recovery. *Energy.* 2010;35:1658-1664. <https://doi.org/10.1016/j.energy.2009.12.012>
- [4] Fuwu Y, Lei X, Yu W. Application of hydrogen enriched natural gas in spark ignition IC engines: from fundamental fuel properties to engine performances and emissions. *Renew Sustain Energy Rev.* 2018;82:1457-1488. <https://doi.org/10.1016/j.rser.2017.05.227>
- [5] Ghazi K. Hydrogen as a spark ignition engine fuel. *Int J Hydrog Energy.* 2002;28:569-577. [https://doi.org/10.1016/S0360-3199\(02\)00150-7](https://doi.org/10.1016/S0360-3199(02)00150-7)
- [6] Iafrate N, Matrat M, Zaccardi M. Numerical investigations on hydrogen-enhanced combustion in ultra-lean gasoline spark-ignition engines. *Int J Engine Res.* 2021; 22:375-389. <https://doi.org/10.1177/1468087419870688>
- [7] Lee S, Yi H, Jang H, Park C, Kim C. Evaluation of emission characteristics of a stoichiometric natural gas engine fueled with compressed natural gas and biomethane. *Energy.* 2021; 216:19376. <https://doi.org/10.1016/j.energy.2021.119766>
- [8] McTaggart-Cowan P, Rogak N, Munshi R, Hill G, Bushe K. Combustion in a heavy-duty direct-injection engine using hydrogen–methane blend fuels. *Int J Engine Res.* 2009;10. <https://doi.org/10.1243/14680874JER02008>
- [9] Rasi S, Läntelä J, Rintala J. Trace compounds affecting biogas energy utilization – a review. *Energy Conv Manag.* 2011;52: 3369-3375. <https://doi.org/10.1016/j.enconman.2011.07.005>
- [10] Sierens R, Demuyneck J, Vancoillie J, Sileghem L, Verhelst S. Efficiency comparison of hydrogen fuelled IC engines with gasoline and methanol fuelled engines. Conference proceedings of Hypothesis IX (paper HYP-024), San José, Costa Rica. 2011.
- [11] Swinbourn N, Li C, Wang F. A comprehensive review on biomethane production from biogas separation and its techno-economic assessments. *Chem Sus Chem.* 2024;17:1-37. <https://doi.org/10.1002/cssc.202400779>
- [12] Teoh Y, How H, Le T, Nguyen H, Loo D, Rashid T et al. A review on production and implementation of hydrogen as a green fuel in internal combustion engines. *Fuel.* 2023;333: 126525. <http://doi.org/10.1016/j.fuel.2022.126525>
- [13] Turns R. An introduction to combustion: concepts and applications. 3rd ed. McGraw-Hill, New York 2012.
- [14] Verhelst S, Wallner, T. Hydrogen-fueled internal combustion engines. *Prog Energy Combust Sci.* 2009;35:490-527. <https://doi.org/10.1016/j.peccs.2009.08.001>
- [15] Wróblewski P, Bratkowski P. Effect of using a combination of coatings on reducing structural defects in the working area of the combustion chamber and on the energy efficiency of a reciprocating internal combustion engine. *Combustion Engines.* 2025;202(3):118-130. <https://doi.org/10.19206/CE-207651>

Prof. Willian Nadaleti, DSc., DEng. – Engineering Center, The Federal University of Pelotas, UFPel, Brazil.
e-mail: willian.nadaleti@ufpel.edu.br



Prof. Ireneusz Szczygiel, DSc., DEng. – Institute of Thermal Technology, Silesian University of Technology, Poland.
e-mail: ireneusz.szczygiel@polsl.pl



Prof. Grzegorz Przybyła, DSc, DEng. – Institute of Thermal Technology, Silesian University of Technology, Poland.
e-mail: grzegorz.przybyla@polsl.pl



Study on effects of LPG addition and EGR application on the combustion and emission characteristics in a dual-fuel diesel engine

ARTICLE INFO

The purpose of this study is to analyze the combustion and exhaust emission characteristics of a four-cylinder dual-fuel diesel engine (AJM 1.9 TDI), operating with diesel as the base fuel and LPG as a premixed, port-injected complement. The engine was modified suitably to run in dual-fuel mode with minimal modifications, without altering the original diesel fuel supply system, engine electronic control logic, and operation algorithms, nor any other factory-installed components. Experiments were conducted under two conditions: with and without the Exhaust Gas Recirculation system (EGR-on and EGR-off). Under each EGR condition, multiple speed/load scenarios were evaluated, replacing diesel with LPG, with a share ranging from 0 to approximately 30% of the total fuel energy. Throughout the experimental runs, in-cylinder pressure (p) data and emissions of NO_x , CO , CO_2 , O_2 , and λ were logged. Based on the collected data, the combustion metrics such as gross mean effective pressure (GMEP), mean in-cylinder temperature (T) traces, net heat release rate (NHRR) profiles, mass fraction burn (MFB) profiles, burn rate (BR) dynamics, crank angle timings ($\phi_{\text{MFB}10}$, $\phi_{\text{MFB}50}$, $\phi_{\text{MFB}90}$) at key MFB stages, combustion duration (CD) and crank angle timing ($\phi_{p,\text{max}}$) of the maximum in-cylinder pressure (p_{max}) were computed and evaluated.

Received: 26 May 2025

Revised: 27 October 2025

Accepted: 31 October 2025

Available online: 22 November 2025

Key words: dual-fuel diesel engine, LPG premixed ratio, internal combustion engine, combustion, emission reduction, alternative fuels

This is an open access article under the CC BY license (<http://creativecommons.org/licenses/by/4.0/>)

1. Introduction

Global energy trends are gradually shifting towards decarbonization and zero-emission targets, driven by tighter emission regulations, growing renewable energy deployment (Fig. 1), and the rise of electric and hydrogen fuel cell vehicles. Yet, traditional internal combustion engines, including those from older generations, still hold a large share of the global market.

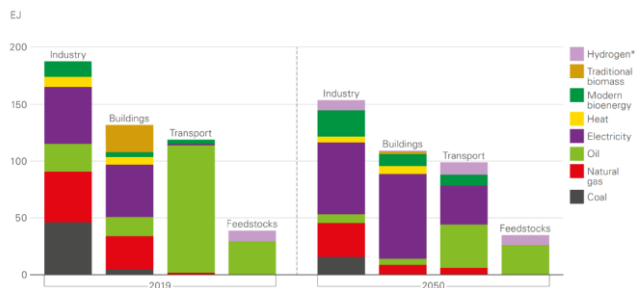


Fig. 1. Energy demand by sector and fuel [3] (* Includes hydrogen-derived fuels)

Diesel engines are widely utilized across various sectors due to their superior thermal efficiency, high power output, durability, and better fuel economy compared to spark-ignition engines. However, a large proportion of internal combustion engines (ICE) in these sectors continue to run on conventional fossil fuels. This leads to serious environmental problems and contributes to the depletion of non-renewable resources, potentially resulting in energy crises and political instability. The transportation sector accounts for approximately 23–28% of global air pollution [1, 4]. Negative consequences of air pollution on human health and the environment have triggered global efforts to reduce conventional ICE's emissions. These concerns, combined

with rising interest in ecological security, have ushered the development of advanced combustion and novel after-treatment technologies. Although these approaches offer effective solutions for reducing harmful compounds in exhaust gases, their implementation is often hindered by economic feasibility and technical complexity, making them less viable for older ICE designs.

Diesel engines are well known for their high output of NO_x and PM pollutants. Combustion in traditional diesel engines, operating in a single-fuel mode (diesel only), initiates with the fuel injection event. It occurs in an environment characterized by a spatially non-uniform distribution of temperature and species concentration, which significantly contributes to NO_x and particulate matter (PM) emissions [24]. The in-cylinder temperature, oxygen concentration, and residence time at high thermal conditions are considered the primary factors contributing to NO_x formation [14, 24]. As highlighted by the author [14, 19], the most commonly used methods to control NO_x emissions include exhaust gas recirculation (EGR), injection timing retardation, staged fuel injection, water injection, catalytic after-treatment, and reduction of premixed burn fraction by reducing ignition delay. EGR is widely regarded as one of the most effective methods currently employed to reduce NO_x emissions in diesel engines. By redirecting a portion of the exhaust gases back into the combustion chamber, the intake charge is diluted, resulting in lower combustion temperatures and, consequently, reduced NO_x formation.

Diesel PM is a complex mixture of solid and liquid phase materials, primarily consisting of carbonaceous material known as soot, a variety of HC's, sulfur compounds and other species [17]. As reported in studies [11, 19, 24], the key contributors to diesel PM formation in the combustion chamber are poor liquid fuel preparation, insufficient air-fuel mixing, and the occurrence of locally rich fuel

regions. It is evident that employing EGR typically leads to increased PM emissions. The trade-off between performance and NO_x -PM emissions in the diesel engine development is widely recognized as a key technical constraint. Relying solely on EGR, without integrating advanced and costly after-treatment systems, prevents older generations of diesel engines from meeting stringent emission regulations. In this context, utilizing alternative fuels in dual-fuel mode (diesel and gaseous fuel), combined with EGR, can provide an effective, practical, and affordable solution for this type of diesel engines.

The dual-fuel strategy involves introducing a secondary fuel, typically in gaseous form, into the intake manifold, where it mixes with the intake air before entering the combustion chamber. This mixture is ignited inside the cylinder by a pilot injection of diesel at the end of the compression stroke. The conversion of lightweight diesel engines to dual-fuel systems requires limited alterations, making the process straightforward and economically viable. Additionally, these engines retain the capability to operate solely on diesel fuel. The operational concept of the dual-fuel supply strategy has been detailed in the previous study [18]. However, for the sake of clarity and completeness, a brief overview is provided in the present paper. In dual-fuel operation, gas flow is controlled by the dual-fuel electronic control unit (DFECU). In contrast, diesel fuel delivery remains under the control of the engine's stock electronic control unit (ECU). According to the user-defined secondary fuel maps, the DFECU adjusts its flow rate and tunes sensor signals from accelerator pedal position (APP), mass air flow (MAF), and manifold absolute pressure (MAP), and transmits these modified signals to the diesel ECU, which correspondingly alters the diesel fuel quantity.

Utilizing alternative gaseous fuels, such as compressed natural gas (CNG), liquefied natural gas (LNG), and liquefied petroleum gas (LPG), is a promising solution for minimizing toxic compounds in exhaust gases and reducing dependence on conventional liquid petroleum fuels [2]. LPG is widely adopted as an alternative energy source employed in households, industry, and transport worldwide. It is regarded not only as a practical substitute for liquid petroleum fuels but also as an effective solution for decreasing harmful emissions such as NO_x and particulate matter [12]. LPG is derived as a by-product from the refining of crude oil and is mainly composed of propane and butane. LPG's high octane number and ignition temperature, along with its low cetane number, inhibit auto-ignition under compression. However, when operated in dual-fuel mode with diesel injected (pilot fuel), the gas ignites effectively. Engines operating on LPG can achieve a higher energy output per unit of fuel than those using diesel, due to LPG's superior calorific value, which may result in lower overall fuel consumption. Moreover, LPG contains negligible amounts of sulfur. The use of diesel fuel in combination with gaseous fuels helps to extend engine life by reducing sulfur dioxide emissions, a primary contributor to corrosion [12, 16]. The main properties of the fuels are given in Table 1.

Despite extensive research on the combustion and emission characteristics of dual-fuel (LPG/diesel) engines, the majority of studies have concentrated on single-cylinder or

laboratory-scale configurations, making a direct transfer of the findings to passenger car applications challenging. For instance, study [16] analyzed the effects of LPG addition on the combustion characteristics of a single-cylinder, four-stroke, direct injection diesel engine under variable compression ratios. Increasing the LPG flow rate from 5 to 20 L/min gradually reduced peak in-cylinder pressure and heat-release rate compared to diesel-only operation, indicating a slight decrease in combustion intensity. Higher compression ratios increased both peak pressure and combustion temperature for all cases, with the diesel-only case achieving the highest values. Emission analysis showed that LPG addition reduced CO, HC, and NO_x emissions compared to diesel-only operation, although these emissions tended to rise at higher compression ratios.

In study [5], the effects of EGR on RCCI combustion were investigated using a single-cylinder, four-stroke diesel engine operating with diesel blended with biodiesel (from waste cooking oils) and a constant 10% LPG fraction for both EGR and non-EGR conditions. Increasing EGR from 0% to 30% resulted in a reduction of peak in-cylinder pressures and heat-release rates, delayed the start of combustion, and extended fuel-air mixing times due to oxygen dilution and lower temperatures. Emission analysis revealed a substantial decrease in NO_x with higher EGR, while CO and HC emissions increased due to slower combustion and local oxygen depletion. The biodiesel content in the fuel blend further reduced NO_x emissions. However, increased CO and HC, indicating a trade-off between emission reduction and incomplete combustion under RCCI with EGR, where the optimal biodiesel fraction depends on balancing this compromise.

Authors [22] studied a four-cylinder, four-stroke turbo-charged marine diesel engine operating in LPG/diesel dual-fuel mode to determine the maximum diesel substitution before knocking occurred. The engine ran without knock at low and medium loads, while full-load conditions caused knocking due to the low cetane number of LPG and the high compression ratio. With the addition of LPG, PM emissions were reduced, but HC and CO emissions increased due to incomplete combustion. NO_x emissions decrease at low and medium loads as the LPG fraction increases, due to ignition delay causing incomplete combustion and lower combustion temperatures. According to the authors [22], NO_x emissions may increase at full load because the higher equivalence ratio reduces air availability compared to lower loads.

The authors [21] made an effort to investigate a four-stroke, naturally aspirated, single-cylinder diesel engine modified for dual-fuel operation using ULSD (ultra-low sulfur diesel) and LPG. The results showed that higher LPG fractions increased peak in-cylinder pressure and heat-release rates due to enhanced premixed combustion. In contrast, the start of combustion was slightly delayed because of LPG's low cetane number and reduced oxygen availability. With EGR addition, combustion was further retarded, and peak pressure decreased slightly, consistent with the thermal effect of recirculated exhaust gases and charge dilution. In terms of emissions, the addition of LPG led to higher HC and CO levels, while soot and NO_x for-

mation were reduced. The application of EGR further lowered NO_x and soot by reducing in-cylinder temperatures, although it slightly increased unburned HC and CO, especially at low engine loads.

Consequently, this study investigates the effects of LPG addition, up to 30% of total fuel energy, and EGR application on the combustion and emission characteristics of a modified Volkswagen Golf IV AJM 1.9 TDI engine. Key parameters including gross: mean effective pressure, in-cylinder pressure, temperature traces, heat release rate, mass fraction burned, burn rate (MFB), crank angle timings at key MFB stages, combustion duration, and peak pressure, as well as NO_x, CO, and CO₂ emissions, were analyzed to provide insights that can support the optimization of older generation diesel engines operating in dual-fuel mode, aiming for improved efficiency and reduced emissions.

Table 1. Fuel properties

Parametr	Unit	Diesel fuel	Butane	Propane
Molecular weight	[g/mol]	170	58.13	44.11
Liquid density at 20°C	[kg/m ³]	800–840	610	501
Liquid viscosity at 25°C	[cSt]	2–4	0.2	0.2
Vapor pressure at 25°C	[bar]	–	8.4	2.1
Boiling temperature	[°C]	125–400	–0.5	–42.1
Self-ignition temperature	[°C]	254	365	470
Cetane number	[–]	40–55	10	5
Lower heating value	[MJ/kg]	36	45.74	46.36
Stoichiometric A/F	[kg/kg]	14,6	14,8	15,7
Latent heat of evaporation	[kJ/kg]	250	390	426
Content of carbon, oxygen and hydrogen	[% by mass]	86/0/14	82.8/0/17.2	75/0/25
Sulfur content	[ppm]	~250	0.01	0.01

2. Experimental setup

The experimental setup consisted of a turbocharged, water-cooled, four-cylinder, four-stroke, direct-injection diesel engine (AJM 1.9 TDI), manufactured by Volkswagen, and equipped with a pump–nozzle injection system. The engine featured a high-pressure exhaust gas recirculation (EGR) system, which directed a portion of the exhaust gases through a cooler before reintroducing them into the intake manifold to reduce nitrogen oxides (NO_x) emissions. The engine was coupled with a Schenck D450-1 hydraulic dynamometer, with the stock electronic control unit (ECU) connected to the dynamometer control unit for precise management of engine speed and torque through dedicated control software. The accelerator pedal signal was electronically emulated to adjust engine speed, while variations in engine load were obtained by applying corresponding torque settings on the dynamometer. The configuration of the test bench is illustrated in Fig. 2, while the engine's technical specifications are provided in Table 2.

The engine was modified for dual-fuel operation by integrating additional ports into the intake manifold for gase-

ous LPG injection, implemented using a standard "auto gas" conversion kit. This kit consisted of an LPG fuel tank with auxiliary parts, a gas filter, fuel supply lines, gas injectors, a gas reducer, sensors, signal emulators, and a dedicated DFECU. As part of the instrumentation setup, the stock air filter was replaced with a laminar flow meter to ensure more accurate airflow measurements. Additionally, to mitigate the impact of intake air temperature variability, the intercooler fan, located downstream of the turbocharger, was replaced with a water-based cooling system. Note that the dual-fuel conversion was implemented without modifying the diesel injection timings, injection patterns, or the engine control logic of the stock ECU. The original diesel system and all factory-installed components remained unmodified, ensuring stable operation in standard DIC mode.

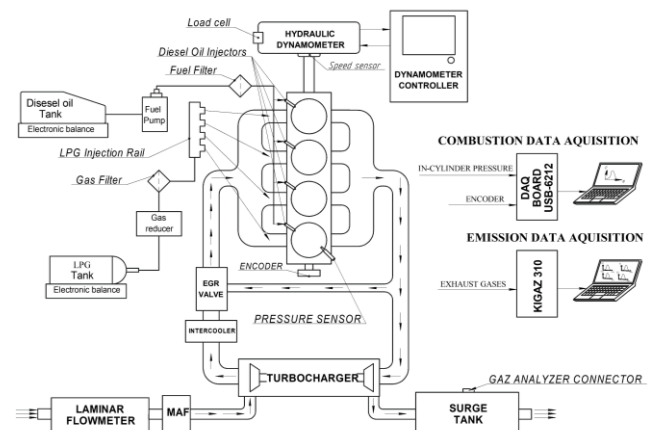


Fig. 2. The schematic diagram of the test bench

Table 2. Engine specifications [9]

Engine parameter	Unit	Specification
Model	[–]	AJM 1.9 TDI
Manufacturer	[–]	Volkswagen
General Details	[–]	Four stroke, compression ignition, water-cooled, direct injection, turbocharger, intercooler
Displacement	[cm ³]	1896
Diesel fuel injector type	[–]	Pump and nozzle unit
Gas fuel injector type	[–]	4-cylinder LPG/CNG injection rail (BARRACUDA)
No. of cylinders	[–]	4
No. of valves per cylinder	[–]	2
Bore	[mm]	79.5
Stroke	[mm]	95.5
Compression ratio	[–]	18:1
Maximum speed	[rpm]	4000
Rated power	[kW]	85
Maximum torque at 1900 rpm	[Nm]	285

In this study, combustion and emission parameters such as in-cylinder pressure and exhaust gases (NO_x, CO, CO₂, O₂, and λ) were measured using a computerized setup. The in-cylinder pressure was measured with the AutoPSI-S fiber-optic sensor from Optrand Inc., while crank angle data were obtained via a CKQH-58 sensor manufactured by LIKA. Data acquisition was performed using the USB-6212 module (National Instruments), with sampling rates set

according to the Nyquist–Shannon sampling theorem to ensure accurate signal reconstruction (Table 3). Fuel consumption was monitored with an AWO electronic balance, while exhaust emissions were measured and logged with a KIGAZ-310 gas analyzer from KIMO.

3. Test scenarios

To assess the effects of LPG addition and EGR application on combustion and emission characteristics, two steady-state operating points (OP) from the dataset described in the previous study [9] were selected. These operating points correspond to the engine’s behavior during the Worldwide Harmonized Light Vehicles Test Procedure (WLTP), specifically within the WLTC 3b cycle, for an unmodified Volkswagen Golf IV equipped with the AJM 1.9 TDI engine. The WLTP is divided into four distinct driving stages: low (urban), medium (suburban), high (extra-urban), and extra-high (highway). Each stage is defined by specific vehicle speed versus time profiles. To replicate these real-world driving conditions on a test bench, the vehicle speed profiles were converted into corresponding engine speed and torque profiles. This conversion was performed using computer simulations based on a simplified longitudinal dynamics model, combined with WLTP gear-shifting logic and a density-based grid clustering approach to identify steady-state operating points that accurately reflect real driving scenarios.

It should be noted that the experiments on the test engine were conducted in the following manner: initial tests were carried out in single-fuel mode, using diesel only, followed by dual-fuel operation with LPG and diesel at the same operating points.

At each OP, experiments were conducted under two conditions: EGR-on and EGR-off. For both cases, four diesel-to-LPG substitution ratios were tested. The experiments are marked OP.1.1 to OP.2.4, where the first digit refers to the operating point and the second to the trial number (see Table 3). It should be noted that during EGR-on test cases, the EGR rate was controlled automatically by the stock ECU. This approach allows the evaluation of engine behavior under dual-fuel conditions with minimal modifications and without any recalibration for LPG usage.

In the dual-fuel setup used in the present study, the quantities of LPG and diesel were inversely adjusted according to engine operating conditions: an increase in LPG was accompanied by a proportional reduction in diesel, and

vice versa, ensuring that the total fuel energy supplied to the engine remained constant.

Substitution ratio (SR) was used as an indicator to quantify the energy share of LPG in the total fuel energy input:

$$SR = \frac{\dot{m}_G \times LHV_G}{\dot{m}_D \times LHV_D + \dot{m}_G \times LHV_G} \times 100\% \quad (1)$$

As previously mentioned, increasing the LPG share in the dual-fuel working concept results in a proportional reduction of diesel injection, which alters the air–fuel ratio. Throughout the experiments, to ensure measurement consistency, the air–fuel ratio (λ) was first measured during diesel-only operation with EGR-on. In dual-fuel mode, λ was maintained at the same level as measured for diesel-only operation for EGR-on. At the same time, for EGR-off, λ was adjusted to match the value used for EGR-on (Fig. 10 and Fig. 11). These adjustments were implemented through modifications in the DFECU control algorithms. It should be noted that, these adjustments were made considering the trade-off between diesel reduction, LPG addition and the limits of λ adjustment via turbocharger operation.

4. Experimental data processing

The in-cylinder combustion dynamics govern the performance and emissions of internal combustion engines. The co-introduction of gaseous fuels with diesel alters combustion dynamics due to differences in the molecular composition, chemical reactivity, and thermophysical properties of the fuels. To evaluate combustion behavior and emission formation, approximately 100 consecutive cycles were sampled and recorded for each experimental trial. These datasets were then averaged and smoothed to minimize noise and reduce sensor uncertainty. The combustion metrics analyzed in this study include (see Fig. 3–Fig. 6, Table 4):

- mean in-cylinder pressure (p) traces
- net heat release rate (NHRR) profiles
- mean in-cylinder temperature (T) traces
- mass fraction burn (MFB) profiles
- burn rate (BR) dynamics
- crank angle timings at key MFB stages (ϕ_{MFB10} , ϕ_{MFB50} , ϕ_{MFB90})
- combustion duration (CD)
- maximum in-cylinder pressure (p_{max}) and its corresponding crank angle ($\phi_{p,max}$)
- gross mean effective pressure (GMEP).

Table 3. Test scenarios

Parameter	Unit	Information							
		1				2			
Operation point	[-]	1	2	3	4	1	2	3	4
Trial	[-]								
Engine speed	[rpm]	1690				2280			
Engine torque	[N·m]	71				145			
Diesel rate EGR-on	[mg/cycle]	19.85	16.96	16.69	15.56	30.98	28.60	25.49	22.85
Diesel rate EGR-off	[mg/cycle]	19.17	17.75	16.65	15.40	31.69	29.49	26.10	22.18
LPG rate EGR-on	[mg/cycle]	0	2.69	2.92	3.96	0	2.20	5.07	7.51
LPG rate EGR-off	[mg/cycle]	0	1.31	2.33	3.49	0	2.04	5.17	8.79
SR EGR-on	[%]	0	14.55	15.92	21.61	0	7.70	17.72	26.25
SR EGR-off	[%]	0	7.40	13.17	19.68	0	6.98	17.67	30.02
Sampling frequency	[kHz]	92				124			

4.1. Computational approach and governing equations

In this study, NHRR was estimated using the Krieger and Borman model [10], derived from the first law of thermodynamics for closed systems and the ideal gas law:

$$\text{NHRR} = \frac{dQ_{\text{net}}}{d\phi} = \frac{\gamma}{\gamma-1} \cdot p \frac{dV}{d\phi} + \frac{1}{\gamma-1} \cdot V \frac{dp}{d\phi} \left[\frac{\text{J}}{\text{deg}} \right] \quad (2)$$

where specific heat ratio (γ), is expressed as follows:

$$\gamma = \frac{c_p}{c_v} \quad (3)$$

Based on the JANAF tables and NASA's polynomial formulation, the specific heat at constant pressure (c_p) is expressed as a function of temperature as follows [15]:

$$c_{p_i}(T) = R \cdot (a_1 + a_2T + a_3T^2 + a_4T^3 + a_5T^4) \left[\frac{\text{J}}{\text{K-mol}} \right] \quad (4)$$

By rearranging the thermodynamic relation between specific heats and the universal gas constant (R), the expression for specific heat at constant volume (c_v) can be expressed as:

$$c_v = c_p - R \left[\frac{\text{J}}{\text{K-mol}} \right] \quad (5)$$

According to the ideal gas equation, the in-cylinder mean gas temperature (T) was calculated in this manner:

$$T = \frac{p \cdot V}{m \cdot R} [\text{K}] \quad (6)$$

The instantaneous cylinder volume is governed by the crankshaft kinematics and can be expressed by the following general equation:

$$V(\phi) = \frac{V}{\varepsilon_s - 1} + \frac{\pi B^2}{4} \cdot (1 + a - s(\phi)) [\text{m}^3] \quad (7)$$

The relationship between piston displacement (s) and crank angle (ϕ) is described by the following expression:

$$s(\phi) = a \cdot \cos(\phi) + \sqrt{(1 - a \cdot \sin(\phi))^2} [\text{m}] \quad (8)$$

The progression of combustion is commonly characterized by the mass fraction burned (MFB). Assuming that the mass of fuel burned is directly proportional to the energy released during combustion (cumulative heat release), MFB was calculated using the following expression:

$$\text{MFB} = \frac{Q_c(\phi)}{\max(Q_c(\phi))} \quad (9)$$

The cumulative heat release, $Q_c(\phi)$, as a function of crank angle, was calculated by integrating the net heat release rate (Q_{net}) over the combustion phase, from intake valve closing (IVC) to exhaust valve opening (EVO):

$$Q_c(\phi) = \int_{\text{IVC}}^{\text{EVO}} \left(\frac{dQ_{\text{net}}}{d\phi} \right) d\phi [\text{J}] \quad (10)$$

The burn rate (BR) is computed by differentiating the mass fraction burned (MFB) with respect to the crank angle (ϕ), as given by the following expression:

$$\text{BR}(\phi) = \frac{d(\text{MFB})}{d\phi} \quad (11)$$

Combustion duration is more often defined as the crank angle interval between 10% and 90% mass fraction burned

(MFB₁₀ to MFB₉₀). This approach excludes the initial and final combustion stages, where the pressure data traces may be unreliable due to signal noise. Additionally, complete combustion (MFB₁₀₀) is rarely achieved as some fuel remains unburned at the end [23]. Therefore, in this study, combustion duration is calculated as follows:

$$\text{CD}_{\text{deg}} = \phi_{\text{MFB90}} - \phi_{\text{MFB10}} [\text{deg}] \quad (12)$$

Hence, combustion duration in milliseconds was obtained by applying the following equation:

$$\text{CD}_{\text{ms}} = \frac{\phi_{\text{MFB90}} - \phi_{\text{MFB10}}}{n \times 0.006} [\text{ms}] \quad (13)$$

The Gross Mean Effective Pressure (GMEP) represents the average effective pressure acting on the piston during the compression and expansion strokes, excluding pumping losses. It provides a useful metric for comparing the performance of an engine under different operating conditions. Mathematically, GMEP can be expressed as:

$$\text{GMEP} = \frac{\sum_{i=1}^{i=180\text{CA}} \frac{(p_1 + p_2)}{2} dV}{V_d} [\text{bar}] \quad (14)$$

5. Combustion: results and discussion

The variation of mean in-cylinder pressure and the net heat release rate as functions of crank angle for each test condition (EGR-on and EGR-off) is illustrated in Fig. 3. It can be observed that, for EGR-off scenarios, for each operating point (OP), an increase in the LPG fraction in the fuel mixture results in slightly higher in-cylinder pressure and a more pronounced heat release rate.

Possible reasons explaining this behavior are:

1. In the dual-fuel combustion mode, LPG in gaseous form is introduced into the intake manifold and mixes with air to create a homogenous, combustible charge. A higher LPG fraction intensifies the premixed combustion phase, resulting in enhanced energy output and elevated in-cylinder pressure [21].
2. LPG is composed primarily of propane and butane, which have higher flame propagation than conventional diesel.
3. It is well known that the introduction of recirculated exhaust gases into the intake manifold leads to charge dilution, thereby reducing the oxygen concentration, which directly affects the upcoming combustion event [7]. Therefore, in EGR-off test cases, an increasing LPG ratio enhances the BR dynamics (Fig. 6a and Fig. 6c), which results in higher mean in-cylinder pressures and temperatures (Fig. 4a and Fig. 4c).

Under EGR-on conditions, a higher proportion of LPG results in reduced mean in-cylinder pressure and temperature compared to diesel-only operation (see Fig. 3 and Fig. 4). This is likely due to a combination of factors that leads to an incomplete and unstable combustion event, such as:

1. Limited oxygen availability from EGR, and the displacement of intake air by LPG, lead to decreased volumetric efficiency and poorer mixing quality of the charge.
2. As it was stated earlier, the author attempted to maintain λ at the same (Fig. 10 and Fig. 11) in both single- and dual-fuel modes through turbocharger system adjust-

- ments. As a result of this approach, the initial cylinder pressure before (BTDC) was altered.
- As gaseous LPG is inducted into the intake manifold, its high latent heat of vaporization absorbs energy, cooling the intake charge and lowering the in-cylinder temperature.
 - Under dual-fuel (LPG/diesel) conditions, the reduction in liquid diesel quantity due to fuel substitution leads to poorer spray atomization and slower droplet development, thereby affecting combustion quality [21]. This effect occurs under both EGR-on and EGR-off conditions. However, this effect is more pronounced during EGR-on operation due to the combined influences of oxygen dilution, charge cooling, and the changes in initial in-cylinder pressure described above.

It should be noted that most of the phenomena described above occur under both EGR-on and EGR-off conditions, although their intensity differs: effects such as oxygen dilution, intake charge cooling, and poorer spray atomization are more pronounced under EGR-on operation, while enhanced premixed combustion and higher burn rates due to increased LPG fractions are more evident under EGR-off conditions.

As illustrated in Fig. 3b (OP.1.4) and Fig. 3c (OP.2.4), the net heat release (NHRR) profiles exhibit a more complex shape. This behavior was observed at high proportions of inducted LPG in the intake charge (approximately 21.61% for OP.1.4-EGR-on and 30.02% for OP.2.4-EGR-off, see Table 3), which were associated with combustion instabilities such as knocking and misfiring. These can be

attributed to a combination of factors, including the physicochemical properties of the fuels, the quality of fuel-air mixture formation, the influence of EGR, and overall combustion dynamics.

Figure 4 shows that the calculated mean temperature follows a trend similar to that of the in-cylinder pressure. Under EGR-off conditions, an increase in LPG fraction leads to higher mean temperatures for both operating points, with OP.1 (Fig. 4a) rising from 1580 K (Trial 1) to 1700 K (Trial 4) and OP.2 (Fig. 4c) increasing from 1680 K (Trial 1) to 1915 K (Trial 4). In contrast, under EGR-on conditions, the mean temperature decreases with the increase LPG content. For OP.1 (Fig. 4b), it drops from 1580 K (Trial 1) to 1420 K (Trial 4), while for OP.2 (Fig. 4d), it fluctuates due to unstable combustion, ranging from 1650 K (Trial 1) to 1695 K (Trial 4), with intermediate values of 1470 K (Trial 2) and 1530 K (Trial 3).

Figure 5 and Figure 6 illustrate the variation in mass fraction burned (MFB) and burn rate (BR) dynamics as functions of crank angle. Variations in combustion behavior can be attributed to previously discussed factors such as fuel properties, poor mixture homogeneity, EGR application, and the lack of optimal engine calibration for better LPG utilization. Compared to DICI mode, increasing the proportion of premixed LPG in dual-fuel mode alters the progression of the burn. It shifts the positions of MFB indicators (see Table 4), thereby modifying both the mass fraction burn profile and burn rate. These changes influence the NHRR, which in turn affects in-cylinder temperature and emission formation.

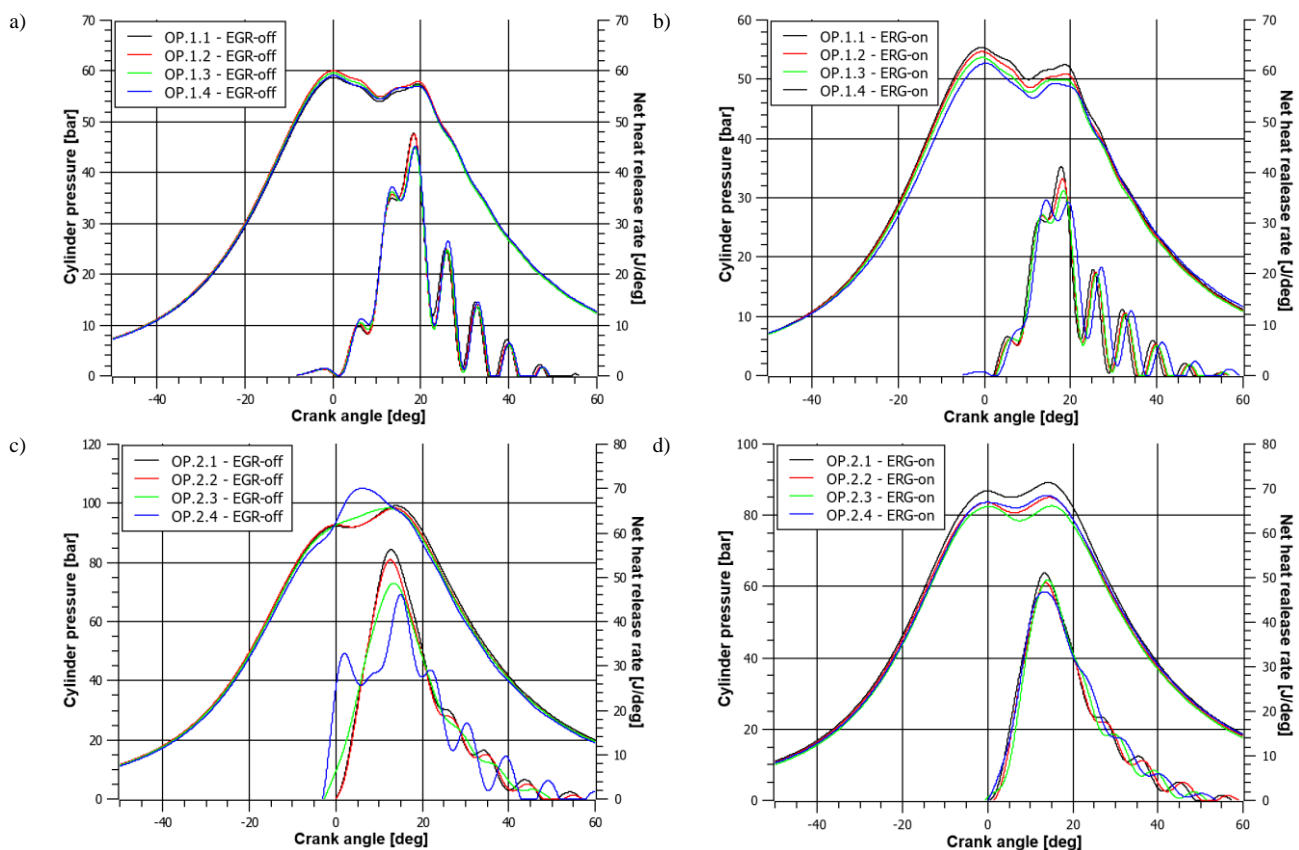


Fig. 3. In-cylinder pressure and NHRR variations

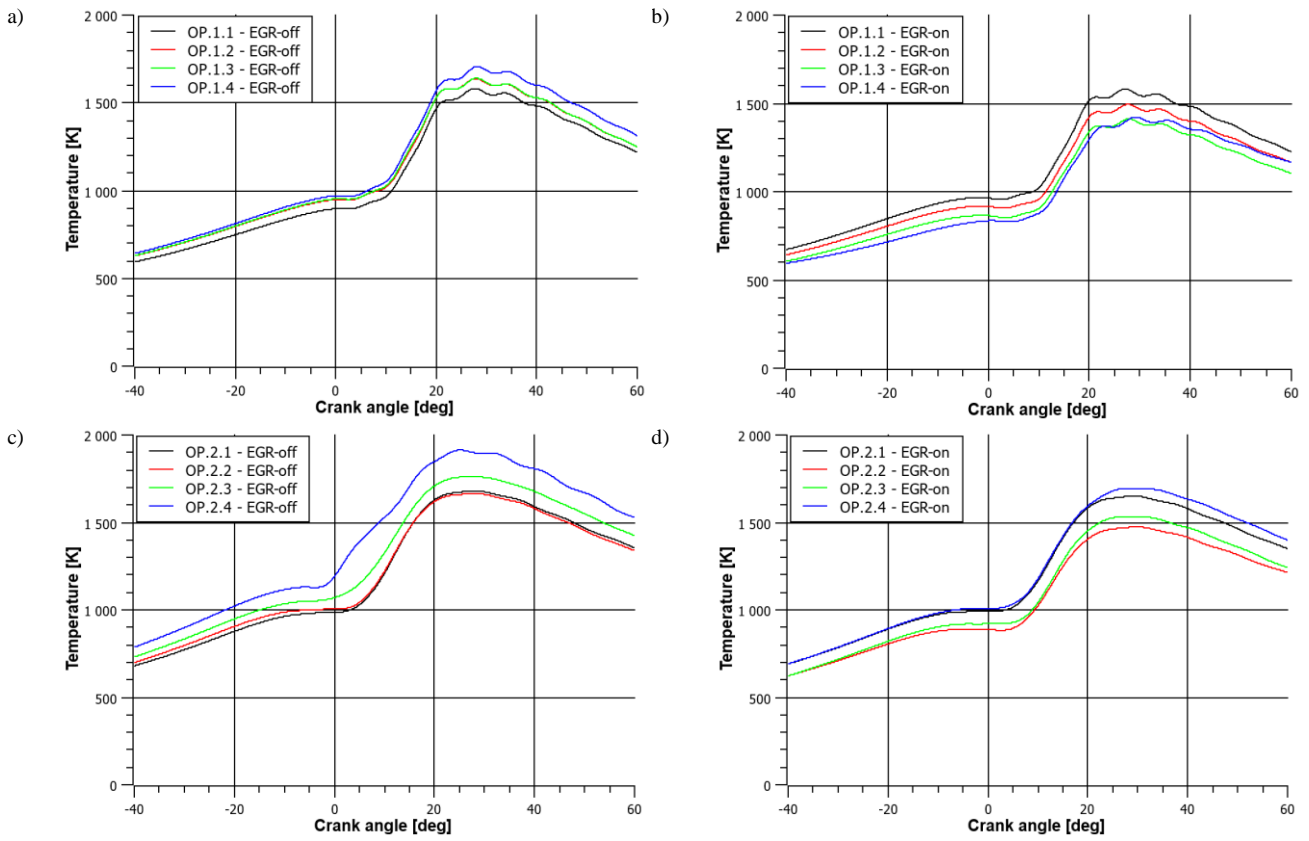


Fig. 4. In-cylinder mean temperature variations

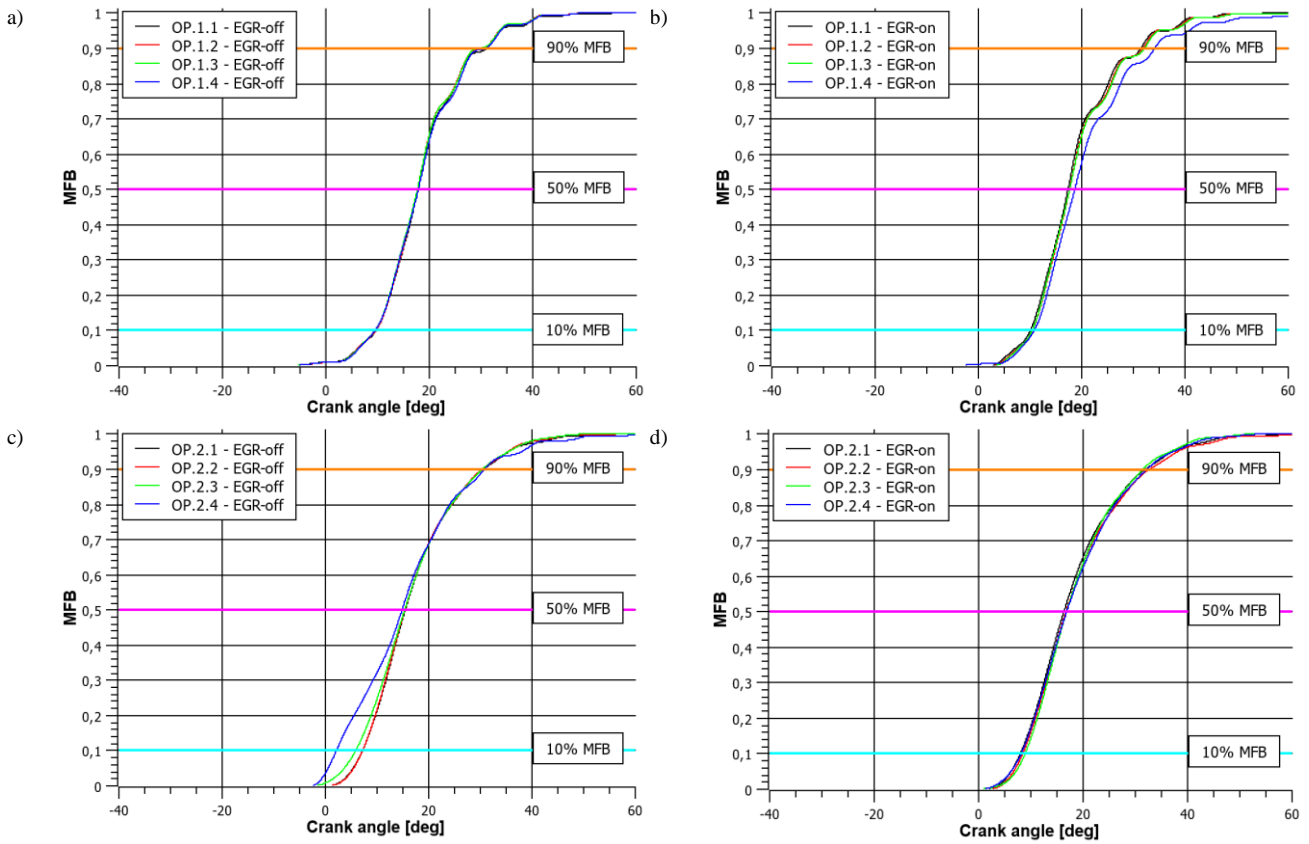


Fig. 5. The mass fraction burn variations

6. Emission: results and discussion

The nitrogen oxides (NO_x) primarily consist of nitric oxide (NO) and a minor amount of nitrogen dioxide (NO₂). These compounds are primarily formed through the high-temperature oxidation of nitrogen in the intake air within the combustion chamber. In particular, NO formation occurs in the post-flame region during the combustion of gaseous fuels [11].

NO_x formation depends on several factors, including in-cylinder temperature and pressure, oxygen content, and the duration of oxidation under high-temperature conditions [16].

Figure 7 indicates that EGR-off test conditions yield higher NO_x emissions as compared to EGR-on. The reintroduction of exhaust gases into the intake charge via the EGR system increases the mixture's specific heat capacity. It dilutes the intake air with inert gases (reducing O₂ availability) and thus negatively affects combustion kinetics [5, 7, 20, 22]. Consequently, in-cylinder pressure and temperature

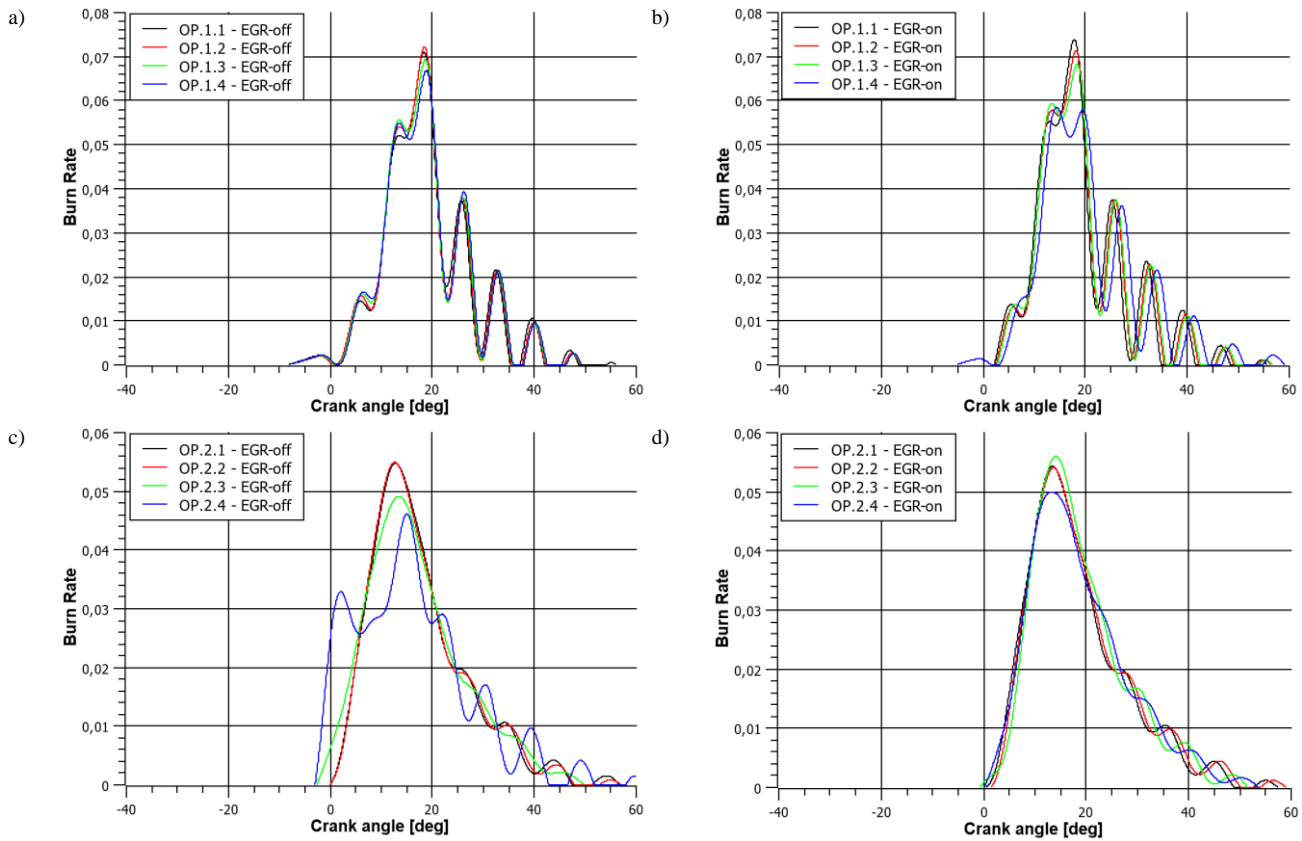


Fig. 6. The burn rate variations

Table 4. Combustion metrics

OP.	Trial number	Test condition	GMEP	p _{max}	φ _{p,max}	φ _{MFB10}	φ _{MFB50}	φ _{MFB90}	CD _{deg}	CD _{ms}
			[bar]	[bar]	[deg]	[deg]	[deg]	[deg]	[deg]	[ms]
1	1	EGR-off	7.01	58.74	0.20	9.72	17.79	31.05	21.33	2.10
	1	EGR-on	5.65	55.39	-0.70	10.06	17.35	31.46	21.40	2.11
	2	EGR-off	6.88	60.06	0.10	9.66	17.71	30.47	20.81	2.05
	2	EGR-on	5.50	54.66	-0.55	10.46	17.63	31.85	21.39	2.11
	3	EGR-off	6.79	59.58	0.20	9.51	17.66	29.22	19.70	1.94
	3	EGR-on	5.42	53.66	-0.50	10.40	17.66	32.11	21.71	2.14
	4	EGR-off	7.07	59.08	0.25	9.52	17.87	30.85	21.34	2.10
	4	EGR-on	5.82	52.70	0.30	10.81	18.66	34.13	23.32	2.30
2	1	EGR-off	11.30	99.21	13.95	7.16	15.46	30.52	23.36	1.71
	1	EGR-on	10.17	89.18	14.25	7.96	16.31	31.78	23.82	1.74
	2	EGR-off	10.77	98.36	13.55	7.17	15.37	30.32	23.16	1.69
	2	EGR-on	9.78	85.02	14.55	8.42	16.71	32.58	24.16	1.77
	3	EGR-off	10.93	98.32	12.10	5.86	15.33	30.38	24.53	1.79
	3	EGR-on	9.85	82.61	15.05	8.88	16.82	31.36	22.48	1.64
	4	EGR-off	10.88	105.03	6.10	2.09	14.84	30.79	28.69	2.10
	4	EGR-on	10.23	85.54	13.80	8.13	16.84	32.12	23.99	1.75

are lowered, and NO_x formation under EGR-on test conditions is reduced. Experimental results confirm this trend (Fig. 7). At Operating Point 1 (OP.1), NO_x emissions decreased from around 340 ppm under EGR-off conditions to approximately 210 ppm with EGR-on. For OP.2, which represents a higher engine speed and load, NO_x levels decline from about 670 ppm (EGR-off) to 510 ppm (EGR-on).

As depicted in Fig. 7, employing LPG in dual-fuel mode further alters NO_x emissions in both EGR-on and EGR-off modes. Based on the findings previously described in this paper, along with insights from the scientific literature, this phenomenon can be explained by the interplay of several factors:

1. In dual-fuel operation mode, increasing the proportion of LPG results in a corresponding decrease in the amount of diesel fed.
2. Due to the gaseous state of LPG, it tends to fill small gaps and crevices inside the cylinder more effectively than liquid diesel.
3. Maintaining a constant level of air–fuel equivalence ratio (λ), along with the factors mentioned in 1 and 2 above, may lead to locally non-uniform or inhomogeneous mixture distribution within the cylinder, which can be considered suboptimal in terms of combustion efficiency and emissions.
4. When LPG is introduced into the intake manifold, its higher latent heat results in greater heat absorption during vaporization, which in turn cools the intake charge. As the LPG proportion increases, this cooling effect becomes more pronounced, resulting in lower in-cylinder temperatures and reduced thermal NO_x formation.
5. LPG, which is primarily a mixture of propane and butane, has a higher laminar flame speed than liquid diesel. These characteristics alter the rate of pressure rise during combustion.
6. In single-fuel mode, the energy is mainly released during the diffusion combustion stage, whereas dual-fuel combustion shifts the energy release toward the pre-mixed combustion stage.
7. The lack of optimization in injection strategy and ECU control algorithms for dual-fuel operation with LPG leads to unstable engine behavior and jerking, thereby negatively affecting mixture formation and combustion quality.

Under EGR-on operation, the addition of premixed LPG further influenced NO_x formation. At Operating Point 1 (OP.1), NO_x concentrations ranged from 210 ppm (Trial 1, no LPG) to 265 ppm (Trial 4, the highest LPG share). In contrast, at OP.2, NO_x initially rose from 510 ppm (Trial 1) to 528 ppm (Trial 2) before decreasing markedly to 382 ppm (Trial 4).

Under EGR-off conditions, increasing the LPG fraction also led to a reduction in NO_x emissions, despite higher in-cylinder pressures and temperatures. At OP.1, NO_x decreased from 340 ppm (Trial 1) to 290 ppm (Trial 4), while at OP.2, it declined from 670 ppm (Trial 1) to 436 ppm (Trial 4).

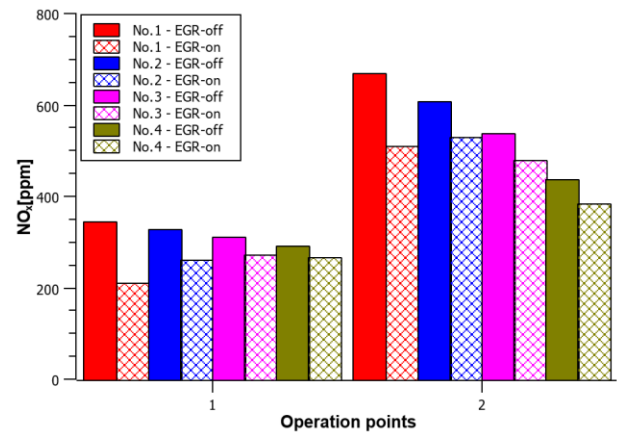


Fig. 7. Variation in nitrogen oxide (NO_x) concentrations corresponding to a specific engine operation point

Carbon monoxide (CO) is a hazardous air pollutant that contributes to environmental degradation and poses significant risks to human health. It is produced as a byproduct of the incomplete combustion of hydrocarbon-based fuels. Figure 10 shows the variation of CO concentrations corresponding to different engine operation test points. Dual-fuel mode yields higher CO emissions compared to single-fuel mode. The formation of CO is facilitated by conditions such as limited oxygen availability, non-optimal air–fuel ratios, poor charge mixing quality and the presence of excess exhaust gases in the combustion chamber, all of which lead to poor combustion [6, 8, 13, 22]. Under EGR-off conditions, CO concentrations increased from 280 ppm to 1874 ppm in OP.1, and similarly, from 354 ppm to 1930 ppm in OP. 2. Under EGR-on operation, CO levels rose from 272 ppm to 1787 ppm in OP.1 and from 106 ppm to 1900 ppm in OP.2. These results indicate that substituting diesel with gaseous LPG promotes incomplete CO oxidation. According to the findings in [6, 8, 13], and other sources, higher CO emissions in exhaust gases can be controlled by adjusting factors such as pilot fuel quantity, injection timing, and EGR rate. Advancing the injection timing improves the oxidation rate of CO, while adjusting the EGR rate enables control over the air–fuel mixture in the intake charge, both of which may contribute to reduced CO emissions.

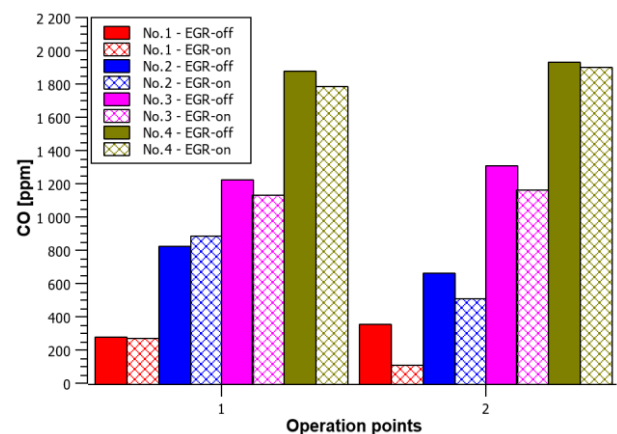


Fig. 8. Variation in carbon monoxide (CO) concentrations corresponding to specific engine operation point

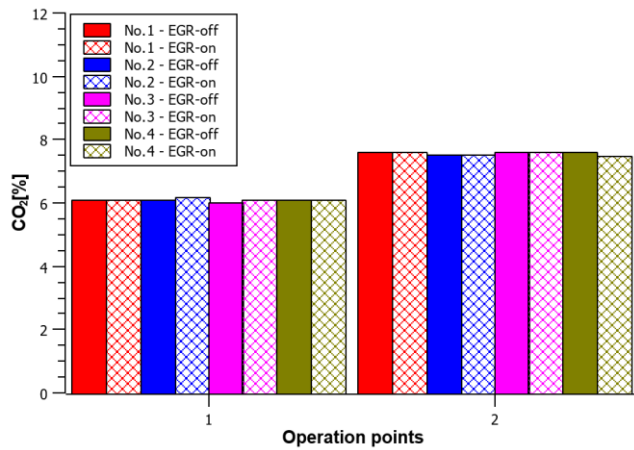


Fig. 9. Variation in carbon dioxide (CO₂) concentrations corresponding to specific engine operation point

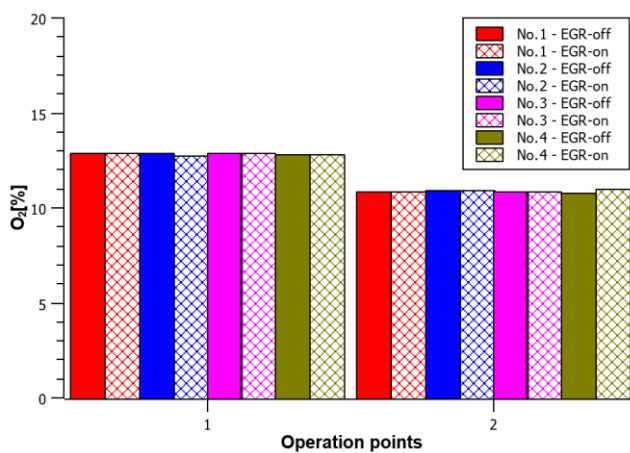


Fig. 10. Variation in oxygen (O₂) content corresponding to specific engine operation point

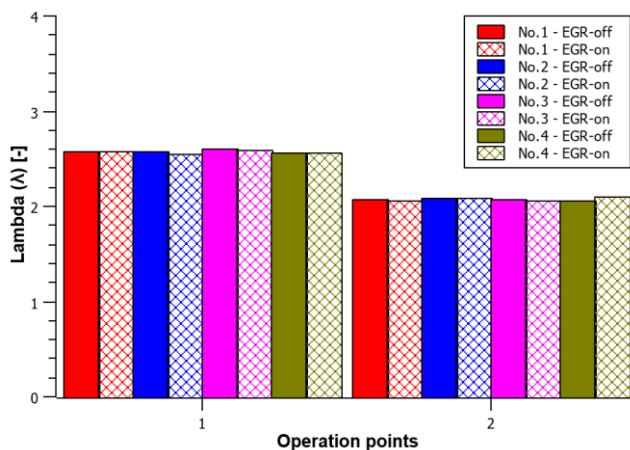


Fig. 11. Variation in air–fuel equivalence ratio (λ) corresponding to specific engine operation point

Carbon dioxide (CO₂) is a major component of exhaust gas recirculation, and its high heat capacity makes it an effective heat absorber during combustion, thereby reducing the maximum combustion temperature [25]. As depicted in Fig. 9, CO₂ levels remain consistent, ranging from 6–6.18% for OP.1 and 7.47–7.6% for OP.2, regardless of the

LPG ratio or EGR condition. This stability is most likely due to the maintenance of a constant air–fuel ratio (AFR) throughout all test trials (Fig. 10 and Fig. 11). Furthermore, analysis of Fig. 9 and Fig. 10 indicates an inverse relationship between CO₂ and O₂ levels in the exhaust gases.

7. Conclusions

The present study experimentally investigates the effects of LPG addition and EGR application on the combustion and emission characteristics of a modified four-cylinder, turbocharged diesel engine (AJM 1.9 TDI) operating in dual-fuel mode. The key conclusions of this investigation are summarized below:

1. The introduction of premixed LPG under EGR-off conditions enhances the premixed combustion phase, resulting in elevated in-cylinder pressures and temperatures, increased burn rates, and a more pronounced net heat release rate. This effect is primarily attributed to the higher laminar flame propagation of LPG. For instance, the peak in-cylinder pressure rose from 58.74 bar to 59.08 bar in OP.1, and from 99.21 bar to 105.03 bar in OP.2. The corresponding mean temperatures increased from 1580 K to 1700 K in OP.1, and from 1680 K to 1915 K in OP.2. In OP.1, the gross mean effective pressure (GMEP) showed minimal variation, ranging from 7.01 bar in Trial 1 to 7.07 bar in Trial 4, with a slight decrease to 6.79 bar in Trial 3, reflecting minor fluctuations in cylinder work as the LPG fraction increased. In OP.2, the corresponding GMEP decreased from 11.3 bar in Trial 1 to 10.88 bar in Trial 4, indicating that although the combustion process intensified and produced higher peak pressures, the overall cycle work was reduced due to changes in combustion timing and mixture distribution. Under EGR-on conditions, combustion is hindered due to charge dilution, reduced oxygen availability, and the cooling effect caused by the vaporization of LPG. These effects hinder fuel atomization and suppress flame propagation, especially at elevated LPG levels. As a result, the maximum pressure decreased from 55.39 bar to 52.70 bar in OP.1 and from 89.18 bar to 85.54 bar in OP.2, accompanied by a reduction in mean temperature from 1580 K to 1420 K in OP.1. For OP.2, the temperature fluctuates due to unstable combustion, ranging from 1650 K to 1695 K, with intermediate values of 1470 K and 1530 K. Correspondingly, the GMEP for OP.1 varied between 5.42 and 5.82 bar. In contrast, for OP.2, GMEP ranged from 10.17 bar to 10.23 bar, with intermediate values of 9.78 bar and 9.85 bar, indicating combustion instability under EGR-on conditions.

2. The formation of NO_x emissions is strongly influenced by in-cylinder temperature, in-cylinder pressure, oxygen availability, and the residence time required for thermal reactions to occur at elevated temperatures. Experimental results confirm that in EGR-off conditions, the engine produces significantly higher NO_x emissions compared to EGR-on conditions. Under EGR-on conditions, the introduction of premixed LPG shows potential for reducing NO_x emissions. At OP.1, NO_x concentrations ranged from 210 ppm (Trial 1) to 265 ppm (Trial 4). In contrast, at OP.2, NO_x initially increased from 510 ppm (Trial 1) to 528 ppm (Trial 2) before decreasing significantly to 382 ppm (Trial 4). This behavior is primarily attributed to the combined

effects of charge dilution, lower in-cylinder temperatures due to LPG vaporization, and reduced diesel fuel input, all of which act to suppress thermal NO_x formation. Notably that, under EGR-off conditions, increasing the LPG fraction leads to a reduction in NO_x emissions despite higher in-cylinder pressures and temperatures. At OP.1, NO_x decreased from 340 ppm (Trial 1) to 290 ppm (Trial 4), while at OP.2, it declined from 670 ppm (Trial 1) to 436 ppm (Trial 4). This phenomenon can be explained by several factors, including a more uniform temperature distribution resulting from the premixed combustion of LPG, which minimizes localized hot spots responsible for NO_x formation. Furthermore, the absence of optimized engine calibration for LPG use and the maintenance of a constant air-fuel equivalence ratio (λ) cause suboptimal fuel-air mixtures, promoting incomplete and unstable combustion.

3. It was observed that carbon monoxide (CO) emissions are higher in dual-fuel mode compared to single-fuel operation, primarily due to the excess of exhaust gases, incomplete combustion caused by limited oxygen availabil-

ity, suboptimal air-fuel ratios, and poor charge mixing quality. Under EGR-off conditions, CO concentrations increased from 280 ppm to 1874 ppm in OP.1, and from 354 ppm to 1930 ppm in OP.2. Similarly, under EGR-on conditions, CO levels rose from 272 ppm to 1787 ppm in OP.1, and from 106 ppm to 1900 ppm in OP.2.

4. Maintaining a constant air-fuel ratio (λ) across all tests resulted in consistent CO_2 levels, regardless of the LPG ratio. CO_2 concentrations ranged from 6 to 6.18% for OP.1 and from 7.47 to 7.6% for OP.2. Additionally, an inverse relationship between CO_2 and O_2 concentrations in the exhaust gases was observed.

The LPG dual-fuel combustion mode may be a promising approach for mitigating toxic emissions in older diesel engine generations. Modifying conventional diesel engines for dual-fuel mode is cost-effective and involves minimal alterations. However, achieving improved engine performance and reduced emissions requires careful adaptation of engine operating conditions, including optimization of the injection strategy and ECU algorithms.

Nomenclature

a_1 – a_7	JANAF polynomial coefficients.	MAP	manifold absolute pressure sensor
APP	accelerator pedal position sensor	MFB	mass fraction burn
B	cylinder bore	m_G, m_D	mass flow rates of gaseous and diesel fuel
BR	burn rate	n	engine revolutions per minute
BTDC	before top dead centre	NHRR	net heat release rate
CD	combustion duration	NO_x	nitrogen oxides
CI	compression ignition	OP	operating point of the engine
CNG	compressed natural gas	ϕ	crank angle
c_p	specific heat at constant pressure	P	mean in-cylinder pressure
c_v	specific heat at constant volume	PM	particulate matter
DFECU	dual-fuel electronic control unit	Q_c	cumulative heat release
DI	direct injection	Q_{net}	total amount of in-cylinder net heat release
DICI	direct injection compression ignition	R	universal gas constant
EGR	exhaust gas recirculation	s	piston displacement
EVO	exhaust valve opening	SR	substitution ratio
GMEP	gross mean effective pressure	T	mean in-cylinder temperature
ICE	internal combustion engine	V	in-cylinder volume
IVC	intake valve closing	WLTP	Worldwide Harmonized Light Vehicles Test Procedure
l	connecting rod length	γ	specific heat ratio
$L_{\text{HVG}}, L_{\text{HVD}}$	lower heating values of gaseous and diesel fuel	ε_s	engine compression ratio.
LPG	liquified petroleum gas	λ	air-fuel equivalence ratio (lambda)
MAF	mass air flow sensor		

Bibliography

- [1] Agency USEP. Inventory of U.S. Greenhouse Gas Emissions and Sinks: 1990-2021. EPA 430-R-. U.S. Environmental Protection Agency 2023. <https://www.epa.gov/ghgemissions/inventory-us-greenhouse-gas-emissions-and-sinks-1990-2021>
- [2] Ashok B, Ashok SD, Kumar CR. LPG diesel dual fuel engine – a critical review. Alexandria Eng J. 2015;54(2):105-126. <https://doi.org/10.1016/j.aej.2015.03.002>
- [3] British Petroleum. BP Energy Outlook 2023, ed. 2023 explores the key trends and uncertainties. Stat Rev World Energy. 2023:1-53. <https://www.bp.com/content/dam/bp/business-sites/en/global/corporate/pdfs/energy-economics/energy-outlook/bp-energy-outlook-2023.pdf>
- [4] Chen X, Wang Z, Pan S, Pan H. Improvement of engine performance and emissions by biomass oil filter in diesel engine. Fuel. 2019;235:603-609. <https://doi.org/10.1016/j.fuel.2018.08.038>
- [5] Elkelawy M, El Shenawy EA, Mohamed SA, Elarabi MM, Bastawissi HAE. Impacts of using EGR and different DI-fuels on RCCI engine emissions, performance, and combustion characteristics. Energy Convers Manag X. 2022;15. <https://doi.org/10.1016/j.ecmx.2022.100236>
- [6] Goldsworthy L. Combustion behaviour of a heavy duty common rail marine Diesel engine fumigated with propane. Exp Therm Fluid Sci. 2012;42:93-106. <https://doi.org/10.1016/j.expthermflusci.2012.04.016>

- [7] Hountalas DT, Mavropoulos GC, Binder KB. Effect of exhaust gas recirculation (EGR) temperature for various EGR rates on heavy duty DI diesel engine performance and emissions. *Energy*. 2008;33(2):272-283. <https://doi.org/10.1016/j.energy.2007.07.002>
- [8] Issa A, Kim J, Chun K, Choi J, Lee W. Investigation of an optimal exhaust gas recirculation rate on a four-stroke spark-ignited LPG engine. *J Energy Inst*. 2025;120:102048. <https://doi.org/10.1016/j.joei.2025.102048>
- [9] Kneba Z, Stepanenko D, Rudnicki J. Numerical methodology for evaluation the combustion and emissions characteristics on WLTP in the light duty dual-fuel diesel vehicle. *Combustion Engines*. 2022,189(2), 94-102. <https://doi.org/10.19206/CE-143334>
- [10] Krieger RB, Borman GL, Engineers AS of M. The computation of apparent heat release for internal combustion engines American Society of Mechanical Engineers, New York 1966.
- [11] Lata DB, Misra A, Medhekar S. Effect of hydrogen and LPG addition on the efficiency and emissions of a dual fuel diesel engine. *Int J Hydrogen Energy*. 2012;37(7):6084-6096. <https://doi.org/10.1016/j.ijhydene.2012.01.014>
- [12] Lata DB, Misra A, Medhekar S. Investigations on the combustion parameters of a dual fuel diesel engine with hydrogen and LPG as secondary fuels. *Int J Hydrogen Energy*. 2011;36(21):13808-13819. <https://doi.org/10.1016/j.ijhydene.2011.07.142>
- [13] Luft S. A dual-fuel compression ignition engine – distinctive features. *Combustion Engines*. 2010;141(2):33-39. <https://doi.org/10.19206/CE-117144>
- [14] Mani M, Nagarajan G, Sampath S. An experimental investigation on a DI diesel engine using waste plastic oil with exhaust gas recirculation. *Fuel*. 2010;89(8):1826-1832. <https://doi.org/10.1016/j.fuel.2009.11.009>
- [15] McBride BJ, Zehe MJ, Gordon S. NASA Glenn coefficients for calculating thermodynamic properties of individual species: National Aeronautics and Space Administration. 2002; 295. <https://ntrs.nasa.gov/search.jsp?R=20020085330>
- [16] Mohsen MJ, Al-Dawody MF, Jamshed W, El Din SM, Abdalla NSE, Abd-Elmonem A et al. Experimental and numerical study of using of LPG on characteristics of dual fuel diesel engine under variable compression ratio. *Arab J Chem*. 2023;16(8):104899. <https://doi.org/10.1016/j.arabj.2023.104899>
- [17] Shahir SA, Masjuki HH, Kalam MA, Imran A, Ashraful AM. Performance and emission assessment of diesel–biodiesel–ethanol/bioethanol blend as a fuel in diesel engines: a review. *Renew Sustain Energy Rev*. 2015;48:62-78. <https://doi.org/10.1016/j.rser.2015.03.049>
- [18] Stepanenko D, Kneba Z. ECU calibration for gaseous dual fuel supply system in compression ignition engines. *Combustion Engines*. 2020;182(3):33-37. <https://doi.org/10.19206/CE-2020-306>
- [19] Thangaraja J, Kannan C. Effect of exhaust gas recirculation on advanced diesel combustion and alternate fuels – a review. *Appl Energy*. 2016;180:169-184. <https://doi.org/10.1016/j.apenergy.2016.07.096>
- [20] Thanh DX, Truong LD, Duy VN. A review of EGR application for automotive industry. *J Innov Bus Ind*. 2024;2(2):117-122. <https://doi.org/10.61552/JIBI.2024.02.007>
- [21] Tira HS, Herreros JM, Tsolakis A, Wyszynski ML. Characteristics of LPG-diesel dual fuelled engine operated with rapeseed methyl ester and gas-to-liquid diesel fuels. *Energy*. 2012;47(1):620-629. <https://doi.org/10.1016/j.energy.2012.09.046>
- [22] Toledo E, Guerrero F, Amador G, Toledo M. Experimental assessment of the performance and fine particulate matter emissions of a LPG-diesel dual-fuel compression ignition engine. *Energies*. 2022;15. <https://doi.org/10.3390/en15239035>
- [23] Wajand JA, Wajand JT. Silniki o zapłonie samoczynnym. Wydawnictwa Naukowo-Techniczne. Warszawa 1988.
- [24] Wang Y, Liu H, Huang Z, Liu Z. Study on combustion and emission of a dimethyl ether-diesel dual-fuel premixed charge compression ignition combustion engine with LPG (liquefied petroleum gas) as ignition inhibitor. *Energy*. 2016;96(x):278-285. <https://doi.org/10.1016/j.energy.2015.12.056>
- [25] Yasin MHM, Paruka P, Mamat R, Ali MH. Fundamental study of dual fuel on exhaust gas recirculation (EGR) operating with a diesel engine. *Appl Mech Mater*. 2015;773-774: 415-419. <https://doi.org/10.4028/www.scientific.net/AMM.773-774.415>

Denys Stepanenko, DEng. – Faculty of Mechanical Engineering and Ship Technology, Gdansk University of Technology, Poland.
e-mail: denstepa@pg.edu.pl



Chemical decarbonisation of diesel engine and its impact on engine oil degradation

ARTICLE INFO

Received: 25 July 2025

Revised: 12 October 2025

Accepted: 13 October 2025

Available online: 27 November 2025

Modern diesel combustion engines are sensitive to damage to the fuel system and to pollution by carbon deposits. Decarbonisation procedures significantly increase engine life and reduce exhaust emissions. In this experiment, decarbonisation was carried out using the chemical set BG 109 EPR, BG 112 DOC and BG 245 on a Skoda Octavia II with a 2.0 TDi diesel engine type CFFB 103 kW (Common Rail). The vehicle had a current odometer reading of 164.882 km. The effect of decarbonisation was monitored during the operation of the vehicle (7 measurements during 7 calendar months during work of 12.716 km). Two main goals of the long-term experiment were to investigate the effect of chemical decarbonisation of the engine on the degradation of the Shell HELIX HX7 5W-30 oil filling and the condition of the fuel system (nozzle injection). The aim of the research was to confirm the hypothesis that cleaning additives have an impact on the rapid degradation of engine oil, especially in heavily worn diesel engines with high mileage.

Key words: technical diagnostic, fuel system, decarbonisation, injectors, tribology

This is an open access article under the CC BY license (<http://creativecommons.org/licenses/by/4.0/>)

1. Introduction

Chemical engine decarbonisation without disassembly is considered the cheapest type of decarbonisation. It is advisable to perform it in regular cycles (approx. 15.000 km) as a prevention against pollution of the combustion chamber. It is also suitable for minor degrees of engine pollution. A significantly dirty engine can be decarbonized just by disassembling it with the use of chemistry, ultrasound or mechanical cleaning. The latest trend is hydrogen decarbonisation without disassembly. Regular decarbonisation is a prerequisite for reliable operation and a long service life of the combustion engine.

The presented work fills the diagnosed gap in the literature on the subject, as it has been observed that there are few works presenting the degradation processes of engine oils during actual operating conditions [27].

Important notice: The research involves the application of commercial products from the brands Škoda, Shell, BG and modern diagnostic equipment. Any marketing promotion of these products is excluded throughout the article. Any attempt to damage the reputation of these brands is also excluded. These commonly used products served exclusively as necessary objects of measurement during research experiments.

2. The issue of nozzle injectors

2.1. The problem of carbonization of injectors

The results of experimental studies obtained by PC processing showed that the aggregate with new EDC units is more economical [2] than mechanical injection units without EDC. Analyses of injection processes in fuel supply systems with common rail systems have shown differences between the time of injection as preset by the controller and the time of injection accomplished in reality by the injection system [11]. The injectors of the Common Rail system make it possible to control the start of the injection and the injected quantity. The opening and closing of the nozzles are solved using an electromagnetic valve or a piezoelectric

element [19]. Only orifice nozzles are used for direct injection of diesel engines. There are two types of orifice nozzles – with a channel and with a seat [7]. The final shape of the orifice nozzle is determined based on engine tests. The hole nozzle is produced with a maximum number of 12 holes with a minimum diameter of 0.2 mm [6]. Among the most thermally stressed and carbon-contaminated parts of the nozzle is the front of the nozzle with holes that extend into the combustion chamber. The temperature of the nozzle face should not fall below 120–140°C during operation, because there is an increased formation of carbon (especially long-term engine idling and low engine speeds are harmful).



Fig. 1. Fuel nozzle operation before and after the use of additives (illustrative photograph) [2]



Fig. 2. Damaged pistons (illustrative photograph)

When fuel is supplied to the engine with air, the temperature of the working medium in the engine cylinder decreases [26, 29]. On the contrary, the optimal performance of the nozzle can also be disturbed by its overheating, especially temperatures exceeding 250°C [29]. The influence of the driver skills was often identified as a previously overlooked factor [3]. Another related factor is the design of the engine's crank mechanism. The piston kinematics parameters can be influenced by adjusting the distance between the crankshaft axis and the axis of the cylinder [14]. Polluted nozzles cause a sharp, uneven jet of the fuel shown in Fig. 1, which may cause melting off of the piston material and consequently damage the engine (Fig. 2) [8, 16]. The quality of the fuel injection also has a great influence on the ignition delay and the roughness of the engine [28]. The starting dose of fuel with the participation of biocomponents causes the penetration of the unburnt part of the atomized fuel into the engine crankcase, and thus into the oil pan, causing destructive secondary reactions with engine oil. [12].

To understand the main function of the nozzle, it is necessary to state its simplified calculation. It assumes that the fuel is incompressible and the injection pressure remains constant [6]:

The nozzle is designed for the fuel dose V_{pal} according to equation (1) [24].

$$V_{pal} = \int_0^{\tau_d} \mu S_{Tr} w_{Tr} d\tau \quad (1)$$

According to equations (2) and (3), the mass flow of fuel in the nozzle - Q_m is calculated. Before that, it is necessary to calculate the speed of the fuel in the nozzle - c (4) [6].

$$Q_m = \mu \cdot \rho_p \cdot S \cdot c \quad (2)$$

$$Q_m = \mu \cdot S \sqrt{2\rho_p(p_v - p_k)} \quad (3)$$

$$c = \sqrt{\frac{2}{\rho_p}(p_v - p_k)} \quad (4)$$

According to equations (5) and (6), the total area of the nozzle openings - S and the diameter of the nozzle openings - d_D are calculated [6].

$$S = \frac{Q_m}{\mu \sqrt{2\rho_p(p_v - p_k)}} \quad (5)$$

$$D_D = \sqrt{\frac{4 \cdot S}{\pi \cdot z_o}} \quad (6)$$

It follows from equations (1) to (6) that carbon deposits result in a decrease in the diameter of the nozzle openings, which significantly decreases their performance parameters. Even a small contamination of the holes has a very sensitive effect on the fuel flow and the quality of the injection.

2.2. The issue of engine oil degradation

Chemical decarbonisation is good for the engine, but may not be good for the oil fill. Aggressive decarbonizing preparations are added to the oil filling and fuel, which can significantly accelerate the degradation of engine oil. Another factor is dissolved carbon deposits that accumulate in the oil fill. Manufacturers of decarbonisation sets declare

that their products do not affect the quality of the oil filling. But reality may be different. Here, there is a large scope for the investigation of engine oil, which is directly and indirectly exposed to chemical decarbonisation.

In tribology, engine oil degradation is expressed by many physical and chemical parameters. The most fragile parameters is, in most cases, kinematic viscosity, TBN and AW additives. And it is necessary to pay great attention to these parameters.

TBN - parameter, which is used to assess the ability to dissolve acid sludge, its level also reflects the life of motor oil. Do not allow the operation of motor oil when the TBN value decreases by more than compared to the value of the reference sample and the manufacturer's motor oil recommendation TBN - the parameter should not fall below the value of 3.5 mg KOH/g [15].

AW additives - total engine oil additives. Engine oil must be usable in the working parts of the engine under all conditions. Ingredients are chemicals of complicated composition. They improve the performance of the base oil. They meet the demanding conditions of modern engines. Reducing the content of additives below 50% is unacceptable [15].

Kinematic viscosity is the primary and essential property of the suitability of a motor oil in a vehicle engine. Motor oil is only suitable for viscosity in the range $\pm 20\%$ of the reference sample and the manufacturer's motor oil recommendation [17]. Fretting in the tribological kinematic pairs under analysis comprises mainly wear products in the form of material build-ups which become softened, oxidised and fragmented over time. Worn products hardened by oxidation as they move around cause further damage in the form of surface abrasion and micropits [1].

For the study of mutual degradation processes, it is appropriate to use statistical-mathematical operations. A proven tool is the application of correlation analysis with the correlation coefficient - r according to equation (7), or of statistical covariance - k (8).

Table 1. Cohen's interpretation of correlation coefficients

Cohen's correlation coefficient scale	
r	correlation level
0.0 - 0.1	trivial correlation
0.1 - 0.3	small
0.3 - 0.5	medium
0.5 - 0.7	big
0.7 - 0.9	very large
0.9 - 1.0	almost perfect

$$r(x, y) = \frac{k(x, y)}{s_x s_y} \quad (7)$$

$$k(x, y) = \frac{1}{n-1} \sum_{i=1}^n (x_i - \bar{x})(y_i - \bar{y}) \quad (8)$$

Assessing the tightness of the dependence using some characteristic that describes to what extent the variable x explains the variability of the variable y is called correlation analysis [9].

3. Experiments, results and discussion

3.1. Characteristics of the experiment objects

Technical diagnostics provide a lot of valuable data about the technical condition of the vehicle and its changes during use. If repeated diagnostic measurements are consistently managed and archived, it is possible to establish a prognosis based on development trends [18].

Our experiment was focused on monitoring the effects of chemical decarbonisation on the injection nozzles and the oil filling of a diesel engine. It had two goals. The first goal was long-term monitoring of the fuel injectors of the 2.0 TDi CFFB 103 kW engine (Fig. 4) and monitoring the fuel supply of individual injectors on the Škoda Octavia II vehicle (Fig. 3). The hypothesis was that chemical decarbonisation would ensure a balanced fuel supply. The second goal was long-term monitoring of the engine oil charge Shell HELIX HX7 5W-30 (Fig. 5) with monitoring of the most sensitive parameters and how they reacted to chemical decarbonisation



Fig. 3. Skoda Octavia II 2.0 TDi



Fig. 4. Engine of the Skoda II 2.0 TDi CFFB

Within this experiment, we would like to draw attention to the fact that the specificity of chemical decarbonisation and thus also of our monitoring is the long-term achievement of the effect (added cleaning additives in oil and fuel) – the effect of decarbonisation was monitored during 7 calendar months during a mileage run-in of 12,716 km. Data were collected from the diagnostic measurements, which were interpreted in tables, graphs and verbal evaluation through mathematical-statistical analysis.

From the point of view of diagnostic means, diagnostic systems are divided into OFF-LINE test diagnostic systems (diagnosed object out of operation) and ON-LINE operational diagnostic systems (diagnostic object in operation) [4, 29].



Fig. 5. Used engine oil and decarbonisation set in the experiment

In our case, tribodiagnosis of the oil filling is an OFF-LINE method, and injector diagnostics is an ON-LINE method. The means of chemical decarbonisation was (commonly available on the Slovak market) a 3-part set of type BG 109 EPR, BG 112 DOC and BG 245 (Fig. 5).

The process of the cleaning procedure consisted of three successive steps:

Step 1: Application of BG 109 EPR preparation into the old oil filling and subsequent operation of the engine for 20 minutes at idling speed. Then followed the draining of the oil filling from the engine with engine flushing.

Step 2: Applying a new oil filling to the engine with the addition of BG 112 DOC preparation.

Step 3: Application (mixing) of the preparation BG 245 into the fuel in the fuel tank.

The vehicle set up in this way was monitored at irregular kilometer intervals (Table 2, Table 2, Table 3) during the run-in of 12,716 km.



Fig. 6. Tribodiagnostic devices Q-1000, Q-3050 and EOBD – Gutmann Mega Macs PC

Tribotechnical diagnostics was carried out in the tribological laboratory (Department of Mechanical Engineering) A. O. S. Gen. M. R. Štefánik in Liptovský Mikuláš. SpectroVisc Q-3050 and FluidScan Q-1000 optical electronic devices were used for this purpose (Fig. 6). Diagnostics of the fuel system was carried out on the measuring station Gutmann Mega Macs PC (Fig. 6), which communicates with the control unit of the vehicle (ECU).

3.2. Diagnostics of injectors

The measuring station, through connectivity via the on-board EOBD port (OBD II), diagnoses active electronic circuits and passive components in the car in accordance with regulation 98/69/EC valid from 1.1.2000 [20].

Gutmann Mega Macs PC enables a wide range of diagnostics. It has a large library of almost all brands and types of cars. As part of the diagnostics of the fuel system, the device offers numerical and graphical measurements of the

performance of the injection nozzles over time (dynamic characteristics).

Table 2. Performance monitoring of injectors

time interval	vehicle operation			fuel quantity deviation			
	initial state (km)	end state (km)	total sum (km)	injector No. 1	injector No. 2	injector No. 3	injector No. 4
08.06–09.06.2021	164,882	165,033	151	1.0	-0.8	0.2	-0.4
09.06–17.06.2021	165,033	165,525	492	1.0	-0.7	0.2	-0.5
17.06–25.06.2021	165,525	166,810	1 285	1.0	-0.6	0.0	-0.4
25.06–08.08.2021	166,810	169,863	3053	0.5	-0.4	0.0	-0.1
08.08–13.09.2021	169,863	170,831	968	0.3	-0.2	0.1	-0.2
13.09–20.12.2021	170,831	177,598	6767	0.1	-0.2	0.2	-0.1

Measurements progress is described in Table 2. Each nozzle performance measurement took place after a certain time ramp-up with an unloaded engine (idling 782–784 revolutions per minute). The car worked in daily operation, mainly on medium-long routes in Central European climatic conditions. The regularly serviced vehicle burned standard fuel – B7 diesel.

3.3. Measurement results

Figure 7 shows on the display of the Guttman Mega Macs PC the condition of the nozzles before chemical decarbonisation from 9. June 2021, with an odometer reading of 164,882 km. The numerical and graphic record shows that the nozzles have a significantly uneven fuel supply due to carbon pollution.

The deviation between nozzle performance ranges from -0.8 to +1.0, which is a large variance (1.8 in absolute value). The ideal variance is 0.0, i.e. no deviation. The accepted maximum deviation in vehicle operation is from +1 to -1. From the above, it follows that the engine has significantly contaminated injectors. According to general recommendations, its operation is within the permitted limit values. The engine is at risk of damage and a reduction in service life.

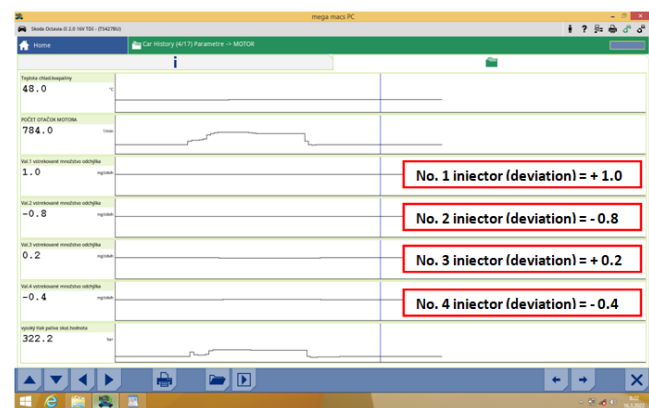


Fig. 7. EOB diagnostic device – condition of nozzles before chemical decarbonisation

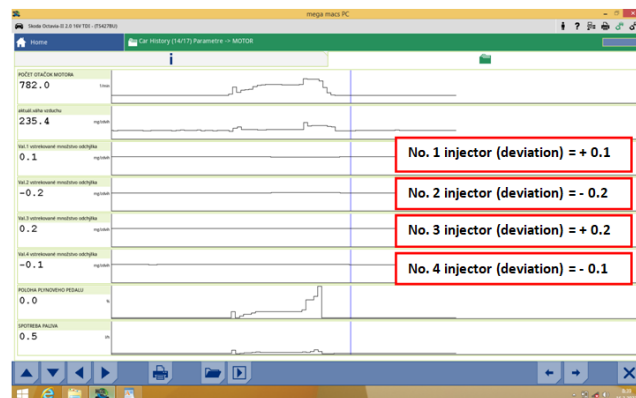


Fig. 8. EOB diagnostic device – condition of nozzles after chemical decarbonisation

The results of the measurements after the decarbonisation procedure are shown in Fig. 8, which is dated 20 December 2021 with an odometer reading of 177,598 km. It follows from the numerical and graphic record that the nozzles have a much more even supply of fuel after the cleaning of carbon deposits than before decarbonisation. The deviation between nozzle performance ranges from -0.2 to +0.2, which is an acceptable variance (0.4 in absolute value).

Graphical interpretation of long-term engine decarbonisation is shown in Fig. 9–11. The change in fuel supply deviation (y) is a function of the mileage (x), i.e. $y = f(x)$. The smoothing techniques used in chemical applications are based, for example, on moving averages or the Savitzky-Golay method [25]. Here, standard tools of mathematical functions and trend curves were used to interpret the results.

Figure 9 graphically shows the reduction of deviation (unevenness) of fuel supply between injector no. 1 and no. 2 depending on the mileage. From a mathematical point of view, this process can be expressed with high accuracy using a simple polynomial regression (eq. (9) and (10)), where the coefficient of determination R^2 reaches high values (0.94 to 0.97). From a practical point of view, injector No. 1 with increased fuel supply compensates for the work of the weaker injector No. 2, which, due to the contamination of the nozzle, delivers a smaller supply of fuel to the combustion chamber of the engine.

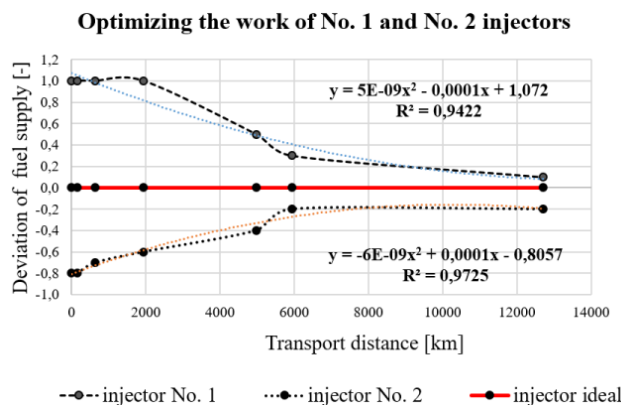


Fig. 9. Ballance of the decarbonisation process of the No.1 and No.2 injectors

For injector No. 1 is the supply of fuel deviation:

$$\text{deviaton} = 5 \cdot 10^{-0.9} \cdot l^2 - 0.0001 \cdot l + 1.072 \quad (9)$$

$(R^2 = 0.9422)$

For injector No. 2 is the supply of fuel deviation:

$$\text{deviation} = -6 \cdot 10^{-0.9} \cdot l^2 + 0.0001 \cdot l - 0.8057 \quad (10)$$

$(R^2 = 0.9725)$

The control unit (EDC – Electronic Diesel Control) can provide this process of optimization and compensation to a certain small extent. With enormously dirty nozzles, even EDC cannot compensate for the uneven work of the injectors.

Differences may also apply to the correction of fuel dosage, as the manufacturer assumes top-down adjustment by means of coding or by earlier disassembly of the nozzle and changing the thickness of the needle wash [22].

The engine is uncultivated, especially at idling speed, and has high mechanical and noise vibrations. Its effectiveness and service life are significantly reduced. The risk of engine damage increases (Fig. 2).

For injector No. 3 is the supply of fuel deviation:

$$\text{deviation} = 4 \cdot 10^{-0.9} \cdot l^2 - 5 \cdot 10^{-0.5} \cdot l + 0.1903 \quad (11)$$

$(R^2 = 0.6404)$

For injector No. 4 is the supply of fuel deviation:

$$\text{deviation} = -3 \cdot 10^{-0.9} \cdot l^2 + 7 \cdot 10^{-0.5} \cdot l - 0.4566 \quad (12)$$

$(R^2 = 0.8302)$

Analogously, similar to Fig. 9, Fig. 10 graphically shows the reduction of deviation (unevenness) of fuel supply between injector no. 3 and no. 4, depending on the mileage. From a mathematical point of view, this process can be expressed with relatively high accuracy using a simple polynomial regression (equations (11), (12)), where the coefficient of determination R^2 reaches acceptable values (0.64 to 0.83).

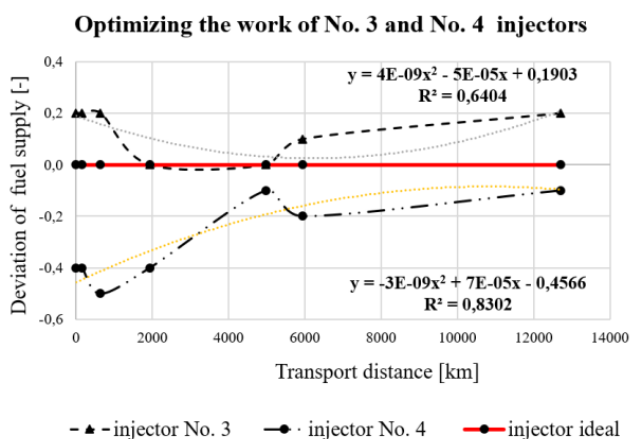


Fig. 10. Balance of the decarbonisation process of the No. 3 and No. 4 injectors

Since the decarbonisation procedure is a complicated process (unevenness of the graphs), defining the decarbonisation process using a simple polynomial regression proved to be the most advantageous. With the help of the regres-

sion function (also expressed by the graph connector Fig. 9, Fig. 10), a relatively accurate approximation of the real state was achieved.

Figure 11 records the overall balance of the decarbonisation process of all four injection nozzles in accordance with Table 1. The change in fuel supply deviation (y) is a function of the mileage (x), i.e. $y = f(x)$. The graphic display shows that the decarbonisation process was most pronounced in the interval from 200 km to 6000 km. At 6000 km, the values stabilized, and later there were no significant changes. The fuel supply deviation of individual nozzles continuously decreased during the entire process, converged to zero and stabilized in the interval $(-0.2, +0.2)$.

From similar studies carried out in the past, it follows that both added additives and the type of fuel used affect the parameters of the injection nozzles.

Among the optical metrics evaluated, only selected macroscopic parameters (spray area and angle) showed sensitivity to fuel composition. Although the spray penetration does not indicate differences, the other indicators in the form of spray area and spray angle significantly indicate changes due to the use of additives [23].

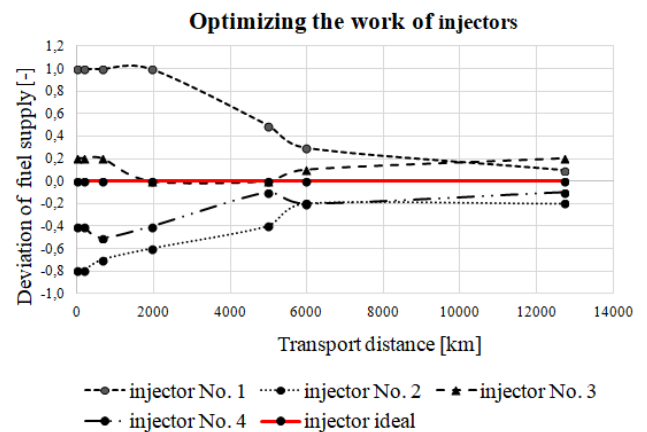


Fig. 11. Balance of the decarbonisation process of the all (four) injectors

3.4. Diagnostics of the oil filling

In the area of the fuel system, chemical decarbonisation has brought positive results.

However, it is questionable how this procedure was reflected in the physical and chemical picture of the oil filling. The situation was also complicated by the decarbonizing oil additive BG 112 DOC, which is being discussed due to the possible disruption of the chemical composition of the engine oil. The use of the intensive fuel additive BG 245 and its possible impact on oil degradation were also questionable.

Tables 3 and 4 record the course of oil charge measurements from new condition to exceeding its service life. (The tables are directly related to each other, and Table 4 is a continuation of Table 3).

These tables provide an overview of the basic physical and chemical parameters of the oil that we monitored and that are most often dealt with in practical tribology. In the gray column (Table 3) are the values of the new oil filling (reference sample), which is compared with the worn sample. Green colored cells in the tables mean satisfactory

results. The red colored cells of Table 4 mean unsatisfactory results. In the table of measurements (Table 4), the unsatisfactory parameter kinematic viscosity at 40°C appears. Since this parameter is unimportant for the operation of an internal combustion engine (it is especially important in industrial machines), we did not pay more attention to it in the research.

Engine oil manufacturers warn customers not to mix various cleaning additives into the oils. It is generally known that it is not recommended to mix oils of other types and brands.

3.5. Measurement results

Similar to the vast majority of cases, this long-term monitoring showed that the most fragile parameter of engine oil was the TBN parameter. But during our monitoring, we also found an abnormal premature drop in kinematic viscosity (Table 5 – red colored cells).

These two most fragile parameters were subjected to deeper analysis. On the basis of correlation analysis (equations 7, 8), the interdependencies between TBN, kinematic viscosity at 100°C and the traveled route were investigated.

Table 3. Engine oil measurement – one life cycle of the oil filling

	8/6/2021 reference sample	9/6/2021	17/6/2021	25/6/2021	allowed values	results for vehicle operation
	mileage of the car: 0 km	mileage of the car: 151 km	mileage of the car: 492 km	mileage of the car: 1285 km		
	total mileage of the car: 164,882 km	total mileage of the car: 165,033 km	total mileage of the car: 165,525 km	total mileage of the car: 166,810 km		
Glycol [%]	0	0	0	0	max. 0	passes
Oxidation [abs/0.1]	12.4	15.1	15.4	17.7	max. 40	passes
Soot [% wt]	0	0.02	0.05	0.07	max. 3	passes
Sulfation [abs/0.1]	17.3	17.7	18.0	19.7	max. 45	passes
Nitration [abs/0.1]	3.9	4.2	5.0	5.7	max. 30	passes
TBN parameter [mg KOH/g]	6.8	6.6	5.8	4.8	min. 3.5	passes
Water content [ppm]	254	132	158	137	max. 5000	passes
Kinematic viscosity at 40°C [mm ² /s]	72.5	69. (-4.1%)	66.6 (-8.1%)	65.9 (-9.1%)	max. difference ±20% compared to the new sample	passes
Kinematic viscosity at 100°C [mm ² /s]	12.6	12.2 (-3.2%)	11.9 (-5.6%)	11.7 (-6.7%)	max. difference ±20% compared to the new sample	passes

Table 4. Engine oil measurement – one life cycle of the oil filling

	8/8/2021	13/9/2021	12/20/2021	allowed values	results for vehicle operation
	mileage of the car: 3053 km	mileage of the car: 968 km	mileage of the car: 6,767 km		
	total mileage of the car: 169,863 km	total mileage of the car: 170,831 km	total mileage of the car: 177,598 km		
Glycol [%]	0	0	0	max. 0	passes
Oxidation [abs/0.1]	18.2	18.3	20.3	max. 40	passes
Soot [% wt]	0.34	0.37	0.48	max. 3	passes
Sulfation [abs/0.1]	22.9	23.0	26.3	max. 45	passes
Nitration [abs/0.1]	10.8	11.5	20.1	max. 30	passes
TBN parameter [mg KOH/g]	3.6	3.5	0.0	min. 3.5	missed
Water content [ppm]	217	119	343	max. 5000	passes
Kinematic viscosity at 40°C [mm ² /s]	61.2 (-15.6%)	59.8 (-17.5%)	44.3 (-38.9%)	max. difference ±20% compared to the new sample	missed
Kinematic viscosity at 100°C [mm ² /s]	11.0 (-12.7%)	10.8 (-14.3%)	8.4 (-33.1%)	max. difference ±20% compared to the new sample	missed

Table 5. Monitoring of the most fragile of the oil filling parameters

Time interval	Vehicle operation			The most fragile parameters on the oil	
	initial state [km]	end state [km]	total sum [km]	TBN [mg KOH/g]	Kinematic viscosity at 100°C [mm ² /s]
08.06.2021	164,882	164,882	0	6.8	12.6
08.06–09.06.2021	164,882	165,033	151	6.6	12.2
09.06–17.06.2021	165,033	165,525	492	5.8	11.9
17.06–25.06.2021	165,525	166,810	1285	4.8	11.7
25.06–08.08.2021	166,810	169,863	3053	3.6	11.0
08.08–13.09.2021	169,863	170,831	968	3.5	10.8
13.09–20.12.2021	170,831	177,598	6767	0.0	8.4

Table 6 shows a very strong (according to Cohen, perfect: $r = 0.9$ to 1) positive correlation of the TBN parameter and kinematic viscosity ν ($r = 0.99$). At the same time, both of these parameters express a very strong inverse correlation with the increase in kilometers ($r = -0.99$).

Table 6. Correlation matrix of the investigated parameters of the engine oil

	Transport distance [km]	TBN [mg KOH/g]	ν at 100°C [mm ² /s]
transport distance [km]	1		
TBN [mg KOH/g]	-0.988381921	1	
ν at 100°C [mm ² /s]	-0.989799344	0.986871717	1

For total base number (TBN):

$$\text{TBN} = -0.0005 \cdot l + 6.3576 \quad (13)$$

$(R^2 = 0.9769)$

For the kinematic viscosity (ν) at 100°C:

$$\nu = -0.0003 \cdot l + 12.363 \quad (14)$$

$(R^2 = 0.9797)$

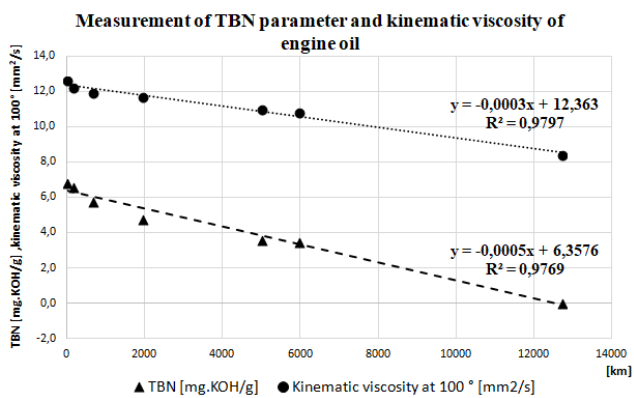


Fig. 13. Course of TBN parameter and kinematic viscosity at 100°C during the life cycle of the oil filling

The course of the most fragile parameters depending on the mileage of the vehicle can be expressed using a simple linear regression. Both parameters are defined by straight line equations and have a linearly decreasing trend (9) (10), where the coefficient of determination R^2 reaches a value of up to 0.98. Their graphic interpretation is in Fig. 13.

The study of the problem shows that the observed parameters (TBN and ν) have an almost ideal linear slope and an almost perfect mutual correlation, which is quite unusual in this respect.

From the theoretical point of view of tribology, this is a significant result. From the practical point of view of tribology, it follows that the oil filling has exceeded its lifetime of the TBN parameter and the kinematic viscosity at 100°C approximately after running for 7000 to 8000 km. Under standard operating conditions (without decarbonisation preparations), the engine used to have an oil life of 12,000 to 15,000 km in the past. The results of the experiment show that the decarbonisation procedure resulted in a very rapid degradation of the engine oil.

3.6. Discussion

It's still true that the most reliable and precise method of diagnosing Common Rail fuel injectors are bench tests. They are carried out on special test benches [10, 21]. In our case, we used a non-disassembly diagnostic method using a portable PC and an EOBD interface. This alternative produced interesting results.

Any flow restriction caused by carbon deposits has, except for defective fuel dispersion, an impact on the lowered fuel supply of the injector into the combustion chamber. In this case the insufficient fuel supply of the injector must be compensated by the other injectors. Such as forced fuel compensation by the engine control unit is undesirable in the long run in terms of uneven engine load, as well as in terms of its durability. The uneven fuel supply between injectors should not exceed 15% while the engine is operating [16].

In general, decarbonisation sets are effective in contaminating injection nozzles. They are highly beneficial and harmless to the fuel system.

After 12,716 km of vehicle operation with applied chemical preparations in the lubrication and fuel system, it is possible to state that the cleaning effect on the injection nozzles is striking and very important for engine operation.

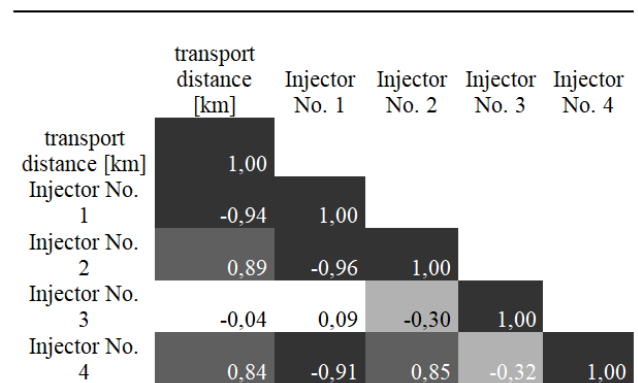


Fig. 12. Correlation matrix of the investigated injectors

In this experiment, in addition to monitoring the long-term chemical decarbonisation of the engine, we also verified the compensation process of the EDC injectors on the Skoda II 2.0 TDi CFFB engine. The fact that the injectors compensate for fuel delivery in pairs, as interpreted in the graphs, cannot be generalized. EDC works on all injectors simultaneously. It should be taken into account that after exceeding the idling speed of the unloaded engine to 1200–1500/minute, all injectors equalize (the sum of fuel supply deviations of all injectors = 0). The correlation analysis in Fig. 12 shows that the weakest injector, No. 1, is most supported by injectors No. 2 and No. 4. There are many strong correlations in the comparison. This method of compensation process depends on the EDC software and may differ from the engine manufacturer

In the case of an oil filling, we cannot talk about the harmlessness of decarbonisation sets.

Although the research results show that the chemical and cleaning effect of decarbonisation preparations accelerates the degradation process of the oil, it should be borne in

mind that the engine had worked almost 165,000 km at the beginning of the measurements and engine management often required the regeneration of the DPF filter. These factors also significantly contributed to the observed oil degradation. Therefore, one must be careful when making hasty conclusions about the significant harmfulness of chemical decarbonisation on the oil filling.

It is still true that it is necessary to strictly follow the recommendations of the manufacturer of the decarbonisation preparation and the manufacturer of the engine oil. It is necessary to be more careful when recommending some manufacturers of cleaning products, as "overdosing the product is not a mistake" (Fig. 14).

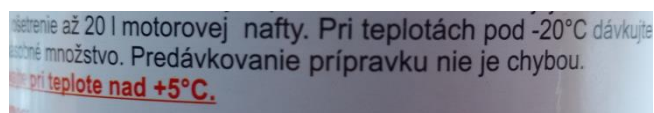


Fig. 14. Cleaning product manufacturer's recommendation: "Overdosing the product is not a mistake"

The vehicle user, in order to quickly clean the engine, often tends to exceed the recommended doses of the chemical product. This often happens with older engines with high mileage, which are heavily clogged with deposits. It is in these engines that the compression space has reduced tightness and there is a significant leakage of fuel with cleaning additives into the engine oil. Cleaning fuel additives in engine oil have a significant anti-detergent effect and damage the lubricating film. Frequent regeneration of

the DPF filter and frequent cold starts of the engine significantly contribute to the undesirable process.

4. Conclusion

The effect of chemical decarbonisation brought very positive results on fuel injectors. An accompanying phenomenon was the undesirable effects of this procedure on engine oil. The results of the experiment show that after the decarbonisation procedure, the injectors had a much more even fuel delivery than before decarbonisation, but decarbonisation resulted in very rapid degradation of engine oil.

In the vehicle's service manual, the Skoda Octavia II car manufacturer recommends changing the oil after two years of operation or after 30,000 km of run-in. From the point of view of the operation of diesel cars, it is recommended to shorten the oil change interval to 7000–10,000 km after chemical decarbonisation of the engine. These recommendations are general and may change depending on the nature and circumstances of the problem.

Reducing the oil change interval in this case indicates potential benefits to the condition of the engine and its components, which in turn can reduce maintenance costs as well as reduce downtime and repairs [5].

Acknowledgements

This article was supported by a scientific research project of the Ministry of Defense of the Slovak Republic entitled: Increasing the capabilities of units within the framework of logistical support for newly introduced equipment of the Armed Forces of the Slovak Republic.

Nomenclature

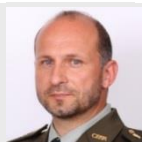
DPF	diesel particulate filter	p_v	injection pressure
ECU	electric central unit	Q_m	weight per unit of time
EDC	electronic diesel control	r	correlation coefficient
EOBD	European on-board diagnostic	R^2	coefficient of determination
OBDII	on board diagnostic	S, S_{Tr}	the size of the flow area of the inj. Holes
TBN	total base number	VV_{pa1}	fuel injection dose
c	fuel output speed	ww_{Tr}	fuel velocity at the injector hole
dD	diameter of injector holes	z_o	the number of injector exit holes
k	statistical covariance	ρ_p	fuel density
l	transport distance	τ_d	duration of injection
p_k	compression pressure in the cylinder	ν	kinematic viscosity

Bibliography

- [1] Barta D, Kowalski S, Dižo J, Dittrich A. The influence of a lubricant medium on the development of fretting wear in an interference fit connection. *Lubricants*. 2024;12(9):327. <https://doi.org/10.3390/lubricants12090327>
- [2] Bulgakov V, Findura P, Kročko V, Nozdrovický L, Korenko M, Kuvachov V. Experimental study of operational properties of two-machine drilling aggregate. *Acta Technologica Agriculturae*. 2018;2:81-86. <https://doi.org/10.2478/ata-2018-0015>
- [3] Cibulová K, Priesner M. Parameters and influences for an evaluation system of trafficability of vehicles on terrain. 3rd International Conference on Challenges to National Defence in Contemporary Geopolitical Situation, Vilnius 2022:14-15. <https://doi.org/10.47459/cndcgs.2022.1>
- [4] Čupera J, Štěrba P. *Automobily – diagnostika motorových vozidel I. (7)*, AVID Brno (CZ), 2013, ISBN 978-80-87143-28-5.
- [5] Gołębiowski W, Zajac G, Sejkorová M, Wolak A. Assessment of oil change intervals in urban buses based on the selected physicochemical properties of used engine oils. *Combustion Engines*. 2024;196(1):15-23. <https://doi.org/10.19206/CE-169807>
- [6] Grohe H. *Benzínové a naftové motory*, ALFA Bratislava (SK), 1985:120-121, 63-030-85.
- [7] Gscheidle R, Fischer R, Heider U. *Příručka pro automechanika*, Haan-Gruiten (CZ), Europa-No. 21632, ISBN 978-3-8085-2163-2.
- [8] *Jazdi lacno s BOOGIE ENERGY PILL*, <https://jazdilacno.webnode.sk/ako-to-funguje/> [ozdravnakura/](https://www.ozdravnakura.com/)
- [9] Jurečková M, Molnárová I. *Štatistika s Excelom, korelačná analýza*, AOS L. Mikuláš, 2005:17-174, ISBN 80-8040-257-4.

- [10] Kluczyk M, Grządziela A. Marine diesel engine common rail injectors monitoring with vibration parameters. *Diagnostyka*. 2019;20(3). <https://doi.org/10.29354/diag/109793>
- [11] Knefel T, Pietras D. Change in parameters and injection times of a divided fuel dose. *Combustion Engines*. 2013; 154(3):51-59. <https://doi.org/10.19206/CE-116985>
- [12] Kowalski S, Cieślowski B, Barta D, Dižo J, Dittrich A. Analysis of the operational wear of the combustion engine piston pin. *Lubricants*. 2023;11(3):12. <https://doi.org/10.3390/lubricants11030100>
- [13] Kreidl M, Šmíd R. *Technická diagnostika, Technická literatura BEN*, Praha, 2006:14-15. ISBN 80-7300-158-6.
- [14] Kukuča P, Barta D, Dižo J, Caban J. Piston kinematics of a combustion engine with unconventional crank mechanism. *MATEC Web of Conferences*. 2018;244:03006. <https://doi.org/10.1051/mateconf/201824403006>
- [15] Lukášik P, Marko M, Droppa P, Marchevka M. The long journeys impact on quality parameters of engine oils in IVECO CROSSWAY buses with CR diesel engines. *Transport Means – Proceedings of the 24-th International Conference*. Kaunas 2020:979-980. <https://transportmeans.ktu.edu/wpcontent/uploads/sites/307/2018/02/Transport-means-A4-II-dalis.pdf>
- [16] Lukášik P, Marko M. Preventive diagnostics of the common rail fuel system injectors. *Science & Military*. 2019;2(14):11-12. ISSN 1336-8885.
- [17] Marko M, Droppa P, Lukášik P, Marchevka M. Tatra-815 engine oils degradation comparison of “Go-Stop“ and standard type of operation. *Transport Means – Proceedings of the 23-th International Conference*. Kaunas 2019:1553. <https://transportmeans.ktu.edu/wpcontent/uploads/sites/307/2018/02/Transport-means-2019-Part-3.pdf>
- [18] Pošta J, Cylek J, Mach R. *Oprávenství a diagnostika II*. Informatorium Praha 2008:185. ISBN 978-80-7333-066-8.
- [19] Pošta J, Kadleček BJ, Fleischhans L. *Oprávenství a diagnostika III*. INFORMATORIUM Praha 2010:104-105. ISBN 978-80-7333-073-6.
- [20] Stěrba P, Čupera J, Polcar A. *Automobily – diagnostika motorových vozidel II*. (8), AVID Brno (CZ), 2011:75-77. ISBN 978-80-87143-19-3.
- [21] Stoeck T. Methodology for common rail fuel injectors testing in case of non-typical faults. *Diagnostyka*. 2020;21(2): 25-30. <https://doi.org/10.29354/diag/122034>
- [22] Stoeck T. Problems of regeneration of modern piezoelectric fuel injectors. *Combustion Engines*. 2022;191(4):3-8. <https://doi.org/10.19206/CE-146700>
- [23] Sz wajca F, Stępień Z, Pielecha I. The influence of alcohol-gasoline blends and deposit control additives on fuel injector contamination in SI DI engines. *Combustion Engines*. 2025; 202(3):131-40. <https://doi.org/10.19206/CE-207120>
- [24] Trnka J, Urban J. *Spařovacie motory*, ALFA Bratislava 1992:205-206. ISBN 80-05-01081-8.
- [25] Veselík P, Sejkorová M, Nieoczym A, Caban J. Outlier identification of concentrations of pollutants in environmental data using modern statistical methods. *Polish Journal of Environmental Studies*. 2020;29(1):853-860. <https://doi.org/10.15244/pjoes/112620>
- [26] Wierzbicki S. Effect of the proportion of natural gas in the feeding dose on the combustion process in a self-ignition engine with a common rail fuel system. *Diagnostyka*. 2018; 19(4):65-70. <https://doi.org/10.29354/diag/99534>
- [27] Zajac G, Gołębiowski W, Szczepanik M, Wolak A, Sejkorová M. Analysis of changes in soot content in engine oils under operating conditions. *Lubricants*. 2023;11(2):89. <https://doi.org/10.3390/lubricants11020089>
- [28] Zdeněk J, Ždánký B, Jetmar J. *Automobily – motory* (3), AVID Brno 2019:115. ISBN 978-80-87143-43-8.
- [29] Zdeněk J, Ždánký B. *Automobily – příslušenství* (4), AVID Brno 2007:250-251. ISBN 978-80-87143-29-2.

Pavol Lukášik, DEng. – Department of Mechanical Engineering, Armed Forces Academy of General M. R. Štefánik Liptovský Mikuláš, Slovak Republic.
e-mail: pavol.lukasik@aos.sk



Vladimir Kadlub, DEng. – Department of Mechanical Engineering, Armed Forces Academy of General M. R. Štefánik Liptovský Mikuláš, Slovak Republic.
e-mail: vladimir.kadlub@aos.sk



Application of ChatGPT in the generation of a numerical performance model of a turbofan engine

ARTICLE INFO

This paper presents a study on the application of ChatGPT 4.0 in developing a numerical model for the performance analysis of a turbofan engine. The modeling process began with general queries regarding numerical approaches to engine simulation. The initial model proposed by ChatGPT appeared plausible but contained significant conceptual errors. Through iterative dialogue and refinement, these errors were gradually identified and corrected, ultimately resulting in a valid engine model. This intermediate model included two rotating components (fan and core spool) and assumed an ideal gas with distinct thermodynamic properties in the cold and hot sections of the engine. Based on this model, ChatGPT successfully generated numerical code for implementation in the MATLAB environment, handling this task with high accuracy and flexibility. Further efforts focused on extending the model to include air extraction for turbine cooling, internal engine bleeds, and the application of a semi-perfect gas model to describe the working fluid more realistically. In these more advanced areas, ChatGPT's performance declined significantly. Despite prompting and corrective guidance, it was unable to produce a fully functional and physically accurate implementation of the enhanced model. The study concludes that while ChatGPT demonstrates strong capabilities in translating well-defined physical models into numerical code, especially within MATLAB, it remains unreliable in constructing or modifying complex thermodynamic models without significant user oversight. Nonetheless, its use can significantly accelerate the implementation phase of numerical engine modeling when guided by an experienced user.

Received: 16 May 2025

Revised: 13 October 2025

Accepted: 23 October 2025

Available online: 15 January 2026

Key words: turbofan engine modeling, ChatGPT in engineering, artificial intelligence applications, gas turbine performance analysis

This is an open access article under the CC BY license (<http://creativecommons.org/licenses/by/4.0/>)

1. Introduction

The generation of accurate, reliable, and above all problem-adequate models constitutes a critical issue in both engineering practice and scientific research. A substantial body of literature is dedicated to the challenges of modeling technical systems as well as to the tools and methodologies employed in this context. This aspect is particularly prominent in aerospace engineering, where model-based investigations play a vital role not only in testing and optimizing existing designs but also in supporting the development of new concepts and their optimisation [35].

The full spectrum of modeling challenges in the field of aeronautics is highly complex due to the vast scope of the subject. The present study focuses on modeling the propulsion system, which is itself a highly complex technical system that requires a multidimensional analytical approach. Consequently, depending on the specific research objectives, engine modeling can be addressed from various perspectives, taking into account both the intended purpose of the study and the required level of model fidelity [23]. Research involving numerical modeling addresses a range of issues, including engine performance, as demonstrated in studies [2, 5, 11, 20, 35]; environmental impact, such as pollutant and greenhouse gas emissions [14, 16–18, 27]; structural integrity assessments [12]; and flow analysis within the engine or its selected components [1, 25, 31, 33]. In many cases, these issues are interrelated, with the results of one type of analysis serving as input data for subsequent analyses. For instance, in [1], the results of gas-dynamic parameter calculations in the engine control stations are used as boundary conditions for flow analysis in the compressor rotor, and the outcomes of this analysis are subse-

quently applied in evaluating engine performance. Similarly, in [16], engine operating parameters obtained from performance calculations are used as input for emissions modeling, while in [12], flow simulations form the basis for the structural analysis of the compressor. Consequently, there is a growing trend toward integrating models operating in different computational domains to improve the efficiency of data exchange between them. This facilitates the development of computational systems that are increasingly becoming complex, multidisciplinary tools.

Steady-state analyses are not always sufficient; in many cases, it is necessary to investigate unsteady phenomena – not only in scenarios involving changes in engine operating conditions, such as acceleration or deceleration, but also under steady-state operation to assess interactions between rotating and stationary components of the engine [31, 33], where unsteady effects are also analyzed. However, such detailed modeling requires significant computational resources and time for model setup and execution, resulting in high research costs. In many cases, a significantly more cost-effective approach is used, involving a variation in the level of model fidelity across engine components – known as the multifidelity approach – as demonstrated in studies [1, 5, 25]. In this method, a selected engine module, such as the compressor flow path [5, 25], is modeled in detail using a more complex model, while other components are represented using simplified methods. This approach enables a substantial reduction in computational time and cost while maintaining high accuracy within the targeted area of investigation.

Engine performance calculations are still predominantly based on quasi-one-dimensional (pseudo-1D) analysis,

which relies on averaged thermodynamic parameters of the flow in the engine's control stations. This approach is represented in studies such as [2, 4, 9–11, 21–23], where flow parameters are determined in selected control sections to evaluate engine performance. The modeling is grounded in the conservation equations of mass, momentum, and energy. At the same time, the processes occurring in individual engine components are characterized using efficiency parameters that account for deviations from idealized, reversible transformations.

A similar approach is employed by dedicated computational tools, such as the GasTurb Program, Gas Turbine Simulation Program (GSP), and the Propulsion Object-Oriented Simulation Software (PROOSIS) [2], which are advanced tools for analyzing the performance of gas turbine engines. Their additional computational modules also enable the determination of other operating parameters of a jet engine, as demonstrated in [14], where the GasTurb software was used to calculate NO_x emissions for the F100-PW-229 engine.

In [2], it was noted that the use of commercial tools requires access to the licenses, which could be expensive. Moreover, users frequently lack access to the program's source code, which prevents them from adapting it to meet the needs of their research, thereby reducing the researcher's role to that of an operator rather than a developer. For this reason, proprietary in-house programs for aero engine performance calculations continue to be developed, based on the laws of physics and chemistry and tailored to specific computational requirements, as demonstrated in studies such as [2, 9–12, 21]. Additionally, the development of numerical methods enables their adaptation for creating new tools in the field of aircraft engine model preparation. For example, in [29], fuzzy logic was employed to develop an engine model, whereas in [19], neural networks were used to construct a compressor map model for engine performance analysis.

In recent years, emerging and rapidly advancing artificial intelligence (AI) technologies have opened up new possibilities for model development and analytical research. Recent advancements in AI, particularly the emergence of Large Language Models (LLMs), have opened new avenues for supporting engineering design and computational tasks [29, 30]. Various tools based on LLMs are currently being developed by companies such as Google, Microsoft, and others. One of the most widely recognized examples is ChatGPT. ChatGPT, in particular, has been explored as a tool for assisting in code development, algorithm generation, and even conceptual design ideation, with early results indicating both its versatility and limitations [6, 28].

Recent studies have shown that LLMs can assist in conceptual design, requirement generation, and early-phase engineering workflows [15]. They facilitate the automation of repetitive tasks, offer support in code generation and debugging, and contribute to technical documentation with high efficiency [28]. Domain-specific tuning, as seen in AviationGPT, further enhances its applicability to specialized tasks, including aviation safety reports and aircraft systems analysis [34].

LLMs are also being considered as collaborative agents in engineering design processes. When used within structured frameworks, they support ideation, generate architectural proposals, and facilitate cross-domain communication [29, 30, 32]. Their ability to process large volumes of data and produce meaningful summaries or insights makes them particularly useful in system-level engineering tasks.

In the context of aviation, artificial intelligence tools, including LLMs, are viewed as key enablers of next-generation operations and training. Their integration is linked to changes in the required skillsets for aviation professionals, with an increasing emphasis on AI literacy and human-machine collaboration [13].

Despite their strengths, the studies also highlight significant limitations. LLMs often produce outputs that are syntactically correct but semantically flawed or factually inaccurate [28, 32]. They may hallucinate technical content, misinterpret standards, or apply inconsistent logic in complex engineering tasks. These risks are particularly critical in safety-sensitive fields, such as aerospace.

Furthermore, performance across different LLM frameworks varies considerably. Their effectiveness in handling highly specific or quantitative engineering tasks remains limited unless paired with dedicated tools or domain-specific training [30]. Human validation and oversight are still essential to ensure correctness and reliability.

This paper examines the practical application of ChatGPT 4.0 in developing a numerical performance model for a turbofan engine. The study employed the free version of ChatGPT, a widely accessible tool used by a broad community of users. The primary objective was to utilize this tool to assist in developing a turbofan engine performance model, which would then be translated into executable code within a selected computing environment – in this case, MATLAB. The aim was to assess the level of model complexity that could be achieved through such an approach, as well as to evaluate the correctness of the resulting model. In doing so, we sought to determine whether a user without prior expertise in this specific domain could generate a valid computational model, potentially applicable to broader tasks such as aircraft performance analysis or numerical simulation-based testing.

2. ChatGPT utilization for turbofan engine calculation

This study investigates whether ChatGPT 4.0, available in its free version at the beginning of 2025, is capable of generating a turbofan engine performance model. The focus is on evaluating the model initially proposed by the tool and assessing how well it aligns with standard methods commonly used for such analyses. The generated results are systematically validated using established and verified computational tools previously developed for this purpose.

In cases where inconsistencies or errors are identified, an iterative dialogue is conducted with the language model to address and correct the issues. All modifications are directly implemented into the computational code and continuously validated against the reference model.

Once a correct elementary performance model is established, further work will focus on its expansion to include elements of more advanced models—for example, incorpo-

rating compressor bleed flows, turbine cooling flows, and working fluid properties modeled using semi-perfect gas formulations. The overall workflow is illustrated in the schematic diagram presented in Fig. 1.

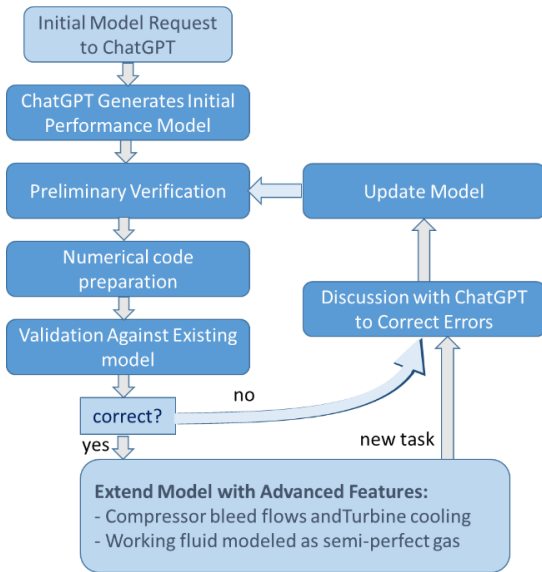


Fig. 1. Workflow for turbofan engine model development using ChatGPT

2.1. Turbofan engine model

In the first stage, ChatGPT was asked to develop a numerical model for calculating the performance of a turbofan engine. The instruction was formulated as follows:

“Could you provide the algorithm for turbofan engine thrust (F) and specific fuel consumption (SFC) calculation for defined bypass ratio (BPR) fan pressure ratio (FPR), compressor pressure ratio (CPR), turbine Inlet Temperature (TIT) mass flow rate. Engine model should include pressure losses and rotating part efficiencies”.

The GPT response provided a computational algorithm that was structured with a clear specification of input data and a numerical model. Input data included fundamental engine parameters such as bypass ratio (BPR), fan pressure ratio (FPR), compressor pressure ratio CPR , turbine inlet temperature TIT , and engine mass flow rate \dot{m}_{total} . Next, parameters characterizing component efficiencies and flow pressure losses were specified. Finally, the input data included ambient conditions, such as air temperature T_0 and pressure P_0 , as well as gas properties, including specific heat capacity, isentropic exponent, and individual gas constants.

A complete computational model of the engine generated by ChatGPT is presented in Fig. 2. It is worth noting that the overall structure of the model was reasonably well-prepared and logically organized, enabling the calculation of the specified parameters: engine thrust (F) and specific fuel consumption (SFC). However, several errors were present in the model, which could have affected the accuracy of the calculations. Incorrect or insufficiently precise formulas are summarized in Table 1.

The formulas presented in Table 1 appear similar to the correct ones but contain errors that would lead to discrepancies between the obtained results and the models found in the literature [4, 8, 23] cited by ChatGPT as the source for

developing the algorithm. Additionally, the specific thrust was defined only in relation to the mass flow rate in the core flow $ST = T/\dot{m}_{core}$, and in the generated equation for specific fuel consumption, the fuel mass flow parameter was used, despite not being determined in the model. Furthermore, the section following the fan, which is conventionally referred to as station 13 in bypass flow and 23 in core flow, is labeled as station 2 in the algorithm prepared by ChatGPT.

Step-by Step Calculations

- Fan and Bypass Stream:**
 - Fan exit pressure and temperature:
$$P_2 = P_0 \text{ FPR}$$

$$T_2 = T_0 \left(1 + \frac{\eta_f}{\eta_c} (\text{FPR}^{(\gamma-1)/\gamma} - 1) \right)$$
 - Bypass flow exit conditions (assuming isentropic expansion in bypass nozzle):
$$P_{\text{bypass exit}} = P_2 \pi_{\text{bypass}}$$

$$T_{\text{bypass exit}} = T_{\text{bypass}}$$
 - Velocity of bypass stream
$$V_{\text{bypass}} = \sqrt{2 \eta_n c_p (T_{\text{bypass exit}} - T_0)}$$
- Core engine (Compressor Combustor and Turbine)**
 - Compressor exit conditions:
$$P_3 = P_2 \text{ CPR}$$

$$T_3 = T_2 \left(1 + \frac{\eta_c}{\eta_f} (\text{CPR}^{(\gamma-1)/\gamma} - 1) \right)$$
 - Turbine exit conditions:
 - Available enthalpy drop across turbine:
$$\Delta h_t = c_p (T_4 - T_3)$$
 - Turbine exit temperature:
$$T_5 = T_4 - \frac{\Delta h_t}{\eta_t}$$
 - Turbine exit pressure
$$P_5 = P_3 \pi_b \left(\frac{T_5}{T_4} \right)^{\gamma/(\gamma-1)}$$
 - Velocity of core exhaust
$$V_{\text{core}} = \sqrt{2 \eta_n c_p (T_5 - T_0)}$$
- Thrust Calculation**

The total thrust is the sum of the momentum flux from the bypass and core stream

$$F = \dot{m}_{\text{bypass}} V_{\text{bypass}} + \dot{m}_{\text{core}} V_{\text{core}} - \dot{m}_{\text{total}} V_0$$

where V_0 is the freestream velocity
- Fuel Flow and Specific Thrust**
 - Fuel-to-air ratio (FAR):
$$\text{FAR} = \frac{c_p (T_4 - T_3)}{\eta_b \text{ LHV}}$$
 - Sopecific Thrust:
$$ST = \frac{F}{\dot{m}_{\text{core}}}$$
 - Specific Fuel Consumption (SFC):
$$\text{SFC} = \frac{\dot{m}_{\text{fuel}}}{F}$$

Fig. 2. Turbofan engine model generated by ChatGPT

Table 1. Incorrect or insufficiently precise formulas generated by Chat GPT

Parameter	Formula given by ChatGPT	Correct formula [8]
Fan exit temperature	$T_2 = T_0 \left(1 + \frac{\eta_f}{\eta_c} (FPR^{(\gamma-1)/\gamma} - 1) \right)$	$T_2 = T_0 \left(1 + \frac{1}{\eta_f} (FPR^{(\gamma-1)/\gamma} - 1) \right)$
Compressor exit temperature	$T_3 = T_2 \left(1 + \frac{\eta_c}{\eta_f} (CPR^{(\gamma-1)/\gamma} - 1) \right)$	$T_2 = T_0 \left(1 + \frac{1}{\eta_c} (CPR^{(\gamma-1)/\gamma} - 1) \right)$
Turbine enthalpy drop	$\Delta h_t = c_p(T_4 - T_3)$	$\Delta h_t = c_p(T_4 - T_5)$
Turbine exit temperature	$T_5 = T_4 - \frac{\Delta h_t}{\eta_t}$	$T_5 = T_4 - \Delta h_t$
Turbine exit pressure	$P_5 = P_3 \pi_b \left(\frac{T_5}{T_4} \right)^{\gamma/(\gamma-1)}$	$P_5 = P_3 \pi_b \left(1 - \frac{1 - T_{t5}/T_{t4}}{\eta_T} \right)^{\frac{\gamma}{\gamma-1}}$
Velocity of core exhaust	$V_{core} = \sqrt{2\eta_n c_p(T_5 - T_0)}$	$V_{core} = \sqrt{2\eta_{n\ core} c_p(T_5 - T_{5\ st})}$
Velocity of bypass stream	$V_{bypass} = \sqrt{2\eta_n c_p(T_{bypass\ ex} - T_0)}$	$V_{bypass} = \sqrt{2\eta_{n\ bypass} c_p * \sqrt{T_{bypass} - T_{bypass\ st}}}$

2.2. Engine computational algorithm in Matlab

ChatGPT was asked to generate an algorithm suitable for execution in the Matlab environment. The algorithm was prepared as a Matlab function, where the engine thrust and specific fuel consumption were generated as output data, while the input data included the fundamental parameters of the turbofan engine and efficiencies of its components. Additionally, ChatGPT suggested input data for the calculations, as presented below, and described the calculation initialization process as shown below:

BPR = 6; % Bypass ratio [-]
 FPR = 1.6; % Fan pressure ratio [-]
 CPR = 30; % Compressor pressure ratio [-]
 TIT = 1400; % Turbine inlet temperature [K]
 m_core = 20; % Core mass flow rate [kg/s]
 eta_f = 0.9; % Fan efficiency [-]
 eta_c = 0.88; % Compressor efficiency [-]
 eta_t = 0.9; % Turbine efficiency [-]
 eta_n = 0.98; % Nozzle efficiency [-]
 pi_b = 0.95; % Burner pressure loss factor [-]
 pi_bp = 0.98; % Bypass pressure loss factor [-]
 T0 = 288; % Ambient temperature [K]
 P0 = 101325; % Ambient pressure [Pa]

[F, SFC] = turbofan_calc(BPR, FPR, CPR, TIT, m_core, eta_f, eta_c, eta_t, eta_n, pi_b, pi_bp, T0, P0);

The proposed data appear reasonable for calculations of an engine from the 1980s–1990s, as noted in [23]. They correspond to operating conditions at zero flight speed under ISA conditions. To adapt these data to the CFM-56-2 present-day engine [3], some parameters proposed by ChatGPT were modified as follows:

FPR = 1.45; % Fan pressure ratio [-]
 CPR = 20; % Compressor pressure ratio [-]
 m_core = 52; % Core mass flow rate [kg/s]
 TIT = 1600; % Turbine inlet temperature [K]

The structure of the proposed computational algorithm was also thoroughly analyzed. In the algorithm, unlike the model presented in Fig. 2, the equations for the temperature behind the fan and compressor were correctly formulated. Additionally, the enthalpy drop across the turbine was properly defined as the temperature drop between sections

4 and 5. This was determined based on the energy demand of the fan and compressor, which is a correct approach that was not included in the presented model. For the pressure calculations behind the turbine, the algorithm, like the model, used the isentropic expansion relationship (without losses).

However, some errors were identified in the prepared algorithm. One issue was the fuel consumption calculation, which, although based on a fairly well-written equation, incorrectly used the turbine efficiency instead of the combustion chamber thermal efficiency. Furthermore, incorrect equations for the exhaust gas velocity were repeated for both engine nozzles. The formula for calculating engine thrust was also incorrectly formulated as follows:

$$F = (m_{bypass} V_{bypass} + m_{core} V_{core}) - m_{total} \sqrt{\gamma R_{air} T_0} \quad (1)$$

The equation (1) includes an incorrect expression for the engine's velocity speed of sound formula $\sqrt{\gamma R_{air} T_0}$ instead of flight speed.

To summarize this section, it is worth noting that ChatGPT developed a plausible turbofan engine model. It includes almost all the required elements characterizing the performance of this type of engine. However, in many cases, errors appear in the provided equations, which will undoubtedly affect the accuracy of the calculations. ChatGPT also developed a function for calculations in the Matlab program. In the developed code, some errors present in the model were eliminated, even though the issue was never discussed. Nevertheless, the resulting computational algorithm still contains formulas that will lead to errors in the obtained calculation data.

2.3. Comparison of engine calculation results

Based on the works [2, 7, 9, 23] a turbofan engine model in Matlab was prepared, which was called ‘‘Correct model’’. This model was used to validate the calculation results from the models prepared by ChatGPT. The data proposed by ChatGPT after mentioned modification was used, supplemented with missing information, such as the combustion chamber efficiency, which was assumed to be 98%, and calculations were performed. The results are summarized in Table 2, along with a comparison to the available data for the CFM-56 engine. The first three parameters

(BPR, m_{total} , OPR) were assumed parameters represent the input data assumed at the same level in the calculations using both models. They are from the range of data given for this engine in [3].

Table 2. Comparison of results from the ChatGPT-developed model, the correct model, and the data for the CFM-56 engine [3]

Parameter	ChatGPT	Correct model	CFM-56-2 data
BPR [-]	6	6	5.9–6
m_{total} [kg/s]	364	364	356–31
OPR [-]	31.9	31.9	30.5–31.8
Takeoff thrust [kN]	13.4	100.6	96–106.7
TSFC [g/(kNs)]	85.26	10.7	10.4–10.7

The ChatGPT algorithm calculation results show significant discrepancies compared to the correct engine model. The calculation errors are at an unacceptable level. The computed takeoff thrust is approximately 8 times lower, and the TSFC is more than 8 times higher than what the correct model should produce.

2.4. Improvement of the model through discussion with ChatGPT

Based on the analysis of errors found in the model, a discussion with ChatGPT was initiated to eliminate them. The discussion started by pointing out that the exhaust gas velocities from both nozzles were being calculated incorrectly. ChatGPT was asked to correct the exhaust gas velocity equations, considering full expansion in the nozzle. The correction provided by ChatGPT was accurate.

The next comment concerned the flight velocity equation used in the calculation of engine thrust. ChatGPT was asked to correct it by introducing the Mach number as an additional variable to determine the flight velocity. Additionally, it was asked to include the dynamic compression at the engine inlet (ram effect) in the calculations of temperature and pressure before the fan. These suggestions were correctly implemented in the engine model.

In the next steps, ChatGPT was asked to consider that the turbine is not ideal and undergoes a non-isentropic process by incorporating the isentropic efficiency in the formula for the pressure behind the turbine. Next was pointed out that for the combustion chamber, the thermal efficiency of the combustion chamber should be used instead of the turbine efficiency. Additionally, it was specified that the flow losses in the bypass duct should be considered in the calculation of the pressure in the external nozzle. Finally, the value of specific heat for the flow in the hot section of the engine was modified to align with typical values used in literature [4, 23].

After implementing all these corrections into the model, ChatGPT was asked to regenerate the function in the Matlab environment. The modified function was used to perform calculations for the previously used CFM-56 engine data set. The calculation results are presented in Table 3. This time, the data shows a sufficient level of agreement with the engine's reference data (see Table 2). The thrust falls within the range of values reported for this engine, and the specific fuel consumption is only slightly below the minimum value. This would require only minor adjust-

ments to the model to achieve results within the expected range.

Table 3. Results from the ChatGPT-corrected model

Parameter	ChatGPT corrected model
Takeoff thrust [kN]	103.8
TSFC [g/(kNs)]	10.1

2.5. Expanding the engine model using ChatGPT

The initially prepared and improved model from ChatGPT underwent further modifications better to align it with the design of the analyzed engine. The modifications were also aimed at using complex computational models of the gas flowing in the engine. The modifications were implemented in stages by sending targeted queries to the system.

Two spool engine model

The first step was to separate the engine calculations into two rotors, as the previously obtained model treated the fan and compressor assembly as a single unit.

To achieve this, the following command was executed: *“Separate the computational model for the fan and compressor assembly into two rotors, assuming that the low-pressure rotor consists of a fan characterized by the Fan Pressure Ratio (FPR) and fan efficiency, as well as a low-pressure compressor defined by the Low-Pressure Compressor Pressure Ratio (LPCPR) and compressor efficiency. The high-pressure assembly consists of a high-pressure compressor with a specified High-Pressure Compressor Pressure Ratio (HPCPR) and efficiency. Both compressors are located in the engine's inner bypass duct”*

This generated a breakdown of the engine compression in the model into three separate modules, but the turbine was still calculated as a single unit. Therefore, the next prompt was to ensure that separate turbines for the high and low-pressure spools were included in the model. After executing this command, a model was created, but the load between the turbines was incorrectly distributed. The load on the high-pressure turbine was defined by the temperature change in the combustion chamber, while the entire power demand for the compressors and fan was assigned to the low-pressure turbine.

This issue was presented to ChatGPT, and it was then asked to correct the problem. Unfortunately, its modifications further degraded the model. It removed turbine efficiency from the pressure calculations and instead applied it to the enthalpy change calculations. At this point, it became necessary to explicitly specify the exact changes that ChatGPT needed to implement to fix the model.

The discussion with ChatGPT regarding the introduction of mechanical efficiency into the model for calculating the balance between the high-pressure turbine and high-pressure compressor, and the low-pressure turbine and low-pressure compressor, plus fan, failed. ChatGPT made changes to the model that did not align with the instructions provided, continuously treating the turbine efficiencies as mechanical efficiencies.

To fix the algorithm, it was necessary to specify explicitly how the calculation of the turbine-compressor balance should be modified, providing the exact equations to be

incorporated. This allowed for the correction of the computational algorithm, accurately representing the operation of a two-shaft engine model.

HPT cooling

The next instruction concerned implementing bleed flows in the engine for turbine cooling, assuming that the entire cooling flow is supplied to the high-pressure turbine and then returns to the main flow.

A prompt was used in the form of: *“Please correct this model to account for a bleed flow of 8% of the core mass flow after the high-pressure compressor. Direct this flow to the high-pressure turbine for cooling. Incorporate the applied cooling into the turbine’s work balance and adjust the combustion chamber calculations to reflect the change in mass flow due to this bleed.”*

High-Pressure Turbine (HPT) Power Calculation with Cooling	
Given:	
Bleed flow fraction: $\dot{m}_{bleed} = \beta \dot{m}_{core}$, where $\beta = 0.08$ (8%)	
Corrected mass flow into the combustor:	
$\dot{m}_{comb} = \dot{m}_{core} (1 - \beta)$	
Total mass flow through the HPT (including cooling air):	
$\dot{m}_{HPT} = \dot{m}_{comb} + \dot{m}_{bleed} = \dot{m}_{core}$	
Since the cooling flow is eventually reintroduced into the turbine stream, the total work extracted by the high-pressure turbine remains the same, but the enthalpy drop calculation must reflect the mixed flow	
Power Balance for HPT	
The high-pressure extracts power to drive the high-pressure compressor (HPC), considering mechanical transmission losses:	
$W_{HPT} = \frac{W_{HPC}}{\eta_{mech,HPT}}$	
where	
$W_{HPC} = \dot{m}_{comb} c_{p,cold} (T_3 - T_{25})$	
Thus, the corrected enthalpy drop in the HPT is:	
$h_{HPT} = \frac{c_{p,cold} (T_3 - T_{25})}{\eta_{mech,HPT}}$	
The exit temperature of the HPT is	
$T_{45} = T_4 - \frac{h_{HPT}}{c_{p,hot}}$	
and the pressure ratio across the turbine considering isentropic efficiency:	
$P_{45} = P_4 \left(1 - \frac{1 - T_{45}/T_4}{\eta_{HPT}} \right)^{\frac{\gamma_{hot}}{\gamma_{hot}-1}}$	

Fig. 3. The turbofan HP spool model modification by ChatGPT for HPT cooling

The task was only partially completed. The mass flow after the compressor was corrected by reducing it for the bleed, but it was not added to the main flow at the high-pressure turbine (HPT). The energy change caused by the addition of the cooling fluid was not accounted for in the turbine’s work calculations. The example of HPT spool calculation modification by ChatGPT for request fulfilment is presented in Fig. 3

Due to the need for further tedious work with the system to fix the model, the decision was made to withdraw from implementing these changes into the model.

Semi-perfect gas model

The next step involved an attempt to modify the gas properties in the engine model presented by ChatGPT.

ChatGPT was requested to incorporate a semi-perfect gas model into the engine calculations and to provide references for the adopted model.

A model was introduced in which gas properties, such as specific heat and the isentropic exponent, were defined as functions of gas temperature, while the individual gas constant was assumed to be a constant value. The source of the applied model was indicated as reference [24], which contains a formulation for the variation of specific heat expressed as a polynomial. The model for calculating specific heat applied by ChatGPT was a 4th degree polynomial:

$$Cp(T) = R(A + BT + CT^2 + DT^3 + ET^4) \quad (2)$$

The polynomial coefficients proposed by ChatGPT are presented in Table 4 where: R – individual gas constant in [J/kg/K] and T – temperature in [K].

Table 4. Polynomial coefficient proposed by ChatGPT

Coefficient	Value
A	0.992313
B	0.236688
C	-0.048898
D	0.004388
E	-0.000106

ChatGPT then prepared Matlab functions for calculating the specific heat: `get_cp`, isentropic exponent `get_gama`, and individual gas constant `get_R` as temperature-dependent variables, and implemented the necessary modifications in the engine model to use these functions for gas parameter calculations.

The gas model, which, according to ChatGPT was dedicated to air, was implemented for calculations involving both air and exhaust gases. However, a different approach was applied: in calculations for the cold flow, the values of `cp` and `gama` were computed based on the inlet temperature of each engine component. In contrast, for the hot flow (turbines), `cp` was calculated at the inlet temperature and used to determine the outlet temperature, while `gama` was computed for the mean temperature and used to calculate the outlet pressure. A code snippet illustrating this part of ChatGPT algorithm is shown in Fig. 4. According to the literature [4, 7], the recommended approach in this regard is to use the mean temperature to determine the gas properties used in the calculations for each individual component. This approach requires the application of iterative calculations.

```

% High-Pressure Compressor (HPC) exit conditions
cp_cold = get_cp(T25);
gamma_cold = get_gamma(T25);
P3 = P25 * HPCPR;
T3 = T25 * (1 + (1/eta_hpc) * (HPCPR^(gamma_cold-1)/gamma_cold - 1));

% Pressure drop in the burner
P4 = P3 * pi_b;

% Fuel-Air Ratio (FAR) with burner efficiency
cp_hot = get_cp(TIT);
LHV = 43e6; % J/kg (jet fuel lower heating value)
FAR = cp_hot * (TIT - T3) / (eta_b * LHV);

% High-Pressure Turbine (HPT) calculations
cp_cold = get_cp(T3);
h_hpt = cp_cold * (T3 - T25) / eta_mech_hpt;
T45 = TIT - h_hpt / cp_hot;
gamma_hot = get_gamma((TIT + T45) / 2);
P45 = P4 * (1 - (1 - (T45/TIT)) / eta_hpt)^(gamma_hot / (gamma_hot - 1));
    
```

Fig. 4. Matlab code for HP shaft components calculation

To address this issue, ChatGPT was first asked to introduce a combustion gas model for calculations in the turbine and exhaust nozzle, taking into account that the working fluid in these sections is the product of hydrocarbon fuel combustion, with the fuel-air mass flow rate being approximately 2% relative to the mass flow rate of the air. This level of fuel burnt mass to airflow mass ratio is typical for turbofan engines and is used in numerous sources in the literature [4, 8, 23, 24].

ChatGPT proposed the model given in Equation (3), where the gas constant R and constant pressure heat value C_p are expressed in [J/kg/K], and the isentropic exponent γ is dimensionless. Based on the provided equations, it developed functions which were then implemented into the engine's computational model.

$$R = 291$$

$$C_p(T) = 1100 + 0.1 T - 10^{-5} T^2 + 10^{-9} T^3 \quad (3)$$

$$\gamma = C_p / (C_p - R)$$

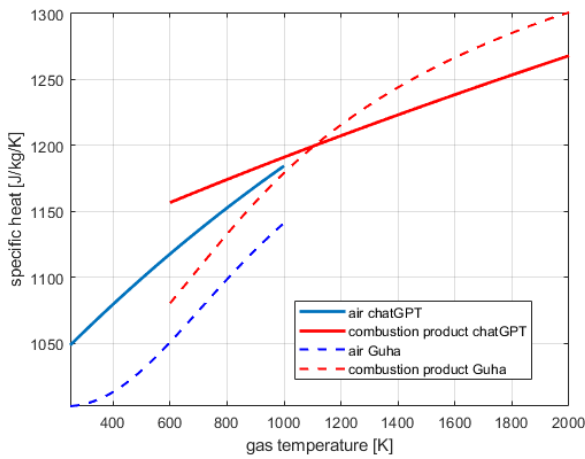


Fig. 5. The results of the specific heat calculations for the gas model proposed by ChatGPT and determined according to the model in [7] for air and combustion product of fuel/air ratio 0.02

To verify the provided equations, a comparison was made with the model presented in [7], which is consistent with the model from reference [24], cited by ChatGPT as the source material. The comparison of the specific heat calculations for air and exhaust gases produced for a mass ratio of 2% fuel to air in the temperature range occurring in a turbofan engine is shown in Fig. 5. The differences in the calculated values are evident, as well as a different pattern of changes in the resulting curves, especially for combustion products.

ChatGPT implemented a semi-perfect gas model across the entire engine simulation by introducing additional functions to compute gas properties. In the case of compressors, the model determined gas parameters based on the inlet temperature to each compressor stage. These values were then used to calculate the component's thermodynamic performance and the properties of the airflow downstream.

For turbines, the methodology applied was inconsistent. While the enthalpy drop across the compressor was calculated using the specific heat evaluated at the mean temperature consistent with standard engineering practices, ChatGPT applied varying approaches in the turbine section.

In some cases, gas properties such as specific heat and the isentropic exponent were determined based on the inlet temperature (Fig. 6 underscore red line); in other instances, these properties were evaluated at the average temperature across the component (Fig. 6 underscore yellow line), and sometimes they were assessed according outlet temperature (Fig. 6 underscore green line). Notably, in certain sections of the engine model, both approaches were used simultaneously for different thermodynamic parameters within the same control volume, leading to internal inconsistencies in the treatment of gas properties.

```
% Fuel-Air Ratio (FAR) with burner efficiency
cp_hot = get_cp_gas(TIT); % Use combustion gas model
LHV = 43e6; % J/kg (jet fuel lower heating value)
FAR = cp_hot * (TIT - T3) / (eta_b * LHV);

% High-Pressure Turbine (HPT) calculations
cp_cold = get_cp(T3);
h_hpt = cp_cold * (T3 - T25) / eta_mech_hpt;
T45 = TIT - h_hpt / cp_hot;
gamma_hot = get_gamma_gas((TIT + T45) / 2); % Use combustion gas model
P45 = ...
P4 * (1 - (1 - (T45/TIT)) / eta_hpt)^(gamma_hot / (gamma_hot - 1));

% Low-Pressure Turbine (LPT) calculations
cp_cold = get_cp((T25 + T02) / 2);
h_lpt = (cp_cold * (T25 - T02) + (1 + BPR) * cp_cold * (T2 - T02)) ...
/ eta_mech_lpt;
T5 = T45 - h_lpt / cp_hot;
gamma_hot = get_gamma_gas((T45 + T5) / 2); % Use combustion gas model
P5 = ...
P45 * (1 - (1 - (T5/T45)) / eta_lpt)^(gamma_hot / (gamma_hot - 1));
```

Fig. 6. Code section implementing semi perfect gas model in the performance calculation for the high-pressure and low-pressure turbines

According to literature [4, 7], the recommended methodology for such thermodynamic simulations involves computing the average specific heat for each component and then using it to derive other gas properties. ChatGPT's implementation deviated from this standard, resulting in inconsistencies in the application of gas property models across engine components. It also influenced the calculation results, which are given in Table 5 after using the model generated by ChatGPT.

It can be observed that, despite the previously identified shortcomings in the model formulation, the results deviate only slightly from the expected values. The thrust is marginally lower than the value obtained in the earlier model (see Table 3) and is 1.8% higher than the results of the "correct model", but it remains within the range specified by the manufacturer (see Table 2). The specific fuel consumption increased to a value outside the manufacturer's specified range, exceeding the maximum limit by nearly 9%. Eliminating the identified modeling deficiencies would undoubtedly improve these results, which are already reasonably close to the actual values. A discussion with ChatGPT was conducted to address this issue; however, the implemented modifications did not yield the desired improvements, and further attempts to correct the model were therefore discontinued in this research.

Table 5. Calculation results for the model generated by ChatGPT with the semi-perfect gas model

Parameter	ChatGPT semi perfect gas model
Takeoff thrust [kN]	102.4
TSFC [g/(kNs)]	11.67

4. Summary and conclusions

The conducted discussion with ChatGPT 4.0 focused on the progressive development and refinement of the turbofan engine performance model, incorporating both thermodynamic and gas property improvements. Starting from a simplified configuration, successive enhancements were introduced to account for non-ideal component efficiencies, realistic bypass and cooling flow modeling, and the implementation of a semi-perfect gas model with temperature-dependent properties.

Throughout the process, ChatGPT was able to generate computational model and provide explanations aligned with general engineering practice. However, numerous issues were encountered, particularly regarding consistent application of gas property calculations, correct distribution of work between turbines and compressors, and the handling of cooling and bleed flows. In several instances, the changes implemented by ChatGPT did not follow the provided instructions or introduced new errors, requiring precise step-by-step guidance and manual corrections.

Despite these challenges, the final model yielded results that were relatively close to those reported by engine manufacturers and validated by other verified simulation models. Thrust levels fell within the expected range, and specific fuel consumption, although slightly higher than desired, remained within an acceptable deviation considering the model limitations.

It was also observed that ChatGPT performed very reliably when implementing requested modifications into the

numerical engine model. Its ability to translate instructions into functioning MATLAB code was consistently accurate and error-free.

In conclusion, while ChatGPT demonstrates a useful capacity for supporting the development of engine performance models, its effectiveness is limited by inconsistency in complex thermodynamic logic and a need for iterative correction when modeling advanced physical processes. This indicates that the data generated by ChatGPT is still not entirely trustworthy. They must be verified by experts, whose intervention is very often necessary to correct and eliminate errors.

As such, at the current stage of development, close user supervision and technical validation remain essential when using LLMs like ChatGPT for engineering design and analysis tasks. However, it is expected that these tools will become increasingly capable and reliable in supporting model development in the near future. Comparative studies between the performance of ChatGPT 3.5 and 4.0 at work show a significant improvement in task execution between these versions [30]; therefore, it is to be expected that the next version of the program will perform even better in this respect.

It should also be noted that the quality of user input – particularly well-structured prompts and precise instructions – plays a critical role in achieving accurate results. While the evolution of human–AI collaboration in this area holds significant potential, it was not the focus of the present study.

Nomenclature

BPR	bypass ratio	p	pressure
CPR	compressor pressure ratio	SFC	specific fuel consumption
F	thrust	T	temperature
FAR	fuel air ratio	TIT	turbine inlet temperature
FPR	fan pressure ratio	TSFC	takeoff specific fuel consumption
h	enthalpy	V	velocity
LLMs	Large Language Models	W	work
OPR	overall pressure ratio		

Bibliography

- [1] Bednarz A, Kabalyk K, Jakubowski R, Bartłomowicz R. Numerical study on sensitivity of turbofan engine performance to blade count of centrifugal compressor impeller. *Energies*. 2023;16(14):5251. <https://doi.org/10.3390/en16145251>
- [2] Catana RM, Dediu G. Analytical calculation model of the TV3-117 turboshaft working regimes based on experimental data. *Appl Sci*. 2023;13(19):10720. <https://doi.org/10.3390/app131910720>
- [3] CFM International. CFM56. Wikipedia. https://en.wikipedia.org/wiki/CFM_International_CFM56#cite_note-cfm56-2-61
- [4] Cumpsty N, Heyes A. Jet propulsion: a simple guide to the aerodynamics and thermodynamic design and performance of jet engines. 3rd ed. Cambridge: Cambridge University Press 2015. <https://doi.org/10.1017/CBO9781316223116>
- [5] Deng W, Xu Y, Ni M, et al. Multi-fidelity simulation of gas turbine overall performance by directly coupling high-fidelity models of multiple rotating components. *J Therm Sci*. 2024;33:1357-1378. <https://doi.org/10.1007/s11630-024-1975-3>
- [6] Ege DN, Øvrebø HH, Stubberud V, Berg MF, Elverum C, Steinert M et al. ChatGPT as an inventor: eliciting the strengths and weaknesses of current large language models against humans in engineering design. *Artificial Intelligence for Engineering Design, Analysis and Manufacturing*. 2025; 39:e6. <https://doi.org/10.1017/S0890060425000010>
- [7] Guha A. An efficient generic method for calculating the properties of combustion products. *P I Mech Eng A-J Power Eng*. 2001;215(3):375-387. <https://doi.org/10.1243/0957650011538596>
- [8] Hill PG, Peterson CR. *Mechanics and thermodynamics of propulsion*. Reading, MA: Addison-Wesley 1965.
- [9] Jakubowski R. Evaluation of performance properties of two combustor turbofan engine. *Eksplot Niezawodn*. 2015; 17(4):575-581. <https://doi.org/10.17531/ein.2015.4.13>

- [10] Jakubowski R, Bednarz A, Rogalski Ł. Study of the effects of heat exchanger location on turbofan engine performance. *Adv Sci Technol Res J.* 2024;18(4):355-368. <https://doi.org/10.12913/22998624/189464>
- [11] Jakubowski R, Jakliński P. A practical approach to modeling and performance analysis of a turboshaft engine using Matlab. *Appl Sci.* 2024;14(23):11373. <https://doi.org/10.3390/app142311373>
- [12] Kabalyk K, Bednarz A, Kantyka K. Fatigue safety factor of a transonic centrifugal compressor impeller subject to blade thickness. *Scientific Reports.* 2025;15:18693. <https://doi.org/10.1038/s41598-025-03776-0>
- [13] Kabashkin I, Misnevs B, Zervina O. Artificial intelligence in aviation: new professionals for new technologies. *Appl Sci.* 2023;13(21):11660. <https://doi.org/10.3390/app132111660>
- [14] Kozakiewicz A, Ludwiczak A. Analysis of nitrogen oxide emissions generated by the F100-PW-229 turbine aircraft engine, performed using the gasturb software. *Problems of Mechatronics Armament Aviation Safety Engineering.* 2025;16(1):9-20. <https://doi.org/10.5604/01.3001.0055.0333>
- [15] Krus P. Large language model in aircraft system design. *Proceedings of the 34th Congress of the International Council of the Aeronautical Sciences;* 2024. Florence. <https://urn.kb.se/resolve?urn=urn:nbn:se:liu:diva-211541>
- [16] Kulczycki A, Przysowa R, Białecki T, Gawron B, Jasiński R, Merksiz J et al. Empirical modeling of synthetic fuel combustion in a small turbofan. *Energies.* 2024;17(11):2622. <https://doi.org/10.3390/en17112622>
- [17] Kuźniar M, Pawlak M, Orkisz M. Comparison of pollutants emission for hybrid aircraft with traditional and multi-propeller distributed propulsion. *Sustainability.* 2022;14(22):15076. <https://doi.org/10.3390/su142215076>
- [18] Maciorowski D, Ludwiczak A, Kozakiewicz A. Hydrogen, the future of aviation. *Combustion Engines.* 2024;197(2):126-131. <https://doi.org/10.19206/CE-178375>
- [19] Loryś SM, Orkisz M. Neural network approach to compressor modelling with surge margin consideration. *Archives of Thermodynamics.* 2022;43(1):89-108. <https://doi.org/10.24425/ather.2022.140926>
- [20] Majka A, Muszyńska-Pałys J. Analysis of the performance of an aircraft powered by hybrid propulsion. *Combustion Engines.* 2023;193(2):45-51. <https://doi.org/10.19206/CE-161107>
- [21] Marszałek N. Performance analysis of turbofan engine with additional combustion chamber fueled by alternative fuel. *Combustion Engines.* 2019;179(4):249-253. <https://doi.org/10.19206/CE-2019-441>
- [22] Marszałek N. The impact of thermodynamics parameters of turbofan engine with ITB on its performance. *Combustion Engines.* 2020;182(3):16-22. <https://doi.org/10.19206/CE-2020-303>
- [23] Mattingly JD, Boyer KM. *Elements of propulsion: gas turbines and rockets.* 2nd ed. Reston, VA: American Institute of Aeronautics and Astronautics 2016.
- [24] McBride BJ, Zehe MJ, Gordon S. *NASA Glenn coefficients for calculating thermodynamic properties of individual species.* Cleveland, OH: NASA Glenn Research Center 2002.
- [25] Muchowski R, Gubernat SM. Influence of axial compressor model simplification and mesh density on surge margin evaluation. *Adv Sci Technol Res J.* 2021;15(3):243-253. <https://doi.org/10.12913/22998624/140541>
- [26] Pasięka M, Grzesik N, Kuźma K. Simulation modeling of fuzzy logic controller for aircraft engines. *Int J Comput.* 2017;16:27-33. <https://doi.org/10.47839/ijc.16.1.868>
- [27] Pawlak M, Kuźniar M. Performance and emission of the aircraft with hybrid propulsion during take-off operation cycle. *Adv Sci Technol Res J.* 2024;18(1):155-166. <https://doi.org/10.12913/22998624/177254>
- [28] Pierson KC, Ha MJ. Usage of ChatGPT for engineering design and analysis tool development. *AIAA SCITECH 2024 Forum.* 2024; Orlando, FL. Reston, VA: American Institute of Aeronautics and Astronautics. <https://doi.org/10.2514/6.2024-0914>
- [29] Pradas Gómez A, Krus P, Panarotto M, Isaksson O. Large language models. *Proceedings of the Design Society.* 2024; 4:2197-206. <https://doi.org/10.1017/pds.2024.222>
- [30] Pradas Gómez A, Panarotto M, Isaksson O. Evaluation of different large language model agent frameworks for design engineering tasks. *Proceedings of the NordDesign 2024;* 2024; Reykjavik, Iceland. Glasgow, UK: The Design Society. 2024:693-702. <https://doi.org/10.35199/NORDDDESIGN2024.74>
- [31] Romagnosi L, Li YC, Mezine M, Teixeira, M, Vilmin S, Anker JE et al. Methodology for steady and unsteady full-engine simulations. *Proceedings of the ASME Turbo Expo 2019 Turbomachinery Technical Conference and Exposition.* Phoenix, USA, 17–21 June 2019.
- [32] Timperley LR, Berthoud L, Snider C, Tryfonas T. Assessment of large language models for use in generative design of model based spacecraft system architectures. *J Eng Des.* 2025;36(4):550-570. <https://doi.org/10.1080/09544828.2025.2453401>
- [33] Ventosa-Molina J, Lange M, Mailach R, Fröhlich, J. Study of relative endwall motion effects in a compressor cascade through direct numerical simulations. *ASME J Turbomach.* 2021;143(1):011005. <https://doi.org/10.1115/1.4049101>
- [34] Wang L, Chou J, Zhou X, Tien A, Baumgartner DM. *AviationGPT: a large language model for the aviation domain.* AIAA SciTech. 2024. <https://doi.org/10.48550/arXiv.2311.17686>
- [35] Wygonik P. Dobór zespołu napędowego do samolotu wielozadaniowego według kryterium zadania lotniczego (in Polish). *Oficyna Wydawnicza Politechniki Rzeszowskiej.* Rzeszów 2024.

Robert Jakubowski, DEng. – Aerospace Technology Department, Rzeszów University of Technology, Poland.

e-mail: robert.jakubowski@prz.edu.pl



Marek Szumski, DEng. – Aerospace Technology Department, Rzeszów University of Technology, Poland.

e-mail: marek.szumski@prz.edu.pl



Performance of a nipa-based fuel blend on a multi-blend capable engine test motorcycle towards renewable biofuel solutions

ARTICLE INFO

The performance of an alternative fuel and its blends into a gasoline engine was evaluated using a developed Multi-Blend Capable Engine (MBCE) from carb to EFI test motorcycle to enhance performance compatibility and environmental concerns of a nipa-based ethanol as renewable alternative feedstock fuel. It shows that the test motorcycle utilizing its stock carburetor systems is compatible up to E30H only, while the EFI modification was found compatible from E10 to 100% nipa hydrous ethanol or E100H as fuel using three different driving modes of the MBCE with decreased power versus speed performance by about 24% and mileage consumption by about 6.0%. However, emissions significantly improved in the test motorcycle with HC and CO meeting Euro 4 standards. The total carbon quantification was found to be 76-225 gCO₂e/km from nipa sap collection up to its utilization as an alternative gasoline fuel engine from E10 to E100H. The study safely recommends implementing up to E30H blend without any adjustments made on carb and EFI system motorcycles. To promote higher blend biofuel adoption in support of SDG 7 Clean and Affordable Energy, the study implies carburetor systems adjustments or EFI conversion for stock carb system motorcycles, while remapping must be made to EFI motorcycles.

Received: 6 August 2025

Revised: 14 October 2025

Accepted: 23 October 2025

Available online: 19 December 2025

Key words: *biofuels, fuel performance, engine performance, emission, carbon quantification*

This is an open access article under the CC BY license (<http://creativecommons.org/licenses/by/4.0/>)

1. Introduction

This research article intends to address some of the gaps in the full implementation of the Philippine Biofuels Act and in other countries with a similar intent [1], which aims to achieve higher anhydrous ethanol (E) blend utilization up to 85% (E85) by 2030, but has remained restricted primarily to E10 since the Act's approval in 2006. Vehicles are believed to be incompatible with higher fuel blend ratios, as evidenced by engine tests that reported difficult engine starts and rusting of metal parts, such as tanks and carburetors [25, 30]. The objective of this endeavour is to initiate performance testing of a nipa-based fuel in a test motorcycle from carbureted (Carb) into modified Electronic Fuel Injected (EFI) fuel system which optimizes the use of higher blends and or as a fuel, parallel to the intent of the Philippines RA 9367 and the United Nation's Sustainable Development Goal's SDG 7 or Affordable and Clean Energy.

Electric Vehicles (EVs) are one of the new trends in transportation [37, 57] nowadays; however, fleet electrification is not the only solution [43]. The importance of Internal Combustion Engines (ICE) should not be neglected, as they continue to be used, especially since the transportation sector is not the major contributor to environmental problems, but rather the energy sector [47]. EVs have their disadvantages, particularly in sourcing raw materials for batteries, which are often acquired through mining. These challenges can potentially be addressed through battery metal recycling [26] and improvements in battery design, as well as by enhancing safety, excitability, or response [17]. Although a lengthy charging system remains an issue, several methods are already underway to address this, such as optimization studies of charging stations [53] and battery performance interventions [16, 54]. Regarding conventional

vehicles, the depletion of fossil fuels for petroleum products poses a prevailing dilemma for internal combustion engines (ICE), where biofuels and blends are expected to help mitigate this issue [5, 41]. In addition to sugarcane and corn, problems with bioethanol feedstock availability can be addressed from promising feedstocks such as sweet sorghum, cassava [28, 38] and other starchy crops [24, 45]. In this study, nipa was utilized as the feedstock for bioethanol production. As regional wars and conflicts affect petroleum supply and costs, considering the promising renewable feedstocks available in each country may support the continued use of internal combustion engines (ICE), provided they are equipped with efficient fuel systems capable of handling varying ethanol blend ratios or even pure ethanol, such as in flex-fuel engines and other Alternative Fuel Vehicles (AFVs) [14].

Several engine performance tests were already conducted in the Philippines [30, 56] and abroad [11, 49] using different fuel blends using either hydrous or anhydrous ethanol on gasoline, where performance and emissions were found to be comparable and more environmentally friendly [33, 58] and as a renewable energy source [23, 32]. However, these blends were conducted at up to 25% ethanol-gasoline ratios except in the study up to E60 [22]. Other tests were also conducted on stationary, motorcycle engines, and passenger cars using a manual variable-fed fuel system up to 100% hydrous [7], fuel injection run by Arduino to E30 [39], and flex-fuel engines [9, 21] in an attempt to investigate the potential of higher fuel blends. Modification of a low-powered motorbike engine from carb to electronic fuel injection (EFI) was also conducted [19], which was found to improve fuel consumption at different speeds on a single fuel blend.

This pioneering test in the Philippines, conducted by modifying a carbureted motorcycle to an EFI test motorcycle or MBCE, utilises fuel blends containing up to 100% nipa-based bioethanol. The ethanol is produced through the distillation of the nipa sap or the sweet juice extracted from the peduncle of *Nypa fruticans*, a mangrove palm species [27]. The study aims to enhance sustainability in the transportation sector by contributing to global efforts to adopt cleaner energy solutions. It aligns with international sustainability goals while addressing local energy needs, reducing dependency on traditional fossil fuels, and mitigating the impacts of fuel price surges caused by conflicts in the Gulf region.

2. Materials and methods

2.1. Introduction

This paper is a continuation study of Mariano Marcos State University (MMSU) and Mapua University, which utilizes nipa sap as a bioethanol feedstock [29]. Performance testing was conducted on a carb modified to EFI to become a Multi-blend Capable Engine (MBCE) test motorcycle. The evaluation focused on power, fuel economy, and emissions using higher gasoline-ethanol fuel blends up to 100% bioethanol in a gasoline engine. A compatibility test was first conducted on the test motorcycle using its stock carburetor with no modifications to determine its compatibility with various fuel blends. Since ethanol, when used as a pure engine fuel or in higher blends, may pose compatibility or drivability issues, the carbureted test motorcycle used in this study was modified to become MBCE, addressing compatibility issues for the full utilization of higher fuel blends.

2.2. Fuel blend feedstock

The formulated blends underwent a neutralization process to address corrosion problems [30, 40] following the distillation of nipa sap, as per protocols developed by MMSU for hydrous (H) ethanol. Commercial E10 gasoline with a 100 RON rating was used as the base fuel blend for nipa bioethanol.

The properties of the nipa-based hydrous ethanol, as well as the formulated blends, were submitted and analyzed by the Department of Energy using ASTM standards to comply with the Philippine National Standards (PNS), as illustrated in Table 1.

Table 1. Properties, methods, and limits of bioethanol as per PNS

Properties	Test method	Limits
Appearance	Visual	Clear and bright
Acidity/alkalinity, pHe	ASTM D6423	6.5–9.0
Density at 20°C, kg/m ³	ASTM D4052	791.5 max
Ethanol content, %v/v	ASTM D5501	99.3 max
Methanol content, %v/v	ASTM D5501	0.5 max
Total acetic acid, %v/v	ASTM D1613	0.007 max
Heating value, MJ/kg	ASTM D4809	26.71 [36]

2.3. Compatibility test of the MBCE on its stock carb system

A compatibility test was first conducted on the carb-type in-use motorcycle, with its specifications listed in Table 2 and an actual photo provided in Fig. 1. The test motorcycle is rated at 10 HP, which is equivalent to approximately 7.5 kW at 8250 rpm.

Table 2. In-use motorcycle’s specifications

Type (color)	Description
Honda XR 125 (Red Orange)	Carb type, 124.7 cc, single cylinder, 4-stroke engine, OHC, air cooled, 8.2 kW at 8250 rpm

Dynamometer tests and mileage runs were conducted to assess fuel blend compatibility, with no modifications or adjustments made to the motorcycle. The motorcycle is expected to run and operate without hard starting or other combustion-related issues to be considered as fuel compatible.



Fig. 1. Honda XR 125 in-use carb type motorcycle

2.4. Modification of the carb type in-use motorcycle to the MBCE test vehicle

Instead of using EFI In-Use motorcycles, the Honda XR 125 was modified to EFI and designated as the MBCE test vehicle, since the use of another In-Use EFI vehicle requires additional modifications aside from the remapping process.



Fig. 2. The MBCE Modification. (a) tank with fuel pump inside, (b) the ECU, (c) switch mode selector, (d) oxygen sensor, (e) CPS (at the other end side), (f) throttle body, (g) TPS manifold, (h) injector manifold

The modification done in the Honda XR 125 in Fig. 2 as shown above include: replacement of the carburetor to FI system with Throttle Body and Throttle Positioning Sensor (TPS) in the manifold connected to the engine head that transmits signal to the Electronic Communication Unit (ECU) and then back to the injectors; installation of crank-

shaft positioning sensor (CPS) for proper timing of the magneto/stator and alignment gears; installation of a new tank and fuel pump, installation of oxygen and temperature sensors; and the use of “Pitsbike” as the Electronic Control Unit or the ECU. Compared to flex-fuel vehicles utilizing blend software and sensors [51, 55]. The MBCE used switch mode optimized into three (3) settings. The switch installed in the steering wheel is set to mode “2”, as shown in Fig. 2c, implying that the MBCE can accommodate fuel blends of 40% to 70% v/v ethanol in gasoline fuel.

The cost of modifying the stock carburetor system to a fuel injection (FI) system, making it an MBCE test vehicle, was 27,000 PHP, or approximately \$500 USD.

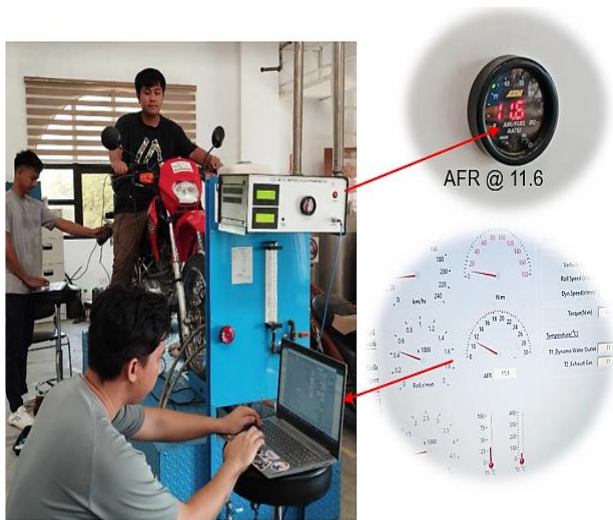


Fig. 3. Remapping and testing of the MBCE motorcycle

The MBCE test vehicle, as shown above in Fig. 3 during dynamometer testing, was equipped with a manual push-button switch to select the most appropriate setting among three different modes. In optimized mode, the MBCE must idle and operate under standard conditions, utilizing all hydrous fuel blends. This mode was remapped on a dynamometer using the ‘Pitsbike’ ECU software.

During the testing, the following switch modes were established: Mode 1 for E10 to E40H; Mode 2 for E40H to E70H; Mode 3 for E70H to E100H. The AFR setting between 11 and 13, using the dynamometer and the “Pitsbike” ECU software, served as an essential indicator to confirm that each mode is at its optimum setting. Remapping is necessary in the modification [10].

Response Surface Methodology (RSM) was employed using Minitab 21 software in this experiment to investigate the effect of ethanol fuel blends with varying ethanol content and vehicle speed on engine performance, specifically dyno power and torque. RSM was used to develop a model based on experimental test data.

Ethanol fuel blend and vehicle speed were taken as input parameters and modelled using Equation 1, a second-order polynomial equation, while dyno power and torque were the responses. Each y response was modelled using a second-order polynomial equation as follows:

$$y = \beta_0 + \sum_{i=1}^k \beta_i X_i + \sum_{i < j} \beta_{ij} X_i X_j + \sum_{i=1}^k \beta_{ii} X_i^2 + \epsilon \quad (1)$$

The i is the linear coefficient, j is the quadratic coefficient, β is the regression coefficient, k is the number of factors, and ϵ is a random error with mean zero [15]. Models were evaluated using Analysis of Variance (ANOVA) to determine the significance of the relationship between the input parameters and responses. Additionally, the quality of the models' fit was assessed using the coefficient of determination (R^2). The models were evaluated based on the significance value (p-value) at a 95% confidence level.

3. Results and discussion

3.1. Ethanol and fuel blend properties

One of the limitations of this study is the use of hydrous ethanol instead of anhydrous ethanol. If testing performs well with hydrous ethanol as a blend, it is expected to perform even better with anhydrous ethanol [46, 52]. Table 3, as shown below, is the Physical and Chemical properties of the nipa bioethanol used in this study.

Table 3. Properties of nipa ethanol

Properties	Results	Remarks
Appearance	Clear and bright	Passed
Acidity/alkalinity, pHe	7.2	Passed
Density 20°C, kg/m ³	809.8	Higher
Ethanol content, % v/v	95.63	Lower
Methanol content, % v/v	0.01	Passed
Total acetic acid, % v/v	0.008	Passed
Heating value, MJ/kg	27.23	Higher

As expected, the ethanol purity used in this study, 95.63%, was lower compared to the PNS of 99.3%, but it was slightly higher in terms of heating value. Important to note in this result is the total acid content of 0.008% compared to the PNS 0.007%, which improves the initial study with 0.001% acid content [30, 52], addressing corrosion issues. The minimum 0.01% to the allowed PNS of 0.50% methanol content proved that the nipa-based bioethanol prepared and utilized in this study is harmless compared to the allowed maximum limit.

All hydrous ethanol fuel blends formulated as presented in Table 4 below exhibit slightly lower densities compared to the maximum 915 kg/m³ allowed with higher water content when compared to the PNS shown in Table 1 above.

The presence of water in hydrous ethanol has a positive influence on combustion characteristics, as shown in Table 4, enhancing octane ratings and reducing the tendency for engine knock [18]. However, hydrous blends have lower heating values, reflecting their reduced energy content per unit of fuel due to the moisture content of the resulting mixture. This impacts fuel efficiency, but is compensated for by a decrease in emissions of particulates and nitrogen oxides, as observed in previous studies on the combustion benefits of hydrous ethanol [6, 20].

3.2. Compatibility comparison of the test motorcycle using the alternative fuel and its blend

The performance curve of the test motorcycle in terms of power versus its speed, both with its stock carburetor and after its modification into MBCE using different fuel blends, is shown in Fig. 4.

Table 4. Physical and chemical properties of fuel blend

Test/analysis	Hydrous alcohol-fuel blend							
	E10	E20H	E30H	E40H	E50H	E60H	E70H	E80H
Density @ 15°C, kg/m ³	761	765	769	773	776	780	785	789
Ethanol content, %v/v	10.1	19.5	34.82	44.89	56.07	65.43	73.08	82.24
Methanol content, %v/v	< 0.1	< 0.1	0.41	0.34	0.32	0.25	0.17	0.11
RON rating	107.8	108	> 110.0	> 110.0	> 110.0	> 110.0	> 110.0	> 110.0
Vapor pressure at 37.80 kPa	48.5	47.4	45.7	44.6	42.8	40.6	36.6	31.6
Water, %v/v	0.098	0.17	0.244	0.357	0.411	0.527	0.609	0.673
Heating value, gross, MJ/kg	43.26	41.67	39.98	38.3	36.69	35.2	33.74	32.08

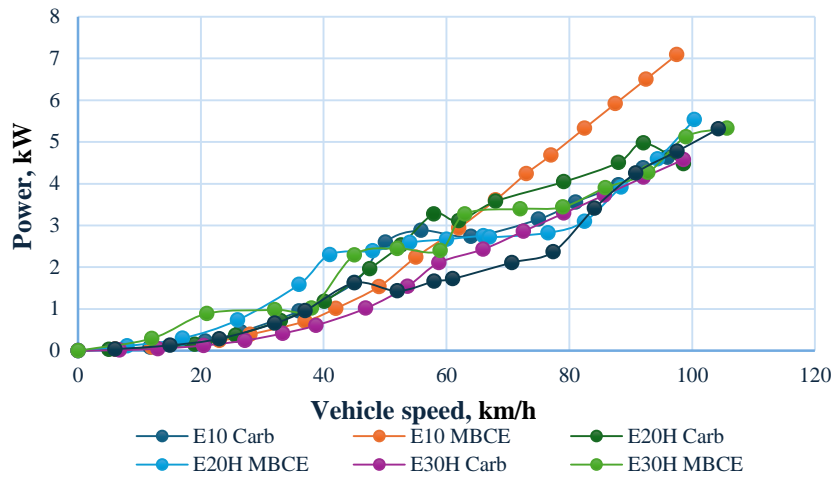


Fig. 4. Performance curve compatibility comparison between carburetor and MBCE-equipped in-use motorcycle

Although MBCE was observed to provide better power performance compared to its speed when compared to Carb, as shown in the figure, it is still considered comparable in terms of performance [42] when hydrous blends are used as fuel. The claim is supported based on the P-value of 0.594, which is greater than 0.05, and the F-value of 0.771, which is less than the F-critical of 2.186.

It is more important to note, as implied in Fig. 4 above, that the test vehicle with its stock carb was only compatible up to E30H, while the MBCE can operate up to E40H.

3.3. Performance of the alternative fuel on the MCBE test motorcycle

In Table 5, the model's evaluation using ANOVA is presented. The models are significant, as indicated by p-values less than 0.05. Thus, the factors have a substantial effect on the responses.

Table 5. ANOVA results for response parameters

Responses	p	F	R ²	Adj R ²
Dyno Power	< 0.01	774.86	0.9594	0.9582
Torque	< 0.01	207.96	0.8683	0.8596

p = significance value; f = f-statistic; R² = coefficient of determination; Adj R² = adjusted coefficient of determination

Additionally, the very high R² values for both models indicate that they fit the responses well. Mode 1 of MBCE was found to have better power performance, approximately 24.9% better than Mode 2 and 25.45% better than Mode 3. The power output performance refers to dynamometer power.

Equations 2 and 3 below present the second-order polynomial equation for determining the response of dyno pow-

er and torque to input parameters. The contour (a) and surface plots (b) were plotted below in Fig. 5 and 6 based on the effect of input parameters on dyno power and torque, respectively.

$$\text{Dyno Power} = 0.284 - 0.02160 \text{ Ethanol Content} + 0.03176 \text{ Vehicle Speed} + 0.000191 \text{ Ethanol Content} \times \text{Ethanol Content} + 0.000220 \text{ Vehicle Speed} \times \text{Vehicle Speed} - 0.000128 \text{ Ethanol Content} \times \text{Vehicle Speed} \quad (2)$$

$$\text{Torque} = 4.81 - 0.1643 \text{ Ethanol Content} + 0.4184 \text{ Vehicle Speed} + 0.001102 \text{ Ethanol Content} \times \text{Ethanol Content} - 0.001814 \text{ Vehicle Speed} \times \text{Vehicle Speed} - 0.000340 \text{ Ethanol Content} \times \text{Vehicle Speed} \quad (3)$$

The succeeding figures, as shown below in Fig. 5 and Fig. 6, demonstrate the flexibility of the MBCE modification in different switch modes capable of utilizing different fuel blends as sustainable engine fuel with decreased fuel economy in km/L, similar to a finding that an increased blend decreases net power [3] and of lower performance [12]. Perhaps due to the diminishing heating values of the increased fuel blends [4, 6, 33].

This trend is also reflected in torque, as shown in Fig. 6, which presents the adverse effect of ethanol on torque. The reduction in torque due to increasing ethanol content is more pronounced and stronger at lower vehicle speeds. This is indicated by the interaction of ethanol content and vehicle speed, where the negative coefficient (-0.000340) slightly reduces torque at high ethanol and high speed, making the ethanol effect more noticeable at lower speeds.

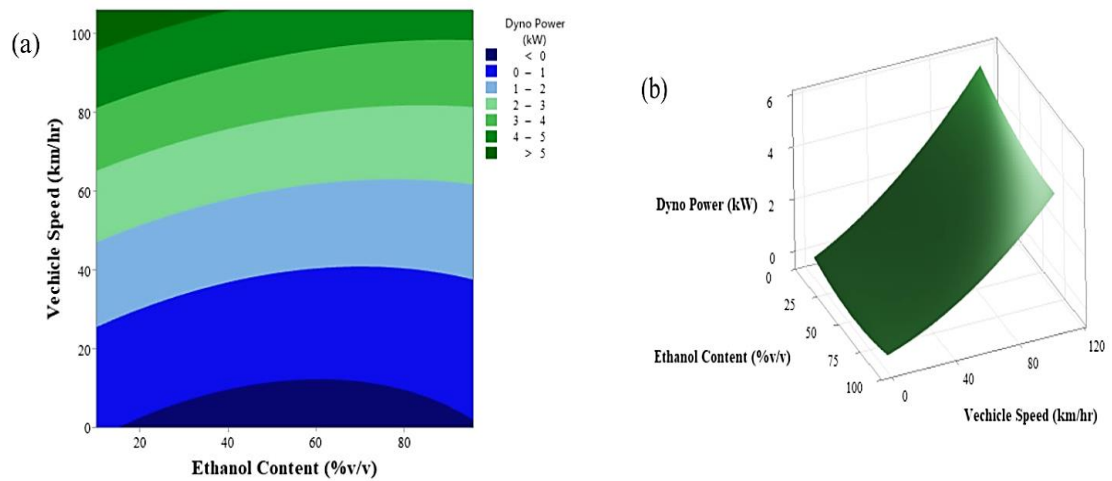


Fig. 5. (a) Contour and (b) surface plot for torque at different ethanol content and vehicle speed

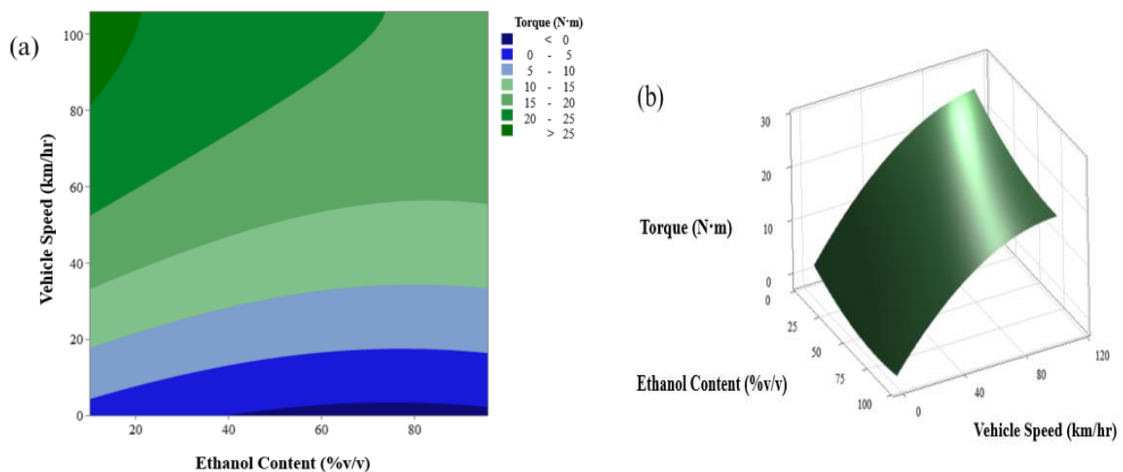


Fig. 6. (a) Contour and (b) surface plot for dyno power at different ethanol content and vehicle speed

Mode 1 of MBCE was found to have a better power performance, approximately 24.9% better than Mode 2 and 25.45% better than Mode 3. The power output performance refers to dynamometer power.

Figure 5a reveals that dyno power is significantly lower at lower vehicle speeds and higher ethanol content. Dyno power tends to reach 5 kW, which corresponds to approximately 61.49% efficiency, based on the 8.13 kW rated power of the test motorcycle with an ethanol content below 40% at around 100 km/h. This is indicated by the negative coefficient for ethanol content (-0.02160), which suggests that increasing ethanol content reduces dyno power. The surface plot in Fig. 5 shows the curve gradually decreasing in dyno power as ethanol content increases.

The trend of decreasing torque as the blend increases, as shown in Fig. 6, is also observed, indicating the adverse effect of ethanol on torque. The reduction in torque due to increasing ethanol content is more pronounced and stronger at lower vehicle speeds. This is indicated by the interaction of ethanol content and vehicle speed, where the negative coefficient (-0.000340) slightly reduces torque at high ethanol and high speed, making the ethanol effect more noticeable at lower speeds.

3.4. MCBE mileage efficiency

Figure 7, as shown below, reflects the performance of the alternative fuel on the MBCE as to mileage economy in kilometres of distance travelled per liter (km/L) of fuel consumed. The MBCE average fuel efficiency in terms of km/lit was measured using a 5 km complete tank method. Trials included two minutes of idling per trial to simulate traffic and city driving, conducted inside the MMSU campus.

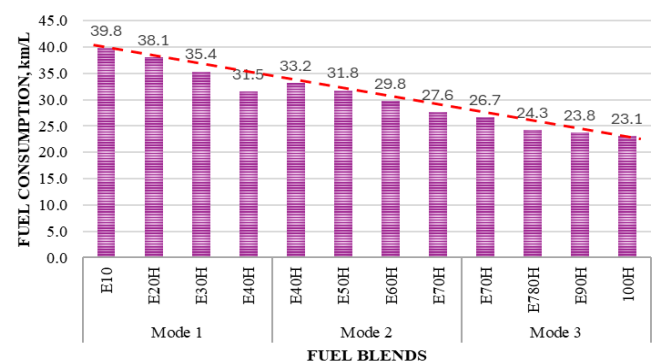


Fig. 7. MTBCE fuel consumption at different modes and fuel blends

The Honda XR125 MBCE's mileage of approximately 40 km/hr, observed using E10 under Mode 1, was close to the mileage of motorcycles in the Philippines. However, the figure implies that as the blend increases with ethanol percentages, its fuel economy decreases, as indicated by the sloping red line trend. The fuel efficiency, in terms of mileage, decreases by approximately 7.76%, 6.15%, and 4.86% for Modes 1, 2, and 3, respectively, for every 10% increase in ethanol content. The said decrease in mileage efficiency was expected due to the lower heating value of the resulting blends [59] as observed in Table 4 above.

3.5. MCBE tailpipe emission using the alternative fuel

In compliance with SDG 7, clean and affordable energy, biofuel offers clean emissions, as implied in Fig. 8, through the decrease in emissions of hydrocarbons (HC) and carbon monoxide (CO), gases known to cause respiratory problems and carcinogens when released into the surroundings [35].

The decreasing amounts of HC and CO, but with increasing CO₂ emissions, as shown in Figs. 8a to 8c, are signs

of better combustion in higher fuel blends [48]. Although E10 already has a very low HC emission of 867 ppm, the emission of every blend continues to decrease, reaching 154 ppm from E10 to E100H, as shown in Fig. 8a. The same observation was noted in Fig. 8b regarding CO emissions, which continuously decrease from 6.46% to 0.98% as E10 to E100H is used, respectively. The HC emissions are very low compared to the Euro 4 standard of 1000 ppm and the 4500 ppm limit [34] on all fuel blends. For CO% emissions, only blends from E80H to E100H passed the CO allowed emission of 2.5% set by the government [34, 44]. Figure 8 shows emission characteristics of MBCE using different fuel blends.

This CO₂ emission can be neutralized by planting trees, as suggested in urban and roadside areas [2]. This can also be adopted in cities in the Philippines. The CO emission can be improved through adjustment of the A/F ratio [33]. The A/F during MBCE testing is more compatible with 11–13 than with the ideal A/F of 14.7.

3.6. Total carbon footprint of fuel blends

Reflected below in Table 6 is the total quantification of CO₂ emissions when used as fuel in the MBCE. The gCO₂/L increases as the blend increases by 6% of the emission for every 10% increase in the blend. The fuel blend's CO₂ quantification used in this study was estimated using the Life Cycle Analysis (LCA) emission of gasoline equal to 2.735 kgCO₂/L from well to wheel [31] obtained from 85 gCO₂/MJ, 43.2 MJ/kg HV, and 745 kg/m³ petrol density, which is slightly higher than the study considering 2.4 kgCO₂/L [13]; and the hydrous nipa-based bioethanol emission of 0.2353 kgCO₂/L to 5.1887 kgCO₂/L from nipa sap collection to utilization [29]. It is important to note that nipa-based total carbon quantification is lower than that of petrol, referring to the minimum value of nipa hydrous bioethanol. Still, it results in greater emissions due to its higher limit compared to petrol emissions (0.2353 < 2.735 > 5.1887 kgCO₂/L).

As to emissions in terms of gCO₂/km, Table 6 also implies a comparable emission factor 76 gCO₂/km based on the testing conducted on the MBCE when compared to the 82.2 gCO₂/km used to estimate the Global Warming Potential (GWP) of CO₂ on motorcycles in Turkey using petrol [8], and in Taiwan at variable mileage at 1838–2098 gCO₂/km [50]. Using pure hydrous ethanol as fuel with 225 gCO₂/km is still low considering the MBCE in this study.

4. Conclusions

In this study, an MBCE motorcycle was evaluated to determine the potential problems associated with the use of higher fuel blends in gasoline engines, particularly in terms of engine drivability and compatibility issues in motorcycles equipped with carburetor and EFI systems.

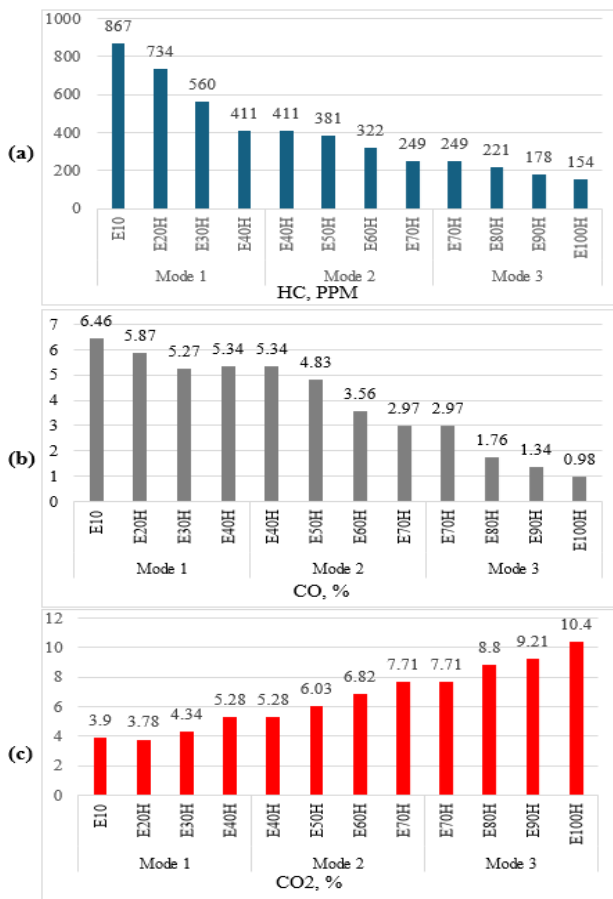


Fig. 8. Emission characteristics of MBCE using different fuel blends

Table 6. Total CO₂e of MCCE on various fuel blends

CO ₂ e	Fuel blend									
	E10	E20H	E30H	E40H	E50H	E60H	E70H	E80H	E90H	E100H
gCO ₂ /L	3012	3231	3597	3844	4114	4342	4531	4757	4944	5189
gCO ₂ /km	76	85	102	122	129	146	164	178	208	225

It was found that the MBCE in its stock carb is only compatible up to E30H without adjustments, while the EFI based on the MBCE is compatible up to E40H. It suggests that to utilize higher fuel blends that include ethanol as a pure engine fuel in EFI, the remapping procedure must be performed on the ECU to make it compatible. In contrast, this study used three different mode switches. The carb type can be compatible only up to 40% blend after carb setting adjustments. Regarding the performance of the MBCE, its power curve showed a decrease of 24.9% and a 25.45% difference in Mode 2 and Mode 3, respectively, compared to Mode 1. The fuel efficiency in terms of mileage was also found to decrease by about 7.76%, 6.15%, and 4.86% for Mode 1, Mode 2, and Mode 3, respectively, using the percentage difference among the blends for every 10% increase in ethanol fuel blends. The exhaust gas emissions are found to be more environmentally friendly, with HC reducing its emissions from 867 ppm to 154 ppm, and its %CO emission decreasing from 6.49% to 0.98%, meeting the Euro standards of 1000 ppm and 2.5%, respectively. The

emission factors of 76 gCO₂e/km to 225 gCO₂e/km for different blends found in this study can be used to estimate GWP. Based on the results, it is recommended that the country can safely proceed to implement fuel blends up to E30H and E40H after the carburetor type motorcycle's system is adjusted or modified to MBCE. Further testing must be conducted on cars and other petrol vehicles.

Acknowledgements

The authors gratefully acknowledge the staff of MMSU (NBERIC and ME dept) for their support and assistance in the production of ethanol, setting and remapping of the test vehicle: Rolando T. Rodrigo, Rein Corpuz Jr., Ruben Nalundasan, Bayani B. Pinpin, Jayrone Niell B. Jamias, Mark Daryl R. Galiza, and Mr. Kevin Lasaten. Also, to MMSU-USAID STRIDE for providing financial assistance for the initial laboratory and dynamometer testing, the Department of Energy for the free physicochemical laboratory Testing, and funding/mechanical testing from Mapua University. Lastly, dedicated to Engr. Christopher Baga.

Nomenclature

Carb	carburetor/carbureted	Fcritical	critical F-value for comparison
E	anhydrous ethanol	F-value	calculated F-statistic from ANOVA
EFI	electronic fuel injection	H	hydrous ethanol
E10-E100	ethanol-gasoline blend using anhydrous ethanol, number =% ethanol	MBCE	multi-blend capable engine
E10H-100H	ethanol-gasoline blend using hydrous ethanol, number =% ethanol	P-value	probability value

Bibliography

- Abel R. Global ethanol-blended-fuel vehicle compatibility study. OSTI 2021.
- Aini N, Shen Z. The effect of tree planting within roadside green space on dispersion of CO₂ from transportation. *International Review for Spatial Planning and Sustainable Development* 2019;7:97-112. https://doi.org/10.14246/irspsd.7.4_97
- Amaral LV, Santos NDSA, Roso VR, Sebastião RCO, Pujatti FJP. Effects of gasoline composition on engine performance, exhaust gases and operational costs. *Renew Sustain Energy Rev.* 2021;135:110196. <https://doi.org/10.1016/j.rser.2020.110196>
- Awad OI, Mamat R, Ibrahim TK, Hagos FY, Noor MM, Yusri IM et al. Calorific value enhancement of fusel oil by moisture removal and its effect on the performance and combustion of a spark ignition engine. *Energy Convers Manag.* 2017;137:86-96. <https://doi.org/10.1016/j.enconman.2017.01.009>
- Awogbemi O, Kallon DVV, Onuh EI, Aigbodium VS. An overview of the classification, production and utilization of biofuels for internal combustion engine applications. *Energies.* 2021;14(18):5687. <https://doi.org/10.3390/en14185687>
- Badawy T, Panithasan MS, Turner JWG, Kim J, Han D, Lee J et al. Performance and emissions evaluation of a multi-cylinder research engine fueled with ethanol, methanol, gasoline Euro-6, E85, and iso-stoichiometric ternary GEM mixtures operated at lean conditions. *Fuel.* 2024;363:130962. <https://doi.org/10.1016/j.fuel.2024.130962>
- Belonio AT, Regalado MJC, Rafael ML, Villota KC, Castillo PR. Design and performance evaluation of a variable-feed hydrous-bioethanol fuel injector for retrofitted engine. *Open Access Library Journal.* 2019;6:e5164. <https://doi.org/10.4236/oalib.1105164>
- Coskun C, Oktay Z. Carbon footprint prediction of vehicle usage in Turkey. *Greenh Gases Sci Technol.* 2020;10:736-758. <https://doi.org/10.1002/ghg.1980>
- De Salvo Junior O, Silva Forcetto AL, Maria Laganá AA, Vaz De Almeida FG, Baptista P. Combining on-road measurements and life-cycle carbon emissions of flex-fuel vehicle. *Renew Sustain Energy Rev* 2024;204:114784. <https://doi.org/10.1016/j.rser.2024.114784>
- Diep HT, Nguyen GB, Mohamad B. Remapping and simulation of EFI system for SI engine using piggyback ECU. *Acta Polytechnica.* 2023;63(2):89-102. <https://doi.org/10.14311/AP.2023.63.0089>
- Dinh Xuan T, Vu Minh D, Hoa BP, Duc KN, Nguyen Duy V. Influence of ethanol-gasoline blended fuel on performance and emission characteristics of the test motorcycle engine. *J Air Waste Manag Assoc.* 2022;72:895-904. <https://doi.org/10.1080/10962247.2022.2064003>
- Erma A, Dugala NS, Singh S. Experimental investigations on the performance of SI engine with ethanol-premium gasoline blends. *Mater Today Proc.* 2022;48:1224-1231. <https://doi.org/10.1016/j.matpr.2021.08.255>
- Eviendy R, Asyari MZ, Sukra ZL, Peranginangin E. Carbon emission and economical impact of conversion Yamaha N-Max 150cc into electric motorcycle. *IOP Conf Ser: Earth Environ Sci.* 2024;1324:012094. <https://doi.org/10.1088/1755-1315/1324/1/012094>

- [14] Ghadikolaie MA, Wong PK, Cheung CS, Zhao J, Ning Z, Yung K-F et al. Why is the world not yet ready to use alternative fuel vehicles? *Heliyon*. 2021;7(7):e07527. <https://doi.org/10.1016/j.heliyon.2021.e07527>
- [15] Ghafari S, Aziz HA, Isa MH, Zinatizadeh AA. Application of response surface methodology (RSM) to optimize coagulation-flocculation treatment of leachate using poly-aluminum chloride (PAC) and alum. *J Hazard Mater* 2009; 163:650-656. <https://doi.org/10.1016/j.jhazmat.2008.07.090>
- [16] Gu J, Kim H-K, Jang S. Study of cooling performance of liquid-cooled EV battery module according to the TIM compression ratio. *Int J Automot Technol*. 2024;25:1485-1502. <https://doi.org/10.1007/s12239-024-00134-3>
- [17] Hasan MK, Mahmud M, Ahasan Habib AKM, Motakabber SMA, Islam S. Review of electric vehicle energy storage and management system: Standards, issues, and challenges. *J Energy Storage*. 2021;41:102940. <https://doi.org/10.1016/j.est.2021.102940>
- [18] Hoth A, Kolodziej CP. Effects of knock intensity measurement technique and fuel chemical composition on the research octane number (RON) of FACE gasolines: Part 2 – effects of spark timing. *Fuel*. 2023;342:127694. <https://doi.org/10.1016/j.fuel.2023.127694>
- [19] Ilyas S, Naveed U, Khalid J. Improving fuel consumption using electronic fuel injection technology for low-powered motorbike engine. 2020 17th International Bhurban Conference on Applied Sciences and Technology (IBCAST), IEEE; 2020:236-243. <https://doi.org/10.1109/ibcast47879.2020.9044560>
- [20] Iodice P, Cardone M. Ethanol/gasoline blends as alternative fuel in last generation spark-ignition engines: a review on CO and HC engine out emissions. *Energies*. 2021;14(13):4034. <https://doi.org/10.3390/en14134034>
- [21] Kumar S, Ramadhas AS, Kumar P, Sithanathan M, Maheshwari M, Kagdiyal V. Fuel economy and emissions of E85 in passenger cars – a move towards flex fuel vehicle. *SAE Int J Adv Curr Pract Mobil*. 2021;3(3):1337-1343. <https://doi.org/10.4271/2021-28-0009>
- [22] Kumbhar SV, Khot SA. Experimental investigations of ethanol-gasoline blends on the performance, combustion, and emission characteristics of spark ignition engine spark ignition (S.I) engine with partial addition of n-pentane. *Mater Today Proc*. 2023;77:647-653. <https://doi.org/10.1016/j.matpr.2022.11.284>
- [23] Kupczyk A, Mączyńska-Sęczek J, Goliż E, Borowski PF. Renewable energy sources in transport on the example of methyl esters and bioethanol. *Processes*. 2020;8(12):1610. <https://doi.org/10.3390/pr8121610>
- [24] Li J, Zhao R, Xu Y, Wu X, Bean SR, Wang D. Fuel ethanol production from starchy grain and other crops: An overview on feedstocks, affecting factors, and technical advances. *Renew Energy*. 2022;188:223-239. <https://doi.org/10.1016/j.renene.2022.02.038>
- [25] Mabumbo D, Mafongoya P. Motorists' perceptions and attitudes towards ethanol blended fuel in Zimbabwe. *J Energy Power Eng*. 2019;13:68-79. <https://doi.org/10.17265/1934-8975/2019.02.003>
- [26] Maisel F, Neef C, Marscheider-Weidemann F, Nissen NF. A forecast on future raw material demand and recycling potential of lithium-ion batteries in electric vehicles. *Resour Conserv Recycle*. 2023;192:106920. <https://doi.org/10.1016/j.resconrec.2023.106920>
- [27] Manzano LFT, Halabaso ER, Aglipay LR, Gamboa FA, Agrupis SC. Evaluation of the physico-chemical and biological properties of fermented Nipa (*Nypa fruticans*) sap under closed and open vessel fermentation system for bioethanol production. *Open Biotechnol J*. 2024;18:1-12. <https://doi.org/10.2174/01187440707318178240809105611>
- [28] Marx S. Cassava as feedstock for ethanol production: a global perspective. *Bioethanol Production from Food Crops*. 2019:101-113. <https://doi.org/10.1016/B978-0-12-813766-6.00006-0>
- [29] Mateo NER, Calderon A, Agrupis S, Manzano LFT, Baga CC, Fagaragan A. Nipa-based bioethanol as a renewable pure engine fuel: a preliminary performance testing and carbon footprint quantification. *Int J Renew Energy Dev*. 2025; 14:39-51. <https://doi.org/10.61435/ijred.2025.60614>
- [30] Mateo NER, Ulep RA, Lucas MP, Agrupis SC, Sagadraca J, Baga C. An overview on the viability of hydrous bioethanol as gasoline fuel blend in the Philippines. The AUN/SEED-Net Joint Regional Conference in Transportation, Energy, and Mechanical Manufacturing Engineering, Singapore: Springer Nature Singapore; 2022:301-314. https://doi.org/10.1007/978-3-031-26365-1_2
- [31] Mattias, E, Serina, A. LCAs of petrol and diesel – a literature review. 2013;58. <https://res.slu.se/id/publ/40431>
- [32] Mendiburu AZ, Lauermaann CH, Hayashi TC, Mariños DJ, Rodrigues Da Costa RB, Coronado CJR et al. Ethanol as a renewable biofuel: combustion characteristics and application in engines. *Energy*. 2022;257:124688. <https://doi.org/10.1016/j.energy.2022.124688>
- [33] Mohammed MK, Balla HH, Al-Dulaimi ZMH, Kareem ZS, Al-Zuhairy MS. Effect of ethanol-gasoline blends on SI engine performance and emissions,” *Case Stud Therm Eng*. 2021;25:100891. <https://doi.org/10.1016/j.csste.2021.100891>
- [34] Morallo NT. Carbon monoxide and hydrocarbon contains of motorcycles: Metro Dumaguete, Philippines. *JPAIR Multidiscip Res*. 2016;25(1):70-79. <https://doi.org/10.7719/jpair.v25i1.390>
- [35] Mueller S, Dennison G, Liu S. An assessment on ethanol-blended gasoline/diesel fuels on cancer risk and mortality. *Int J Environ Res Public Health*. 2021;18(13):6930. <https://doi.org/10.3390/ijerph18136930>
- [36] Muhaji, Sutjahjo DH. The characteristics of bioethanol fuel made of vegetable raw materials. *IOP Conf Ser Mater Sci Eng*. 2018;296:012019. <https://doi.org/10.1088/1757-899x/296/1/012019>
- [37] Muratori M, Alexander M, Arent D, Bazilian M, Cazzola P, Dede EM et al. The rise of electric vehicles – 2020 status and future expectations. *Prog Energy*. 2021;3:022002. <https://doi.org/10.1088/2516-1083/abe0ad>
- [38] Oktem A, Oktem AG. Bioethanol obtained from soluble sugars in sweet sorghum, influencing properties and their interrelationships. *Ind Crops Prod*. 2024;221:119351. <https://doi.org/10.1016/j.indcrop.2024.119351>
- [39] Paenpong PP. Development of electronic fuel Injection system through the use of Arduino Mega 2560 microcontroller. *Journal of Engineering and Innovation*. 2023;16(1):34-43.
- [40] Park IJ, Yoo YH, Kim JG, Kwak DH, Ji WS. Corrosion characteristics of aluminum alloy in bio-ethanol blended gasoline fuel: Part 2. The effects of dissolved oxygen in the fuel. *Fuel*. 2011;90:633-639. <https://doi.org/10.1016/j.fuel.2010.09.049>
- [41] Priya, Deora PS, Verma Y, Muhal RA, Goswami C, Singh T. Biofuels: An alternative to conventional fuel and energy source. *Mater Today*. 2022;48:1178-1184. <https://doi.org/10.1016/j.matpr.2021.08.227>
- [42] Reddy KVMK, Reddy BM, Reddy KCS, Kartheek P, Adarsh TS. Comparative investigation of electronic fuel injection in two-wheeler applications: a review. *IOP Conf Ser Mater Sci Eng*. 2021;1116:012073. <https://doi.org/10.1088/1757-899x/1116/1/012073>

- [43] Sacco R, Frigo MM. The future of light-duty vehicles in Brazil: tendencies and challenges for a greener fleet. *Revista Brasileira de Energia*. 2023;29(2):160-180. <https://sbpe.org.br/index.php/rbe/article/download/783/562>
- [44] Salison AJP, Taguiam JEC, Gaspay SMA, Villar JJS, Javier SFD, Ballarta JN. Estimation of energy demand and emissions from the tricycle sector in Quezon city, Philippines. *Transp Res Procedia*. 2025;82:2444-2459. <https://doi.org/10.1016/j.trpro.2024.12.197>
- [45] Sanni A, Adegboyega O, Yahya S. Sustainability analysis of bioethanol production from grain and tuber starchy feedstocks. *ScienceOpen Preprints*. 2022. <https://doi.org/10.14293/s2199-1006.1.sor-.ppp0ent.v1>
- [46] Shirazi SA, Abdollahipoor B, Martinson J, Reardon KF, Windom BC. Physiochemical property characterization of hydrous and anhydrous ethanol blended gasoline. *Ind Eng Chem Res*. 2018;57:11239-11245. <https://doi.org/10.1021/acs.iecr.8b01711>
- [47] Souza Alvarenga D, Santos N, Rückert Roso V, Teixeira Malaquias AC, Baeta JG. Internal combustion engines and biofuels: Examining why this robust combination should not be ignored for future sustainable transportation. *Renew Sustain Energy Rev*. 2021;148:111292. <https://doi.org/10.1016/j.rser.2021.111292>
- [48] Suarta IM, Baliarta ING, Rahtika IPGS, Sunu PW. The role of hydrogen bonds of the azeotropic hydrous ethanol fuel composition to the exhaust emissions. *J Phys Conf Ser*. 2018;953:012070. <https://doi.org/10.1088/1742-6596/953/1/012070>
- [49] Tola E Al-Gaadi Alameen ZZIK, Zeyada AA. Hydrous ethanol-gasoline blends as alternative fuels for spark ignition engine: fuel properties and engine performance. *International Energy Journal* 2022:245-254. <https://parc.ksu.edu.sa/sites/parc.ksu.edu.sa/files/imces/abstract-iej.pdf>
- [50] Tsai J-H, Yao Y-C, Huang P-H, Chiang H-L. Fuel economy and volatile organic compound exhaust emission for motorcycles with various running mileages. *Aerosol Air Qual Res*. 2018;18:3056-3067. <https://doi.org/10.4209/aaqr.2018.07.0264>
- [51] Volpato O, Theunissen F, Colli G, Nelson CS. New flex fuel management and components for motorcycles. *SAE Technical Paper 2008-36-0227*. 2008. <https://doi.org/10.4271/2008-36-0227>
- [52] Wang X, Gao J, Chen Z, Chen H, Zhao Y, Huang Y et al. Evaluation of hydrous ethanol as a fuel for internal combustion engines: a review. *Renew Energy*. 2022;194:504-525. <https://doi.org/10.1016/j.renene.2022.05.132>
- [53] Wu H, Calderon AD. A study on the construction of charging stations on freeways using a road section power consumption model. 2024 8th International Conference on Green Energy and Applications (ICGEA), IEEE; 2024:72-79. <https://doi.org/10.1109/icgea60749.2024.10560595>
- [54] Xu B, Calderon AD. Volume optimization simulation design of permanent magnets for new energy electric vehicles. 2023 9th International Conference on Mechanical and Electronics Engineering (ICMEE), IEEE; 2023:196-202. <https://doi.org/10.1109/icmee59781.2023.10525288>
- [55] Yu ASO, Nascimento PTS, Nigro FEB, Frederick BWB, Varandas A, Vieira SFA et al. The evolution of flex-fuel technology in Brazil: the Bosch case. *PICMET 2010 Technology Management for Global Economic Growth*. 2010:1-11.
- [56] Yu JL, Quiros EN. Performance characteristics of Philippine hydrous ethanol-gasoline blends: preliminary findings. *ASME 2019 13th International Conference on Energy Sustainability*, American Society of Mechanical Engineers. 2019. <https://doi.org/10.1115/es2019-3824>
- [57] Yuan M, Thellufsen JZ, Lund H, Liang Y. The electrification of transportation in energy transition. *Energy*. 2021;236:121564. <https://doi.org/10.1016/j.energy.2021.121564>
- [58] Yusuf AA, Inambao FL. Progress in alcohol-gasoline blends and their effects on the performance and emissions in SI engines under different operating conditions. *Int J Ambient Energy*. 2021;42:465-481. <https://doi.org/10.1080/01430750.2018.1531261>
- [59] Zhang Z, Jiaqiang, Chen J, Zhu H, Zhao X, Han D et al. Effects of low-level water addition on spray, combustion and emission characteristics of a medium speed diesel engine fueled with biodiesel fuel. *Fuel*. 2019;239:245-262. <https://doi.org/10.1016/j.fuel.2018.11.019>

Nathaniel Ericson Mateo, PME, MSME – Faculty of Mechanical Engineering, Mariano Marcos State University (MMSU), Philippines.
e-mail: nrmateo@mmsu.edu.ph



Shirley Agrupis, PhD Biology – Program Leader of National Bioenergy Research and Innovation Center, Mariano Marcos State University, Philippines.
e-mail: shirleyagrupis@yahoo.com



Aldrin Calderon, DEng. – Faculty Mechanical, Manufacturing, and Energy Engineering, Mapua University, Philippines.
e-mail: adcalderon@mapua.edu.ph



Kendrick Cyrus Acidera, BSME – Faculty Mechanical Engineering, Mariano Marcos State University, Philippines.
e-mail: kcacidera@mmsu.edu.ph



Loreli Faye Manzano, BSChE – Science Research Specialist of National Bioenergy Research and Innovation Center, Mariano Marcos State University, Philippines.
e-mail: lmanzano@mmsu.edu.ph



Mariusz J. NIEŚCIORUK 
Andrei-Alexandru BOROIU 
Gustavo OZUNA 
Agustín Brau ÁVILA 
Przemysław KUBIAK 
Marek WOZNIAK 
Krzysztof SICZEK 

The use of hydrogen to supply combustion engines – part 1

ARTICLE INFO

Hydrogen is used to supply various internal combustion engines, as well as to fuel cells, which are employed in various vehicles. The goal of the present study was to review the state of art relative to the application of H₂ in the automotive industry. The review focuses on out-of-engine studies on the effect of H₂ combustion processes, internal combustion engines supplied with H₂, and vehicles utilizing fuel cells. Challenges in applying fuel cells to actual vehicles include limited flexibility in controlling power flow in the PEMFC + B setup, significant power flow losses, which complicate the management of energy systems in case of. The PEMFC + B + UC configuration, as well as a low power density of batteries. A drawback of H₂ engines is the emission of NO_x, which can be lowered by exhaust gas treatment. Fuel cell vehicles (FCVs) can be a clean energy alternative to gasoline-powered cars. However, their development depends on H₂ fuel availability and the expansion of refueling infrastructure.

Received: 22 April 2025

Revised: 26 September 2025

Accepted: 21 November 2025

Available online: 14 January 2026

Key words: *hydrogen, combustion engines, fuel cell, exhaust gas emissions*

This is an open access article under the CC BY license (<http://creativecommons.org/licenses/by/4.0/>)

1. Introduction

Stringent emission standards, with pollution levels closely linked to the combustion quality of existing internal combustion engines (ICEs), force manufacturers to develop new fuel injection solutions and adapt existing ones to meet more stringent standards [13]. Furthermore, other solutions are being sought to meet stringent emission standards. Nowadays, hydrogen (H₂) is increasingly being used to power ICEs in various types of vehicles and stationary applications. The development of the energy and transportation sectors has increased interest in using fuels derived from renewable sources, rather than fossil fuels.

Menes [68] conducted a synthetic review of the political framework, specifically the operational plans and initiatives, along with national leadership for the advancement of H₂ technologies and efficiency in 19 countries.

Gis and Gis [36] explored the circumstances surrounding the adoption of hydrogen in transportation in North-western Europe. Taking into account various technical aspects –including hydrogen refueling stations (HRS) and fuel cell electric vehicles (FCEVs), and economic factors (such as H₂ usage costs), the following countries were included: Belgium, Denmark, France, Germany, the Netherlands, Norway, and England. In Poland, significant fuel and energy corporations (including Orlen, Lotos, PGNiG, and ZE PAK Capital Group) are highly interested in the application of H₂ in transportation, while vehicle manufacturers such as Solaris and Autosan are focused on developing vehicles with fuel cells (FCs). It was discovered that the optimal placement of basic H₂ refueling stations is situated along the TEN-T corridors traversing Poland. The sequence of such locations is as follows: 1 – Poznań, 2 – Warsaw, 3 – Białystok, 4 – Szczecin, 5 – Łódź region, 6 – Tricity, 7 – Wrocław, 8 – Katowice region, 9 – Kraków.

Sikora and Orliński [98] observed that on 28 March 2023, the EU Council approved a rule imposing strict CO₂

emission norms for new cars and vans; therefore, from 2035 onward, only electric or H₂-fueled cars and vans will be eligible for registration. Notably, hydrotreated vegetable oil was excluded as a fuel from the Fit for 55 package regarding cars and vans. This type of fuel can replace diesel with HVO fuel without affecting the fuel injection (FI) control system and also has significant potential to reduce greenhouse gas emissions.

Various techniques used for the extraction of H₂ from biomass are reviewed in [74].

Skobiej [99] reviewed the most recent studies and progress in utilizing H₂ as fuel for internal combustion engines. The review thoroughly examined H₂'s ability to enhance combustion efficiency, particularly when mixed with NH₃ or CH₄. Essential findings emphasize H₂'s potential to reduce detrimental emissions, such as CO, HC, and soot, while it may increase NO_x emissions due to elevated combustion temperatures. The article also examines different H₂ injection methods, such as direct injection (DI), which surpasses port fuel injection (PFI) by notably improving power production and fuel efficiency. Additionally, the research highlights the importance of adjusting H₂ ratios in dual-fuel ICEs to achieve a balance between efficiency and emissions. These findings underscore the importance of H₂ in future decarbonization initiatives, with ongoing studies focused on reducing NO_x emissions while maintaining high efficiency.

Wesołowski et al. [130] suggested producing H₂ through the gasification of electronic waste in a steam environment to create syngas, which can serve as a H₂ source after isolation processes. They showcased the outcomes of gasifying electronic waste, which includes plastic components or epoxy resins, detailing the composition of the syngas produced during recycling and evaluating the possibilities of this waste processing for fueling transportation.

Matla et al. [66] examined the current understanding of H₂ combustion systems, which are now quite popular, primarily because of the advanced production technology and comparatively low recycling costs of FCs. The authors examined existing solutions that address challenges associated with H₂ production, storage, and transport. They stated that the forecasted threefold increase in H₂ production by 2050, driven by decreasing production costs, promotes research focused on its application as a fuel for H₂ ICEs.

Stępień [103] reported that H₂, being a zero-emission fuel, enables the construction of a piston ICE that meets the criteria for "Zero Emission Vehicles" regarding CO₂ emissions. The piston ICE powered by H₂ could serve as a bridging technology for powertrains, particularly in trucks and off-road vehicles, competing with both electric drives and FCs. The author offered a comprehensive examination of the potential advancement and distribution of H₂-fueled ICEs in automobiles.

A separate development group consists of vehicles utilizing hydrogen via FCs, known as fuel-cell electric vehicles (FCEVs) [28], some of which are in the early stages of development. Daszkiewicz and Kołodziejek [24] examined the option of utilizing ultracapacitors, batteries, or FCs to enhance the efficiency of a rail vehicle's powertrain. The choice of the right solution relies on the vehicle's intended purpose and its traction features. Zadrąg et al. [134] simulated dynamic loads on the propulsion system of ships equipped with unconventional power systems – reformed methanol FCs (RMFCs).

The present study reviews the state of art regarding the application of H₂ in the automotive industry. The review focuses on out-of-engine studies on the effect of H₂ combustion processes, internal combustion engines supplied with H₂, and vehicles powered by FCs.

2. Out-of-engine studies on the effect of H₂ combustion process

2.1. General overview and key mechanisms

Out-of-engine studies on H₂ combustion processes are conducted numerically or on test stands, including dedicated burning chambers.

Habib et al. [38] compared various H₂ combustion mechanisms elaborated by various researches, including GR13.0 [116], Dagaut et al. [22], ÓConaire et al. [75], Zsély et al. [138], Davis et al. [25], Saxena & Williams [94], Sun et al. [105], Li et al. [58], Ahmed et al. [2], USC-II [126], Konnov [52], Rasmussen et al. [86], Starik et al. [102], NUIG-NGM [42], Hong et al. [45], SanDiego [21], Burke et al. [18], CRECK [114], Kéromnès et al. [49].

ÓConaire et al. [75] developed a comprehensive kinetic model for H₂/O₂ combustion across a wide range of temperatures (298–2700 K), pressures (0.05–87 atm), and equivalence ratios (0.2–6). This extensive system and evaluation examined combustion characteristics across a range of temperatures, from low to high, and pressures, from sub-atmospheric to elevated, for fuel-lean to fuel-rich mixtures. Their rigorous assessment provided insights into essential reaction pathways across various combustion conditions, relevant to both basic kinetics and real-world applications.

Li et al. [59] conducted an in-depth analysis of the chemical reaction dynamics for H₂/O₂ combustion, referencing previous research [15] and utilizing new kinetic and thermodynamic data. Their mechanism was tested under various experimental conditions, including shock tubes, flow reactors, and laminar premixed flames. They determined that the H + OH + M reaction is crucial, particularly for simulating high-pressure flame propagation, as flame speeds were matched by employing different transport coefficients from the literature, with adjustments made to the rate within acceptable uncertainty.

The mechanism of the H₂/O₂ reaction is essential for both basic kinetics studies and practical combustion applications such as fire safety, energy conversion, and stimulus [59]. The application of H₂ as a fuel in these sectors requires knowledge of its oxidation chemistry. Moreover, the fundamental reactions involving the species H, O, OH, HO₂, and H₂O₂ are crucial for forming the reactive radical pool that initiates oxidation in HC fuels. Thus, enhancing H₂/O₂ kinetics provides a better understanding of the combustion process and advances H₂-oriented technologies in various sectors [75]. The H₂/O₂ reaction mechanism is explained in [59].

2.2. Recent advances in H₂ combustion chemistry

Recently, several studies have enhanced the comprehension of H₂ combustion chemistry [53]. In the reaction H₂ + OH = H₂O + H, studies [67, 106, 129], showed strong consistency with prior experimental findings. Nonetheless, the discrepancies in the determined rate constants were greater than those used in kinetic models from 2015 [53], making it difficult to choose a revised expression. An experimental investigation conducted between 295 and 701 K on the reaction OH + OH = H₂O + O, which is not part of a [53, 118, 119] H₂ kinetic mechanism, found that the rate constant from the study by Sangwan and Krasnoperov [93] below 834 K was less than other recorded measurements. The low-temperature rate constant was in agreement with the theoretical study conducted by Nguyen and Stanton [72]. Another study [5] suggested a fit to such data, indicating strong alignment with high-temperature tests by Wooldridge et al. [131] and a reverse rate from Sutherland et al. [107]. Hong et al. [44] also supported the findings of Wooldridge et al. [131].

Konnov [52] analyzed recent proposals by Burke and Klippenstein [19, 51] regarding the influence of chemically termolecular reactions, such as H + O₂ + R, on H₂ combustion kinetics under typical conditions. These reactions require careful consideration for inclusion in mechanisms, as they alter reactivity and laminar flame speeds. To investigate this, a comprehensive H₂ combustion mechanism was assessed to mitigate increased chain termination from these reactions while preserving or enhancing model performance. Revised kinetic investigations led to the inclusion of four new reactions and modifications to three rate constants, although this significantly decreased the computed burning velocities compared to experiments and earlier models, primarily due to termolecular reactions. The introduction of a theoretical transport database from Jasper et al. [47, 48] greatly improved the accuracy of the revised model, aligning it closely with experimental burning speed data

for H₂+air flames at atmospheric pressure, representing a notable advancement over previous models [54]. The system included new termolecular reactions and revised rate constants for existing reactions. These chemical changes did not significantly affect the mechanism's ability to simulate H₂ self-ignition and oxidation behavior in flow reactor setups.

Olm et al. [76] systematically evaluated 19 H₂ combustion mechanisms using an extensive experimental dataset, including ignition delays, species profiles, and burning speeds. They established error function values to assess the effectiveness of each mechanism across different test datasets, with values closer to one indicating better performance.

According to the average error function values, the K eromn es [49] mechanism provides the most accurate predictions for ignition delay times and burning speeds, while the flow reactor data was best represented by the Starik [102] mechanism. Overall, the K eromn es-2013 mechanism demonstrated the highest efficiency, closely followed by NUIG-NGM [42], Konnov [52], and Li et al. [58].

2.3. CFD modeling and engine performance findings

Simulations in computational fluid dynamics (CFD) indicate that DI ICEs achieve a 40% increase in brake power, resulting from a 30.6% improvement in volumetric efficiency. Additionally, DI systems reduce NO_x emissions by 36% compared to port fuel injection (PFI) with H₂ at an optimal air/fuel (A/F) ratio (λ) of 1.5. The research also highlights H₂'s superior efficiency in reducing fuel consumption – by 71.8% compared to CH₄ and 67.2% compared to coke oven gas (COG) – due to its higher heating value per unit mass [71]. The significant 71.8% decrease in brake-specific fuel consumption observed with H₂ DI compared to CH₄ is mainly attributed to H₂'s higher energy density. The precision of the DI system further amplifies this effect by optimizing the combustion process, minimizing fuel waste, and increasing thermal efficiency. These results were obtained for an optimal A/F ratio ($\lambda = 1.5$), maximizing the benefits of H₂'s exceptional combustion properties.

2.4. Influence of H₂ enrichment and combustion strategies

Gharehghani et al. [35] numerically studied the effect of H₂ enrichment on the operational range and combustion characteristics of a spark-ignition (SI) ICE powered by natural gas (NG). They found that misfiring occurred at equivalence ratios of approximately 0.61, 0.48, and 0.42 for H₂ fractions of 0%, 30%, and 50%, respectively. Combustion durations were 70, 47, and 45° crank angle for H₂ contents of 0%, 30%, and 50%, respectively, at the same equivalence ratio ($\Phi = 0.625$). The highest brake-specific NO_x was observed at $\Phi = 0.83$ ($\lambda = 1.2$), and this value was nearly unaffected by the H₂ fraction. Increasing the H₂ fraction reduced emissions of CO, HC, and CO₂. Adding 30% H₂ reduced CO₂ emissions by 10.2%, while a 50% H₂ fraction led to a 22.7% reduction.

Matla et al. [66] proposed a conceptual H₂ combustion system for ICEs, utilizing a prechamber to improve combustion parameters and overall engine efficiency. As noted

in [65], a split combustion chamber solution enhances the controllability of the combustion process in H₂ ICEs. Such a system is theoretically more efficient than any previously known solution. It was determined that the compression ratio (CR) and the degree of mixture depletion have the most significant impact on the H₂ combustion process. Their influence on H₂ knock formation was assessed, which can be categorized as severe knock (highly undesirable) or mild knock, depending on the level of pressure oscillations in the combustion chamber; in the latter case, combustion improvement is possible.

Brze anski et al. [14] studied the combustion of H₂-air mixtures with varying compositions. After H₂ DI was introduced into an isochoric combustion chamber, the mixture formed during the combustion process. The effect of fuel dose distribution before and after ignition on fire front development and pressure behavior in the isochoric chamber was analyzed. Management of the H₂-air mixture's combustion, primarily related to flame front velocity and heat release rate, can be achieved by using DI and initiating combustion during fuel injection. This method enables the delivery of stoichiometric mixtures to ICEs, significantly increasing the heat produced by the engine without entering the abnormal combustion zone. This can enable high engine performance compared to engines running on lean mixtures. Filming and pressure recording in the isochoric chamber were used to study combustion, demonstrating the effectiveness of this approach for analyzing mixture formation and combustion.

2.5. Advanced injection strategies and emissions control

Using CFD modelling, Shi et al. [96] analyzed how different injection parameters – including the amount of H₂ per pulse, the inter-pulse interval, and the width of the minor injection pulse – affect engine efficiency and emissions. The results indicate that split DI enhances mixture stratification, resulting in faster and more efficient combustion than single injection. Increasing the mass fraction of post-injection and the interval between injections further improves combustion, as a longer minor injection pulse width enhances engine efficiency by enriching the mixture near the spark plug. However, while this approach reduces HC and CO emissions to nearly negligible levels, it increases NO_x emissions.

Shahpouri et al. [95] reported that to minimize NO_x and soot emissions from engines running on hydrogen, an engine can be enhanced with a hardware-in-the-loop (HIL) configuration, thereby reducing calibration work for the engine. Furthermore, optimal model-based combustion control (MCC) can lower engine-out emissions. Both HIL and MCC methods need rapid and precise models for NO_x and soot emissions. The precision of a rapid physics-based engine model utilizing premixed combustion relies on forecasting the laminar flame speed (LFS). The authors forecasted LFS using an artificial neural network (ANN) machine learning (ML) approach. The LFS model and the engine combustion model are validated for both an H₂ SI engine and an H₂-diesel CI engine. The black-box and gray-box models for soot and NO_x emissions were created for the H₂-diesel engine utilizing ANN, support vector machine (SVM), and Gaussian process regression (GPR) techniques

with various feature sets, and are then compared to a standard one-dimensional physics-based NO_x model. The gray-box emission models were ideal for engine HIL configurations where precision is crucial. The black-box models were appropriate for model-based real-time control of H_2 combustion when computational power is restricted.

2.6. Syngas combustion and engine adaptation

Hagos et al. [39] analyzed the properties of three distinct syngases derived from major gasification products of low and medium calorific values, comparing them to CNG and H_2 . Syngases, especially those with a medium calorific value, have an adiabatic flame temperature similar to that of H_2 , resulting in increased NO_x emissions. Syngases have a much lower stoichiometric A/F ratio compared to CNG and H_2 , which may increase brake specific fuel consumption (BSFC).

Fiore et al. [29] reported that syngas fuel serves as an intermediary phase in the transition from carbon-based to H_2 -derived fuels. Syngas-powered dual-fuel engines achieve notable standard fuel savings. Syngas has low knocking propensity and allows the use of high compression ratios (CRs). Its broad flammability range favors lean combustion. Dual-fuel CI engines, homogeneous charge spark ignition engines, and DI SI engines are highly sensitive to the physical and chemical properties of syngas, such as CO and H_2 content, laminar flame speed, broad flammability range, and lower density compared to air. The authors also noted that large-eddy simulations or even direct numerical simulations should be conducted, and models require further improvement and validation. Models addressing turbulence-chemistry interaction should be tested, especially for high-speed DI of syngas. Multicomponent diffusion models should be included, as H_2 diffuses much faster than other mixture components. Intake and exhaust processes, typically neglected in syngas port-injection engine simulations, must be considered, as a significant part of power derating is linked to reduced volumetric efficiency. These processes must be included in high-fidelity data assessment.

Paykani et al. [78] examined the impact of syngas use on the performance and emissions of SI, CI, HCCI, and advanced dual-fuel engines like reactivity-controlled compression ignition (RCCI) engines. Many factors affecting both syngas and engine properties significantly influence the prospective benefits of syngas use in ICEs. Variations in the H_2 fraction of syngas have limited its broad application. Additional gaseous components, such as CO_2 , N_2 , and CH_4 , in syngas may negatively impact engine combustion. The key reasons for power loss in SI engine are the low energy density of syngas/air blends and reduced volumetric efficiency due to air replacement. Adding high H_2 -content syngas as a secondary fuel improved combustion and performance compared to low H_2 -content syngas. Using high CRs in syngas-powered engines reduced power loss without increasing knocking. DI of syngas can also eliminate power derating, avoiding issues related to reduced volumetric efficiency and unintentional pre-ignition or surface ignition in the intake system.

2.7. Material issues: hydrogen embrittlement

As noted by [89], the intended replacement of conventional fuel in combustion engines with H_2 may cause hydrogen embrittlement, particularly in various steel-based materials, depending on material type, structure, and operating conditions. The authors described the process of electrochemical hydrogenation, similar to galvanic coating of metals used in the automotive industry. They assessed how hydrogenation duration affects the properties and microstructure of austenitic steel. They found that the material was strengthened by electrochemical hydrogenation in a 0.5M H_2SO_4 solution. The increase in strength was directly related to the amount of H_2 supplied. However, the typical features of hydrogen embrittlement, such as localized brittle fracture areas reported in the literature, were not observed in the analyzed material.

2.8. Summary and research directions

Several mechanisms describing H_2 combustion have been published recently, exhibiting varying degrees of complexity and accuracy.

Various out-of-engine studies on the effect of H_2 combustion have utilized CFD methods, investigating not only pure H_2 but also gases containing high H_2 content, such as syngases.

The application of combustion engines fuelled with H_2 and fuel cells (FCs) in vehicles is discussed in the following subchapters.

The use of the dual-fuel ICEs supplied with fuel and H_2 is presented in Part 2 of this review. It can be noticed that the efficiency of such ICEs can be enhanced, for example, by applying new solutions to their injection system, such as a hypocycloid mechanism in the drive of pumping sections of high-pressure pumps for diesel combustion engines and the others [9, 12, 64].

3. Combustion engines supplied with H_2

Escalante and Fernandez [27] stated that in ICEs fueled by H_2 , the emissions from air/ H_2 mixtures primarily consist of CO_2 and NO_x . For NO_x , higher emissions occur because H_2 combustion produces higher flame temperatures and flame speeds than other fuels, such as gasoline. Emissions of unburned hydrocarbons (UHC) result from the heating of lubricant oil and the use of oil-based coolants. The thermal efficiency of a H_2 -fueled engine (38.9%) exceeds that of a gasoline engine (25%). The power output by a H_2 -fueled test engine reached 80% of the output of a gasoline engine. At light loads, H_2 combustion can minimize NO_x emissions and prevent abnormal combustion phenomena by shortening the injection duration and delaying the spark timing. Spark-ignition (SI) engines can operate efficiently with air- H_2 mixtures at equivalence ratios between 0.3 and 0.9, using compression ratios (CR) above 12:1, exhaust gas recirculation (EGR), shorter injection durations, and delayed spark timing. Nearly ideal functioning of compression-ignition (CI) engines requires increasing CR, using EGR, and primarily employing a combustion inducer (such as diesel) while adding an H_2 mixture to achieve the desired power output. Replacing hydrocarbons requires research on CI engines powered by H_2 and diesel, operating at CR above 15:1, using natural gas (NG) injectors, and variable

H₂ loads, starting from low loads until minimal HC levels are achieved, utilizing a combustion initiator.

From an engine design perspective, the primary modifications suggested for using H₂ as a fuel include:

- Replacement of injectors: Larger injection volume capacity is needed. The low density of H₂ necessitates rapid injection of larger fuel quantities. NG injectors can be modified to operate with H₂.
- Improved temperature management: The high combustion speed of H₂, compared to gasoline and diesel requires enhanced temperature control, such as cooling around nozzles, spark plugs, and cylinder heads.
- Mixtures: Using H₂ combustion alongside hydrocarbons is recommended as an initial phase of H₂ integration. Light blends with about 5–10% H₂ by volume can serve as a starting point for a gradual, clean transition from traditional fuels.

Verhelst et al. [120] stated that due to its physical and chemical characteristics, H₂ is primarily employed in SI applications and is regarded as a baseline. The power output of an H₂ ICE is lower than that of a gasoline engine due to H₂'s low volumetric energy density. H₂ occupies more engine volume, reducing the possible air intake per cylinder. This negative effect is partly offset by the higher heating value and stoichiometric air-to-fuel ratio, but it may still lead to a 17% reduction in power output. Although port fuel injection (PFI) has lower theoretical performance than other mixing systems, it remains the only system used in demo cars due to its simplicity and injector availability.

The authors further explained that the wide flammability range of H₂ benefits load control strategy, enabling a 'qualitative' load control approach that eliminates the need for throttling and associated losses. In this case, the A/F ratio is raised to decrease performance at partial loads, which works similarly to a diesel engine. Running the ICE with very lean mixtures additionally helps reduce NO_x emissions. Reintroducing exhaust gases (EGR) to the inlet is another method to lower the performance at part-load operations without throttling. The presence of the inert exhaust gases also reduces the amount of air and fuel in the engine. H₂ enables stable ICE operation with higher EGR levels than gasoline due to its broader flammability range and faster flame speed. The maximum power per engine displacement can be increased by raising inlet pressure using supercharging or turbocharging, with turbocharging being preferred for efficiency. However, the reduced throttle response and lower exhaust energy with H₂ compared to traditional fuels create challenges for turbocharged H₂ ICEs. Control methods based on power density or ICE efficiency are typically integrated into lean-burn and stoichiometric strategies. At low loads, the ICE operates with varying air-to-fuel (A/F) ratios, yielding high efficiency and very low emissions. When a specific power requirement is exceeded, the operation shifts to throttled stoichiometric mode. The performance achieved by this load control approach was reflected in a single-cylinder ICE map at BMW, later scaled to 12 cylinders in a demo car [122]. The map showed optimal performance between 4 and 6 bar IMEP (indicated mean effective pressure) with an indicated thermal efficiency (ITE) of 42%. This maximum efficiency is

paired with a large portion of the map showing ITE values above 38%. However, the maximum torque reached about 10.3 bar IMEP, indicating lower power density compared to similar gasoline ICEs, mainly due to low inlet charge density and combustion limitations.

The authors also noted that the broad flammability range, high flame speed, and low ignition energy of H₂ improve engine efficiency but can also cause unwanted combustion events. The most common is 'backfire' - premature ignition of the H₂-air mixture during the intake stroke, leading to combustion in the intake system and possible failure. Preventing early ignition requires eliminating ignition sources such as hot spark plug electrodes and exhaust valves, and modifying the ICE. Keeping ignitable mixtures away from ignition sources is another way to prevent backfire. In this case, variable valve timing and carefully managed injection timing are used to prevent backfire by introducing a cooling period with fresh air and minimizing H₂ during the initial intake phase [1, 60]. Pre-ignition can also occur when the inlet valves are closed and the charge is compressed, resulting in extremely high pressures and potential damage. Ultimately, self-ignition (knock) of the unburned mixture can occur, as in any SI ICE. In an H₂ ICE, knock is less likely than in gasoline engines, but its effects may be more severe due to the high burning speed of H₂ mixtures.

H₂ PFI has been applied in various demonstration vehicles, either modified from existing models or purpose-built for H₂. Modifications for H₂ operation focus on the fuel system (from storage to injection) and engine control unit programming. Quantum Tecstar converted over 30 vehicles for H₂, using the Toyota Prius hybrid as a base. Two compressed H₂ tanks replace the gasoline tank, preserving the vehicle's interior. The Prius engine is turbocharged to boost H₂ performance. The Quantum H₂ Prius offers similar drivability to the gasoline version, with a range of 100–130 km and compliance with SULEV II emissions standards [121].

Designing a dedicated H₂ vehicle required additional hardware considerations [125].

Shinde and Karunamurthy [97] observed that current PFI and DI H₂ ICEs provide favorable brake thermal efficiency compared to gasoline ICEs. H₂ properties are better suited for gasoline-type engines, but specific adjustments are needed to utilize H₂'s potential fully. For DI, a late injection strategy is recommended for optimal combustion. Efficiency losses must be minimized. EGR increases ICE efficiency, and further dehumidifying EGR improves it; thus, arrangements for EGR dehumidification are suggested. Downsizing the engine increases efficiency but also raises NO_x emissions, requiring a balance between NO_x and efficiency. Research should focus on hybrid fueling systems combining DI and PFI to enhance efficiency and lower emissions.

H₂-fueled ICEs have demonstrated higher-brake thermal efficiency than those using fossil fuels. However, irregular combustion such as backfiring in H₂-injected engines, limits performance improvements due to H₂'s low ignition energy and high flame speed. Volumetric efficiency drops significantly during backfire, and damage to intake and fuel injection systems can occur. Backfire is triggered by residual

exhaust gas at high temperatures, hot spots, and irregular spark plug discharge, which promote pre-ignition of the H₂-air mixture. Gao et al. [32] analyzed factors leading to backfire, including incorrect valve and injection timing and high A/F ratios, and reviewed backfire control methods, discussing their pros and cons. The main causes are excessive residual exhaust gas, slow combustion, and uneven H₂ distribution near intake valve seats. Backfire control strategies require specific conditions to remain effective; outside these, they may negatively impact results. Power loss is almost unavoidable for naturally aspirated ICEs when backfire prevention is implemented. Various strategies are recommended to mitigate performance loss, and multi-objective optimization is proposed to achieve the best overall efficiency.

BMW created the H₂ 7 car with a dual-fuel system that allows for operation on either H₂ or gasoline. In H₂ mode, it uses a variable A/F ratio lean-burn strategy for low and medium loads, and a throttled stoichiometric approach for high loads. Approximately 8 kg of H₂ are stored in a cryogenic tank in the trunk, providing a range of 200 km. Emission tests of a mono-fuel H₂ 7 variant showed very low emissions. Using a special after-treatment system with two catalysts (one for stoichiometric and one for minimizing NO_x spikes during transitions), the car achieved drive-cycle NO_x emissions of 0.0008 g/mi, just 3.9% of the SULEV II threshold [43].

Vogel [124] developed a large diesel engine with H₂ DI into the combustion chamber, achieving high power density and reduced exhaust emissions. Combustion occurred via self-ignition, following the diesel principle, with H₂ as the energy source, allowing CO₂-free operation.

Prechtl and Dorer [83] reported that H₂'s properties and use in high-power, large-displacement engines led to the concept of an engine with internal mixture formation and CI. A system developed by MAN B&W used electro-hydraulic control for injection. H₂ was injected at high pressure in gaseous form, with experiments and 3D flow simulations performed. The ignition process was modelled in 1D chemical simulations. Combustion in a diesel ICE is feasible, and the mixing system is key for effective H₂ combustion in large diesel ICEs.

Rottengruber et al. [88] performed studies on a DI H₂-powered diesel engine, injecting H₂ at high pressure near top dead center and igniting by self-ignition. This was systematically tested on a single-cylinder engine. Combustion was analyzed using custom software to generate pressure curves and engine mechanics, and a computational model was developed to predict NO_x emissions.

Some researchers have investigated various H₂-fueled engines (see Table 1).

Brzeżański and Rodak [15] conducted theoretical and experimental work on a Kipor 186F SI ICE modified for H₂. The engine utilized an H₂ DI system in the combustion chamber, enabling the regulation of heat release rate. H₂ DI, compared to inlet channel injection, greatly expanded the engine's operational range and prevented knocking. The right DI approach enabled combustion with a lower excess air coefficient, approaching stoichiometric conditions. This increased maximum cylinder pressure and improved engine

parameters, with no resultant knocking. The DI approach, employed during both the compression and combustion phases, enables H₂ to replace hydrocarbon fuels in ICEs fully.

Brzeżański and Rodak [16] also analyzed NO_x formation during H₂-air combustion in an SI ICE. They developed a strategy for generating and combusting H₂-air mixtures, ensuring low NO_x. This approach limits the N and O₂ reaction during operation. Preliminary tests have shown that this injection strategy enables progress monitoring. Unlike previous H₂ supply systems, this method allowed stoichiometric combustion without anomalies or auto-ignition. Monitoring the heat release rate and in-cylinder pressure rise was also possible. These engine parameters strongly influenced burning characteristics and NO_x emissions. The developed system avoided knocking and allowed full NO_x emission monitoring. Burning progress and NO_x propensity can be evaluated by average pressure rise. Tests over a wide H₂-air mixture range ($\lambda = 2.03\text{--}1.05$) showed that NO_x generation depends more on temporary pressure rise (and thus temperature) than O₂ availability. The H₂ injection strategy, which allows injection during either the compression or both compression and combustion phases, depending on the operating point, significantly influences operating parameters and NO_x emissions, and could inform regulatory guidance.

Szlachetka et al. [109] simulated a gaseous fuel delivery system in a Wankel engine using a zero-dimensional model of the injector set, with gaseous H₂ injected into the RX 50 Wankel engine's intake manifold. The study was conducted at 3700 rpm and an inlet pressure of 0.4 MPa. Pressure time profiles in the fuel pipe and injector-to-intake tubing were analyzed. Maximum pressure fluctuations in the fuel rail reached 0.016 MPa at injector closure. Notable changes in fuel flow in the pipe to the intake manifold were observed, up to 0.002 kg/s. The maximum average injector mass flow was 0.00325 kg/s.

Mitianiec [69] noted that Wankel engines may be attractive in automotive applications due to their small size, compactness, simple design, smooth operation, and reduced vibration resulting from inertia forces. The main drawback is significant pollution (HCs, CO) and high BSFC, which can be addressed by H₂ DI and, in aviation, by using high-octane fuel in DI systems. The researcher simulated thermodynamic processes during scavenging, utilizing engine geometry, initial and boundary conditions to compute pressure, temperature, density, heat exchange, and volume as a function of piston angle in a zero-dimensional model. Mixture formation during compression-phase injection provided insights into air excess ratio. The model can be used for various fuels. Using H₂ lowers emissions but also reduces efficiency.

The author concluded that:

1. While the inlet port is opened, only a brief moment is available to fill the chamber with fresh air. Emission discharge continues longer due to high pressure, depending on the outlet port area. Rotor contact points should be minimized for effective sealing.

2. For naturally aspirated rotary Wankel engines, volumetric efficiency remains below 1.0 due to emissions that hinder air flow into the chamber.
3. Fuel injection must occur during the compression phase to minimize fuel waste.
4. A gasoline-homogeneous mixture engine produces more internal work (and power) than an H₂ engine, due to gasoline's higher caloric value under the same settings.
5. The mass of charge in the naturally aspirated Wankel engine varies slightly with engine speeds.
6. Exhaust pressure within in the port is largely unaffected by the fuel at the speed.
7. The engine achieves peak power at high speeds, specifically 12,000 rpm in this case.
8. To achieve high overall efficiency, a DI fuel layout is needed for stratified charge.
9. The scavenging process is crucial for ported engines.

Szwaja [110] studied knocking in an H₂-powered engine. Knocking intensity was defined as in-cylinder pressure fluctuations (sampled at 100 kHz) and processed with high-pass filtering (cutoff at 3.5 kHz). The study used a CFR engine with variable CR (6–14). A sharp rise in pressure pulsation amplitude was observed as CR rose from 11 to 12, attributed to auto-ignition of the H₂-air mixture at the end of SI-controlled combustion. The dual nature of H₂ knock combustion was proposed. Pressure pulsation intensity during regular combustion (without H₂ auto-ignition) showed an exponential relationship with CR, directly related to the temperature of the H₂-air mixture at ignition.

Kovar et al. [55] evaluated H₂-fueled engines, focusing on mixture formation, combustion of air-H₂ mixtures with varying A/F ratios, NO_x emissions, and power characteristics. Studies were conducted on a single-cylinder test engine (naturally aspirated and supercharged) and a six-cylinder turbocharged engine. Main technical challenges in H₂ engine development are (i) reduced power due to lower volumetric energy density of H₂/air mixtures, and (ii) issues like backfire and early ignition. Engine concepts like turbocharging, intercooling, and internal blending with A/F equivalence ratio $\Phi < 0.5$ can increase efficiency while keeping NO_x low. The safest H₂-powered engine system utilizes an in-cylinder fuel mixer, where air is drawn in first, followed by H₂ DI into the cylinder. No backfire was observed in lab tests (even when H₂ was introduced before inlet valve closure at ~1 MPa).

Szwajca et al. [111] examined a two-stage passive H₂ combustion setup for knock studies under various conditions. Experiments with a single-cylinder AVL 5804 engine assessed the effect of center of combustion (CoC) and excess A/F ratio (λ) on knocking and its metrics. Tests at 1500 rpm, with CoC (2–18°CA aTDC) and $\lambda = 1.25$ –2.0, showed strong knock at $\lambda = 1.25$ –1.5, requiring higher λ to suppress it. Knocking depended more on λ than on CoC.

Lee et al. [57] studied H₂ DI, assessing three mixing methods: homogeneous, lean homogeneous, and lean-stratified in a single-cylinder ICE. Results show that H₂'s significant heat loss requires delaying combustion. The lean-stratified charge (LSC) mode, designed to reduce high-temperature zones near the cylinder wall, achieved the highest BTE (34.09%) at low loads. However, this also

increased NO_x emissions, illustrating the trade-off between efficiency and emissions in H₂ DI systems.

Bao et al. [11] tested a 2.0L turbocharged H₂ DI ICE, achieving 120 kW at 4400 rpm and 340 N·m at 2000 rpm. Peak BTE was 42.6% with a mildly lean A/F ratio ($\lambda = 1.91$) at 2000 rpm. NO_x emissions dropped by over 99.5% at speeds below 2000 rpm and by about 90% at 4400 rpm, with two-thirds of cases achieving NO_x below 20 ppm using an NH₃-SCR after-treatment system. This confirms that H₂ DI ICEs can deliver high power, efficiency, and near-zero emissions.

Wróbel et al. [132] reviewed advances in H₂ combustion vehicle technology, highlighting prototypes and summarizing key features (see Table 2). Since H₂ engine drivelines are mechanically similar to conventional ones, they are ideal for operators in challenging environments or those seeking stable maintenance costs. H₂ engine development is promising for applications that do not require dense refueling infrastructure. H₂ combustion vehicles tolerate varying H₂ quality, operate in harsh conditions, are reliable and user-friendly, and are mature, tested technology that ensures independence from rare earth metals. The main drawback is NO_x emissions, requiring exhaust treatment.

According to [87], just a year after its prototype was revealed in October 2021, HYVIA presented the H₂-powered Renault Master Van H2-TECH at the Paris Motor Show 2022. Its main advantages are zero emissions, a 5-minute refueling time, and a 400 km range. The Master Van H2-TECH is a spacious van with 12 m³ cargo capacity, a 30 kW FC, a 33 kWh battery, and tanks for 6.4 kg of H₂.

Various strategies are employed to enhance H₂ combustion and ICE efficiency while minimizing harmful emissions, including optimized A/F ratios, sophisticated injection systems, and EGR. These methods aim to enhance combustion efficiency, reduce NO_x emissions, and minimize the production of other pollutants [34, 77, 104].

Optimized combustion can be realized via:

- Control of the air-fuel mixture is essential, as accurate management of this ratio is crucial. Operating the engine in a "fuel-lean" mode (with surplus air) can enhance efficiency. The rapid flame speed of H₂ enables stable combustion, even under lean conditions [6, 31, 50, 70, 84, 133].
- Injection techniques, particularly high-pressure DI systems, provide enhanced control over the timing of combustion and fuel distribution, resulting in improved efficiency and performance [34, 99].
- Stratified combustion, which employs stratified or spark-assisted diffusive combustion, can enhance combustion features and improve thermal efficiency [34].
- The timing of ignition, as sophisticated ignition systems can be employed to enhance the timing of combustion, ensures it occurs at the most efficient moment within the engine cycle [7, 34, 137].

Emission control can be realized via:

- EGR lowers combustion temperatures, which aids in reducing the creation of NO_x [3, 34, 50, 77],.
- Catalytic converters, because although hydrogen burning mainly generates water. Catalytic converters can also minimize NO_x emissions [34, 104, 113, 117].

Table 1. Selected combustion engines supplied with H₂

Refs	Type of engine	Combustion system	Bore × stroke [mm]	Displacement [dm ³]	CR [-]	Power output [kW]/speed [rpm]
[15, 16]	Kipor 186F, Single-cylinder, vertical 4-stroke, forced air cooled diesel	Single-cylinder, vertical 4-stroke, forced air cooled diesel. DI system. Modified by Heron chamber in the piston for a strong swirl during compression.	86 × 70	0.406	Original 19.3, after modification of burning space 15.1	Continuous 6.6, Maximum 7.4/3600
[110]	CFR Waukesha Single cylinder SI 4- 4-stroke water cooling		8.26 × 11.43	0.611	4.5–18.5	
[55]	OKC-Octane Single cylinder SI 4-stroke both naturally aspirated and supercharged	gas DI		0.61	8:1	
[55]	LIAZ ML637ENE 6-cylinder SI 4-stroke turbocharged		130 × 150	11.946	12:1	160/2000
[111]	AVL 5804 1-cyl., 4-valve, SI, TJI, supercharged	H ₂ supplied from cylinder to main chamber at 6.5 bar. Two tanks in series before injector to reduce pressure pulsation.	85 × 90	0.5107	14.5:1	
[57]	Single-cylinder SG–DISI	Highly pressurized H ₂ injected from three cylindrical vessels via modified piezo-actuated gasoline injector, with fire arrester and H ₂ detector.	85 × 88			
[11]	4-stroke, DI H ₂ -fueled			1		

Table 2. Selected prototype cars with H₂-fuelled ICEs (based on [132])

Model	Engine	H ₂ Tank	Range (km)
Ford P2000 (2001)	ICE 2.0 l straight-four engine Zetec (port injection)	Compressed (87 dm ³ , 250 bar, 1.5 kg)	100
Ford Shuttle Bus (2004)	ICE 6.8 l V10 Triton	Compressed (350 bar, 29.6 kg) *	240–320
ETEC Chevrolet Silverado (2004)	ICE 6.0 l V8	Compressed (3 × 150 dm ³ , 350 bar, 10.5 kg) *	230–260
Toyota Quantum Prius (2005)	ICE 1.4 l straight-four engine (electronic multi point H ₂ injection)	Compressed (1.6 kg)	100–130
Toyota Corolla (racing vehicle) (2021)	ICE 1.6 l 3-cylinder turbo with intercooler	Compressed	
Lexus RC F designed vehicle (2022)	ICE 5.0 l V8		

* Note: The higher brake specific fuel consumption BSFC is due to the relatively larger size and car weight of these vehicles.

- Lean burn approaches, which involve operating the engine in a lean manner, enhance efficiency and decrease the release of specific emissions [4, 26]. Modifications to the engine can be focused on [7, 77, 85]:
- Material enhancements, as the combustion of H₂ can be detrimental to engine parts. Changes such as reinforced valves and seats, upgraded connecting rods, and altered inlet manifolds are frequently required.
- Elevated voltage ignition, as H₂ needs a more powerful spark to ignite. Therefore, ignition coils with higher voltage might be needed.

- The injectors' design, as they are meant for gaseous fuels, is essential for the efficient delivery of H₂. Additional considerations specific to H₂ include [33, 62, 104, 108, 112]:
- Lubrication plays a crucial role in engines supplied with H₂, as the low lubricity of H₂ can create difficulties. A careful choice of lubricating oils, along with possibly other additives, may be necessary.
- Combustion instabilities, as in H₂ burning, may be susceptible to them. Sophisticated control methods are necessary to ensure consistent and reliable performance.
- H₂ embrittlement, as H₂ may induce it in specific metals. The selection of materials and the design of the engine need to consider this. Improvements in performance can be reached via:
- Turbocharging and supercharging, which can enhance the volume of air drawn into the ICE, boosting power production [23, 34, 99, 135].
- Dual-fuel operation realized by combining H₂ with fuels, like NG to rise efficiency and lower emissions [10, 99].
- Incorporation of nanomaterials into H₂ to enhance thermal conductivity and heat transfer [81].

4. Vehicles with fuel cells (FCs)

Pramuanjaroenkij and Kakaç [82] reported that H₂ can be supplied to fuel cells (FCs) to generate electricity for powering vehicles, resulting in zero greenhouse gas emissions and requiring no direct combustion.

FCs serve as energy-conservation technologies for the 21st century, applicable to mobile, stationary, and especially FC electric vehicles (FCEVs), which are classified as zero-emission vehicles. H₂ FC vehicles, which use hydrogen as a power source, are also referred to as hydrogen electric vehicles or FC electric vehicles. Many individuals mistakenly thought that FCs were batteries; however, FCs

can continuously generate electric power as long as they receive a constant fuel supply. Batteries can supply electrical energy only as long as their stored charge permits; once depleted, they provide no further energy. FCs have been utilized in various applications, including unmanned aerial vehicles (UAVs), unmanned underwater vehicles (UUVs), as well as automobiles, trucks, and buses. Over the past five years, research on FCs has focused on catalysts and membranes, fluid flow fields, motors and converters in FC vehicles, sensors and controls, cooling methods for FCs, machine learning applications, modeling, simulations of FC vehicles, and especially energy management systems within these vehicles.

As noted in [41], the path to widespread acceptance of hydrogen fuel cell vehicles (HFCVs) is fraught with challenges. Central to these issues are the substantial costs associated with vehicle manufacturing and H₂ FC technology, insufficient refueling infrastructure, and concerns regarding the efficiency and environmental impact of H₂ generation. Despite these challenges, technological advancements, economies of scale, and significant investments in research and development (R&D) could help overcome these barriers.

Stakeholder involvement is essential for advancing HFCVs. Car manufacturers such as Toyota, Hyundai, Honda, and Mercedes-Benz are continuously improving their HFCV models, demonstrating strong commitment to this technology. However, a broader transition to HFCVs requires a more comprehensive set of actions and collaborations, including public education initiatives, development of H₂ infrastructure, and funding for research to improve the cost and efficiency of HFCVs.

Government initiatives and policies also play a significant role in the adoption of HFCVs. Governments can promote the development of HFCVs through financial incentives, infrastructure development, clear regulations and standards, and public awareness campaigns. Governments must integrate HFCVs into their broader energy, environment, and economic strategies to ensure balance and consistency. The advancement of HFCVs is closely linked to the broader expansion of the hydrogen economy.

Fang et al. [28] evaluated the current status of fuel-cell electric vehicles (FC-EVs), ongoing research, and the associated challenges and opportunities. Proton-exchange membrane fuel cells (PEMFCs) and solid oxide fuel cells (SOFCs) face significant obstacles to widespread adoption. PEMFC vehicles are challenged mainly by high costs, limited durability, and infrastructure gaps. The reliance on expensive platinum-based catalysts increases production costs, while degradation from catalyst poisoning and membrane failure affects long-term viability. Additionally, the lack of H₂ refueling stations is a significant barrier to the adoption of PEMFC vehicles.

In contrast, SOFCs do not require costly platinum group catalysts; however, SOFC vehicles face challenges related to high operating temperatures, fuel flexibility, system complexity, and stack degradation. Operating at 500–1000°C, SOFCs encounter issues with thermal management and material compatibility. Ensuring efficient operation with various fuel types, optimizing system design, and minimizing stack degradation are crucial for advancing

SOFC technology. Collaborative R&D efforts are crucial for addressing these challenges and accelerating the adoption of both PEMFC and SOFC vehicles as sustainable transportation solutions.

Günaydın et al. [37] compared passenger and commercial H₂ FC vehicles with internal combustion engine (ICE) cars, plug-in hybrid electric vehicles, and battery electric vehicles, focusing on well-to-wheel efficiency, range, fuel consumption, refueling/recharging time, emissions, and vehicle costs. They found that while battery electric vehicles (BEVs) lead the passenger vehicle market due to lower costs and expanding infrastructure, HFCVs are well-suited for commercial vehicles, offering fast refueling and long range. The transition to HFCVs faces hurdles, including limited infrastructure compared to gasoline and electric systems, as well as the higher cost of hydrogen production relative to gasoline and electricity, both of which must be addressed for widespread adoption. The increasing use of renewable energy may reduce electricity costs for electrolysis, thereby lowering overall hydrogen production costs and facilitating the generation of green hydrogen. Recent years have seen significant growth in hydrogen infrastructure and electrolysis capacity worldwide, particularly in Asia-Pacific countries. Enhanced government incentives and investments, along with financial support for consumers and manufacturers, are vital for increasing HFCV adoption. Additionally, R&D efforts are crucial for advancing hydrogen infrastructure and production technologies.

Baba et al. [8] examined the use of FCs and energy management in hybrid vehicles. FC vehicles offer significant advantages over battery-electric vehicles in terms of range, energy efficiency, charging time, and adaptability to different climates. The classification and a brief overview of HEVs/FCs are provided, followed by a summary of FC HEVs that illustrate various hybrid vehicle configurations.

Topological categorization

Hybridization refers to the integration of two energy sources and one propulsion type, or two types of propulsion. In HEVs, this means combining electric and thermal propulsion. In FCEVs, the system starts with the battery supplying energy to the DC bus [63]. The DCU maintains steady bus voltage and delivers propulsion energy to the motor drive converter. The DC/AC converter controls motor speed and torque, and the motors convert electrical energy into kinetic energy [80].

- 1) Complete FCEV framework: The FC stack serves as the sole energy source, comprising a DC-DC converter, fuel tank, FC stack, inverter, and electric motor [40], which provides high efficiency, a simple design, system reliability, and a user-friendly driving experience [40].
- 2) FC + Battery integration: This design includes a unidirectional DC-DC converter (UDC) connected to the storage system and an inverter directly linked to the motor. The storage system provides the high current needed for engine startup [40, 91].
- 3) FC + Ultracapacitor (UC) hybridization: This configuration utilizes an ultracapacitor to extend the life of the storage system, but its low energy density limits its application to short-term use [90].

- 4) FC + (Battery + UC) hybridization: This setup includes an FC connected to the DC bus, with two DC-DC converters (one unidirectional and one bidirectional) located between the FC and the capacitor [80, 90].
- 5) FC + battery + PV hybridization: A hybrid system combining FC, battery, and photovoltaic (PV) sources, with the storage system linked to the DC bus via a bidirectional converter. PV power depends on solar radiation and temperature [73].

Such topologies were presented in Fig. 1.

According to Voelckner [123], since 2015, three H₂-fueled vehicles have been available for purchase from major automakers: the Honda Clarity FC, Hyundai Nexo SUV, and Toyota Mirai. However, Honda has discontinued all Clarity models. Hyundai has sold only about 1600 Nexo SUVs in six years, and Toyota has sold approximately 14,300 Mirai sedans in the U.S. over two generations, sometimes relying on substantial discounts to boost sales. In 2025, Honda will launch the CR-Ve: FCEV, an improved compact crossover with a hydrogen FC (co-developed with GM) and a larger battery for plug-in charging, offering 29 miles of electric range and 241 miles from the FC. It will be available for lease in California only, with an expected annual volume of 300 vehicles.

According to [127], there are two main types of pure electric vehicles using FCs as their primary electricity source: FC electric vehicles (FCEVs) and FC hybrid electric vehicles (FCHEVs). The primary challenges in FC electric mobility include low FC efficiency, cold start issues, difficulties with hydrogen storage, the need for cost reduction, safety risks, and traction system problems.

Waseem et al. [128] noted that energy storage for electric vehicles can be achieved using various technologies, including lithium-ion batteries (LIBs), lead-acid batteries (LABs), solid-state batteries (SSBs), FCs, and ultracapacitors (UCs).

Samuel et al. [92] analyzed a hydrogen FC vehicle based on the Toyota Mirai and confirmed its fuel efficiency using real-world test data. This validated model was used to calculate fuel efficiency for actual driving cycles recorded in Mexico City in 2019, encompassing three distinct drive cycles that accurately reflect real urban driving conditions.

On February 28, 2024, at the 16th Expo Foro Movilidad in Mexico, FOTON unveiled the HC12 hydrogen fuel cell bus, the first hydrogen FC bus in Mexico. The HC12 features a 120 kW fuel cell engine and a 35 MPa hydrogen system, offering a range of up to 550 km (400 km from hydrogen, 150 km from electricity). It is emission-free, environmentally adaptable, highly safe, and fuel-efficient, making it ideal for medium- to long-distance transport, luxury tourism, and group services [30].

Thanks to hydrogen technology and larger, lightweight hydrogen tanks totaling 51.2 kg, the Solaris Urbino 18 H₂ bus excels on long routes. The BALLARD FCmove HD+ FCs, rated at 100 kW, achieve 57% efficiency and can operate for over 30,000 hours between -25°C and +50°C. The bus is powered by a 240 kW motor, delivering 1470 Nm of continuous torque and 2100 Nm peak torque [100]. Such buses have been tested in Brasov, Romania, and can be refueled in 5–10 minutes, offering a range of around 350

km. The cost is approximately EUR 700,000, which is about EUR 100,000 more than the electric model. The Solaris hydrogen bus has also been tested in Cluj-Napoca and Târgu Mureș [46].

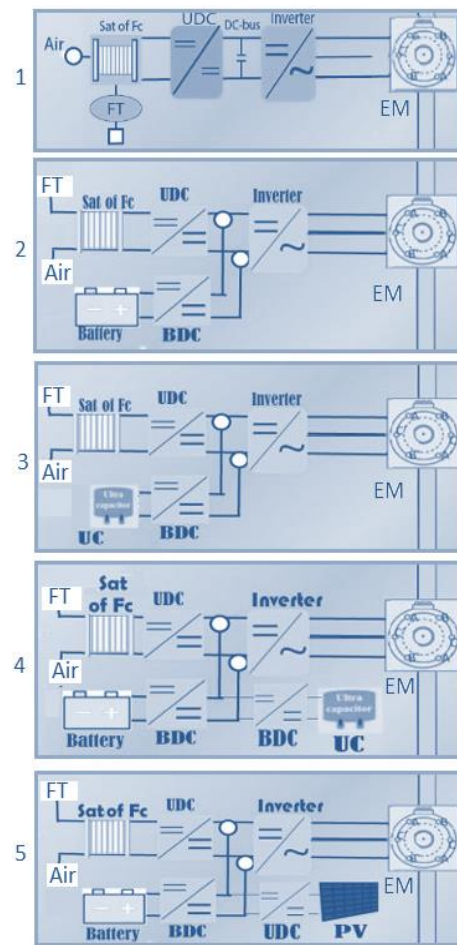


Fig. 1. Topologies of vehicles with fuel cells (FCs): 1 – The complete FCEV framework, 2 – The FC design + Battery integration, 3 – The FC arrangement + UC hybridization, 4 – The FC + (Battery + UC hybridization) set, 5 – The FC arrangement + Battery + PV hybridization arrangement

Currently, two major technical challenges for H₂ FCs are the high cost of catalysts and the frequent replacement of membrane materials that do not meet durability requirements [136]. According to [20], dynamic loading and FC costs are the main barriers to the successful commercialization of FCEVs and FCHEVs.

Issues related to hydrogen transportation can be addressed with innovative storage materials that are lightweight, strong, cost-effective, and suitable for long-distance, high-capacity delivery. For example, Zhang Jinying's team at Xi'an Jiaotong University utilized graphene for hydrogen storage, addressing challenges related to storage and transport. By using NaH or LiH as raw materials and controlling the encapsulation area of graphene, they achieved stable hydrogen release via interfacial nanovalue control [56]. Using NaH or LiH as fuel allows for higher hydrogen storage density and is suitable for other gases as well. These materials offer strong chemical stability and mechanical strength, making them suitable for high-

temperature applications and emergency power for vehicles, drones, and semi-mobile devices [56].

Proton exchange membranes are essential for all types of H₂ FCs, but are very expensive. The widely used RSO₃H (R = organic group) Nafion membrane, produced by DuPont, has a high cost and limited ion transport, which raises the price of H₂ FC vehicles. The catalysts used are also extremely expensive, costing twice as much as gold, further limiting the advancement of H₂ FCs [136].

Brzeżański et al. [17] conducted initial tests, approximately 2.5 hours in duration, on the Toyota Mirai FC powertrain in a thermoclimatic chamber at temperatures ranging from –10°C to –18°C, simulating winter conditions in temperate climates. They found that the operating principles and methods of the FC power unit differ significantly from those of combustion engines. Since climate conditions greatly affect FC performance, testing in a thermoclimatic chamber was necessary. During the tests, the drive system and electrical components were covered with condensed water, but no operational disruptions were observed.

Pielecha et al. [79] examined a Toyota Mirai model with a FC hybrid system (see Table 3), which shares many design features with hybrid cars. Innovative FC technologies were implemented, including compressed hydrogen tanks and advanced control systems. The study analyzed FC operation during ignition and driving, focusing on the hydrogen injection method of the three fuel injectors. The relationship between the FC and the high-voltage battery was also examined. It was demonstrated that increasing the electric motor's supply voltage at high torque levels results in a threefold voltage gain (up to approximately 650 V), doubling the drive system's torque compared to standard values.

Table 3. Toyota Mirai vehicle drive system characteristics [115]

Parameter		Value
Vehicle	mass	1850 kg
	maximum speed	179 km/h
Vehicle range	type approval cycle	approx. 550 km (NEDC test)
FC	type	PEM (polymer electrolyte)
	power	114 kW
	power density	2.0 kW/kg; 3.1 kW/dm ³
	cell number	370
Electric motor	humidification	internal circulation
	type	synchronous AC
	maximum power	113 kW
	maximum torque	335 N·m
Battery	type	NiMH
H ₂ storage	volume of tanks	front – 60 dm ³ , back – 62.4 dm ³
	pressure/mass	70 MPa/5 kg H ₂
Refueling	time	3 min

Małek [61] reported that the method of supplying fuel to the FC cathode significantly affects the durability and efficiency of hydrogen energy conversion. FCs are inherently variable systems. The researchers studied a Nexa FC module (1.2 kW net output). To control the pump's airflow, a master-slave regulator was designed, featuring a sub-

regulator that works in conjunction with a brushless motor speed controller to adjust the airflow. A separate brushless motor was connected to the main regulator output. This approach allowed testing of different airflow regulation techniques independently of the initial controller's protocols. Airflow regulation of the PEM FC enabled identification and maintenance of the peak net power output of the FC stack, regardless of variations in controlled object parameters and external conditions. Adaptive extremum control with bi-factor assessment enabled automatic adjustment of controller parameters in response to changing system characteristics, improving both the value and speed of finding the optimum operating point.

While the development and market introduction of FC electric vehicles are progressing rapidly, several challenges remain for their practical application in vehicles, limiting the widespread adoption of FC technology in automotive powertrains. The main issues are [101]:

- Limited flexibility in power flow control in PEMFC + battery systems
- Significant power flow losses in PEMFC + battery + ultracapacitor configurations, complicating energy management
- Low battery power density results in larger, more expensive battery systems and increased vehicle mass.

5. Summary

Several mechanisms describing H₂ combustion have been developed recently, exhibiting varying degrees of complexity and accuracy. Further studies are needed to facilitate the incorporation of such mechanisms into AI-based modeling of H₂ combustion and control algorithms for real applications, including internal combustion engines (ICEs).

Future research might focus on increasing H₂ production from renewable sources, investigating novel materials or production techniques that reduce the costs of fuel cells (FCs) and H₂ generation, improving storage and distribution methods, and advancing materials science to lower FC costs. Additionally, it is crucial to perform a life-cycle assessment of hydrogen fuel cell vehicles (HFCVs), especially focusing on the recycling or disposal of proton exchange membrane (PEM) materials, the long-term environmental benefits and trade-offs, and the potential for partnerships among governments, industry stakeholders, and academia to address ongoing technical and economic challenges.

The growth of the market for H₂ internal combustion engine (H₂ICE) vehicles heavily depends on advancements in H₂ infrastructure and the establishment of appropriate legal regulations. Further studies are needed for H₂ engines, particularly focusing on the development of exhaust gas treatment technologies to reduce NO_x emissions.

Fuel cell vehicles (FCVs) can reduce emissions and provide a clean energy alternative to gasoline-powered cars. However, their development depends on the availability of H₂ fuel and the expansion of refueling infrastructure.

Nomenclature

A/F	air-fuel	FI	fuel injection
BSFC	brake specific fuel consumption	HEV	hybrid electric vehicle
CI	compression ignition	ICE	internal combustion engine
CNG	compressed natural gas	NG	natural gas
CR	compression ratio	PFI	port fuel injection
DI	direct injection	SI	spark ignition
FC	fuel cell		

Bibliography

- [1] Abele AR. Quantum hydrogen storage systems, Sacramento, CA 2006.
- [2] Ahmed SS, Mauß F, Moréac G, Zeuch T. A comprehensive and compact n-heptane oxidation model derived using chemical lumping. *Phys Chem Chem Phys*. 2007;9:1107-1126. <https://doi.org/10.1039/B614712G>
- [3] Aldajah S, Ajayi OO, Fenske GR, Goldblatt IL. Effect of exhaust gas recirculation (EGR) contamination of diesel engine oil on wear. *Wear*. 2007;263:93-98. <https://doi.org/10.1016/j.wear.2006.12.055>
- [4] Alrazen HA, Abu Talib AR, Adnan R, Ahmad KA. A review of the effect of hydrogen addition on the performance and emissions of the compression – Ignition engine. *Renew Sustain Energy Rev*. 2016;54:785-796. <https://doi.org/10.1016/j.rser.2015.10.088>
- [5] Altinay G, Macdonald RG. Determination of the rate constant for the $\text{OH}(\text{X}^2 \text{Pi}) + \text{OH}(\text{X}^2 \text{Pi}) \rightarrow \text{H}_2\text{O} + \text{O}(\text{P})$ reaction over the temperature range 295 to 701 K. *J Phys Chem A*. 2014;118:38-54. <https://doi.org/10.1021/jp409344q>
- [6] Aritra C, Suhail D, Bijan KM. Combustion performance and emission characteristics of hydrogen as an internal combustion engine fuel. *J Aeronaut Automot Eng JAAE*. 2014;1:1-6.
- [7] Ayissi MZ, Newen IA, Alloune R, Bitondo D. Effects of gasoline and hydrogen blends on exhaust gas emissions and fuel consumption from gasoline internal combustion engines. *J Combust*. 2022;2022:1-10. <https://doi.org/10.1155/2022/5526205>
- [8] Baba MA, Labbadi M, Cherkaoui M, Maaroufi M. Fuel cell electric vehicles: a review of current power electronic converters topologies and technical challenges. *IOP Conf Ser Earth Environ Sci*. 2021;785:012011. <https://doi.org/10.1088/1755-1315/785/1/012011>
- [9] Bajerlein M, Bor M, Karpiuk W, Smolec R, Spadło M. Strength analysis of critical components of high-pressure fuel pump with hypocycloid drive. *Bull Pol Acad Sci Tech Sci*. 2020;1341-1350. <https://doi.org/10.24425/bpasts.2020.135380>
- [10] Bakar RA, Widudo, Kadirgama K, Ramasamy D, Yusaf T, Kamarulzaman MK et al. Experimental analysis on the performance, combustion/emission characteristics of a DI diesel engine using hydrogen in dual fuel mode. *Int J Hydrog Energy*. 2024;52:843-860. <https://doi.org/10.1016/j.ijhydene.2022.04.129>
- [11] Bao L, Sun B, Luo Q, Li J, Qian D, Ma H et al. Development of a turbocharged direct-injection hydrogen engine to achieve clean, efficient, and high-power performance. *Fuel*. 2022;324:124713. <https://doi.org/10.1016/j.fuel.2022.124713>
- [12] Bor M, Borowczyk T, Idzior M, Karpiuk W, Smolec R. Analysis of hypocycloid drive application in a high-pressure fuel pump. *MATEC Web Conf*. 2017;118:00020. <https://doi.org/10.1051/mateconf/201711800020>
- [13] Bor M, Borowczyk T, Karpiuk W, Smolec R. Determination of the response time of new generation electromagnetic injectors as a function of fuel pressure using the internal photoelectric effect. 2018 Int. Interdiscip. PhD Workshop IIPhDW, Swinoujście: IEEE; 2018. <https://doi.org/10.1109/iiphdw.2018.8388385>
- [14] Brzeżański M, Papuga T, Rodak Ł. Analysis of creation and combustion process of hydrogen-air mixtures by optical method in isochoric chamber. *Combustion Engines*. 2017; 170:121-125. <https://doi.org/10.19206/CE-2017-320>
- [15] Brzeżański M, Rodak Ł. Investigation of a new concept of hydrogen supply for a spark-ignition engine. *Combust Engines*. 2019;178:140-143. <https://doi.org/10.19206/CE-2019-324>
- [16] Brzeżański M, Rodak Ł. Influence of the method of creating a hydrogen-air mixture on the emission of nitrogen oxides in a spark-ignition engine. *Combustion Engines*. 2019;178: 224-227. <https://doi.org/10.19206/CE-2019-339>
- [17] Brzeżański M, Szałek A, Szramowiat M. Tests of the vehicle's power unit with fuel cells at a reduced ambient temperature. *Combustion Engines*. 2019;179:65-69. <https://doi.org/10.19206/CE-2019-410>
- [18] Burke MP, Chaos M, Ju Y, Dryer FL, Klippenstein SJ. Comprehensive H_2/O_2 kinetic model for high-pressure combustion. *Int J Chem Kinet*. 2012;44:444-474. <https://doi.org/10.1002/kin.20603>
- [19] Burke MP, Klippenstein SJ. Ephemeral collision complexes mediate chemically termolecular transformations that affect system chemistry. *Nat Chem*. 2017;9:1078-1082. <https://doi.org/10.1038/nchem.2842>
- [20] Chandran M, Palanisamy K, Benson D, Sundaram S. A review on electric and fuel cell vehicle anatomy, technology evolution and policy drivers towards EVs and FCEVs market propagation. *Chem Rec*. 2022;22:e202100235. <https://doi.org/10.1002/tcr.202100235>
- [21] Combustion Research Group. The San Diego Mechanism: chemical kinetic mechanisms for combustion applications. 2014.
- [22] Dagaut P, Lecomte F, Mieritz J, Glarborg P. Experimental and kinetic modeling study of the effect of NO and SO_2 on the oxidation of CO/H_2 mixtures. *Int J Chem Kinet*. 2003; 35:564-575. <https://doi.org/10.1002/kin.10154>
- [23] Das LM. Hydrogen engines: design, performance evaluation, combustion analysis, and exhaust emissions. 1st ed. Newark: John Wiley & Sons, Incorporated; 2025.
- [24] Daszkiewicz P, Kołodziejek D. Comparison and analysis of modern combustion powertrain systems of rail vehicles. *Combustion Engines*. 2024;196:46-53. <https://doi.org/10.19206/CE-171385>
- [25] Davis SG, Joshi AV, Wang H, Egolfopoulos F. An optimized kinetic model of H_2/CO combustion. *Proc Combust Inst*. 2005;30:1283-1292. <https://doi.org/10.1016/j.proci.2004.08.252>
- [26] Davy M, Evans RL, Mezo A. The ultra lean burn partially stratified charge natural gas engine. *SAE Technical Paper* 2009-24-0115. 2009. <https://doi.org/10.4271/2009-24-0115>

- [27] Escalante Soberanis MA, Fernandez AM. A review on the technical adaptations for internal combustion engines to operate with gas/hydrogen mixtures. *Int J Hydrog Energy*. 2010;35:12134-12140. <https://doi.org/10.1016/j.ijhydene.2009.09.070>
- [28] Fang T, Vairin C, Von Jouanne A, Agamloh E, Yokochi A. Review of fuel-cell electric vehicles. *Energies*. 2024;17:2160. <https://doi.org/10.3390/en17092160>
- [29] Fiore M, Magi V, Viggiano A. Internal combustion engines powered by syngas: a review. *Appl Energy*. 2020;276:115415. <https://doi.org/10.1016/j.apenergy.2020.115415>
- [30] FotonMotor. The first hydrogen fuel cell bus in Mexico originated from Foton 2024. <https://www.fotonmotor.com/newsDetaila799d935.html>
- [31] Fu Z, Li Y, Wu W, Li Y, Gao W. Experimental study on the combustion and emission performance of the hydrogen direct injection engine. *Int J Hydrog Energy*. 2024;61:1047-1059. <https://doi.org/10.1016/j.ijhydene.2024.02.276>
- [32] Gao J, Wang X, Song P, Tian G, Ma C. Review of the backfire occurrences and control strategies for port hydrogen injection internal combustion engines. *Fuel*. 2022;307:121553. <https://doi.org/10.1016/j.fuel.2021.121553>
- [33] Gao N, Geng Z, Zhao W, Geng L, Dong F, Huang D. Review on the combustion and emission characteristics of hydrogen engine. *Int J Hydrog Energy*. 2025;143:121-146. <https://doi.org/10.1016/j.ijhydene.2025.05.321>
- [34] Gao W, Fu Z, Li Y, Li Y, Zou J. Progress of performance, emission, and technical measures of hydrogen fuel internal combustion engines. *Energies*. 2022;15:7401. <https://doi.org/10.3390/en15197401>
- [35] Gharehghani A, Hosseini R, Mirsalim M, Yusaf TF. A computational study of operating range extension in a natural gas SI engine with the use of hydrogen. *Int J Hydrog Energy*. 2015;40:5966-5975. <https://doi.org/10.1016/j.ijhydene.2015.03.015>
- [36] Gis M, Gis W. The current state and prospects for hydrogenisation of motor transport in Northwestern Europe and Poland. *Combustion Engines*. 2022;190(3):61-71. <https://doi.org/10.19206/CE-144560>
- [37] Günaydin ÖF, Topçu S, Aksoy A. Hydrogen fuel cell vehicles: Overview and current status of hydrogen mobility. *Int J Hydrog Energy*. 2025;S0360319925004562. <https://doi.org/10.1016/j.ijhydene.2025.01.412>
- [38] Habib MA, Abdulrahman GAQ, Alqaity ABS, Qasem NAA. Hydrogen combustion, production, and applications: A review. *Alex Eng J*. 2024;100:182-207. <https://doi.org/10.1016/j.aej.2024.05.030>
- [39] Hagos FY, Aziz ARA, Sulaiman SA. Trends of syngas as a fuel in internal combustion engines. *Adv Mech Eng*. 2014;6:401587. <https://doi.org/10.1155/2014/401587>
- [40] Hames Y, Kaya K, Baltacioglu E, Turksoy A. Analysis of the control strategies for fuel saving in the hydrogen fuel cell vehicles. *Int J Hydrog Energy*. 2018;43:10810-10821. <https://doi.org/10.1016/j.ijhydene.2017.12.150>
- [41] Hassan Q, Azzawi IDJ, Sameen AZ, Salman HM. Hydrogen fuel cell vehicles: opportunities and challenges. *Sustainability*. 2023;15:11501. <https://doi.org/10.3390/su151511501>
- [42] Healy D, Kalitan DM, Aul CJ, Petersen EL, Bourque G, Curran HJ. Oxidation of C1–C5 alkane quaternary natural gas mixtures at high pressures. *Energy Fuels*. 2010;24:1521-1528. <https://doi.org/10.1021/ef9011005>
- [43] Heller K, Ellgas S. Optimization of hydrogen internal combustion engine with cryogenic mixture formation. Graz, Austria: 2006, 49-58.
- [44] Hong Z, Cook RD, Davidson DF, Hanson RK. A shock tube study of $\text{OH} + \text{H}_2\text{O}_2 \rightarrow \text{H}_2\text{O} + \text{HO}_2$ and $\text{H}_2\text{O}_2 + \text{M} \rightarrow 2\text{OH} + \text{M}$ using laser absorption of H_2O and OH . *J Phys Chem A*. 2010;114:5718-5727. <https://doi.org/10.1021/jp100204z>
- [45] Hong Z, Davidson DF, Hanson RK. An improved H_2/O_2 mechanism based on recent shock tube/laser absorption measurements. *Combust Flame*. 2011;158:633-644. <https://doi.org/10.1016/j.combustflame.2010.10.002>
- [46] Hydrogen Central. Hydrogen bus tested on the streets of Romania 2021. <https://hydrogen-central.com/hydrogen-bus-romania/>
- [47] Jasper AW, Kamarchik E, Miller JA, Klippenstein SJ. First-principles binary diffusion coefficients for H, H_2 , and four normal alkanes + N_2 . *J Chem Phys*. 2014;141:124313. <https://doi.org/10.1063/1.4896368>
- [48] Jasper AW, Miller JA. Lennard-Jones parameters for combustion and chemical kinetics modeling from full-dimensional intermolecular potentials. *Combust Flame*. 2014;161:101-110. <https://doi.org/10.1016/j.combustflame.2013.08.004>
- [49] Kéromnès A, Metcalfe WK, Heufer KA, Donohoe N, Das AK, Sung C-J et al. An experimental and detailed chemical kinetic modeling study of hydrogen and syngas mixture oxidation at elevated pressures. *Combust Flame*. 2013;160:995-1011. <https://doi.org/10.1016/j.combustflame.2013.01.001>
- [50] Kim J, Chun KM, Song S, Baek H-K, Lee SW. The effects of hydrogen on the combustion, performance and emissions of a turbo gasoline direct-injection engine with exhaust gas recirculation. *Int J Hydrog Energy*. 2017;42:25074-25087. <https://doi.org/10.1016/j.ijhydene.2017.08.097>
- [51] Klippenstein SJ. From theoretical reaction dynamics to chemical modeling of combustion. *Proc Combust Inst*. 2017;36:77-111. <https://doi.org/10.1016/j.proci.2016.07.100>
- [52] Konnov AA. Remaining uncertainties in the kinetic mechanism of hydrogen combustion. *Combust Flame*. 2008;152:507-528. <https://doi.org/10.1016/j.combustflame.2007.10.024>
- [53] Konnov AA. On the role of excited species in hydrogen combustion. *Combust Flame*. 2015;162:3755-3772. <https://doi.org/10.1016/j.combustflame.2015.07.014>
- [54] Konnov AA. Yet another kinetic mechanism for hydrogen combustion. *Combust Flame*. 2019;203:14-22. <https://doi.org/10.1016/j.combustflame.2019.01.032>
- [55] Kovar Z, Scholz C, Beroun S, Nydrle M, Drozda H, Blazek J et al. Hydrogen piston engines: R&D, experiences. *Combustion Engines*. 2006;125:28-36. <https://doi.org/10.19206/CE-117350>
- [56] Lamb KE, Webb CJ. A quantitative review of slurries for hydrogen storage – slush hydrogen, and metal and chemical hydrides in carrier liquids. *J Alloys Compd*. 2022;906:164235. <https://doi.org/10.1016/j.jallcom.2022.164235>
- [57] Lee S, Kim G, Bae C. Effect of mixture formation mode on the combustion and emission characteristics in a hydrogen direct-injection engine under different load conditions. *Appl Therm Eng*. 2022;209:118276. <https://doi.org/10.1016/j.applthermaleng.2022.118276>
- [58] Li J, Zhao Z, Kazakov A, Chaos M, Dryer FL, Scire JJ. A comprehensive kinetic mechanism for CO , CH_2O , and CH_3OH combustion. *Int J Chem Kinet*. 2007;39:109-136. <https://doi.org/10.1002/kin.20218>
- [59] Li J, Zhao Z, Kazakov A, Dryer FL. An updated comprehensive kinetic model of hydrogen combustion. *Int J Chem Kinet*. 2004;36:566-575. <https://doi.org/10.1002/kin.20026>
- [60] Liu X, Liu F, Zhou L, Sun B, Schock H. Backfire prediction in a manifold injection hydrogen internal combustion engine. *Int J Hydrog Energy*. 2008;33:3847-3855. <https://doi.org/10.1016/j.ijhydene.2008.04.051>

- [61] Małek A. Adaptive search for a PEM fuel cell maximum net power. *Combustion Engines*. 2011;145:49-57. <https://doi.org/10.19206/CE-117101>
- [62] Manigandan S, Ryu JI, Praveen Kumar TR, Elgendi M. Hydrogen and ammonia as a primary fuel – a critical review of production technologies, diesel engine applications, and challenges. *Fuel*. 2023;352:129100. <https://doi.org/10.1016/j.fuel.2023.129100>
- [63] Marei MI, Lambert S, Pick R, Salama MMA. DC/DC converters for fuel cell powered hybrid electric vehicle. 2005 IEEE Veh. Power Propuls. Conf., Chicago, USA. 2005: 556-559. <https://doi.org/10.1109/VPPC.2005.1554614>
- [64] Masood M, Mehdi SN, Ram Reddy P. Experimental investigations on a hydrogen-diesel dual fuel engine at different compression ratios. *J Eng Gas Turbines Power*. 2007;129: 572-578. <https://doi.org/10.1115/1.2227418>
- [65] Matla J. Possible applications of prechambers in hydrogen internal combustion engines. *Combustion Engines*. 2022; 191(4):77-82. <https://doi.org/10.19206/CE-148170>
- [66] Matla J, Kaźmierczak A, Haller P, Trocki M. Hydrogen as a fuel for spark ignition combustion engines – state of knowledge and concept. *Combustion Engines*. 2024;196:73-79. <https://doi.org/10.19206/CE-171541>
- [67] Meisner J, Kästner J. Reaction rates and kinetic isotope effects of $H_2 + OH \rightarrow H_2O + H$. *J Chem Phys*. 2016;144: 174303. <https://doi.org/10.1063/1.4948319>
- [68] Menes M. Program initiatives of public authorities in the field of hydrogenation of the economy in a global perspective, as of the end of 2020. *Combustion Engines*. 2022;189: 18-29. <https://doi.org/10.19206/CE-142170>
- [69] Mitianiec W. Modelling and simulation of working processes in Wankel engine with direct hydrogen injection system. *Combustion Engines*. 2015;161:42-52. <https://doi.org/10.19206/CE-116890>
- [70] Muraki H, Zhang G. Design of advanced automotive exhaust catalysts. *Catal Today*. 2000;63:337-345. [https://doi.org/10.1016/S0920-5861\(00\)00477-6](https://doi.org/10.1016/S0920-5861(00)00477-6)
- [71] Musy F, Ortiz R, Ortiz I, Ortiz A. Hydrogen-fuelled internal combustion engines: direct injection versus port-fuel injection. *Int J Hydrog Energy*. 2024;S0360319924028106. <https://doi.org/10.1016/j.ijhydene.2024.07.136>
- [72] Nguyen TL, Stanton JF. Ab Initio thermal rate calculations of $HO + HO = O(^3P) + H_2O$ reaction and isotopologues. *J Phys Chem A*. 2013;117:2678-2686. <https://doi.org/10.1021/jp312246q>
- [73] Nguyen V-L. Couplage des systèmes photovoltaïques et des véhicules électriques au réseau: problèmes et solutions. Université de Grenoble, 2014.
- [74] Nieścioruk MJ, Bandrow P, Szufa S, Woźniak M, Siczek K. Biomass-based hydrogen extraction and accompanying hazards–review. *Molecules*. 2025;30:565. <https://doi.org/10.3390/molecules30030565>
- [75] Ó Conaire M, Curran HJ, Simmie JM, Pitz WJ, Westbrook CK. A comprehensive modeling study of hydrogen oxidation. *Int J Chem Kinet*. 2004;36:603-622. <https://doi.org/10.1002/kin.20036>
- [76] Olm C, Zsély IGY, Pálvölgyi R, Varga T, Nagy T, Curran HJ, et al. Comparison of the performance of several recent hydrogen combustion mechanisms. *Combust Flame*. 2014; 161:2219-2234. <https://doi.org/10.1016/j.combustflame.2014.03.006>
- [77] Paluch M, Noga M. Influence of hydrogen addition on performance and ecological parameters of a spark-ignition internal combustion engine at part load typical for urban traffic. *Adv Sci Technol Res J*. 2025;19:262-270. <https://doi.org/10.12913/22998624/199738>
- [78] Paykani A, Chehrmonavari H, Tsolakis A, Alger T, Northrop WF, Reitz RD. Synthesis gas as a fuel for internal combustion engines in transportation. *Prog Energy Combust Sci*. 2022;90:100995. <https://doi.org/10.1016/j.pecs.2022.100995>
- [79] Pielecha I, Cieślík W, Szałek A. The use of electric drive in urban driving conditions using a hydrogen powered vehicle – Toyota Mirai. *Combustion Engines*. 2018;172:51-58. <https://doi.org/10.19206/CE-2018-106>
- [80] Pires VF, Cordeiro A, Foito D, Silva JF. High step-up DC–DC converter for fuel cell vehicles based on merged quadratic boost–čuk. *IEEE Trans Veh Technol*. 2019;68:7521-7530. <https://doi.org/10.1109/TVT.2019.2921851>
- [81] Polat F, Sarıdemir S, Gad MS, El-Shafay AS, Ağbulut Ü. Enhancing diesel engine performance, combustion, and emissions reductions under the effect of cerium oxide nanoparticles with hydrogen addition to biodiesel fuel. *Int J Hydrog Energy*. 2024;83:884-896. <https://doi.org/10.1016/j.ijhydene.2024.08.031>
- [82] Pramanjaroenkij A, Kakaç S. The fuel cell electric vehicles: the highlight review. *Int J Hydrog Energy*. 2023;48: 9401-9425. <https://doi.org/10.1016/j.ijhydene.2022.11.103>
- [83] Prechtl P, Dorer F. Wasserstoff-Dieselmotor mit Direkteinspritzung, hoher Leistungsdichte und geringer Abgasemission: Teil 2: Untersuchung der Gemischbildung, des Zünd- und des Verbrennungsverhaltens. *MTZ – Mot Z*. 1999;60: 830-837. <https://doi.org/10.1007/BF03226544>
- [84] Premkartikkumar SR, Annamalai K, Pradeepkumar AR. Using hydrogen as a fuel in automotive engines – an investigation. *IJITR Int J Innov Technol Res*. 2013;1:90-93.
- [85] Rameez PV, Mohamed Ibrahim M. A comprehensive review on the utilization of hydrogen in low temperature combustion strategies: combustion, performance and emission attributes. *J Energy Inst*. 2024;113:101511. <https://doi.org/10.1016/j.joei.2023.101511>
- [86] Rasmussen CL, Hansen J, Marshall P, Glarborg P. Experimental measurements and kinetic modeling of $CO/H_2/O_2/NO_x$ conversion at high pressure. *Int J Chem Kinet*. 2008; 40:454-480. <https://doi.org/10.1002/kin.20327>
- [87] RenaultGroup. The Renault Master Van H2-Tech, a hydrogen-powered utility vehicle 2022. <https://www.renaultgroup.com/en/magazine/energy-and-motorization/everything-there-is-to-know-about-hydrogen-vehicles>
- [88] Rottengruber H, Wiebicke U, Woschni G, Zeilinger K. Wasserstoff-Dieselmotor mit Direkteinspritzung, hoher Leistungsdichte und geringer Abgasemission: Teil 3: Versuche und Berechnungen am Motor. *MTZ – Mot Z*. 2000;61:122-128. <https://doi.org/10.1007/BF03226557>
- [89] Rutkowska-Gorczyca MJ, Dziubek M, Wiśniewski M. Response of hydrogen charging diffusion of the austenitic stainless steel AISI 310s. *Combustion Engines*. 2024;198: 68-73. <https://doi.org/10.19206/CE-186591>
- [90] Sadoun R. Intérêt d'une Source d'Energie Electrique Hybride pour véhicule électrique urbain– dimensionnement et tests de cyclage. Ecole Centrale de Lille, 2013.
- [91] Sakka MA, Van Mierlo J, Gualous H, Lataire P. Comparison of 30KW DC/DC converter topologies interfaces for fuel cell in hybrid electric vehicle, Barcelona, Spain: 2009, p. 1–10.
- [92] Samuel S, Gonzalez-Oropeza R, Cedillo Cornejo E. Hydrogen fuel cell vehicle for Mexico City. 2020. SAE Technical Paper 2020-01-1169. 2020. <https://doi.org/10.4271/2020-01-1169>
- [93] Sangwan M, Krasnoperov LN. Disproportionation channel of self-reaction of hydroxyl radical, $OH + OH \rightarrow H_2O + O$,

- studied by time-resolved oxygen atom trapping. *J Phys Chem A*. 2012;116:11817-11822. <https://doi.org/10.1021/jp308885j>
- [94] Saxena P, Williams FA. Testing a small detailed chemical-kinetic mechanism for the combustion of hydrogen and carbon monoxide. *Combust Flame*. 2006;145:316-323. <https://doi.org/10.1016/j.combustflame.2005.10.004>
- [95] Shahpouri S, Gordon D, Hayduk C, Rezaei R, Koch CR, Shahbakhti M. Hybrid emission and combustion modeling of hydrogen fueled engines. *Int J Hydrog Energy*. 2023;48:24037-24053. <https://doi.org/10.1016/j.ijhydene.2023.03.153>
- [96] Shi C, Ji C, Ge Y, Wang S, Yang J, Wang H. Effects of split direct-injected hydrogen strategies on combustion and emissions performance of a small-scale rotary engine. *Energy*. 2021;215:119124. <https://doi.org/10.1016/j.energy.2020.119124>
- [97] Shinde BJ, K. K. Recent progress in hydrogen fuelled internal combustion engine (H2ICE) – a comprehensive outlook. *Mater Today Proc*. 2022;51:1568-1579. <https://doi.org/10.1016/j.matpr.2021.10.378>
- [98] Sikora M, Orliński P. Hydrotreated vegetable oil fuel within the Fit for 55 package. *Combustion Engines*. 2024;197(2):3-8. <https://doi.org/10.19206/CE-174554>
- [99] Skobiej K. A review of hydrogen combustion and its impact on engine performance and emissions. *Combustion Engines*. 2025;200(1):64-70. <https://doi.org/10.19206/CE-195470>
- [100] Solaris Bus & Coach. Solaris Urbino 18 hydrogen 2025. https://www.solarisbus.com/public/assets/content/firma/onas/nowy_profil_firmy/Urbino_18_hydrogen_EN.pdf?_gl=1*_1ufe3y8*_up*MQ.*_ga*MTg1MjI5OTcxMy4xNzQ0NjMzNDc4*_ga_JKWEFR8KTK*MTc0NDYzMzQ3Ny4xLjAuMTc0NDYzMzQ3Ny4wLjAuMA
- [101] Sorlei I-S, Bizon N, Thounthong P, Varlam M, Carcadea E, Culcer M et al. Fuel cell electric vehicles—a brief review of current topologies and energy management strategies. *Energies*. 2021;14:252. <https://doi.org/10.3390/en14010252>
- [102] Starik AM, Titova NS, Sharipov AS, Kozlov VE. Syngas oxidation mechanism. *Combust Explos Shock Waves*. 2010;46:491-506. <https://doi.org/10.1007/s10573-010-0065-x>
- [103] Stepien Z. A comprehensive overview of hydrogen-fueled internal combustion engines: achievements and future challenges. *Energies*. 2021;14:6504. <https://doi.org/10.3390/en14206504>
- [104] Stepien Z. Analysis of the prospects for hydrogen-fueled internal combustion engines. *Combustion Engines*. 2024;197(2):32-41. <https://doi.org/10.19206/CE-174794>
- [105] Sun H, Yang SI, Jomaas G, Law CK. High-pressure laminar flame speeds and kinetic modeling of carbon monoxide/hydrogen combustion. *Proc Combust Inst*. 2007;31:439-446. <https://doi.org/10.1016/j.proci.2006.07.193>
- [106] Sun P, Zhang Z, Chen J, Liu S, Zhang DH. Well converged quantum rate constants for the $H_2 + OH \rightarrow H_2O + H$ reaction via transition state wave packet. *J Chem Phys*. 2018;149:064303. <https://doi.org/10.1063/1.5046890>
- [107] Sutherland JW, Patterson PM, Klemm RB. Rate constants for the reaction, $O(3P)+H_2O \rightarrow OH+OH$, over the temperature range 1053 K to 2033 K using two direct techniques. *Symp Int Combust*. 1991;23:51-57. [https://doi.org/10.1016/S0082-0784\(06\)80241-9](https://doi.org/10.1016/S0082-0784(06)80241-9)
- [108] Szamrej G, Karczewski M. Exploring hydrogen-enriched fuels and the promise of HCNG in industrial dual-fuel engines. *Energies*. 2024;17:1525. <https://doi.org/10.3390/en17071525>
- [109] Szlachetka M, Wendeker M, Czarnigowski J, Jakliński P, Grabowski Ł. A simulation research of a hydrogen injection system for a Wankel engine. *Combustion Engines*. 2010;141:114-122. <https://doi.org/10.19206/CE-117153>
- [110] Szwaja S. Hydrogen resistance to knock combustion in spark ignition internal combustion engines. *Combustion Engines*. 2011;144:13-19. <https://doi.org/10.19206/CE-117118>
- [111] Szwajca F, Gawrysiak C, Pielecha I. Effects of passive pre-chamber jet ignition on knock combustion at hydrogen engine. *Combustion Engines*. 2024;198:110-122. <https://doi.org/10.19206/CE-189738>
- [112] Taib NM, Abu Mansor MR, Wong WY. Hydrogen combustion in transportation and power generation. In: Su'ait MS, Jarimi H, Noor SAM, editors. *ACS Symp. Ser.*, 1499, Washington, DC: American Chemical Society; 2025:169-192. <https://doi.org/10.1021/bk-2025-1499.ch010>
- [113] Teoh YH, How HG, Le TD, Nguyen HT, Loo DL, Rashid T et al. A review on production and implementation of hydrogen as a green fuel in internal combustion engines. *Fuel*. 2023;333:126525. <https://doi.org/10.1016/j.fuel.2022.126525>
- [114] The CRECK Modelling Group. *Hydrogen/CO Mech. Version 2012*.
- [115] Toyota Europe. *Outline of the Mirai 2017*. www.toyota-europe.com
- [116] University of California – Berkeley. *GRI-Mech 3.0 1999*.
- [117] Ustolin F, Paltrinieri N, Berto F. Loss of integrity of hydrogen technologies: A critical review. *Int J Hydrog Energy*. 2020;45:23809-23840. <https://doi.org/10.1016/j.ijhydene.2020.06.021>
- [118] Varga T, Nagy T, Olm C, Zsély IGY, Pálvölgyi R, Valkó É et al. Optimization of a hydrogen combustion mechanism using both direct and indirect measurements. *Proc Combust Inst*. 2015;35:589-596. <https://doi.org/10.1016/j.proci.2014.06.071>
- [119] Varga T, Olm C, Nagy T, Zsély IGY, Valkó É, Pálvölgyi R et al. Development of a joint hydrogen and syngas combustion mechanism based on an optimization approach. *Int J Chem Kinet*. 2016;48:407-422. <https://doi.org/10.1002/kin.21006>
- [120] Verhelst S, Demuynck J, Sierens R, Scarcelli R, Matthias NS, Wallner T. Update on the progress of hydrogen-fueled internal combustion engines. *Renew Hydrog Technol*. 2013;381-400. <https://doi.org/10.1016/B978-0-444-56352-1.00016-7>
- [121] Verhelst S, Wallner T. Hydrogen-fueled internal combustion engines. *Prog Energy Combust Sci*. 2009;35:490-527. <https://doi.org/10.1016/j.peccs.2009.08.001>
- [122] Verhelst S, Wallner T, Eichlseder H, Naganuma K, Gerbig F, Boyer B et al. Electricity powering combustion: hydrogen engines. *Proc IEEE*. 2012;100:427-439. <https://doi.org/10.1109/JPROC.2011.2150190>
- [123] Voelcker J. Hydrogen fuel-cell vehicles: everything you need to know. *Car Driv*. 2024. <https://www.caranddriver.com/features/a41103863/hydrogen-cars-fcev/>
- [124] Vogel C. Wasserstoff-Dieselmotor mit Direkteinspritzung, hoher Leistungsdichte und geringer Abgasemission: Teil 1: Konzept. *MTZ – Mot Z*. 1999;60:704-708. <https://doi.org/10.1007/BF03226534>
- [125] Wallner T, Lohsebusch H, Gurski S, Duoba M, Thiel W, Martin D et al. Fuel economy and emissions evaluation of BMW Hydrogen 7 Mono-Fuel demonstration vehicles. *Int J Hydrog Energy*. 2008;33:7607-7618. <https://doi.org/10.1016/j.ijhydene.2008.08.067>
- [126] Wang H, You X, Ameya JV, Davis SG, Laskin A, Egolfopoulos F et al. *USC Mech Version II. High-temperature combustion reaction model of H₂/CO/C₁-C₄ compounds*. 2007.

- [127] Waseem M, Amir M, Lakshmi GS, Harivardhagini S, Ahmad M. Fuel cell-based hybrid electric vehicles: An integrated review of current status, key challenges, recommended policies, and future prospects. *Green Energy Intell Transp.* 2023;2:100121. <https://doi.org/10.1016/j.geits.2023.100121>
- [128] Waseem M, Lakshmi GS, Sreeshobha E, Khan S. An electric vehicle battery and management techniques: comprehensive review of important obstacles, new advancements, and recommendations. *Energy Storage Sav.* 2025;4:83-108. <https://doi.org/10.1016/j.enss.2024.09.002>
- [129] Welsch R. Rigorous close-coupling quantum dynamics calculation of thermal rate constants for the water formation reaction of $H_2 + OH$ on a high-level PES. *J Chem Phys.* 2018;148:204304. <https://doi.org/10.1063/1.5033358>
- [130] Wesołowski M, Hamid M, Mońka P, Janicka A. Analysis of the potential of electro-waste as a source of hydrogen to power low-emission vehicle powertrains. *Combustion Engines.* 2024;196:126-133. <https://doi.org/10.19206/CE-169494>
- [131] Wooldridge MS, Hanson RK, Bowman CT. A shock tube study of the $OH + OH \rightarrow H_2O + O$ reaction. *Int J Chem Kinet.* 1994;26:389-401. <https://doi.org/10.1002/kin.550260402>
- [132] Wróbel K, Wróbel J, Tokarz W, Lach J, Podsadni K, Czerwiński A. Hydrogen internal combustion engine vehicles: a review. *Energies.* 2022;15:8937. <https://doi.org/10.3390/en15238937>
- [133] Xiao T, He A, Pei X, Pan M, Wang X, Hu Z. Research on hydrogen-fueled turbojet engine control method based on model-based design. *Processes.* 2023;11:3268. <https://doi.org/10.3390/pr11123268>
- [134] Zadrag R, Socik P, Kniaziewicz T, Zacharewicz M, Bogdanowicz A, Wirkowski P. Analysis of simulated dynamic loads of a ship propulsion system of a non-conventional power system. *Combustion Engines.* 2024;197(2):158-168. <https://doi.org/10.19206/CE-184139>
- [135] Zhao F, Sun B, Yuan S, Bao L, Wei H, Luo Q. Experimental and modeling investigations to improve the performance of the near-zero NOx emissions direct-injection hydrogen engine by injection optimization. *Int J Hydrog Energy.* 2024;49:713-724. <https://doi.org/10.1016/j.ijhydene.2023.09.039>
- [136] Zhou A. Review of hydrogen fuel cell vehicle research. *Acad J Eng Technol Sci.* 2022;5. <https://doi.org/10.25236/AJETS.2022.050908>
- [137] Zhu D, Shu B. Recent progress on combustion characteristics of ammonia-based fuel blends and their potential in internal combustion engines. *Int J Automot Manuf Mater.* 2023;20. <https://doi.org/10.53941/ijamm0201001>
- [138] Zsély IGY, Zádor J, Turányi T. Uncertainty analysis of updated hydrogen and carbon monoxide oxidation mechanisms. *Proc Combust Inst.* 2005;30:1273-1281. <https://doi.org/10.1016/j.proci.2004.08.172>

Mariusz J. Nieścioruk, MEng. – mjniescioruk AEI, Poland.

e-mail: mariusz.j@niescioruk.eu

Prof. Andrei-Alexandru Boroiu, DSc., DEng. – Faculty of Mechanics and Technology, National University of Science and Technology, Politehnica Bucharest, Romania.

e-mail: andrei.boroiu@upb.ro



Prof. Gustavo Ozuna – Department of Industrial Engineering and Systems, Hermosillo 83000, University of Sonora, Mexico.

e-mail: gozuna@industrial.uson.mx



Prof. Agustín Brau Ávila, DSc., DEng. – Department of Industrial Engineering and Systems, Hermosillo 83000, University of Sonora, Mexico.

e-mail: agustin.brau@unison.mx



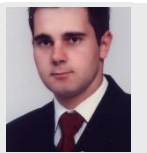
Przemysław Kubiak, DSc., DEng. – Institute of Vehicles and Construction Machinery Engineering, Warsaw University of Technology, Poland.

e-mail: przemyslaw.kubiak@pw.edu.pl



Marek Wozniak, DEng. – Department of Vehicles and Fundamentals of Machine Design, Lodz University of Technology, Poland.

e-mail: marek.wozniak.1@p.lodz.pl



Krzysztof Siczek, DSc., DEng. – Department of Vehicles and Fundamentals of Machine Design, Lodz University of Technology, Poland.

e-mail: ks670907@p.lodz.pl



Xymena GROSS 
 Jakub TOMASZ 
 Manuela SKOWRON 
 Beata KURC 
 Ewelina RUDNICKA 
 Natalia SZYMLET 
 Lukasz RYMANIAK 

The electrochemical route to sustainable transport

ARTICLE INFO

Received: 18 June 2025
 Revised: 10 November 2025
 Accepted: 18 November 2025
 Available online: 29 December 2025

The electrification of mopeds is a growing concern in urban transportation. Due to their intended use, they represent a prime area for implementing alternative energy storage solutions. Recent research has focused on the use of metal sulfides as anode materials in sodium-ion cells, as well as on carbon materials derived from biomaterials for use in electrochemical supercapacitors. Capacitive properties of these materials were evaluated using techniques such as galvanostatic charge-discharge (GCD) and cyclic voltammetry (CV). The cycling tests demonstrated high reversibility of reactions and strong specific capacitance, indicating good electrochemical performance. GCD analysis of sodium-based systems revealed high initial potentials and efficiency exceeding 90%, suggesting their suitability for long-term applications. Additionally, tests of supercapacitors indicated pseudocapacitive behaviour, further confirming the effectiveness of the studied materials. Overall, the results highlight the strong potential of sodium-ion technologies for energy storage, particularly in applications that require durability, such as electric mopeds.

Key words: *energy consumption, metal sulphides, scooter, sodium-ion cells, sustainable transport*

This is an open access article under the CC BY license (<http://creativecommons.org/licenses/by/4.0/>)

1. Introduction

Ongoing urbanization, the growing population in metropolitan areas, and increasing congestion of road infrastructure pose significant challenges in ensuring sustainable transport. The rise in individual mobility – driven by dynamic economic development and increasing affluence of societies – has led to a steady increase in the number of vehicles operating on public roads. It is estimated that by 2050, the global number of motor vehicles could double [20]. At the same time, transportation remains one of the primary sources of greenhouse gas emissions, particulate matter, and nitrogen oxides, which impact both the global climate and local air quality [4, 18].

According to the European Environment Agency, the transport sector currently accounts for approximately 30% of the European Union's total energy consumption. It generates 20–25% of total CO₂ emissions, 10% of PM₁₀, and as much as 45% of NO_x emissions [3]. A significant portion of these pollutants is concentrated in densely populated urban areas, contributing to the increased incidence of cardiovascular and respiratory diseases. The World Health Organization (WHO) reports that 90% of the urban population breathes air that exceeds permissible pollution levels, resulting in increased mortality due to cancer, cardiovascular, and pulmonary conditions [24].

In view of these circumstances, the development of electromobility – including L-class single-track vehicles – is becoming one of the key solutions for reducing emissions and improving urban quality of life [11]. A particularly prominent role within this segment is played by electric mopeds and motorcycles, which, in contrast to internal combustion vehicles, do not emit toxic compounds and are characterized by lower energy consumption, reduced operating costs, and a favorable acoustic profile.

According to, the latest Mordor Intelligence report [14], the global market value of electric scooters and motorcycles in 2024 was estimated at USD 38.6 billion, with a projected Compound Annual Growth Rate (CAGR) of 11.1% between 2024 and 2029 (Fig. 1). The fastest market growth is observed in Asia-Pacific countries – especially China, India, and Indonesia – where two-wheelers constitute a primary mode of daily transportation represent a dominant mode of daily transportation.



Fig. 1. Forecasted compound annual growth rate (CAGR) of the electric scooter and motorcycle market by global region, 2025–2030 [14]

In Europe, an increasing number of cities are implementing sustainable mobility strategies that promote the use of light electric vehicles by introducing low- and zero-emission zones, offering free parking, or allowing access to bus lanes. This trend is also evident in Poland, where the number of registered L1e-B class single-track vehicles, as well as those offered through vehicle-sharing schemes, continues to grow.

Despite the rapid advancement of electric drive technologies, energy storage remains a significant challenge. Batteries, as a key component of electric vehicles, are still characterized by limited energy density, relatively high

mass, and substantial environmental impact during both production and disposal stages. Breakthrough solutions in battery cell technologies – combining high durability, safety, low unit cost, and reduced dependence on critical raw materials – are still lacking. In parallel with electrification, research is continually being conducted into the development of vehicle powertrains including improving combustion processes in conventional engines and the use of hydrogen fuels [15, 22].

With the growing trend toward electrification of urban transportation, electric mopeds are emerging as a key area for implementing alternative energy storage solutions. Among these, sodium-ion cells represent a promising and cost-effective alternative to traditional lithium-based batteries. Environmental regulations, limited lithium resources, and rising market prices are driving the search for efficient and sustainable energy sources, making sodium-ion technology a compelling candidate. These cells are gaining significant attention from researchers and technologists due to their potential for widespread adoption. Recent studies have focused on the use of metal sulphides as viable anode materials in Na-ion cells, as well as on carbon materials derived from biomaterials for use in electrochemical supercapacitors. This information serves as the foundation for this work, which aims to evaluate selected power sources for scooters used in the city.

The study introduces an eco-friendly and low-energy fabrication approach that employs locust bean gum as a natural binder for sodium-ion electrodes. For lignin-based capacitor materials, we utilised a simplified synthesis route, highlighting the potential of various sustainable methods in electrochemical energy storage.

2. Literature review

A review of the scientific and technical literature reveals a growing focus on the energy and environmental efficiency of single-track vehicles, including L1e-B class electric scooters, when operated under real-world conditions. Particular attention is given to studies that encompass not only energy consumption but also operational constraints and the life cycle of the vehicle and its key components.

In the study by [7], a comparative analysis was conducted of energy consumption and pollutant emissions generated by electric scooters and their conventional counterparts in urban environments, under actual traffic conditions. Based on field measurements, the average energy consumption of an electric scooter was determined to be 2.8 kWh/100 km, which is nearly eight times lower than the energy equivalent of fuel consumption for an internal combustion vehicle. The authors also observed significantly lower CO₂ emissions (14.17 g/km compared to 31.81 g/km), as well as more than a sixfold reduction in operating costs. A notable observation included the higher average acceleration of the electric scooter and lower speed variability during operation, both of which positively influence drivetrain efficiency in urban settings.

The issue of energy consumption throughout the full life cycle of a vehicle was thoroughly addressed in a study by [19], which conducted an LCA (Life Cycle Assessment) for an electric scooter used in a sharing system. The authors reported an average energy consumption of 0.034 kWh/km

(3.4 kWh/100 km), which, assuming a total mileage of 50,000 km, corresponds to an energy usage equivalent to 1.25 full battery discharge cycles. The study demonstrated that the greatest environmental burden arises not from the use phase, but from the production and replacement of the energy storage system. This highlights the crucial role of battery durability and energy efficiency in evaluating the total environmental impact of electric vehicles.

From a cost and operational perspective, the study by [8] provides an important contribution. It presents an optimized Total Cost of Ownership (TCO) model for light electric two-wheelers, accounting for variable local conditions such as topographical route profiles, load characteristics, charging infrastructure availability, and type of use (private, fleet, or municipal). The analysis suggests that drivetrain configurations and battery specifications should be carefully tailored to real-world usage conditions. The application of standardized systems may lead to a substantial decline in energy efficiency and increased operational costs.

In the context of the vehicle's complete life cycle, a less frequently addressed but highly relevant issue is the management of used battery packs. Eduardo et al. (2025) [2] conducted a comparative analysis of several "end-of-life" scenarios for batteries used in electric scooters, encompassing both mechanical and chemical recycling methods, as well as secondary use in low-voltage energy storage systems. The study concluded that a properly selected end-of-life strategy for batteries can significantly reduce the vehicle's environmental footprint and lessen its dependency on critical raw materials, such as lithium, nickel, and cobalt, whose availability and prices are subject to high market volatility.

3. Methodology

The systems under investigation were analysed through cyclic voltammetry using the G 1000 Potentiostat/Galvanostat/ZRA from Gamry Instruments (USA). The voltammograms obtained from these tests provided insight into the reversibility of redox processes within the cells and the cyclic stability of the capacitors.

To evaluate the specific capacity and initial coulombic efficiency of the tested systems, galvanostatic charge-discharge experiments were conducted using the ATLAS 0691 MBI testing unit (Atlas-Sollich, Poland). These assessments were conducted under a range of current densities.

The specific energy values for each system have been calculated, enabling their application analysis.

4. Electrochemical analysis of selected power sources

4.1. Na-ion cells with highly efficient anodes

The electrode material incorporates one of three base compounds: CuO, SnS [16], and CoS₂. In each system, the electrolyte used is a 0.8 M solution of NaPF₆ in EC: DMC (1:1). An aqueous solution of LBG was employed as the binder. Acetylene black (AB) was used as the conductive additive in the analysed systems.

Galvanostatic curves recorded at a current density of 10 mA/g exhibit distinct plateau regions (Fig. 2).

These plateaus correspond to processes occurring during cell operation, which are the insertion of sodium ions into the anode material and the conversion of the active material. Both processes are reversible. The plateau appears at potentials of approximately 2 V, 1.5 V and 0.5 V. The plateau observed at the lowest potential (0.5 V) corresponds to the decomposition reaction of copper oxide into metallic copper [1].

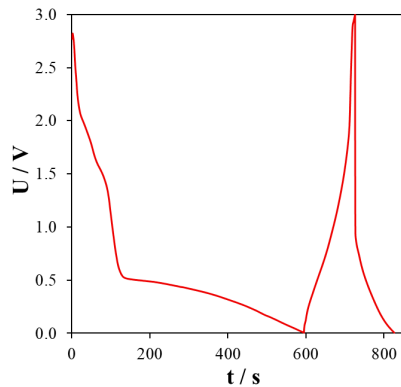


Fig. 2. Graph for an CuO Na-ion half-cell GCD for a current density of 10 mA/g

Galvanostatic charge/discharge testing at a current density of 50 mA/g indicates sustained high reversibility of the intercalation and deintercalation processes (Fig. 3). The observed plateau regions correspond to cyclically occurring reactions during cell operation.

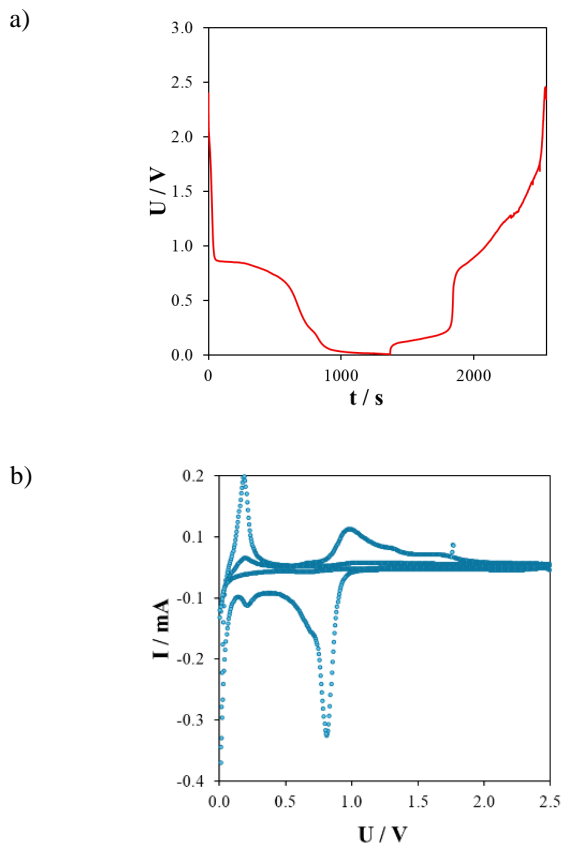


Fig. 3. Graphs for an SnS Na-ion half-cell (a) GCD for a current density of 50 mA/g; (b) cyclic voltammetry at a scan rate of 0.5 mV/s

The specific capacities of the analysed material reached 935 mAh/g during sodiation and 482 mAh/g during desodiation in the first cycle. These values decreased to approximately 295 mAh/g by the fifth cycle. At the same time, the coulombic efficiency of the system stabilized above 95% after the fifth cycle. This system demonstrates satisfactory cycling stability and high efficiency in the reversible electrochemical processes.

The cyclic voltammetry curves of the analysed system indicate morphological changes occurring during the first cycle. These changes are associated with electrochemical reactions taking place during cell operation and with the formation of a passivation layer on the electrode surface [23]. The peaks observed in the first cycle do not reappear in subsequent cycles. However, the following cycles exhibit high reproducibility.

The experimental tests with CoS₂ material began with subjecting the system to galvanostatic charging/discharging with a current of 50 mA/g. The capacity for the sodium ion insertion cycle was 1611 mAh/g, while for disinsertion, it reached a value of 867 mAh/g.

During this cycle, two plateaus were observed (Fig. 4). The first occurred during cell charging at a potential of 1.051 V, and the second during discharging at a potential of 1.78 V.

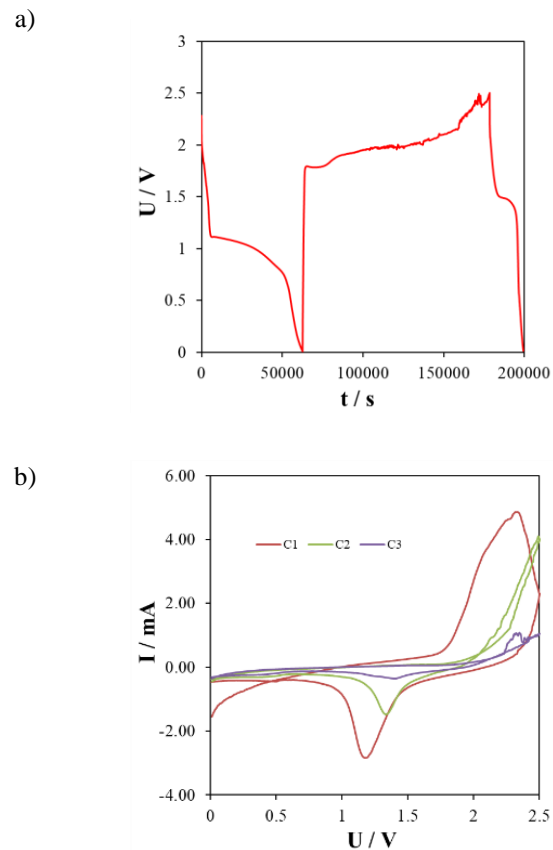


Fig. 4. Graphs for an CoS₂ Na-ion half-cell (a) GCD for a current density of 50 mA/g; (b) cyclic voltammetry at a scan rate of 0.5 mV/s

The next stage of the research involved subjecting the system to cyclic voltammetry at a scanning rate of 0.5 mV/s (Fig. 4b). As can be observed, with each subsequent cycle,

the intensity of the anodic and cathodic peaks decreases. This indicates lower capacity values compared to the first cycle, as well as decreasing reversibility of the process.

In the first cycle, a reduction peak was observed at a potential of 1.15 V, corresponding to conversion and melting reactions, respectively. During the conversion reaction, a sulphur compound is formed with metallic sodium, while the active material of the electrode is reduced to metallic cobalt. As a result of the melting reaction, an alloy is formed between sodium and cobalt, which can lead to the accumulation of a significant amount of sodium cations on the electrode surface and thus an increase in the volume of the electrode material.

4.2. Bio-based capacitor

Figure 5 shows the CV curves for the 5th, 10th and 20th cycles of operation of the lignin-based capacitor. The preparation method followed the procedure reported in [9]. The shape of the curves deviates from a perfect rectangle, which may indicate the presence of pseudocapacitive processes occurring in parallel with typical ion adsorption or limitations in charge transport in the pores of the material [6]. However, the observed curves indicate good reversibility of the electrochemical reactions and a specific capacitance of 63 F g⁻¹. Slight changes in signal intensity across successive cycles indicate high cyclic stability of the tested material, confirming its potential for long-term use in electrochemical capacitors.

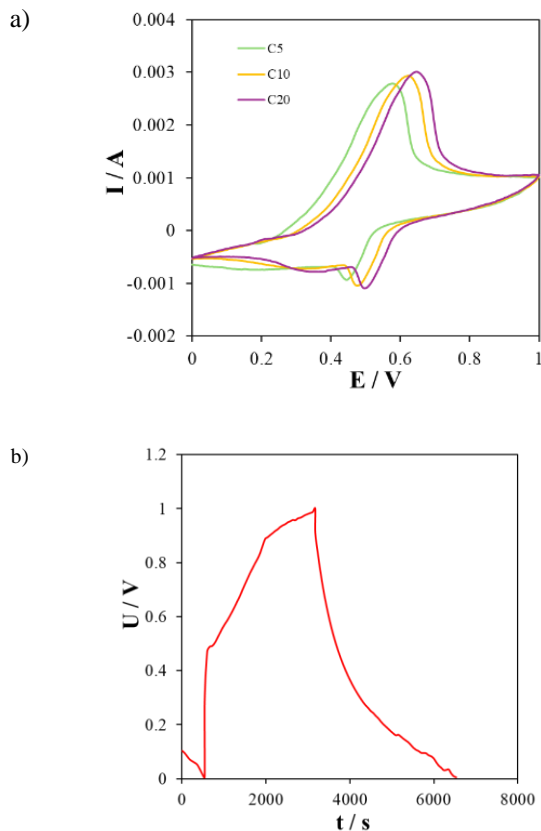


Fig. 5. Graphs for an lignin-based electrochemical capacitor (a) cyclic voltammetry at a scan rate of 10 mV/s; (b) GCD for a current density of 50 mA/g

Additionally, galvanostatic charge-discharge (GCD) measurements were performed at a constant current of 10 mA/g. The obtained curve does not show a perfectly linear course, which may also indicate the participation of pseudocapacitive phenomena. The small voltage difference between the end of charging and the beginning of discharging confirms the low internal resistance of the system. At the same time, the long discharging time indicates good charge storage capacity [5].

The results obtained by CV and GCD methods indicate the favourable electrochemical properties of the lignin-derived material and its suitability as an electrode component in capacitors [10].

5. Power values of the obtained devices

To accurately assess the energy parameters of the devices obtained (Table 1), the energy values were normalized to the mass of the active electrode material. In the case of Na-ion cells, the specific energy (E_s) was determined using formula 1, while in the case of capacitors, formula 2 was used.

$$E_s = \frac{U \cdot It}{m} \quad (1)$$

$$E_s = \frac{1}{2} C_s U^2 \quad (2)$$

Table 1. Key parameters for obtained systems

Parameter	CuO	SnS	CoS ₂	Capacitor
E _s (Wh/kg)	356	613	809	10.3

The proposed battery configurations exhibit comparable manufacturing costs, attributable to the assumed availability of the specified materials [17]. The presented results indicate that a CoS₂ battery is the most suitable option for a single-track vehicle, offering the highest specific energy (gravimetric energy density) of 809 Wh/kg. To provide better insight into the achieved performance, the obtained capacitance results were compared with recent data reported for analogous systems employing different synthesis routes (Table 2). The vehicles under consideration are compact, which is among their principal advantages; consequently, the propulsion systems cannot be substantially enlarged without compromising functionality. It is therefore reasonable to employ an auxiliary battery module weighing 5 kg, which can be accommodated in the cargo space or integrated into the vehicle body. According to the literature survey, such a battery would enable a driving range of approximately 150 km, which is sufficient for the daily operation of an urban moped.

Table 2. Comparison of specific capacity and capacitance values obtained in this work with data reported in the recent literature for analogous electrolytes

System	Capacity	Literature value	Reference
CuO / Na-ion	164 mAh/g	525 mAh/g	[21]
SnS / Na-ion	295 mAh/g	839 mAh/g	[13]
CoS ₂ / Na-ion	867 mAh/g	861 mAh/g	[25]
Lignin-based capacitor	63 F/g	311 F/g	[12]

Although the obtained capacities are slightly lower than the top-reported values in the literature, they were achieved using significantly simplified and environmentally friendly synthesis routes that did not require high-temperature activation, template-assisted methods, or multi-step pyrolysis. In particular, the CoS₂-based electrode exhibits a specific capacity higher than that of the optimized composite systems, while being much easier to fabricate and scale up.

The CuO- and SnS-based electrodes also exhibit stable electrochemical behavior with capacities suitable for practical sodium-ion applications, underscoring the effectiveness of the proposed preparation process. The lignin-derived carbon electrode shows promising capacitive performance in alkaline electrolyte, which can be further enhanced through structural optimization, confirming its potential as a sustainable alternative to conventional carbon materials.

6. Conclusions

Urban scooters are gaining prominence within the European Union's transport systems, and their electrification is a key element of sustainable mobility. Given the current constraints on the supply of rare earth metals, particularly lithium, exploring alternative battery chemistries is imperative. This study has demonstrated that environmentally friendly and simplified fabrication methods can yield high-performance electrochemical materials suitable for light

electric vehicle applications. The investigated sulphide-based systems (SnS and CoS₂) and the novel eco-friendly LBG binder exhibited high initial specific capacities and satisfactory cycling stability, confirming their strong potential as anode materials for Na-ion batteries with good reversibility of intercalation–deintercalation processes.

The CuO oxide material demonstrated comparable electrochemical activity, supporting its role as a stable and efficient conversion-type electrode in sodium-ion systems.

The bio-based capacitor prepared using lignin-derived carbon exhibited excellent cyclic stability and reversibility, demonstrating that renewable materials can effectively replace conventional electrodes and marking a significant step toward sustainable energy storage technologies.

Among the evaluated solutions, the CoS₂-based battery is identified as the most advantageous, owing to its favorable energy-to-mass ratio and comparable production cost. A 5 kg module is estimated to provide a range of approximately 150 km per charge, which is sufficient for daily urban use. Moreover, the proposed materials exhibit favorable recyclability characteristics. Future work will focus on developing physical prototypes and integrating them with an L1e-B category urban two-wheeler propulsion system.

Acknowledgements

The study presented in this article was performed within statutory research (No. 0415/SBAD/0362).

Bibliograph

- [1] Cao K, Jin T, Yanga L, Jiao L. Recent progress in conversion reaction metal oxide anodes for Li-ion batteries. *Mater Chem Front.* 2017;1:2213-2242. <https://doi.org/10.1039/C7QM00175D>
- [2] Eduardo S, Recklies EA, Nikolic M, Severengiz S. A comparative life cycle assessment of end-of-life scenarios for light electric vehicles: a case study of an electric moped. *Sustainability.* 2025;17(15):6681. <https://doi.org/10.3390/su17156681>
- [3] European Commission. White Paper on transport: Roadmap to a Single European Transport Area – Towards a competitive and resource-efficient transport system. 2011 (accessed on 2025 Jun 16). <https://eur-lex.europa.eu/legal-content/EN/TXT/?uri=celex:52011DC0144>
- [4] European Environment Agency (EEA). Greenhouse gas emissions from transport in Europe. 2022 (accessed on 2025 Jun 16). <https://www.eea.europa.eu/en/analysis/indicators/greenhouse-gas-emissions-from-transport-1762418495/greenhouse-gas-emissions-from>
- [5] Khan HR, Ahmad AL. Supercapacitors: overcoming current limitations and charting the course for next-generation energy storage. *J Ind Eng Chem.* 2025;141:46-66. <https://doi.org/10.1016/j.jiec.2024.07.014>
- [6] Kinkelin SJ, Röder F, Vogel K, Steimecke M, Bron M. A fundamental study on cyclic voltammetry at porous carbon thin-film electrodes, *Electrochim Acta.* 2024;488:144183. <https://doi.org/10.1016/j.electacta.2024.144183>
- [7] Koossalapeerom T, Satiennam T, Satiennam W, Leelapatra W, Seedam A, Rakpukdee T. Comparative study of real-world driving cycles, energy consumption, and CO₂ emissions of electric and gasoline motorcycles driving in a congested urban corridor. *Sustainable Cities and Society.* 2019;45:619-627. <https://doi.org/10.1016/j.scs.2018.12.031>
- [8] Korzilius O, Borsboom O, Hofman T, Salazar M. Optimal design of electric micromobility vehicles. 2021 IEEE International Intelligent Transportation Systems Conference (ITSC); 2021:1677-1684. <https://doi.org/10.1109/ITSC48978.2021.9564429>
- [9] Kurc B, Pięłowska M, Fuć P, Szymlet N, Gross X, Piasecki A. Utilizing kraft lignin–derived hard carbon as an innovative bio-electrode in electrochemical capacitors. *Ionics (Kiel).* 2024;30(11):7431-7451. <https://doi.org/10.1007/s11581-024-05770-4>
- [10] Kurc B, Pięłowska M, Rymaniak Ł, Fuć P. Modern nanocomposites and hybrids as electrode materials used in energy carriers. *Nanomaterials.* 2021;11(2):538. <https://doi.org/10.3390/nano11020538>
- [11] Laskowski P, Zimakowska-Laskowska M, Zasina D, Wiatrak M. Comparative analysis of the emissions of carbon dioxide and toxic substances emitted by vehicles with ICE compared to the equivalent emissions of BEV. *Combustion Engines.* 2021;187(4):102-105. <https://doi.org/10.19206/CE-141739>
- [12] Li H, Yuan D, Tang C, Wang S, Sun J, Li Z et al. Lignin-derived interconnected hierarchical porous carbon monolith with large areal/volumetric capacitances for supercapacitor. *Carbon.* 2016;100:151-157. <https://doi.org/10.1016/j.carbon.2015.12.075>
- [13] Mei J, Han J, Wu F, Pan Q, Zheng F, Jiang J et al. SnS@C nanoparticles anchored on graphene oxide as high-performance anode materials for lithium-ion batteries. *Front Chem.* 2023;10:1105997. <https://doi.org/10.3389/fchem.2022.1105997>
- [14] Mordor Intelligence. Electric Scooter and Motorcycles Market – Growth, Trends, and Forecasts (2024–2029). 2024 (accessed on 2025 Jun 16). <https://www.mordorintelligence.com/industry-reports/electric-scooters-market>

- [15] Pielecha I, Sidorowicz M. Effects of mixture formation strategies on combustion in dual-fuel engines – a review. *Combustion Engines*. 2021;184(1):30-40. <https://doi.org/10.19206/CE-134237>
- [16] Rudnicka E, Galiński M, Jakóbczyk P. Enhanced electrochemical performance of SnS–PPy–carbon black composite with a locust bean gum as a binder as in anode in lithium-ion batteries. *J Appl Electrochem*. 2024;54(9):1945-1956. <https://doi.org/10.1007/s10800-024-02079-y>
- [17] Ruppert J, Voß P, Ihlbrock L, Palm J, Lux S, Leker J. Analyzing material and production costs for lithium-ion and sodium-ion batteries using process-based cost modeling – CellEst 3.0. *J Power Source Adv*. 2025;36:100190. <https://doi.org/10.1016/j.powera.2025.100190>
- [18] Sawczuk W, Merkisz-Guranowska A, Rilo Cañas AM, Kołodziejcki S. New approach to brake pad wear modelling based on test stand friction-mechanical investigations. *Eksploat Niezawodn*. 2022;24(3):419-426. <https://doi.org/10.17531/ein.2022.3.3>
- [19] Schelte N, Severengiz S, Schünemann J, Finke S, Bauer O, Metzen M. Life cycle assessment on electric moped scooter sharing. *Sustainability*. 2021;13(15):8297. <https://doi.org/10.3390/su13158297>
- [20] Statista. Number of motor vehicles worldwide from 2006 to 2023. Statista; 2024 (accessed on 2025 Jun 16). <https://www.statista.com/statistics/281134/number-of-vehicles-in-use-worldwide/>
- [21] Sun X, Luo F. Facile fabrication of large-area CuO flakes for sodium-ion energy storage applications. *Molecules*. 2024;29:2528. <https://doi.org/10.3390/molecules29112528>
- [22] Szwajca F, Pielecha I, Mielcarzewicz D. Experimental investigation on the influence of passive/active pre-chamber injection strategy on the hydrogen knock limit. *Combustion Engines*. 2025;203(4):32-41. <https://doi.org/10.19206/CE-207382>
- [23] Vafaeian S, Fattah-Alhosseini A, Keshavarz MK, Mazaheri Y. The influence of cyclic voltammetry passivation on the electrochemical behavior of fine and coarse-grained AISI 430 ferritic stainless steel in an alkaline solution, *J Alloys Compd*. 2016;677:42-51. <https://doi.org/10.1016/j.jallcom.2016.03.222>
- [24] World Health Organization (WHO). Ambient (outdoor) air quality and health. 2021 (accessed on 2025 Jun 16). [https://www.who.int/news-room/fact-sheets/detail/ambient-\(outdoor\)-air-quality-and-health](https://www.who.int/news-room/fact-sheets/detail/ambient-(outdoor)-air-quality-and-health)
- [25] Zheng H, Pei M, Qiu R, Ma D, Deng S, Jiao X et al. High-capacity and high-rate sodium storage of CoS₂/NiS₂@C anode material enabled by interfacial C-S covalent bond and Mott–Schottky heterojunction. *Chem Eng J*. 2023;476:146801. <https://doi.org/10.1016/j.cej.2023.146801>

Xymena Gross, Eng. – Faculty of Chemical Technology, Poznan University of Technology, Poland.
e-mail: xymena.gross@student.put.poznan.pl



Beata Kurc, DEng. – Faculty of Chemical Technology, Poznan University of Technology, Poland.
e-mail: beata.kurc@put.poznan.pl



Jakub Tomasz, Eng. – Faculty of Chemical Technology, Poznan University of Technology, Poland.
e-mail: jakub.tomasz@student.put.poznan.pl



Ewelina Rudnicka, DEng. – Faculty of Chemical Technology, Poznan University of Technology, Poland.
e-mail: ewelina.rudnicka@put.poznan.pl



Manuela Skowron, MEng. – Faculty of Chemical Technology, Poznan University of Technology, Poland.
e-mail: manuela.skowron@doctorate.put.poznan.pl



Natalia Szymlet, DEng. – Faculty of Civil and Transport Engineering, Poznan University of Technology, Poland.
e-mail: natalia.szymlet@put.poznan.pl



Prof. Łukasz Rymaniak, DSc., DEng. – Faculty of Civil and Transport Engineering, Poznan University of Technology, Poland.
e-mail: lukasz.rymaniak@put.poznan.pl



Spray structures formed by a multi-nozzle injector during the injection of a multi-component surrogate synthetic fuel under flash-boiling conditions

ARTICLE INFO

Received: 8 July 2025

Revised: 14 November 2025

Accepted: 18 November 2025

Available online: 19 December 2025

The introduction of synthetic fuels into spark-ignition direct-injection engines requires a deeper understanding of the injection and spray formation process. It also includes spray formation under flash-boiling conditions, which has not been of primary importance so far. This research focuses on experimental studies of spray propagation and its morphological features when moderate flash boiling is achieved. Our main objective is to verify this effect in a multiple-nozzle injection system for a selected synthetic fuel. It is accomplished by increasing the fuel temperature. The results showed that the spray structure changed slightly due to flash-boiling, but the secondary effects related to the rapid vaporisation of the injected fuel, such as spray collapse, were not observed.

Key words: *combustion engines, synthetic fuels, flash-boiling, spray propagation, spray collapse*

This is an open access article under the CC BY license (<http://creativecommons.org/licenses/by/4.0/>)

1. Introduction

Due to the tightening of global regulations aimed at reducing greenhouse gas emissions, synthetic fuels can serve as an alternative to conventional fuels. Fossil fuel combustion remains one of the primary sources of anthropogenic CO₂ emissions and air pollution, underscoring the need to reduce its carbon footprint [9, 17]. In 2024, fossil fuels accounted for nearly 60% of the world's electricity generation [13]. In the transportation sector, up to 95% of the global transportation energy comes from petroleum-based liquid fuels, and by 2040, it is expected to represent between 80% and 90% [14]. Additionally, the stricter regulations on greenhouse gases (GHG) and exhaust emissions from internal combustion engines are meant to increase society's interest in improving the efficiency of combustion-based systems [26]. Among the viable alternatives to achieve this goal is by integrating renewable energy in the transport sector [9].

This integration is possible because hydrocarbons with similar chemical and physical properties to conventional fuels, called synthetic fuels, can be synthesized from the electrolysis of water and carbon dioxide captured from the air or industrial processes [7].

Synthetic fuels can be classified into one of the following categories: production process, feedstock, application, sustainability, or chemical composition [21]. Synthetic fuels derived from renewable electricity (through hydrogen generation in water electrolysis) and raw materials are called electro-fuels or e-fuels [26]. They are of special interest as they can be treated as a sustainable alternative to conventional fuels.

According to Uchida et al. [27], e-fuels can be produced with a chemical composition similar to that of conventional fuels, i.e. drop-in fuels for use in existing and next-generation engines, without significant design changes. However, some e-fuels can be substantially different, and

they may require dedicated engines or new combustion concepts. According to the authors, these types of fuels are expected to accelerate the decarbonisation process.

Some processes to produce e-fuels include methanol-to-gasoline (MtG) for a gasoline surrogate, paraffinic fuels (Fischer-Tropsch FT process) for gasoline or Diesel; and polyoxymethylene dimethyl ethers (OMeX) representing a Diesel alternative [19, 27]. As a result of e-fuel production, for example, through the Fischer-Tropsch (FT) process, a mixture is formed that contains a wide range of chemical compounds, primarily consisting of olefins and paraffins with straight carbon chains [19]. Therefore, different chemical and physical properties of individual components in fuel mixtures influence the atomisation, mixture formation and combustion processes.

By implementing synthetic fuels, the carbon dioxide emissions related to their use are lower than the carbon dioxide captured during their production, resulting in a reduction of GHG emissions and achieving carbon-neutral or carbon-negative cycles when electrolysis is used with renewable energy [7]. Other benefits include the capability of utilising installed infrastructure for the storage and transportation of conventional fuels, as well as the possibility of extending the life cycle of current vehicles in operation. Reducing costs associated with developing specific infrastructure is a significant advantage, particularly in comparison to other technologies, such as battery or fuel cell electric vehicles [21].

As one may conclude, synthetic fuels can be identified as a viable alternative to conventional fuels within the transportation sector, with the benefit of reducing greenhouse gas and pollutant emissions. Moreover, their production could accomplish carbon-neutral or carbon-negative cycles. Additionally, the capability of using installed infrastructure facilitates their implementation compared to other technologies under investigation.

However, to facilitate the large-scale application of synthetic fuels, further research is still needed to determine optimal operating conditions, taking into account possibly different air-fuel mixture preparation processes. It needs to include possible flash-boiling, which has been previously shown to alter the atomisation and mixture formation processes.

Flash-boiling is a process related to the rapid phase change of the injected liquid, which may improve atomisation and mixture formation under internal conditions [4, 5]. It can be obtained by increasing the fuel temperature (prior to the injection) or by decreasing the ambient pressure (to which the liquid is injected) [1, 28].

The effects on the atomisation process due to flash-boiling are correlated with the saturation pressure of the injected liquid [4].

In general, a more complex relation is expected for multi-component fuels due to the different boiling points of each component, along with their varying molecular interactions. Furthermore, the saturation pressure curve for this type of mixture differs from that of pure components, exhibiting a dependence on molar fractions, pressure, and temperature. Fixing the molar fraction, the pressure-vs-temperature graph can be divided into two curves, the bubble curve and the dew curve, separated by the critical point [25]. Moreover, considering that the flash-boiling phenomenon is defined as a liquid being injected into an environment where the pressure is lower than the saturation pressure, causing superheating and violent evaporation, the bubble curve is crucial for understanding its behavior in multi-component fluids, as this line corresponds to the saturated liquid line. The dew curve, in turn, corresponds to the saturated vapour line.

Neroorkar and Schmidt [20] presented a model to determine the vapour-liquid equilibrium (VLE) characteristics of gasoline-ethanol blends, enabling flash-boiling injection simulations. The results obtained by the model were compared with experimental data and other previously validated models, exhibiting good agreement in the saturation pressure predictions for different ethanol contents. This pressure is used to determine the flash-boiling intensity through the ambient-to-saturation pressure ratio. Hutchison and Wallace [11] investigated the flash-boiling effect of surrogate and commercially available fuels on fuel volatility and particle emissions. The authors utilised the DWSIM chemical process simulation software to calculate the bubble point pressure of surrogate fuels at various temperatures, thereby determining the flash-boiling intensity. The numerical results obtained were validated with the dry vapour pressure (DVPE) experimental results.

Zeng et al. [29] used the ambient-to-saturation pressure ratio to identify three different regions: non-flash-boiling, transitional flash-boiling, and flare flash-boiling.

Xu et al. [28] evaluated flash-boiling characteristics for four different fuels, varying injection pressure, ambient pressure and fuel temperature. The authors presented a relationship between spray penetration and width, as well as the ambient-to-saturation pressure ratio and the air-to-liquid density ratio, under different flash-boiling regimes.

Hwang et al. [12] compared the spray characteristics of iso-octane with those of a multi-component gasoline surrogate under three different engine conditions: high density, flash-boiling, and early-injection conditions. Spray collapse was observed for the gasoline surrogate under flash-boiling and early-injection conditions, resulting in higher liquid and vapour spray penetration than iso-octane.

Kannaiyan and Sadr [15] compared the variation in spray parameters between two gas-to-liquid (GTL) synthetic fuels and Jet A-1 aviation fuel at injection pressures of 0.3 and 0.9 MPa. The results of the experiments show that there were no significant differences between the fuels in terms of the effective spray cone angle and global Sauter mean diameter (SMD). However, in the near nozzle region, especially at higher injection pressures, a variation in droplet velocity, Weber number (We), and mean droplet diameter (d_{10}), droplet disintegration and dispersion are identified. One of the reasons presented by the authors is related to differences in kinematic viscosity and surface tension between the fuels.

Cui et al. [8] compared the spray and combustion characteristics of methanol and *n*-heptane under subcooled and flash-boiling conditions. They used a two-hole injector, which operated under an injection pressure of 10 MPa. An increase in plume interference and spray angle, along with a reduction in unburned hydrocarbons, was observed for methanol under flash-boiling conditions.

Regarding the atomisation and vaporisation mechanisms of sprays under flash-boiling conditions, the following processes are defined: nucleation of bubbles, bubble growth, vaporisation, and droplet breakup [24]. Additionally, Robinson and Judd [22] defined four phases present in the bubble growth process: surface tension (ST), transition (T), inertia-controlled (IC), and heat transfer-controlled (HT).

Saha et al. [23] investigated the behaviour of a single droplet of oxymethylene ethers (OME_x) e-fuels under flash-boiling conditions, taking into account that, depending on the molecular characteristics of the e-fuels, their thermo-physical characteristics present a considerable variation compared to conventional fuels. The authors reported that for OME_1 under low superheat conditions, only the surface tension and transition phases were observed in the bubble growth process; however, under moderate and high superheat conditions, the inertia-controlled phase was also observed. Finally, when comparing bubble growth between dimethyl ether (DME), OME_1 and OME_4 , it was concluded that DME exhibited the fastest bubble growth rate.

Badawy et al. [3] evaluated the ambient-to-saturation pressure ratio reduction effect on the spray characteristics for four fuels (iso-octane, ethanol, methanol, and commercial grade gasoline). Although spray collapse was observed for all fuels at low ambient-to-saturation pressure ratios, no direct relationship was established with the variations observed in spray penetration, cone angle, axial velocity, and Sauter mean diameter.

Li et al. [18] investigated the impact of low ambient temperature on the spray characteristics of methanol by varying both ambient and fuel temperatures, demonstrating

that spray collapse under flash-boiling conditions is delayed when the ambient temperature is reduced.

Huang et al. [10] compared the spray characteristics (spray tip penetration and spray area) of gasoline and five synthetic fuels (ethanol-to-gasoline, G40, bio-naphtha, DMC, and bio-ethanol), under two different fuel temperatures, 25°C and 200°C. At 25°C, separation between the plumes was distinguished for all the fuels, but the ethanol-to-gasoline and bio-ethanol exhibited a higher penetration than the other fuels. At 200°C, bio-ethanol and G40 fuels presented the highest tip penetration. This study highlights the variations in spray morphology depending on the fuel; however, the impact of spray collapse on the final results was not addressed.

This study evaluates the morphological changes of synthetic fuel sprays when the flash-boiling conditions are reached. The analysis focused on comparing global spray structures and detecting a possible propensity for spray collapse. The bubble point calculation was performed following the approach presented by Hutchison and Wallace [11] for surrogate fuels. Experimental research on the injection and atomisation of a multi-component synthetic fuel under flash-boiling conditions was conducted using a constant-volume chamber and a high-speed camera.

2. Experimental setup

In the present research on the injection process of a synthetic fuel, a Bosch HDEV5.2 six-hole injector with a hole diameter of 0.35 mm was used. The injector was mounted in a constant volume chamber (CVC) with optical access. A round quartz window was placed in front of the camera to prevent fuel from splashing over the camera optics. As tests were performed only at an ambient pressure and temperature environment, the other side of the vessel was left open for easier operation. The back wall of the chamber (with respect to the camera) was covered with black material to decrease background scattering and improve the sharpness of the observed fuel spray.

Flash-boiling conditions were obtained by increasing the fluid temperature prior to the injection. The fuel temperature range was 25–120°C, and its upper value was limited by the injector’s manufacturer-recommended operating temperature [6]. A constant injection pressure of 5 MPa was maintained in all tests.

Pressurisation of the system was based on a gas booster (Haskel, Single Acting – Single Stage model 86980), which increased the nitrogen pressure up to 5 MPa (gauge) pressure. The nitrogen pressure was monitored by a digital pressure gauge (Wika, model CPG1500).

To achieve refuelling at a controlled pressure and avoid air entrainment in the fuel line, a dedicated fuel line was implemented with an air-driven liquid pump (Maximator MSF111L). The nitrogen used to pressurise the fuel container was separated from the fuel by a piston designed and manufactured in stainless steel. It prevented nitrogen from dissolving in the fuel.

The injector opening time was set to 1.5 ms. The opening currents were set according to the manufacturer’s specifications [6] at 9.4 A with a 704 μs pickup time and 3.4 A with a 696 μs hold-on time.

The injection process was recorded at a frequency of 20,000 frames per second using a Photron FastCam SA1.1 camera equipped with a Nikon AF NIKKOR 24–85 mm 1:2.8-4 D lens, with the aperture fully open. To ensure adequate illumination, the chamber was illuminated by two LED lamps (Amaran 200D) operating at full power and fitted with Fresnel lenses. A photograph of the experimental setup presenting its main components is shown in Fig. 1.

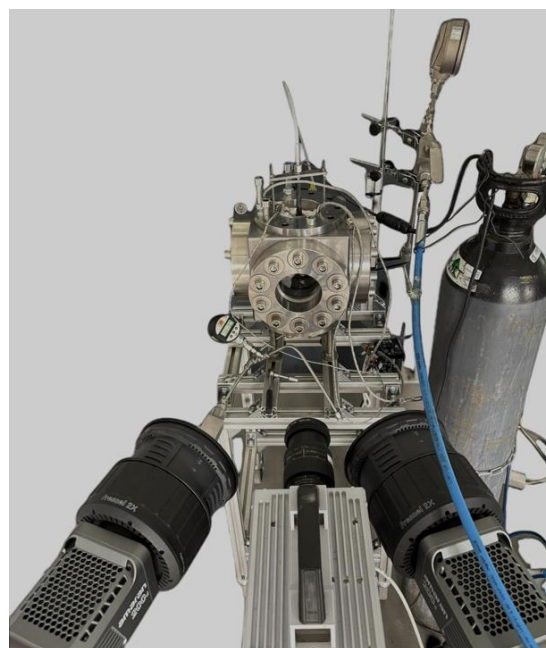


Fig. 1. Experimental setup – a photograph presenting main components: a constant volume chamber, high-speed camera and LED lamps (with Fresnel lens)

Figure 2 illustrates the arrangement of the setup and the interaction between its components.

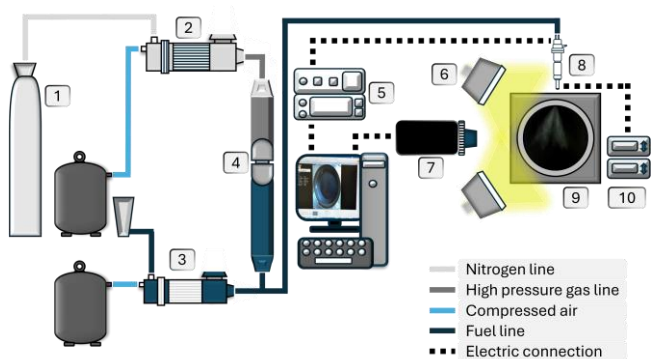


Fig. 2. Experimental setup: 1 – nitrogen tank, 2 – gas booster, 3 – fuel pump, 4 – piston, 5 – injection control unit, 6 – LED lamp, 7 – high-speed camera, 8 – injector, 9 – constant volume chamber, 10 – electric heater PID control

Image capture was performed using dedicated software provided by Photron, specifically PFV 4.4. The image recorded by the camera had a resolution of 564 × 564 pixels, and the injector was positioned so that its tip was visible within the camera’s field of view.

The fuel temperature was controlled using two electric heaters connected to PID controllers, based on the indica-

tion from two J-type thermocouples. The injector temperature was set according to the calibration performed previously for the high-boiling-point silicone oil [2]. The uncertainty of the temperature measurement and control system's components is shown in Table 1.

Table 1. Temperature control system's components

Component	Uncertainty
Dewetron EPAD2	$\pm 0.3^\circ\text{C}$
EMS-3710 N (j-type thermocouple input)	$\pm 1^\circ\text{C}$

To study the structural and physical effects of flash-boiling, a synthetic fuel composition is presented in Table 2. *n*-heptane, toluene, and *n*-octane, as the main components, are used to study the flash-boiling structural and physical effects in multi-component synthetic fuels.

Table 2. Fuel composition

Component	Volume fraction [%]
<i>n</i> -heptane	40
<i>n</i> -octane	40
toluene	10
<i>n</i> -hexane	6
ethylbenzene	2
<i>m</i> -xylene	2

The density and viscosity of the synthetic fuel were 722–730 $\frac{\text{kg}}{\text{m}^3}$ at 15°C and 0.45 mPa · s at 40°C, respectively.

In this study, similar to previous research [16], an inverse parameter (called the superheat index factor) is used instead of the ambient-to-saturation pressure ratio to describe the potential flash-boiling intensity. The superheat index factor R_p , is defined as the ratio of the saturation pressure P_{sat} for a given liquid temperature T_l to the ambient pressure P_a .

$$R_p = \frac{P_{\text{sat}}(T_l)}{P_a} \quad (1)$$

Following the methodology from Hutchison and Wallace [11], the R_p ratio was evaluated using an ambient pressure 0.1 MPa and the saturation vapour pressure of the liquid as the bubble pressure for each liquid temperature T_l .

The bubble pressure curve was evaluated using the Soave-Redlich-Kwong equation of state, also implemented in the DWSIM software, which proved to be sufficiently accurate for describing the bubble pressure curve when compared to the validated results from UNIFAC-NIST bubble points. Table 3 and Fig. 3 summarise the R_p results.

Table 3. Fuel temperature, saturation pressure, and the superheat index

T_l [°C]	P_{sat} [MPa]	R_p [-]
60	0.02	0.19
90	0.06	0.55
120	0.13	1.34

The parameter that varied between series of tests was the temperature of the injected liquid. The injector and heaters were thermally insulated using glass wool. The time

required to stabilise the liquid temperature inside the injector was experimentally determined to be 20 minutes. Subsequent test series were conducted at a stabilisation time of 30 minutes. Test within a single series (for the same temperature) were performed at intervals of 1 minute. The first test in each series was not considered in the analysis. The required temperature setpoint relative to the actual temperature of the injected liquid was previously determined through a calibration procedure.

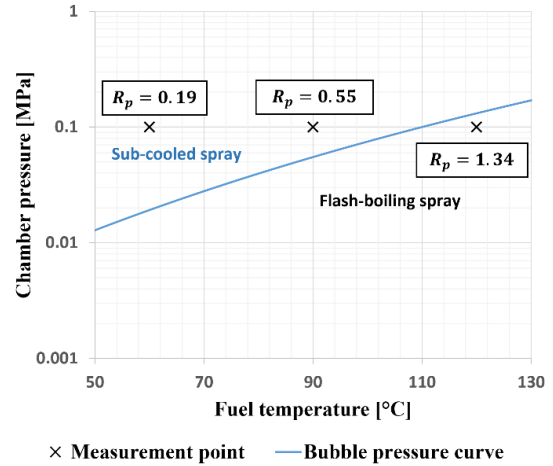


Fig. 3. Preheat ratio factor and flash-boiling regime

3. Results

The experimental investigation of the injection and atomisation of a synthetic fuel under subcooled and flash-boiling conditions provided detailed information on the dynamics of these processes. The studies performed using a multi-component surrogate synthetic fuel were focused on qualitative and quantitative analysis of the spray structures.

Figure 4 compares the selected spray images, after the background subtraction and the application of the artificial colour scale, with colours corresponding to the scattered light intensity detected by the camera pixels.

For the fuel temperatures 25°C and 60°C, the differences between the spray clouds seem to be marginal, and it is observed for each considered time after the start of injection. As the fuel temperature increases from 25 to 120°C, an increase in the area covered by the spray becomes visible. Moreover, the scattering signal intensity along the spray axis and the spray area increased. At a fuel temperature of 120°C, initially separated regions of the spray cloud begin to merge, and the separation distance between the plumes is reduced. On this basis, it can be stated that at a temperature of 120°C, the individual plumes become wider due to rapid vaporization, which intensifies the breakup of the liquid jet and promotes finer droplet detachment with an increased radial-to-axial momentum ratio. However, the effects of flash-boiling, in this case, are not profound.

The spray structures were also evaluated quantitatively. For this purpose, three parameters were selected: spray tip penetration (STP), spray area, and spray width. The definition of STP, maximum width, and maximum area are presented in Fig. 5.

In Figure 5a, spray tip penetration, considered a macro parameter, is defined as the maximum distance reached by the fuel spray within the chamber. The maximum width parameter represents the maximum horizontal extent of the spray, defined as its overall width. The spray area refers to the largest area covered by the fuel (white colour) visible in Fig. 5b.

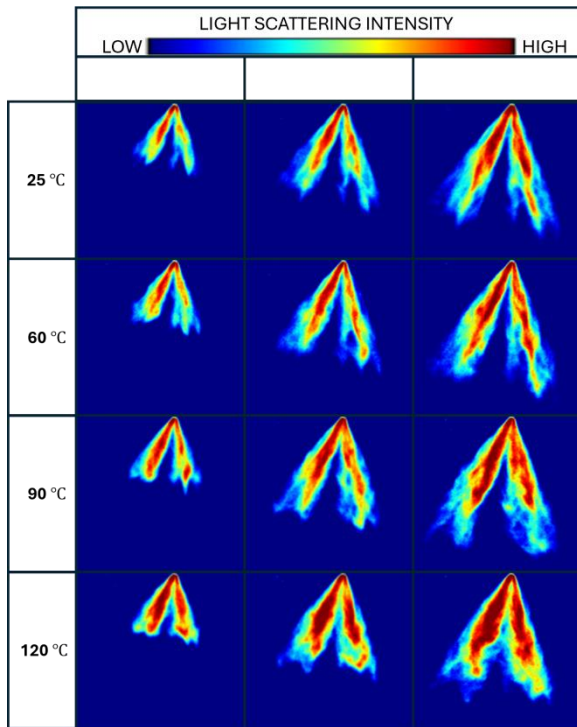


Fig. 4. Spray clouds at 0.5, 1.0, and 1.5 ms after start of injection (ASOI) at varying fuel temperature

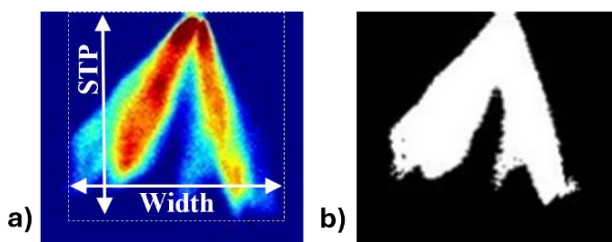


Fig. 5. Definition of: a) STP and spray width, b) spray area (white pixels)

Figures 6–8 present the results of spray tip penetration (STP), spray area, and spray width, respectively, for selected time points.

According to the results, the STP, spray area, and spray width measured for the multi-component synthetic fuel depend on the fuel temperature. The biggest differences were observed at 1.5 ms after the start of injection (ASOI). Heating fuel up to 120°C leads to considerable changes in the macro parameters of the spray. After full development of the fuel sprays (1.5 ms), the highest STP was observed for fuel temperatures of 90 and 60°C. For fuel at 120°C, the STP is slightly smaller; the spray area and maximum width of the fuel spray are the largest compared to those at other temperatures.

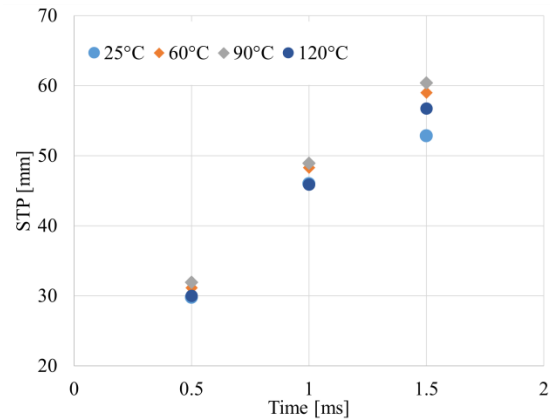


Fig. 6. Spray tip penetration of fuel spray at 0.5, 1.0, and 1.5 ms after start of injection

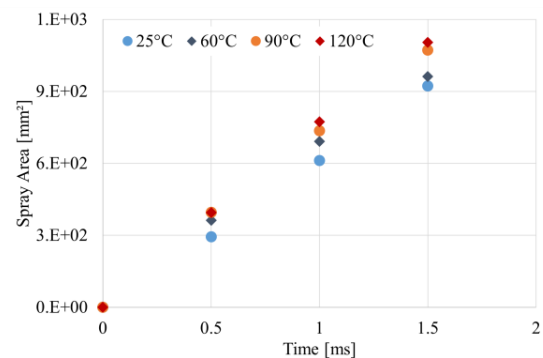


Fig. 7. Spray area at 0.5, 1.0, and 1.5 ms after start of injection

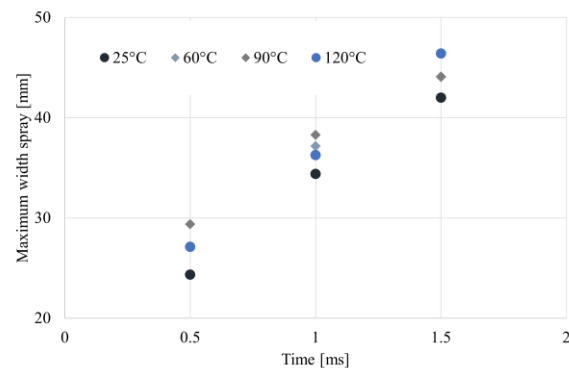


Fig. 8. Maximum spray width at 0.5, 1.0, and 1.5 ms after start of injection

Both qualitative and quantitative analyses reveal the differences between the spray structures, suggesting possible effects from flash-boiling. The reduced spray tip penetration, increased spray area and width, as well as the reduced separation distance between the individual spray plumes, are in accordance with the flash-boiling effects observed by other researchers.

This agreement enables linking the observed changes with the rapid vaporisation, which intensifies the breakup of the liquid jet and promotes the formation of smaller droplets with an increased radial-to-axial momentum ratio. However, as the observed changes in the spray structures were not substantial, it is necessary to consider that other factors, such as reduced surface tension and viscosity, may also play a role.

4. Summary and conclusions

This paper presents the results of experimental studies of multi-component synthetic fuel sprays formed under flash-boiling conditions. The experimental studies were carried out on a dedicated test stand equipped with a multi-hole injector, a constant-volume chamber, and a high-speed camera used to visualise the sprays forms inside the constant-volume chamber. The acquired images were used to compare the spray structures in both qualitative and quantitative manners, and to draw conclusions about the possible effect of flash-boiling on the injection and atomisation of the considered synthetic fuel.

The results showed that the spray structure was sensitive to temperature changes, especially in the highest range (from 90 to 120°C), possibly resulting in flash-boiling. However, the secondary effects related to the rapid vaporisation of the injected fuel, in the form of spray collapse, were not observed, and the changes were not profound.

In general, the key observations related to the changes in spray morphology can be summarised as follows:

- At the highest studied temperature (120°C), the spray area and the scattering signal intensity visibly increased, suggesting enhanced atomisation and smaller droplets
- The individual plumes became thicker, and the separation distance between them decreased. Nevertheless, the plume separation was still observed even for the highest studied temperature
- The highest STP was observed for fuel temperatures of 60 and 90°C, under subcooled conditions
- Under flash-boiling conditions (120°C) and after full development of multi-component synthetic fuel sprays

(1.5 ms), the spray tip penetration STP was slightly reduced. In contrast, the spray area and spray width were increased compared to other fuel temperatures.

All those observations suggest an effect of flash-boiling, even though the superheat index R_p was relatively low (1.34). However, the observed changes were not substantial, and the plume separation, visible even at the highest temperature, indicates that no significant near-nozzle effects from flash-boiling were present.

Nevertheless, in terms of possible cross-flowing air in an engine combustion chamber, even those small effects could influence the mixture formation, as smaller droplets, due to the increased importance of aerodynamic drag, exchange momentum with the ambient gas more effectively.

These aspects, in turn, suggest two important possible next steps in further research. Firstly, further studies are required to determine whether a further reduction in plume separation and spray collapse can be observed at lower ambient pressures (and increased superheat index) for this fuel. The second research could be oriented on the possible cross-flow effects on the altered sprays. Even slightly modified sprays can interact differently with the cross-flowing air. Such changes, in turn, could profoundly affect spray evolution in a combustion chamber, influencing the performance of the combustion process and engine emissions.

Acknowledgements

This study was funded by the National Science Centre, Poland, within the framework of the OPUS programme, grant number: 2018/29/B/ST8/01356.

Nomenclature

ASOI	after start of injection	MtG	methanol-to-gasoline
CVC	constant volume chamber	OMEx	polyoxymethylene dimethyl ethers
d_{10}	mean droplet diameter	R_p	superheat index
DME	dimethyl ether	SMD	Sauter mean diameter
DVPE	dry vapour pressure equivalent	STP	spray tip penetration
FT	Fischer-Tropsch	TD	thermal-diffusion controlled
G-E	gasoline – ethanol	T_1	liquid temperature
GHG	greenhouse gases	VLE	vapour-liquid equilibrium
GTL	gas-to-liquid	W_e	Weber number
IC	inertia-controlled		

Bibliography

- [1] Atac OF, Moon S, Jeon J. Unraveling the initial flash boiling spray formation at the same superheated index achieved by altering ambient pressure and fuel temperature independently. *Int J Heat Mass Transf.* 2021;169:120897. <https://doi.org/10.1016/j.ijheatmasstransfer.2020.120897>
- [2] Bachanek J, Rogóż R, Pachler K, Tatschl R, Teodorczyk A, Kapusta ŁJ. Experimental study and empirical modelling of direct-injection n-heptane sprays formed under flash-boiling conditions. *Int J Heat Mass Transf.* 2025;236:126282. <https://doi.org/10.1016/j.ijheatmasstransfer.2024.126282>
- [3] Badawy T, Xu H, Li Y. Macroscopic spray characteristics of iso-octane, ethanol, gasoline and methanol from a multi-hole injector under flash boiling conditions. *Fuel.* 2022;307:121820. <https://doi.org/10.1016/j.fuel.2021.121820>
- [4] Bar-Kohany T, Arogeti M, Malka A, Sher E. Advances in liquid atomization via flash boiling – a global overview. *Energies.* 2023;16(19):6763. <https://doi.org/10.3390/en16196763>
- [5] Bar-Kohany T, Levy M. State of the art review of flash-boiling atomization. *At Sprays.* 2016;26(12):1259-1305. <https://doi.org/10.1615/atomizspr.2016015626>
- [6] Bosch Motorsport. HP Injection Valve HDEV 5.2. <https://www.bosch-motorsport.com/content/downloads/Raceparts/en-GB/49510539208591115.html#Tabs=9007199304263179/>
- [7] Cremades LV., Oller L. Techno-environmental feasibility of synthetic fuels in ground transportation. Application to the Spanish automobile fleet in 2035. *Energy Reports.* 2024;11:5466-5474. <https://doi.org/10.1016/j.egy.2024.05.032>

- [8] Cui M, Nour M, Fu J, Zhang W, Wang G, Xu H, et al. Fundamental investigation of methanol flash boiling combustion under direct injection conditions. *Combust Flame*. 2025;276. <https://doi.org/10.1016/j.combustflame.2025.114147>
- [9] Deutz S, Bongartz D, Heuser B, Kätelhön A, Schulze Langenhorst L, Omari A et al. Cleaner production of cleaner fuels: Wind-to-wheel-environmental assessment of CO₂-based oxymethylene ether as a drop-in fuel. *Energy Environ Sci*. 2018;11(2):331-343. <https://doi.org/10.1039/c7ee01657c>
- [10] Huang W, Oguma M, Kinoshita K, Abe Y, Tanaka K. Investigating spray characteristics of synthetic fuels: comparative analysis with gasoline. *Int J Automot Manuf Mater*. 2024;2-2. <https://doi.org/10.53941/ijamm.2024.100008>
- [11] Hutchison BRM, Wallace JS. Influence of fuel volatility on particulate matter emissions from a production DISI engine. *Fuel*. 2021;303:121206. <https://doi.org/10.1016/j.fuel.2021.121206>
- [12] Hwang J, Karathanassis IK, Koukouvinis P, Nguyen T, Tagliante F, Pickett LM et al. Spray process of multi-component gasoline surrogate fuel under ECN Spray G conditions. *Int J Multiph Flow*. 2024;174:104753. <https://doi.org/10.1016/j.ijmultiphaseflow.2024.104753>
- [13] International Energy Agency. *Global Energy Review 2025 – Natural Gas*. 2025. <https://www.iea.org/reports/global-energy-review-2025/global-trends>
- [14] Kalghatgi G, Agarwal AK, Senecal K, Leach F. Introduction to engines and fuels for future transport. *Energy, Environment, and Sustainability*. 2022:1-5. https://doi.org/10.1007/978-981-16-8717-4_1
- [15] Kannaiyan K, Sadr R. Experimental investigation of spray characteristics of alternative aviation fuels. *Energy Convers Manag*. 2014;88:1060-1069. <https://doi.org/10.1016/j.enconman.2014.09.037>
- [16] Kapusta ŁJ. Understanding the collapse of flash-boiling sprays formed by multi-hole injectors operating at low injection pressures. *Energy*. 2022;247:123388. <https://doi.org/10.1016/j.energy.2022.123388>
- [17] Letcher TM. Introduction with a focus on atmospheric carbon dioxide and climate change. *Future Energy: Improved, Sustainable and Clean Options for Our Planet*. 2020:3-17. <https://doi.org/10.1016/b978-0-08-102886-5.00001-3>
- [18] Li X, Xiang L, Wang L, Wang Z, Hu Y. Experimental study on macroscopic and microscopic characteristics of flash boiling methanol spray under extremely cold conditions. *Energy Convers Manag*. 2025;333:119780. <https://doi.org/10.1016/j.enconman.2025.119780>
- [19] Liu G, Larson ED. Comparison of coal/biomass co-processing systems with CCS for production of low-carbon synthetic fuels: methanol-to-gasoline and Fischer-Tropsch. *Energy Procedia*. 2014:7315-7329. <https://doi.org/10.1016/j.egypro.2014.11.768>
- [20] Neroorkar K, Schmidt D. Modeling of vapor-liquid equilibrium of gasoline-ethanol blended fuels for flash boiling simulations. *Fuel*. 2011;90(2):665-673. <https://doi.org/10.1016/j.fuel.2010.09.035>
- [21] Ram V, Salkuti SR. An overview of major synthetic fuels. *Energies*. 2023;16. <https://doi.org/10.3390/en16062834>
- [22] Robinson AJ, Judd RL. Bubble growth in a uniform and spatially distributed temperature field. *Int J Heat Mass Transf*. 2001;44(14):2699-2710. [https://doi.org/10.1016/S0017-9310\(00\)00294-5](https://doi.org/10.1016/S0017-9310(00)00294-5)
- [23] Saha A, Grenga T, Deshmukh AY, Hinrichs J, Bode M, Pitsch H. Numerical modeling of single droplet flash boiling behavior of e-fuels considering internal and external vaporization. *Fuel*. 2022;308:121934. <https://doi.org/10.1016/j.fuel.2021.121934>
- [24] Senda J, Hojyo Y, Fujimoto H. Modeling on atomization and vaporization process in flash boiling spray. *JSAE Rev*. 1994;15(4):291-296. [https://doi.org/10.1016/0389-4304\(94\)90209-7](https://doi.org/10.1016/0389-4304(94)90209-7)
- [25] Smith JM, Ness HC Van, Abbott MM, Swihart MT. Introduction to chemical engineering thermodynamics eighth edition. 8 ed. New York: McGraw-Hill 2018:68-132.
- [26] Stępień Z. Synthetic automotive fuels. *Combustion Engines*. 2023;192(1):78-90. <https://doi.org/10.19206/CE-152526>
- [27] Uchida N, Onorati A, Novella R, Agarwal AK, Abdul-Manan AFN, Kulzer AC et al. E-fuels in IC engines: a key solution for a future decarbonized transport. *Int J Eng Res*. 2025. <https://doi.org/10.1177/14680874251325296>
- [28] Xu M, Zhang Y, Zeng W, Zhang G, Zhang M. Flash boiling: easy and better way to generate ideal sprays than the high injection pressure. *SAE Int J Fuels Lubr*. 2013;6(1):137-148. <https://doi.org/10.4271/2013-01-1614>
- [29] Zeng W, Xu M, Zhang G, Zhang Y, Cleary DJ. Atomization and vaporization for flash-boiling multi-hole sprays with alcohol fuels. *Fuel*. 2012;95:287-297. <https://doi.org/10.1016/j.fuel.2011.08.048>

Henry Andrés Porras Perucho, MSc. – Faculty of Power and Aeronautical Engineering, Warsaw University of Technology, Poland.

e-mail: henry.porras_perucho.dokt@pw.edu.pl



Joanna Grochowalska, DEng. – Faculty of Mechanical Engineering and Ship Technology, Gdańsk University of Technology, Poland.

e-mail: joanna.grochowalska@pg.edu.pl



Cláudio Manuel Vianna Moreira, BSc. – Faculty of Sciences, Physics Department, University of Lisbon, Portugal.

e-mail: clauvmoreira@gmail.com



Łukasz Jan Kapusta, DEng. – Faculty of Power and Aeronautical Engineering, Warsaw University of Technology, Poland.

e-mail: lukasz.kapusta@pw.edu.pl



Łukasz Boruc, DEng. – Faculty of Power and Aeronautical Engineering, Warsaw University of Technology, Poland.

e-mail: lukasz.boruc@pw.edu.pl



Analysis of the possibilities of using alternative fuel mixtures as a substitute for conventional fuels

ARTICLE INFO

Received: 18 June 2025
Revised: 13 October 2025
Accepted: 21 November 2025
Available online: 13 December 2025

In the face of growing requirements to reduce exhaust emissions and the need for more ecological solutions in the transportation sector, increasing attention is being paid to alternative fuels. This article examines the potential of using fuel mixtures containing bio-components, in particular alcohols and Sustainable Aviation Fuel (SAF), as a substitute for conventional fuels. The research focuses on two key aspects: composition of the fuel mixture and exhaust emissions. The research results aim to determine whether the proposed alternative fuel mixture can be an effective and more environmentally friendly alternative to conventional fuels, while maintaining suitable operating properties. The results of this work can be a valuable contribution to the development of sustainable fuel technologies, helping to reduce the negative impact of transportation on the environment.

Key words: *alternative fuels, exhaust gases analyzer, spark ignition engines, ethanol blends, emission reduction*

This is an open access article under the CC BY license (<http://creativecommons.org/licenses/by/4.0/>)

1. Introduction

In recent years, the global transportation sector has been facing growing pressure to reduce its environmental footprint due to the urgent need to mitigate climate change and comply with increasingly stringent emission standards. Road transport, in particular, remains a significant contributor to greenhouse gas emissions, as well as the production of nitrogen oxides (NO_x), carbon monoxide (CO), and particulate matter (PM), which not only exacerbate global warming but also have a substantial impact on air quality and public health. In this context, the development and implementation of alternative fuels have become a central focus of research and innovation.

Among various approaches to fuel decarbonization, blending conventional fossil-based fuels with renewable or oxygenated components such as alcohols or esters offers a relatively accessible and scalable strategy. Bioethanol, derived from biomass, is already widely used in gasoline blends (e.g., E10, E85). At the same time, ethyl acetate, a volatile organic ester, has emerged as a promising additive due to its oxygen content and combustion-enhancing properties. Simultaneously, aviation kerosene (Jet A-1), although not renewable, is of interest as a high-energy-density component that may stabilize combustion when used in multi-component blends, especially in experimental or transitional fuel systems.

This study aims to analyze the potential of alternative multi-component fuel blends – specifically those containing ethanol, ethyl acetate, and Jet A-1 – to act as viable substitutes for conventional gasoline. The research is focused on two key aspects: the composition of the proposed blend and its impact on pollutant emissions. A particular emphasis is placed on how such mixtures influence the formation of carbon monoxide and nitrogen oxides during combustion, as these are critical indicators of both efficiency and environmental impact.

The article is structured as follows. Section 2 presents a comprehensive literature review that summarizes existing

research on alcohol-based fuels, oxygenated additives, and the role of hydrocarbon carriers, such as Jet A-1. Section 3 outlines the methodology for selecting alternative fuel components. Section 4 outlines the experimental methodology and test setup used to evaluate fuel performance and emissions. Section 5 discusses the results of laboratory tests, comparing the proposed blend against a conventional gasoline baseline. Finally, Section 6 concludes by assessing the feasibility of implementing alternative fuels in practical automotive applications and outlines directions for further research.

2. Biocomponents in engine fuels

2.1. Introduction

Among the various bio-components explored for fuel blends, ethanol remains prominent due to its capacity to enhance combustion efficiency and reduce toxic emissions. Analytical studies, such as those by Balat et al. and Srinivasan and Saravanan, have revealed that ethanol-gasoline blends, like E10 and E20, not only exhibit favorable ignition and combustion properties but also contribute to reductions in both CO and HC emissions. Ethanol's remarkable ability to enhance complete combustion is attributed to its molecular structure, which contains both carbon and significant amounts of oxygen, resulting in overall lower emissions when blended with gasoline [9, 10].

Moreover, the potential incorporation of other oxygenates such as ethyl acetate further enhances the stability and performance of these fuel blends. Ethyl acetate has been noted for improving volatility, thus enabling better cold-start capabilities, while reducing soot and particulate matter emissions – a characteristic highlighted in comparative studies of alcohol-blended fuels [3].

Additionally, the exploration of Jet A-1 kerosene in blends with ethanol and gasoline brings forth intriguing considerations regarding fuel properties, particularly with respect to volatility and heat release characteristics. The research indicates that the addition of Jet A-1 could miti-

gate particulate matter emissions while simultaneously stabilizing combustion under varying temperature and pressure conditions. Studies conducted within this scope suggest that although small proportions of Jet A-1 might lead to an increase in CO emissions due to incomplete fuel vaporization, the overall combinatory effects on emissions may warrant further investigation [6].

2.2. Ethanol

The use of ethanol, particularly in various proportions such as E10 (10% ethanol), E20 (20% ethanol), and E85 (85% ethanol), has been the subject of extensive research to assess its impact on emissions in spark-ignition engines. One of the primary benefits associated with higher ethanol content in fuel blends is the reduction in carbon monoxide (CO) emissions, largely attributed to ethanol's higher oxygen content. Studies demonstrate that the presence of oxygenate compounds in the fuel promotes more complete combustion, resulting in lower CO emissions across several engine test conditions. For instance, Wu et al. reported that variations in ethanol blending can result in significant reductions in CO emissions, with reductions of 20% to 25% when moving from gasoline to E10 blends, a trend also consistent with findings from Cesur et al., who highlighted the benefits of enhanced combustion characteristics provided by alcohol-based fuels [2, 12].

On the other hand, the effect of ethanol blends on nitric oxides (NO_x) emissions demonstrates a more complex relationship. At moderate ethanol concentrations, such as E10 and E20, studies indicate that while CO emissions decrease, NO_x emissions can increase due to higher combustion temperatures resulting from richer fuel blends. However, for high ethanol blends such as E85, the evaporative cooling effect of ethanol tends to lower combustion temperatures, potentially mitigating the rise in NO_x emissions observed at lower ethanol concentrations. This dual effect of ethanol on NO_x emissions is corroborated by multiple studies, including findings from He et al., Wu et al., and Syarifudin et al., where they reported that while NO_x can increase under certain conditions, the overall emissions profile changes favorably in terms of CO and hydrocarbons (HC) with increased ethanol content [3, 11, 13].

Moreover, unburned hydrocarbons, often exacerbated during cold starts, present another dimension to the emissions profile associated with ethanol-rich blends. Ethanol has lower volatility than traditional gasoline, resulting in delayed vaporization under colder starting conditions, which in turn can contribute to elevated HC emissions. Nevertheless, modern engine management systems have evolved to offset such undesirable effects by optimizing fuel injection and ignition timing. Research by Sasongko and Wijayanti indicated that incorporating ethanol enhances combustion due to increased oxygen availability, thereby leading to a significant reduction in hydrocarbons under optimal conditions [4, 11].

2.2. Jet A-1 kerosene as a fuel blend component

The inclusion of Jet A-1 kerosene into spark-ignition fuel blends introduces possibilities for altering emission profiles and enhancing fuel efficiency. Jet A-1's low volatility and high energy density create a stabilizing influence

when blended with more volatile fuels, such as ethanol. Research indicates that such blends can result in lower NO_x emissions due to decreased combustion temperatures when designed judiciously. Moreover, the cooling characteristics of Jet A-1, combined with the combustion enhancements offered by alcohols, could create a unique synergistic effect beneficial to emission profiles [3].

Further analysis indicates that while Jet A-1 enhances combustion stability in ethanol blends, the interplay of fuel properties necessitates meticulous calibration of the air-fuel ratios and ignition timing. While higher ethanol blends may elevate the potential for aldehyde emissions, particularly acetaldehyde, concurrent evaluations challenge the emissions profiles against other regulated pollutants [9]. Continued scrutiny of potential detrimental emissions, in conjunction with the benefits of increased oxygen content, necessitates a balanced approach that emphasizes optimizing combustion parameters for both environmental compliance and vehicle performance.

2.3. Alternative fuel blends as gasoline substitutes

The integration of alternative fuels, such as ethanol and ethyl acetate, into gasoline presents a distinctive avenue for reducing greenhouse gas emissions. Studies have shown that when evaluated within the specific context of combustion efficiency, fuels blended with 10% to 20% ethanol can significantly reduce CO emissions and improve overall combustion outcomes when appropriately tuned [1, 13]. Ethanol-laden fuels not only satisfy the demand for more sustainable energy solutions but also demonstrate compatibility with existing fuel infrastructures, particularly for lower ethanol blends like E10. However, transitioning to higher blends, such as E85, necessitates evaluating potential evaporative emissions and incomplete combustion issues arising from the higher alcohol content, especially under high-temperature conditions [3, 8].

There's a compelling argument for developing additional research and long-term assessments of these alternative blends. During cold starts, as highlighted in several studies, including those of Solanki et al. and Elfasakhany, the challenges of managing varying vaporization properties necessitate focused insights for practical use, underscoring a gap that remains to be addressed before the widespread adoption of high-ethanol-content fuels [4, 10]. Further delineation of these effects will be critical in assessing the emissions trade-offs associated with the adoption of such biofuel alternatives.

2.4. Impact of fuel blends on pollutant emissions

A discernible trend is that particulate matter emissions tend to decrease with increasing ethanol concentrations, as evidenced by empirical data showing that E10 leads to significant reductions in PM emissions relative to conventional gasoline. The oxygenate characteristics of ethanol enable more efficient combustion, reducing the formation of soot and aromatic compounds and resulting in lower particulate emissions [7, 12].

Nevertheless, moving toward higher ethanol blends introduces complex dynamics related to aldehyde emissions, particularly acetaldehyde, which can reportedly increase by 50-70% when shifting from gasoline to E40 or higher

Table 1. Parameters of potential blend components

	Mass fraction	RON	Calculated RON	Specific energy [MJ/kg]	Calc. specific energy [MJ/kg]	Flame speed [m/s]	Calc. flame speed [m/s]	Flame temperature [°C]	Calc. flame temperature [°C]
Gasoline	0	95	0	46	0	0.50	0	2100	0
Ethyl acetate	0.28	118	32.85	27	7.52	0.45	0.13	2100	584.66
Kerosene (Jet A-1)	0.22	30	6.65	44	9.75	0.35	0.08	2100	465.34
Methanol	0	112	0	20	0	0.45	0	1900	0
Ethanol	0.50	111	55.50	27	13.50	0.50	0.25	1900	950
Total	1								

blends. This necessitates careful monitoring and potential integration of advanced after-treatment systems designed to capture and reduce unregulated pollutants in these fuel blends [3, 12]. Furthermore, temperature effects – especially with blends containing E20 to E40 – demonstrate cooling due to ethanol evaporation, which counteracts the formation of NO_x emissions. This can translate into reductions in NO_x emissions compared to gasoline, aligning well with regulatory frameworks that mandate lower emissions standards [5, 13].

In summary, while the move toward higher ethanol blends showcases the promise of decreased CO and HC emissions, specific operational parameters must be optimized to avoid potential pitfalls, such as increased aldehyde emissions, and to strike a balance between emissions outcomes for regulated and unregulated pollutants. The complexities of combustion dynamics necessitate extensive future research focused on fine-tuning engine configurations, optimizing fuel management systems, and developing after-treatment solutions to mitigate any unintended consequences of emissions.

3. Selection of fuel components

Based on a literature review, components were selected and then analyzed to select the appropriate proportions. The composition of the analyzed mixture was determined using a spreadsheet that contained fuel parameters and the Solver add-on, with established boundary conditions for the mixture. All calculations were performed for each component of the mixture by multiplying its properties by its mass fraction. The values were then summed to obtain the properties for the entire mixture. To achieve NO_x reduction, the average flame temperature for the fuel was set to a maximum of 2000 degrees. The average flame propagation velocity, calculated based on the mass fraction of components, was set to a minimum of 0.4 m/s. The value of the octane number for the mixture was set to a minimum of RON 95. The specific energy was not set as a target and the goal of the solver solution was to obtain the highest possible value. After the analysis, the weight composition of the mixture was set as follows: 50% ethanol, 28% ethyl acetate, and 22% JET A-1 kerosene, which was later named E50EA28K22. The calculations and parameters are presented in Table 1.

Kerosene is primarily used as an ingredient to increase calorific value. The octane number and combustion speed when using only alcohols are higher than in the case of adding kerosene, however, in the aspect under consideration, there is no need to obtain a higher octane number than

standard E10 petrol. In contrast, without kerosene participation, there is a significant decrease in specific energy, resulting in higher fuel consumption. The calculated decrease in calorific value (Equation 1) compared to petrol is approximately 33%. Table 2 presents the expected emission levels resulting from the combustion of the fuels. This table was taken into consideration when choosing fuel blend components and helped achieve the expected results.

$$\Delta SE = \left(1 - \frac{CSE}{SE}\right) \times 100\% \quad (1)$$

$$\Delta SE = \left(1 - \frac{30.77}{46}\right) \times 100\%$$

$$\Delta SE \approx 33.11\%$$

where: ΔSE – specific energy difference [%], CSE – calculated specific energy of the blend [MJ/kg], SE – specific energy of gasoline [MJ/kg].

Table 2. Assumed emission profiles

Fuel	CO ₂ [g/MJ]	CO	NO _x	HC	PM
Gasoline	~73	High	Medium	High	Medium
Kerosene (Jet A-1)	~72	High	Medium	Medium	Medium
Ethanol	~69	Medium	Low	Medium	Low
Methanol	~67	Medium	Low	Medium	Low
Ethyl acetate	~65	Medium	Medium	Medium	Low

4. Description of the measuring station and measurement methodology

In order to carry out the measurements, a test stand was built, containing a power generator in which engine fuel mixtures were burned. Diagram of the measuring system is shown in Fig. 1.

The measuring station comprises a Honda EU22 generator and a Stage V-compliant single-cylinder combustion engine with a displacement of 120 cm³, as well as an AC generator with a nominal power of 2.2 kW. To generate a torque load on the combustion engine, resistors were electrically connected in the generator circuit to measure the generated electrical power. Fuel consumption was measured by measuring the mass loss of the fuel container in defined time intervals using a Radwag APP 35.3Y.1 precision scale ($d = 0.1$ g). The measurement of exhaust component concentrations was performed using a Horiba PG-300 and a MAHA MET6.3 exhaust gas analyzer. The measuring ranges of the analyzers are presented in Table 3.

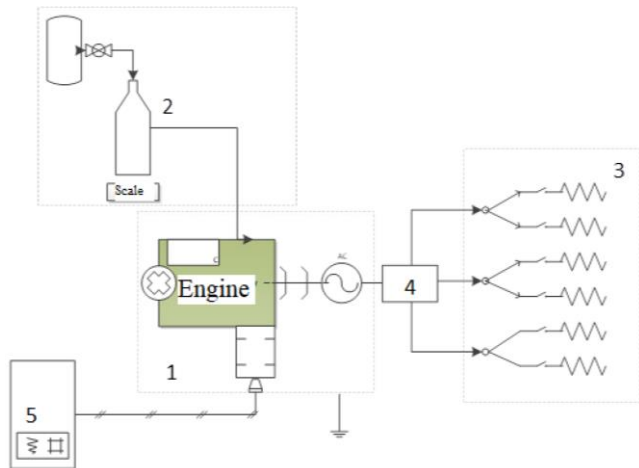


Fig. 1. Measuring system: 1 – generator, 2 – mass fuel consumption measurement system, 3 – resistive load, 4 – wattmeter, 5 – exhaust gas analyzers

Table 3. Measuring ranges

Device		Range	Repeatability
Horiba PG300	CO	0–10,000 ppm	±0.5% FS
	CO ₂	0–20% vol	±0.5% FS
	NO	0–2500 ppm	±0.5% FS
	SO ₂	0–200 ppm	±0.5% FS
MAHA MET 6.3	HC	0–30,000 ppm	±0.5% FS
	Lambda	0–9.9	–
	O ₂	0–25% vol	±0.02% FS

Six measurement points were determined for different electrical load configurations. Due to the difference in energy delivered per unit mass for the tested fuels, it was necessary to adjust the throttle opening angle. This was achieved using a lever to obtain an excess air coefficient of 1. Adjustment was necessary for each load change. After setting the appropriate throttle opening angle value, the unit was operated for about 2 minutes to stabilize the values on the exhaust gas analyzers. Then, fuel consumption and the values of the measured compounds in the exhaust gases were recorded. For each fuel, the measurements at all points were repeated three times in order to obtain an average of the measurements.

5. Results

Table 4 presents data read from the wattmeter, exhaust gas analyzers, and calculated fuel consumption for E10 petrol. At point 6, the NO measurement range for the analyzer was exceeded. However, this point is not taken into

account in the final comparison due to probable measurement inaccuracy.

The average results for the E50EA28K22 blend are shown in Table 5. Measurement point number 6 was rejected because the engine did not achieve sufficient torque to maintain the specified load for the tested alternative mixture. This is due to the lower calorific value of the fuel. Therefore, the average of 5 points was taken for comparison.

Comparison of the fuels for each corresponding measuring point is shown in Table 6. Point number 6 is included for transparency regarding each fuel blend; however, it is not considered in the comparison. The average change was calculated and is shown in Fig. 2. The average emission changes of E50EA28K22 relative to E10 are as follows:

- Nitrogen oxides (NO_x) – E50EA28K22 showed a reduction of ~30% in NO_x emissions. This is attributed to the cooling effect of ethanol evaporation and lower combustion temperatures compared to gasoline. The high oxygen content of the blend also promotes more complete combustion at lower temperatures.
- Hydrocarbons (HC) – Unburned hydrocarbon emissions decreased by ~10% for the alternative blend. Ethanol and ethyl acetate enhance oxidation during combustion, thus reducing HC emissions.
- Carbon monoxide (CO) – CO emissions were reduced by approximately 5% with the alternative blend. This is likely due to the high oxygen content of ethanol and ethyl acetate, which supports more complete combustion and reduces the formation of partial oxidation products, such as CO.
- Sulfur dioxide (SO₂) – A significant increase in SO₂ (~65%) was observed with the E50EA28K22 blend. This is directly linked to the sulfur content in Jet A-1, which remains much higher than the ultra-low sulfur levels mandated for gasoline. This result underscores the need for cleaner kerosene alternatives such as Sustainable Aviation Fuels (SAF).
- Carbon dioxide (CO₂) – CO₂ emissions increased by about 10%. This is consistent with the reduced CO levels and indicates a more complete oxidation of carbon-containing compounds to CO₂, a sign of improved combustion efficiency.

Lambda values for both fuels remained centered around 1, confirming stoichiometric combustion. The throttle adjustments and real-time lambda monitoring ensured consistent excess air levels, validating the methodology and reproducibility of the experimental results. The comparison only shows average changes for different fuels, serving as a summary indicator of relative trends.

Table 4. Results for gasoline E10

Measuring point	Average									
	Assumed electrical power	Electrical power	Fuel consumption	HC	Lambda	NO	CO	CO ₂	O ₂	SO ₂
[-]	[W]	[W]	[g/s]	[ppm]	[-]	[ppm]	[ppm]	[% vol]	[% vol]	[ppm]
1	0	0	0.15	228	1.027	27	8070	4.56	8.81	73.40
2	650	708	0.17	133	0.984	95	8570	6.96	6.62	20.10
3	850	907	0.17	111	0.988	195	8914	9.05	4.72	17.50
4	1300	1377	0.18	86	0.976	1232	7703	13.22	1.31	13.70
5	1500	1556	0.19	71	0.995	1914	5285	14.27	0.75	12.50
6	2150	2166	0.25	69	0.995	2803	4519	14.54	0.52	12.50

Table 5. Results for E50EA28K22 blend

Average										
Measuring point	Assumed electrical power	Electrical power	Fuel consumption	HC	Lambda	NO	CO	CO ₂	O ₂	SO ₂
[-]	[W]	[W]	[g/s]	[ppm]	[-]	[ppm]	[ppm]	[% vol]	[% vol]	[ppm]
1	0	0	0.19	222	1.023	23	8414	5.43	8.58	66.27
2	650	708	0.22	127	0.981	69	8842	8.26	5.84	34.50
3	850	908	0.22	91	0.983	121	9136	9.62	4.87	29.20
4	1300	1377	0.25	76	0.981	820	6832	13.90	1.13	26.83
5	1500	1556	0.27	62	1.003	1253	3920	14.61	0.78	25.40
6	2150	1717	0.30	64	1.009	1523	3381	14.69	0.75	24.67

Table 6. Comparison of the E50EA28K22 to gasoline E10

Average										
Measuring point	Electrical power	Fuel consumption	HC	Lambda	NO	CO	CO ₂	O ₂	SO ₂	
[-]	[W]	[%]	[%]	[%]	[%]	[%]	[%]	[%]	[%]	
1	0	26.8	-2.6	-0.4	-16.0	4.3	19.2	-2.6	-9.7	
2	708	35.0	-4.5	-0.3	-27.4	3.2	18.7	-11.8	71.6	
3	907	29.3	-18.0	-0.5	-38.2	2.5	6.3	3.2	66.9	
4	1377	36.3	-12.0	0.5	-33.5	-11.3	5.1	-14.0	95.9	
5	1556	41.7	-12.2	0.8	-34.5	-25.8	2.4	4.0	103.2	

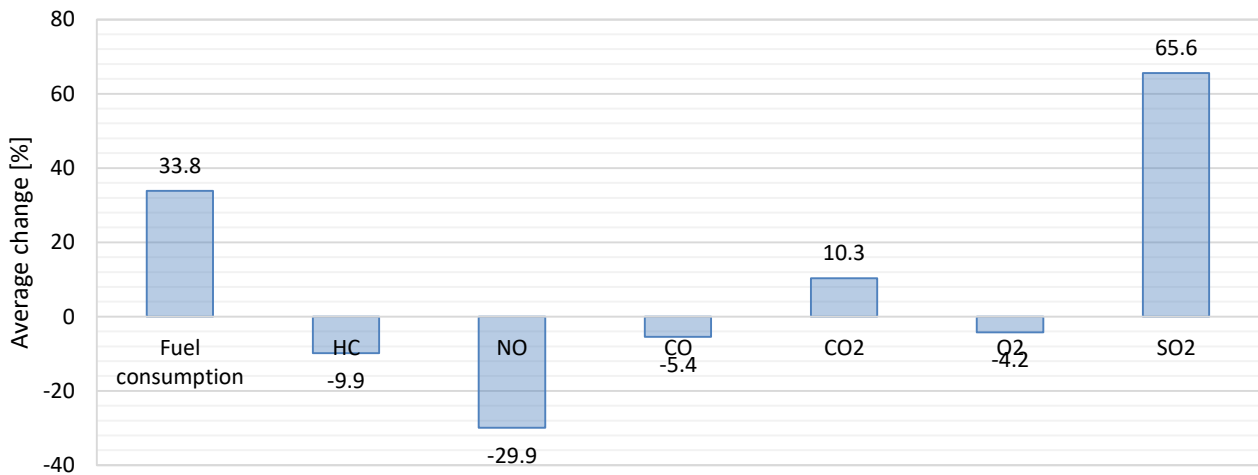


Fig. 2. Average change in comparison of the fuels

The addition of kerosene to the fuel causes a significant increase in sulfur dioxide, due to the fuel's chemical composition. The ASTM D1655 standard specifies a maximum sulfur content of 3000 ppm in aviation kerosene. This is 300 times more than the allowable content for gasoline, which is 10 ppm. Typically, the sulfur content in JET A-1 is lower, at around 500 ppm. Additionally, since the kerosene content in the mixture is only 22%, chemical analyses must be performed to determine the exact sulfur content. The studies focused only on the emission of sulfur dioxide during combustion.

Table 7 shows measured fuel consumption and electrical power for E10 gasoline. Later, specific fuel consumption was calculated using Equation 2. The same data is shown for E50EA28K22 blend in Table 8. The first measurement point is not taken into account because the generator was operating without an electrical load, so the generat-

ed electrical power is equal to 0. However, this does not mean that the engine generates zero power; due to the measurement of only electrical power, it is not possible to determine the mechanical power. If the power is assumed as 0, the specific fuel consumption will also be 0, which is not in accordance with reality.

Table 7. Fuel consumption of E10 gasoline

E10			
Measuring point	Fuel consumption	Electrical power	Specific fuel consumption
[-]	[g/s]	[W]	[g/kWh]
2	0.17	708	838.86
3	0.17	907	676.71
4	0.18	1377	480.91
5	0.19	1556	440.81
6	0.25	2166	420.09

Table 8. Fuel consumption of E50EA28K22

E50EA28K22			
Measuring point	Fuel consumption	Electrical power	Specific fuel consumption
[-]	[g/s]	[W]	[g/kWh]
2	0.22	708	1132.82
3	0.22	908	874.80
4	0.25	1377	655.27
5	0.27	1556	624.54
6	0.30	1717	634.68

$$g_u = \frac{G_u \cdot 3600000}{N_u} \quad (2)$$

where: g_u – specific fuel consumption [g/kWh], G_u – mass fuel consumption [g/s], N_u – electrical power [W].

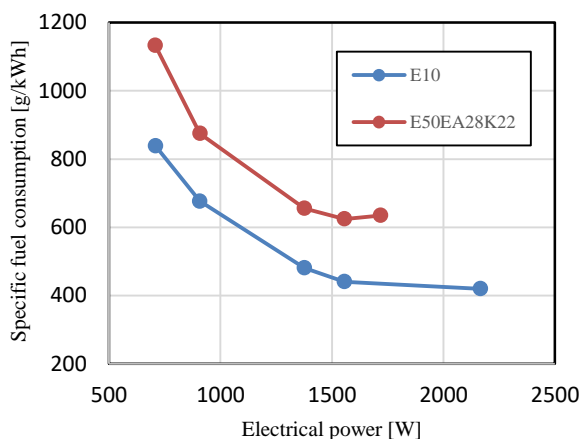


Fig. 3. Specific fuel consumption

The test results showed a clear increase in fuel consumption for the E50EA28K22 blend compared to conventional E10 gasoline (Figure 3). This was anticipated due to the lower specific energy content of the alternative mixture. On average, specific fuel consumption increased by approximately 34%, necessitating a greater mass of fuel to maintain the same power output. This trade-off highlights a limitation in energy density but may be justified by improvements in emission performance.

Nomenclature

CO carbon monoxide
 CO₂ carbon dioxide
 HC hydrocarbons
 NO nitrous oxide

PM particulate matter
 RON research octane number
 SAF sustainable aviation fuels
 SO₂ sulfur dioxide

Bibliography

[1] Bielaczyc P, Szczotka A, Woodburn J. A study of gasoline-ethanol blends influence on performance and exhaust emissions from a light-duty gasoline engine. SAE Technical Paper 2012-01-1052. 2012. <https://doi.org/10.4271/2012-01-1052>

[2] Cesur I, Eren B, Zengin A. Reducing emissions and promoting environmental sustainability in spark-ignition engines

6. Conclusions

This study demonstrates the potential of a novel multi-component fuel blend composed of 50% ethanol, 28% ethyl acetate, and 22% Jet A-1 kerosene as a feasible substitute for conventional E10 gasoline in spark-ignition engines. The blend was engineered to balance octane requirements, flame speed, and combustion temperature while maximizing energy efficiency within the constraints of regulated emissions.

Key findings include:

- Reduced Emissions: The alternative blend significantly lowered NO_x emissions (by ~30%) and unburned hydrocarbons (by ~10%) compared to E10, indicating more complete and cleaner combustion due to the oxygen-rich alcohols.
- Increased Fuel Consumption: Due to its lower specific energy, the blend required a higher fuel mass flow to maintain equivalent power output, resulting in a ~34% increase in fuel consumption.
- Trade-off in SO₂ Emissions: The addition of Jet A-1 increased sulfur dioxide emissions, highlighting a trade-off between calorific value enhancement and environmental impact, especially regarding sulfur content.
- Feasibility for Transition Fuels: Despite limitations, the blend meets standard octane requirements (RON 95) and performs within acceptable emission limits, making it a strong candidate for use in transitional or supplementary fuel systems.
- Substitution of Jet A-1 with Sustainable Aviation Fuels (SAF): SAFs derived from biomass, waste oils, or synthetic pathways offer lower sulfur content and improved lifecycle emissions profiles. Their use could mitigate the SO₂ emissions observed with Jet A-1 while maintaining the desired combustion stability.

Future research should focus on long-term engine durability, cold-start performance, and after-treatment systems to mitigate sulfur-related emissions. By replacing Jet A-1 kerosene with Sustainable Aviation Fuel, future fuel designs can better align with both regulatory emissions targets and sustainability goals. It should also be performed on a dynamometer with a combustion engine, which will allow for the analysis of exhaust gases at different loads and with different rotational speeds.

- [4] Kumar R, Chaurasia O. A review on performance and emissions of compression ignition engine fueled with ethanol-diesel blend. *Journal Européen Des Systèmes Automatisés*. 2019;52(2):205-214. <https://doi.org/10.18280/jesa.520214>
- [5] Qadiri U, Wani M. Performance combustion and emission characteristics of 3-cylinder SI engine fuelled conventional gasoline, ethanol blends, and micro-emulsion used as an alternative fuel. *Math Model Eng Probl*. 2019;6(4):541-549. <https://doi.org/10.18280/mmep.060409>
- [6] Sasongko M. and Wijayanti W.. Effect of ethanol addition on the performance and exhaust emissions of a spark ignition engine. *J Mech Eng Sci*. 2017;11(2):2734-2742. <https://doi.org/10.15282/jmes.11.2.2017.14.0248>
- [7] Seggiani M, Prati M, Costagliola M, Puccini M, Vitolo S. Bioethanol-gasoline fuel blends: exhaust emissions and morphological characterization of particulate from a moped engine. *Journal of the Air & Waste Management Association*. 2012;62(8):888-897. <https://doi.org/10.1080/10962247.2012.671793>
- [8] Sharudin H, Abdullah N, Najafi G, Mamat R, Masjuki H. Investigation of the effects of iso-butanol additives on spark ignition engine fuelled with methanol-gasoline blends. *Appl Therm Eng*. 2017;114:593-600. <https://doi.org/10.1016/j.applthermaleng.2016.12.017>
- [9] Solanki T, Jain S, Goyal A. Analysis on emissions of gasoline engine with different ethanol blends at different compression ratio. *Ymer Digital*. 2022;21(08):18-28. <https://doi.org/10.37896/ymer21.08/04>
- [10] Srinivasan C, Saravanan C. Emission reduction on ethanol-gasoline blend using fuel additives for an SI engine. *Energy Sources Part A: Recovery Utilization and Environmental Effects*. 2013;35(12):1093-1101. <https://doi.org/10.1080/15567036.2011.584114>
- [11] Syarifudin S, Sanjaya F, Fatkhurrozak F, Usman M, Sibagariang Y, Köten H. Effect methanol, ethanol, butanol on the emissions characteristics of gasoline engine. *Automotive Experiences*. 2021;4(2):62-67. <https://doi.org/10.31603/ae.4641>
- [12] Wu T, Chang C, Wu T, Shen Y. Emission characteristics of ethanol blending fuels from a laboratory gasoline engine. *Applied Mechanics and Materials*. 2012;253-255:2227-2230. <https://doi.org/10.4028/www.scientific.net/amm.253-255.2227>
- [13] Wu T, Hsu Y, Wu T. Comparisons of alcohol blending fuels' emission from a laboratory gasoline engine. *Adv Mater Res*. 2013;772:536-542. <https://doi.org/10.4028/www.scientific.net/amr.772.536>

Kacper Leśny, MEng. – Faculty of Mechanical Engineering, Wrocław University of Science and Technology, Poland.
e-mail: kacper.lesny@pwr.edu.pl



Adriana Włóka, MEng. – Faculty of Mechanical Engineering, Wrocław University of Science and Technology, Poland.
e-mail: adriana.wloka@pwr.edu.pl



Radosław Włostowski, DEng. – Faculty of Mechanical Engineering, Wrocław University of Science and Technology, Poland.
e-mail: radoslaw.wlostowski@pwr.edu.pl



Prof. Andrzej Kazmierczak, DSc., DEng. – Faculty of Mechanical Engineering, Wrocław University of Science and Technology, Poland.
e-mail: andrzej.kazmierczak@pwr.edu.pl



A model of a fuel spray parameter in a marine diesel engine

ARTICLE INFO

Received: 13 June 2025
Revised: 10 December 2025
Accepted: 11 December 2025
Available online: 11 January 2026

This work presents an empirical model of one of the main parameters describing fuel spray evolution in a marine diesel engine – spray cone angle in the early stage of spray formation. The model was formulated based on experimental data obtained in a constant volume chamber with optical access. Laboratory experimental studies were conducted to determine the parameters of fuel spray in marine diesel engine-relevant air densities. The Mie scattering spray visualization technique was employed to capture the propagation process of the liquid fuel. Furthermore, a model of the evolution over time of the spray cone angle is formulated, where the existing literature models of the spray cone angle are defined as constant. The calculation results for the spray cone angle were verified against the experimental data for the spray cone angle.

Key words: *marine diesel engine, marine fuel injector, fuel spray, mathematical model, spray cone angle*

This is an open access article under the CC BY license (<http://creativecommons.org/licenses/by/4.0/>)

1. Introduction

Piston internal combustion engines with compression ignition (CI) are the dominant types of engines used for propulsion in the marine sector. Among those engines, one can distinguish low-speed two-stroke engines and medium- and high-speed four-stroke engines. It is essential to note that marine engines can differ significantly in design from those used in automotive applications [3, 14].

Despite ongoing efforts to implement alternative fuels and propulsion systems aboard marine ships, marine diesel engines continue to primarily burn heavy fuel oil (HFO) and marine diesel oil (MDO) [21, 25]. These fuels can differ in physical properties, such as density and viscosity, compared to conventional diesel oil. The combustion of these fuels produces exhaust gases containing nitrogen oxides (NO_x), sulfur oxides (SO_x), carbon oxides (CO_x), and particulate matter (PM), which significantly contribute to air pollution in the maritime environment [10, 23]. Pollution resulting from marine engine emissions was the driving force behind the introduction of Annex VI to the MARPOL 73/78 Convention by the International Maritime Organization (IMO), which regulates permissible emission levels. Notably, the IMO has announced plans to reduce total greenhouse gas emissions from maritime transport by 50% by 2050, compared to 2008 levels [11].

Considering the trend towards introducing alternative fuels and achieving low-emission targets in compression-ignition marine engines, there is a growing need to conduct research on fuel spray behavior [22, 26].

The processes of fuel injection and atomization in internal combustion engine cylinders are critical, as they directly influence air-fuel mixing, ignition, and combustion behavior. Moreover, the distinct structural characteristics of marine diesel engines with direct fuel injection, in contrast to those used in the automotive sector, necessitate a detailed understanding of the fuel injection and spray formation processes that occur inside the cylinders.

The formation of the fuel spray injected directly into the cylinder of a marine diesel engine depends on the injector

nozzle's design parameters, fuel properties, and the conditions existing during injection [8]. One of the key parameters responsible for jet and droplet disintegration is the air density to which the fuel is injected.

When the fuel is injected at high pressure into the combustion chamber of a marine diesel engine, it is atomized into droplets and forms a characteristic conical spray shape. The shape and internal structure of the atomized fuel spray influence subsequent combustion processes inside the cylinder. The fuel spray propagates deeper into the chamber, increasing in both axial and radial directions. The fuel spray geometry is described by parameters that define its outer dimensions and internal structure. These parameters are classified into macro- and micro-groups. Macro parameters include the spray tip penetration (STP) and spray cone angle (SCA), whereas a typical micro-parameter used for evaluating atomization quality is the mean droplet diameter. The structure of the fuel spray pattern in the cylinder depends on the injector design features and operating pressure parameters. For example, higher injection pressure improves break-up of the fuel jet, but may also increase spray penetration and the risk of fuel impingement on the cylinder walls [18]. The authors [18] also presented the results of a study on the effect of the SCA on NO_x and soot emissions. As the SCA increased, NO_x emissions decreased, whereas soot emissions increased. On the other hand, changes in nozzle geometry affect the angle of the fuel spray. Tang et al. [20] demonstrated the influence of different nozzle k-factor on the spray angle as a function of time, for fuel injection pressure of 200 MPa and a backpressure of 5 MPa. It should be noted that the k-factor is defined as the ratio of the difference between the inlet and outlet diameters of the nozzle to its length [20]. Their study showed that for all tested nozzles, the fuel spray angle decreased rapidly within the first 0.1 ms, corresponding to the initial phase of injection. After approximately 0.2 ms, the spray cone angle stabilized. This spray behavior is characteristic of high injection pressures. Moreover, it was found that an increase in the k-factor results in a linear increase in the

average fuel spray angle. Therefore, the ability to predict the structure of the injected fuel based on injection conditions and fuel type becomes important.

The values of fuel spray parameters are typically determined using models that combine physical principles with empirical relationships derived from experimental data [12]. These models typically consider the type of fuel, nozzle outlet diameter, and injection and ambient conditions. As a result, they are well correlated with the specific conditions under which they were developed. Therefore, applying these models to different conditions – such as alternative fuel types or other nozzle geometries – may not be valid under different conditions.

STP models account for the temporal and spatial variability of the fuel spray as it propagates into the cylinder. The SCA of the atomized spray is typically described as a constant value of a fully developed fuel spray, which remains unchanged over time [1, 4, 9]. From a general perspective, the mathematical models of SCA described in the literature include fuel and gas density in the cylinder, as well as the geometrical parameters of the fuel spray injector.

This is due to the fact that at high fuel injection pressures, the spray cone angle reaches a steady value very quickly after the start of injection, as observed in the test results described by [16, 20]. In [12], Kegl et al. proposed a model to calculate the spray angle of mineral diesel and rapeseed oil biodiesel. In developing the spray cone angle model, the authors considered the change of this parameter over time. It should be noted that the injection pressure was 17 MPa.

Marine diesel engines feature cylinders of much larger size than those used in automotive applications [17]. As such, effective combustion requires that the correct amount of fuel be delivered and atomized in the whole chamber volume. To maximize combustion efficiency, the fuel must be evenly distributed throughout the large combustion chamber. A high-viscosity spray injected into the marine diesel engine cylinder undergoes both primary and secondary break-ups influenced by chamber backpressure, nozzle geometry, and initial spray velocity. Due to the large scale of the marine diesel engine spray, changes in the SCA during the early stage of fuel spray development may be considerable.

In marine diesel engines with autoignition, the combustion process initiates with the injection and subsequent creation of a small portion of an air-fuel mixture capable of autoignition. The fuel injection begins shortly before the piston reaches top dead center (TDC), and the ignition is usually initiated before the entire volume of fuel is introduced. The injection continues during the initiated combustion process, significantly influencing the further characteristics of late-stage combustion and emissions. Consequently, analyzing the early development and radial expansion of the fuel spray during the initial stages of injection is crucial for creating an air-fuel mixture capable of autoignition.

The purpose of this study is to develop a new mathematical model that describes changes in the SCA of a marine diesel engine fuel injector as a function of time. To achieve this, high-speed imaging was employed in a series of experimental tests.

2. Experimental setup

The experimental setup consisted of three main modules [5–7]:

- a constant-volume chamber
- a visualization system based on a high-speed camera and global illumination to record the Mie scattering signal
- a pressure fuel supply system for the injector.

The test constant-volume chamber was cubic in shape and provided optical access from two sides. It is worth noting that the constant-volume chamber system is a fundamental piece of experimental research equipment in studies on fuel atomization and combustion. The marine diesel fuel injector was mounted on top of the chamber and tilted in relation to the chamber axis to increase the spray observation distance. The main design parameters of the chamber are presented in Table 1 and in [5]. The record propagation of fuel spray was carried out through one of the chamber's viewing windows, while the remaining three were covered to minimize light reflections.

Table 1. The main design parameters of the constant-volume chamber [5]

Parameter	Unit	Value
Length/width	mm	200 × 200
Diameter of the viewing window	mm	100
Number of access windows	–	4
Maximum backpressures	MPa	5

The parameters and methodology were included earlier in [5–7]. The chamber was filled with inert nitrogen gas during the tests. The tests were conducted at ambient temperature. Two levels of backpressure conditions were considered (p_B): 3.2 MPa and 4.3 MPa. A marine diesel fuel injector was used for the four-stroke marine diesel engine. An investigation was conducted on three different nozzle outlet diameters: 0.285 mm, 0.325 mm, and 0.375 mm, corresponding to L/D ratios of 10.9, 9.5, and 8.3, respectively. All the nozzle holes had a cylindrical shape. The spray analysis was performed using a single active nozzle hole, while the other holes were plugged. A commercial diesel fuel was used in the study and measured before the tests. The density was 816.1 kg/m³ (at 40°C) and the viscosity was 2.35 mPa·s. The injector's opening duration was 40 ms, and was calibrated to open at three different pressures (p_o): 15 MPa, 25 MPa, and 35 MPa.

To visualize the spray evolution inside the constant-volume chamber, image acquisition was performed using a high-speed camera (Photron SA1.1), operating at 15,000 frames per second. Two 250 W halogen lamps were used to illuminate the chamber. Sample images obtained during the experiment are shown in Fig. 1. The marine fuel injector was supplied with fuel by a high-pressure common-rail system, which maintained a pressure of approximately 50 MPa upstream of the injector. The system featured a specialized solenoid valve with a short opening time of 10 ms mounted before the fuel injector. Fuel pressure was measured using a piezoresistive pressure sensor (Kistler 4067E) [13]. Each test was repeated three times to eliminate gross errors and to confirm the correctness of the measurement method. The macrostructures of the diesel spray were analyzed using DaVis 8.4 software from the recorded images.

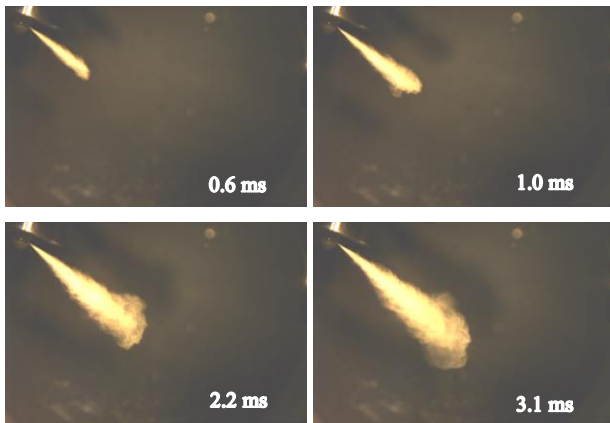


Fig. 1. The example raw images of diesel fuel spray captured at different times after start of injection, L/D: 10.9, p_o : 15 MPa, p_B : 4.3 MPa

3. Results and discussion

One of the macro parameters of the diesel spray from a marine diesel engine injector is the spray cone angle (SCA). It should be noted that SCA (together with STP) is a parameter that provides information about the volume (assuming axial symmetry of the spray) occupied by the atomised fuel within the cylinder space. The top of the cone is located at the injector nozzle outlet, while its base corresponds to the leading edge part of the spray front. The SCA of the diesel fuel spray is defined as the apex angle whose arms mark the outer boundary of the spray. The definition of SCA is illustrated in Fig. 2.

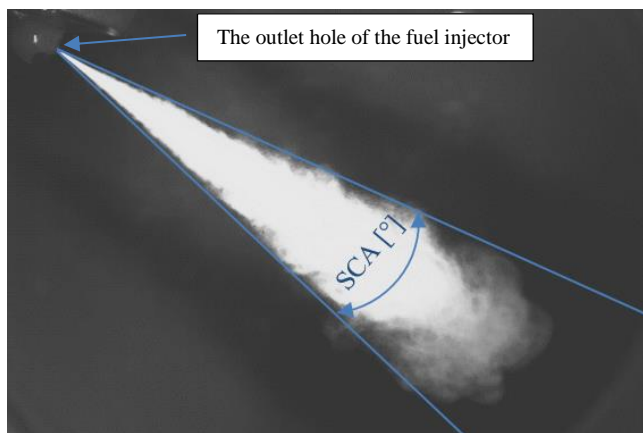


Fig. 2. The definition of SCA

In the experimental tests, the injection and atomization of diesel fuel from an injector into a constant-volume chamber were recorded. The propagation of the fuel spray was recorded from the start of injection until the end of the process. Fig. 3 presents sample results of SCA measurements from three repetitions. Significant differences in the shape of the recorded fuel spray were observed between 0 and 0.134 ms. As a result, the large discrepancy in spray cone angle values during this period made the analysis unreliable. Therefore, the first three measurements were excluded from further analysis of the early stage of the fuel spray development.

According to the results in Fig. 3, the SCA of the diesel fuel spray increases over time. From the start of injection, the spray penetrates the chamber at a high initial velocity,

driven by the pressure differential between the injection pressure and the chamber's backpressure gas. The greater this pressure difference, the more kinetic energy is imparted to the fuel. As the spray continues to propagate, it undergoes secondary break-up, leading to a widening of the spray cone angle. This growth continues up to approximately 1.2 ms, after which the cone angle stabilizes. The duration of this development phase depends on the specific injection conditions.

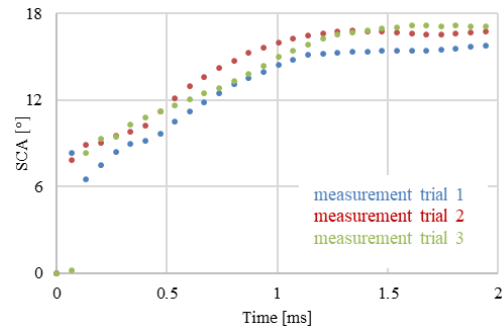


Fig. 3. The spray cone angle for L/D: 10.9, p_o : 15 MPa, p_B : 3.2 MPa

Figures 4, 5, and 6 present the arithmetic mean of the SCA over time for different L/D ratios, opening pressures (p_o), and backpressures in the constant-volume chamber (p_B). It should be noted that the analysis of the SCA characteristic was conducted [7], but only for a single backpressure condition in a constant-volume chamber. The average was calculated from three experimental trials for each injection condition. The error bars for each point represent the maximum and minimum spray cone angle values relative to the mean for that case.

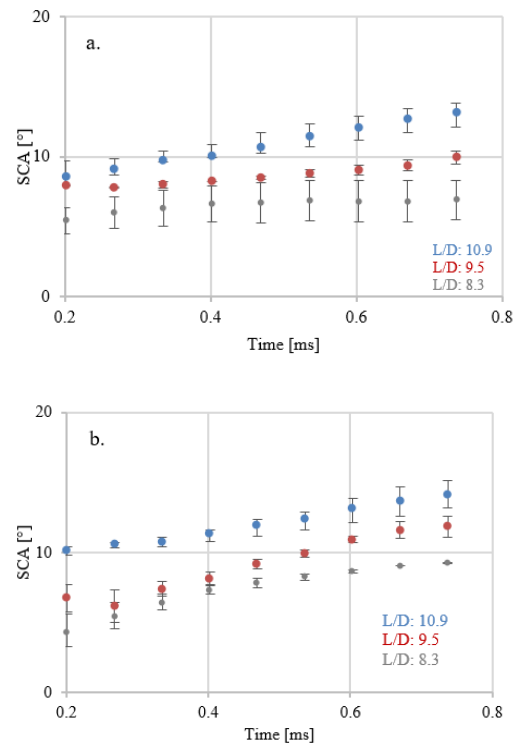


Fig. 4. The selection example of SCA results depending on L/D for p_o : 15 MPa, p_B : a) 3.2 MPa b) 4.3 MPa

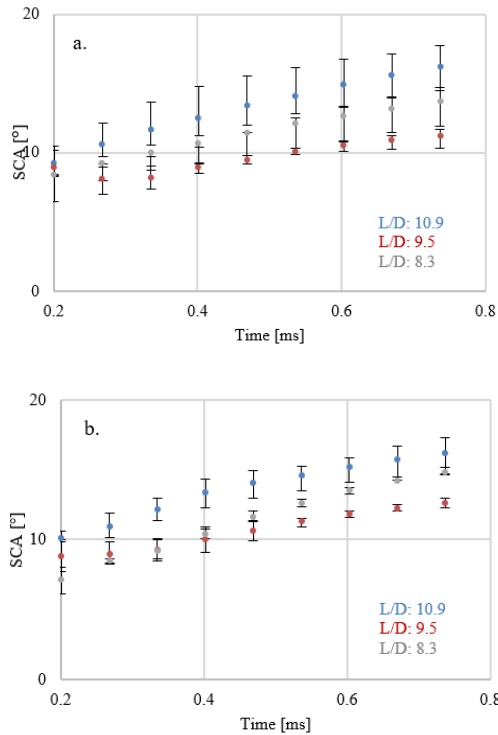


Fig. 5. The selection example of SCA results depending on L/D for p_0 : 25 MPa, p_B : a) 3.2 MPa b) 4.3 MPa

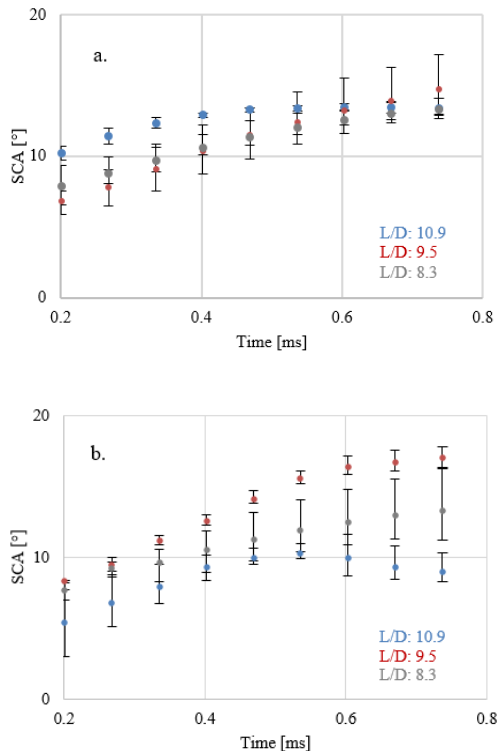


Fig. 6. The selection example of SCA results depending on L/D for p_0 : 35 MPa, p_B : a) 3.2 MPa b) 4.3 MPa

First, the influence of marine diesel injector geometry on the SCA of injected diesel fuel during the initial phase of injection was analyzed. According to the results presented in Figs. 4–6, an increase in the L/D ratio of the fuel injector resulted in an increase in the spray cone angle. The largest value of spray cone angles was recorded for the L/D ratio of

10.9 in most observed cases. Decreasing the L/D ratio, which implies an increase in the outlet hole diameter, resulted in smaller spray cone angles, due to changes in flow conditions within the nozzle. A change in the geometry of the injector nozzle orifice (i.e., a change in the L/D ratio) affects the initial spray behavior because the mass flow rate is altered [15]. Moreover, it influences the possibility of decay or development of turbulence and cavitation in the flow along the nozzle [2].

For an opening pressure of 35 MPa and backpressure 4.3 MPa, the decrease in cone angle was observed for L/D = 10.9, as shown in Fig. 6b. This pressure combination created highly favorable conditions for fuel jet break-up. Droplets at the spray boundaries likely evaporated, and smaller droplets were more rapidly decelerated by the increased chamber backpressure. The presented results confirm the influence of the outlet hole geometry on the initial spray structure.

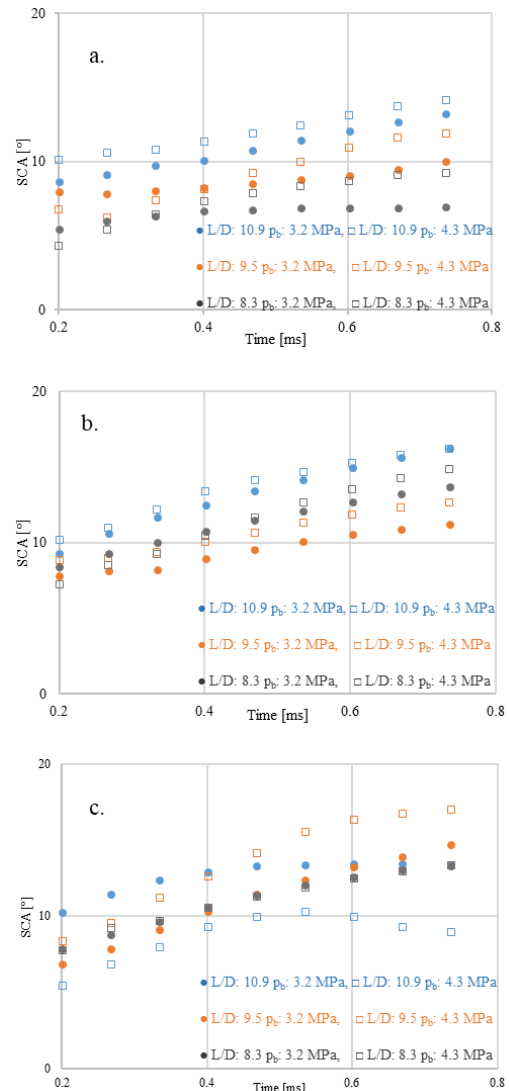


Fig. 7. The SCA results depending on L/D and p_B for : p_0 : a) 15 MPa, b) 25 MPa, c) 35 MPa

Based on the experimental results presented in Fig. 7, it can be concluded that an increase in aerodynamic resistance in the constant-volume chamber has a significant influence

on the propagation of the injected fuel. In this work, and partly in previous works [5–7] on the atomization process of diesel oil from a marine engine injector, the effect of backpressure in a constant-volume chamber on macro parameters was analyzed. Figure 7 presents the experimental results of SCA, considering all factors, including L/D ratio, opening pressures, and backpressures (3.2 MPa and 4.3 MPa). According to the presented experimental results, the area occupied by the injected and atomized diesel spray increases with the increase of the gas pressure in the constant-volume chamber. This is a typical trend in the formation of fuel spray geometry when the gas density in the constant-volume chamber is increased [5–7, 19]. This behavior of fuel spray is consistent with the predictions of the general atomization theory for high-pressure fuel injectors.

A higher gas density leads to the more rapid dissipation of the initial axial spray energy, promoting radial dispersion and disintegration of droplets, thereby increasing the spray cone angle. Furthermore, a decrease in spray velocity is observed, which is attributed to the increased aerodynamic forces in the constant-volume chamber at a backpressure of 4.3 MPa compared to a backpressure of 3.2 MPa. Furthermore, increasing the opening pressure also contributes to greater SCA values, as evidenced in Fig. 7. As part of earlier analyses of selected data, the velocity of the fuel spray in the initial stage was investigated [5].

3.1. Model of spray cone angle

Based on the analysis of the experimental results, presented in the previous section, it was noticed that the SCA changes over time during the initial phase of injection. In addition, the value of this SCA will be influenced by the changing diameters of the outlet holes, the backpressures in the constant-volume chamber, and the injector opening pressure. This became the basis for developing a mathematical model to predict the temporal variation of the spray cone angle of a diesel spray from a marine engine injector during the initial stage of injection.

The mathematical model of SCA was constructed using a general modeling approach based on the collected experimental data. First, the modeling problem was formulated, and simplifying assumptions were defined. The goal was to develop a time-dependent mathematical model of the SCA evolution during the early stage of fuel injection. The following assumptions were made: constant fuel density and viscosity, and constant test temperature. In the next step, the model variables were defined as: L/D ratio, backpressure (p_B), and opening pressure (p_o). Based on the analysis of the experimental results, the general form of the model was identified as nonlinear with a logarithmic character. A preliminary analysis of the approximation of results to the selected mathematical function was presented in earlier work [7]. Therefore, logarithmic approximation was applied. The final form of the model was adopted as Equation (1):

$$SCA = A \cdot \ln \left[1 + (L/D)^C \cdot p_o^B \cdot p_B^D \cdot t \right] \quad (1)$$

Parameters A, B, C, and D are coefficients adjusted to fit the function to the experimental results.

Table 2 presents the standard errors and 95% confidence intervals. It can be observed that the estimated model pa-

rameters A, B, C, and D fall within these intervals. To construct the nonlinear time-dependent mathematical model of SCA, an optimization function was used to minimize the coefficient of determination (R^2). The *NonLinearModelFit* function from Mathematica software was applied [24]. The coefficient of determination R^2 for the time-dependent SCA model during the early stage of fuel spray was 0.987. To validate the model, the computed results were compared with the experimental data.

Table 2. The parameters of the mathematical model

Parameter	Determined value of parameter	Standard error	Confidence interval 95%
A	4.94	0.23	4.49–5.38
B	0.87	0.04	0.80–0.95
C	2.75	0.07	2.60–2.89
D	0.70	0.09	0.52–0.88

As shown by the results, the model-predicted SCA values (derived from Eq. (1)) are in close agreement with the experimental values. The mean relative errors between the experimental and modeled SCA results range from 5.1% to 16.6%. The example results from the computations were compared with the experimental data (Fig. 8).

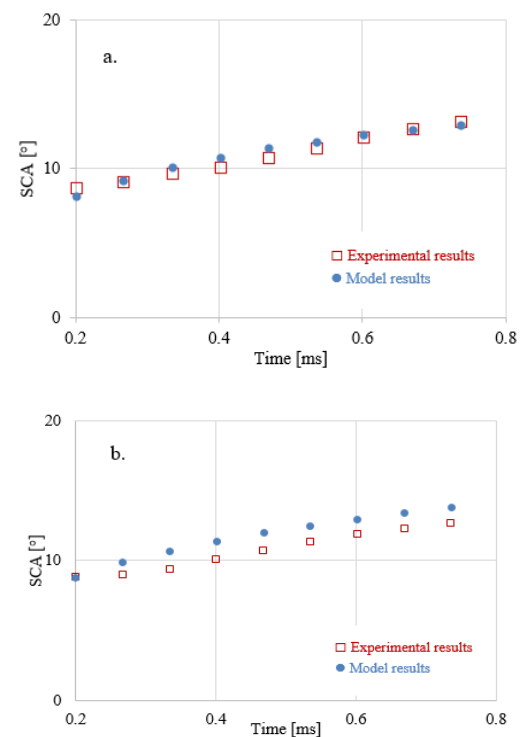


Fig. 8. Example results from the computations were compared with the experimental data: a) L/D: 10.9, p_o : 15 MPa, p_B : 3.2 MPa, b) L/D: 9.5, p_o : 25 MPa, p_B : 4.3 MPa

4. Conclusions

This article presents the results of experimental investigations of the diesel fuel spray formation by a marine diesel engine injector. The focus was on the early stage of spray development, as it is a crucial period for the initial air-fuel mixture formation and its spontaneous autoignition. The primary considerations concerned the influence of various nozzle orifices, backpressures in the constant-volume

chamber, and opening pressures of the marine diesel fuel injector on the behavior of the spray cone angle (SCA) of diesel fuel spray. Based on these results, the following conclusions can be drawn:

- The SCA for diesel fuel injection from a marine diesel engine injector changes over time in the early stage of spray formation in a repeatable manner, which correlates with the nozzle dimensions and injection conditions
- Increasing the L/D ratio of the injector nozzle orifice leads to an increase in SCA
- Increasing the gas density in the constant-volume chamber results in an increase in the SCA.

The final outcome of this study is a formulated mathematical model for calculating the time-varying SCA for a marine injector during the early spray stage of diesel fuel injection. The model accounts for the L/D ratio of the injector orifice, variations in fuel pressure during injection, and

changes in backpressure in the constant-volume chamber. Therefore, the presented mathematical model of SCA can be used for a rough estimation of the SCA when one of these parameters changes. The data generated by the model can be used as an input for 3D computational fluid dynamics (CFD) modeling of injection and atomization processes for the considered marine injector. It should be noted that this model was formulated based on specific values of experimental parameters; therefore, it shouldn't be applied outside the considered ranges of those parameters without prior validation.

The results presented in this article were obtained as part of doctoral research work.

Acknowledgements

The authors thank Prof. Jerzy Kowalski for his support and collaboration, and Dr. Piotr Jaworski for technical support in experimental procedures.

Nomenclature

CFD computational fluid dynamics
 CI compression ignition
 SCA spray cone angle

STP spray tip penetration
 TDC top dead center

Bibliography

- [1] Arrègle J, Pastor J, Ruiz S. The influence of injection parameters on diesel spray characteristics. SAE Technical Paper 1999-01-0200, 1999. <https://doi.org/10.4271/1999-01-0200>
- [2] Baumgarten C. Mixture formation in internal combustion engines. 1st ed. Berlin/Heidelberg: Springer-Verlag 2006.
- [3] Carlton J. Marine propellers and propulsion. 2nd ed. Bodmin, Cornwall: Elsevier Butterworth-Heinemann 2007.
- [4] Delacourt E, Desmet B, Besson B. Characterisation of very high pressure diesel sprays using digital imaging techniques. *Fuel*. 2005;84(7-8):859-867. <https://doi.org/10.1016/j.fuel.2004.12.003>
- [5] Grochowalska J. Analysis of the macrostructure of the fuel spray atomized with marine engine injector. *Combustion Engines*. 2019;179(4):80-85. <https://doi.org/10.19206/CE-2019-413>
- [6] Grochowalska J, Jaworski P, Kapusta ŁJ, Kowalski J. A new model of fuel spray shape at early stage of injection in a marine diesel engine. *Int J Numer Methods Heat Fluid Flow*. 2022;32(7):2345-2359. <https://doi.org/10.1108/HFF-05-2021-0349>
- [7] Grochowalska J, Jaworski P, Kapusta Ł. Analysis of the structure of the atomized fuel spray with marine diesel engine injector in the early stage of injection. *Combustion Engines*. 2023;195:97-103. <https://doi.org/10.19206/CE-168394>
- [8] Guan W, Chen X, Zhang Y, Li H, Wu J, Chen X et al. Effect of asymmetric structural characteristics of multi-hole marine diesel injectors on internal cavitation patterns and flow characteristics: a numerical study. *Fuel*. 2021;283:119324. <https://doi.org/10.1016/j.fuel.2020.119324>
- [9] Hiroyasu H, Arai M. Structures of fuel sprays in diesel engines. SAE Technical Paper 900475, 1990. <https://doi.org/10.4271/900475>
- [10] Hu N, Zhou P, Yang J. Reducing emissions by optimising the fuel injector match with the combustion chamber geometry for a marine medium-speed diesel engine. *Transp Res Part D Transp Environ*. 2017;53:1-16. <https://doi.org/10.1016/j.trd.2017.03.024>
- [11] International Maritime Organization (IMO). IMO approves net zero regulations. London: IMO. <https://www.imo.org/en/MediaCentre/PressBriefings/pages/IMO-approves-netzero-regulations.aspx>
- [12] Kegl B, Lešnik L. Modeling of macroscopic mineral diesel and biodiesel spray characteristics. *Fuel*. 2018;222:810-820. <https://doi.org/10.1016/j.fuel.2018.02.169>
- [13] Kistler. Piezoresistive high pressure sensor. 2014. <https://www.kistler.com/PL/en/piezoresistive-pressure-sensor/C00000143>
- [14] Kowalski J. Model of the combustion process in the marine 4-stroke diesel engine. *Mechanik*. 2015;10:833/49-833/58.
- [15] Park J, Kim D, Park S. Effects of nozzle L/D on near-field development and macroscopic spray characteristics of common-rail diesel sprays. *Int J Automot Technol*. 2020;21(3):657-666. <https://doi.org/10.1007/s12239-020-0063-2>
- [16] Park Y, Hwang J, Bae Ch, Kim K, Lee J, Pyo S, Effects of diesel fuel temperature on fuel flow and spray characteristics. *Fuel*. 2015;162:1-7. <https://doi.org/10.1016/j.fuel.2015.09.008>
- [17] Payri R, Gimeno J, Bracho G, Vaquerizo D. Study of liquid and vapour phase behavior on diesel sprays for heavy duty engine nozzles. *Appl Therm Eng*. 2016;107:365-378. <https://doi.org/10.1016/j.applthermaleng.2016.06.159>
- [18] Prabhakara Rao G, Raju VRK, Srinivasa Rao S. Effect of fuel injection pressure and spray cone angle in DI diesel engine using CONVERGE™ CFD code. *Procedia Eng*. 2015;127:295-300. <https://doi.org/10.1016/j.proeng.2015.11.372>
- [19] Salvador FJ, Gimeno J, De la Morena J, González-Montero LA. Experimental analysis of the injection pressure effect on the near-field structure of liquid fuel sprays. *Fuel*. 2021;292:120296. <https://doi.org/10.1016/j.fuel.2021.120296>
- [20] Tang C, Feng Z, Zhan C, Ma W, Huang Z. Experimental study on the effect of injector nozzle K factor on the spray characteristics in a constant volume chamber: near nozzle spray initiation, the macroscopic and the droplet statistics. *Fuel*. 2017;202:583-594. <https://doi.org/10.1016/j.fuel.2017.04.078>

- [21] Tay ZY, Konovessis D. Sustainable energy propulsion system for sea transport to achieve United Nations sustainable development goals: a review. *Discov Sustain.* 2023;4:20. <https://doi:10.1007/s43621-023-00132-y>
- [22] Uchida N, Onorati A, Novella R, Kumar Agarwai A, Abdul-Manan AFN, Kulzer AC et al. E-fuels in IC engines: a key solution for a future decarbonized transport. *Int J Engine Res.* 2025;26(11):1675-1702. <https://doi:10.1177/14680874251325296>
- [23] Viana M, Hammingh P, Colette A, Querol X, Degraeuwe B, de Vlieger I et al. Impact of maritime transport emissions on coastal air quality in Europe. *Atmos Environ.* 2014;90:96-105. <https://doi:10.1016/j.atmosenv.2014.03.046>
- [24] Wolfram Language & System. *NonLinearModelFit*. Documentation Center. 2022. <https://reference.wolfram.com/language/ref/NonlinearModelFit.html>
- [25] Zacharewicz M, Kniaziewicz T. Model tests of a marine diesel engine powered by a fuel-alcohol mixture. *Combustion Engines.* 2022;189(2):83-88. <https://doi:10.19206/CE-143486>
- [26] Zincir BA, Arslanoglu Y. Comparative life cycle assessment of alternative marine fuels. *Fuel.* 2024;358(Pt A):129995. <https://doi:10.1016/j.fuel.2023.129995>

Joanna Grochowalska, DEng. – Faculty of Mechanical Engineering and Ship Technology, Gdańsk University of Technology, Poland.
e-mail: joanna.grochowalska@pg.edu.pl



Łukasz Jan Kapusta, DEng. – Faculty of Power and Aeronautical Engineering, Warsaw University of Technology, Poland.
e-mail: lukasz.kapusta@pw.edu.pl



Impact of spark plug type on the cycle-to-cycle variability in an internal combustion gas engine

ARTICLE INFO

Received: 20 June 2025
Revised: 12 December 2025
Accepted: 12 January 2026
Available online: 12 January 2026

An experimental study was conducted using a single-cylinder gas engine to determine the impact of spark plug type on engine cycle-to-cycle repeatability. Two types of spark plugs were used for the analysis: the first was a flat electrode spark plug, and the second was a conventional spark plug with a side electrode, designated as “J”. The tests were carried out over an air excess ratio range of 1.0 to 1.4 and an ignition coil charging time range of 1.5 ms to 5 ms, at a constant engine speed of 1500 rpm and a load of 6 bar IMEP. The results indicate a significant improvement in engine repeatability when using a spark plug with a flat ground electrode. An average reduction of 61% in the IMEP variability coefficient was achieved in the air excess range of 1.0–1.3. The use of a spark plug with a side electrode “J” resulted in a reduction in the sensitivity of engine operation to changes in the mixture composition and coil charging time.

Key words: *ignition system, cycle-to-cycle variation, gas engines, lean burn*

This is an open access article under the CC BY license (<http://creativecommons.org/licenses/by/4.0/>)

1. Introduction

Spark-ignition gas engines are a crucial component in the development of drive systems and power generation systems, primarily due to their potential to reduce CO₂ and NO_x emissions [5, 24]. Gas engines are most commonly fuelled by natural gas, whose main component is methane. As a gaseous motor fuel, it has a lower ability to quickly initiate and sustain combustion reactions than conventional gasoline [2]. That fact leads to greater susceptibility to combustion instability. It has a negative impact on the possibility of burning lean mixtures, which can improve energy and environmental performance [16].

The combustion of lean mixtures is particularly beneficial when using advanced ignition systems, including laser plasma ignition systems, pre-chamber combustion systems, or hydrogen enrichment of 5–30% [7, 11, 18, 19]. This allows mixtures with an air excess ratio greater than 1.8 to be burned [6]. By further diluting the mixture, it is possible to reduce NO_x emissions by up to 75–90% and improve thermal efficiency by 2–9% [3, 13]. Increasing the excess air ratio above the stoichiometric composition is associated with a decrease in combustion temperature and heat release rate, affects ignition initiation disturbances, and increases susceptibility to loss of combustion process repeatability from cycle to cycle [10].

Due to the limitations resulting from working with lean mixtures, one approach to improving combustion stability is to modify the design of the spark plug and the configuration of the ignition system. In experimental studies [1], Abdel-Rehim compared four types of spark plugs and found that the configuration without a ground electrode reduced the coefficient of variation (COV) of IMEP by 23.8% and increased IMEP by 4.4% compared to the reference spark plug. Sjerić and co-authors [20] performed a numerical analysis of the effect of spark plug geometry on cyclic combustion variability, comparing a classic J-gap spark plug with an iridium spark plug with a thin central electrode. They showed that the use of an iridium spark

plug reduced COV(IMEP) by up to 13.5% and reduced fuel consumption by approximately 1.25% in the partial load range of the engine.

Li et al. [14] compared single and twin spark plug configurations in a natural gas-fueled SI engine, analyzing the combustion process at different λ values and EGR ratios. It was demonstrated that the use of twin spark plugs reduced combustion time by ~20–30% and accelerated the achievement of CA50 (e.g., from 21.77°C_A to 16.58°C_A at $\lambda = 1.5$), resulting in improved combustion stability and increased maximum pressure compared to the single-spark system.

In a study by Gu et al. [8], the effect of spark plug orientation on combustion stability under severely lean conditions in a single-cylinder SI engine was analyzed using three spark plug settings relative to the flow direction. It was demonstrated that the optimal orientation (90° relative to the flow direction) increased the stable combustion limit from $\lambda = 1.78$ to $\lambda = 1.96$ at 2000 rpm, and significantly improved the combustion rate and heat distribution throughout the cycle.

Zhang and Chen [25] conducted optical studies of methane combustion at various ignition energies and spark plug gaps, examining the impact of these parameters on cyclic variability and flame formation under lean-burn conditions. They demonstrated that increasing the ignition energy and using a larger gap (1.20 mm) significantly improves combustion stability, reducing the coefficient of variation of the IMEP and extending the lean mixture limit to $\lambda = 1.4$.

To identify the phenomena responsible for combustion instability, model studies replicating the conditions of ignition and flame propagation are necessary, as confirmed by the results of experimental work on the dynamics of combustion reactions [4, 17, 26]. At the same time, engine testing under real conditions is of key importance, as it allows the impact of design solutions on the performance and environmental indicators of the unit to be assessed [13, 21].

Cyclic combustion variability (CCV) arises from turbulence fluctuations, local variations in mixture composition, and random disturbances in flame initiation and propagation, resulting in each engine cycle operating under slightly different physical and chemical conditions. As a result, even with constant control parameters, fluctuations in pressure and combustion rate occur, leading to differences in IMEP, Pmax, and combustion phase between successive cycles [12].

The non-repeatability of engine operation is most often described using statistical indicators, such as COV(IMEP), COV(Pmax), and COV(CA50), which enable the determination of the dispersion of energy and phase combustion parameters from one cycle to the next [15]. However, COV(IMEP) and COV(CA50) limits are not the same for all cases; they depend on the type of engine, fuel, and cylinder configuration. In single-cylinder gas engines, COV(IMEP) often exceeds 3–5% during lean-burn operation, reflecting higher susceptibility to cyclic combustion variability. In multi-cylinder production units, fluctuations in individual cylinders are partially compensated, resulting in lower observed values of these indicators [9].

The current state of knowledge suggests that surface spark plug designs, such as those analyzed in this article, have not been previously studied on an engine in terms of their impact on cyclic combustion variability and ignition stability. Previous work by the authors [23] included optical identification of electrical discharge in a constant volume chamber (CVC), which showed that a flat electrode spark plug generates a larger arc surface area, higher luminescence intensity, and shorter discharge duration compared to a conventional spark plug. These effects favor improved ignition of lean mixtures, especially in gas engines. However, CVC model studies did not allow for an unambiguous assessment of the impact of this design on the combustion process in the cylinder and the repeatability of engine operation; therefore, it was necessary to extend the analysis to include tests of the actual combustion process in a piston unit.

In the next stage, the authors focused on the parameters of ignition system control (including coil energy and saturation time) [22]. The presented article combines both approaches, spark plug type analysis and ignition parameter analysis, conducting comprehensive engine tests under lean-burn conditions to assess the impact of spark plug geometry on combustion stability during the cycle and improve engine performance indicators.

2. Research methodology

2.1. Spark plug geometries under investigation

To determine the impact of spark plug electrode section geometry on the repeatability of the combustion process in a gas engine, two different spark plugs were used, differing in shape and the degree of exposure of the discharge zone. The first variant is a spark plug generating a half-surface discharge, designated as SPF. In contrast, the second variant is a conventional spark plug with a side electrode of the “J” type, designated as SPJ (Fig. 1). The technical data for both spark plugs are presented in Table 1.



Fig. 1. View of SPF and SPJ spark plugs used for the engine tests

Due to the absence of a side ground electrode, the SPF spark plug is designed for engines with rotary pistons and high-performance engines operating under high thermal loads. The SPJ spark plug used is a modern classic design, widely used in most SI engines.

Table 1. Technical data of the tested spark plugs

Parameter	SPF	SPJ
Model No.	NGK LMAR8BI-9	NGK R0465B-10
Central electrode	iridium	nickel
Ground electrode	platinum	–
Electrodes gap	0.9 mm	1.3 mm

Previous experimental studies conducted in an isochoric chamber using both spark plugs have shown that the arc generated by the SPF spark plug is characterized by a higher energy concentration, resulting from a shorter discharge time. In contrast, the SPJ spark plug allows for a geometrically stable arc; at a lower energy concentration, the discharge phase is longer than in the case of SPF.

2.2. Engine test stand and measurement apparatus

The tests were conducted on a single-cylinder AVL 5804 research engine (Fig. 2) adapted for gas fuel. The engine had an open hemispherical combustion chamber, indirect fuel injection, an independent engine control system, and external electric supercharging. The technical data are presented in Table 2.

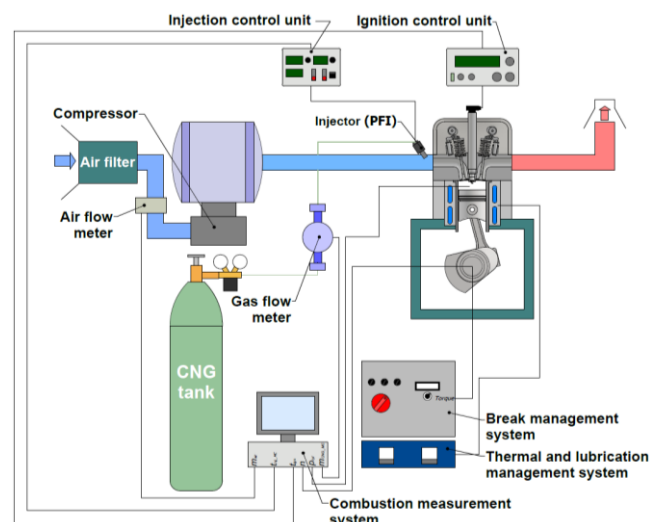


Fig. 2. Schematic of the test bench equipped with an AVL 5804 test engine

The AVL IndiSmart DAQ system with an AVL 365C angle sensor, an AVL GH14D combustion pressure transducer (0–250 bar, $\pm 0.3\%$ FS), a Micro Motion ELITE Cori-

olis flow meter (0.1–2 kg/h, $\pm 0.25\%$ RD), and an ABB Sensy-Flow thermal air flow meter (0–720 kg/h, $\pm 1\%$ RD).

Table 2. Technical data for the AVL 5804 single-cylinder test engine

Type	AVL 5804 R1 DOHC PFI
Bore \times stroke	85 \times 90 mm
Compression ratio	15
Displacement	0.5107 dm ³
Cooling system	liquid – dual-circuit system with heat exchanger
Intake system	28 mm electronically controlled throttle valve Mechanical supercharging

2.3. Scope of research and data processing

At each measurement point, a series of 100 consecutive engine cycles was recorded. The scope of the tests included a constant rotational speed with a gradual change in the air excess ratio from $\lambda = 1.0$ to 1.4, achieved by adjusting the throttle opening. The fuel dose was adjusted to achieve approximately 6 bar IMEP and remained constant throughout the entire test. The ignition discharge energy was adjusted by varying the ignition coil charging time from 1.5 ms to 5.0 ms. The λ value was determined based on the mass flow rate of air and fuel supplied to the engine. The ignition timing was adjusted individually for each engine operating point during testing to ensure a combustion center position of CA50 = 8° aTDC. For the recording of 100 consecutive cycles, the ignition timing was fixed. For each configuration, the values of COV(IMEP), CA50 variability, and COV(Pmax) were calculated. The weighted distance method was used to develop contour maps.

3. Results and discussion

3.1. Cycle-to-cycle variation in in-cylinder pressure curves

The combustion process in a spark ignition engine is characterized by natural uniqueness, which results in cyclical unevenness of pressure waves in the cylinder, directly resulting from the characteristics of heat release. Figure 3 illustrates an example series of 100 consecutive cycles recorded at $\lambda = 1.0$ (stoichiometric charge) and a coil charging time of 3 ms, corresponding to the SPF spark plug marked in red, while those for the SPJ spark plug are marked in blue; the bold line represents the average curve for a given set of cycles. Under the conditions presented, the SPF spark plug was characterized by a smaller spread of Pmax values, which was 3.62 bar lower than for the SPJ spark plug. Since very good repeatability indices characterize the use of stoichiometric mixtures, the visible differences primarily result from changes in the spark plug, rather than from variations in mixture formation conditions.

The pressure curve in the cylinder has a significant influence on the rate of pressure increase in the initial phase (CA10–CA20), especially in the case of gas supply, as methane has a higher ignition temperature than traditional gasoline. Cycle-to-cycle variability is primarily influenced by engine operating conditions such as load, rotational speed, charge homogenization degree, and mixture composition as determined by the λ coefficient, as well as spark discharge energy.

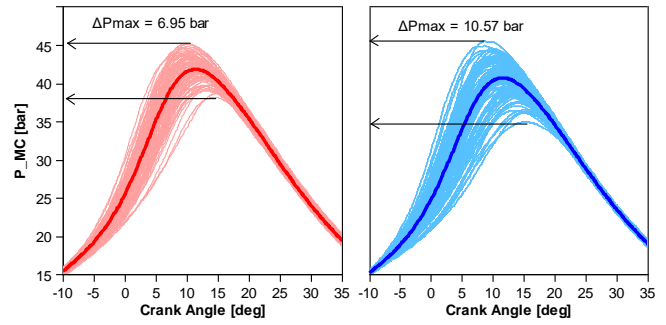


Fig. 3. Cylinder pressure for 100 cycles, at lambda 1.0 and coil charging time 3 ms. Results for SPF – red lines, SPJ – blue lines

3.2. Statistical distribution of IMEP for varying excess-air equivalence ratios

The non-repeatability of the combustion process, as demonstrated in the previous chapter, results in different IMEP values being obtained in successive engine cycles. Figure 4 illustrates the distribution of IMEP values obtained from 100 cycles for various degrees of mixture lean ($\lambda = 1.0$ –1.4) at a constant coil charging time of 3 ms.

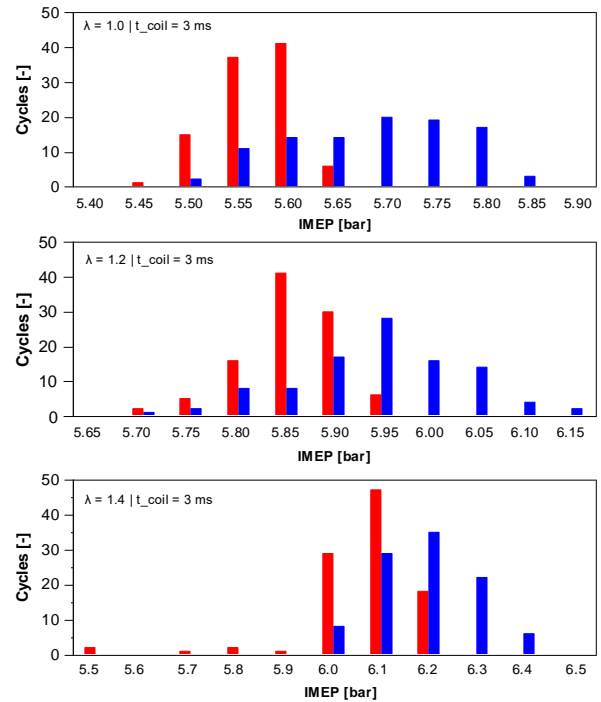


Fig. 4. The influence of the air excess coefficient λ on the dispersion of the mean indicated pressure IMEP

Throughout the entire λ range presented, higher IMEP values were obtained using the SPJ spark plug, while lower values were obtained for the SPF spark plug. Mixture leaning using the SPF spark plug in the range of $\lambda = 1.0$ –1.2 does not cause significant changes in the distribution. However, when burning the leanest loads, near the flammability limit, some cycles exhibit reduced IMEP values. In the case of the SPJ spark plug, a symmetrical distribution was obtained each time, but it was characterized by a significantly higher degree of dispersion than for the SPF spark plug.

Based on the above distributions, it can be concluded that the use of an SPF spark plug in stoichiometric and

slightly lean mixtures reduces the dispersion in IMEP values from cycle to cycle. The increased energy concentration in the arc generated by the SPF helps to eliminate the negative effects of mixture heterogeneity and intensify the charge kinetics in the vicinity of the electrodes. However, the shortening of the arc glow phase of this spark plug, despite the increased power concentration, has a negative effect on engine performance with lean mixtures. The short exposure time of the electric arc causes a delay in the CA0–CA10 phase, resulting in cycles with a reduced IMEP value. Under these conditions, using an SPJ spark plug with a stable and longer arc is a better solution.

3.3. Influence of λ and ignition energy on combustion repeatability

The best measure of engine non-repeatability is the IMEP variability coefficient. It is most widely used because it represents the measurable energy effect of the combustion process transferred to the crankshaft, whose kinematics and dynamics are directly felt by the user. Load depletion slows down combustion and increases the energy required to initiate ignition. Figure 5 shows the COV_{IMEP} curve as a function of λ for three coil charging times, corresponding to maximum charging currents from 5.4 A to 10.5 A.

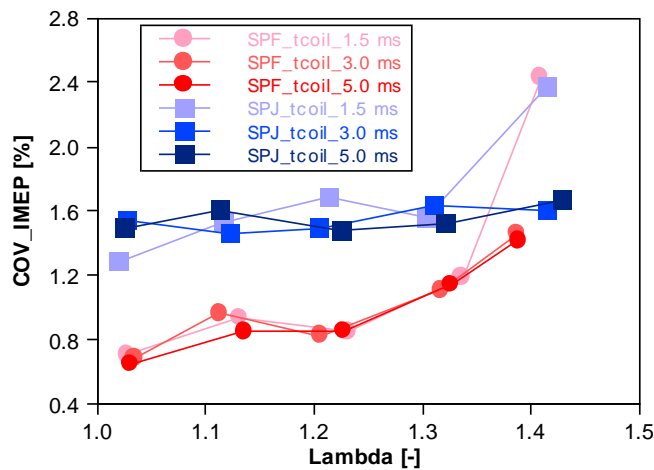


Fig. 5. The influence of the air excess ratio and ignition coil saturation time on the IMEP coefficient of variation (COV_{IMEP})

As λ increases, COV_{IMEP} increases, indicating that engine repeatability deteriorates; however, within the range of $\lambda = 1.0$ – 1.3 , these changes are mild. There is a clear advantage of the SPF spark plug, for which COV_{IMEP} values more than twice as low were obtained in this range. At maximum mixture lean, a charging time of 1.5 ms proves insufficient for both spark plugs – the ignition energy is too low, resulting in a loss of operating stability (typically above 5% COV_{IMEP}). The graph also shows that the charging time has a much greater impact in the case of the SPJ spark plug, while for SPF above 3 ms its impact is practically negligible. The SPJ spark plug ensures relatively stable COV_{IMEP} values along the entire λ characteristic, while for SPF, an increase in λ causes a significant increase in COV_{IMEP}, although the level of variability itself remains significantly lower than for SPJ. Since SPF enables very stable operation with richer mixtures, any deviation in

the λ value is clearly visible. In the case of SPJ, the overall level of stability is lower, and changes in λ have a smaller relative impact on the COV_{IMEP} value.

3.4. Two-dimensional interpolated maps of combustion variability indicators

To more fully illustrate the impact of control parameters on engine repeatability, contour maps were developed based on the measurement points, marked with red markers on the graphs. Figure 6 shows the relationship between the λ coefficient and the coil charging time t_{coil} as a function of the COV_{IMEP} value for the SPF (a) and SPJ (b) spark plugs. Both maps utilize the same color scale, enabling a direct comparison of the results.

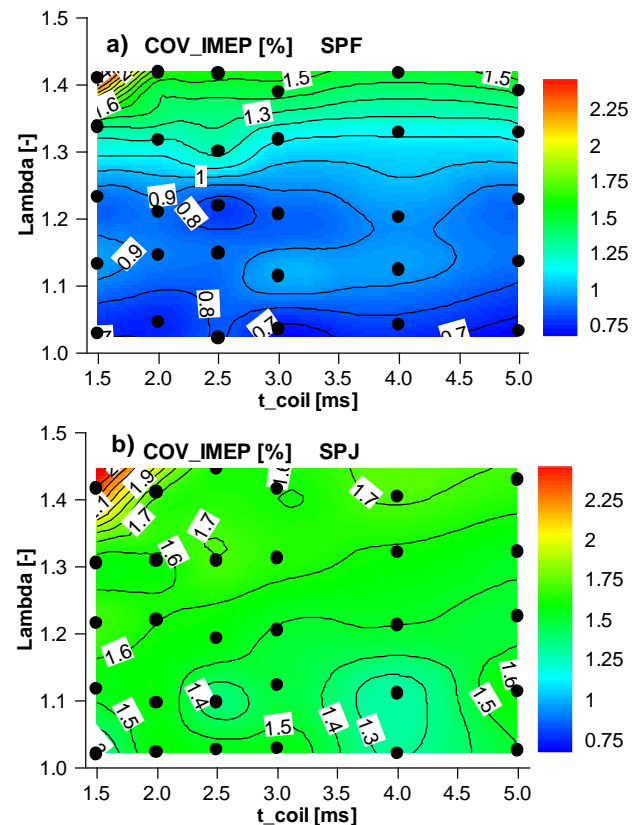


Fig. 6. Contour maps of the IMEP coefficient of variation (COV_{IMEP}) as a function of the air excess coefficient λ and ignition coil charging time: a) SPF spark plug, b) SPJ spark plug

In the case of the SPF spark plug, the range of low COV_{IMEP} values (0.75–1.00%) dominates, while for the SPJ spark plug, the range corresponding to values of approximately 1.5% prevails. For SPF, a clear influence of λ increase on COV_{IMEP} increase is observed. In contrast, for SPJ, the λ coefficient does not show a significant impact across the entire analyzed engine operating range. In both cases, a coil charging time of 1.5 ms proves insufficient, which prevents stable operation in lean mixture regions. The short discharge time in the SPF spark plug ensures high repeatability of the combustion process, but at the same time increases sensitivity to changes in control parameters. In contrast, the SPJ spark plug is characterized by poorer repeatability but shows less susceptibility to changes in operating conditions.

In the case of COV_CA50 (Fig. 7), the predominance of positive values is interpreted as less variability in the position of the combustion center for the SPJ spark plug. This is due to a longer glow phase and a more stable discharge, which reduces sensitivity to local differences in the mixture in the initial phase of flame development. The differences between the spark plugs gradually disappear at the extreme measurement points, where the boundary conditions of combustibility limit the influence of the control parameters.

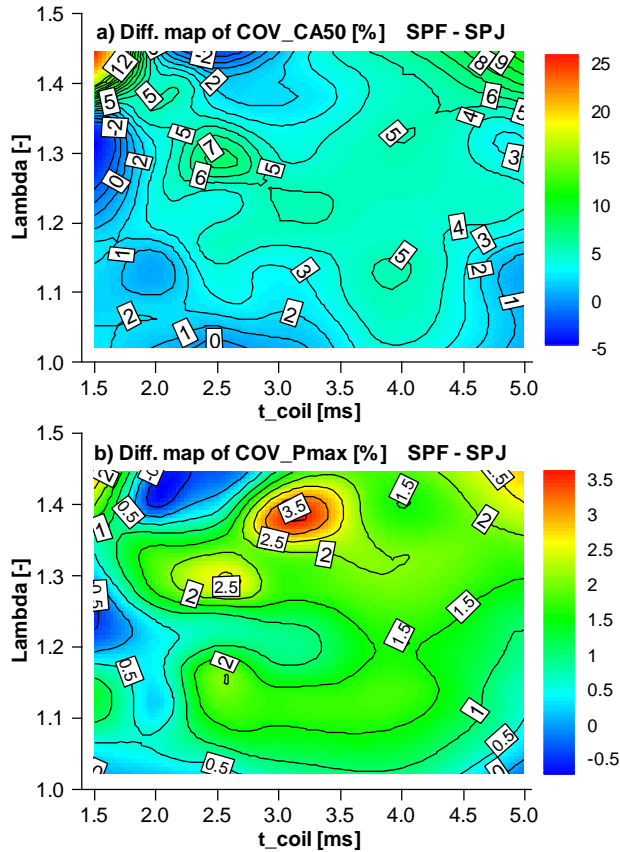


Fig. 7. Differential maps of coefficients of variation: a) COV_CA50 and b) COV_Pmax, determined as the difference between the values obtained for the SPF and SPJ spark plugs (SPF – SPJ)

For the COV_Pmax indicator, the map also shows lower values across the entire analyzed area for the SPJ spark plug. However, these differences are much smaller than in the case of COV_CA50, because Pmax is a parameter that is more strongly dependent on the average combustion rate and thermodynamic conditions in the TDC region, and to a lesser extent on local differences in ignition initiation. As a result, the stability of Pmax for both spark plugs differs less clearly, which reflects the limited sensitivity of this indicator to changes in electrode geometry.

3.5. Scatter analysis of the CA50–IMEP relationship

The analysis of the CA50 scatter relative to IMEP allows for the simultaneous assessment of combustion phase variability and indicated operation, providing a precise tool for identifying cyclical process instability. Figure 8 shows the sets of points obtained for different values of λ at a constant coil charging time of 3 ms, illustrating the effect of mixture depletion on the co-occurrence of CA50 and

IMEP deviations. The last panel represents the operating point with the lowest stability, reflecting the maximum dispersion of cycles under conditions of a mixture close to the flammability limit.

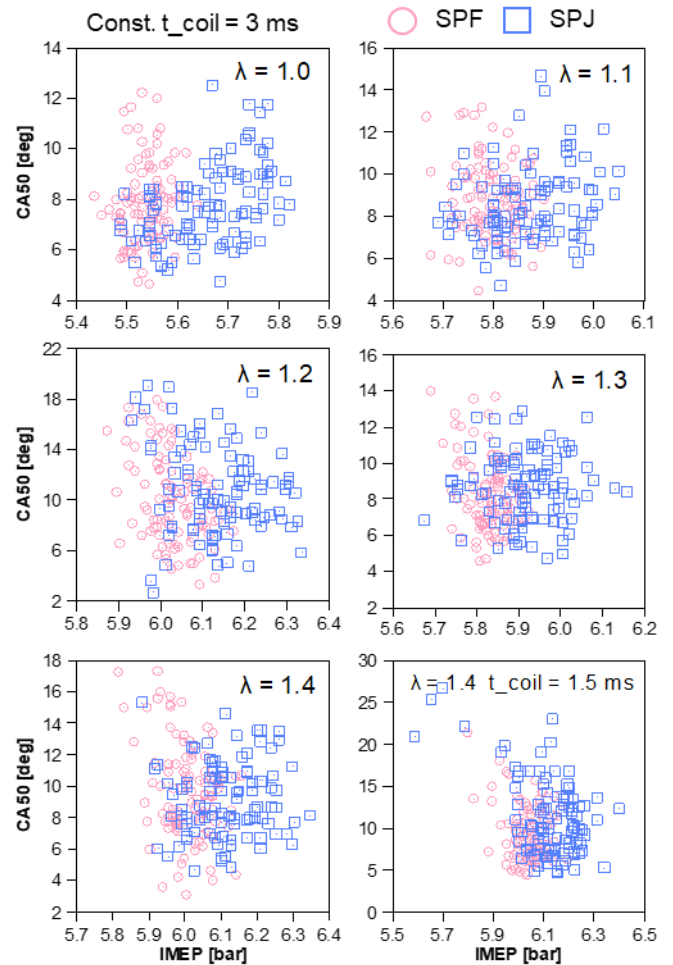


Fig. 8. Cycle-by-cycle spread of the CA50 angle relative to the mean indicated effective pressure IMEP for different values of λ and for the extreme case $\lambda = 1.4$ and $t_{coil} = 1.5$ ms

For both spark plugs, the CA50 (IMEP) relationship exhibits characteristics typical of SI engines, in which slight deviations of the combustion center position from the set value (CA50 = 8° aTDC) result in changes in IMEP due to modifications to the effective duration of the main combustion phase. In the case of the SPF spark plug, the scatter of points is significantly smaller, confirming a more repeatable achievement of the set combustion phase and lower sensitivity of IMEP to small deviations in CA50. For SPJ, the distribution of points is wider, indicating greater energy variation among cycles with comparable CA50 offsets.

As λ increases, both the range of IMEP values and the CA50 dispersion gradually increase, with the effect of mixture depletion being more pronounced for the SPJ spark plug. Higher λ values cause a slowdown in the early combustion phase, which is reflected in greater point dispersion and increasing sensitivity of the CA50(IMEP) relationship to slight fluctuations in ignition initiation. For the SPF spark plug, the observed increase in variability is milder, which confirms the beneficial effect of a higher concentra-

tion of discharge energy on the stabilization of the early combustion phase with moderately lean mixtures.

In the final case, corresponding to operation near the stability limit, the CA50(IMEP) relationship undergoes a significant expansion, and the dispersion structure loses its regular character. For both spark plugs, especially at lower ignition energies, cycles with significantly reduced IMEP appear, despite ignition control ensuring a nominal CA50 of 8° aTDC. This phenomenon is typical for operation with a mixture of limited reactivity, in which minor disturbances in combustion initiation can lead to a significant reduction in the combustion rate in the CA0–CA10 phase, and thus to the formation of cycles with low energy quality. As a result, this point represents the operating condition with the lowest stability, consistent with the observed maximum dispersion of CA50 and IMEP.

4. Summary

The results of research on the impact of spark plug type on the repeatability of gas engine operation from cycle to cycle are presented in this paper. The use of two different spark plugs were compared: a conventional spark plug widely used in SI and DI engines, and one that does not have a classic “J” electrode. As a result of the research conducted under conditions of variable air excess ratio and coil charging time, the following conclusions were drawn:

1. Significant impact of spark plug design on engine repeatability from cycle to cycle under variable λ conditions in the range of 1.0–1.4 and coil charging time of 1.5–5 ms.
2. In the range of λ 1.0–1.3, using an SPF spark plug, significantly lower values of the coefficient of variation of the indicated mean pressure were obtained.
3. Changing the coil charging time does not significantly affect the tested engine repeatability; however, a value below 2 ms does not ensure the required engine repeatability under the poorest conditions.
4. Despite the improvement in engine repeatability represented by COV_IMEP, an increase in the dispersion of other thermodynamic indicators of engine repeatability (COV_CA50, COV_Pmax) was observed.
5. Shortening the discharge time using SPF results in an increase in the concentration of electric arc energy. However, shortening the discharge causes high sensitivity of the early combustion phase CA0–CA10 to local charge dynamics, which translates into an increase in the CA50 and Pmax variability coefficients.
6. The use of an SPJ spark plug, which generates a more stable discharge over a longer period, helps reduce the impact of engine operating conditions (λ , t_{coil}) on cycle-to-cycle repeatability.

Nomenclature

CA0–CA10	interval 0% to 10% mass fraction burned	EGR	exhaust gas recirculation
CA50	crank angle of 50% fuel burned	IMEP	indicated mean effective pressure
CCV	cyclic combustion variability	Pmax	maximum in-cylinder pressure
COV	coefficient of variation	SI	spark-ignition
COV(CA50)	coefficient of variation of CA50	SPF	surface plug with flat electrode
COV(IMEP)	COV of indicated mean effective pressure	SPJ	spark plug with J-gap electrode
COV(Pmax)	COV of maximum in-cylinder pressure	t_{coil}	ignition coil charging time
CVC	constant volume chamber	λ	excess air coefficient

Bibliography

- [1] Abdel-Rehim AA. Impact of spark plug number of ground electrodes on engine stability. *Ain Shams Eng J.* 2012;4(2): 307-316. <https://doi.org/10.1016/j.asej.2012.09.006>
- [2] Amirante R, Distaso E, Tamburrano P, Reitz RD. Laminar flame speed correlations for methane, ethane, propane and their mixtures, and natural gas and gasoline for spark-ignition engine simulations. *Int J Engine Res.* 2017;18(9): 951-970. <https://doi.org/10.1177/1468087417720018>
- [3] Atibeh PA, Brear MJ, Dennis PA, Orbaiz PJ, Watson HC. Lean limit combustion analysis for a spark ignition natural gas internal combustion engine. *Combust Sci Technol.* 2013;185(8):1151-1168. <https://doi.org/10.1080/00102202.2013.769785>
- [4] Bueschke W, Skowron M, Szwajca F, Wislocki K. Flame propagation velocity in 2-stage gas combustion system applied in SI engine. *IOP Conf Ser: Mater Sci Eng.* 2018; 421: 042009. <https://doi.org/10.1088/1757-899x/421/4/042009>
- [5] Cho HM, He BQ. Spark ignition natural gas engines – a review. *Energy Convers Manag.* 2006;48(2):608-618. <https://doi.org/10.1016/j.enconman.2006.05.023>
- [6] Clasen K, Melaika M, Koopmans L, Dahlander P. High load lean SI-combustion analysis of DI methane and gasoline using optical diagnostics with endoscope. *SAE Technical Papers.* 2021-24-0046. 2021. <https://doi.org/10.4271/2021-24-0046>
- [7] Fichtner J, Ninow J, Kapischke J. Simultaneous reductions in NOx emissions, combustion instability, and efficiency loss in a lean-burn CHP engine via hydrogen-enriched natural gas. *Energies.* 2025;18(16):4339. <https://doi.org/10.3390/en18164339>
- [8] Gu Q, Xu M, Ye C, Hung D, Li X. Investigation of the Impacts of spark plug orientation on combustion stability under lean SI operation. *SAE Technical Papers.* 2020-01-1121. 2020. <https://doi.org/10.4271/2020-01-1121>
- [9] Han SB. Investigation of cyclic variations of IMEP under idling operation in spark ignition engines. *KSME International Journal.* 2001;15(1):81-87. <https://doi.org/10.1007/bf03184801>
- [10] Jung D, Sasaki K, Iida N. Effects of increased spark discharge energy and enhanced in-cylinder turbulence level on lean limits and cycle-to-cycle variations of combustion for SI engine operation. *Appl Energy.* 2017;205:1467-1477. <https://doi.org/10.1016/j.apenergy.2017.08.043>
- [11] Kheyrollahi J, Jafarmadar S, Khalilarya S, Niaki SRA. Improvement of performance and emission in a lean-burn

- gas fueled spark ignition engine by using a new pre-chamber. *Environ Prog Sustain Energy*. 2021;40(5). <https://doi.org/10.1002/ep.13637>
- [12] Kosmadakis GM, Rakopoulos DC, Rakopoulos CD. Assessing the cyclic-variability of spark-ignition engine running on methane-hydrogen blends with high hydrogen contents of up to 50%. *Int J Hydrog Energy*. 2021;46(34):17955-17968. <https://doi.org/10.1016/j.ijhydene.2021.02.158>
- [13] Kurtyka K, Pielecha J. Cold start emissions from a gasoline engine in RDE tests at different ambient temperatures. *Combustion Engines*. 2020;181(2):24-30. <https://doi.org/10.19206/CE-2020-204>
- [14] Li Y, Yang F, Linxun X, Liu J, Wang J, Duan X. Influences of the control parameters and spark plug configurations on the performance of a natural gas spark-ignition engine. *Fuel*. 2022;324:124728. <https://doi.org/10.1016/j.fuel.2022.124728>
- [15] Páv K. Implication of cycle-to-cycle variability in SI engines. *MECCA Journal of Middle European Construction and Design of Cars*. 2018;16(1):10-17. <https://doi.org/10.1515/mecdc-2018-0002>
- [16] Paykani A. Comparative study on chemical kinetics mechanisms for methane-based fuel mixtures under engine-relevant conditions. *Energies*. 2021;14(10):2834. <https://doi.org/10.3390/en14102834>
- [17] Pielecha I. The influence of petrol injection parameters on the structure of geometry of fuel spray injected from outward-opening injectors. *Fuel*. 2018;222:64-73. <https://doi.org/10.1016/j.fuel.2018.02.133>
- [18] Pielecha I, Szwajca F. Combustion of lean methane/propane mixtures with an active prechamber engine in terms of various fuel distribution. *Energies*. 2023;16(8):3608. <https://doi.org/10.3390/en16083608>
- [19] Richardson SW, McMillian MH, Woodruff SD, Worstell T, McIntyre DL. Laser spark ignition of a blended hydrogen-natural gas fueled single cylinder engine. *ASME 2006 Internal Combustion Engine Division Spring Technical Conference*. 2006;411-419. <https://doi.org/10.1115/ices2006-1397>
- [20] Sjerić M, Taritaš I, Kozarac D. Effect of spark plug geometry on the cyclic combustion variability and fuel consumption of gasoline engines. *J Energy Eng*. 2017;143(6). [https://doi.org/10.1061/\(ASCE\)EY.1943-7897.0000492](https://doi.org/10.1061/(ASCE)EY.1943-7897.0000492)
- [21] Sobczak J, Kamińska M, Ziółkowski A, Rymaniak Ł, Szymlet N. Analysis of pollutant emissions of a railbus based on Real Train Emissions measurements. *Combustion Engines*. 2025;201(2):22-33. <https://doi.org/10.19206/CE-201217>
- [22] Szwajca F, Wisłocki K, Różański M. Analysis of energy transfer in the ignition system for high-speed combustion engines. *Energies*. 2024;17(20):5091. <https://doi.org/10.3390/en17205091>
- [23] Szwajca F, Wisłocki K. Experimental identification of the electrical discharge on a surface gap spark plug. *Combustion Engines*. 2023;195(4):104-108. <https://doi.org/10.19206/CE-168296>
- [24] Vipartas T, Rimkus A, Stravinskas S, Pitrenas A, Matulis A. Spark ignition (SI) engine energy and ecological performance using natural gas and late intake valve close (LIVC). *Appl Sci*. 2025;15(11):6185. <https://doi.org/10.3390/app15116185>
- [25] Zhang X, Chen L. The synergy effect of ignition energy and spark plug gap on methane lean combustion with addressing initial flame formation and cyclic variation. *ACS Omega*. 2023;8(7):7036-7044. <https://doi.org/10.1021/acsomega.2c07897>
- [26] Zheng J, Bhatnagar K, Khurana M, Zhang P, Zhang BY, Linga P. Semiclathrate based CO₂ capture from fuel gas mixture at ambient temperature: Effect of concentrations of tetra-n-butylammonium fluoride (TBAF) and kinetic additives. *Appl Energy*. 2018;217:377-389. <https://doi.org/10.1016/j.apenergy.2018.02.133>

Filip Szwajca, DEng. – Faculty of Civil and Transport Engineering, Poznan University of Technology, Poland.

e-mail: filip.szwajca@put.poznan.pl



Prof. Krzysztof Wisłocki, DSc., DEng. – Faculty of Civil and Transport Engineering, Poznan University of Technology, Poland.

e-mail: krzysztof.wislocki@put.poznan.pl



Application of 3D-printed metal pistons in internal combustion engines: advantages and challenges

ARTICLE INFO

Received: 19 May 2025
Revised: 25 November 2025
Accepted: 10 December 2025
Available online: 11 January 2026

The application of 3D-printed metal pistons in internal combustion engines (ICE) presents significant advantages, including enhanced design flexibility, weight reduction, and improved thermal management. This innovative manufacturing technique enables the creation of complex geometries and tailored surface textures, contributing to better fuel efficiency and reduced emissions. Moreover, it opens new possibilities for customised piston design in advanced combustion strategies. However, challenges such as material anisotropy, surface roughness, and long-term reliability must be addressed to ensure consistent and safe performance under demanding engine conditions. Ongoing research in material science, process optimisation, and post-processing techniques is essential for overcoming these hurdles and realising the full industrial potential of 3D-printed pistons in modern ICE technology.

Key words: 3D printing, metal pistons, internal combustion engines, fuel efficiency, manufacturing challenges

This is an open access article under the CC BY license (<http://creativecommons.org/licenses/by/4.0/>)

1. Introduction

The growing demand for improved fuel efficiency and reduced emissions has become a central driver of innovation in internal combustion engine (ICE) technology, prompting academia and industry to seek transformative solutions [43]. Among these innovations, additive manufacturing (AM) of metal pistons stands out as a revolutionary advancement, offering unprecedented freedom in design optimization and functional integration. Unlike conventional casting or forging techniques, which constrain the geometric complexity and material distribution within pistons, 3D printing enables engineers to fabricate components with complex internal lattice structures, conformal cooling channels, and tailored surface textures that were previously unachievable [24, 36]. These capabilities facilitate significant enhancements in thermal management, mass reduction, and combustion dynamics—all of which contribute to higher power output, improved fuel economy, and lower pollutant emissions.

Furthermore, 3D printing enables the precise customization of piston geometries to suit advanced combustion strategies, such as homogeneous charge compression ignition (HCCI) or direct fuel injection, resulting in more uniform combustion and reduced engine knock. This level of customization, combined with the potential to integrate sensor networks for real-time monitoring of mechanical stress, temperature, and pressure, positions 3D-printed pistons at the forefront of smart engine components. However, despite the promise, this technological shift also introduces various engineering and economic challenges, including material anisotropy, surface roughness, long-term reliability, and cost-effectiveness in mass production. These challenges necessitate ongoing research in material science, process optimization, and post-processing techniques to ensure performance consistency and durability under demanding engine conditions.

This paper aims to comprehensively explore the benefits, technical limitations, and industrial prospects of 3D-

printed metal pistons, highlighting recent progress in additive manufacturing technologies and examining how these components could reshape the future of internal combustion engines [53]. By addressing both the opportunities and constraints of this approach, the discussion seeks to provide a realistic yet forward-looking assessment of additive manufacturing's role in advancing next-generation engine systems.

2. Literature review

The integration of additive manufacturing (AM) into the design and production of internal combustion engine (ICE) components represents a paradigm shift in engineering. AM enables the fabrication of highly complex geometries, weight-optimized structures, and functionally graded materials that were previously unattainable using conventional casting or forging techniques. These capabilities are particularly advantageous in piston design, where thermal management, mechanical strength, and lightweight are simultaneously critical.

Recent reviews by [11, 25, 49] indicate that piston-grade alloys are primarily processed using laser powder bed fusion (LPBF), due to its high dimensional accuracy and compatibility with AlSi10Mg, Ti6Al4V and nickel-based superalloys. Electron beam melting (EBM) offers improved control of residual stress, while directed energy deposition (DED), frequently discussed by [5], is increasingly used for repairing worn piston crowns and ring grooves. Each AM technique produces characteristic microstructures and defect distributions that directly influence fatigue, thermomechanical resistance and post-processing requirements.

Kolganov et al. [30] and Adamou et al. [2] report that AM facilitates the production of robust engine components such as cylinder heads and combustion chambers. The design freedom offered by AM supports the integration of internal vanes, lattice cooling structures, and advanced fuel injection features, which collectively improve combustion uniformity and reduce emissions of NO_x and unburned

hydrocarbons. In micro-gas turbines, for instance, such designs have already yielded measurable performance and emission benefits.

A growing body of work, including studies by [8, 41], emphasizes the importance of design-for-additive-manufacturing (DfAM) in engine components. Principles such as load-path alignment, minimization of overhangs, control of heat-affected zones, and orientation-aware topology optimization enable the integration of conformal cooling channels, lattice-reinforced skirts, and variable-thickness crowns. These design adaptations improve stiffness and reduce thermal gradients compared to cast pistons.

Dolan et al. [14] and Dongre et al. [16] demonstrated that 3D-printed pistons, particularly heavy-duty diesel engines, can incorporate optimized ribbed and honeycomb structures that reduce mass while maintaining stiffness. These designs are feasible exclusively due to AM's topology optimisation capability, which efficiently redistributes material load. Selvaraj et al. [42] validated such designs using finite element modelling, confirming mechanical gains with no stress concentration in critical regions. AM also enables multi-material printing – for example, combining high-strength tool steels with copper alloys to enhance thermal conductivity without compromising structural integrity. Gray et al. [22] report the successful production of OEM-grade components, such as aluminum cylinder heads, using laser powder bed fusion (LPBF) with reduced porosity and high dimensional accuracy.

The LPBF microstructure of AlSi10Mg is characterised by melt-pool bands, fine cellular silicon networks and rapid-solidification dendrites, as extensively described by [15, 19, 40]. This architecture contributes to high as-built strength yet also introduces anisotropy and stress-raising interfaces. Typical AM defects, such as gas pores, lack-of-fusion voids, and keyhole porosity, are strongly correlated with crack initiation under cyclic loading, making microstructural control essential for piston-grade applications.

Despite AM's advantages, fatigue performance remains a bottleneck, particularly for alloys such as AlSi10Mg, which are commonly used in piston applications. Romano et al. [40] and Dan et al. [10] demonstrate that the fatigue strength of such components is influenced by defect size and distribution, which are attributed to porosity and layer-by-layer fabrication. However, post-processing treatments, such as T6 heat treatment, polishing, and nano-alloying (e.g., TiB₂ reinforcement), have significantly enhanced fatigue life. Machine learning-assisted studies [34] further indicate that surface roughness is dominant in the elastic fatigue regime.

Build orientation and process parameters have a decisive influence on fatigue performance. Ngnkou [15] and Zhang [51] show that specimens built at 0° consistently outperform those built at 90°, due to fewer lack-of-fusion defects and more favourable melt-pool alignment. Studies by [19, 40] demonstrate that optimizing scan speed, hatch spacing, and volumetric energy density reduces defect size and scatter, significantly increasing the high-cycle fatigue limit.

The following table summarizes influential studies and their contributions to developing 3D-printed pistons and AM applications in ICE.

Table 1. Summary of key studies on additive manufacturing in piston design and internal combustion engines [2, 10, 14, 16, 22, 30, 31, 40, 42]

Focus area	Key contributions
General AM in ICE components	Enables durable, complex engine parts
AM combustion chambers and emissions	Improved fuel-air mixing; reduced NO _x
3D printed pistons: geometry and cooling	Advanced geometries; improved cooling
Topology optimization of piston design	Weight reduction with maintained strength
Structural modeling of optimized pistons	FEA-validated piston stiffness gains
Fatigue modeling of AlSi10Mg pistons	Defect-based fatigue life predictions
Nano-alloying to improve fatigue life	Nanostructure enhancement of fatigue resistance
LPBF cylinder heads and crankcases	OEM-grade AM components with low porosity
Heat treatment for AM consistency	Improved microstructure and mechanical reliability

Table 1 illustrates that the development of 3D-printed pistons encompasses a range from general structural innovations to fine-tuned fatigue resistance and emission optimization. A key observation is the trend toward multi-material solutions and structural simulations, which suggests a maturing field transitioning from feasibility to application-specific refinement.

Residual stress accumulation is another critical issue highlighted in AM literature. Reviews by Liu [33] and Martina [35] demonstrate that steep thermal gradients during LPBF generate high tensile stresses at the surface, thereby increasing distortion risk and reducing fatigue life. Mitigation strategies include substrate preheating [52], chessboard scanning or low-power strategies [7], and topology-optimised supports [9]. These approaches can substantially reduce stress magnitudes and improve dimensional stability of piston components.

Thermo-mechanical analyses reveal that pistons fabricated using AM encounter steep temperature gradients – often exceeding 300°C between the crown and skirt. Velugula [47] reports localized thermal stresses of up to 270 MPa in diesel and spark-ignition pistons. Fully coupled FEA simulations by Valera [45] and Selvaraj [42] demonstrate that topology-optimised and lattice-reinforced AM pistons exhibit lower peak temperatures and more uniform stress distributions compared with cast counterparts. Functional grading and porosity control, as explored by Najibi & Alizadeh [37], further mitigate thermal strain and delay crack initiation.

Research continues to push boundaries in multi-material integration, in-situ sensing, and automated quality assurance. Challenges like cost scalability, surface finish control, and regulatory certification remain. However, the innovation trajectory supports the broader adoption of AM in mainstream piston production and other high-performance ICE components.

This critical review underscores that while AM technologies offer transformative benefits for piston design and performance, significant engineering challenges remain to be overcome. Further research is necessary for multi-material printing, durability under real engine conditions, and cost-effective scalability.

Multi-material and functionally graded approaches are emerging as a promising route for next-generation piston architectures. Fracchia [20] and Tian [44] demonstrate that graded aluminium alloys with region-specific silicon content or ceramic reinforcement improve thermal resistance in the crown while maintaining ductility in the skirt. Studies on hybrid steel–copper and aluminium–copper architectures, supported by recent work by Dan [10] and Gray [22], confirm substantial gains in heat dissipation without compromising load-bearing capacity. AM thus shifts piston design toward spatially optimised material distributions rather than uniform alloy selection.

3. Design workflow for additively manufactured pistons

The successful development of additively manufactured pistons requires more than selecting a suitable alloy or printing process; it also necessitates careful consideration of the material properties and the printing process. Modern engineering practice relies on a structured, multi-stage workflow that integrates mechanical requirements, thermal constraints, geometry optimisation and post-processing. This workflow links engine-specific loads with AM-specific design rules, ensuring both manufacturability and in-service durability.

Load-path analysis and topology optimisation

The workflow begins with evaluating the piston's load paths under peak cylinder pressure, thermal gradients, and inertial forces. Conventional finite element analyses are used to identify high-stress regions around the crown, bowl rim and ring belt. Topology optimisation enables systematic redistribution of material, removing low-load regions while reinforcing structural paths [3, 16]. These methods have already demonstrated substantial stiffness improvements for lightweight AM geometries.

Integration of internal features is enabled exclusively by AM

Based on the optimized geometry, additive manufacturing enables engineers to embed features unattainable through casting, such as conformal cooling channels positioned close to the crown surface, thereby reducing thermal peaks and improving heat extraction efficiency [6, 18]. Similarly, self-supporting lattice structures can be integrated into the skirt, pin boss or crown regions to reduce weight while maintaining rigidity or damping vibrations [29]. Such features directly address the thermal-mechanical bottlenecks of conventional pistons.

Thermo-mechanical validation using FEM and coupled simulations

Before manufacturing, the optimised piston is validated under realistic thermo-mechanical loading conditions. Recent simulation studies have reported temperature differences exceeding 300°C between the crown and skirt in

heavy-duty and SI engines, resulting in local stress concentrations exceeding 250 MPa [47]. Fully coupled CFD–FEA analyses demonstrate that AM-optimised crowns exhibit more uniform temperature distribution and reduced distortion compared with cast pistons [42]. Accurate wall and piston boundary temperatures are essential for such coupled simulations; concise wall-temperature models calibrated using measurements in the cylinder head, liner and piston have therefore been widely used to support thermal boundary-condition definition [46]. These simulations prevent design iterations at the manufacturing stage and ensure that AM features do not introduce stress concentrations or geometries that are prone to failure.

Post-processing and property enhancement

Finally, the printed piston undergoes a tailored post-processing chain to achieve the required microstructure, density and fatigue strength. HIP treatments eliminate internal pores, while heat treatments, such as T6, modify the Si-rich network in AlSi10Mg. Targeted surface machining or polishing reduces roughness, which is known to be a primary factor in fatigue initiation [10, 34]. These steps are crucial for achieving repeatability and long-term durability under engine thermal cycling conditions.

Together, these four stages provide a systematic framework for transitioning AM pistons from prototype to functional, engine-ready components. They also demonstrate that additive manufacturing is not merely a replacement for casting, but a design-driven process that requires coordinated optimisation of geometry, materials, thermal management and process parameters.

4. Advantages of 3D-printed metal pistons

One of the most transformative advantages of 3D-printed metal pistons lies in the multifaceted improvements in design, efficiency, and sustainability that additive manufacturing enables. A primary benefit is the significant weight reduction achieved through topology optimization, which strategically removes material from low-stress regions, resulting in lower reciprocating mass, reduced inertial forces, and decreased friction [4]. These changes contribute to improved fuel economy, enhanced engine responsiveness, and reduced mechanical wear due to better dynamic balance. Coupled with this is the potential for enhanced thermal management by integrating complex internal structures, such as lattice geometries and conformal cooling channels, which dramatically increase heat dissipation capacity [32]. By mitigating thermal stress, these innovations extend the piston's operational lifespan and enable higher compression ratios that improve power output and efficiency while reducing the risk of engine knock and premature component failure [21].

Moreover, 3D printing facilitates customized geometry that optimizes combustion by tailoring the piston crown and combustion chamber shape to promote ideal air-fuel mixing and flame propagation. This customization supports advanced combustion modes such as homogeneous charge compression ignition (HCCI) and direct injection, which are instrumental in reducing NO_x emissions and unburned hydrocarbons [23]. The technology also supports the integration of embedded sensors directly into piston compo-

nents, enabling real-time monitoring of temperature, pressure, and mechanical strain [28]. These "smart pistons" empower predictive maintenance and adaptive engine control, ultimately increasing reliability and performance under varying operational conditions.

Economically, 3D printing is ideal for small-batch, high-precision production, as it eliminates costly tooling and significantly shortens the development cycle [48]. This makes it particularly attractive for motorsports, prototyping, and custom engine applications. Additionally, multi-material capabilities enable the fabrication of pistons with functionally graded materials (FGMs), allowing high-strength, heat-resistant alloys to be applied selectively to high-load zones (e.g., crown) while maintaining lightweight materials in other regions (e.g., skirt). This fine-tuned material distribution maximizes performance without compromising structural integrity. Lastly, the sustainability aspect of additive manufacturing cannot be overstated. Compared to traditional subtractive machining methods, 3D printing significantly reduces material waste by depositing only the necessary material, aligning with global trends in resource efficiency and environmentally responsible engineering.

5. Challenges of 3D-printed metal pistons

Despite the promising advantages of 3D-printed metal pistons, several challenges must be addressed to ensure their widespread and reliable adoption in high-performance and mass-market engines. One critical issue is material porosity, which can significantly reduce the mechanical strength and fatigue resistance of additively manufactured components. These internal voids, inherent in many powder bed fusion processes, compromise structural integrity and can lead to premature failure under cyclic loading. However, advanced post-processing methods such as hot isostatic pressing (HIP) and carefully optimized printing parameters have shown considerable effectiveness in minimizing porosity and improving part density [50]. Another inherent challenge is the anisotropic mechanical behavior introduced by the layer-by-layer nature of 3D printing. This directionality can result in non-uniform stress distribution and localized weaknesses under operational loads [17]. To counteract this, engineers must pay close attention to build orientation and apply thermal treatments or mechanical post-processing to enhance isotropy and ensure consistent performance.

Moreover, the long-term durability of 3D-printed pistons remains a subject of scrutiny. Exposure to prolonged thermal and mechanical stress can exacerbate residual stresses and fatigue issues, requiring more comprehensive research into material behavior over time and under realistic engine conditions [13]. In addition to internal material issues, the surface finish of 3D-printed pistons is often rougher than that of conventionally machined parts, which can elevate friction levels and accelerate wear during engine operation [21]. This necessitates applying secondary finishing techniques, such as precision machining, surface polishing, or functional coatings, to enhance tribological performance and extend the component's lifespan. Lastly, while 3D printing is advantageous for low-volume and customized applications, its economic viability for large-scale production is still limited. The high cost of metal

powders, energy-intensive processes, and comparatively slower build rates pose challenges to cost efficiency when compared with traditional casting or forging methods [38]. Therefore, detailed cost-benefit analyses and advancements in high-speed additive manufacturing systems are vital for transitioning from prototyping to commercial-scale production. Addressing these limitations through multidisciplinary engineering efforts will be essential for the broader implementation of 3D-printed pistons in the automotive and aerospace sectors.

6. Material selection for 3D-printed pistons

The advancement of additive manufacturing has opened new pathways for optimizing the design and performance of internal combustion engine components, particularly pistons. Among the most promising developments is the application of 3D-printed metal pistons, which enables unprecedented design flexibility, weight reduction, and thermal efficiency [1, 26]. Material selection plays a pivotal role in the success of such components, as pistons must withstand extreme mechanical and thermal stresses while maintaining low weight and high durability [39].

Various metallic materials are currently being explored for 3D printing pistons, each with unique strengths and trade-offs. For example, AlSi10Mg, a lightweight aluminum alloy, has been successfully employed by companies like Mahle Powertrain in producing pistons for Formula 1 engines, offering significant weight savings and optimized geometry [56]. Meanwhile, Koenigsegg has adopted titanium-based components in its Jesko engines to reduce mass and increase mechanical performance at high rpm [54]. In more extreme environments, such as aerospace propulsion, Inconel 718 is preferred for its superior heat resistance and fatigue strength, albeit at an increased density and manufacturing expense [50].

A notable trend in this domain is the move toward multi-material 3D printing, where materials like CuCrZr are integrated for advanced heat dissipation, paired with strong structural alloys such as maraging steel or titanium. Research consortia, including GE Additive and NASA, are studying these functionally graded structures for next-generation propulsion systems [55].

The following table provides a comparative overview of key metallic materials used in metal additive manufacturing, supporting informed material selection for piston design. Properties such as tensile strength, thermal conductivity, and density are included, followed by a visual comparison chart to facilitate design decision-making.

As Table 2 shows, while AlSi10Mg offers excellent printability and acceptable strength, its limited heat resistance may constrain use in heavy-duty diesel or turbocharged gasoline engines. Conversely, Inconel 718 provides high fatigue resistance at elevated temperatures, making it suitable for aerospace and high-performance applications, albeit with compromises in weight and cost. CuCrZr stands out due to its high thermal conductivity, supporting hybrid solutions where localized heat dissipation is critical. Figure 1 further illustrates the complex trade-offs between density, thermal performance, and mechanical strength, highlighting the need for application-specific optimization.

Table 2. Comparative table of metal materials for 3D-printed pistons

Material	Tensile strength [MPa]	Melting point [°C]	Thermal conductivity [W/m·K]	Density [g/cm ³]	Advantages	Limitations	Common applications
AlSi12	320–400	575–585	140–160	2.65–2.68	High thermal conductivity, low weight, good castability and fluidity, high corrosion resistance	Lower mechanical strength compared to AlSi10Mg, limited ductility under fatigue.	Heat exchangers, engine pistons, housings, thin-walled structures
AlSi10Mg	320–380	580–600	140–160	2.65	Lightweight, good thermal conductivity, excellent printability	Limited high-temperature resistance	Automotive pistons, motorsports
Ti6Al4V (Titanium Alloy)	900–1100	~1600	6–8	4.43	High strength-to-weight ratio, corrosion-resistant	Expensive, low thermal conductivity	Aerospace, high-performance racing engines
Inconel 718 (Nickel Alloy)	1000–1240	~1350	6–11	8.19	Exceptional heat resistance, fatigue strength	Heavy, costly, hard to machine	Jet engines, turbine pistons
316L Stainless Steel	480–620	~1370	15–25	7.99	Cost-effective, corrosion-resistant, and good wear resistance	High density, only moderate thermal properties	Industrial pistons, structural components
CuCrZr (Copper Alloy)	300–450	~1080	300–350	8.96	Excellent thermal conductivity, good for thermal regulation	Lower mechanical strength, heavy	Thermal management zones, hybrid structures
Maraging Steel (e.g., 1.2709)	1900–2100	~1400	20–25	8.00	Extremely high strength, good post-processing performance	High weight, relatively poor thermal performance	Long-life pistons, tool inserts, aerospace parts

Figure 1 compares the key physicochemical properties of metal alloys used to produce 3D printed pistons, including tensile strength, melting point, thermal conductivity, and density. Analysis of the graph indicates significant differences in parameters that determine the use of a given material in specific operating conditions.

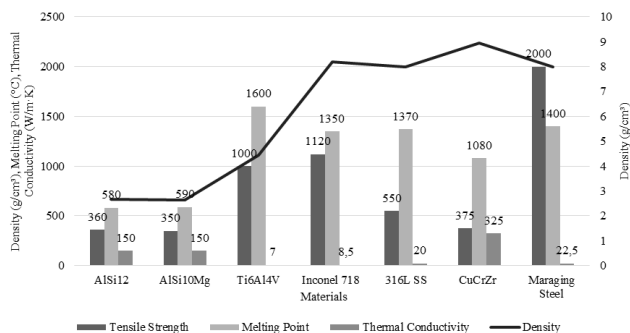


Fig. 1. Comparison of parameters of metal powders for 3D printing

For example, CuCrZr is characterized by the highest thermal conductivity (~325 W/m K), which makes it an excellent choice for piston zones requiring intensive heat dissipation. However, its density (~8.96 g/cm³) and moderate mechanical strength (~325 MPa) limit its use as the primary structural material.

In turn, Ti6Al4V is distinguished by an excellent strength-to-weight ratio (up to 1100 MPa at a density of 4.43 g/cm³). However, its low thermal conductivity (only 7 W/mK) requires the support of additional cooling systems.

Inconel 718 and Maraging Steel offer the highest strength values (1120 and 2000 MPa, respectively) and resistance to high temperatures. However, their weight and

difficulty in processing limit their use in specialized environments, such as aviation or high-performance engines.

AlSi10Mg and AlSi12, despite having relatively lower mechanical properties, offer a low specific weight and high thermal conductivity, which makes them widely used in lightweight structures of pistons in combustion engines.

This comparison confirms that there is no "ideal" material that would meet all the requirements at the same time. The alloy selection should be adapted to the specific operating profile – a high-performance engine will require properties different from those of a unit for a city or agricultural vehicle. Therefore, hybrid structures and gradient materials (FGM), combining the advantages of several alloys in one structure, are gaining increasing importance.

7. Industrial applications and prospects

The use of 3D-printed metal pistons is gaining traction in motorsports and aerospace industries, where performance gains outweigh production costs [26]. As the technology matures, improved manufacturing efficiency and material advancements could make it viable for mainstream automotive applications.

Future research should focus on refining printing techniques, developing superior metal powders, and enhancing post-processing methods to address existing challenges. Collaborations between industry and academia will play a crucial role in accelerating the adoption of this technology [27].

8. Conclusion

Additive manufacturing presents a transformative approach to piston production, unlocking unprecedented design flexibility, functional integration and performance enhancements across a wide range of internal combustion engine applications [1, 12, 26, 53]. The literature reviewed

in this paper shows that metal AM processes – in particular LPBF – already enable the manufacture of geometrically complex pistons and related components such as cylinder heads and combustion chambers [2, 22, 30]. These components can integrate lattice-reinforced structures, conformal cooling channels, and tailored combustion-bowl geometries, supporting higher power density, improved fuel efficiency, and lower pollutant emissions compared to conventionally cast designs [4, 14, 32].

At the same time, the analysis of fatigue behaviour, residual stresses and microstructural features confirms that 3D-printed pistons cannot simply be treated as one-to-one replacements for traditional pistons made from the same nominal alloy. Defect size and distribution, surface roughness, and build orientation have a first-order influence on fatigue life, particularly for AlSi10Mg, which remains the most widely used alloy for AM pistons [10, 34, 40]. Residual stresses originating from steep thermal gradients and layer-wise solidification add further complexity, requiring careful control of process parameters and the use of post-processing operations such as HIP, heat treatment and precision finishing [13, 31, 38]. These findings underscore that AM pistons must be engineered as integrated systems, in which geometry, material state, and process history are jointly optimised.

The proposed design workflow for additively manufactured pistons synthesizes current best practices into four stages: load-path analysis and topology optimization, integration of AM-specific internal features, thermo-mechanical validation, and post-processing tailored to fatigue and tribological requirements. This framework demonstrates that AM is not merely an alternative production route, but a design-driven paradigm in which structural optimisation and thermal management are embedded from the outset of the development process. In parallel, advances in material selection – from AlSi10Mg and Ti6Al4V to Inconel 718, maraging steels and CuCrZr-based solutions – open the way for multi-material and functionally graded pistons that exploit spatially optimised property distributions [39, 50, 54–56].

From an industrial perspective, the current technology readiness level is highest in motorsports, prototyping, and specialized high-performance engines, where the benefits of rapid design iteration and performance gains outweigh the higher manufacturing costs [54–56]. In volume production, economic barriers remain significant due to the high price of metal powders, energy-intensive processing, and relatively low build rates compared to casting and forging [38, 50]. Nevertheless, as AM equipment productivity improves and experience with robust process windows grows, hybrid deployment scenarios – such as AM for prototype and small-series pistons, combined with conventional manufacturing for mainstream models – appear increasingly realistic.

Looking ahead, further research is needed in several areas to realize the potential of 3D-printed pistons fully. First, there is a clear need to bridge the gap between coupon-level fatigue data and long-term durability of full-scale pistons tested under representative engine duty cycles. Second, multi-physics simulation frameworks must be extended to account for microstructural anisotropy, graded materials and residual stress fields inherent to AM components. Third, design rules and certification procedures must evolve to address internal lattices, conformal channels, and multi-material architectures that do not fit within the assumptions of existing standards. Finally, comprehensive techno-economic and life-cycle assessments are essential to quantify the actual cost, environmental impact and supply-chain implications of deploying AM pistons at scale [1, 12].

In summary, additively manufactured metal pistons are unlikely to replace conventional pistons across all applications in the near term. However, for high-value, performance-critical, or highly customized engines, they already offer a compelling pathway to integrate advanced geometries, intelligent sensing, and tailored material architectures that would be impossible to realize otherwise. With continued progress in process stability, material systems, design methodologies and validation protocols, 3D-printed pistons have the potential to become a key enabler of next-generation internal combustion engines rather than a mere manufacturing curiosity.

Bibliography

- [1] Abdulhameed O, Al-Ahmari A, Ameen W, Mian SH. Additive manufacturing: challenges, trends, and applications. *Adv Mech Eng.* 2019;11(2):1687814018822880. <https://doi.org/10.1177/1687814018822880>
- [2] Adamou A, Costall A, Turner JWG, Jones A, Copeland C. Experimental performance and emissions of additively manufactured high-temperature combustion chambers for micro-gas turbines. *Int J Engine Res.* 2023;24(4):1273-1289. <https://doi.org/10.1177/14680874221082636>
- [3] Andronov V, Pitrmuc Z, Zajíc J, Šotka P, Beránek L, Bock M. Conformal cooling as a support tool for eliminating local defects in high-pressure die casting series production. *Prog Addit Manuf.* 2025;10(2):1511-1528. <https://doi.org/10.1007/s40964-024-00721-x>
- [4] Andronov V, Šimota J, Pelikán L, Beránek L, Novák V. Analysis of strength properties of 3D printed lightweight structures made of AlSi10Mg material. *IOP Conf Ser: Mater Sci Eng.* 2021;1178(1):012002. <https://doi.org/10.1088/1757-899X/1178/1/012002>
- [5] Armstrong M, Mehrabi H, Naveed N. An overview of modern metal additive manufacturing technology. *J Manuf Processes.* 2022;84:1001-1029. <https://doi.org/10.1016/j.jmapro.2022.10.060>
- [6] Arrivabeni EB, Tomasoni D, Giorleo L, Barbato MC. A methodology for mould conformal cooling channels optimization exploiting 3D printing. *ESAFORM 2021.* 2021. <https://doi.org/10.25518/esaform21.3894>
- [7] Bian P, Shi J, Liu Y, Xie Y. Influence of laser power and scanning strategy on residual stress distribution in additively manufactured 316L steel. *Optics & Laser Technology.* 2020; 132:106477. <https://doi.org/10.1016/j.optlastec.2020.106477>
- [8] Blakey-Milner B, Gradl P, Snedden G, Brooks M, Pitot J, Lopez E et al. Metal additive manufacturing in aerospace: a review. *Materials & Design.* 2021;209:110008. <https://doi.org/10.1016/j.matdes.2021.110008>
- [9] Cheng L, Liang X, Bai J, Chen Q, Lemon J, To A. On utilizing topology optimization to design support structure to prevent residual stress induced build failure in laser powder bed

- metal additive manufacturing. Additive Manufacturing. 2019;27:290-304.
<https://doi.org/10.1016/j.addma.2019.03.001>
- [10] Dan C, Cui Y, Wu Y, Chen Z, Liu H, Ji G et al. Achieving ultrahigh fatigue resistance in AlSi10Mg alloy by additive manufacturing. Nat Mater. 2023;22(10):1182-1188.
<https://doi.org/10.1038/s41563-023-01651-9>
- [11] DeRoy T, Wei HL, Zuback JS, Mukherjee T, Elmer JW, Milewski JO et al. Additive manufacturing of metallic components – process, structure and properties. Prog Mater Sci. 2018;92:112-224.
<https://doi.org/10.1016/j.pmatsci.2017.10.001>
- [12] Despeisse M, Ford S. The role of additive manufacturing in improving resource efficiency and sustainability. In: Umeda S, Nakano M, Mizuyama H, Hibino H, Kiritsis D, Von Cieminski G (eds). Advances in Production Management Systems: Innovative Production Management Towards Sustainable Growth. Cham: Springer International Publishing; 2015:129-136.
https://doi.org/10.1007/978-3-319-22759-7_15
- [13] Diniță A, Neacșa A, Portoacă AI, Tănase M, Ilinca CN, Ramadan IN. Additive manufacturing post-processing treatments, a review with emphasis on mechanical characteristics. Materials. 2023;16(13):4610.
<https://doi.org/10.3390/ma16134610>
- [14] Dolan R, Budde R, Schramm C, Rezaei R. 3D printed piston for heavy-duty diesel engines. SAE Technical Paper 2024-01-3717. 2024. <https://doi.org/10.4271/2024-01-3717>
- [15] Domfang Ngnekou JN, Nadot Y, Henaff G, Nicolai J, Kan WH, Cairney JM et al. Fatigue properties of AlSi10Mg produced by additive layer manufacturing. Int J Fatigue. 2019; 119:160-172. <https://doi.org/10.1016/j.ijfatigue.2018.09.029>
- [16] Dongre G, Kshirsagar P, Kulat S, Kulkarni B, Kulkarni V, More S. Topology optimisation of piston. IJRASET. 2023; 11(5):2978-2983.
<https://doi.org/10.22214/ijraset.2023.51449>
- [17] Eriksson M, Lervåg M, Sørensen C, Robertstad A, Brønstad BM, Nyhus B et al. Additive manufacture of superduplex stainless steel using WAAM. MATEC Web Conf. 2018; 188:03014.
<https://doi.org/10.1051/mateconf/201818803014>
- [18] Feng S, Kamat AM, Pei Y. Design and fabrication of conformal cooling channels in molds: review and progress updates. Int J Heat and Mass Transf. 2021;171:121082.
<https://doi.org/10.1016/j.ijheatmasstransfer.2021.121082>
- [19] Ferro P, Fabrizi A, Berto F, Savio G, Meneghello R, Rosso S. Defects as a root cause of fatigue weakening of additively manufactured AlSi10Mg components. Theor Appl Fract Mech. 2020;108:102611.
<https://doi.org/10.1016/j.tafmec.2020.102611>
- [20] Fracchia E, Gobber FS, Rosso M, Actis Grande M, Bidulská J, Bidulský R. Junction characterization in a functionally graded aluminum part. Materials. 2019;12(21):3475.
<https://doi.org/10.3390/ma12213475>
- [21] Garcia CR, Rumpf RC, Tsang HH, Barton JH. Effects of extreme surface roughness on 3D printed horn antenna. Electron Lett. 2013;49(12):734-736.
<https://doi.org/10.1049/el.2013.1528>
- [22] Gray J, Depcik C, Sietins JM, Kudzal A, Rogers R, Cho K. Production of the cylinder head and crankcase of a small internal combustion engine using metal laser powder bed fusion. J Manuf Process. 2023;97:100-114.
<https://doi.org/10.1016/j.jmapro.2023.04.054>
- [23] Gruden DO. Combustion chamber layout for modern Otto engines. SAE Technical Paper 811231. 1981.
<https://doi.org/10.4271/811231>
- [24] Heitzman RC. Design of an articulated piston for Caterpillar® 3500 engines utilizing computer-aided design and analysis. J Eng Gas Turbines Power. 1990;112(3):276-279.
<https://doi.org/10.1115/1.2906492>
- [25] Herzog D, Seyda V, Wycisk E, Emmelmann C. Additive manufacturing of metals. Acta Mater. 2016;117:371-392.
<https://doi.org/10.1016/j.actamat.2016.07.019>
- [26] Jared BH, Aguilo MA, Beghini LL, Boyce BL, Clark BW, Cook A et al. Additive manufacturing: toward holistic design. Scr Mater. 2017;135:141-147.
<https://doi.org/10.1016/j.scriptamat.2017.02.029>
- [27] Javaid M, Haleem A, Singh RP, Suman R, Rab S. Role of additive manufacturing applications towards environmental sustainability. Adv Ind Eng Polym Res. 2021;4(4):312-322.
<https://doi.org/10.1016/j.aiepr.2021.07.005>
- [28] Jiménez M, Romero L, Domínguez IA, Espinosa MDM, Domínguez M. Additive manufacturing technologies: an overview about 3D printing methods and future prospects. Complexity. 2019;2019(1):9656938.
<https://doi.org/10.1155/2019/9656938>
- [29] Khan N, Riccio A. A Systematic review of design for additive manufacturing of aerospace lattice structures: current trends and future directions. Prog Aerosp Sci. 2024;149: 101021. <https://doi.org/10.1016/j.paerosci.2024.101021>
- [30] Kolganov KA, Mikryukov IV, Markov AS. Development of a technology for the manufacturing of parts/components of an internal combustion engine involving additive manufacturing methods. Silovoe i energeticheskoe oborudovanie Avtonomnye sistemy. 2019;2(3):166-184.
<https://doi.org/10.32464/2618-8716-2019-2-3-166-184>
- [31] Laleh M, Sadeghi E, Revilla RI, Chao Q, Haghdad N, Hughes AE et al. Heat treatment for metal additive manufacturing. Prog Mater Sci. 2023;133:101051.
<https://doi.org/10.1016/j.pmatsci.2022.101051>
- [32] Liu H, Ma J, Tong L, Ma G, Zheng Z, Yao M. Investigation on the potential of high efficiency for internal combustion engines. Energies. 2018;11(3):513.
<https://doi.org/10.3390/en11030513>
- [33] Liu Y, Shi J, Wang Y. Evolution, control, and mitigation of residual stresses in additively manufactured metallic materials: a review. Adv Eng Mater. 2023;25(22):2300489.
<https://doi.org/10.1002/adem.202300489>
- [34] Maleki E, Shamsaei N. A comprehensive study on the effects of surface post-processing on fatigue performance of additively manufactured AlSi10Mg: an augmented machine learning perspective on experimental observations. Additive Manufacturing. 2024;86:104179.
<https://doi.org/10.1016/j.addma.2024.104179>
- [35] Martina F, Roy MJ, Szost BA, Terzi S, Colegrove PA, Williams SW et al. Residual stress of as-deposited and rolled wire+arc additive manufacturing Ti-6Al-4V components. Mat Sci Technol. 2016;32(14):1439-1448.
<https://doi.org/10.1080/02670836.2016.1142704>
- [36] Mattarelli E, Fontanesi S, Rinaldini C, Valentino G, Iannuzzi S, Severi E et al. Combustion optimization of a marine DI diesel engine. SAE Technical Paper 2013-24-0020. 2013.
<https://doi.org/10.4271/2013-24-0020>
- [37] Najibi A, Alizadeh P. Nonlinear transient thermal stress investigation of 2D-FG porosity long cylinder sector. Commun Nonlinear Sci Numer Simul. 2025;142:108558.
<https://doi.org/10.1016/j.cnsns.2024.108558>
- [38] Panda BK, Sahoo S. Numerical simulation of residual stress in laser based additive manufacturing process. IOP Conf Ser: Mater Sci Eng. 2018;338:012030.
<https://doi.org/10.1088/1757-899X/338/1/012030>
- [39] Pfeifer A, Gericke M, Heinze T. Synthesis and characterization of novel water-soluble 6-deoxy-6-(2-amino-2-(hydroxy-

- methyl)propane-1,3-diol)cellulose derivatives. *Adv Ind Eng Poly Res.* 2020;3(2):77-82.
<https://doi.org/10.1016/j.aiepr.2020.02.001>
- [40] Romano S, Brückner-Foit A, Brandão A, Gumpinger J, Ghidini T, Beretta S. Fatigue properties of AlSi10Mg obtained by additive manufacturing: defect-based modelling and prediction of fatigue strength. *Eng Fract Mech.* 2018; 187:165-189.
<https://doi.org/10.1016/j.engfracmech.2017.11.002>
- [41] Schoeffmann W, Knollmayr C, Mehrabi K. Additive manufactured components in engine and fuel cell applications – from prototyping to dedicated production design. *Euro PM2024 Proceedings. EPMA 2024.*
<https://doi.org/10.59499/EP246281384>
- [42] Selvaraj G, Yessian S, Ramalingam S, Dharani Kumar S, Gopal G, Sharma S et al. Investigation on topology-optimized compressor piston by metal additive manufacturing technique: analytical and numeric computational modeling using finite element analysis in ANSYS. *Open Physics.* 2023;21(1):20220259.
<https://doi.org/10.1515/phys-2022-0259>
- [43] Stojanovic B, Glisovic J. *Automotive engine materials.* In: Reference Module in Materials Science and Materials Engineering. Elsevier 2016.
<https://doi.org/10.1016/B978-0-12-803581-8.01946-9>
- [44] Tian X, Zhao Z, Wang H, Liu X, Song X. Progresses on the additive manufacturing of functionally graded metallic materials. *J Alloys Compd.* 2023;960:170687.
<https://doi.org/10.1016/j.jallcom.2023.170687>
- [45] Toledo Valera JD, Zavos A, Nikolakopoulos PG. Thermal and structural improvements of a motorcycle piston using a fully coupled thermo-mechanical FEM simulation. *Int J Engine Res.* 2025;26(7):973-983.
<https://doi.org/10.1177/14680874241297781>
- [46] Torregrosa AJ, Olmeda P, Degraeuwe B, Reyes M. A concise wall temperature model for DI diesel engines. *Appl Therm Engineering.* 2006;26(11–12):1320-1327.
<https://doi.org/10.1016/j.applthermaleng.2005.10.021>
- [47] Velugula R, Thiruvallur Loganathan B, Varadhaiyengar L, Asvathanarayanan R, Mittal M. An analysis of mechanical and thermal stresses, temperature and displacement within the transparent cylinder and piston top of a small direct-injection spark-ignition optical engine. *Energies.* 2023; 16(21):7400. <https://doi.org/10.3390/en16217400>
- [48] Wasti S, Adhikari S. Use of biomaterials for 3D printing by fused deposition modeling technique: a review. *Front Chem.* 2020;8:315. <https://doi.org/10.3389/fchem.2020.00315>
- [49] Wei HL, Mukherjee T, Zhang W, Zuback JS, Knapp GL, De A et al. Mechanistic models for additive manufacturing of metallic components. *Prog Mater Sci.* 2021;116:100703. <https://doi.org/10.1016/j.pmatsci.2020.100703>
- [50] Weissbach R, Praegla PM, Wall WA, Hart AJ, Meier C. Exploration of improved, roller-based spreading strategies for cohesive powders in additive manufacturing via coupled DEM-FEM simulations. *Powder Technol.* 2024;443:119956. <https://doi.org/10.1016/j.powtec.2024.119956>
- [51] Zhang J, Li J, Wu S, Zhang W, Sun J, Qian G. High-cycle and very-high-cycle fatigue lifetime prediction of additively manufactured AlSi10Mg via crystal plasticity finite element method. *Int J Fatigue.* 2022;155:106577. <https://doi.org/10.1016/j.ijfatigue.2021.106577>
- [52] Zhao L, Santos Macías JG, Dolimont A, Simar A, Rivière-Lorphèvre E. Comparison of residual stresses obtained by the crack compliance method for parts produced by different metal additive manufacturing techniques and after friction stir processing. *Additive Manufacturing.* 2020;36:101499. <https://doi.org/10.1016/j.addma.2020.101499>
- [53] Zhou L, Miller J, Vezza J, Mayster M, Raffay M, Justice Q et al. *Additive manufacturing: a comprehensive review.* *Sensors.* 2024;24(9):2668. <https://doi.org/10.3390/s24092668>
- [54] Koenigsegg Automotive AB. *Jesko Engine Development Report.* 2021.
- [55] GE Additive & NASA. *Advancing Aerospace with Additive Manufacturing.* 2022.
- [56] Mahle Powertrain. *Pistons Manufactured with 3D Printing for Formula 1 Applications.* 2020.

Piotr Laskowski, DEng. – Faculty of Automotive and Construction Machinery Engineering, Warsaw University of Technology, Poland.
 e-mail: piotr.laskowski@pw.edu.pl



Marcin Wojs, DEng. – Faculty of Automotive and Construction Machinery Engineering, Warsaw University of Technology, Poland.
 e-mail: marcin.wojs@pw.edu.pl



Analysis of the quality of vehicle fleet data as input for modeling emissions and dispersion of pollutants emitted by combustion engine vehicles

ARTICLE INFO

Received: 21 June 2025

Revised: 22 December 2025

Accepted: 6 January 2026

Available online: 15 January 2026

Reliable modeling of emissions and dispersion of pollutants emitted in exhaust gases from motor vehicles is highly challenging due to the presence of multiple variables and inconsistencies in input data quality across different stages of the process. This article focuses on the vehicle fleet. It has been demonstrated that the structure of the vehicle fleet in a given area varies depending on the data collection methods and sources, which ultimately determines the dispersion results. This issue becomes particularly significant in urban environments, where the intensity of road traffic is high, and ventilation conditions are often poor, partly due to the formation of street canyons by dense urban development. The modeling was conducted at a selected intersection in Wrocław for various fleet structure scenarios. The results were compared with the results of pollutant concentrations from a nearby air quality monitoring station. The Copert emission model and emission factors from the European EMEP/Corinair database were used. In contrast, the GRAL model, a CFD model (suitable for urban dispersion modeling), was used to simulate pollution dispersion.

Key words: road transport, emission modelling, air quality, dispersion modelling, fleet structure analysis

This is an open access article under the CC BY license (<http://creativecommons.org/licenses/by/4.0/>)

1. Introduction

Air pollution is one of the most serious threats to public health and the climate worldwide. In particular, urban traffic is considered a key source of emissions of harmful substances such as nitrogen oxides (NO_x), carbon monoxide (CO), volatile organic compounds (VOCs), particulate matter (PM, including soot), and greenhouse gases (GHG), including carbon dioxide (CO₂), nitrous oxide (N₂O) and methane (CH₄). Numerous reports by Polish environmental protection authorities, such as the National Centre for Environmental Protection (KOBiZE) and the Chief Inspectorate for Environmental Protection (GIOŚ), indicate that road transport contributes significantly to air pollution [9, 13]. They show, among other things, that although transport accounts for about 33% of total nitrogen oxide emissions nationwide, this figure is significantly higher in large cities, reaching about 43% in Warsaw, for example.

Due to the inability to directly measure emissions from all vehicles participating in traffic, as well as the presence of other sources of the same pollutants, such as exhaust fumes from individual building heating systems, it is challenging to determine the impact of motorization on air quality precisely. Therefore, emission estimation methods should be used for this purpose, usually involving emission modelling techniques. Modelling the emission and dispersion of pollutants from combustion engine vehicles is a complex issue that requires high-quality input data on the vehicle fleet [8]. The reliability of modelling results depends to a large extent on the accuracy of information on fleet composition, traffic patterns and vehicle technical characteristics [10, 14]. This literature review presents the current state of knowledge on the quality of vehicle fleet data and its impact on the accuracy of modeling emissions and pollutant dispersion in the urban environment. Traditional approaches to collecting vehicle fleet data rely mainly on official registration statistics and traffic surveys [10].

However, studies show significant discrepancies between different data sources. A study conducted in Toronto found that the emission factors obtained from models were twice as high as those estimated using trace measurements for CO and NO_x [19]. Similarly, an analysis of mobility data during the pandemic revealed a 60% discrepancy between data from mobile applications and actual traffic measurements [8]. This means that a critical approach to the fleet structure must be incorporated into the model. In general, it should be emphasized that the assessment of the impact of motor vehicle traffic using modeling consists of two consecutive steps: emission modeling and pollutant dispersion modeling. At each of these stages, input data from various sources is entered. In emission models, these include traffic intensity, road type and geometry, and vehicle fleet structure (division into categories, age, engine size, etc.). Any error made at this stage is then carried over to the pollutant dispersion modelling stage, where another error is also generated. It is therefore essential to ensure the best possible quality of input data at each stage in order to minimise the final error.

Research confirms the significant impact of fleet data quality on emission modelling results. Sensitivity analysis has shown that greenhouse gas emissions from light vehicles can vary by -2% to 11%, and conventional pollutants by -47% to 228% compared to baseline values. For heavy-duty vehicles, the variability can be -21% to 55% for GHG and -32% to 174% for CAP, respectively [14]. These significant differences highlight the crucial role of accurate fleet characteristics data. A comparison of two popular emission models, MOVES and FIVE, showed significant differences in emission estimates. The MOVES model showed lower systematic errors for ozone and PM_{2.5} at the national level, while FIVE performed better at the urban scale due to higher NO_x emissions in urban areas [8]. These differences are partly due to different approaches to charac-

terising the vehicle fleet in each model. It should be emphasised that accurate validation of emission model results is extremely difficult, if not impossible.

In Europe, the dominant models are COPERT (Computer Programme to Calculate Emissions from Road Transport) and HBEFA (Handbook Emission Factors for Road Transport) [5, 20]. Shi et al. published a study presenting highly detailed CO₂ emission maps for road transport in 20 major European cities (France, Germany, the Netherlands) for the year 2023. The authors applied Floating Car Data (FCD), utilizing machine-learning algorithms to extrapolate GPS samples into actual traffic volumes, and combined these with the COPERT model to calculate emission factors [15]. While the COPERT model is widely used across EU countries, the HBEFA model is typically applied only in some of them, primarily in Germany, Austria, France, Switzerland, and Sweden [4]. In Slovakia, for instance, HBEFA-based emission factors were used in a study on the introduction of LNG buses in urban transport, demonstrating that this tool is also applied in other European countries [6].

Recent comparative analyses integrating COPERT and HBEFA indicate that both models tend to overestimate NO_x emissions relative to field measurements. However, COPERT reproduces traffic conditions in highly urbanized environments more accurately, which confirms its calibration to European measurement campaigns [5]. However, the advantage of COPERT and HBEFA in European applications stems primarily from their close alignment with the characteristics of the vehicle fleet, emission standards, and traffic structures specific to EU member states, which are harmonized under the regulations of the European Environment Agency (EEA). In contrast, MOVES and FIVE were designed primarily to support the U.S. emission inventory system and air-quality policy, using fleet, fuel, and activity data characteristic of the United States [18].

Accurately estimating the impact of road traffic on air quality in cities is a complex and challenging process. Selected issues are briefly described below.

Lack of reliable and detailed data on the fleet – designing effective emission reduction policies is hindered by insufficient and unreliable data on the composition of the vehicle fleet (e.g., age, engine type, emission control technology) and its actual activity [10, 17]. Fluctuations in model estimates of emissions often result from local factors such as variable fleet composition, the presence of external sources of pollution and changing traffic intensity [12]. An overly general classification of vehicles, such as treating all heavy traffic as a single category, may not accurately reflect the actual distribution of emissions.

The evolution of the vehicle fleet – the increasing popularity of vehicles with gasoline direct injection (GDI) engines, which are fuel-efficient but also increase emissions of soot and toxic substances – poses a new challenge [19]. Furthermore, the growing share of electric vehicles (EVs) and hybrids is altering the emissions profile, while simultaneously leading to a significant increase in electricity demand, which necessitates an assessment of the environmental impact of electricity production. This introduces new complexi-

ties, such as changing the boundaries of the analysis system (e.g. from ‘tank-to-wheel’ to ‘well-to-wheel’) [2, 19].

Limitations of models and measurement data – the accuracy of roadside emission and pollutant concentration inventories is largely dependent on the quality of the emission factors (EFs) used. Models such as MOVES, although based on data from vehicle inspection programmes and dynamometer tests, may not take into account the full range of real-world driving conditions (e.g. variable speeds, acceleration and braking), which can lead to NO_x emissions being overestimated by as much as 50–100% compared to actual measurements [3]. Vehicle emissions vary significantly depending on vehicle type, age, distance traveled, fuel type, combustion processes, and other factors (e.g. tire and brake wear), as well as local weather conditions such as temperature and humidity. Traffic conditions (e.g. traffic density, road conditions, vehicle type) can vary dramatically over short distances (1–10 km) and in short intervals (e.g., hourly). Additionally, factors such as the engine's technical condition and the driver's driving style also impact the amount of emissions [7, 16].

Ageing fleet in developing countries – in many developing countries, the problem of vehicle emissions is exacerbated by an ageing vehicle fleet and less stringent environmental regulations [1, 14].

The aim of this article is to highlight issues with the availability and quality of data on the structure of the vehicle fleet in assessing the impact of road traffic on air quality in urban conditions, using the example of Wrocław. An innovative combination of data sources for modelling emissions from road traffic has been used in the paper. Most models available in the literature rely on the statistical structure of the vehicle fleet. This article demonstrates how different input data sources for the model can significantly influence the final results of modeling the impact of road transport on air quality in urban conditions.

2. Materials and methods

2.1. Analysis of the fleet of vehicles moving around Wrocław

The most critical component in modelling traffic-related emissions is the introduction of the vehicle fleet. An appropriate selection of the fleet structure – especially in terms of vehicle age (compliance with Euro standards), propulsion and fuel type, engine displacement, and other characteristics – is pivotal for the quality of the modelling. Identifying a suitable data source for the composition of the fleet is challenging for several reasons. Ideally, actual measurement data that precisely reflects the fleet structure for the area being modeled and is synchronized in time would be used. However, obtaining such data for every case, especially at a larger scale, is highly challenging, time-consuming, and requires considerable human resources, often with associated error margins (for example, due to variability in driver behaviour and changes in traffic conditions and congestion). In practice, the approach most commonly used is to model traffic emissions using statistical data. However, multiple statistical data sources exist. One example is the national statistics, which consider the entirety of the registered vehicle fleet across Poland. However,

national statistics may not always accurately reflect the local context, such as a specific city or a given road segment.

A second approach is to use more regionalised data, for example, the data from the Central Register of Vehicles and Drivers (CEPiK) for the city of Wrocław, as shared by the Municipal Office of Wrocław. However, analyses have shown that this data is also subject to certain limitations. First, local CEPiK databases retain records of vehicles for five years, even if those vehicles have been withdrawn from service. A vehicle is only removed from the database after five years of inactivity (e.g., after no technical inspection), potentially skewing statistics towards an overestimation of older vehicles. Another issue is the fact that many people using the city are not residents – for example, those commuting from nearby smaller towns such as Trzebnica, Oława, or Oleśnica, or students and young professionals who drive vehicles registered in their hometowns. The third challenge is data completeness. Whereas the author had access to the CEPiK database for Wrocław for the years 2015–2017, which included almost all necessary information for accurate emission modeling (year of manufacture, vehicle category, fuel/powertrain, and engine displacement), more recent data lacked certain crucial details. Even within the 2015–2017 dataset, errors were identified – for example, incorrect classification of light commercial vehicles (incorrectly classified as heavy trucks, special-purpose vehicles, or ‘other’), and the absence of a ‘Light Duty Vehicles’ category. Moreover, in the case of articulated trucks, the fact that a vehicle is registered in Wrocław does not necessarily mean that it operates within the city. Figure 1 presents a summary of vehicles registered in Wrocław, based on CEPiK data for the years 2015, 2017, and 2021. Notably, the total number of registered vehicles increased sharply over this period (2015: 394,550 vehicles, 2017: 495,306, 2021: 613,938), and approximately 80% of the total comprised passenger cars (2015: 79%, 2017: 80%, 2021: 81%).

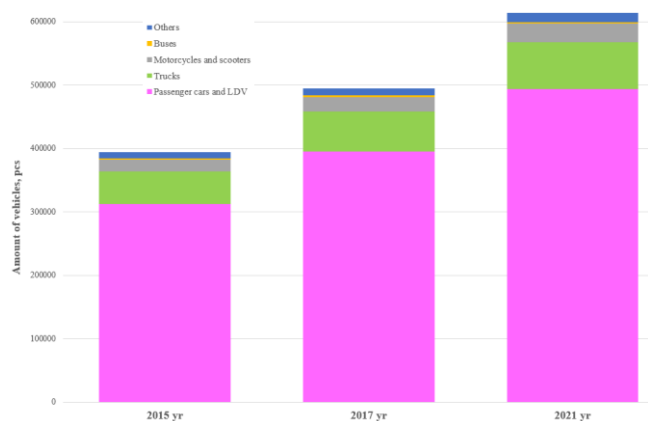


Fig. 1. Vehicles registered in Wrocław according to CEPiK data, broken down by category for 2015, 2017, and 2021 (author’s compilation based on CEPiK data for Wrocław)

A third important source of fleet data, in the author’s view, is through direct observations conducted in actual

traffic conditions. To this end, in April 2023, a study was conducted in which license plate numbers were recorded along one of the main streets in the center of Wrocław, near the intersection of Oławska and Podwale Streets. Three half-hour measurement periods were conducted: one in the morning on a Sunday, one at noon on a Sunday, and one in the afternoon of a working day. The focus was not to measure traffic intensity, but to capture the composition of the vehicle fleet, selecting times with relatively smooth traffic flow to maximise the number of registrations. In total, nearly 1000 license plate numbers were recorded and compiled into a spreadsheet. A request was then submitted to the central CEPiK office in Gliwice to obtain data for those vehicles, including: vehicle category, year of manufacture, engine displacement, fuel/powertrain type, alternative fuel, and status (registered/inactive). A statistical analysis was conducted using the received data. At first glance, this approach appears advantageous compared to relying on pre-existing statistics due to its higher data quality. However, such studies are time-consuming, require significant human resources for data recording and processing, and involve a lengthy wait for the data to be released. Moreover, the sample size is a limitation – approximately 1000 observed vehicles account for only a small fraction of those using Wrocław’s roads. For example, only one articulated lorry was registered, making statistical analysis challenging. To achieve better statistical significance, more such studies would be required, preferably conducted across multiple locations simultaneously, which further increases resource demands.

Additionally, a fee must be paid to CEPiK for data access. Considering the dynamic changes in the composition of the vehicle fleet, such studies must be conducted frequently. Similar studies were conducted in 2022 by the Wrocław Municipal Office as part of analyses related to the implementation of the Clean Transport Zone. In Section 3.1, the results of that study are compared with those from the author’s observations.

2.2. Location of analysis

The analyses were conducted in the area of the intersection of Powstańców Śląskich Street, Hallera Street, and Wiśniowa Avenue. This location was selected for several reasons. First, it is an intersection of some of the city’s main thoroughfares. Powstańców Śląskich Street is a primary route leading out of the city towards the A4 motorway. Secondly, this intersection hosts an air quality monitoring station operated by the State Environmental Monitoring network under the auspices of the Chief Inspectorate of Environmental Protection. This is a typical ‘traffic’ station dedicated to measuring pollutants arising from vehicular activity. This allows for a direct comparison between the dispersion results and actual observed air pollution levels. Notably, in recent years, this station has registered the highest nitrogen oxides (NO_x) concentrations across Wrocław. An additional advantage of the site is the presence of cameras from the Intelligent Transport System (ITS), which significantly facilitates the acquisition of actual traffic data. Figure 2 presents the selected area of analysis, with the air quality monitoring station marked in red.



Fig. 2. Selected area of analysis (basemap: www.geoportal.gov.pl)

2.3. Emission modeling using the Copert model

The first stage of the analysis involved emission modeling for the vehicle fleet in the vicinity of the intersection. The European Copert model was used for this purpose. Copert operates in conjunction with the EMEP/Corinair emission factor database. To build the model, the following data were required:

- road sections and their lengths
- number of traffic lanes in each direction
- vehicle fleet composition (in percentages)
- traffic flow on each lane
- vehicle speed (set to the local speed limit of 50 km/h).

The analyses were conducted for three fleet scenarios:

- 1) CEPIK data for Wrocław (2021) – ‘Fleet 1’
- 2) Municipal Office of Wrocław traffic survey data (2022) – ‘Fleet 2’
- 3) Author’s traffic survey data (2023) – ‘Fleet 3’.

Traffic flow data were based on measurements conducted on the selected date, 17 August 2022. This date was chosen due to its proximity to the data years (2021–2023), and because it was a summer date with no significant additional emissions from heating (there is a nearby area of single-family homes), making it ideal for focusing exclusively on vehicular emissions. This date also coincided with the highest recorded NO₂ concentrations at the monitoring station (Fig. 3).

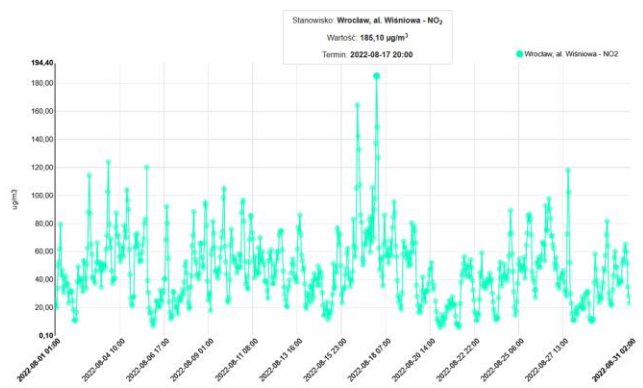


Fig. 3. Variations in NO₂ concentrations measured in 2022 at the air quality monitoring station located on Wisłowa Avenue (source: https://powietrze.gios.gov.pl/pjp/current/station_details)

Figure 4 presents assumptions about lane counts and traffic directions. Table 1 summarizes the average daily traffic for each direction, as well as the segment lengths.

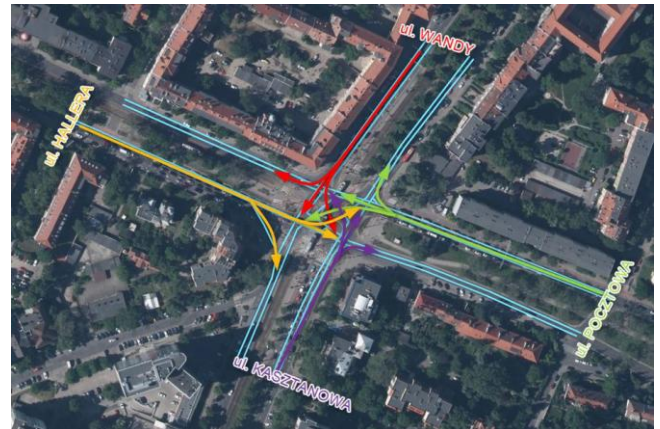


Fig. 4. Analysed road stretches and traffic directions per lane

Table 1. Average daily traffic and stretch lengths

Stretch	Number of vehicles, pcs/day	Number of vehicles, pcs/hour	Length of stretch, m
Wandy_crossroad_left	2724	114	126.1
Wandy_crossroad_straight	8171	341	136.6
Wandy_crossroad_right	2724	114	132.4
Hallera_crossroad_left	2407	101	216.3
Hallera_crossroad_straight	14206	592	198
Hallera_crossroad_right	2328	97	172.2
Kasztanowa_crossroad_left	4808	201	134.7
Kasztanowa_crossroad_straight	9875	412	140.1
Kasztanowa_crossroad_right	3292	138	99.7
Pocztowa_crossroad_left	2406	101	233.2
Pocztowa_crossroad_straight	10055	419	225.5
Pocztowa_crossroad_right	3352	140	175.3
Crossroad_Wandy_line1	2407	101	98.4
Crossroad_Wandy_line2	13226	552	95.3
Crossroad_Hallera_line1	12779	533	131.4
Crossroad_Hallera_line2	4808	201	128.1
Crossroad_Kasztanowa_line2	2406	101	109.8
Crossroad_łącznik	8171	341	45
Crossroad_Kasztanowa_line1	2328	97	46.8
Crossroad_Pocztowa_line1	2724	114	163.8

Measurements of NO_x (including NO₂), CO, and PM_{2.5} are performed automatically by the nearby air quality station. In the context of combustion-related pollutants from vehicular traffic, NO₂ was selected for this analysis. PM was omitted due to its potential distortion by re-suspended dust caused by traffic (no rain was recorded that day), making PM measurements unsuitable for direct attribution.

2.4. Dispersion modeling using the GRAMM/GRAL model

For dispersion modeling, the GRAMM/GRAL model, developed in Austria, was used. This is a Computational Fluid Dynamics (CFD)-based numerical model, well-suited for low wind speeds and complex terrain, making it ideal for

capturing the effects of buildings and other topographical features on airflow and the dispersion of pollutants [11].

In addition to emission data, the model required:

- terrain topography and land-use data
- meteorological data, sourced from the Institute of Meteorology and Water Management (<https://dane.imgw.pl/datastore>)
- spatial and infrastructural data, sourced from the Wrocław Development Office.

The GRAMM/GRAL model features an integrated GIS (Geographic Information System) module, enabling the precise input of spatial details, including building and terrain characteristics, making it highly suitable for such analyses. The same modelling settings were used across all three fleet scenarios.

3. Results and discussion

3.1. Fleet composition

The three analysed fleets vary significantly in composition. In terms of vehicle category distribution, 'Fleet 1' and 'Fleet 2' are similar (Fig. 5), whereas 'Fleet 3' (derived from the author's observations) diverges, likely due to its relatively small sample size compared with the actual traffic volume. According to numerous statistical analyses, passenger cars comprise roughly 80% of the total urban traffic fleet.

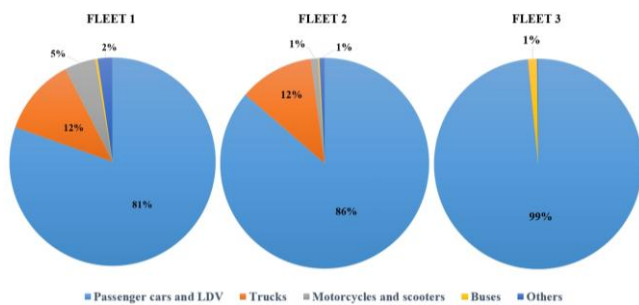


Fig. 5. Distribution of the vehicle fleet by category

Slight variations were also observed in fuel and propulsion types (Fig. 6). Due to data gaps, a comprehensive analysis of the City Office data was not possible. However, the available statistics align closely with those from the CEPiK database. In both instances, nearly 80% of the fleet used conventional fuels (gasoline or diesel), with hybrids and LPG vehicles treated as a separate category.

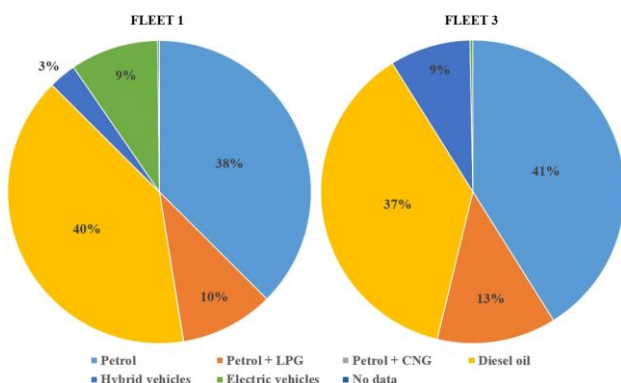


Fig. 6. Fleet composition by fuel or drive system

More significant differences emerged when analyzing the age and emission standard (Euro class) of the vehicles. The CEPiK database (2021) indicated a very high proportion of older vehicles, with over half not meeting the Euro 3 standard. In contrast, the data collected by the Wrocław City Office and the author's survey indicated that roughly three-quarters of the local fleet meets Euro 4 or higher standards (Fig. 7).

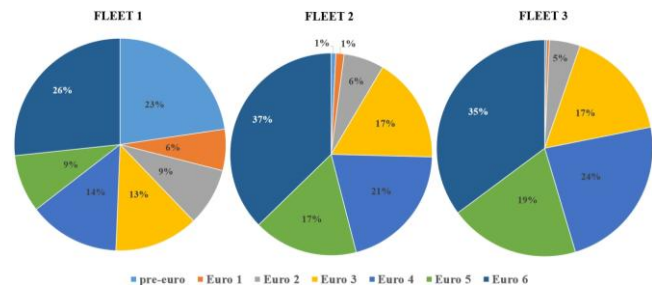


Fig. 7. Fleet composition by Euro standard

3.2. Modeling results

The modeling of the spread of pollutants in the air was carried out to verify the quality of data for the analyzed fleets. For this purpose, in the model, in addition to the standard network of receptors, which calculates the concentrations of substances in the air, an additional point was introduced: the location of the monitoring station, where the calculations were also performed. Figure 8 shows an example of the distribution of nitrogen dioxide concentrations in the modelling area for fleet 2. At the same time, Table 2 presents a summary of the modeling results, along with information on the concentrations recorded at the station. Since the model calculated the average daily maximum concentration value averaged over 1 hour, the concentration values were also averaged over the entire day of 17.08.2022.



Fig. 8. NO₂ dispersion results for fleet 2

Table 2. Average daily traffic and stretch lengths

	Concentration, µg/m ³			
	Monitoring station	Modeling, fleet 1	Modeling fleet 2	Modeling fleet 3
NO ₂	86.1	116.2	93.6	49.2

As shown in Table 2, the calculations for fleet 1 were significantly overestimated. The nitrogen dioxide concentration calculated at the monitoring station location was overestimated by about 2 times. This is most likely due to the fact that a large part of the fleet was classified as vehicles meeting low Euro standards, and as a result, the calculated emissions were greatly overestimated. In turn, the calculations for fleet 3 indicated underestimated results. The too-small sample of vehicles most likely causes this situation. It should be noted that 99% of this fleet were passenger cars, while trucks and buses with large-capacity engines are also a significant source of exhaust emissions in the city. The closest result was obtained for fleet 2. The calculated concentration is not ideal, but close to the measured one. It is essential to consider that modeling the spread of exhaust gases from vehicle traffic is often marred by numerous errors at various stages. Additionally, it should be emphasised that fleet 2 also had some errors in the data or gaps. Nevertheless, as can be seen from the analyses carried out, it was the best source of data.

4. Summary and conclusions

Assessing the impact of road traffic on air quality is a challenging endeavor, fraught with uncertainties related to statistical data, emission factors, and inconsistencies in other input data. The primary objective of this paper was to assess the quality of fleet data from different sources – statistical data from the CEPiK database, measurement data collected by the Wrocław City Office, and the author's own survey. The results clearly demonstrate that selecting an accurate vehicle fleet structure is crucial for accurately modeling traffic-related air pollution. The analyses revealed numerous data quality issues:

- misclassification of vehicles (e.g., a Fiat Seicento registered as a truck)
- incomplete or missing data

- discrepancies between available data and the classification required by the EMEP/Corinair emissions database
- misassigning Euro emission standards due to relying on the year of production rather than official Euro category. In Poland, the Euro standard is not specified in the vehicle's registration documents, which may lead to errors (e.g., a 2001 car might already be Euro 4 compliant, despite Euro 3 being in force at the time). Similar issues arise with Euro 6 vehicles registered in 2015, when the standard came into force mid-year.

Among the analysed vehicle-fleet data sources, the best-performing dataset was 'Fleet 2', originating from fleet measurements conducted by the Wrocław Municipal Office in real urban traffic. The results obtained for 'Fleet 3' were underestimated, most likely due to an insufficient sample size. In contrast, highly overestimated results were produced using 'Fleet 1'. This was caused by the presence of many old vehicles in the dataset (not meeting any emission standards) which, in reality, no longer operate on public roads. Therefore, to ensure a reliable assessment of the impact of road transport on urban air quality, it is recommended to use vehicle-fleet data that are as representative of real conditions as possible and based on the largest feasible statistical sample.

The study confirms that the most reliable source of data for estimating emissions is direct measurement of the actual traffic fleet in the area of interest. However, obtaining a sufficiently large sample for statistical reliability is challenging, resource-intensive, and time-consuming.

Acknowledgements

This work was supported by data obtained courtesy of the Wrocław City Hall, as well as free public data and from the paid Central Register of Vehicles and Drivers (Poland) database.

Nomenclature

CEPiK	Central Register of Vehicles and Drivers (Poland)	GRAMM	Graz Mesoscale Model
CFD	computational fluid dynamics	ITS	intelligent transport system
CH ₄	methane	KOBiZE	National Centre for Emissions Management
CO	carbon monoxide	NO	nitrogen monoxide
EEA	European Environment Agency	NO ₂	nitrogen dioxide
GHG	greenhouse gases	NO _x	nitrogen oxides (mixture)
GIOS	Chief Inspectorate for Environmental Protection (Poland)	N ₂ O	nitrous oxide
GRAL	Graz Lagrangian Model	PM	particulate matter
		VOC	volatile organic compounds

Bibliography

- [1] Alotaibi S, Almujiab H, Mohamed KAA. Towards cleaner cities: estimating vehicle-induced PM_{2.5} with hybrid EBM-CMA-ES modeling. *Toxics*. 2024;12:827. <https://doi.org/toxics12110827>
- [2] Angelis ED, Carnevale C, Di Marcoberardino G. Low emission road transport scenarios: an integrated assessment of energy demand, air quality, GHG emissions, and costs. *T-ASE* 2022; 19(1):37-47. <https://doi.org/10.1109/TASE.2021.3073241>
- [3] De Nunzio G, Laraki M, Thibault L. Road traffic dynamic pollutant emissions estimation: from macroscopic road information to microscopic environmental impact. *Atmosphere*. 2021; 12(53). <https://doi.org/10.3390/atmos12010053>
- [4] German Environment Agency: HBEFA Traffic Situations. Application guidelines. 2025. <https://doi.org/10.60810/openumwelt-8047>
- [5] Heni L, Haj-Salem H, Lebacque J-P. Integration and Comparative Analysis of COPERT and HBEFA emission models

- coupled with the BIDIM-GSOM traffic model for large-scale networks. *Transp Res Proc.* 2025;86:361-370. <https://doi.org/10.1016/j.trpro.2025.04.046>
- [6] Jurkovic M, Kalina T, Skrucany T. Environmental impacts of introducing LNG as alternative fuel for urban buses – case study in Slovakia. *Promet – Traffic&Transportation.* 2020;32(6):837-847. <https://doi.org/10.7307/ptt.v32i6.3564>
- [7] Lindhjem CE, Pollack AK, DenBleyker A. Effects of improved spatial and temporal modeling of on-road vehicle emissions. *J Air & Waste Manage Assoc.* 2012;62(4):471-484. <https://doi.org/10.1080/10962247.2012.658955>
- [8] Ma S, Tong D, Harkins C. Impacts of on-road vehicular emissions on U.S. air quality: a comparison of two mobile emission models (MOVES and FIVE). *J Geophys Res Atmospheres.* 2024;129(20). <https://doi.org/10.1029/2024JD041494>
- [9] Ministry of Climate and Environment: ‘National balance of SO₂, NO_x, CO, NH₃, NMLZO, heavy metals and TZO emissions for the years 1990–2022. Summary report. Warsaw 2024.
- [10] Oanh NTK, Huy LN, Permadi DA. Assessment of urban passenger fleet emissions to quantify climate and air quality co-benefits resulting from potential interventions. *Carbon Management.* 2018;9(4):367-381. <https://doi.org/10.1080/17583004.2018.1500790>
- [11] Oettl D. Quality assurance of the prognostic, microscale wind-field model GRAL 14.8 using wind-tunnel data provided by the German VDI guideline 3783-9. *J Wind Eng Ind Aerodyn.* 2015;142:104-110. <https://doi.org/10.1016/j.jweia.2015.03.014>
- [12] Orth S, Russel AG. Assessment of light-duty versus heavy-duty diesel on-road mobile source emissions using general additive models applied to traffic volume and air quality data and COVID-19 responses. *J Air & Waste Manage Assoc.* 2023;75(5):374-393. <https://doi.org/10.1080/10962247.2023.2185315>
- [13] Polish Association for New Mobility: ‘Report: Transport air pollution. Strategies for measuring and reducing transport emissions – actions from local to national level’. Warsaw 2024.
- [14] Reyna JL, Chester MV, Ahn S. Improving the accuracy of vehicle emissions profiles for urban transportation greenhouse gas and air pollution inventories. *Environ Sci Technol.* 2014;49(1):369-376. <https://doi.org/10.1021/es5023575>
- [15] Shi Q, Ciais P, Megel N. High spatiotemporal resolution traffic CO₂ emission maps derived from floating car data (FCD) for 20 European cities (2023). *Earth Syst Sci Data Discuss.* 2025; in review. <https://doi.org/10.5194/essd-2025-458>
- [16] Szczotka A, Puchałka B, Bielaczyc P. Influence of drivers’ driving style on the uncertainty of measurements of exhaust emissions on a chassis dynamometer. *AUTOBUSY – Technika, Eksploatacja, Systemy Transportowe.* 2018;19(12):675-679. <https://doi.org/10.24136/atest.2018.476>
- [17] Wang L, Chen X, Xia Y. Operational data-driven intelligent modelling and visualization system for real-world, on-road vehicle emissions – a case study in Hangzhou City, China. *Sustainability.* 2022;14(9):5434. <https://doi.org/10.3390/su14095434>
- [18] web.jrc.ec.europa.eu/policy-model-inventory/explore/models/model-copert/ (accessed on 2025-12-01).
- [19] Xu J, Wang J, Hilker N. Comparing emission rates derived from a model with those estimated using a plume-based approach and quantifying the contribution of vehicle classes to on-road emissions and air quality. *J Air & Waste Manage Assoc.* 2018;68(11):1159-1174. <https://doi.org/10.1080/10962247.2018.1484395>
- [20] Yu C, Yang X, Mu J. A systematic review of urban road traffic CO₂ emission models. *Carbon Footprints.* 2025;4:17:1-23. <https://doi.org/10.20517/cf.2025.12>

Maria Skrełowicz, DEng. – Faculty of Mechanical Engineering, Wrocław University of Science and Technology, Poland.
e-mail: maria.skretowicz@pwr.edu.pl



ROCKET TECHNOLOGIES

Suborbital Rocket
ILR-33 AMBER 2K



Łukasiewicz
Institute
of Aviation

SATELLITE TECHNOLOGIES

SPARK (Spacecraft Platform Architecture
for Research and Key-enabling missions)

AVIATION TECHNOLOGIES

Aerobatic Glider I-45 JAY



The Łukasiewicz Research Network - Institute of Aviation offers a wide range of specialized research, engineering services and products. We provide comprehensive solutions, ranging from dedicated analyzes, simulations, engineering design, through the selection, testing and certification of materials and structures, to rapid prototyping and additive manufacturing.

al. Krakowska 110/114, 02-256 Warsaw, Poland
e-mail: info@ilot.lukasiewicz.gov.pl / www.ilot.lukasiewicz.gov.pl



Publisher:

**Polish
Scientific
Society
of Combustion
Engines**



**ISSN: 2300-9896
eISSN: 2658-1442**

Combustion Engines

Polskie Towarzystwo Naukowe Silników Spalinowych



www.combustion-engines.eu